21st Edition

ISSN 1454 - 8003

PROCEEDINGS OF INTERNATIONAL CONFERENCE OF HYDRAULICS, PNEUMATICS, TOOLS, SEALING ELEMENTS, FINE MECHANICS, SPECIFIC ELECTRONIC EQUIPMENT &MECHATRONICS

HERVEX 2014

HERVEX

November 2014
21st Edition

INTERNATIONAL CONFERENCE AND EXHIBITION

HERVEX 2014

Hydraulics| Pneumatics|
Sealing Elements| Fine Mechanics| Tools|
Specific Electronic Equipment & Mechatronics

CALIMANESTI - CACIULATA, NOVEMBER 5 - 7, 2014

HERVEX 2014

ORGANIZERS

HYDRAULICS AND PNEUMATICS RESEARCH INSTITUTE
BUCHAREST, ROMANIA

KOMAG INSTITUTE OF MINING TECHNOLOGY, GLIWICE, POLAND

CHAMBER OF COMMERCE AND INDUSTRY VALCEA, ROMANIA

PARTNERS

DEVELOPMENT AND ASSESSMENT INSTITUTE IN WASTE WATER
TECHNOLOGY, AACHEN, GERMANY

WROCLAW UNIVERSITY OF TECHNOLOGY, POLAND

“POLITEHNICA” UNIVERSITY OF BUCHAREST, ROMANIA

”GHEORGHE ASACHI” TECHNICAL UNIVERSITY OF IASI, ROMANIA

TECHNICAL UNIVERSITY OF CLUJ-NAPOCA, ROMANIA

“POLITEHNICA” UNIVERSITY OF TIMISOARA, ROMANIA

MEDIA PARTNERS

Tehnica Instalaţiilor

INSTAL NEWS.RO

T&T

HIDRAULICA
HYDRAULICS-PNEUMATICS-TRIBOLOGY-ECOLOGY-SENSORICS-MECHATRONICS

PNEUMATYKA.com

Partener European

CONFERENCE HELD UNDER THE PATRONAGE OF

Comité Européen des Transmissions Oléohydrauliques et Pneumatiques
CETOP

Published by - Hydraulics and Pneumatics Research Institute, Bucharest, Romania
- Chamber of Commerce and Industry Valcea, Romania

INTERNATIONAL CONFERENCE AND EXHIBITION

HERVEX 2014

IS SUPPORTED BY:

MINISTRY OF NATIONAL EDUCATION - STATE AUTHORITY FOR SCIENTIFIC RESEARCH, TECHNOLOGICAL DEVELOPMENT AND INNOVATION

NATIONAL PROFESSIONAL ASSOCIATION OF HYDRAULICS AND PNEUMATICS IN ROMANIA - “FLUIDAS”

COMMITTEES

HONORARY COMMITTEE

Ahmet SERDAROGLU– President of European Fluid Power Committee – CETOP

Rudolf SCHEIDL –Institute of Machine Design and Hydraulic Drives, Johanes Kepler University, Linz, Austria

Henryk CHROSTOWSKI – Wroclaw University of Technology, Poland

Humbertus MURRENHOFF – Institute for Fluid Power Drives and Controls at Aachen University, Germany

PhD.Eng. Petrin DRUMEA – President of National Professional Association of Hydraulics and Pneumatics “FLUIDAS”, Romania

ORGANIZING COMMITTEE

Eng. Gheorghe RIZOIU – General Manager of Chamber of Commerce and Industry Valcea, Romania

PhD. Eng.Gabriela MATACHE – Hydraulics and Pneumatics Research Institute in Bucharest, Romania

Assoc.Prof. PhD.Eng. Erol MURAD – “POLITEHNICA” University of Bucharest, Romania

Prof. PhD. Eng. Dan OPRUTA – Technical University of Cluj-Napoca, Romania

Assoc.Prof. PhD.Eng. Constantin CHIRITA – Technical University “Gheorghe Asachi”- Iasi, Romania

Prof. PhD. Eng. Ilare BORDEASU – “Politehnica” University in Timisoara, Romania

Assoc.Prof. PhD.Eng. Constantin RANEA – Ministry of National Education, Romania

Dr inz. Antoni KOZIEL – KOMAG Institute of Mining Technology, Gliwice, Poland

Dr inz. Krzysztof NIESPIALOWSKI - KOMAG Institute of Mining Technology, Gliwice, Poland

Dr inz. Edward PIECZORA – KOMAG Institute of Mining Technology, Gliwice, Poland

PhD. Eng. Elmar DORGELOH – Manager of Development and Assessment Institute in Waste Water Technology at RWTH Aachen University, Germany

PhD. Eng. Krzysztof KEDZIA – Wroclaw University of Technology, Poland

SCIENTIFIC PROGRAMMEE COMMITTEE

PhD.Eng. Mohamed HAJJAM – University of Poitiers – IUT Angouléme, France

PhD.Eng. Zygmunt DOMAGALA – Wroclaw University of Technology, Poland

Dr inz. Malgorzata MALEC – KOMAG Institute of Mining Technology, Gliwice, Poland

Dr inz. Krzysztof STANKIEWICZ - KOMAG Institute of Mining Technology, Gliwice, Poland

Prof. Stanislaw SZWEDA – KOMAG Institute of Mining Technology, Gliwice, Poland

Prof. Teodor WINKLER – KOMAG Institute of Mining Technology, Gliwice, Poland

PhD.Eng. Amadio BOLTZANI – “ASSOFLUID”, Italy

PhD.Eng. Gabriela MATACHE – Hydraulics and Pneumatics Research Institute in Bucharest, Romania

Eng. Radu ALEXANDRU – FESTO S.R.L., Romania

Prof. PhD.Eng. Valeriu BANU – S.M.C. Romania

Prof. PhD.Eng. Doru CALARASU – Technical University “Gheorghe Asachi”- Iasi, Romania

Eng. Ioan CAMPEAN – S.C. HIDROSIB S.A. Sibiu, Romania

PhD.Eng. Tudor CRACIUNOIU – S.C. ICTCM S.A. Bucharest, Romania

Eng. Mircea DANCIU – PARKER HANNIFIN Corporation Romania

Prof. PhD.Eng. Gheorghe GHEORGHE – General Manager – National Institute of Research and Development in Mechatronics and Measurement Technique (INCDMTM), Bucharest, Romania

Prof. PhD.Eng. Vasile JAVGUREANU – Technical University of Moldova, Chisinau, Republic of Moldova

PhD.Eng. Ioan LEPADATU – Hydraulics and Pneumatics Research Institute in Bucharest, Romania

Eng. Leopold LUPUSANSCHI- S.C. CEROB S.R.L. Bucharest, Romania

Prof. PhD.Eng. Pavel MACH – Technical University of Praga, Czech Republic

PhD.Eng. Daniel MARIN- S.C. FAST ECO S.A. Bucharest, Romania

PhD.Eng. Adrian MIREA – SC ROMFLUID SA, Bucharest, Romania

Eng. Ioan MOLDOVEANU – Festo S.R.L., Bucharest, Romania

PhD.Eng. Andrei DRUMEA – “POLITEHNICA” University of Bucharest, Romania

Prof. PhD.Eng. Johann NICOLICI – Technical University of Viena, Austria

Eng. Cristian SEN – SUSZI – INDUSTRIAL SRL Constanta, Romania

Prof. PhD.Eng. Ion DAVID- Technical University of Civil Engineering in Bucharest, Romania

PhD.Eng. Ion PIRNA – General Manager of National Institute of Research – Development for Machines and Installations Designed to Agriculture and Food Industry – INMA, Bucharest, Romania

PhD.Eng. Mircea PRICOP- S.C. HESPER S.A. Bucharest, Romania

Prof. PhD.Eng. Liviu VAIDA – Technical University of Cluj-Napoca, Romania

Prof. PhD.Eng. Nicolae VASILIU – “POLITEHNICA” University of Bucharest, Romania

Eng. Nicolae TASU – HANSA FLEX, Romania

Prof.PhD.Eng. Paul SVASTA – “POLITEHNICA” University of Bucharest, Romania

Phd.Eng. Catalin DUMITRESCU – Manager of Hydraulics and Pneumatics Research Institute in Bucharest, Romania

Prof. PhD.Eng. Rudolf SCHEIDL – Institute of Machine Design and Hydraulic Drives, Johanes Kepler University, Linz, Austria

Eng. Valentin CISMARU – President of Chamber of Commerce and Industry Valcea, Romania

Assoc.Prof. PhD.Eng. Constantin CHIRITA – Technical University “Gheorghe Asachi”- Iasi, Romania

Prof. PhD.Eng. Alexandru MARIN – “POLITEHNICA” University of Bucharest, Romania

SECRETARY

Valentin MIROIU – Hydraulics and Pneumatics Research Institute in Bucharest, Romania

Mgr. Anna OKULINSKA – KOMAG Institute of Mining Technology, Gliwice, Poland

Cristina NUICA – Chamber of Commerce and Industry Valcea, Romania

EXHIBITION ORGANIZING COMMITTEE

Lorena MATEESCU – Chamber of Commerce and Industry Valcea, Romania

PhD.Eng. Ioan LEPADATU – Hydraulics and Pneumatics Research Institute in Bucharest, Romania

SPECIALIZED REVIEWER COMMITTEE

PhD.Eng. Heinrich THEISSEN – Institute for Fluid Power Drives and Controls, Aachen University, Germany

PhD.Eng. Petrin DRUMEA – President of National Professional Association of Hydraulics and Pneumatics “FLUIDAS”, Romania

Assoc.Prof. PhD.Eng. Constantin RANEA – Ministry of National Education, Romania

CONTENTS

SECTION I: INDUSTRIAL HYDRAULICS AND MECHATRONICS

SECTION II: MOBILE HYDRAULICS AND TRIBOLOGY

SECTION III: HYDRAULIC SYSTEMS

SECTION IV: ENVIRONMENT, ECOLOGY AND RENEWABLE ENERGY

SECTION V: EDUCATION AND TRAINING IN FLUID POWER

ISSN 1454 - 8003
Proceedings of 2014 International Conference of Hydraulics and Pneumatics - HERVEX
November 5 – 7, Calimanesti-Caciulata, Romania

STUDY OF FLOW FORCES ACTING ON THE SPOOL OF SOLENOID DIRECTIONAL CONTROL VALVE

Janusz RAJDA[1], Elżbieta RAJDA[2]

[1] PONAR Wadowice S.A., janusz.rajda@ponar-wadowice.pl

[2] elzbieta.rajda@ponar-wadowice.pl

Abstract: *This paper concerns the issue of flow forces acting on the spool of a directional control valve during its overdrive. These forces have significant influence on the performance curves of the valve operating limit. Bench testing of axis component flow forces for different types of spools, performing various connection configurations of a solenoid directional control valve was conducted in order to determine their actual values as a function of the spool displacement. The test cycle was repeated for three various designs of the valve body in order to provide a comparative assessment. In addition, the performance curves of the operating limit were obtained to confirm the results.*

Keywords*: directional control valve, flow force, valve operating limit*

1. Introduction

Hydraulic drives and controls are widely used in various industries. Their special feature is that the actuators can produce high forces and torques at a relatively low mass and high density of the transmitted power. Another important advantage is the fact that the solenoid operated versions are well suited for use with electronic and microprocessor-based control systems. Directional control valves are used to control the direction of flow of the working fluid and are found in almost every hydraulic system. Usually, they control the working motion of the hydraulic cylinders or motors, and turn on/off a specific branch of the system. The most commonly used types of directional control valves are: spool types, four-port and subplate mounted versions, according to ISO 4401, electrically direct operated by solenoids. Hence the interest of scientific research and industrial centers in continuous improvement of their performance [6]. During development design of directional control valves and their comparative evaluation both experimental testing methods and computer flow simulation method based on the analysis of CFD [1, 2] are used. The latter methods are continuously developed, but still must be verified by experimental studies [3, 4]. The subject of this paper is the experimental study of flow forces acting on the spool of the directional control valve subplate mounted according to ISO 4401-05. The value and direction of the forces can be one of the criteria for the assessment of its design and having a decisive influence on the scope of the valve operating limit [5, 7, 8].

2. Construction and operation of the spool type directional control valve subplate mounted according to ISO 4401-05

As an object of the study the popular four-port solenoid operated directional control valve coded WE10 [12] which is subplate mounted according to the ISO 4401-05 standard [9] was chosen, often referred to as CETOP05. Standard subplate mounting pattern allows for easy assembly and disassembly of the valve without unnecessary dismantling the pipelines. It also allows the use of the valves from different manufacturers [11, 12, 13, 14]. Directional control valves WE10 are relatively simple and cheap solutions of direct solenoid operated valves. They are very popular in the industry. They can be operated by the solenoids with different supply voltage. The most widely used are DC powered solenoids, usually with a voltage of 24 V. Fig. 1 shows the design and operation of this type of directional control valve. The spool (2), with specially adopted shape is moved along the hole of the body (1) by means of solenoids (3) to the end position, allowing the change of the configuration of connections between the four ports of the valve. Return of the spool to the starting position is possible due to the centering springs (4), after the power is turned off at the solenoid. Various spools can be used interchangeably with one valve body. This allows for performance of different configurations of the connections between the four ports: *P, A, B, T* (T_A, T_B).

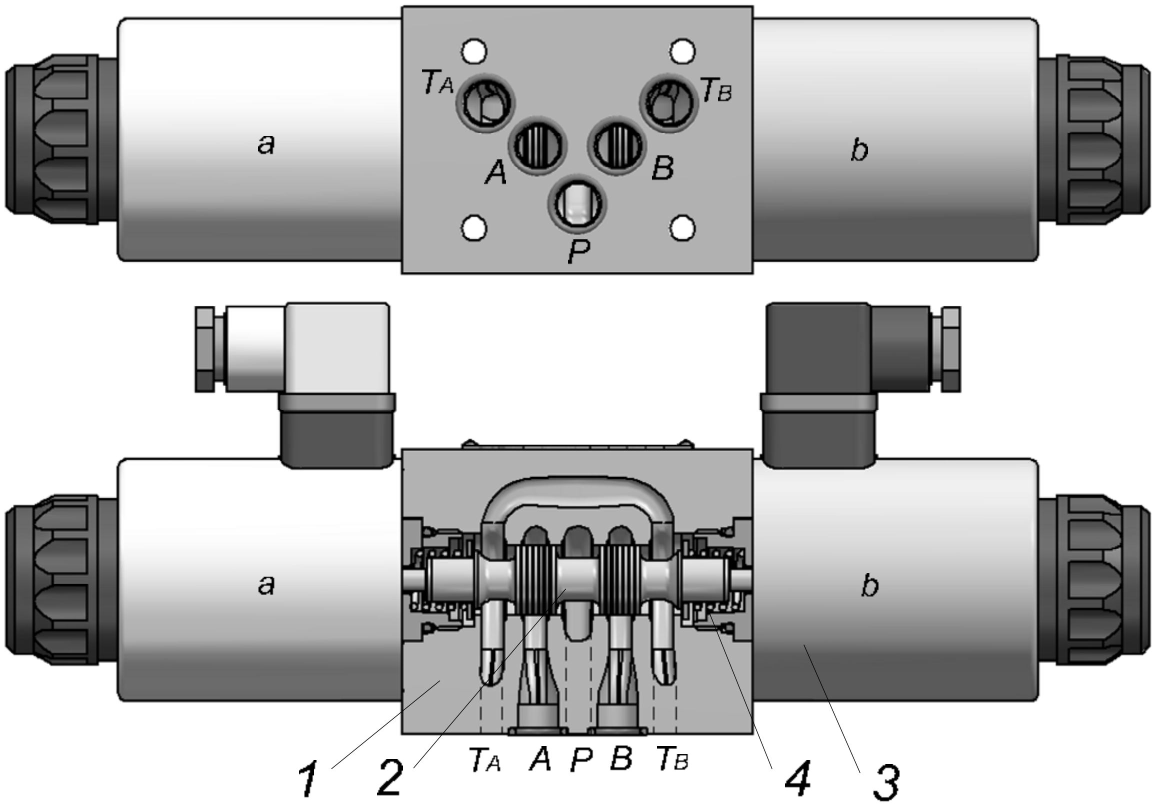

Fig. 1. Directional control valve subplate mounted to ISO 4401-05 standard: 1 - body, 2 - spool, 3 - solenoid, 4 - spring.

A characteristic of this valve is that according to the standard ISO 4401-05 [9], it has a doubled drain port T_A and T_B (Fig. 2). Control of the hydraulic actuator movement requires often the use of additional valves to have leak-proof cut-off, pressure and speed of movement limited. The subplate mounting type allows for stacking of additional modular valves between the directional control valve and the subplate. For this reason, it is assumed that, in reality, only one drain port is connected to the system the port T_A. Therefore, the standard subplates are manufactured with connection of only one drain port (T_A). This means that even with the implementation of symmetric configuration of connections for this type of valve, both pressure drops and flow forces will not be symmetrical at solenoids *a* and *b* override. This fact makes it difficult to optimize the pressure-flow performance of the valve for this size of connection pattern.

ISSN 1454 - 8003
Proceedings of 2014 International Conference of Hydraulics and Pneumatics - HERVEX
November 5 – 7, Calimanesti-Caciulata, Romania

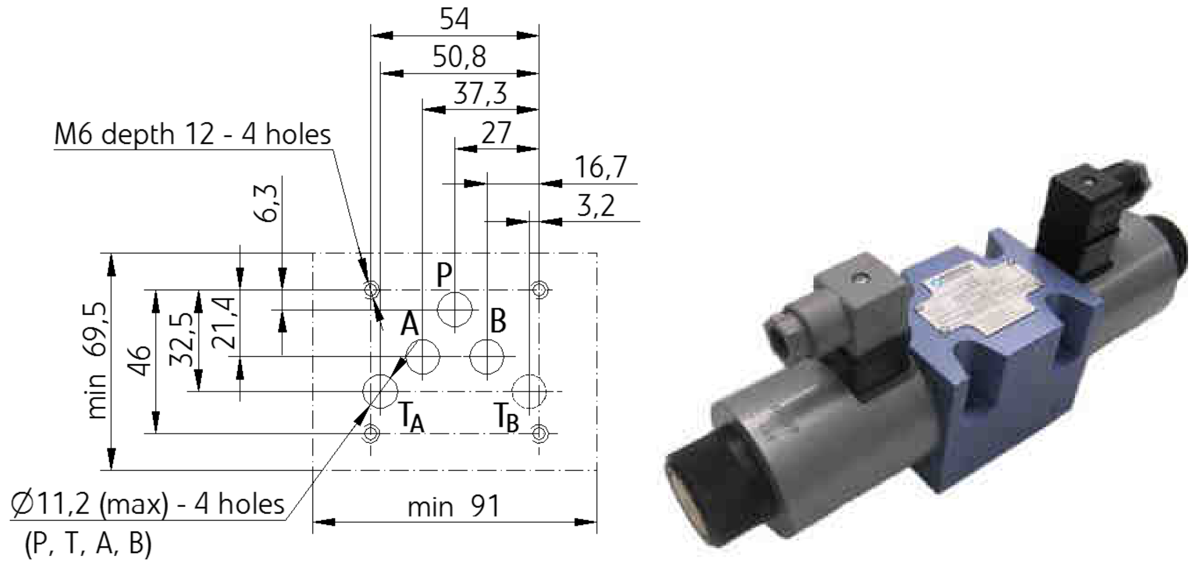

Fig. 2. Connection pattern to ISO 4401-05 and view of directional control valve [11].

Flow force study presented in this paper has been carried out for a typical valve where port T_A was connected to a drain line and the port T_B was cut off.

3. Basic technical features of spool type directional control valves

The basic technical features describing spool type solenoid operated directional control valves include:

- maximum working pressure,
- pressure drop,
- operating limit.

The first technical feature - maximum working pressure - is associated mainly with the use of strength materials and rigid body structure. Maintaining the proper rigidity of the body results from the application of the smallest possible clearance between the control spool and the body, in order to minimize internal leakage. For the spool type valves, maximum operating pressure range from 31.5 MPa to 35 MPa.

Considering pressure drop at the valve, improvement of this feature is somewhat more difficult. Largely, it comes down to design of the body with a possibly large cross-section of the channels and such their configuration that the pressure drop at the valve is as small as possible. The valve spool shape also affects pressure drop, in particular control edge spacing and shape of the recesses in the spool. The occurrence of pressure drop is a disadvantageous phenomenon. It causes an energy loss which turning into heat makes the temperature rise in the working fluid, and that in turn requires the use of cooling system. Sample flow resistance curves for the valve to ISO 4401-05 are shown in Fig. 3.

ISSN 1454 - 8003
Proceedings of 2014 International Conference of Hydraulics and Pneumatics - HERVEX
November 5 – 7, Calimanesti-Caciulata, Romania

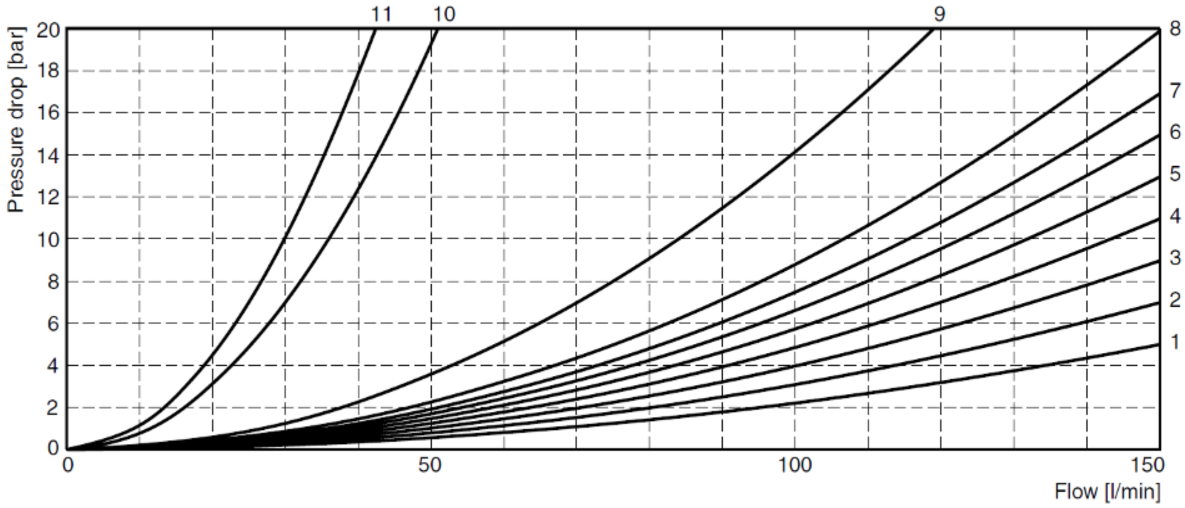

Fig. 3. Sample pressure drop curves for different configurations and flow paths of directional control valves subplate mounted to ISO 440-05 [12].

Operating limit of the directional control valve is the technical feature most commonly illustrated as a curve in a coordinate system - the volumetric flow rate vs. pressure. It consists of the points corresponding to the limit values of pressure and flow rate for which the valve is still able to correctly operate. The proper operation of the valve is expressed by the possibility of spool shift between the neutral position and the end position and vice versa. Sample curves of the performance limit for the valve to ISO 4401-05 are shown in Fig. 4.

a) b)

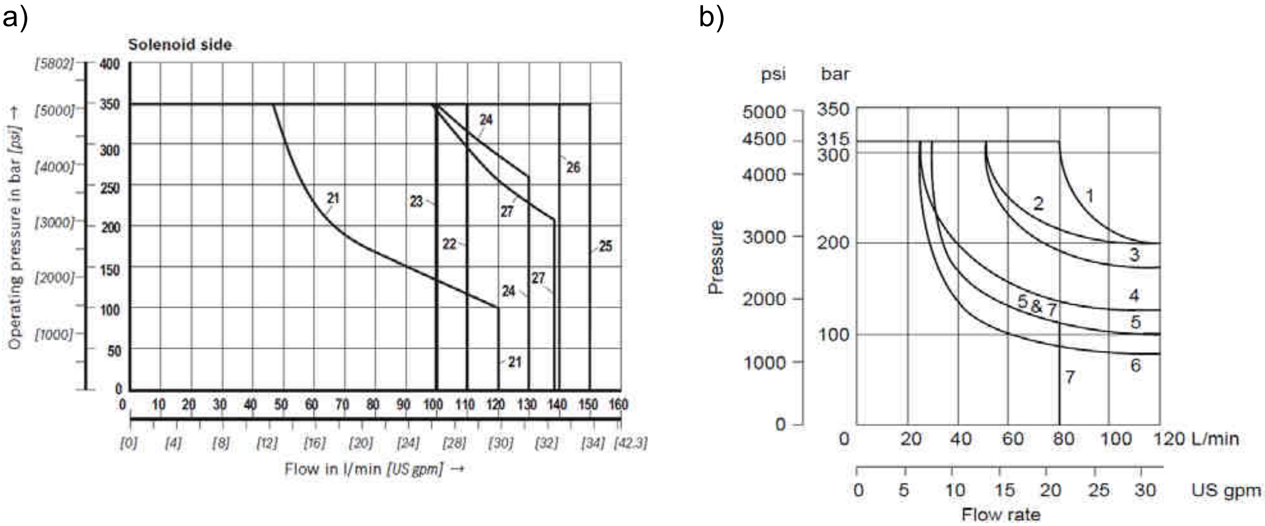

Fig. 4. Sample curve of the operating limit for directional control valve subplate mounted ISO 4401-05: a) with DC solenoid [13], b) with AC solenoid [14].

The operating limit of the valve is affected by more factors than the flow resistance. In addition to the design of the communication channels of the body and the spool, force characteristics of the control solenoids and return springs have significant impact on the performance range of the valve.

To summarize the undertaken analysis of the basic technical features for spool type directional control valves, we can see that design of the body has the significant impact on them. In addition, if the valve complies with ISO 4401, it is necessary to keep the dimensional connection pattern and the corresponding limits of overall body dimensions. Thus, the body design solution must fulfill various technical requirements and, therefore, remains a key component of any directional control valve.

4. Balance of forces acting on the spool of directional control valve

Operating limit of the spool valve, during flow of the working fluid at its override, is directly related to the balance of forces acting on the spool.

During the override the spring centered spool of solenoid operated directional control valve is affected on its movement direction by the following forces:

- solenoid force F_e,
- centering spring force F_s,
- flow force F_h,
- inertia force of moving masses of components of the valve (spool, solenoid armature, retainer and spring) F_i,
- viscous friction force F_v,
- dry friction force F_f.

Fig. 5 shows the forces acting on the spool at its override during the flow of working fluid.

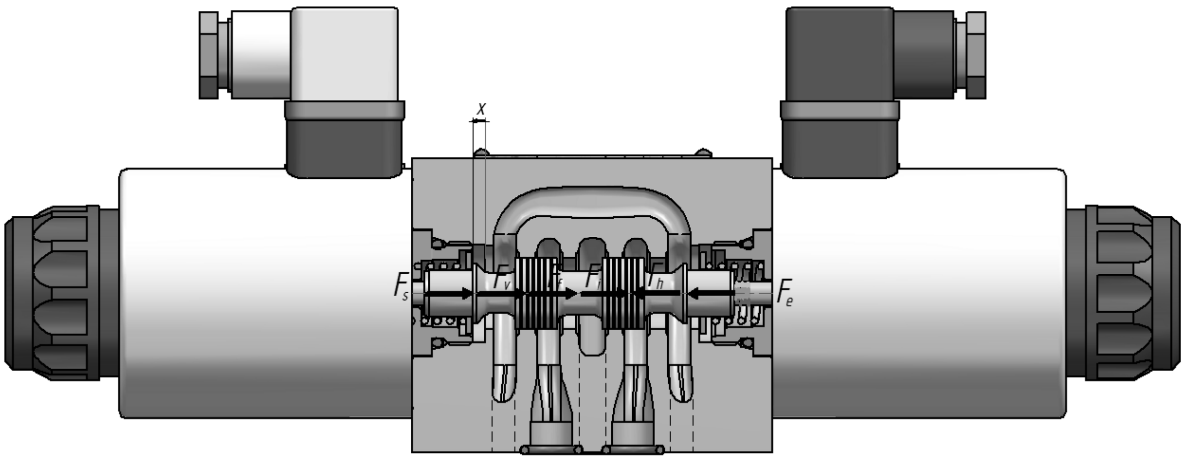

Fig. 5. Forces acting on the spool at its override.

The balance of these forces was included in the formula (1).

$$F_e + F_h = F_s + F_i + F_v + F_f \tag{1}$$

The components are described by following formulas:

$$F_s = F_{s0} + k_1 \cdot x \tag{2}$$

where: F_{s0} – preload force of the centering spring, k_1 - stiffness coefficient of the spring, x - displacement of the spool from the neutral position (frequently called as a stroke),

$$F_v = k_2 \cdot \frac{dx}{dt} \tag{3}$$

where: k_2 - attenuation coefficient of the spool movement,

$$F_f = k_3 \cdot F_n \tag{4}$$

where: F_n - resultant value of the normal force acting on valve spool, k_3 - replacement of dry friction coefficient,

$$F_i = m_s \cdot \frac{d^2x}{dt^2} \tag{5}$$

where: m_s - resultant mass of the valve spool, retainer and spring.

For the given design of the directional control valve, the solenoid is normally a constant element, assumed as *a priori*. Solenoid force F_e as a function of a pusher movement can be thus determined on the base of technical features declared by the manufacturer of solenoid or directly measured the force performance at a suitable bench. In the case of the centering spring force F_s the force performance curve is generally linear. This force performance curve can be determined by calculation or experiments in a similar way as for the performance curve of the solenoid. Spring force features are chosen according to the performance curve of the solenoid for obtaining the best operating limit for the particular valve spool.

Viscous friction force F_v depends on the design details (clearance between the spool and the hole in the body), working conditions (fluid viscosity) and the speed of movement of the spool. Inertia force F_i follows from Newton's second law and depends on the mass of the spool and moving along with it valve components, and acceleration of the movement of those masses. It can be seen that the forces F_i and F_v will attain small values, if velocity and acceleration of the spool override will be relatively small, e.g. with manual control. Dry friction force F_f is a function of the resultant normal forces acting on the spool during its override. The resultant value of the normal force consists, among others, of the normal component of the flow force and the force from the static pressure, which pushes the spool to the wall of the hole of the body. In addition, the dry friction force will depend on design details such as the number and shape of the relief grooves on the spool, surface roughness of the spool and the hole in the body. Determination of the value of force F_f by direct experiment is relatively difficult. You can expect that when measuring the flow forces hysteresis of values of axial forces at the spool movement back and forth occurs. On this basis we will assess its value.

The value of the flow forces acting at the direction of spool movement can be analytically determined from the principle of momentum conservation for hydraulic fluid stream.

$$F_h = \rho \cdot [Q_1(v_{Q1}\cos\alpha_1 - v_{Q2}\cos\alpha_2) - Q_4(v_{Q4}\cos\alpha_4 - v_{Q5}\cos\alpha_5)] \tag{6}$$

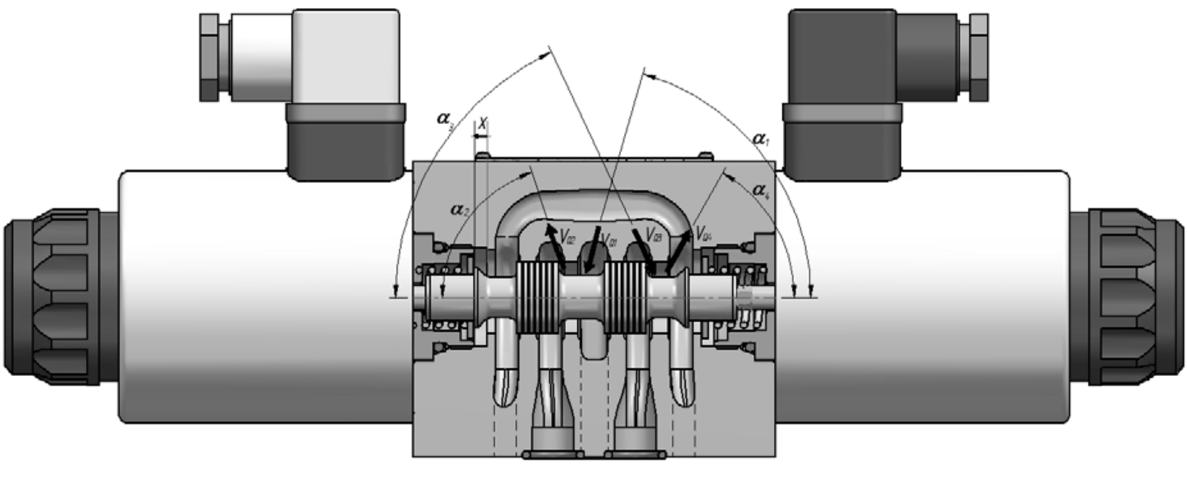

Fig. 6. Liquid stream velocity vectors in the control slots.

However, this equation contains the unknown as the working fluid velocity v_1, v_2, v_3, v_4, in the control slots of the valve and their directions expressed by the angles α_1, α_2, α_3, α_4 (Fig. 6). Correct determination of these unknowns makes a lot of difficulties. This requires separate experiments or usage of the ready-made results from similar studies. It is also possible to determine these parameters through CFD analysis. However, in each case assumes a one-dimensional flow model, a and thus, the results can be roughly approximate. The analysis of three-dimensional flow forces at the current opportunities can be carried out using the CFD software. To determine the complete characterization of the flow forces all of these analyzes must be repeated for the successive positions of the spool, which is very time-consuming. Furthermore, due to the complexity of the issues, the results of analysis should be subjected to experimental verification.

To summarize the analysis carried out so far, we can conclude that:

- flow force value at the given type of solenoid and the specified centering spring is crucial for the operating limit of directional control valve,
- design leading to the reduction of flow forces acting at the direction of the spool axis should be the main task to improve the operating limit of directional control valve,
- the value of flow force acting at the direction of the spool movement during its override can be considered one of the criteria for assessing the design of the valve.

The above statements lead to a conclusion that the assessment of the flow forces acting at the valve spool experimentally is necessary to conduct research to improve the operating limit of directional control valve.

5. Experimental method of the flow forces assessment

For the experiments, a special measuring device was designed and manufactured. The cross-section of 3D model is shown in Fig. 7. To test the flow forces the solenoids and springs were removed from the directional control valve. Instead, a displacement transducer LVDT (3) and a force sensor (4) were installed. These elements were pivotally connected with the valve spool (2). The valve spool was held in a predetermined position by the force sensor, which could measure a force in either direction (compression or tension). Since the solenoids and springs were removed, the test could include the impact forces associated with the flow of working fluid and friction of the spool. In order to reduce influence of the friction forces, the spool with maximum radial clearance within acceptable tolerances was made.

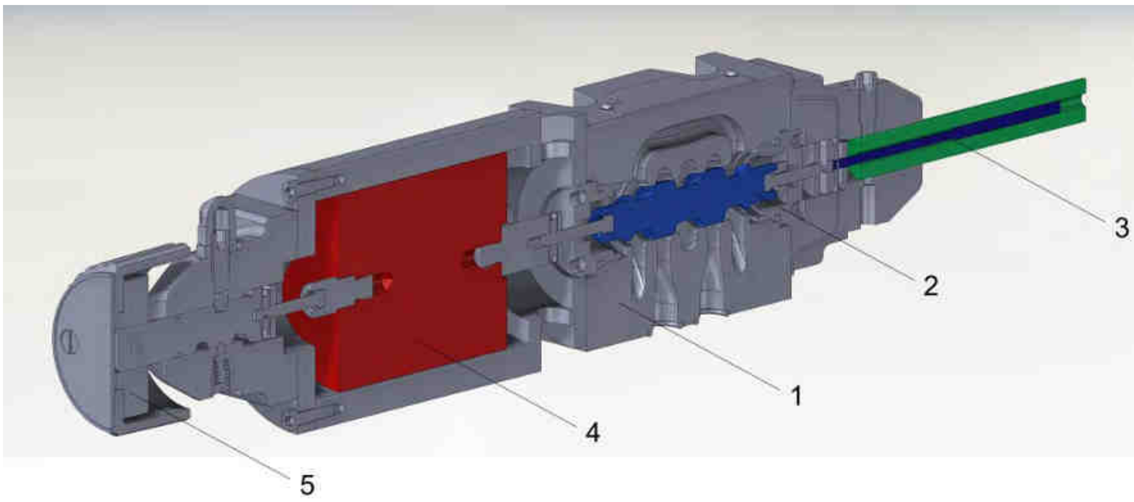

Fig. 7. Cross-section of a 3D model – measuring device and directional control valve with transducers: 1 - valve body, 2 - spool, 3 - LDVT transducer, 4 - force sensor, 5 - screw device.

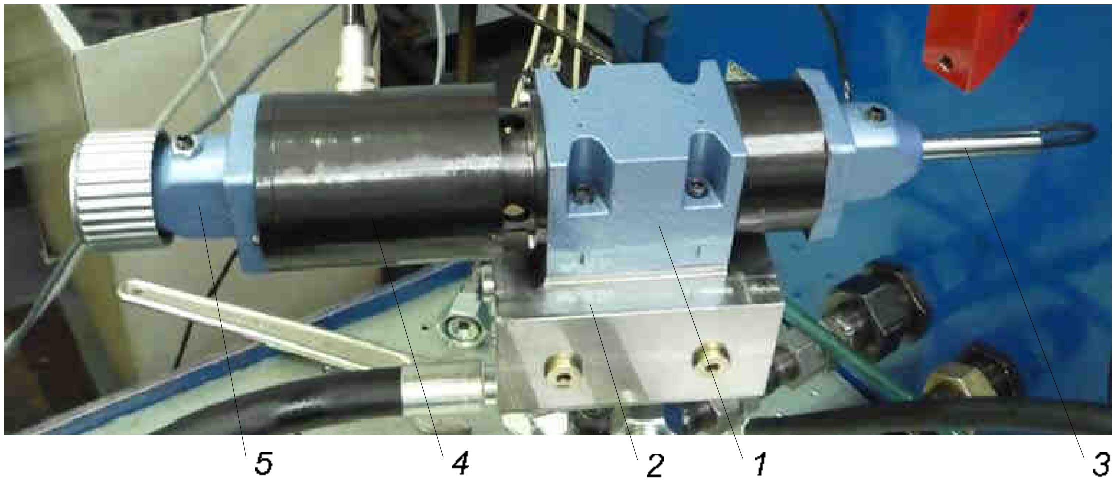

Fig. 8. Directional control valve with force and displacement measuring devices: 1 - valve body, 2 - subplate, 3 - LDVT transducer, 4 - force sensor body, 5 - screw device.

Fig. 8 shows the directional control valve with force and displacement measuring devices built in on the test bench.

6. Measurement of flow forces for standard solution

Using the designed and built device, measurements of the flow forces acting at the direction of movement of the spool for directional control valve WE10 with a standard body, for various types of spools (Fig. 9a, 9b). Schematic diagram of valve port connections in a hydraulic system of the test bench is shown in Figure 9c. The experiments were carried out on a test bench with a kinematic oil viscosity of 41 cSt keeping its constant value during the test by stabilizing its temperature.

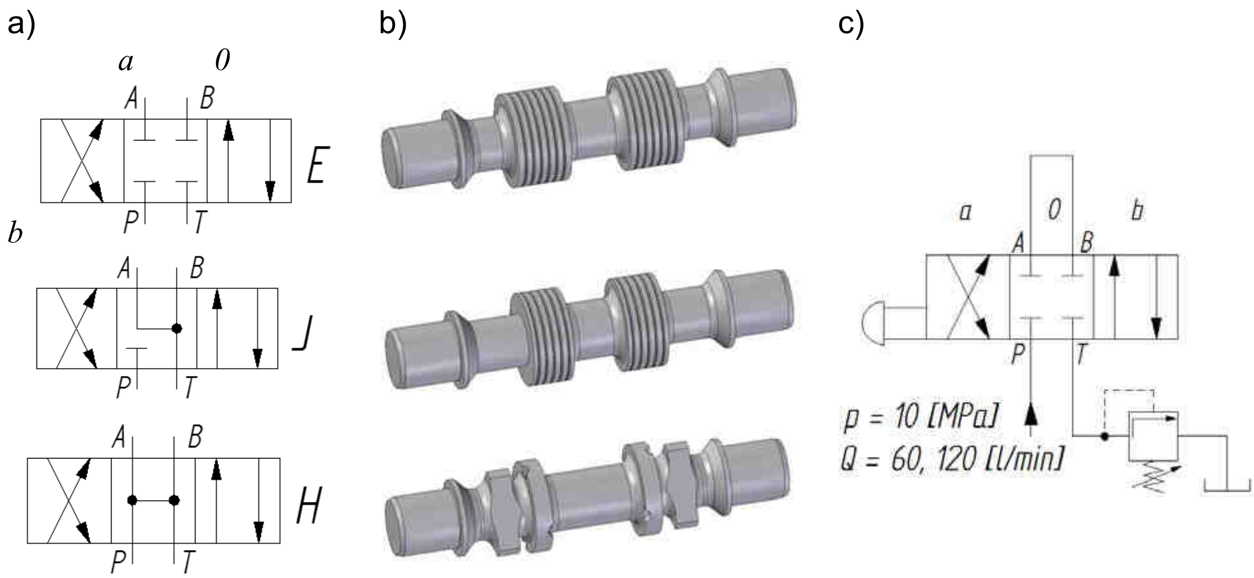

Fig. 9. Testing of spool types E, J, H of directional control valve WE10: a) schemes of connections, b) view, c) valve port connections of WE10 during the test.

Each experiment was conducted for a complete cycle of the spool movement, which included override from the neutral position *0* to end one *a*, return to the neutral position, and then override to the end position *b* and return to the initial position *0*. The overrides were performed in a smooth manner and at the rate of approximately 50 times slower than at the real valve solenoid operated. As a result, the viscous friction forces, as well as the mass inertia forces can be omitted at the measurement results. Unfortunately, the dry friction force existing at the time of measurement cannot be completely eliminated.

The experimental tests were carried out for two values of volumetric flow rate Q = 60 dm^3/min and Q = 120 dm^3/min.

Fig. 10 - 12 present graphs of the flow force for volume flow rate Q = 120 dm^3/min. Positive values of spool displacement from the neutral position corresponds to *PA-BT* connections, negative - *PB-AT*.

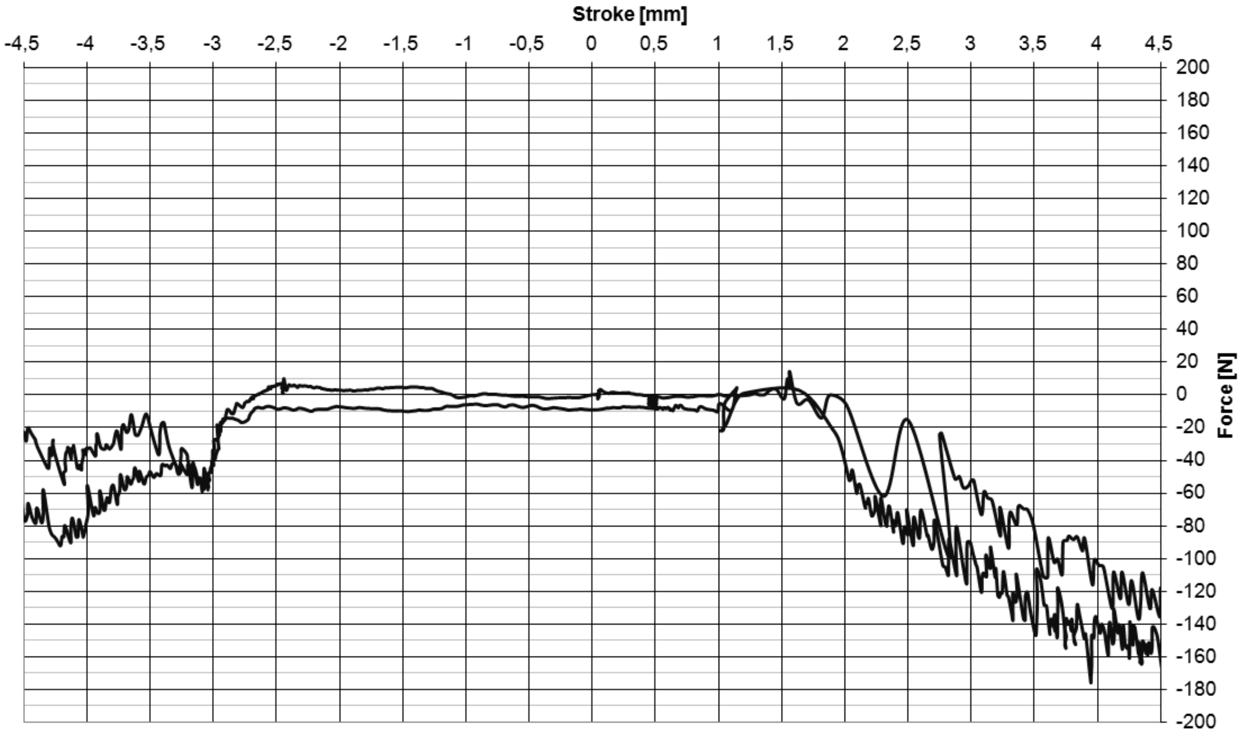

Fig. 10. Flow force of a directional control valve WE10E-standard, at Q = 120 dm^3/min.

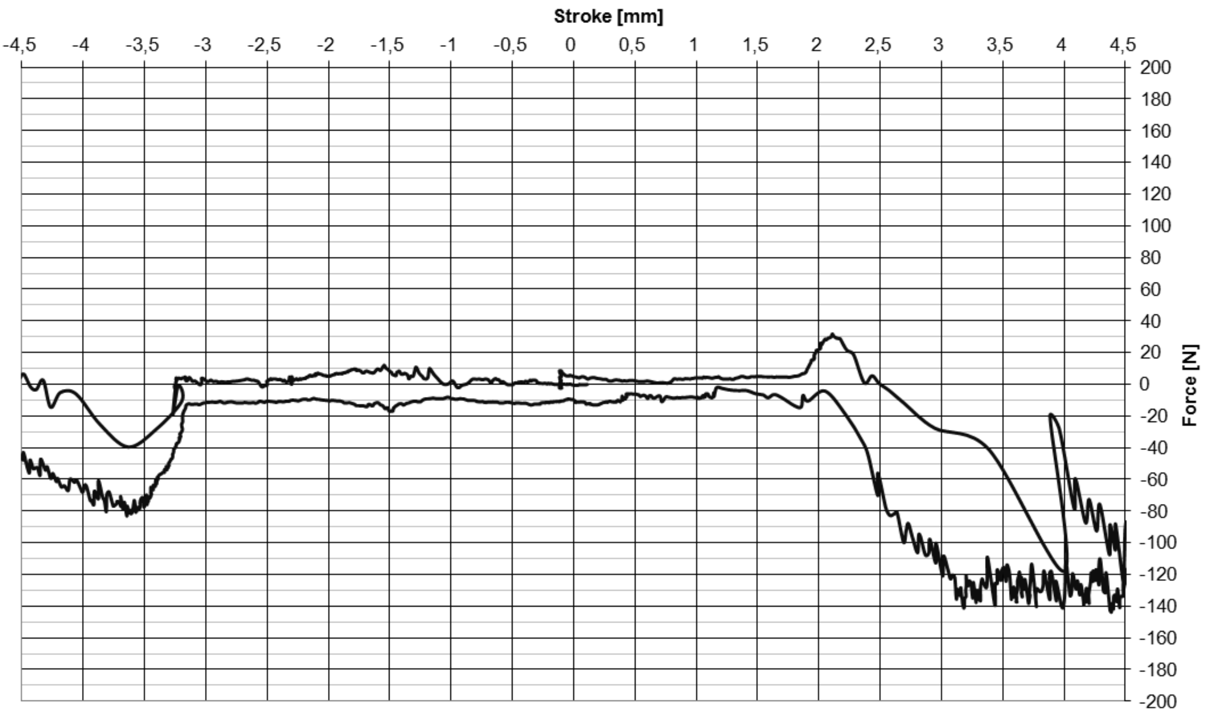

Fig. 11. Flow force of a directional control valve WE10J-standard, at Q = 120 dm^3/min.

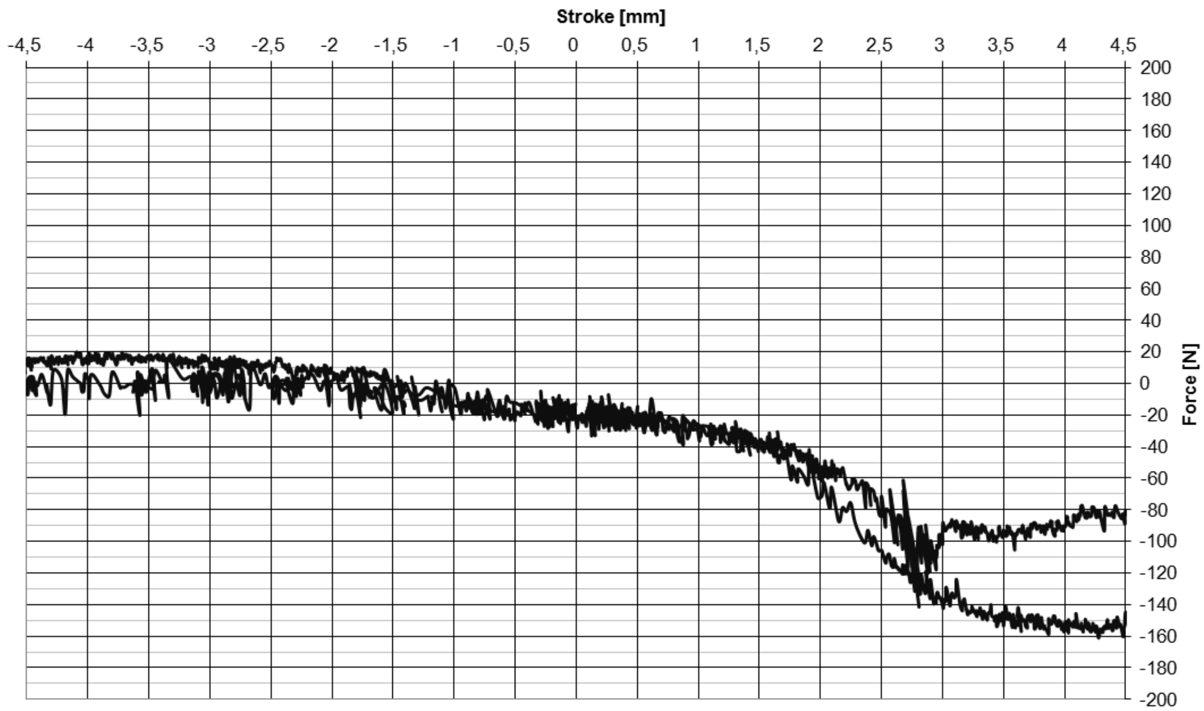

Fig. 12. Flow force of a directional control valve WE10H-standard, at Q = 120 dm^3/min.

Hysteresis of flow force corresponds to twice the value of dry friction force, which is a function of the normal component of the forces acting on the valve spool. Maximum value of the axial force is about 160 N for WE10E, about 140 N for WE10J and about 155 N for WE10H - 155 N. Fig. 13

shows, for comparison, a chart of force for WE10H for the volumetric flow rate Q = 60 dm^3/min flow force reaches maximum value of approximately 55 N.

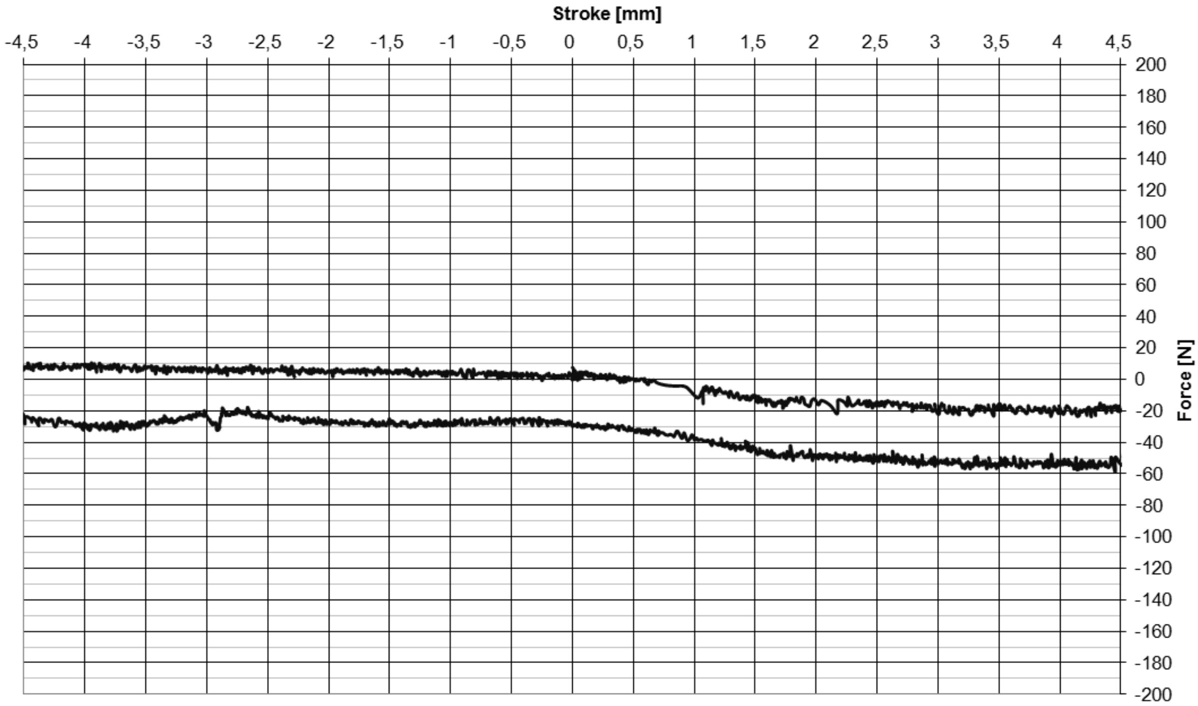

Fig. 13. Flow force of a directional control valve WE10H -standard, at Q = 60 dm^3/min.

7. Flow forces measurements of different valve bodies

Using the built experimental device comparative measurements of flow forces for the spool "H" in the set of three different designs of the communication channels in the valve body WE10:

- WE10H-standard (existing design of body),
- WE10H-leader (body produced by one of leading producers),
- WE10H-new (innovative body design).

All three assembled sets differed thus only by the body. Directional control valve WE10H-leader was built on the basis of the valve body of one of the leading manufacturers for research purposes only and we can not evaluate performance of the complete valve based on the test results of the research. The designation of WE10H-leader was given by analogy.

The results of tests carried out for the volumetric flow rate Q = 120 dm^3/min are shown in Fig. 12, Fig. 14 and Fig. 15.

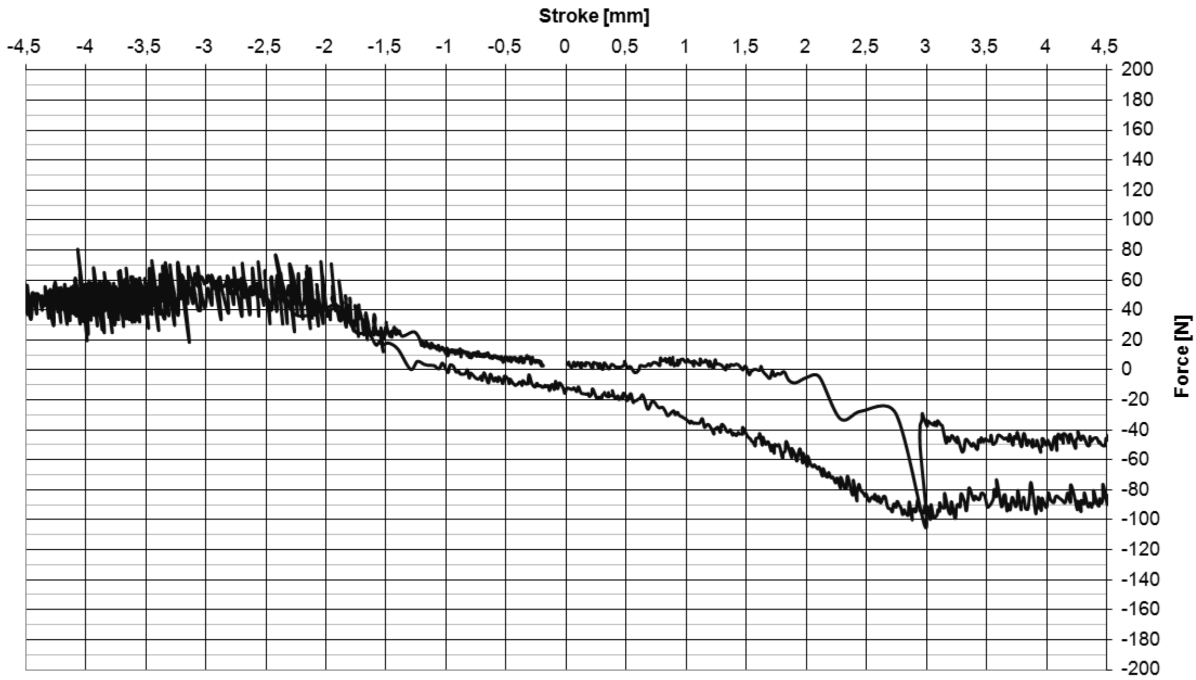

Fig. 14. Flow force of WE10H-leader directional control valve, at Q = 120 dm^3/min.

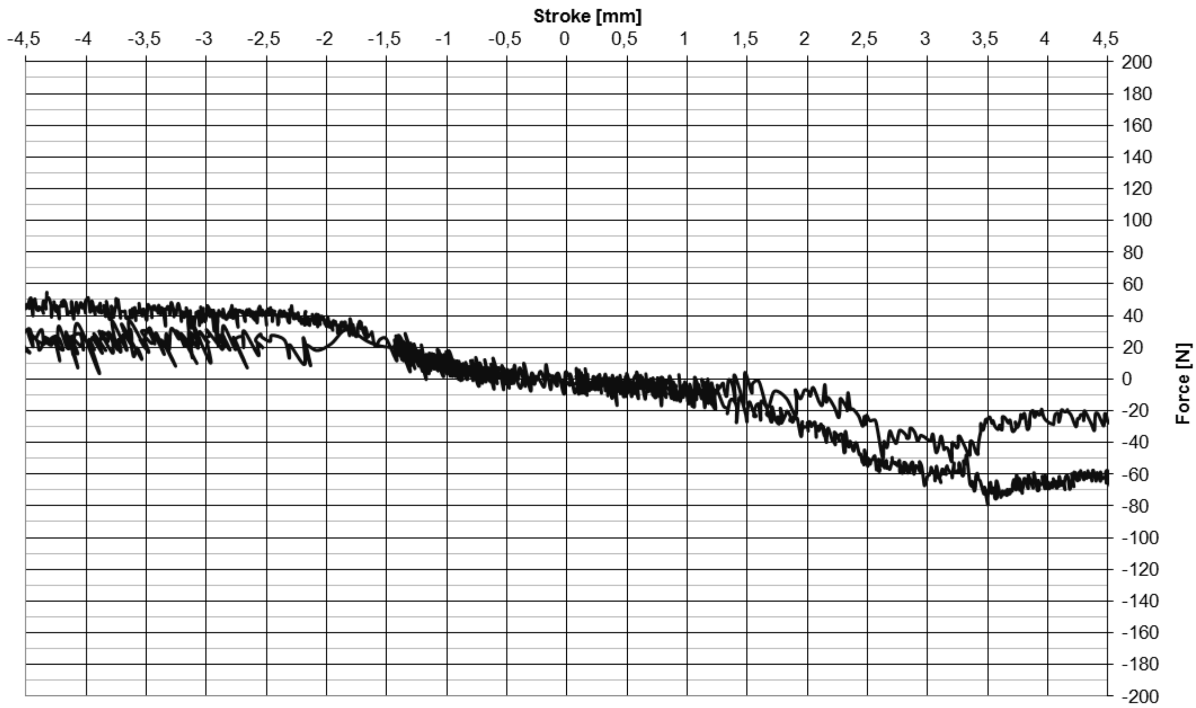

Fig. 15. Flow force of the WEH10-new directional control valve, at Q = 120 dm^3/min.

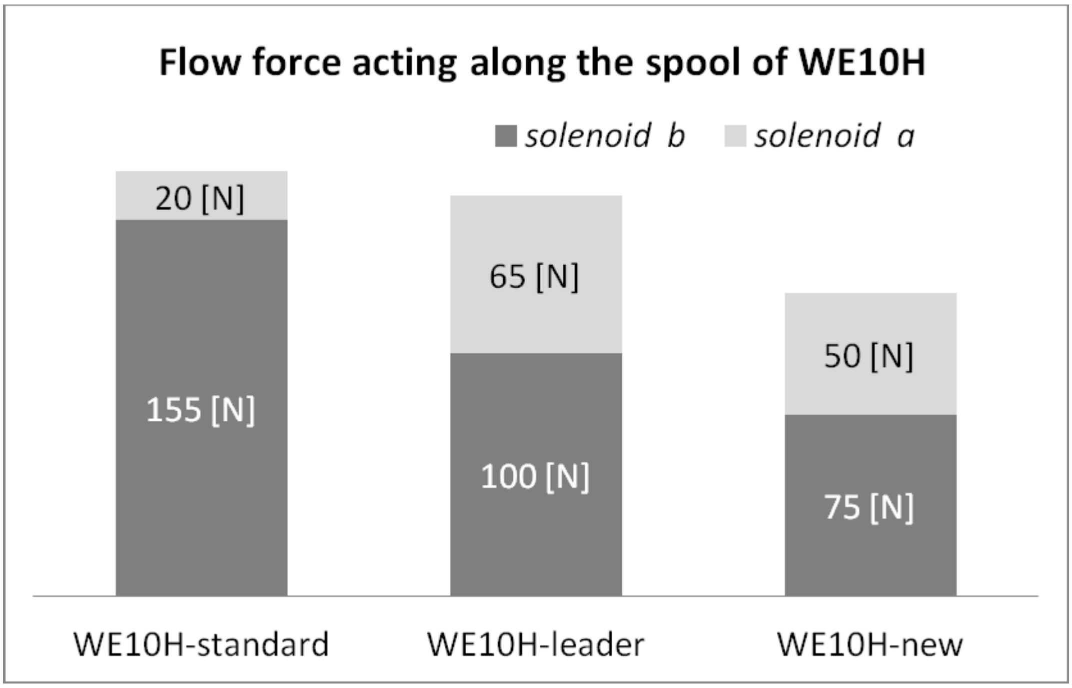

Fig. 16. Comparison of maximum flow force values for three various directional control valve WE10H (for Q = 120 dm^3/min).

Comparison of the greatest values of flow forces for individual design solutions of the bodies are shown in Fig. 16. For all solutions, the flow force reaches the highest values for the connection configuration accomplished by solenoid *b*. The most preferred solution in this respect is the WE10-new body. It reduces the maximum value of the flow force by 25% compared to the solution WE10-leader and more than 50% compared to WE10-standard. In the case of connection configuration made by solenoid *a* the smallest value of the flow force shows directional control valve WE10H-standard and reaches force value of about 60% lower than the solution WE10H-new, and this compared to WE10H-leader demonstrates the value of this force about 23% less. Considering the maximum range of the flow forces for both solenoids, the best solution also proves to be WE10-new body, which is better than 25% WE10-leader and 29% of WE10-standard. Furthermore, in terms of force symmetry for both the connection configuration under consideration, the best solution is also WE10H-new.

8. Defining operating limits for different bodies of the valve

In order to determine the relationship between the smaller of the axial component of the flow forces and the improvement in operating limits of the directional control valve, for three different designs of internal channels of the valve body, comparative tests were carried out. In order to make direct comparisons of the experimental results of the operating limits, directional control valves were assembled from identical components, with the exception of the bodies. The experiments were conducted in compliance with ISO 6403 [10] and consisted in determining limit values of volumetric flow rates and the corresponding pressure at which the valve was able to work properly. For the all tested valves, a combination *PA-BT* was crucial (energized solenoid *b*). The resulting operating limits for this connection are shown on the chart (Fig. 17). The best results were achieved by the directional control valve WE10H-new. In terms of working pressures up to 10 MPa, when compared to the WE10H-leader, they are better by about 12%, and to WE10H-standard as much

ISSN 1454 - 8003
Proceedings of 2014 International Conference of Hydraulics and Pneumatics - HERVEX
November 5 – 7, Calimanesti-Caciulata, Romania

as 40%. This confirms the test results of the flow forces. A summary of flow forces values and operating limits at the pressure of 10 MPa is shown in Fig. 18.

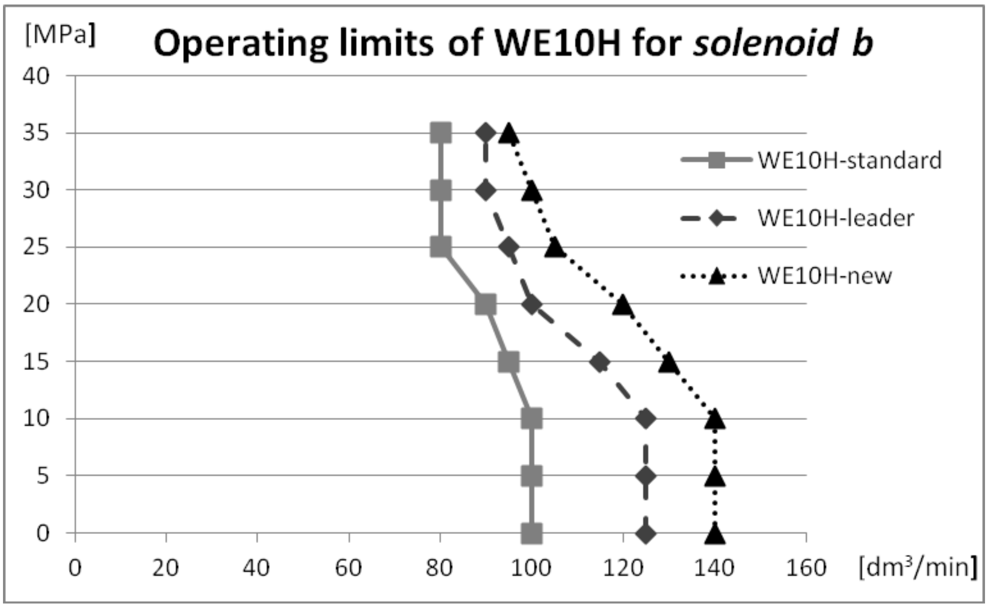

Fig. 17. Operating limit chart for three various body designs of WE10H

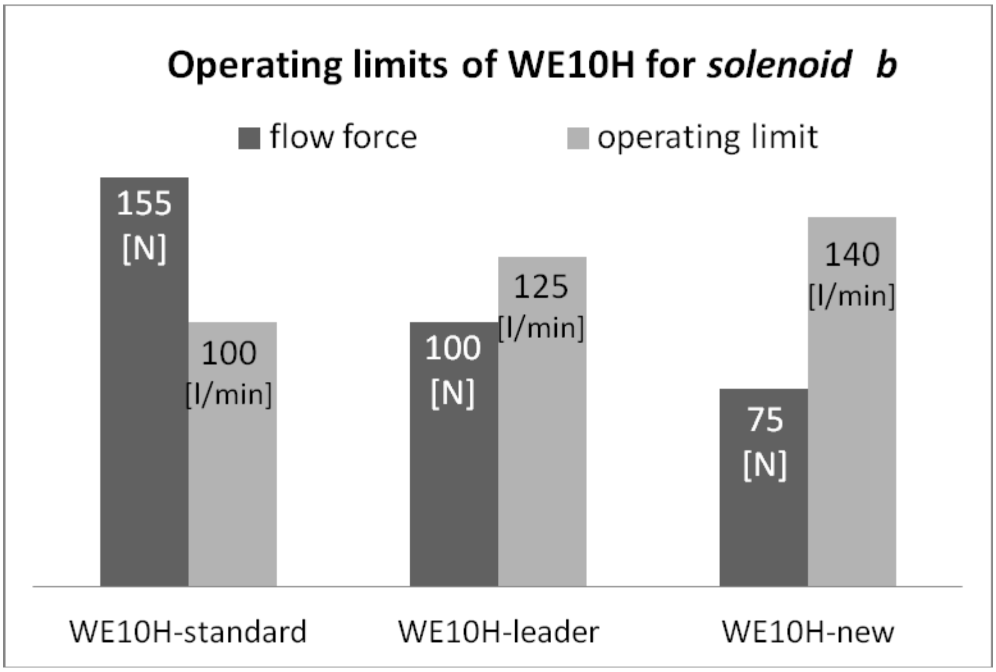

Fig. 18. Flow force and operating limit chart for three various body designs of WE10H at pressure *p* = 10 [MPa].

9. Summary and conclusions

The paper presents the problem of flow forces acting on the spool of solenoid direct operated directional control valve. Balance of the forces acting on the spool determines one of the main technical features of the valve, which is the operating limit. Assuming that the designer has the solenoid with a specific force performance and a suitably chosen centering spring, the only way to achieve significant improvement of valve operating limits is to reduce the flow force acting along the axis of the spool. Therefore, when designing the valve, the information about its maximum value and its value changes as a function of the spool displacement becomes crucial. The paper discusses the measurement of the flow force component acting along the axis of the valve spool. The research was conducted on a four-port directional control valve subplate mounted (ISO 4401-05), for the spools of various connection configurations. Additionally, a comparative study of directional control valve WE10H was conducted using various valve bodies: a standard, an innovative version and one of the leading manufacturers designs. Innovative design of the communication channels in valve body WE10H-new allows a large reduction of unfavorable flow forces of up to more than 50% compared to the previous solution, and compared to the solution of leading manufacturer by 25%. This is reflected in operating limits of directional control valve WE10H by 40% and 12% accordingly.

Thereby, it has also been confirmed that the relative reduction of the value of the flow forces acting along the spool axis can be one of the criteria for evaluation of the quality of design of the directional control valve body.

REFERENCES

[1] R. Amirante, P.G. Moscatelli, L.A. Catalano, "Evaluation of the flow forces on a direct (single stage)", Energy Conversion and Management, 48 (2007), 942–953
[2] R. Amirante, G. Del Vescovo, A. Lippolis, "Evaluation of the flow forces on an open centre directional control valve by means of a computational fluid dynamic analysis", Energy Conversion and Management, 47 (2006), 1748–1760
[3] M. Domagala , E. Lisowski, "Optimization hydraulic components using fluid-solid interaction simulation", Proceedings of 4th FPNI-PhD Symposium, 151-159, Florida-Sarassota, 2006
[4] E. Lisowski , J. Rajda, "CFD analysis of pressure loss during flow by hydraulic directional control valve constructed from logic valves", Energy Conversion and Management, 65 (2013), 285–291
[5] E. Lisowski , W. Czyżycki, J. Rajda, "Three dimensional CFD analysis and experimental test of flow force acting on the spool of solenoid operated directional control valve", Energy Conversion and Management, 70 (2013), 220–229
[6] Renn J-C, Kao T-C, "Application of CFD to design a power-saving hydraulic directional two-land-four-way-valve", Proceedings of the 1st international conference on computational methods in fluid power technology", 26–28, Melbourne 2003
[7] G. Del Vescovo, A. Lippolis, "Three-dimensional analysis of flow forces on directional control valves", Int J Fluid Power, 2003, 4(2)
[8] J. R. Valdes, M. J. Miana, J. L. Nunez, T. Putz, "Reduced order model for estimation of fluid flow and flow forces in hydraulic proportional valves", Energy Conversion and Management, 49 (2008), 1517–1529
[9] ISO 4401:2005 – Hydraulic fluid power – Four-port directional control valves – Mounting surfaces,
[10] ISO 6403:1988 Hydraulic fluid power – Valves controlling flow and pressure – Test methods
[11] Directional spool valve type WE10 electrically operated, Ponar Wadowice, WK 499 780, 07.2013,
[12] Directional Control Valve Series D3W Catalogue HY11-3500/UK, Parker Hannifin Corporation, UK.indd RH 28.11.2013
[13] Directional spool valves, direct operated, with solenoid actuation, Type WE10,Rexroth Bosch Group, RE 23340, Edition: 2013-06
[14] Wet Armature Solenoid Operated Directional Control Valves, Model DG4V-5, 20 Series, Eaton Vickers.

ISSN 1454 - 8003
Proceedings of 2014 International Conference of Hydraulics and Pneumatics - HERVEX
November 5 – 7, Calimanesti-Caciulata, Romania

HYDRAULIC ACTUATION USED FOR BRIDGE SEISMIC ISOLATION

Florin NEDELCUŢ[1], Fănel ŞCHEAUA[2], Gavril AXINTI[3]

"Dunărea de Jos" University of Galati, MECMET Research Center

[1]florin.nedelcut@ugal.ro
[2]fanel.scheaua@ugal.ro
[3]gaxinti@ugal.ro

Abstract: *This paper presents a solution for isolation of bridge structures against seismic motions effects based on the use of hydraulic devices. This solution can provide a certain level of seismic energy dissipation, adequate for bridge or viaduct type structures. The adaptive isolation system used it is expected to improve the behavior of structures during seismic ground motions. The system is composed by hydraulic fluid dampers, mounted between bridge pier and superstructure pathway. A hydraulic fluid damping device consists of a cylinder with piston, being filled with a viscous fluid, ordinarily mineral oil or silicone oil. A specific translational motion at the piston rod is forcing the viscous fluid to circulate inside the cylinder through a certain number of orifices practiced in the piston. A simplified tridimensional model for hydraulic dissipation device was introduced in computational fluid dynamics (CFD) analysis performed using ANSYS-FLOWIZARD software, with the purpose to highlight the fluid motion within the cylinder chambers. A translational motion was imposed at the piston rod, which simulates the occurrence of an earthquake. The hydraulic dissipation system is capable of limiting the superstructure response for a large variety of seismic ground motions.*

Keywords*: hydraulic device, seismic energy dissipation, viscous fluid, CFD, piston*

1. Introduction

A bridge or viaduct structure type represents a major objective of public interests that realize the connection between human communities and beyond their resistance over time these structures must be capable to withstand the destructive action of natural events such as earthquakes. Today's modern structures except the component materials of certified quality may have some special devices mounted inside the structural frameworks that are able to change the structural response in case of earthquakes. These devices mounted between the bridge pier and pathway creates a disconnection between the two structural elements, thus the efforts coming from the ground are not transmitted vertically to the superstructure in the occurrence of an earthquake. Thereby, special isolation systems are used mounted at the base of building structures, mainly composed of elastomeric bearings or sliding bearings, which often requires safety devices to ensure displacements limitation when high magnitude earthquakes arise. These protection systems are represented by hydraulic devices which can provide also an energy dissipation level.

2. Configuration of a composed seismic isolation system

A bridge or a viaduct represent a structure, designed by civil engineers, intended to allow crossing over an natural obstacle like a river, or a valley. The bridge structure can be built of concrete, metal, masonry, with the following configuration:

Superstructure - the upper part of the bridge that takes over the loads from road or rail traffic;

Infrastructure - the bridge component part that sustains the superstructure and takes over the loads from the superstructure and transmits them to the ground, consisting of abutment and piles;

The engineers must take into account the efforts from traffic but also those derived from seismic actions that once appeared may affect the stability of the structure. Therefore are beginning to be introduced in use the isolation systems mounted inside the bridge structural frames which can provide a visible enhanced stability during seismic activities. An isolation solution that can be used successfully for bridge seismic isolation is represented by the use of elastomeric bearings in combination with hydraulic devices for anchorage and displacements limitation. These systems are positioned between the bridge superstructure and infrastructure. The elastomeric supports ensure disconnection between piers and superstructure, so as infrastructure to be able to move within the limits allowed by the isolation system in the occurrence of an earthquake, while hydraulics ensure sustainable connection between the superstructure and piers, but also limitation of large displacements. In Figure 1 it is presented a bridge or viaduct structure isolated against seismic actions with a composed isolation system. It can be observed that the pathway is placed on the elastomeric bearings, while hydraulic devices are mounted as connection elements between the superstructure and the bridge piers.

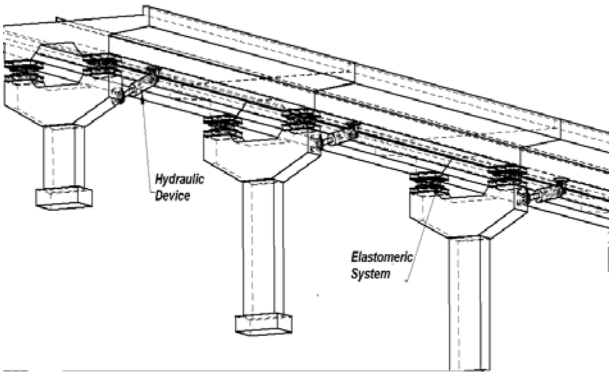

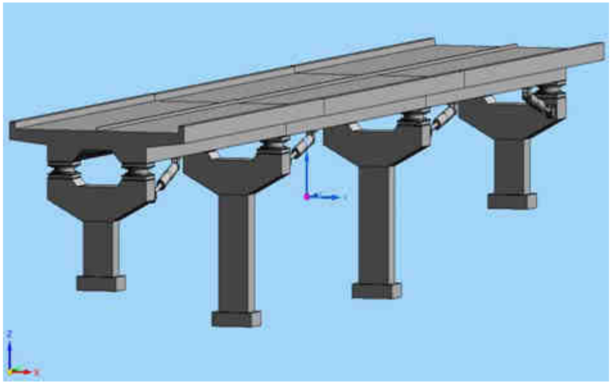

Figure 1. Bridge seismic isolated with elastomeric system with hydraulic devices

The isolation system consists of a combination between a certain numbers of hydraulic dissipation devices named otherwise fluid viscous dampers and elastomeric supports. Usually, the hydraulic dissipation device is placed between structural frames therefore are limiting the lateral movements and avoiding their shearing effects. Consequently, a hydraulic dissipation device converts the mechanical energy into caloric energy (heat), transmitted to the external environment trough cylinder walls. The hydraulic damping device acts as a seismic energy dissipation device combined with a lateral (horizontal) displacement restraint.

3. Simplified hydraulic device model

The hydraulic system is being shown as a plunger-cylinder filled with fluid by a certain value of viscosity, having a very low compressibility factor, that may act to decrease relative displacements occurring between structural elements which are attached to. Inside the piston there are practiced a number of orifices in order to allow fluid flow between the cylinder chambers. The fluid used inside the device cylinder is usually represented by mineral oil or silicone oil. In Figure 2 it is presented a three-dimensional model for hydraulic dissipation device used in bridge or viaduct seismic isolation.

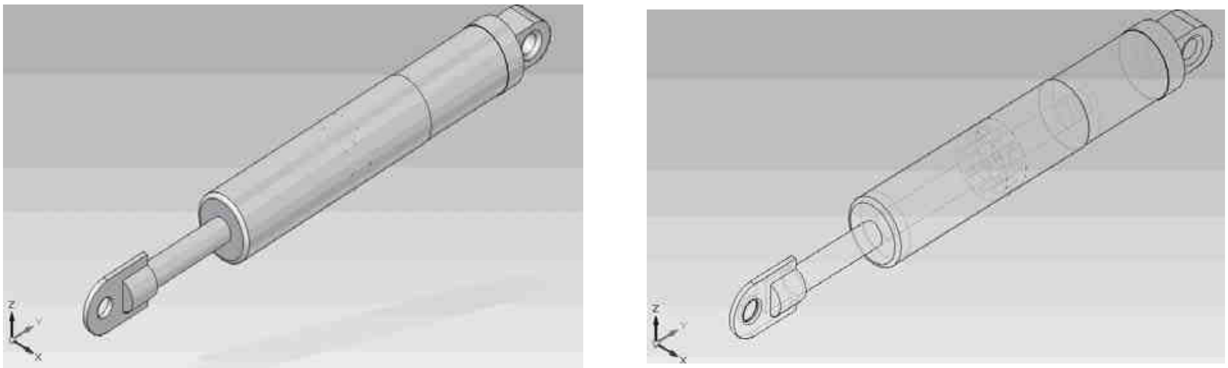

Figure 2. Hydraulic dissipation device model

In the occurrence of an earthquake hydraulic system become operational by repeated compression-tension translational motions. Because of the working fluid properties in terms of viscosity and internal friction at the fluid particles level occurring inside the cylinder, the device responds with a resistance to piston movement. The resistance force takes over and passively consumes a part of seismic energy transmitted by earthquake to superstructure improving in this way the structural response during seismic actions.

Also, the addition of the hydraulic device into the structure is altering the seismic induced movements, inducing a delay of a quarter of period.

4. Results

A simplified 3D model of seismic energy dissipation device was introduced into a computational fluid dynamics analysis (CFD) using ANSYS-FLOWIZARD software. The purpose of this study was to highlight the fluid particles motion inside the cylinder chambers when connected to the superstructure. The three-dimensional model of the hydraulic dissipation device was a simplified one, according to the practical requirements of the study. The fluid taken into consideration for the CFD analysis was a high-viscosity silicone-oil type, with a viscosity of 29.1 kgm-1·s-1 and a density of 970.0 kg/m3 [1].

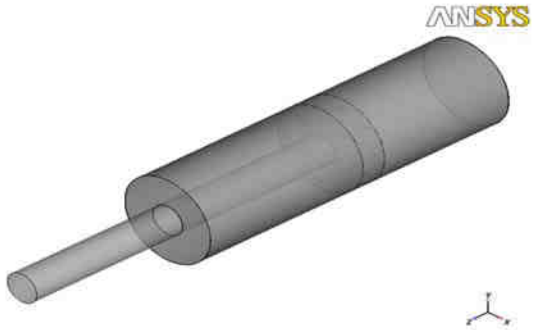

*a). **Three-dimensional model for hydraulic dissipation device***

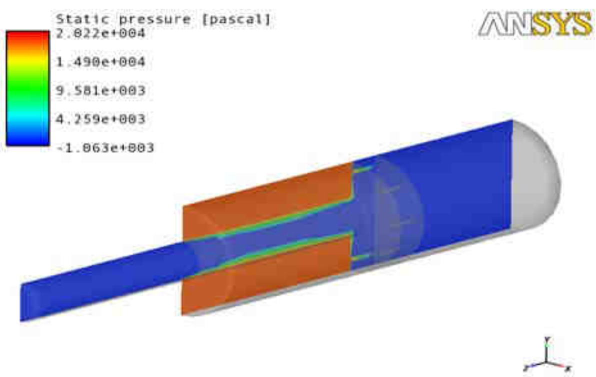

*b). **Static pressure values***

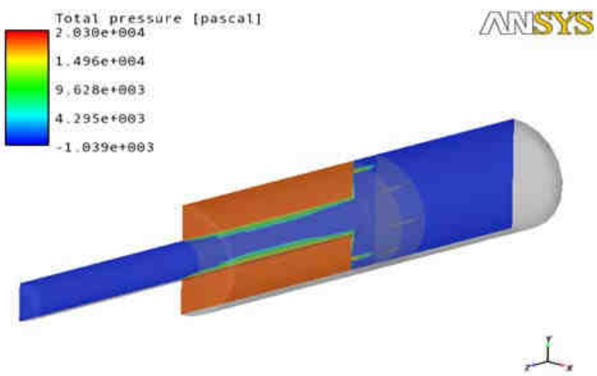

*c). **Total pressure values***

ISSN 1454 - 8003
Proceedings of 2014 International Conference of Hydraulics and Pneumatics - HERVEX
November 5 – 7, Calimanesti-Caciulata, Romania

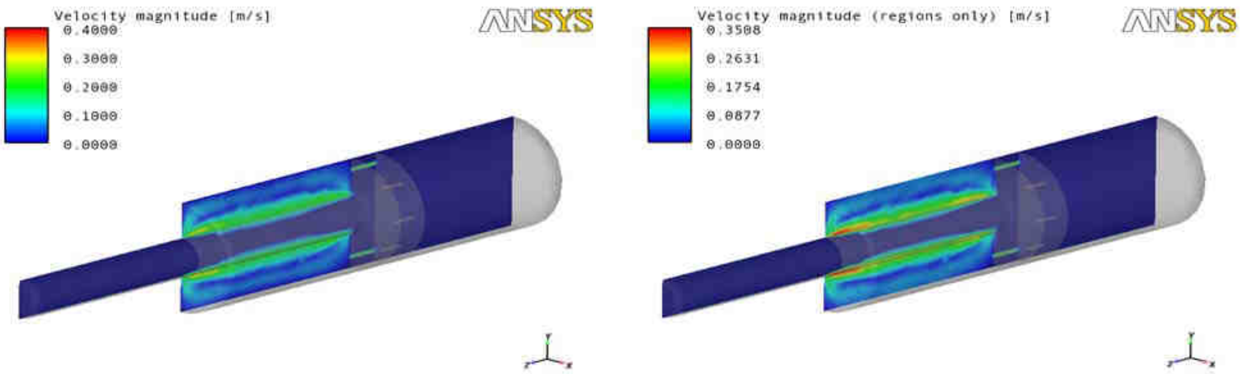

d). ***Velocity magnitude values*** e). ***Velocity magnitude values on regions***

Figure 3. Computational fluid dynamics analysis results

The fluid material properties in terms of density, viscosity, specific heat and thermal conductivity are important because the loads and energy dissipation during operation of the device is mainly based on these properties. The initial input data concerning the material properties used in hydraulic device operation for both fluid region and internal solid model are declared in Table 1.

Table 1 Region Properties

Name	Type	Compressible flow	Rotating Machinery	Material Properties
fluid.1	Fluid	No	No	Name=ulei-siliconic. Viscosity=29.1 kg/m-s, Specific Heat=1601.0 J/kg-K, Thermal Conductivity=0.159 W/m-K, Density=970.0 kg/m3
solid.2	Solid	not applicable	not applicable	Name=steel. Specific Heat=502.48 J/kg-K, Thermal Conductivity=16.27 W/m-K, Density=8030 kg/m3

Variable	Value
Mesh type	Tetrahedral mesh
Total number of cells	126622
Tetrahedral cells	126622

The temperature is almost constant for the speed range studied, with only 12 ºC higher than that of the environment. The mesh of the 3D hydraulic device model had 126622 tetrahedral cells.

5. Conclusions

Avoiding the effects of seismic activities is the aim of bridge and viaduct structural designers mainly. In order to accomplish this goal various systems have been developed capable to isolate the structure from earthquake destructive action. In this study it was proposed an isolation solution for bridges or viaducts using a system consisting of elastomeric supports and hydraulic devices.

Hydraulic devices provides an amount of seismic energy dissipation, but also can be successfully used to limit the superstructure displacements during an earthquake. The composed system is therefore capable of simultaneously limiting the superstructure response, but also for limiting the loads, for a large variety of seismic ground motions.

REFERENCES

[1] AASHTO, *Guide specifications for seismic isolation design*, Washington, DC., 2000
[2] G., Axinti, A. S., Axinti, Acționări hidraulice și pneumatice, Vol III, Editura “Tehnica-Info” Chișinău 2009
[3] G. Axinti, F. Nedelcut, F. Scheaua, *Study on the working principle of a hydraulic energy dissipation device,* Proceedings of 2012 International Conference of Hydraulics and Pneumatics - HERVEX, Calimanesti-Caciulata, Romania
[4] http://www.alga.it/uploads/474_catalogo_FD_rev4.pdf

ISSN 1454 - 8003
Proceedings of 2014 International Conference of Hydraulics and Pneumatics - HERVEX
November 5 – 7, Calimanesti-Caciulata, Romania

HYDRAULIC DRIVE SYSTEM FOR A TRAINING SIMULATOR OF FLIGHT ATTENDANTS

Radu RADOI[1], Ioana ILIE[1], Marian BLEJAN[1]

[1] INOE 2000 – IHP, Bucharest

Abstract: *The Hydraulic Drive System was designed and realized by INOE 2000 – IHP for Regional Air Services – Tuzla Airport. It will be used for the Cabin Emergency and Escape Trainer CEET B732 for the Sea Survival School. The hydraulic drive system realizes a fine tuning position by means of a single rod cylinder driven by an asymmetrically directional proportional control valve.*

Keywords*: hydraulic drive, training simulator, proportional valve*

1. Introduction

The hydraulic drive system that acted on *Cabin Emergency and Escape Trainer CEET B732* contains: a hydraulic power unit, two manual valves, two hydraulic cylinders, two encoders and an electrical panel. The hydraulic power group is realized in a compact structure and has a 7.5 kW electric pump, a 100l tank, and also the electrohydraulic devices that mean two proportional directional control valves, the safety valve, level and temperature sensors. The power group is placed in the simulator hold, that is, in fact, the front part of a 737 Boeing fuselage. In the training classes, instructors drive the simulator in various training scenarios. Through the selection switch the automation system commands hydraulics and also monitors the operating parameters: cylinder displacement, oil temperature, tank oil level. On the front of electric panel there are light that warn the operator about the system function: if the system is ready, the system works, a failure has occurred.

2. Features and the system schematic.

Figure no. 1 shows the hydraulic drive system schematic. The each part of schematic has been chosen in order to obtain the necessary flow and pressure to lift up the simulator at 100 mm/s maximum speed. On the schematic is shown the 100l fluid tank FT, the hydraulic pump P, the electric motor EM, the level and temperature switch, the thermostat T, the return flow filter RLF, the tank breather filter TBF, the pressure relief valve PRV mounted on a manifold HP2, the electrical acted 4/2 valve HDV, the pressure gauge PG, two 4/3 proportional directional control valves PDV, the ball valve unit, hose break valve, the restrictor R1, two wire encoders SE and electrical enclosure with automation system AS . On the command console there is a switch with the trainer selects the scenarios and lights that warn about the system status or failures.

The main system features are:

- Three –phase power supply 400V/50Hz
- Working fluid: mineral hydraulic oil HL 46
- Maximum working pressure: 100 bar
- Hydraulic cylinders stroke: 400 mm
- Maximum speed of two cylinders working simultaneous: 100 mm/s

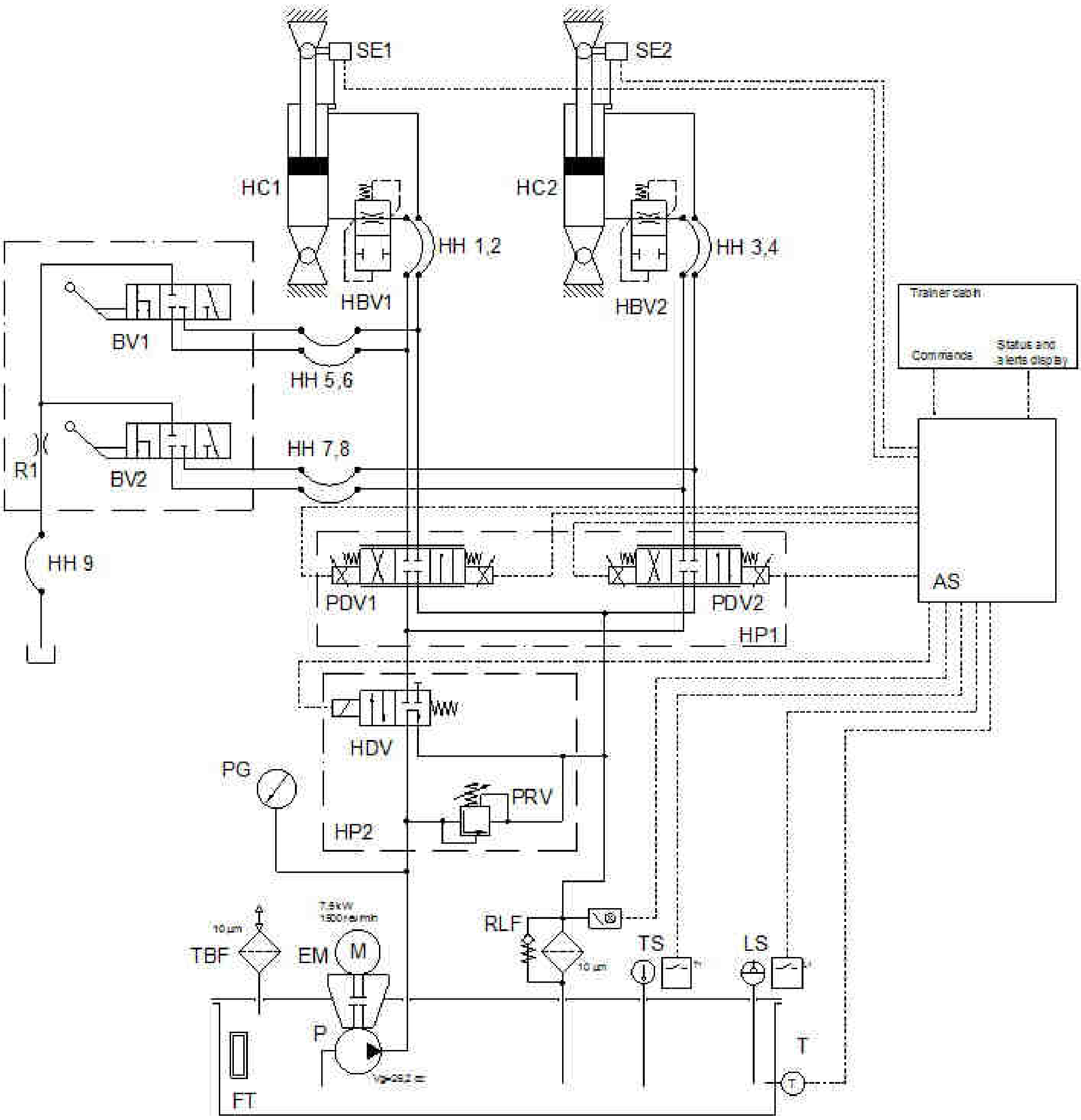

Figure 1. Schematic of hydraulic drive system

3. System description and operation

The hydraulic drive system consist of hydraulic power unit, two hydraulic cylinders with wire encoders, pipes and houses to connect cylinders to the power unit, the manifold block that contains restrictors in order to lift down the simulator in blackout condition, automation system and the operator console. The hydraulic power unit (shown in figure no. 2) is placed in simulator hold and contains the 7.5 kW gear pump and the 100 l oil tank which are mounted on the lid the hydraulic equipment (figure no.3). The electrical enclosure with automation system is placed near hydraulic power unit. This one contains electrical power supply, circuit breakers, the programmable logic controller, and the driver for control valve electromagnets.

Figure 2 Hydraulic equipment in the simulator hold

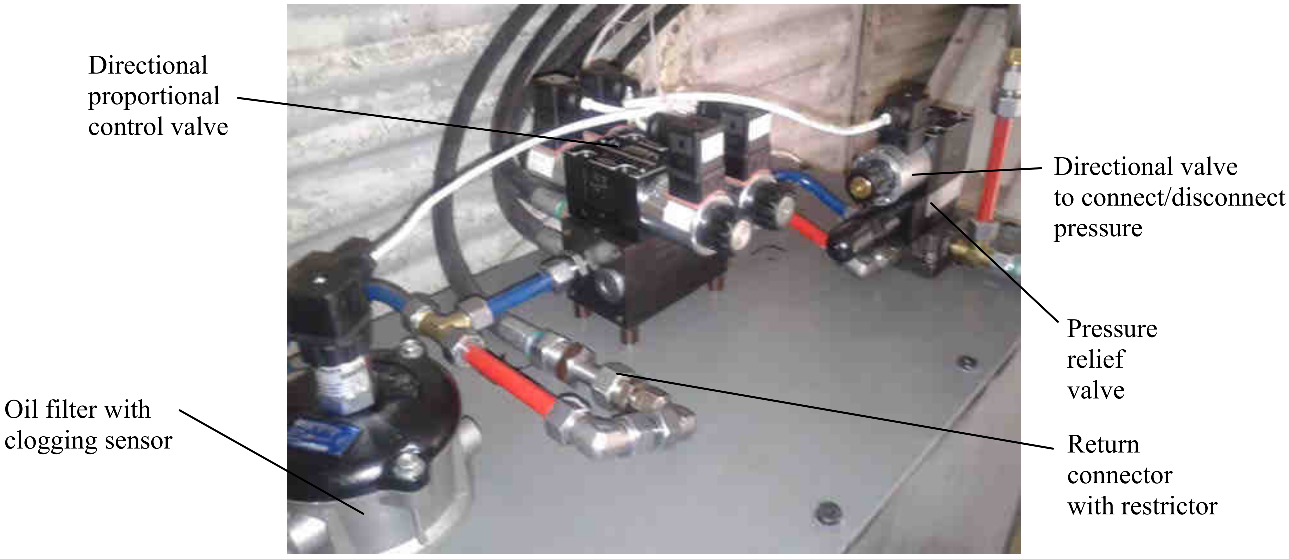

Figure 3 Layout of hydraulic equipment on hydraulic power unit

Figure no. 4 shows the hydraulic cilinder position under the simulator. The cylinders are mounted between two mounting brackets through bolts. The bottom mounting bracket are embedded in concrete slab, and the top one is welded to the support of the simulator. The picture also shown the wire encoder with cylinder stroke is measured and connection housing which contains the hose break valve of cartridge type.

Figure no. 5 shows the ball valves unit that lift down the simulator in case of electric power failure. There is placed between hydraulic power unit and hydraulic cylinders. The ball valve allows connecting cylinder rooms and through the flow restrictor unloading oil from the large cylinder room to the tank. This unloading circuit was provided both to avoid ending up suspended simulator in case of electric break and also to help mounting and dismounting cylindrical supports.

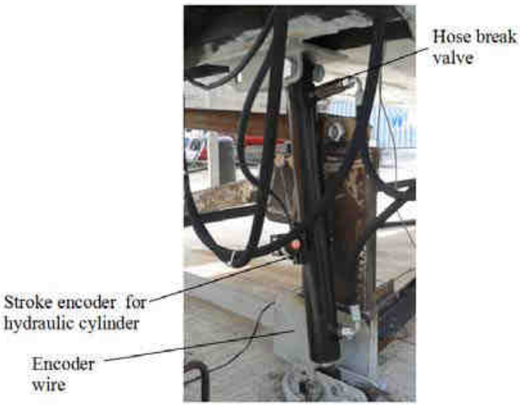

Figure 4 Hydraulic cylinder mounted between the support and the simulator frame

Figure 5 Ball valves for lift down the simulator in case of electric power failure

Figure no 7 shows the sketch with side view of the simulator, it can be seen the support, it's front joint and the cylinders placement under simulator. Figure no. 8 shows movements of the simulator accorded to cylinders drive. A synchronous command for both cylinders causes vertical motion for simulator and also a pitch movement for the front joint. An asynchronous command for cylinders causes lateral movement, yaw and roll movements.

Figure 6

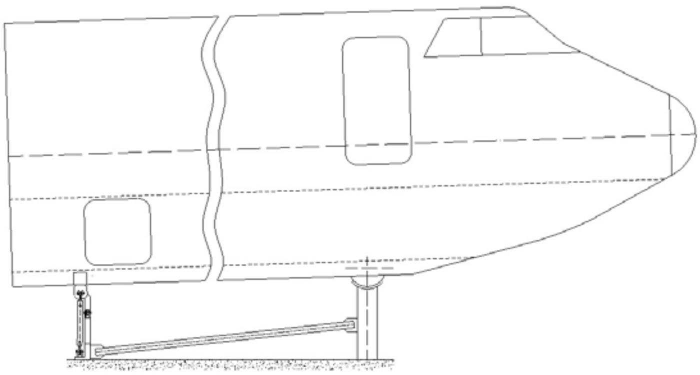

Figure 7 - Sketch with side view of the simulator

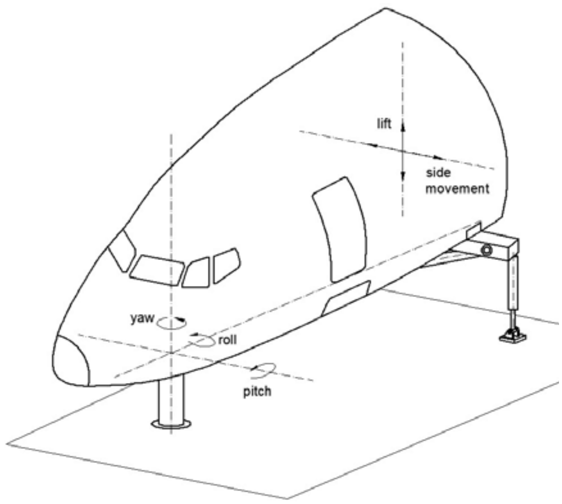

Figure 8 - Movements of the simulator

The automation system is built on a Schneider Electric Programmable Controller Twido TWDLCAE40DRF type. The software that has been implemented allows adjusting the position of the two cylinders based on predefined scenarios. The operator selects a particular training scenario and the PLC drives electromagnets of the proportional control valves through the OEM module. In order to adjust the position of the cylinders there are used two wire encoders in a closed loop structure. A training scenario involves change position for cylinders' rod within a predetermined time. Figure no. 9 shows dynamic response- error correction at step input signal.

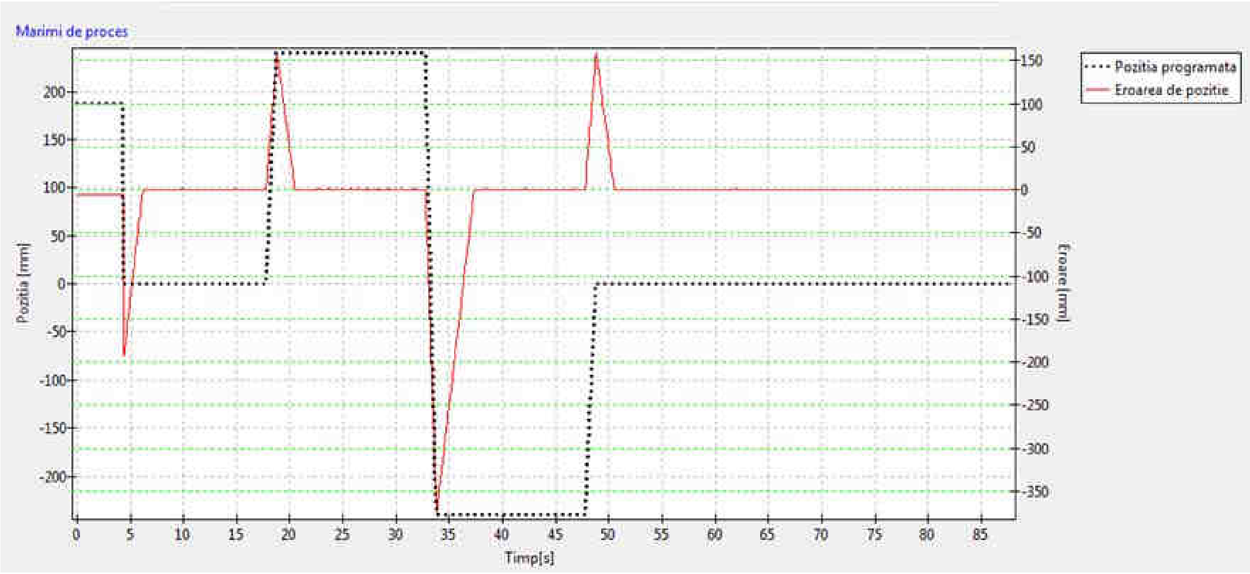

Figure 9 Dynamic response - error correction at step input signal

4. Conclusions

The hydraulic drive system realizes a fine tuning position by means of a single rod cylinder driven by an asymmetrically directional proportional control valve. The control system is software implemented on a Twido PLC that allows both scenarios management and also the closed loop algorithm.

REFERENCES

[1] Ravi Doddannavar, Andries Barnard, "Practical Hydraulic Systems", Elsevier Science & Technology Books, March 2005, ISBN: 075066276X
[2] http://insidepenton.com/machinedesign/AdvHydMotionDesignPractices-Paso.pdf
[3] http://www.schneider-electric.com/products/ww/en/3900-pac-plc-other-controllers/3920-controllers-plc-for-commercial-machines/533-programmable-controller-twido/
[4] http://machinedesign.com/archive/nascar-simulators-keep-it-real

ISSN 1454 - 8003
Proceedings of 2014 International Conference of Hydraulics and Pneumatics - HERVEX
November 5 – 7, Calimanesti-Caciulata, Romania

EXPERIMENTAL RESEARCH ABOUT DYNAMIC BEHAVIOR OF AN ELECTRO-HYDRAULIC AXIS

Adrian MIREA[1], Ioana ILIE[2]

[1]SC ROMFLUID S.A., Bucharest

[2] INOE 2000 – IHP, Bucharest

Abstract
The paper presents the experimental results obtained in dynamic tests of an electro-hydraulic axis. Tests have been made in the Servo technique Laboratory of INOE 2000 –Hydraulics and Pneumatics Research Institute on the specialized stand. The experimental results are comparable to those obtained by numerical simulation for the tested axis.

Keywords: *electrohydraulic axis, dynamic behavior, mathematical model*

1. Structure of electro-hydraulic axis and testing equipment

The main parts of the tested electro-hydraulic axis (figure no. 1), and there are: a MOOG servo-valve (SV), a double acting cylinder (Scil), a displacement transducer (TC) needed for close control loop. The schematic for testing equipment shown in figure no. 1 are properly both for steady state and also for dynamic tests. The hydraulic power supply contains a hydraulic pump (P), a geared motor (M), safety valve (S) that control the equipment pressure value, a pressure line filter (F). As a self-acting regulator is used the servo-controller (SC) that compares and processes signals from displacement transducer and wave form generator (GF). The output signal from the servo-controller is applied on the servo-valve torque motor in order to control the cylinder rod position. All signals occurring in the testing process are transmitted through the data acquisition system (SA to the computer on which data is stored in standard form, database type. The pressure values are measured by pressure transducers (TP) mounted on the servo-valve ports (P, T, A, B), and the flow value are monitored by a flowmeter (Q). In order to create load on the cylinder rod (Scil) is used another cylinder that have on their hydraulic circuit pairs of dissipative: throttle valve (DR) and check valve (SS). The load on the cylinder rod (Scil) is monitored by the force transducer (TF).

The mathematical model for this electro-hydraulic system contains the following equations:

- *The servo-valve transfer function*:

$$H_{SV}(s) = \frac{\Delta x(s)}{\Delta i(s)} = \frac{Kix}{\frac{s^2}{\omega_n^2} + \frac{2\zeta}{\omega_n} s + 1} \tag{1}$$

K_{ix} *= 8.25 m/A,* amplification factor;
x - displacement of valve slide;
ω_n = 377 rad/s servo-valve natural pulsation;
ζ = 0.7, ξ - damping factor.

- *Equation of continuity of flows servo-valve – hydraulic cylinder (Scil):*

$$A_P \dot{y} + k_{lp} P + \frac{A_p^2}{R_h} \dot{P} = \begin{cases} b_d c_{dd} \left(|x| - x_0\right) signx \sqrt{\frac{p_S - |P|}{\rho}}; |x| > x_0 \\ 0; |x| = x_0 \end{cases} \tag{2}$$

$b_d = \pi d_{SV} \alpha_d$ section of flow through valve slide;
d_{SV} = 6 mm diameter of the servo-valve slide;

ISSN 1454 - 8003
Proceedings of 2014 International Conference of Hydraulics and Pneumatics - HERVEX
November 5 – 7, Calimanesti-Caciulata, Romania

α_d = 0.4 - coefficient of utilization of flow section;
c_{dd} = 0.6 – flow coefficient;
A_p = 15x10^{-4} m^2 – active face of cylinder piston that have diameter D=0,43 x10^{-2} m ;
k_{lp} - internal leakage coefficient inside the hydraulic cylinder;
$y, \dot{y}, \ddot{y}$ - position, speed, and acceleration of the cylinder piston (SCil);
P - pressure drop between A şi B connections of the SCil;
R_h - equivalent stiffness of the hydraulic path between servo-valve and cylinder: $R_h = 2\frac{\varepsilon_l}{\vartheta_0}A_p^2$;

$\dot{P}$ - rate of change over time of pressure drop P;
ε_l = 10000 daN/cm^2 modulus of the fluid elasticity;
ϑ_0 = 0.785x10^{-5} m^3 – of the hydraulic path between servo-valve and cylinder;
x - displacement of valve slide ;
P_S – the hydraylic power supply pressure;
ρ = 900 kg/m^3 – oil density.

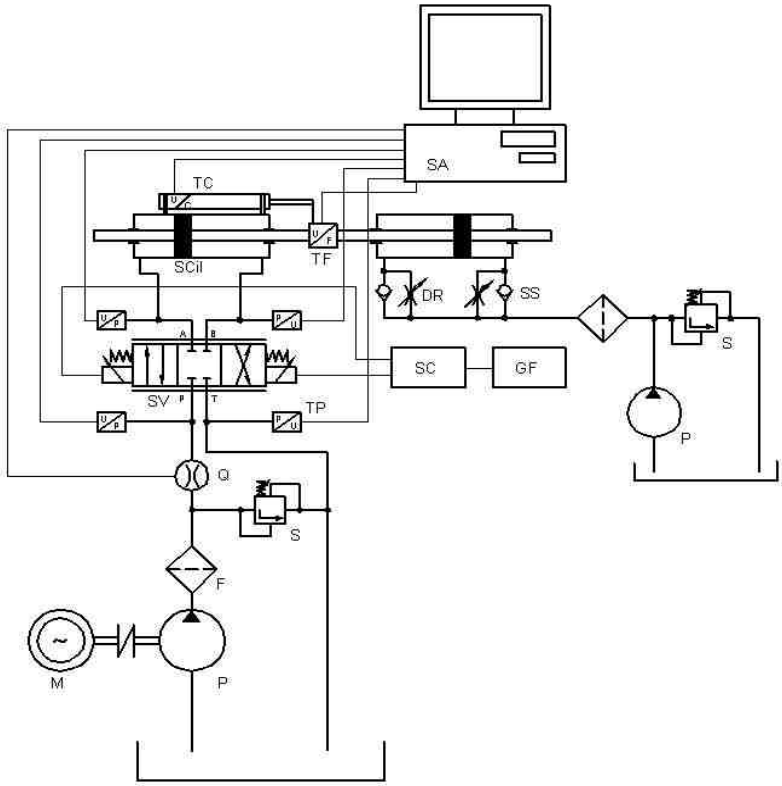

Legend:
SA- data acquisition system;
SC- servo-controller;
GF- wave form generator;
SCil- hydraulic cylinder;
SV- servovalve;
TP- pressure transducer;
TC- displacement transducer;
TF- force transducer;
DR- throttle valve;
SS- check valve;
Q – flow metter;
S- safety valve;
F - pressure line filter;
P- hydraulic pump;
M- electric motor

Fig. 1. Schematic for testing equipment

Equation of piston displacement in the hydraulic cylinder:

$$m_p \ddot{y} = PA_p - F_f - F_{sarcina} \qquad (3)$$

$m_p \cong 4$ kg, weight-acted mobile part;
$F_f = F_{fs} + F_{fv}$ the friction at the cylinder piston;
$F_{fs} = F_{fs0}\,\mathrm{sign}\,\dot{y}$ Coulomb friction load;
F_{fs0} – modulus of Coulomb friction load;

$F_{fv} = k_{fv}\dot{y}$ viscous friction; $F_{fs} << F_{fv}$,

$F_{sarcina}$ - load on the cylinder rod.

The simulation schedule obtained in MATLAB-SIMULINK by implementing the mathematical model is shown in fig. no.2. Parameters used on the simulation process, other than the below mentioned ones, are:

- displacement transducer constant $K_{pozitie}$ = 1 m;
- amplification factor of the PID controller K_P,
- servo-valve conversion U-I coefficient, K_{ui} = 0.015 A/V

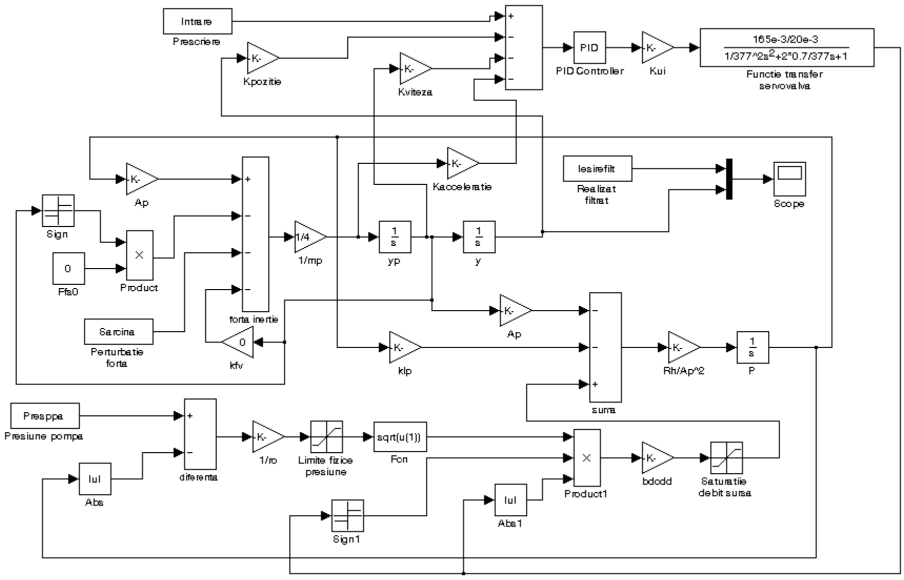

Fig.2 The MATLAB-SIMULINK simulation schedule

2. The experimental results obtained in dynamic tests
2.1 The response to step input signal

In order to obtain this dynamic behavior of the electro-hydraulic axis, the input signal is a step one between $-I_{max}$ and $+I_{max}$. The experimental results are shown in 2.1 ….2.4 charts.

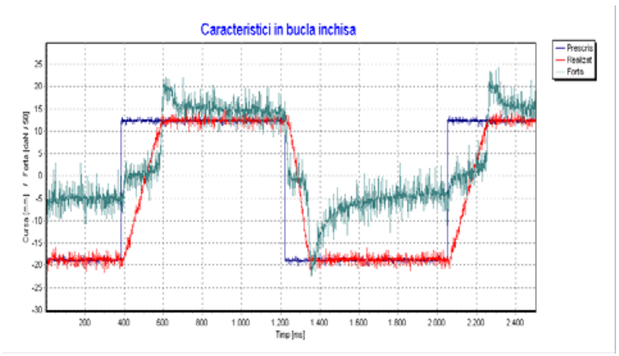

Chart no. 2.1
Step response: -20mm ….+15mm
Load: F=75daN
T_{oil} 40˚ C
Responding time 200 ms

Chart no.2.1 values

Time	Set point [mm]	Accomplished [mm]	P_p [bar]	P_a [bar]	P_b [bar]	P_t [bar]	Load [N]
1	-18.8965	-17.627	72.31487	32.07697	47.66868	0.05292	-369.663
2	-18.1641	-19.9219	74.04882	33.74157	47.33576	-0.00777	-321.112
3	-18.8477	-18.6523	75.0025	31.18919	47.72417	-0.07713	-237.883
....							
65	-18.8477	-18.6035	73.44194	32.96475	48.0016	-0.04245	-265.626
66	-18.6523	-19.2871	75.43599	32.3544	47.89063	-0.0858	-269.094
67	-19.0918	-18.3594	76.38966	32.96475	48.44549	-0.00777	-276.03
....							
137	-18.7988	-18.457	75.34929	34.4074	48.22354	-0.05112	-234.415
138	-18.6523	-19.9219	76.12957	34.29643	48.66744	0.104939	-230.947
139	-18.3105	-18.0176	75.17589	34.019	48.66744	0.148288	-54.0836
....							
621	12.59766	11.52344	74.8291	68.19869	2.280717	-0.5713	792.0856
622	12.8418	12.10938	72.74836	68.08771	2.780096	-0.29387	996.6921
....							
2497	12.30469	12.54883	76.04287	62.65004	12.2128	-0.0858	760.8745
2498	12.30469	12.20703	75.69608	62.42809	12.93413	0.018241	743.5349
2499	12.06055	13.13477	75.52268	61.92871	12.87864	-0.01644	941.2056
2500	11.81641	12.06055	72.92175	60.65252	12.37926	-0.02511	639.4977

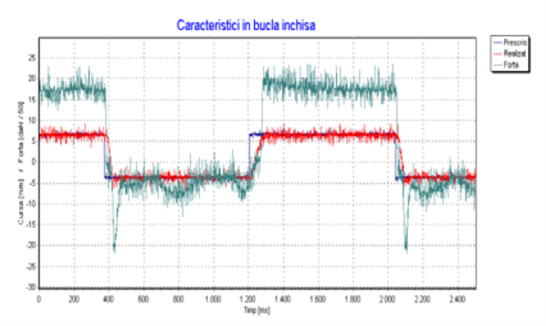

Chart no 2.2
Step response: -5mm …+5mm
T_{oil} 40˚ C
Responding time = 30ms on the unload cylinder chamber and a responding time = 120ms on the load cylinder chamber

Chart no.2.2 values

Time	Set point [mm]	Accomplished [mm]	P_p [bar]	P_a [bar]	P_b [bar]	P_t [bar]	Load [N]
1	6.445313	6.347656	73.52864	66.36763	8.439719	0.018241	941.2056
2	6.591797	6.542969	72.40157	65.92374	8.217773	-0.04245	875.3154
3	6.591797	5.761719	72.22817	66.42312	8.051314	-0.01644	951.6093
....							
324	6.933594	6.933594	73.44194	65.70179	6.608665	-0.09447	965.481
325	7.03125	6.738281	74.30892	66.20117	6.719638	0.000902	719.2596
326	6.835938	6.640625	71.1878	67.58833	7.718395	0.200306	726.1954
....							
1026	-3.51563	-3.51563	72.14147	34.51838	46.39249	-0.12048	-88.7627
1027	-3.36914	-4.78516	70.84101	34.12997	45.56019	-0.02511	-182.396
......							
2497	-4.3457	-3.71094	73.44194	27.47159	49.83265	-0.01644	-210.139
2498	-4.10156	-1.5625	74.8291	27.24964	50.55398	-0.00777	-348.856
2499	-3.80859	-3.75977	74.9158	27.4161	51.99663	-0.11181	-348.856
2500	-3.71094	-3.71094	74.13552	27.47159	51.60822	-0.10314	-355.791

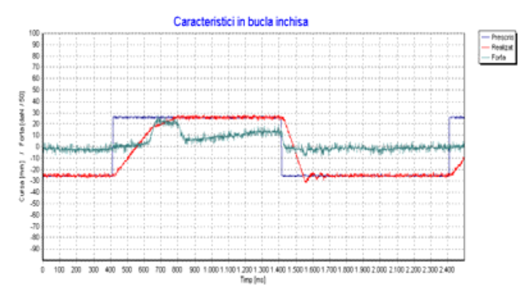

Diagram 2.3
Step response: -25mm…+25mm and a lower load
T_{oil} 40˚ C
Responding time = 300ms

Chart no.2.3 values

Time	Set point [mm]	Accomplished [mm]	P_p [bar]	P_a [bar]	P_b [bar]	P_t [bar]	Load [N]
1	-25.3906	-25.293	98.41087	54.10511	60.70801	-0.2852	-88.7627
2	-25.3418	-25.1953	100.8384	54.38255	60.26412	-0.31121	-189.332
3	-25.6348	-25.293	100.7517	54.27157	60.76349	-0.12914	-154.653
…….							
733	25.39063	21.04492	96.93701	90.55975	6.220259	0.703153	1010.564
734	25.97656	22.50977	95.89663	89.83842	6.220259	0.642464	903.0586
735	25.97656	24.70703	96.15673	92.16886	4.999556	0.607785	1138.876
…………..							
1980	-25.4395	-25.4883	99.88473	51.83017	61.92871	-0.25919	-119.974
1981	-25.4883	-25.1465	98.49756	51.38627	61.48482	-0.30254	-119.974
1982	-25.1465	-24.6582	98.75766	51.99663	62.48358	-0.34589	-95.6985
…….							
2498	25.83008	-10.9863	91.47505	84.62269	9.715909	0.78985	36.08199
2499	25.73242	-10.5957	92.42873	84.06783	9.54945	0.703153	32.61408
2500	25.73242	-10.4492	92.60212	84.90012	10.9921	0.919897	18.74245

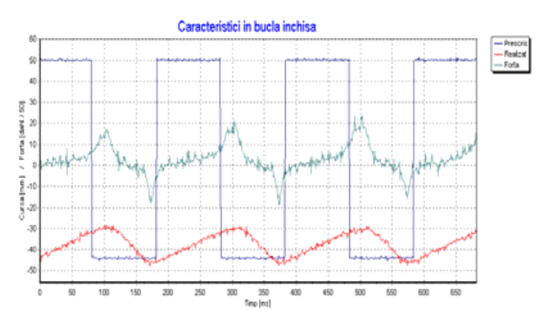

Chart no. 2.4
Step response: -45mm…+50mm
High frequency.
At this frequency (6 Hz) the axis doesn't realized the program.

Chart no.2.4 values

Time	Set point [mm]	Accomplished [mm]	P_p [bar]	P_a [bar]	P_b [bar]	P_t [bar]	Load [N]
1	49.46289	-43.3594	68.93366	63.37136	10.65918	-1.18686	-50.6157
2	50.48828	-45.3125	66.76622	64.48109	8.939098	-1.35158	119.3117
3	50.39063	-42.9688	67.89329	62.53906	8.217773	-0.97878	-95.6985
…..							
450	50.09766	-36.084	68.41347	62.87198	5.332475	0.182967	185.202
451	49.90234	-35.0586	67.2864	63.75977	5.831854	0.330353	341.2578
452	49.41406	-37.4023	68.15338	63.59331	6.275746	0.200306	60.35733
………							

1232	50.68359	-37.8418	72.22817	65.86825	5.110529	0.009571	-88.7627
1233	49.02344	-37.5488	69.36715	64.8695	7.440962	0.04425	133.1834
1234	49.95117	-38.7695	67.80659	64.09268	7.274503	-0.07713	-36.7441
....							
2497	-44.043	-32.0313	70.14743	70.02974	3.057528	-0.63199	885.7191
2498	-44.043	-32.1289	70.32082	68.53161	3.113015	-0.52795	913.4624
2499	-44.1406	-32.0313	69.88733	65.97923	2.336204	-0.60598	937.7377
2500	-43.6523	-32.666	68.58687	67.25542	2.502663	-0.63199	993.2242

2.2 The response to sinus input signal

In order to obtain this dynamic behavior of the electro-hydraulic axis, the input signal is a sinus one variable between $-I_{max}$ and $+I_{max}$. The experimental results are shown in 2.5 ,2.6 charts.

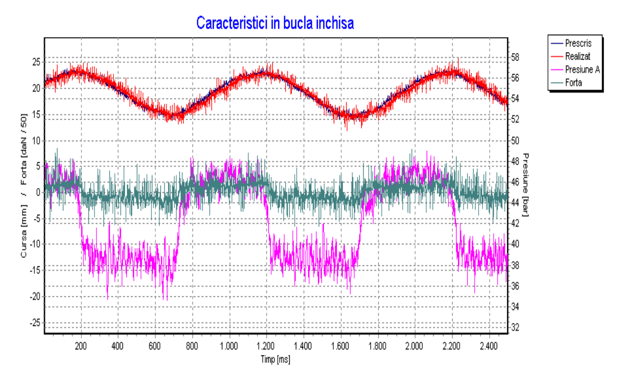

Chart no. 2.5
The response to sinus input signal
Frequency= 1Hz.
Amplitude = 10mm.
At this frequency(a lower one) the displacement of the axis follow the input signal.

Chart no.2.5 values

Time	Set point [mm]	Accomplished [mm]	P_p [bar]	P_a [bar]	P_b [bar]	P_t [bar]	Load [N]
1	20.99609	18.21289	69.97403	47.83514	38.01403	0.564436	-81.8268
2	21.14258	20.75195	72.05478	49.00036	37.68111	0.79852	129.7155
3	20.75195	21.43555	70.58092	49.83265	37.62562	1.197329	171.3303
4	21.67969	20.89844	71.70799	47.66868	38.125	0.81586	46.48571
......							
820	16.11328	17.08984	73.44194	45.22727	39.7896	-0.39791	-40.212
821	17.28516	15.67383	72.31487	45.89311	38.9573	-0.62332	-140.781
822	17.38281	18.26172	72.22817	45.17179	38.23597	-0.38057	39.54989
......							
1278	21.97266	22.11914	71.96808	38.23597	44.33949	-0.32855	-50.6157
1279	21.77734	22.2168	70.58092	37.45916	44.17303	-0.30254	-36.7441
1280	22.07031	23.19336	71.36119	38.125	44.06206	-0.21584	63.82524
......							
2473	17.57813	17.96875	73.09515	38.90181	43.72914	0.113609	-50.6157
2474	17.67578	17.87109	72.66166	38.29146	44.17303	0.304343	-12.4687
2475	17.57813	17.96875	71.70799	39.3457	43.17427	0.399711	-33.2761

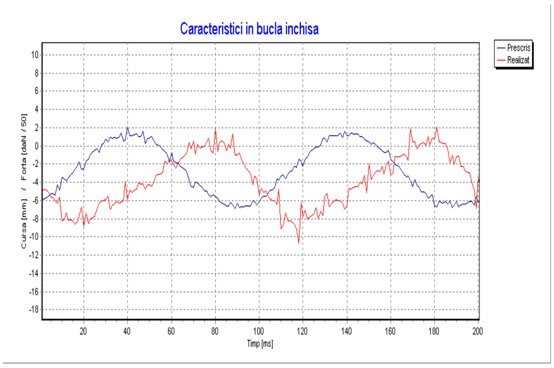

Chart no. 2.6

The response to sinus input signal
Frequency= 15Hz.
Amplitude = 7mm.
At this frequency the displacement of the axis doesn't follow the input signal.

Chart no.2.6 values

Time	Set point [mm]	Accomplished [mm]	P_p [bar]	P_a [bar]	P_b [bar]	P_t [bar]	Load [N]
1	-5.66406	-4.63867	60.87078	18.8157	49.05584	4.561199	-67.9552
2	-5.9082	-4.98047	59.83041	17.76145	49.72168	3.711562	-36.7441
3	-5.85938	-4.78516	61.47766	18.20534	49.16681	3.260734	4.870827
4	-5.71289	-4.88281	61.04417	18.53826	49.27779	2.567153	-57.5515
5	-5.51758	-5.12695	61.99785	18.03888	49.2223	2.029627	-5.53289
.....							
1045	0.146484	-3.36914	68.15338	63.92623	5.942827	-0.52795	-12.4687
1046	0	-2.92969	68.06668	62.42809	3.279474	-0.03378	95.0364
1047	-0.19531	-3.02734	66.93961	64.4256	3.889826	0.80719	4.870827
......							
1706	-1.36719	-8.1543	59.05013	53.66122	10.04883	-0.97011	-2.06499
1707	-0.97656	-8.20313	60.78408	53.82768	9.327504	-1.01346	-22.8724
......							
2497	-1.51367	-8.78906	65.63915	61.48482	8.384233	-1.09149	49.95361
2498	-0.97656	-8.54492	61.30427	57.4343	9.161044	-1.03947	195.6057
2499	-1.85547	-6.64063	57.92306	51.83017	8.1068	-1.29089	-57.5515
2500	-0.58594	-9.22852	62.25794	55.32582	9.604936	-1.15218	-64.4873

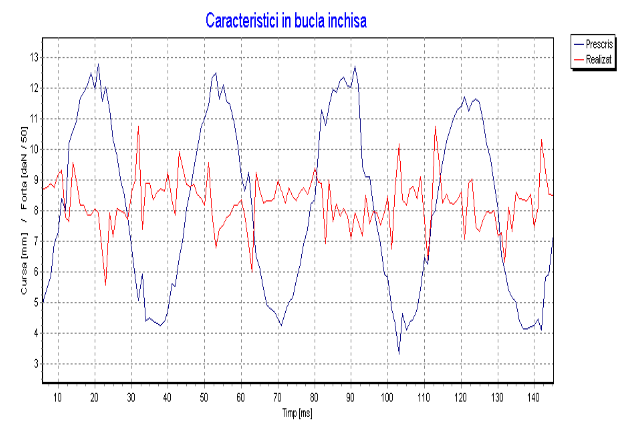

Diagram 2.7

The response to sinus input signal
Frequency= 30Hz.
Amplitude = 9mm.
At this frequency the displacement of the axis doesn't follow the input signal.

3. Conclusions

The experimental results obtained are comparable to the theoretically ones obtained in numerical simulation. Deviations predictable between the experimentally and theoretically data are determined by the lower functional performances of some hydraulic equipment used and doesn't have a notable influence over the final result.

The dynamic and static behavior of the electro-hydraulic axis depend both on temperature of working oil and also on main features of hydraulic components. The mathematical model could be considered completely validated because the experimental data are matches in 95% with the numerically ones.

REFERENCES

[1]. Mazilu I., Marin V. – Sisteme hidraulice automate , Editura Academiei, Bucureşti, 1982
[2]. Merritt H. – Hydraulic Control systems, John Wilez and Sons, 1967
[3]. Adrian Mirea; Gabriel Rădulescu, Gabriela Matache – Cercetări teoretice asupra unităţilor de translaţie pe o axă - Simpozionul internaţional de hidraulică, pneumatică, etanşări, mecanică fină, scule, dispozitive şi echipamente electronice specifice, mecatronică –HERVEX 2006
[4]. M.Comes, P. Drumea, M. Blejan, A.V. Mirea Positioning systems tuning interface using proportional hydraulic drives - The 4th International Symposium for Informatics and Technology in Electronic Modules Domain, SIITME 98, Bucharest
[5]. P. Drumea, A. Mirea, A. Marin, P.Svasta - Quality control management for electrohydraulic equipment with top dynamic performances– HRTC 2000 – The international Workshop 2000, march 13-14, 2000
[6]. A. Drumea, Al. Vasile, P. Svasta, I. Ilie, Modelling and Simulation of Simple Mechatronic System - Position Control Solution Based on Linear Variable Inductor Displacement Transducer, 2nd Electronics System-Integration Technology Conference ESTC08, Greenwich, London, UK, September 1-4, 2008, ISBN 978-1-4244-2814-4, pp. 225-229.
[7]. Petrin Drumea, Mircea Comes, Adrian Mirea, Dănică Dobrin, Mechatronic positioning system with the velocity controL, MTM 2002, LVIV, Ukraina
[8]. Mircea Comes, Andrei Drumea, Adrian Mirea, Alexandru Marin, Servohydraulic actuator as a mechatronic system, MTM 2001, Romania

ISSN 1454 - 8003
Proceedings of 2014 International Conference of Hydraulics and Pneumatics - HERVEX
November 5 – 7, Calimanesti-Caciulata, Romania

DRIVE INSTALLATION OF HARMONY FLOW WITH ONE BIG CONDENSER

Prof.dr. eng. Carmen BAL[1], assist. drd. eng. Carmen Ioana IUHOS[2]

[1] Technical University of Cluj Napoca, carmen.bal@dppd.utcluj.ro;

[2,] Technical University of Cluj Napoca, bic-tkd@yahoo.com

Abstract: *In this paper we propose to analyses the alternative flow in the parallel installation including the capacity, and the friction resistance In this paper we show the caloric effect due to the displacement of the low in the friction resistance calculate. We propose to calculate the section of the friction resistance in the drive installation assembly connection with one big condenser c_m and one friction resistance were we know the capacity and the flow and sonic pressure.*

***Keywords**:* sonic pressure, sonic flow, friction resistance, sonic condenser, temperature etc

1. Introduction

Gogu Constantinescu great inventor spent an enormous energy to convince the world that are compressible fluids with more than accepted, and this is essential for the propagation of vibrations through the liquid. As stated right from its appearance, sonicity is in correspondence with electricity and sonic transmissions are similar to AC power transmission.

Considering the above analogy true, compress liquids is equivalent to demonstrating accumulation of electric charge in a capacitor. Sonic vibration transmission is achieved, and at the beginning it was thought that the vibration energy is an energy degrading not only can convert heat. It was unthinkable that a vibration system can achieve high efficiency mechanical work.

Sonic actuation permits the optimal combination between the ease of processing electric signals (of low energy) and the high-power sonic actuation, which eliminates the greatest parts in a classical hydraulic system (such as hydraulic reservoirs, control systems for pressure, flow, direction, etc), resulting in an actuation which melts the virtues of low-energy signal processing and the high-output, small-volume, economical and compact sonic actuation

It should be mentioned that this approach of the problem makes the sonicity theory a particular case of power transmission through „displacement", which means the fluid, instead of flowing continuously from generator to they actuator, evolves harmonically in time at various wavelengths and frequencies.

In the new system, energy is transmitted from one point to another by covering distances which can be large, by applying periodical compressions which generate longitudinal vibrations in columns of solids, liquids and gases. The energy transmitted through these periodical longitudinal pressure and volume vibrations is in fact power transmission through sonic waves.

This concept enables obtaining thermal effects through fluid motion or/and synchronous, non-synchronous, single-phase actuation when using a small volume of non-polluting fluid, such as water. The effect of this solution is that one can eliminate the individual equipment for flow and pressure adjustment and control by transferring them in the modern domain of computerized electronic control.

2. Experimental consideration about the caloric effects in the harmonic installation

We considered the sonic system formed by with one big capacity cylinder noted C_M and one friction resistance C_f (figure 1). Is formed by sonic generators who are connecting by the friction resistance R_f. with a pipe, this resistance is connected also by a pipe to the capacity cylinder. The capacity of cylinder are $V= 2405{,}282 \cdot 10^3$ mm^3 [2]. [2].

ISSN 1454 - 8003
Proceedings of 2014 International Conference of Hydraulics and Pneumatics - HERVEX
November 5 – 7, Calimanesti-Caciulata, Romania

After the work of the experimental dates obtained from the three sensor place in the system, are results the primary histograms, presented in the figure 2. This illustrated the evolution of the pressure to the generators and the two extremity of the condenser. Also, we can see the speed of the generators. Pressure evolution curves reveal a phase shift between the pressure at the condenser pressure generator**.**

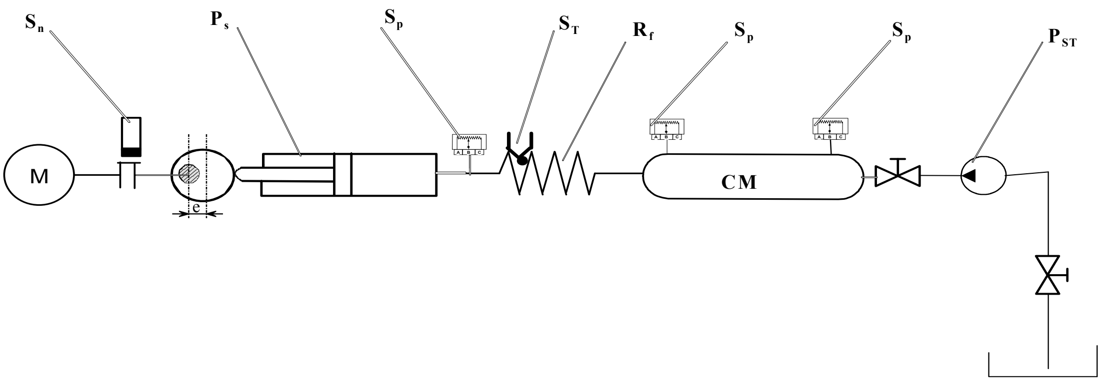

Fig. 1 The harmonic installation with the friction resistance

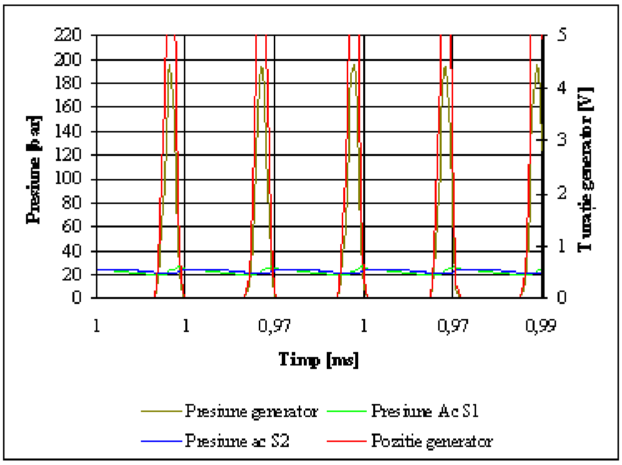

Fig. 2 The variation of the pressure in time in the case of the installation

In the experimental graphics we are noted with:

ΔG – the variation of the generator pressure;

ΔS_1 – the variation of the pressure obtained by the first sensor of pressure place to the left of the capacity cylinder

ΔS_2 – the variation of the pressure obtained by the right sensor of pressure placed to the capacity cylinder;

T – temperature

In figures 3 and 4 we are represented the variation of diagrams of the pressure and temperature in time and speed for the static pressure static pressure 0,75E+05 Pa.

It appears that the pressure are on condenser pressure sensors are equal to the 50E+05 Pa, after the pressure to the pressure sensor 1 increases to the 120 E+05 Pa. The generators pressure is a rapidly growing 250E + 05 Pa reached, at which time the stop of the electric motor occurs. Since starting speed was great 1600rev/min , has been a sudden increase of the temperasture friction at the surface friction ressistance. (heating phenomenen due to friction), the temperature reaching 85 ^{0}C.

After 50 seconds of turning off the system when it occurs

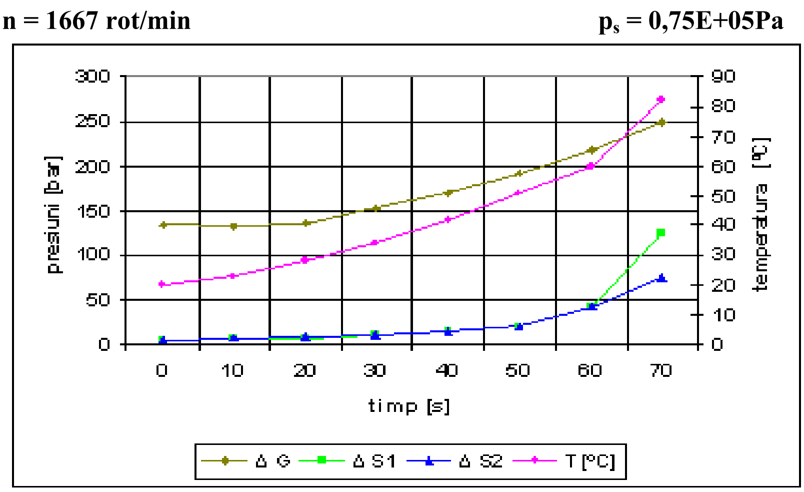

Fig. 3 Diagram of pressures and temperature variation of speed according to the static pressure of 0,75E+05 Pa

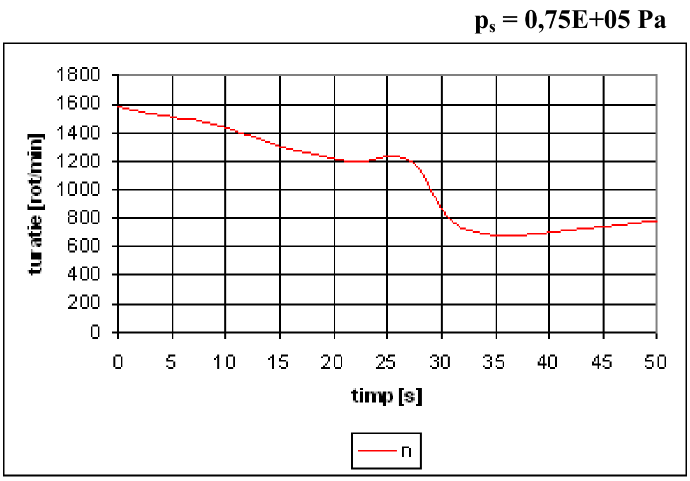

Fig. 4 The variation of revolution in time to the static pressure 0,75E+05 Pa

Figures 5 and 6 are plotted diagram of the variation in pressure and temperature versus time and speed for static pressure 1E + 05 Pa. It is noted the pressure that the pressure on the cylinder pressure sensors are equal and pressure stabiliyes at 50E + 05Pa, the pressure fluctuation generastor is verry large variation in speed due to start at 834 rev/min and decreased to 275rev/min, as result of a pressure the 160E+05 Pa to the generator, when the electric motor taken off. Temperature reached after nearly a minute from start to 80ºC

Figures 7 and 8 are plotted diagram of the variation in pressure and temperature versus

n = 1667 rot/min **p_s = 1E+05Pa**

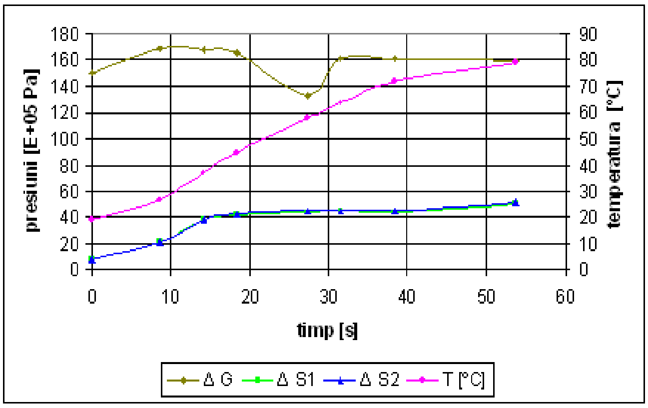

Fig. 5. Diagram of pressures and temperature variation of speed according to the static pressure of 1E+05 Pa

time and speed for the static pressure of 1.25 + 05 Pa. It appears that the pressures are on

p_s = 1E+05Pa

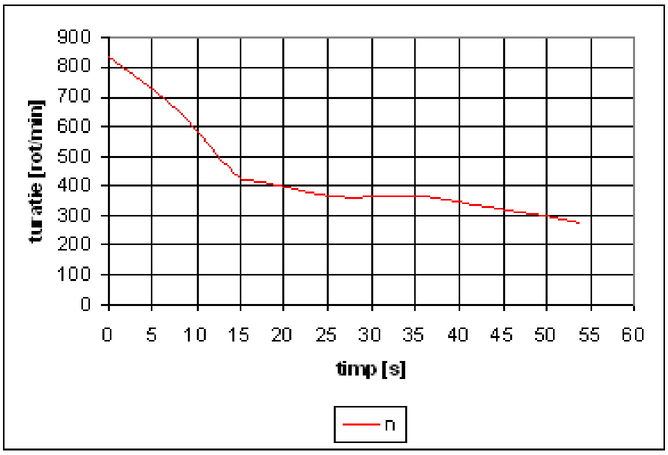

Fig. 6. The variation of revolution in time to the static pressure 1E+05 Pa

cylinder pressure sensors are equal to 20E + 05 Pa after the pressure sensor 1 increases to 125 E + 05 Pa pressure generator is a fast growing reaching 260E + 05 Pa, at stopping the electric motor is time and speed for static pressure 1E + 05 Pa.

It is noted that the pressure on the cylinder pressure sensors are equal and pressure stabilizes at 50E + 05 Pa, the pressure fluctuation generator is a very large variation in speed due to start at 834 rev/ min and decreased to 275 rpm/ min as a result of a pressure generator is a fast growing reaching 260E + 05 Pa, at stopping the electric motor is produced.

Since starting speed was great - 1667 rev / min has been a sudden increase of temperature

n = 1667 rot/min **p_s = 1,25E+05Pa**

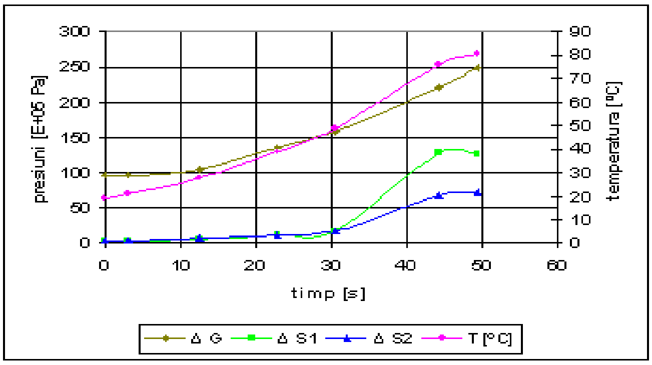

Fig. 7 Diagram of pressures and temperature variation of speed according to the static pressure of 1,25E+05 Pa

at the surface friction resistance (due to the phenomenon of frictional heating), the temperature reached 80 ° C after 50 seconds of turning off the system when it occurs.

p_s = 1,25E+05Pa

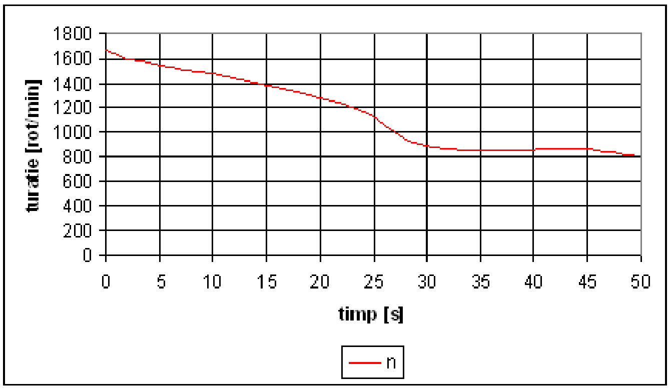

Fig. 8 The variation of revolution in time to the static pressure 1,25E+05 Pa

3. Conclusions

Analyzing charts above we can draw the following conclusions:

1. The greatest influence on increasing pressure and the temperature in the system has the higher speed so that it is higher to start the fastest growing pressures and temperature resistance friction;
2. The static pressure in the system to a lesser extent affect the temperature rise;
3. As the electric motor stops after a short period of operation is not recommended for making the stand consists of a friction resistance and a cylinder.

REFERENCES

[1]. Constantinescu, G., (1985), *The theory of the sonicity*, Bucureşti, Ed.Academiei.
[2] Carmen Bal, (2007)**,** *Caloric effect in the circuits by harmonic flow****,*** Cluj Napoca, Ed. ALMA MATER.
[3] Carmen Bal, (2006), *Research and contributions about the drive systems with the harmonic flow*, The doctoral thesis Technical University of Cluj Napoca.
[4] Pop I. Ioan**,** Carmen Bal, Marcu Lucian ş.a.**,** (2007), *The sonicity applications. Experimental results*, Iaşi**,** Ed. Performantica.

ISSN 1454 - 8003
Proceedings of 2014 International Conference of Hydraulics and Pneumatics - HERVEX
November 5 – 7, Calimanesti-Caciulata, Romania

EXPERIMENTS REGARDING THE PARAMETERS OF POWER OPTIC DEVICES

Irina BACIS[1], **Cristina MARGHESCU**[1], **Andrei DRUMEA**[1]

[1] University “Politehnica” of Bucharest; irina.vasile@cetti.ro; cristina.marghescu@cetti.ro

Abstract: *The purpose of this paper is to present the experiments conducted on a platform developed for the analysis of the coupling and alignment of optical devices, of the emitted optical power, of the losses on optical fibre and at receivers, of the various devices emitting optical flow. On this platform it is possible to conduct experiments to determine the losses in the coupling optic elements, fibre types, lengths, splitters, connections extended through reflow of zone, receivers.*

Keywords*: power optic device, optical fibre, laser diode*

1. Introduction

An optical transmission system is a means of transferring information between fixed points on a fiber optic cable; the information is in the form of bits or symbols in the case of digital systems and in the form of analog waveforms for analog systems [1]. There are numerous transmission techniques available today. These transmissions require a complex study regarding the behavior of the transmission chain especially when using high power laser diodes to cover great distances (500 km) [2]. To study the basic technical aspects of optical transmission systems and the particular characteristics related to a local communication network, a communication system was implemented with the possibility of accessing from a computer without the use of any additional elements. The computer, through specialized software, sets the pulse frequency, duty cycle and current intensity for the high power 1055 Fabry-Perot laser diode.

The light beam obtained, modulated in impulse, is sent to the fiber optic through the coupler, that is coaxial with the optical source and allows the easy connection and disconnection of the fiber optic to the transmitter. An incident ray - perpendicular on the section of the fiber, does not change its direction at the refraction (n) in another environment, but changes its speed [4]. For air N = 1 and the speed of light is 300,000 km/sec, and for glass n = 1.5 and in this case the speed changes in accordance with the formula:

$$\frac{c_0}{\upsilon_{glass}} = \frac{n_{glass}}{n_{air}} \tag{1}$$

This leads to a velocity in fiberglass of 200,000 km / s.

At reception, the fiber is guided by a similar coupling to send light on the electro-optical receiver (photodiode, phototransistor) which converts it in current pulses. These are amplified and decoded to recompose the transmitted signal or information.

2. Structure for the characterization of an optical system

As we have already mentioned, characterization of transmission through an optical system using a computing system can be achieved with a platform that can deliver current pulses controlled by a computer with specialized software that sets the pulse frequency, duty cycle and current intensity.

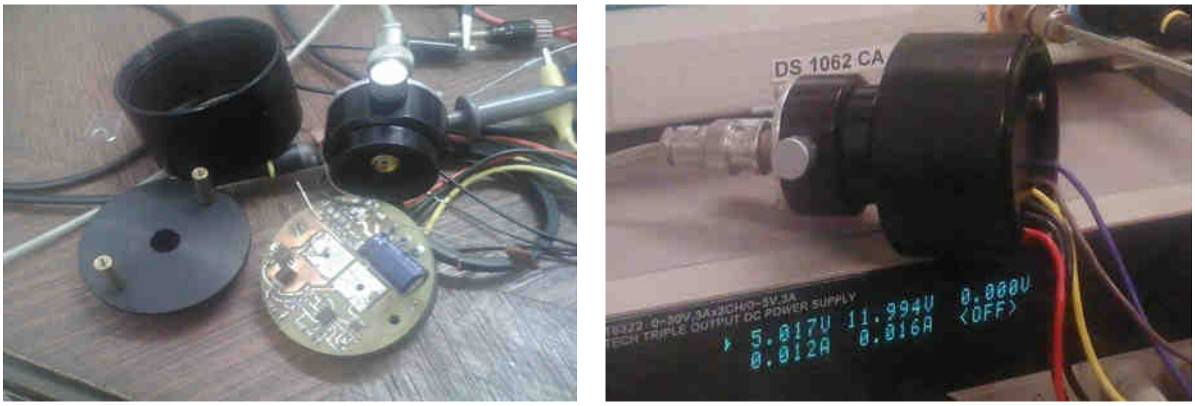

a) b)

Figure 1. *Experimental laser emission structure with Fabry - Perot diode:*
a) The structures subsystems e; b) The assembled transmitter coupled with the optical receiver powered from a source

In order to simplify the procedure a specialized platform was implemented. A Fabry-Perot power laser diode was used, operating in impulse with $\mu\varphi$=1055 nm, Ith=40 mA and Iop=750 mA on a single-mode optical fiber of type SFM 128 with EM optical coupling type connected through alignment. Two types of measurements were conducted to demonstrate the usefulness of the experimental structure.

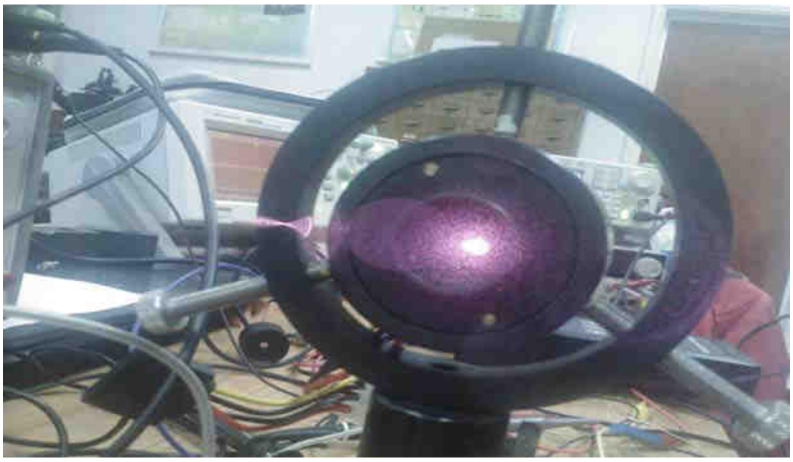

Figure 2 *Laser emitting device supplied from a PC source*

The structure was controlled on input (VIN) with impulses obtained from a generator which generates impulses where the fill factor could be set to 10% and a frequency of 10 MHz, so an impulse of 0.1 μs.

The current through the power diode was determined by measuring the voltage across a resistor with a value of 0.25 Ω using an oscilloscope. The values are presented in Table 1, and the variation is illustrated in Figure 3.

Table 1. *Current as function of command voltage*

Command voltage [mV]	0	50	100	150	200	250	300	350
Input I_D[mA]	5	38	75	115	155	200	245	290

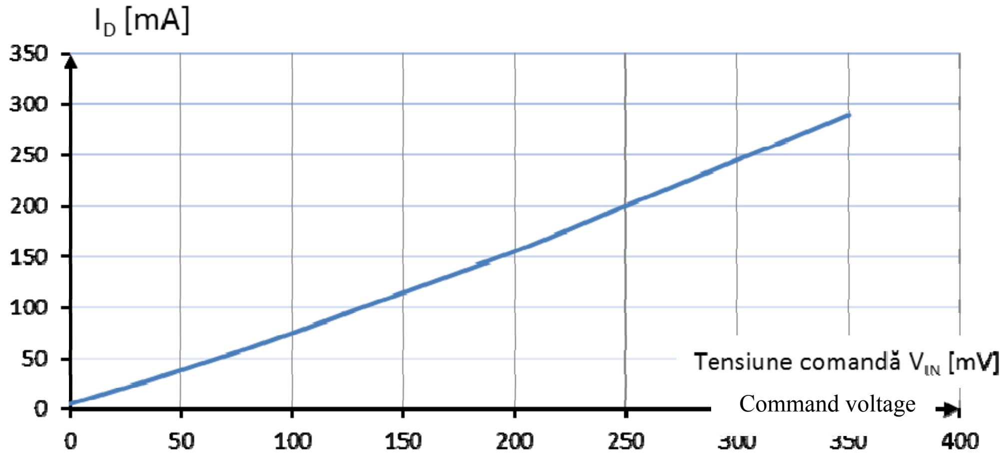

Figure 3. *Current through the laser diode as function of command voltage*

The amplitude of the voltage impulses was measured at the output of an optical detector with receiver diode in a built-in amplifier with a load resistor of 50 kΩ. The values are presented in Table 2, and in Figure 4.

Table 2. *Voltage variation at the output of the optical detector as function of current impulse through the laser diode*

Input current in the laser diode [mA]	5	20	40	60	80	120	160	180
V_{out} receiver optic device [mV] without load	0	15	130	180	200	200	200	200

It can be observed that the voltage is limited due to optical detector saturation.

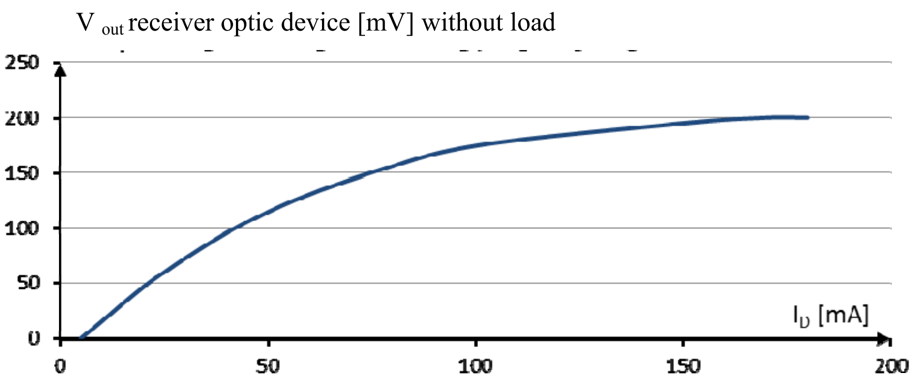

Figure 4.*Voltage variation at the output of the optical detector as function of current impulse through the laser diode*

In the second stage measurements were conducted to determine the optical power injected into the fiber optic and received on the receiver cell of a power meter. The values are presented in Table 3. When using an adapted power meter with a 50 ohm load, the received power is dependent on the value of the current and is not limited. We can also observe that the 1055 FPL diode begins to emit optical power after the current through exceeds 40 mA (see Figure 5).

Table 3 *Power variation measured with a Power-meter with 50 Ω load as function of current pulses through the laser diode*

Input current I_D[mA]	5	30	60	80	100	180	300	600
Power [mW] for 50Ω	0	0	0.130	3.7	9.5	15	30	55

Another parameter of the optical coupling that can be measured on the experimental structure is the irradiance. Table 4 presents the values obtained, and in Figure 6 respectively.

Table 4. *Irradiance function of distance at I_D=200 mA*

Distance [mm];	10	50	100	120	150	200	300
Power [μW]	100 0	500	260	190	115	60	18

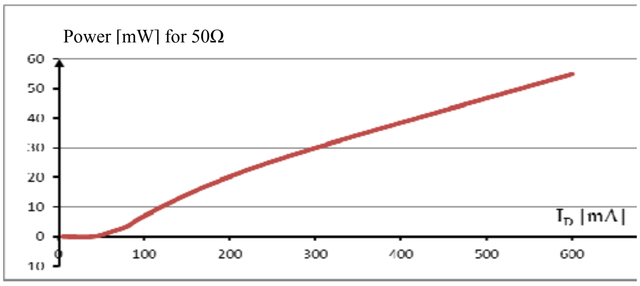

Figure 5. *Power variation measured with a Power-meter with 50 Ω load as function of current pulses through the laser diode*

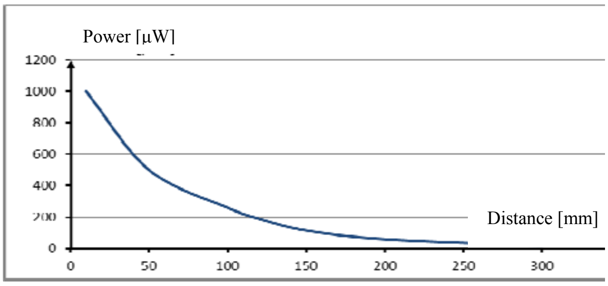

Figure 6. *Irradiance function of distance at ID=200 mA*

3. Determination of optimal cutting angle for fiber continuity

In real life situations optical fibre must often be cut. Extending certain segments due to network reconfiguration or as a result of damage requires welding the optical fiber. Regardless of how much the ends are polished the resulting surfaces are not perfect and some burrs or dirt remain which behave like reflectors for the optical wave. We performed experiments on a single-mode optical fiber of type SFM 128 with EM type optical coupler connected through alignment (see Figure 7). Following several attempts made by cutting the fiber under certain angles using a device the optimal angle to section the two endings so that the optical power loss is minimal or the coupling from the melting zone to be maximum resulted.

***Figure 7**. Measurement structure of the angle under which fibre is debited for determination of optical power transmitted depending on the angle φ*

***Figure 8** Platform for measuring the power injected into the fiber*

***Table 5.** Variation of optical power in case of fiber cutoff function of the angle φ*

φ cutoff angle of the optical fibre [degrees]	70	75	80	82	85	90	95	100
Power [mW] at 50Ω	33	45	51	50	45	40	35	32

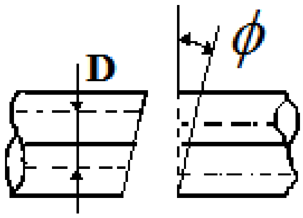

a)

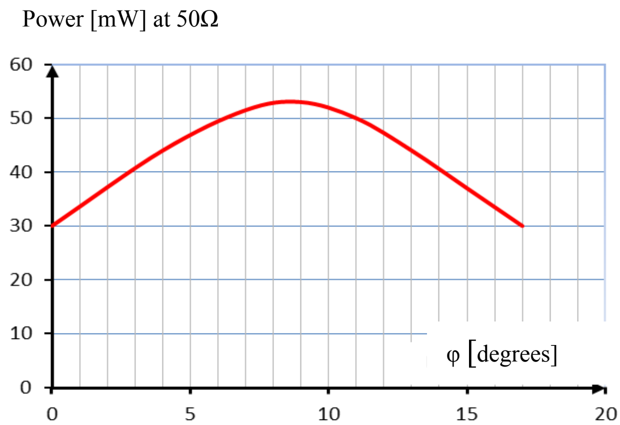

b)

***Figure 9** a) φ angle; b) Variation of optical power in case of fiber cutoff function of the angle φ*

4. Conclusions

The study of the transmission through fiber is needed to understand the phenomena that occurs in optical fiber connections and elements which have a decisive role in achieving a quality transmission through these joints.

It is possible to perform experiments to determine the losses in the optical coupling elements, fiber types, lengths, splitters, using the platform.

ACKNOWLEDGMENT

Presented work was supported by a grant of the Romanian National Authority for Scientific Research CCCDI - UEFISCDI, Project number: PN-II-PT-PCCA-2013-4-1673.

REFERENCES

[1] I. Bacis, L. Filip, "Curs operator pe fibra optica", Centrul de instruire si Documentare ROMTELECOM , Bucuresti 2003;
[2] P. Schiopu, N. Grosu; "Masuratori optoelectronice";Editura Matrix ROM 2011; Bucuresti, ISBN 978-973-755-694-3
[3] R. J Bates,"Optical Switching and Networking Handbook", McGraw-Hill, New York, 2001
[4] J. Hecht, "City of Light, The Story of Fiber Optics", Oxford University Press, New York, 1999.
[5] A. Drumea, "Control of Industrial Systems Using Android–Based Devices", Proceedings of the 36th International Spring Seminar on Electronics Technology, Alba Iulia, Romania, 8–12 May 2013; pp. 405–408.
[6] B. Mihailescu, I.Plotog, P.Svasta, M.Vladescu, "VPS Control Module EMC Modeling and Evaluation", 2010 9th International Symposium on Electronics and Telecommunications (ISETC)
[7] C. Tamas, M.Pantazica, C. Grecu, I. Marghescu, "Integrated Circuits Characterization Platform (ICCP)", 36th International Spring Seminar on Electronics Technology – ISSE 2013

ISSN 1454 - 8003
Proceedings of 2014 International Conference of Hydraulics and Pneumatics - HERVEX
November 5 – 7, Calimanesti-Caciulata, Romania

SENSORICS USED IN THE DIAGNOSIS OF GEARBOXES

Nicolae Florin ROTARU[1], Liviu Ioan VAIDA[2]

[1] Technical University of Cluj-Napoca, nicolae.rotaru@termo.utcluj.ro

[2] Technical University of Cluj-Napoca, liviu.vaida@termo.utcluj.ro

Abstract: *This paper describes a concept for the analysis of gearbox vibrations using a modern method of a fault diagnosis. The faults analysed constitute a spontaneous discharge of energy, just like some mechanical vibrations produced by a piece from a gearbox.*

Keywords*: diagnosis, vibration analysis, piezoelectric sensor*

1. Introduction

In terms of machinery and modern equipment, a new concept is increasingly more developed. It is about the maintenance of state function. The interventions on the machinery are made only when the machine condition has deteriorated beyond a certain point. We must determine the condition of the machine in every moment of its operation.

Such a concept can be applied also in the track of the gearboxes.

Vibration analysis which produces the body wave perceived on gearboxes can be used as a criterion of assessment for the technical state of these machines.

The essential problem in the developing of a system for the anomalies diagnosis is to select from all the information resulting from this analyse those who give a direct appreciation about the technical conditions of the pump components. There are some technical possibilities to capitalize this information which must be correlated with the faults which produced the body wave change.

One possibility is that the operation of the gearbox to be monitored, having in view constantly the evolution of the vibration or the noise. Their essential changing can be interpreted as being caused by an abnormal growth of some states (for example wear).

Experimental research has confirmed that the body vibrations are even more intense as the energy source that produces them is stronger.

Increasing complexity of product and the large number of components which generally are technical designed to have the duration of operation, are arguments that justify the possibility of increasing the number of accidental falls of the installation in which the product is component part.

The condition of the product worsens because of the wear of different components, leading to the situation in which performances required are not provided by the system, and therefore it can not be used anymore. This wear, which does not involve a substantial change in the functional parameters occurs gradually over time, and leads to a certain limit, irreversible damage to the installation.

The analysis of the signal produced by the body wave range in frequency domain can be used for the surveillance of gearboxes, control of the technical state and the diagnosis of fault product.

2. Technical description of the gearbox selected for equipment with sensor

To establish a system for diagnosis of the wear (anomalies) it is necessary to establish first of all a set of measurements of the function that defines the oscillatory process (body wave) for the new gearbox (reference), which correspond to all requirements imposed by the execution project.

To study the gearbox anomalies we have chosen a box with variable speed whose gear shift can be made automatically by an electrical plate.

Transmission with continuous variation of transmission report, called CVT (Continuously Variable Transmission) are composed of, in addition to classical mechanism of adaptation and transfer of power flux, mechanical converter with continuum variation of the transmission report.

Mechanical converters used for the CVT assembly are mechanical systems where the successively transformation of the energy is done in the same forms of energy (mechanical energy).

Mechanical converters used for CVT assembly are based on the principle of power flow between the input unit and the output through a link, rigid or flexible, which by changing the position from these two elements determine the gear ratio change. The only applicable solution in the production of series is that of the converters with pulleys with variable diameters, with flexible intermediate element, continuous or articulated.
The variable spindle speed modifies the transmission report by changing the radius of the metal strap on the two pulleys. The control of radius is made by positioning the moving parts of those two pulleys (figure 1).

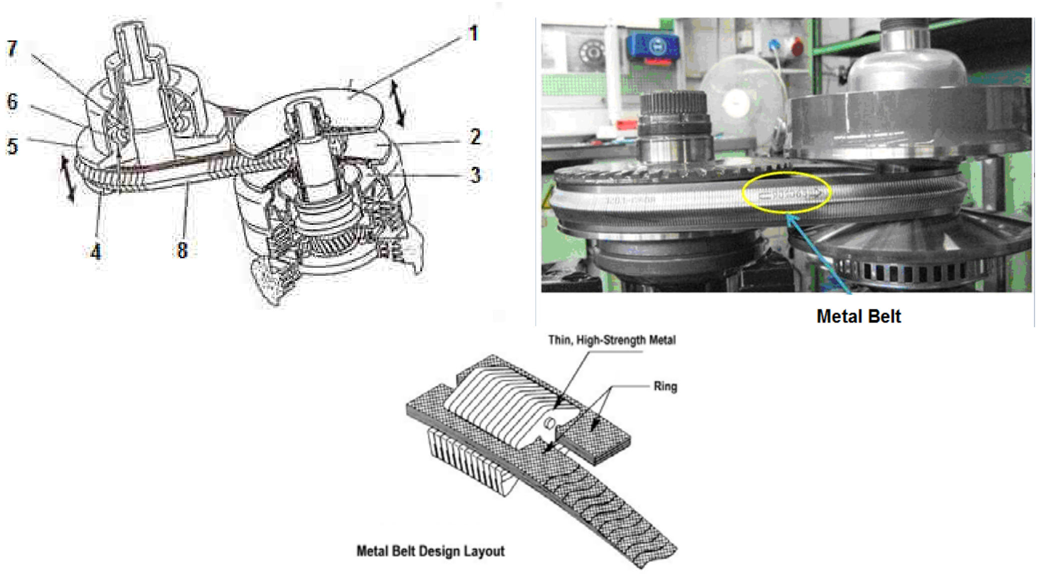

***Fig. 1** Converter for CVT transmission 1,2- half pulleys; 3-liners for primary hydraulic cylinder; 4-fixed half pulley; 5- mobile semi pulley; 6- secondary hydraulic cylinder; 7-coil springl; 8-strap*

The converter is composed by a primary pulley, a secondary one or driven, both of having the sloping sides and joined together by means of a belt of trapezoidal metal; the two pulleys have variable opening, are therefore composed of a fixed half-pulley and a mobile one.
The semi principal mobile pulley moves axially because it is driven by oil pressure controlled by the hydraulic command group, while the secondary pulley moves axially in the opposite direction to the primary one (that is, when one closes the other opens) by the action of an internal spring on the closure and due to the pressure exerted by the thrust belt to open; depending on the pilotage made

ISSN 1454 - 8003
Proceedings of 2014 International Conference of Hydraulics and Pneumatics - HERVEX
November 5 – 7, Calimanesti-Caciulata, Romania

by the electro command group, the mobile part of the principal wheel will open or will closed while the mobile part of the secondary wheel will do the same but in the opposite direction; therefore, the drive belt will have the position of "climbing" on a wheel and "down" on the other to convey a specific gear ratio that changes continuously from short to the long or "overdrive" given the variation of the contact radius of the steel belt on the drive wheel.
The speed converter modify the transmission report by changing the radius of the winding metal strap on the two pulleys. The control of the winding radius is made by positioning the moving parts of the two pulleys.
The planetary mechanism (Figure 2) provides the coupling and the uncoupling of the transmission engine and also it helps to reverse the direction of rotation on the reversing side.

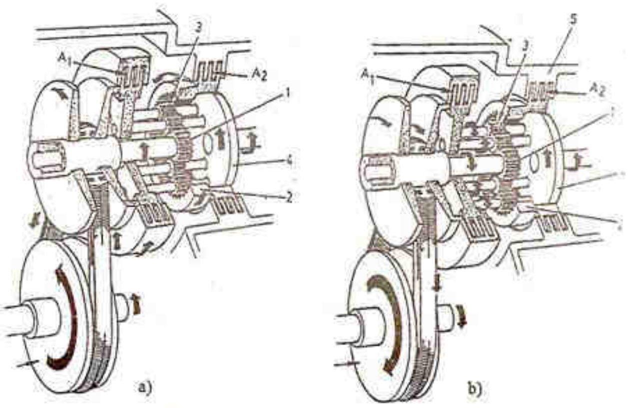

Fig. 2 Reversing mechanism 1,2-planetary wheels; 3-double satellites; 4-bearing arm; 5-transmission case; A1, A2-clutch lock

A1 clutch used for the went before realise the blocking of the planetary unit (direct drive) by binding the bearing arm to the dimmer (the driven wheel 1).
A2 clutch for reverse immobilizes the second crown of the planetary mechanism in relation to transmission case.
To reduce the radial gauge of the clutch are used multiple discs, which works in oil. The raising of disks packages is done hydraulically.
Clutch operation is totally automated by the hydraulic command, so no driver intervention is required.
The kinematics organizational chart for the CVT transmission is shown in Figure 3 and Figure 4 cross section.

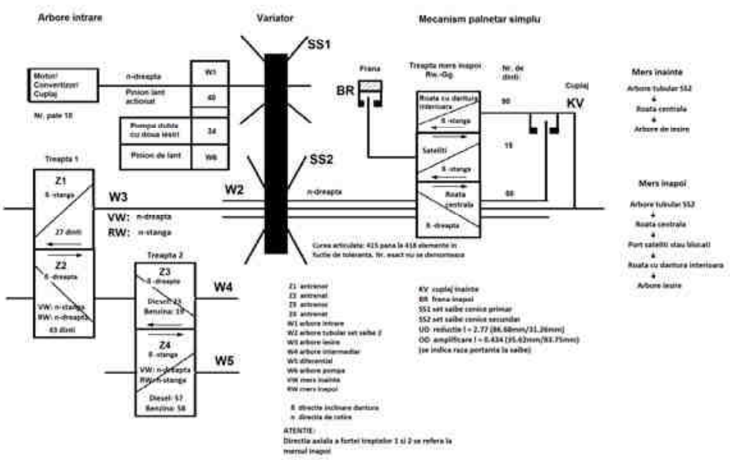

Fig.3 - The kinematics organizational chart for the CVT transmission

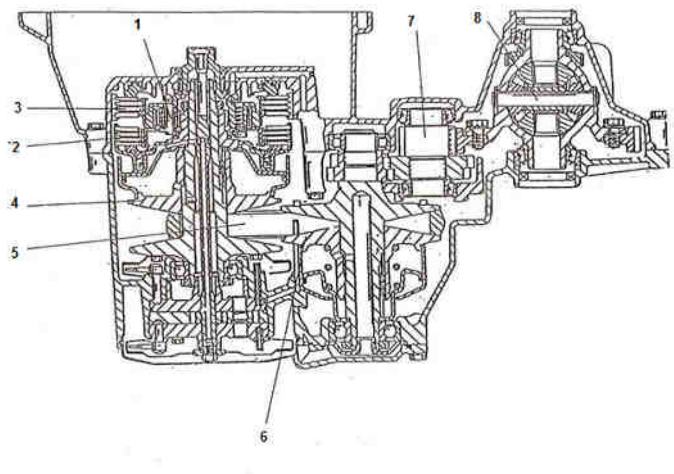

Fig. 4 Section 1-differential planetary gear; 2- clutch used for the went before; 3- clutch for reverse; 4-primary pulley; 5-metal belt; 6-secondary pulley ans.; 7-mechanism of the engine deck; 8-differential

3. Presentation of the test stand and the sensors chosen

To demonstrate the validity of the comparative analysis of the evolution of function that describes the oscillatory process, we have designed a stand just like in the diagram (Fig. 5) for measurements in case that in the gearbox there are replaced some components with increasing degrees of wear.

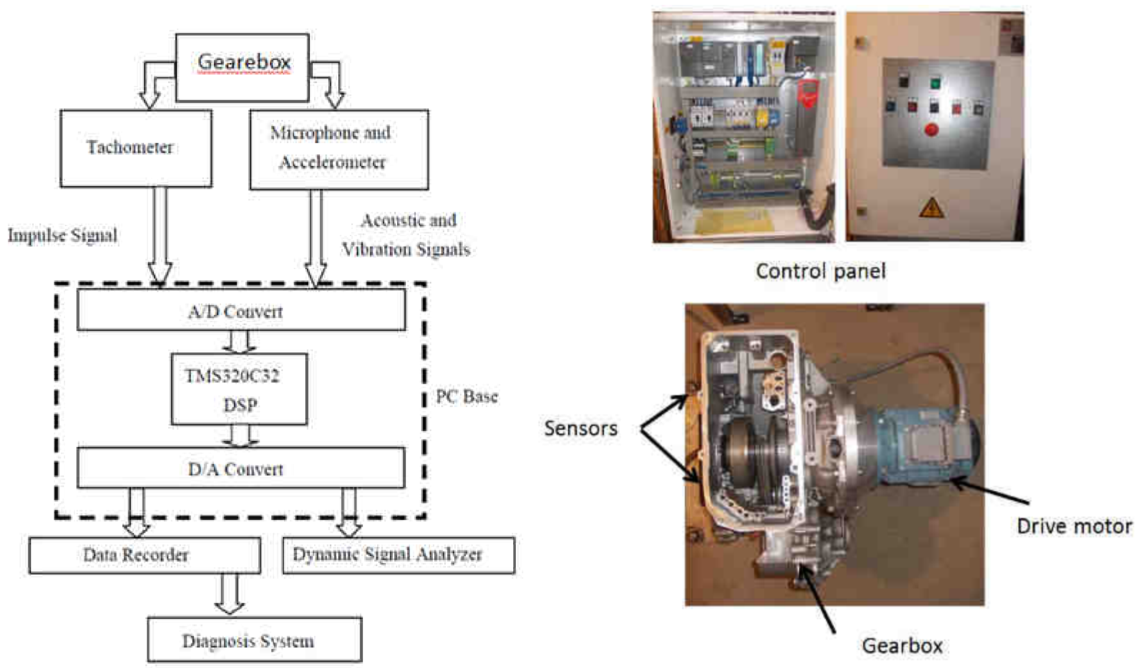

Fig. 5 Trial stand

Control panel (figure 5) command a drive motor for the gearbox, thus allowing control speed and direction of rotation; control panel can control and can change the gear ratio by controlling a solenoid valve which control the speed shifting.

Using a piezoelectric acceleration sensor applied on a gearbox the casing oscillations are recorded and then they are transformed into electrical signals time. These signals contain information that can be recovered using a frequency-analyzer.

Appreciation of the machine results from qualitative interpretation of the measurements by comparison with the frequency spectrum determinant on a new gearbox without abnormal wear without functional abnormalities.

The results of these measurements are stored in a database.

Database must also include information on the evolution of the function that describes the process when the wears progresses in time.

Because the causes of failure of a gearbox have mechanical origin, its vibration is the safest parameter used to control her condition.

For further diagnosis gearbox we will make some measurements and we will interpret the spectrograms (compared to those recorded in the new gearbox) of the oscillatory process for components with different levels (established) of wear.

4. Conclusions

The appreciation of the machine results from the qualitative interpretation of measurements by comparison with the frequency spectrum determinant on a new gearbox without abnormal wear and without functional abnormalities.

Such analysis systems can be introduced to control the quality of the gearbox directly to the manufacturer.

Using this method for checking the transmission quality, is reduced considerably the cost of test. The method is very good, thus we are able to provide to product warranty.

REFERENCES

[1] A. Potolea, “ Posibilitati si realizari in diagnoza pompelor cu pistoane axiale“, Cluj-Napoca 2002, PhD thesis;
[2] A. Darabont, I.Iorga, M.Ciodaru, “Masurarea zgomotului si a vibratilor in tehnica”, Editura Tehnica, Bucuresti, 1983.
[3] L. Deacu, L. Kerekes, “Studiu privind utilizarea fenomenului de emisie acustica in aplicatii industriale”, UTCN, Cluj Napoca, 1997.
[4] L. Deacu, s.a., “Tendinte noi in tehnica proportionala”, Hidraulica, Cluj Napoca, 1998
[5] http://www.rasfoiesc.com/inginerie/tehnica-mecanica/TRANSMISII-CU-VARIATOR-MECANIC26.php

ISSN 1454 - 8003
Proceedings of 2014 International Conference of Hydraulics and Pneumatics - HERVEX
November 5 – 7, Calimanesti-Caciulata, Romania

PROCESSING SIMULATION OF HYDRAULIC BLOCKS NCMT

Vasile ALEXA[1], József SÁROSI[2], Sorin RAŢIU[3]

[1] Faculty of Engineering Hunedoara, Politehnica University of Timisoara, Romania, vasile.alexa@fih.upt.ro

[2] Technical Institute, Faculty of Engineering, University of Szeged, Hungary, sarosi@mk.u-szeged.hu

[3] Faculty of Engineering Hunedoara, Politehnica University of Timisoara, Romania, sorin.ratiu@fih.upt.ro

Abstract: *In this paper we will present the design of technology for mechanical cutting module subsystem Prismatic Machining in CATIA V5 R20 for a hydraulic plate of the hydraulic actuation system. The ultimate goal of virtual processing is to obtain numerical processing file management components on CNC machines.*

Keywords: *hydraulic blocks, CATIA V5 R20, simulation, NCMT*

1. Introduction

The mere presence of a hydraulic pump, motor and other components and devices is not sufficient to ensure system functionality. To ensure the system functions, hydraulic agent circulated among its elements.

The transport of hydraulic fluid in an installation is carried out by connecting elements (pipes), which hydrostatic systems are connected with each other or with the installation components by means of a coupling system, which must provide tightness working pressure of the system.

The coupling of the various elements of the structure can be achieved using a hydrostatic pipes, hydraulic plates or blocks by means of modulation.

Modular hydraulic blocks are typified elements, parallelepiped-shaped, aimed at realizing hydraulic circuits in different variants without pipes. They allow surface mounting devices on three sides, the fourth being found holes connecting block the installation.

The connection is usually through pipes and for this reason this surface wears the name of part of connecting the pipes. The other two surfaces, the upper and lower, serve to assembly block on the vertical, in column (with other blocks).

Links between appliances mounted on a block enable typically realization a technical working cycles.

The block shown schematically in Figure 1 performs the cycle: working quickly advance, advance work, rapid withdrawal.

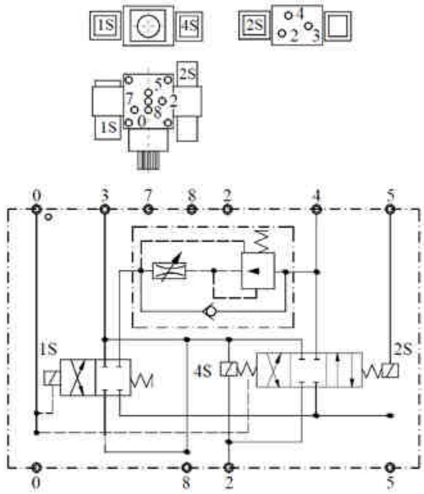

Fig.1. *Diagram of a hydraulic block*

2. General overview of CATIA V5R20 Machining Subsystem

Machining subsystem contains modules that allow the simulation of various types of workpieces on machine tools with numerical control:

- on the lathe (Lathe Machining module);
- on the milling machines in Cartesian coordinates (Prismatic Machining)
- on the milling machines with 3 and 5 axis (Surface Machining, Advanced Machining) etc.

The ultimate goal of a simulation and 'virtual working' is to get the numeric file management workpiece on NC machines.

The subsystem of CATIA Machining provides complete solutions for solving all these steps, meeting users with a large palette of tools to make the design more efficient. Working with modules provided by this subsystem is simple and is done mainly through orders placed through icons on the toolbars and menus associated entities. Regardless of how they work to achieve a processing assisted NCMT any working strategy for NC programming contains all the following items (file type) that are part of CATProcess structure (Figure 2):

- define the geometry of the part to be processed, modeling performed and saved in a file CATPart;
- assembly semiproduct-component achieved in a CATProduct file, the file that contains the links between the defined geometries;
- defining working strategy for processing assisted NCMT, achieved in an NC program file type CATProcess where the program is transferred to the NC a machine tool equipment.

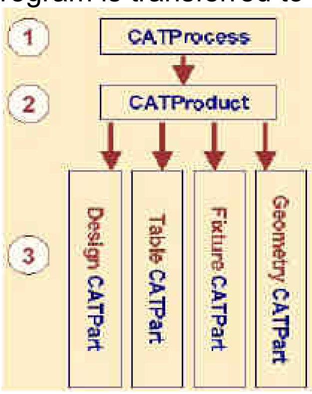

Fig. 2 *The structure of the elements CATProcess*

In principle, effectively generating tool path for machining parts CNC machines supposes a logical succession of steps, such as:

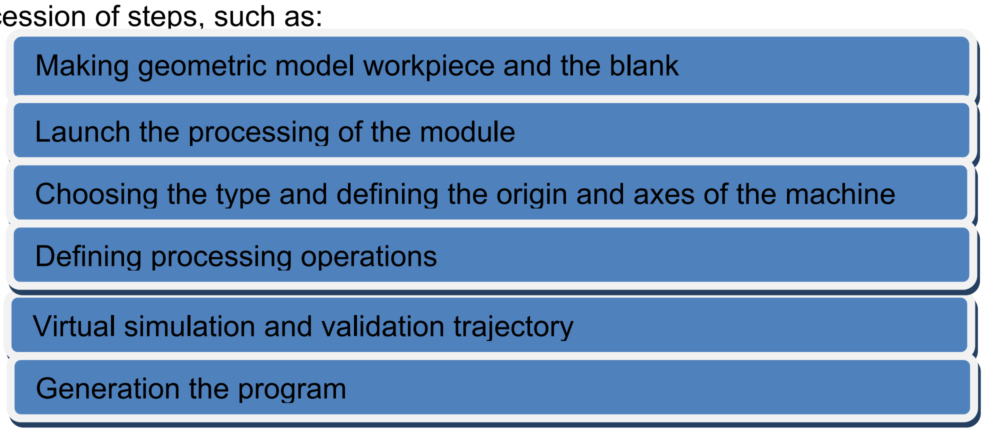

Fig.3. *The logical sequence of steps for processing hydraulic block*

The links between the three elements of the program structure makes any change in a file automatically to changes in other files which makes the programming time processing assisted NCMT have a reduced duration and the accuracy and quality of NC program is very high. All this leads to increased productivity and at relatively low cost.

Another important element in achieving the NC program and strategy is one that concerns the selection and specification of cutting tools that are done processing. Cutting tools can be chosen from a catalog of tools, which can be retrieved from a manufacturer or may be specifically designed and made by technology-programmer.

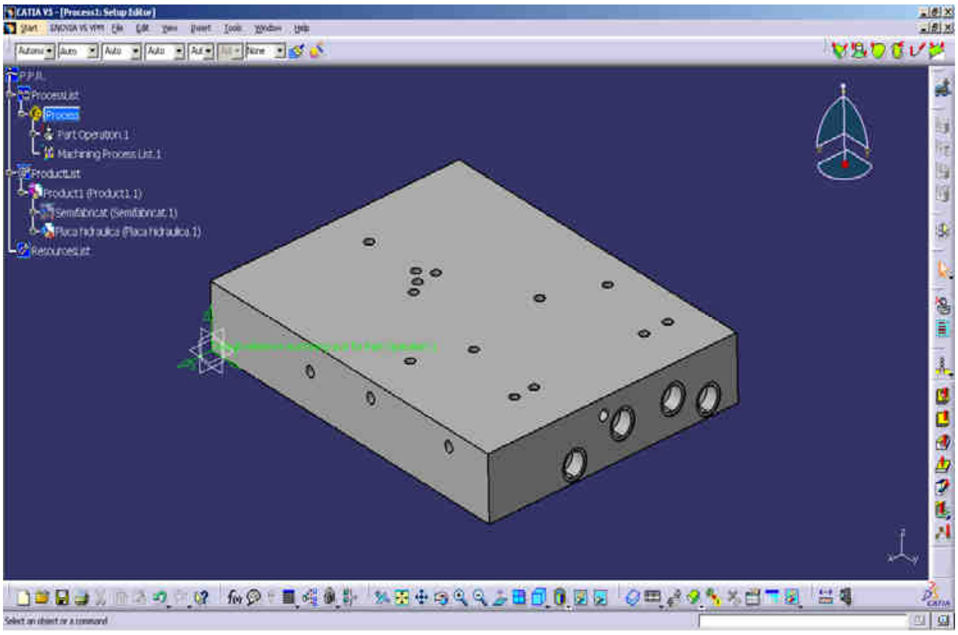

Fig.4. *Interface of the subsystem Machining*

The display of the module (figure 4) provides a modern interface, with a simple structure, showing the following: the main menu graphics window for viewing entities in the process (model, tool, path etc.), toolbars, status bar and the shaft specifications.

The shaft specification provides easy access to process entities, grouped by category, while providing information associated with those entities.

3. Simulation the processing hydraulic block about Machining Prismatic module

Machining the workpiece of the subsystem using the NCMT is done to obtain numerical file-management program and related documentation processing technology that workpiece.

This piece is processed on a milling machine coordinates, so we start the processing Prismatic Machining module (milling in cartesian coordinates). It will go through the following steps:

a) *Determining the dimensions of the hydraulic block and operation phases*

For the workpiece to be processed, the blank is obtained by cutting from sheet metal and has the form shown in Figure 5 blank is installed in the device, and this in turn on the router table using fasteners and specific guidance.

Workpiece machining milling machine in Cartesian coordinates, it is necessary the following sequence of processing next stages.

b) *Choosing machine tools*

It is envisaged that the working parts are needed technological processes of milling, drilling and boring, therefore choose the box **Machine Editor**, a milling machine called a 3-axis coordinate Machine.1 (by pressing).

For this machine is selected, the spindle tab, change the coordinates of a point tool - Home Point (X = 0, Y = 0, Z = 200). In determining these values take into account the length of tools and toolholders used, the thickness of the piece, the size and shape of the workpiece clamping device.

Numerical Control tab you can select customization options simulated machine tool application to be similar to the real owner used to track processing. The **Post Processing** field can choose a specific postprocessor numerical control equipment and the field plates **Post Processing** words vocabulary words recognized by the device.

Maximum feed rate is specified in the Max field machining feedrate and rapid positioning speed is indicated in field **Rapid feedrate**.

c) *work piece and the blank*

Selecting and work piece assembly is done by pressing **Product** or **Part**. It displays a dialog from which you can choose and blank piece ensemble consisting of previously saved. Ensemble obtained is composed of two overlapping parts and the corresponding view, the blank is shown transparent (Figure 5). The set is available in desktop and specifications tree branch product list.

The axis machining **Reference** button opens a dialog box where you can choose an orthogonal system of axes belonging blank. The vertical axis Z is parallel to the spindle axis.

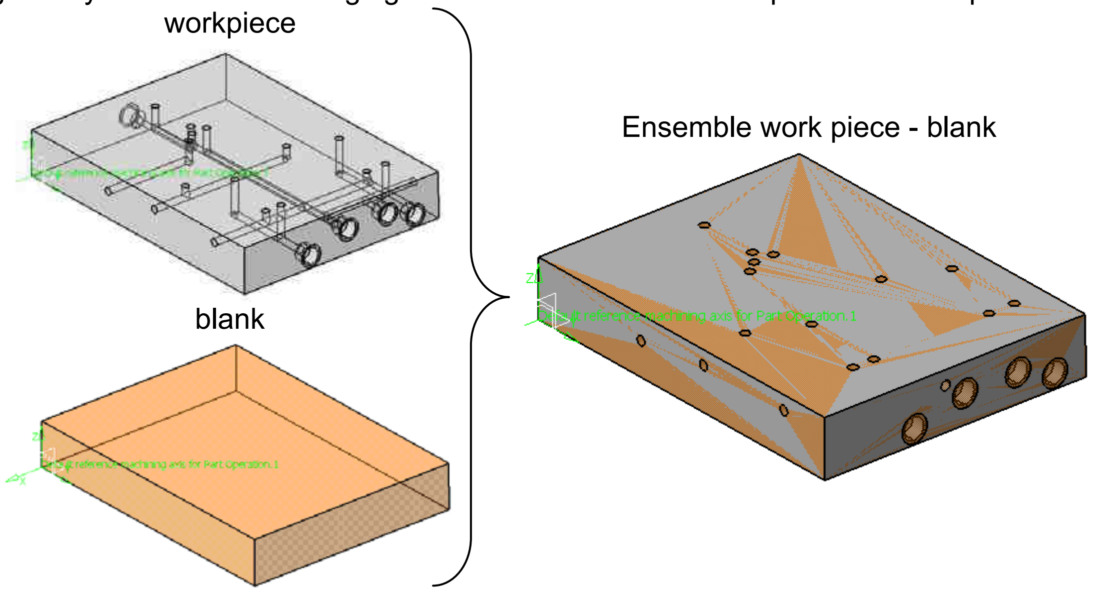

Fig.5. *Ensemble work piece - blank*

d) ***processing design phase***

For processing holes, Prismatic Machining module provides a specific tool, called Drilling, available in Axial Machining Operations toolbar (Figure 6). Window dialog box shown in Figure 7 Renaming drilling operation in D 22.

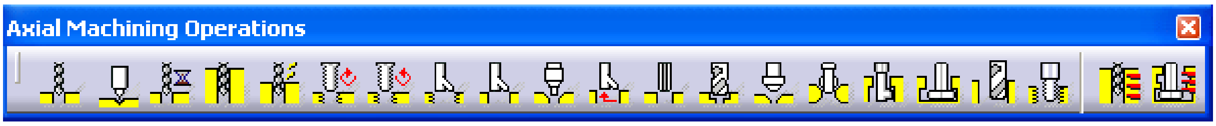

Fig.6. *Axial Machining Operations Toolbar*

ISSN 1454 - 8003
Proceedings of 2014 International Conference of Hydraulics and Pneumatics - HERVEX
November 5 – 7, Calimanesti-Caciulata, Romania

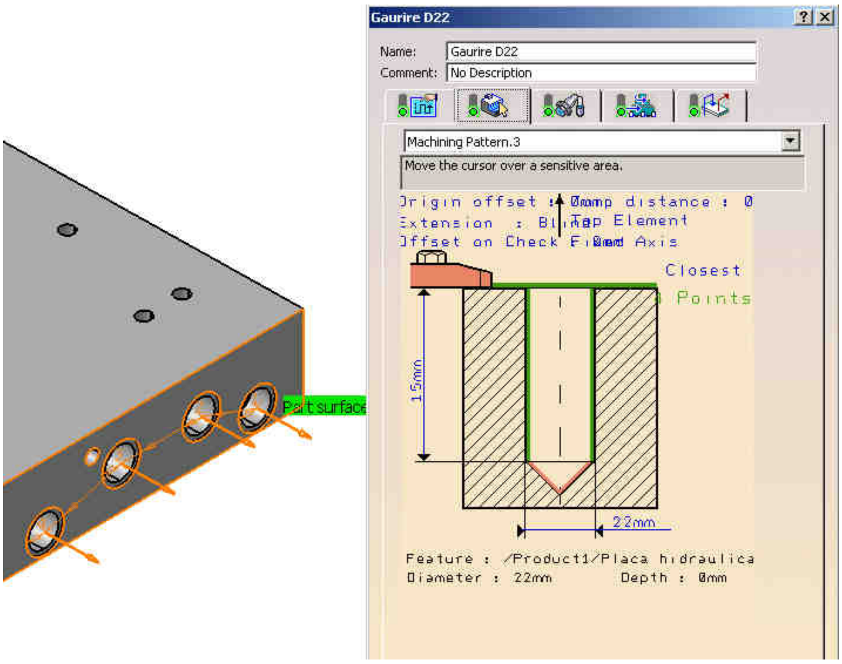

Fig.7. *Driling dialog box, Geometry tab*

In the dialog box tabs are present five (Strategy, Geometry, Tool Selection, Feeds and Speeds and Macro Definition), each having a status indicator symbolized by three LEDs (red, yellow and green). If all the information in a tab complete, its light turns green, meaning the possibility of simulation processing. Red LED informs the fact that more information is required, and the card is necessary to verify that the operation / phase.

Inner cylindrical surface size D28 x 1 mm are obtained by Counter boring used as a rotary cutting tool Lamare diameter 28 mm provided with a guide pin diameter D10. Order this purpose is called **Counter Boring** on additional toolbar **Axial Machining Operations** (fig. 4).

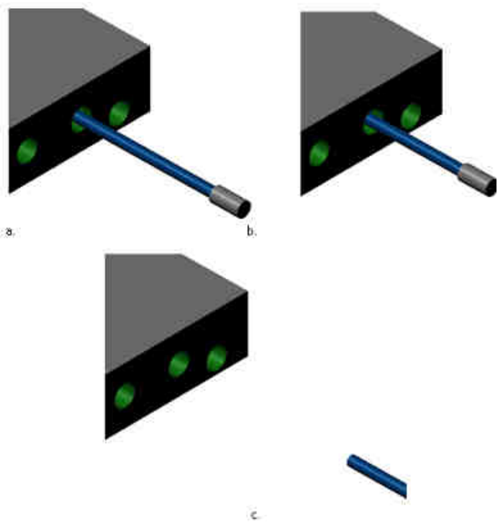

Fig. 8. *Sequences during simulation phase deep drilling D10:*
(a), (b) intermediate stage, (c) final stage

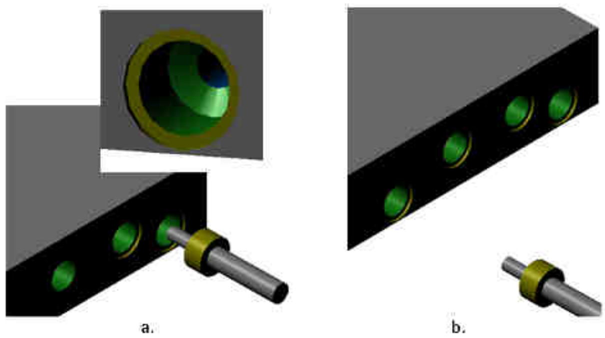

Fig. 9. *Sequences during simulation operation counter boring:*
(a) an intermediate stage, with an enlarged detail of the area obtained, (b) final stage

In terms of size cutting tool, choose a Lamare cutter diameter 28 mm provided with a guide pin diameter D10, form, and size is shown in Figure 5 cutting tool is renamed in the Name field: Rotary Counter Boring D28. To establish machined surfaces switches **Geometry** tab. Select the surface of the workpiece (**Part Surface**), and then the processed surfaces are selected position four edges of the circular surface to limit the depth of hole.

e) ***determining the order of operations***

To specify the processing steps in the proper order, set the path for mechanical design, CATIA provides a tool for ordering operations by priority. By default, the priority values are not user-accessible, but it has the possibility of changing their table after selecting the option Access sequencing rules settings menu **Tools - Options - Machining Program**.

The bar **Manufacturing Optimization Program** Rules Manager tool is used (fig. 10) to access the first list of options (fig. 11).

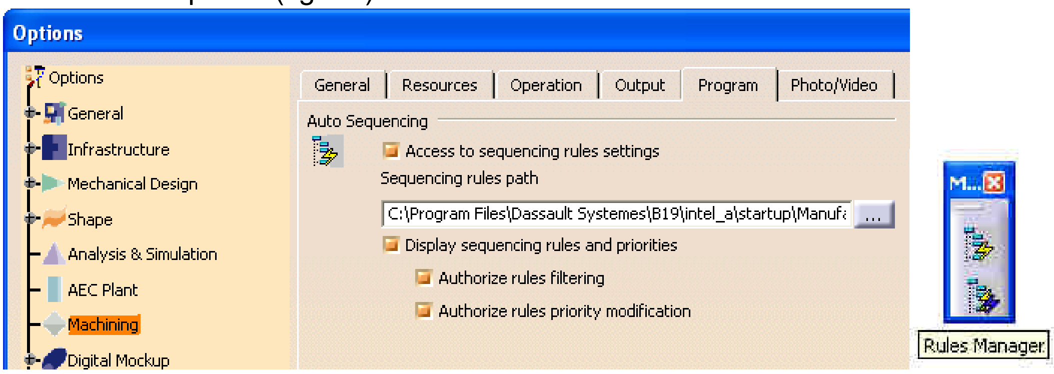

Fig.10. *Checking Access option sequencing rules settings and toolbar Manufacturing Optimization Program*

In this list, uncheck all options except the first two (sort by type of operation and after the cutting tool diameter in the case when two or more identical operations); These options are some rules for sorting operations.

If workpiece was chosen priorities in Figure 12, ie, their order is drilling D22, D10 and deep drilling counter boring D 28x1.

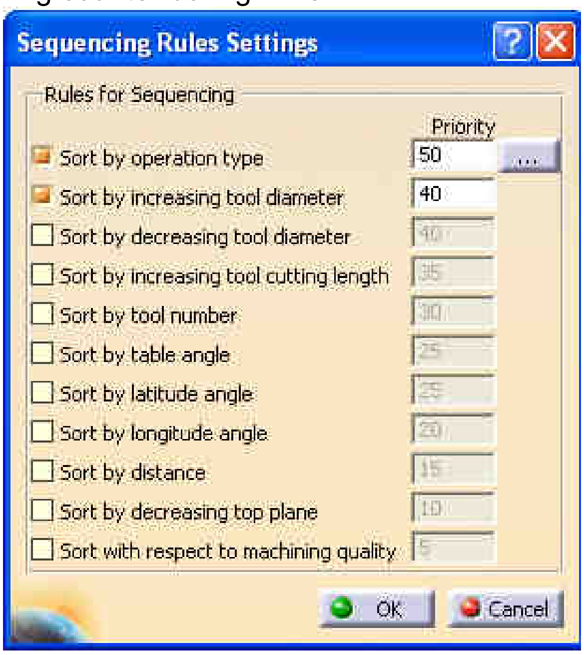

Fig. 11. *Window Sequencing Rules Settings*

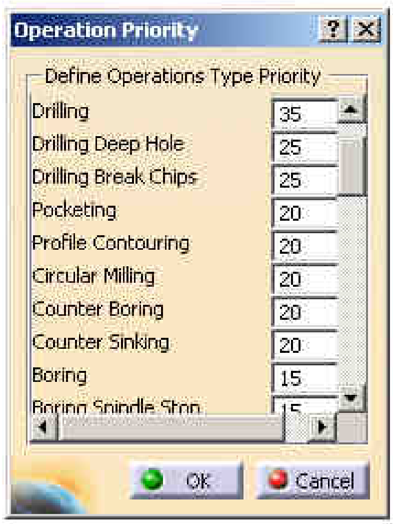

Fig. 12. *Window Operation Priority*

f) processing virtualization

To simulate processing program is running right click on tree branch **Manufacturing Program.1** specifications (fig. 13). From the available list item is chosen for **Manufacturing Program.1** object to open a new options menu then select **Start Video Tool Path Simulation** using. From this list you can select **Generate NC Output Interactively** command to generate machine code simulation result of processing phases

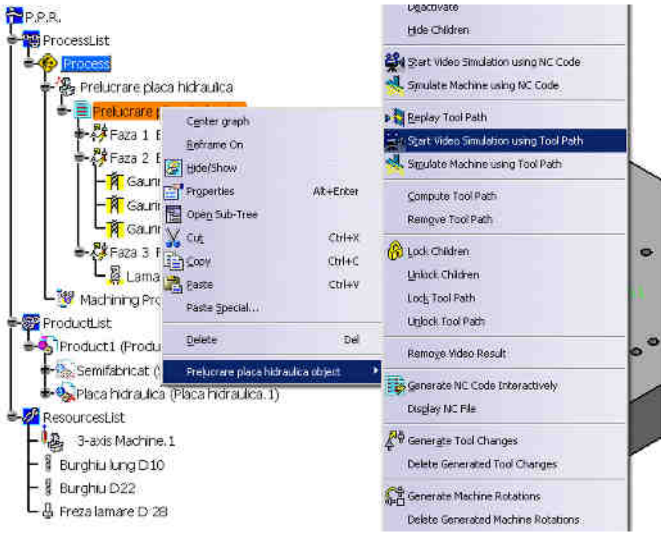

Fig.13. *Launch processing simulation*

After selecting the option Start Video Tool Path Simulation using a dialog box is displayed and the 3D model of the blank (Fig.14).

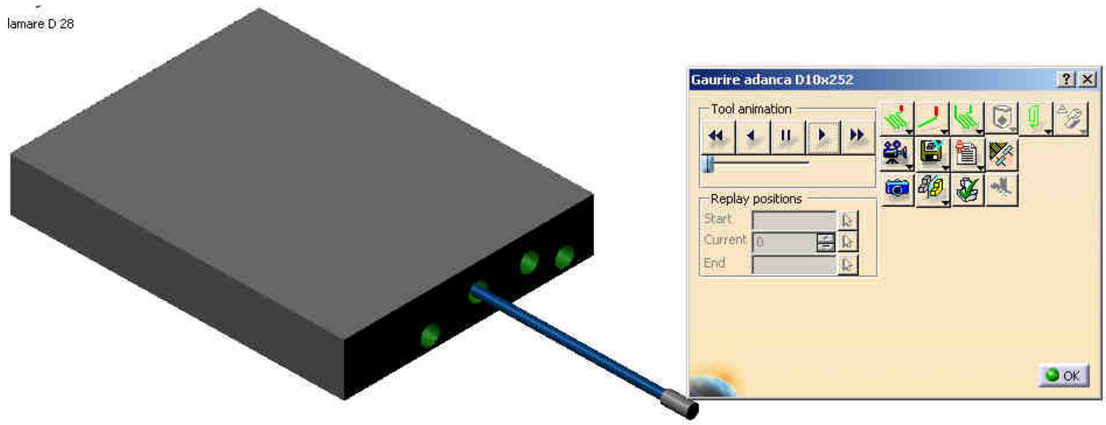

Fig. 14. *Simulation processing*

g) CNC program generation

After simulating the processing piece is necessary to generate CNC program for processing it. the program Generation of is done with the command Generate NC Output Interactively, Waters Manufacturing Program.1 option menu. Order or Generate NC Code in Batch Mode on the toolbar NC Output Management (fig. 15).

Fig. 15. *Toolbar NC Output Management*

ISSN 1454 - 8003
Proceedings of 2014 International Conference of Hydraulics and Pneumatics - HERVEX
November 5 – 7, Calimanesti-Caciulata, Romania

Open the window in Figure 16, the settings and selections are as shown: **CATProcess Input** field contains the saved file after the processing the validation process, the **Selection** field program is selected (**Manufacturing Program.1**) NC Data Type list of options is choose the type of **APT** code.

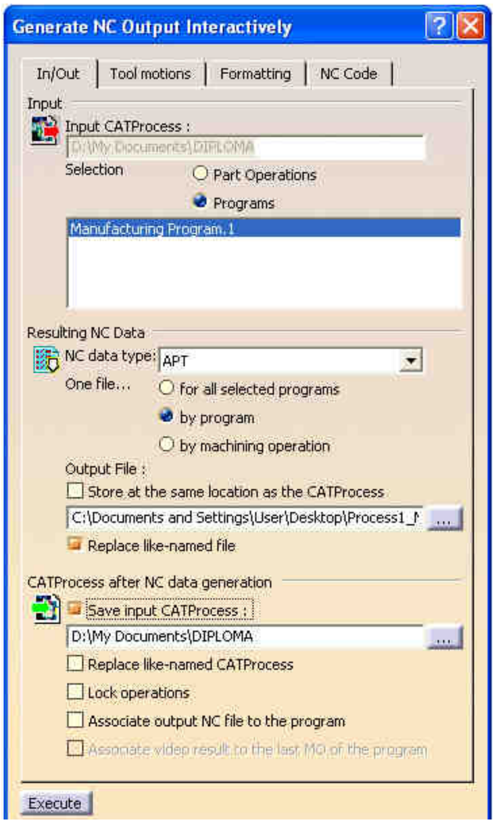

Fig.16. *Window Generate NC Output Interactively*

Below the **Output File** field is set path where files will be saved resulting from the generation program. By pressing **Execute**, CATIA interpret and compile all the options and parameters defined above.

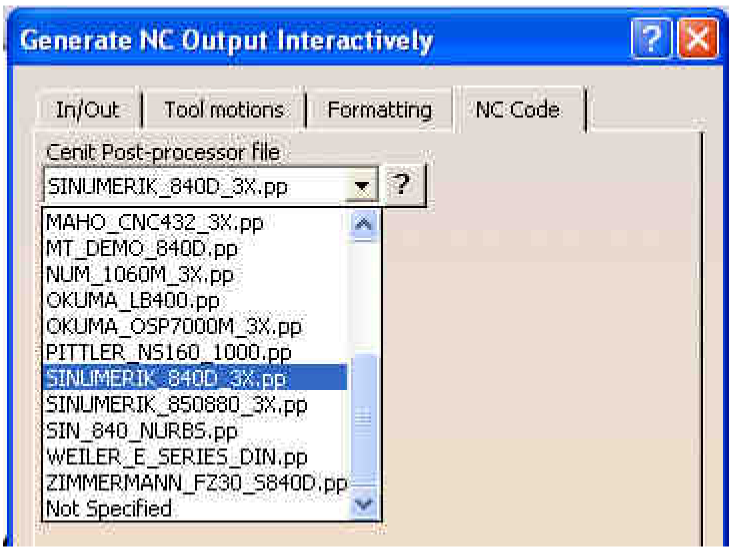

Fig.17. *The choice of numerical control equipment*

If the field is selected **NC Data Type**, then you need to choose the **NC Code** tab (fig. 17) postprocessor of machine tools. If you choose a 3-axis milling machine, fitted with **Sinumerik 840D**, then the **Execute** button in the tab **In/Out** will generate NC code type.

4. Conclusions

Subsystem of CATIA **Machining** provides complete solutions for solving all these steps, meeting users with a wide range of tools to make the design more efficient. Working with modules provided by this subsystem is simple and is done mainly through orders placed through icons on the toolbars and menus associated entities.

The links between elements of the program structure make any changes in a file automatically to changes in other files which makes the programming time processing assisted NCMT have a shortened NC precision and quality of the program is very high. All this leads to increased productivity and relatively low cost.

REFERENCES

[1] Botez, E., s.a. – Maşini-unelte şi agregate, Ed. Tehnică, Bucureşti, 1977, vol. I, II
[2] Boangiu, Gh., s.a. – Maşini-unelte şi agregate, Ed. Didactică şi Pedagogică, Bucureşti, 1985
[3] N. Vasiliu, ş.a. , Acţionări hidraulice şi pneumatice, Vol.I, Editura Tehnică, Bucureşti, 2005
[4] Cioată, V. G. – Proiectare asistată de calculator cu Catia V5, Ed. Mirton, Timişoara, 2009
[5] SÁROSI J.: Accurate Positioning of Pneumatic Artificial Muscle at Different Temperatures Using LabVIEW Based Sliding Mode Controller, 9th IEEE International Symposium on Applied Computational Intelligence and Informatics (SACI 2014), Timisoara, Romania, 15-17 May, 2014, pp. 85-89
[6]
[7] ***, CATIA V5R14, V5R16, V5R19, User Guide - documentaţie de firmă, Dassault Systemes
[8] ***, www.catia.com
[9] Ghionea, I. G., Proiectare asistată în CATIA V5. Elemente teoretice şi aplicaţii, Ed. Bren, Bucureşti, 2007
[10] Sham Tickoo, Vicky Raina, CATIA V5R17 for Designers, CADCIM Technologies, USA, 2007
[11] Ivan, N. V., s.a. – Sisteme CAD/CAPP/CAM. Teorie şi aplicaţii, Ed. Tehnică, 2004
[12] Lee, K., Principles of CAD/CAM/CAE Systems. Addison Wesley Longman, Inc., USA, 1999

ISSN 1454 - 8003
Proceedings of 2014 International Conference of Hydraulics and Pneumatics - HERVEX
November 5 – 7, Calimanesti-Caciulata, Romania

ON USING PERSONAL COMPUTERS TO CONTROL MECHATRONIC SYSTEMS

Mihai AVRAM[1], Constantin BUCSAN[1], Alina Rodica SPANU[1]

"Politehnica" University of Bucharest, 313 Spl. Independentei, Bucharest, mavram02@yahoo.com

Abstract: *The mechatronic systems used for research purposes, in laboratory conditions, in order to test experimental models, are usually very complex and they can be controlled with a personal computer. The paper deals with establishing the structure of the control block when a personal computer is used to control a mechatronic system. There are taken into account situations when a data acquisition board is used and also when specialized input/output modules are used. Two examples of mechatronic systems controlled using personal computers are presented along with the advantages and disadvantages of such systems.*

Keywords: *mechatronic system, personal computer, control.*

1. Introduction

The central element of a mechatronic system is the command block that controls and optimizes the system. The command block is usually based on a programmable automaton, a microcontroller, a personal computer or an industrial computer, according to the complexity of the system and its purpose [1].

There is an important difference between the industrial systems, working in tough conditions, and the research systems, working in research laboratories.

The complex industrial systems use industrial computers, which combine the flexibility and universality of a personal computer with the error tolerance and safety of a programmable automaton. Complex processes are controlled with both industrial computers and programmable automatons.

Many systems have the command block built around a microcontroller, this being an efficient solution for a mechatronic system.

2. Command blocks using personal computers

Very complex systems, used mostly in research activities, in laboratory conditions, for testing experimental models, are controlled using a personal computer, accomplishing various tasks: process control, signal analysis and processing, control of serial and parallel ports, results displaying, graphic presentations etc.

If the controlled process implies a hostile environment, the data processing must be carried out at a safe distance from the controlled system. Another problem is the great number of transducers (for position, force, pressure, flow rate, temperature etc. measurement) distributed through the system, from which data must be gathered, and also the digital and/or analog commands that must be transmitted to the actuators of the system (classic electro-magnets, proportional electro-magnets, step-by-step motors, c.c. servo-motors, piezoelectric actuators etc.). This means a large number of connections.

When the command system is built around a personal computer, two options can be made:

- a personal computer, a data acquisition board and adequate software;
- a personal computer, specialized input/output modules and adequate software.

The first variant is the well known computer aided data acquisition. The acquisition board is usually inserted into a slot on the PC mother board, in order to be directly connected to the data bus and to be able to perform real time processing. The connections with the transducers and the actuators within the system are made using an external connecting board. There is also the variant of an external data acquisition module, usually connect through the USB port.

The acquisition boards usually contain signal conditioning circuits, multiplexers, A/D and D/A converters etc. The resolution of the converters must be in accordance with the measuring demands.

Using specialized input/output modules is an efficient solution for the command block, even when the controlled system works in a hostile environment. The input/output modules contain analog and digital I/O circuits and can be configured according to the needs of the controlled mechatronic system. The I/O modules can work in industrial conditions (large temperature variations: -40^0C to 70^0C, vibrations and shocks, oil vapors, dust, impurities etc.) so they are placed near the controlled system and can be connected to a PC using Ethernet, RS232, RS485, Foundation Fieldbus protocols. The producers guarantee very good electric isolation between inputs and outputs and also between the channels.

The transducers and the actuators within the controlled system are directly connected to the I/O modules, so the mechatronic system is simplified, the costs are reduced, the installation time is shorter and the sensibility to disturbances is lower.

The configuration of a FieldPoint type I/O system is easy to perform using *FieldPoint Explorer* software, which allows the configuration of the programmable settings of the system: the input range (for an analog input module), the sampling rate, the output range (for an analog output module). The software allows defining I/O objects (one or more I/O channels) and uses an interactive interface for reading and writing the characteristic values of these objects, in order to check the correct installation and configuration of the system.

3. Examples of mechatronic systems controlled using a personal computer

Figure 1 shows a pneumatic positioning system controlled by a personal computer by means of a PCI-6025 data acquisition board (from National Instruments) plugged on the motherboard of the computer [2]. The transducers and the actuators within the controlled system are connected to connection board P_C.

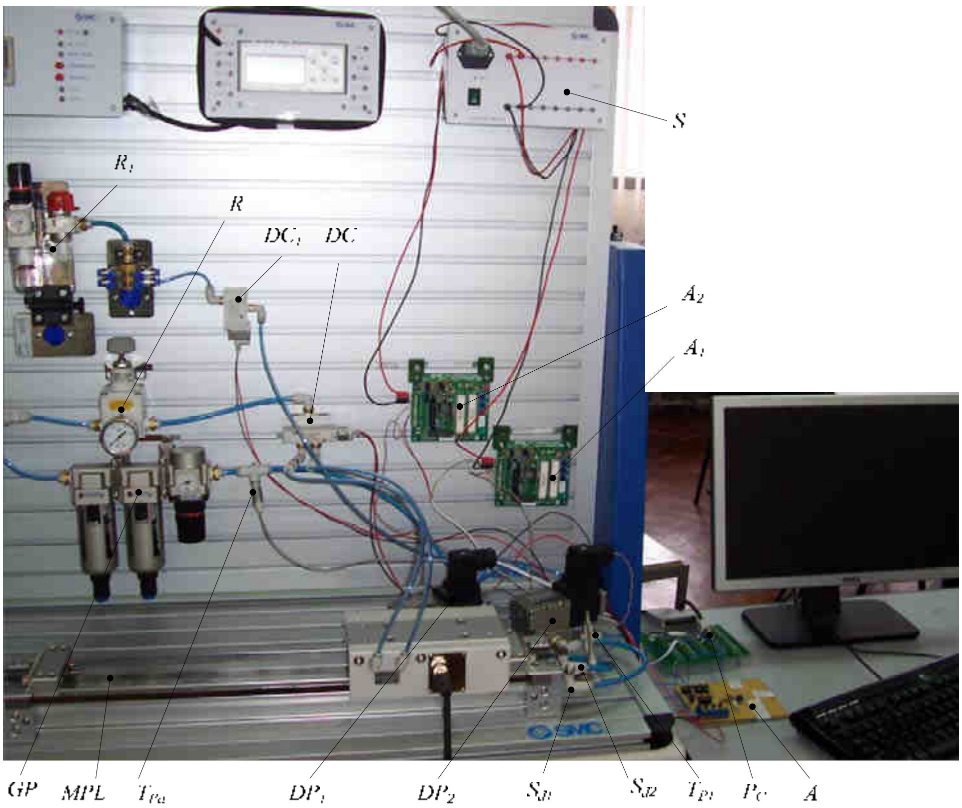

Figure 1: Mechatronic system controlled by a PC and a data acquisition board

The controlled system has the following configuration:

- a pneumatic linear motor *MPL*, with integrated position transducer and braking system;
- two 3/2 proportional distributors DP_1 and DP_2;
- a 5/2 classic distributor *DC,* with preferential position, electrically controlled,
- two one-way valves, relievable, S_{d1} and S_{d2}, pneumatically controlled, one for each circuit of the motor;
- a 3/2 classic distributor DC_1, with preferential position, electrically controlled, used to command the valves S_{d1} and S_{d2};
- two pressure transducers T_{Pa} and T_{P1};
- two pressure regulators *R* and R_1;
- two electronic amplifiers A_1 and A_2 and an adapter A;
- a 24V power supply *S*.

The system assures the positioning of the actuated load in any point of the working stroke with an imposed accuracy. The working program [3] was developed using LabView programming environment and a series of necessary algorithms [4].

Figure 2 shows a pneumatic positioning system controlled by FieldPoint modules. The system has the following characteristics:

- the pneumatic liniar motor has a special structure, beeng rodless;
- two particular proportional drossels [5] are used to control the flow rate and so to control the moving speeds.

The controlled system has the following configuration:

- a pneumatic linear motor *MPL*;
- two proportional pnneumatic drossels *DPP_1* and *DPP_2*, one for each circuit;
- a pozition transducer *Tp*;
- two one-way valves, relievable, pneumatically controlled, *Sd_1* and *Sd_2*;
- two one-way valves *Ss_1* and *Ss_2*;
- two classic pneumatic distributors, *DC3/2* şi *DC5/3*;
- a high voltage amplifier, with adjustable voltage in the range *0...1000 V*, used to feed the piezoelectric actuators – *HVPZT*;
- four FieldPoint modules – *FP_I/O*;
- a pessure regulator *RP*;
- a PC which communicates with the *I/O* modules using the *RS232* serial port and running LabView programming environment.

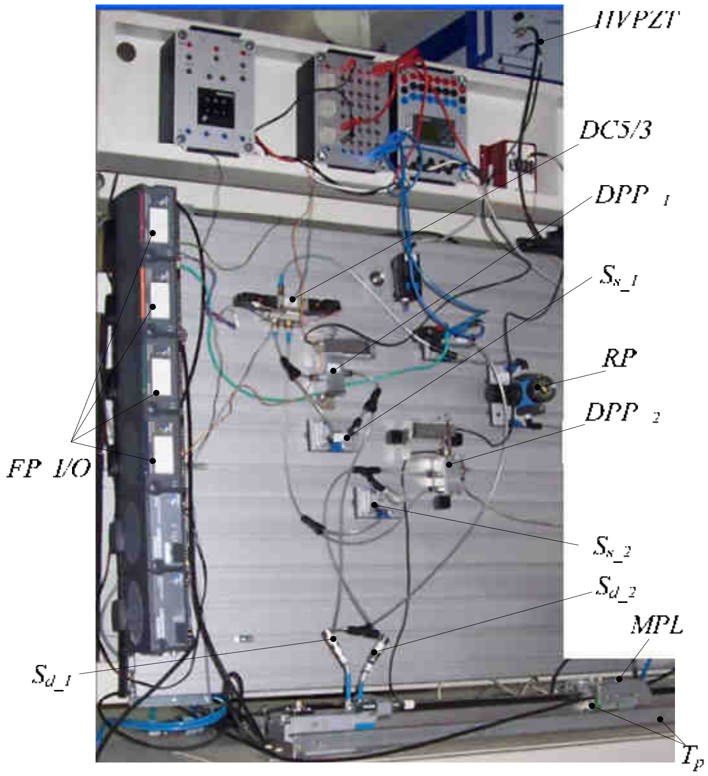

Figure 2: Mechatronic system controlled by a PC and I/O modules

A liniar measuring system type *LIMES L1* from Kübler was used for position controlling. This system is connected to the *0* axis of the module *FP-QUAD-510*.

Two voltages u_{PIEZO_1} and u_{PIEZO_2} in the range *0...10V* are generated in order to control the proportional pneumatic drossels *DPP_1* and *DPP_2*. These voltages are the input signals of the *HVPZT* amplifier, which feeds the piezoelectric actuators type P-287, integrated in the structure of the proportional drossels. The module *FP-AO-210* is used for this task.

The designed and built system is, considering its hardware and software structure, a complex experimenting and testing system, with all the tasks controlled by the computer. The hardware structure consists of high performance equipment and the software structure consists of special developed programming environments for data acquisition and control (LabVIEW and FieldPoint).

One of the advantages of the system is that the experimental results can be directly visualized on the PC monitor while measuring, this being very important for experimental research. The results can also be stored in different types of files, allowing further data processing and printing of testing reports on the tested pneutronic system, independent of human operator presence.

4. Conclusions

The mechatronic systems used for research purposes, in laboratory conditions, in order to test experimental models, are usually very complex and they can be controlled with a personal computer.

A data acquisition board can be used to gather data from the transducers and to control the system. This way, a cheaper and more flexible system results.

Using specialized I/O modules, a higher performance but more expensive system is obtained.

REFERENCES

[1] Avram M., Bucsan C., Sisteme de actionare pneumatice inteligente, Editura Politehnica PRESS, Bucuresti, 2014;
[2] Avram M., Bucşan C., Pneutronic Positioning Unit - Part 1: Design and Working Principle, Romanian Review of Precision Mechanics, Optics and Mecatronics 2009 (19), No.36; pag.7…10;
[3] Avram M., Constantin V., Constantin B., Pneutornic Positioning Unit, Part 2: The control algorithms, Romanian Review of Precision Mechanics, Optics and Mecatronics, 2010 (20), No.37, pag.39…42;
[4] Avram M., Constantin V., Constantin B., Pneutornic Positioning Unit, Part 3: The Application Software, Romanian Review of Precision Mechanics, Optics and Mecatronics, 2010 (20), No.38, pag.105…106;
[5] Avram, M. Bucşan, C. Duminica, D. Bogatu, L. & Spânu, A.R, Pneumatic Proportional Valve with Piezoelectric Actuator, Vol. 10, ISSN 1726-9687, ISBN 978-3-901509-84-1, Editor: B. Katalinic, Publisher DAAAM International Vienna, Vienna, 2011.

ISSN 1454 - 8003
Proceedings of 2014 International Conference of Hydraulics and Pneumatics - HERVEX
November 5 – 7, Calimanesti-Caciulata, Romania

MAINTENANCE, REPAIR AND PERFORMANCE TESTING OF COMPONENTS IN INSTALLATIONS WITH HYDRAULIC DRIVE

Ph.D. Eng. Cătălin DUMITRESCU [1], Ph.D. Eng. Corneliu CRISTESCU[1], Dipl.Eng. Radu SAUCIUC[1], Dipl.Eng. Liliana DUMITRESCU[1]

[1]Hydraulics and Pneumatics Research Institute INOE 2000-IHP, Bucharest, ROMANIA,

e-mail: dumitrescu.ihp@fluidas.ro, cristescu.ihp@fluidas.ro, sauciuc.ihp@fluidas.ro, lilianad.ihp@fluidas.ro

Abstract: *Maintenance of hydraulic equipment has positive implications on the lifespan of the equipment and systems they contain. In some situations, although it made an adequate maintenance, there are necessaire to perform repairing (planned or unplanned) of components and after that it is necessary to know how close the performances of the equipment repaired are, compare with those of the new one. Article makes some considerations on the main causes of occurrence of faults in hydraulic installations and presents an example of a complex device (hydraulic pump) that has been repaired and tested.*

Keywords*: maintenance, fluid power, hydraulics, hydraulic equipments, testing*

1. Introduction

Proper maintenance, although it is seen as an activity that is not always necessary, helps to avoid future costs related to emergency repairs (unscheduled), reduced production and even the possibility of accidents. Besides these general considerations, in the field of hydraulics can act specifically considering the particularities of the hydraulic apparatus and systems [1].

Leading cause of faults in hydraulics (70 to 80%, according different sources) is improper quality of the working fluid. The latter must pay attention both during use in the plant, as before, by maintaining it in optimal conditions.

The fluid filtering fineness in a hydraulic equipment is imposed by the component which requires the cleanest oil (and best filtering class); for example, a hydraulic installation which use servo-valves or proportional directional valves needs an oil with ISO 15/13/10 contamination class [2]. At the running of the hydraulic equipment it is required to detect the flaws from their very initial stage, before causing malfunctions to the equipment, sometimes this meaning even during the maintenance, revision and repair operations.

Generally, in maintenance works, an important role is played by the check-up of the oil temperature and level of the contents of impurities.. The overheating and high level of noise, generated by certain component parts, is obvious signs that it is necessary to make a revision or even some general repair. The revision and repair activities sometimes lead to important interventions upon the hydraulic components, implying the replacement of certain parts or elements from the general structure, which can lead to a change in the working performance of these components. The general objective of the revision and repair is to prevent malfunction and prolong the lifespan of the hydraulic equipment [3]. The maintenance of the hydraulic installations represents an assembly of activities which aim to maintain in good operational conditions the equipment by means of the following works: planned repairs; maintenance; accidental repairs (not planned); monitoring the behaviour during use of the equipment; the supply with spare parts and materials required for repairs and maintenance; the elaboration of the technical documentation for repairs and maintenance and the modernization of the equipment [4, 5].

2. Troubleshooting and repairing of the hydraulic installations

2.1. The diagnostic of the flaws at hydraulic installations

This is conditioned by the assimilation of the general knowledge regarding the hydraulic drives as well as of the knowledge in detail of the operational scheme of the installation. The diagnose starts from the effect found, generated by one or more factors. The diagnose process is a complex one, which takes into account associated effects and in correlation with the effect found, on the basis of some logical hypothesis, leads to the initial cause. Hence the flaw is spotted, for determining its cause, can be performed measurements for noise, pressure and flows. For this, starting from the designing stage of the installation, it is required to be provided special couplings for manometers and flow meters. The flaw tracking is made by successive checkings of the hydraulic parts analyzed. It is not possible to use an order of checking, for all cases. In the first stage, the checkups are made only by means of manometers which provide qualitative information regarding the found flaw. For obtaining quantitative information, it is necessary to perform flow measurements as well, requiring a more complex test and diagnose apparatus, developed by well known companies like PARKER [6] and HYDAC [7] - Fig.1 and 2.

Figure 1: Testing and diagnosting Sensocontrol from PARKER

Figure 2: HMG 510 Portable Data Recorder from HYDAC

The analysis of the flaws is alleviated, if the return lines to the tank and drainage are made of transparent plastic tubing. In this way, may be noticed the leaks and the fluid return, and it is possible to evaluate accurately the working correctness of the delivery elements and the losses by drainage. It is also useful to collect general information about the operational mode, maintenance volume, previous flaws and repairs.

2.2. The characteristic flaws of the hydraulic installations

Generally, at a hydraulic installation are distinguished two types of flaws:

- Flaws found at the periodical checkups and which at the moment when found, did not resulted to have been damaged any component;
- Flaws found as a result of the deterioration of a component system.

From the first category of flaws, characteristic to the hydraulic power installations, the most common are the following: Improper external seal; Overheating of the operational fluid or certain components; Abnormal noise appeared at a certain component or at the whole installation.

2.2.1 The improper external or internal seals

The faulty external seals on the pressure circuits are easy to be found, whenever noticing hydraulic fluid leaks. For example, the improper seal of the circuit of admission-aspiration of the pump, in the case of depressurization, cannot be found directly, but by its effects, the uneven mode of operation of the pump, pump s overheating, foaming hydraulic fluid and noise. This flaw is found by measuring the depression at the pump entry. Its decrease from the value set during the normal work, indicate the aspiration of fake air. Generally, the lack of a proper external and internal seal may come from flaws of the sealing systems of the hydraulic components and couplings from the installation.

2.2.2. The overheating of the hydraulic fluid

This flaw is detected by means of a thermometer placed usually on the oil reservoir, or by hand touch for temperatures up to 500 C. When this value is exceeded it is signaled that something had happened in the proper operation and it is required an examination of the entire installation. The excessive heating of the hydraulic fluid may be generated by the incorrect supply of the pump, by the pump s wear, the debiting for a long time through a drossel or stroke, a malfunction of the cooling installation. Another source of heating may be pump s wear. This can be caused by a normal wear phenomenon after a long time of work or it is caused by improper use of the pump with fluid contaminated with impurities, or in an inadequate mode of admission aspiration which produced the premature wear of the pump.

2.2.3. The increase of the noise level

Another frequently met flaw is the increase of noise over the admitted limit. The potential sources are: the incorrect supply of the pump, vibrations generated by the defected couplings of the bodies in motion, the noises produced by the pressure valves or vibrations of the pressure pipes which have no adequate fixation, in relation with wavelength of the system oscillations.

2.3. Troubleshooting

The correct diagnose of the flaws and causes as well as the good quality remediation, provide the proper work of the installation in the initial conditions of performance, preventing the reoccurrence of the same flaw or of a derived one and in the case of replacing an aggregate, it confers reliability equal with that of the replaced one. As general rule regarding the interventions in the hydraulic installations, is that of following the requirements regarding the purity of the operational fluid. If the rules are not properly observed, this may very probably lead to the malfunction of the hydraulic installation. After occurring a major flaw it is required the check-up of the content of impurities from the hydraulic fluid. If it is exceeded the admitted limit of impurities, the installation needs washing and cleaning thoroughly. For determining the impurity class of the hydraulic fluid used at the hydraulic installations, prestigious firms developed the necessary apparatus, which can detect fast the content of impurities and to which class or category it belongs in an ISO or NAS class. For example, PARKER, [8], developed a system of monitoring and analyze of the impurities, LCM 20 Contamination Monitor, shown in Fig. 3, which can analyze separately a sample of fluid, or may be connected on line in derivation or directly in the hydraulic installation. At the end of the testing, this apparatus generates a document with the number of particles found for each category of sizes and to which class it belongs.

Figure 3: LCM 20 Contamination Monitor from PARKER

In the case of repairing some hydraulic pumps and motors, the repair is, generally, made by replacing the component parts and subassemblies with some original ones and more rarely by manufacturing and metallizations and rectifications of the parts. After repairing the hydraulic pumps and motors, these must be checked and tested on an adequate stand, on which to be possible to check their technical performances as well as the lack of the abnormal noise and overheating. The stand must also offer conditions for the adjustment of the control devices with which are these equipped (pressure, flow, power compensators etc.) for adjusting them in accordance with the needs.

3. The repairing and testing of a pump with axial pistons

Within a complex technological installation, the drive of some mechanical systems is hydraulicaly performed, having as main source of fluid under pressure pumps with axial pistons, with pressure compensator. The technological complex is older, but lately it has been modernized, the main components replaced - the old hydrostatic pumps with new axial pistons pumps PV 092 produced by PARKER. During the actual stage of revision, for shortening its time, a pump with axial pistons has been replaced with a new one, identical with the former, the old pump being subsequently repaired. After about a month of work, the new pump started to produce overheat and the noise during work became abnormal, fact which determined the responsible factors to disassemble it from the installation and replace the new pump with the old one which works acceptably. The client complained about the impossibility of adjusting the pressure level of the regulator-compensator and the displacement geometrical volume of the pump. The new pump was brought at INOE 2000-IHP, which undertook the action of diagnose, troubleshooting and testing. Because at the date when the pump was disassembled, the color of the fluid from the tank of the installation was dark, were taken samples of hydraulic oil and made tests for finding the impurities contained in the fluid, by means of a PARKER apparatus. The result was surprising, cause the quantity and size of the impurities was from class 12 NAS 1638, equivalent with 22/21/18 to ISO 4406, which was far over the accepted limit of about 7 NAS Class. The oil it, also, contained water. According to the producer’s catalogue (PARKER), the filtering requirements for the hydraulic oil is in general of class 19/13 to ISO 4406, equivalent with class 8 NAS 1368 and for component parts with higher lifespan it is of 16/13 to ISO 4046, equivalent with class 5 NAS 1638. Taking into account these facts, it was very obvious that the conditions of work of the new pump were not appropriate, even dangerous for a new pump with minimum adjustments and little use. Therefore, was recommended, to the beneficiary company, to replace completely the hydraulic oil from tank.

3.1. The diagnose of the hydrostatic pump

The hydrostatic pump with axial pistons, which was investigated, is a pump with pressure compensator type PV 092, (fig. 4), manufactured by PARKER [6]. The main technical data of the pump are: pump code PV 092; type - with axial pistons; displacement 92 cm3/rot; max pressure 350 bar; nominal pressure 280 bar; max rev. 3000 rot/ min.

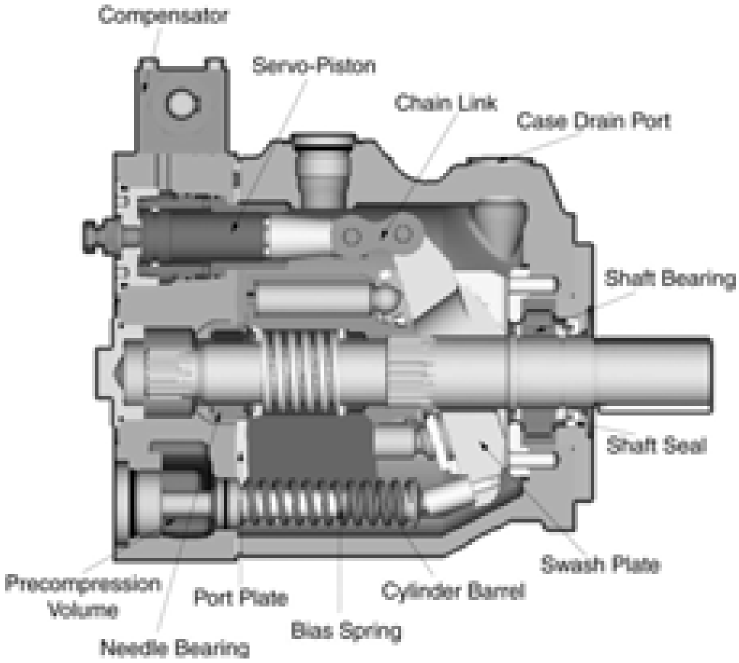

Figure 4: The hydrostatic pump with axial pistons

After dissembling and examining, were found the following: the component parts are not much damaged; the port plate is in a good condition; the pressure plate presents scratches of 5-10 μm, insignificant for work; the assembly pistons plate with bronze coating is good, but the crimping of a piston is deteriorated, cause a semicircular piece broke. Very probably the break produced cause of a material flaw (blows, inclusions) or the existence of certain internal tensions. From the way, it looks the break occurred during disassembly cause neither the detached parts nor the adjacent parts have scratches or traces. The last motion from the crimping of the pistons are a bit bigger than normal, being possible to produce in certain conditions some noise. On the pump casing were noticed rust stains, probably cause there is water in the oil, but the consequences were not very serious. At a careful examination, on the shaft cannot be seen any blue areas which to put into evidence the occurrence of a high temperature and an overheating of the pump. The bearing with cylindrical balls type NU NJ 2209 E YVL (di = 45 mm; De = 85 mm; l = 23 mm) has an axial loose of 0.8 mm, quasi-normal, which could generate some beats if the pump's coupling cannot provide the coaxial connection between motor and pump. The interior ring of the bearing has an axial loose between it and the shut safety ring Seeger of 0.3 mm, which can generate some sort of banging during work. The pressure compensator was in good condition. It was found that it was attempted to regulate pressure at a different level, but the method for performing that action was not properly known by the operator, thus being unable to perform it.

3.2. The repair of the detected flaws

After diagnosing the pump, for repairing the flaws, were proposed and performed the following operations for improving the pump condition:
1. Purchase a complete kit of axial pistons from the manufacturer and assemble it in the pump body;
2. Adjust decrease the axial loose of the interior ring of the ball bearing by inserting a flat ring which ensures a second support for the interior ring thicker with 0,2...0,3 mm;
3. If it is necessary, the ball bearing will be replaced with another with a lower loose between the rings;
4. The testing of the pump on the stand, watching carefully the eventual occurrence of over noise and overheating during work, as well as the possibilities of adjustment of the pressure

compensator depending on the desired pressure value and the possibility of performing an adjustment variation of the pump's displacement, depending on the pre-set flow.
After drawing the conclusions at testing, it is decided if the pump may be or not recommended to be assembled in the hydraulic installation.

3.3. Testing on stand of pump's workability and adjustability

After repairing it, the pump with axial pistons and pressure compensator was mounted on the stand for testing the pumps with variable flow, stand from the Lab for testing hydraulic apparatus for high pressure from IHP.

3.3.1 The pump's testing objectives and scheme

The testing of the pump had focused on the following objectives:
- The possibility of adjusting the pump's flow by the variation of the displacement /geometrical volume;
- The possibility of adjusting pressure at the pressure compensator/regulator;
- Watch the way the pump works, with all normal values.

For testing the workability and adjustability, the pump was mounted on a stand, according to the scheme of fig. 5.

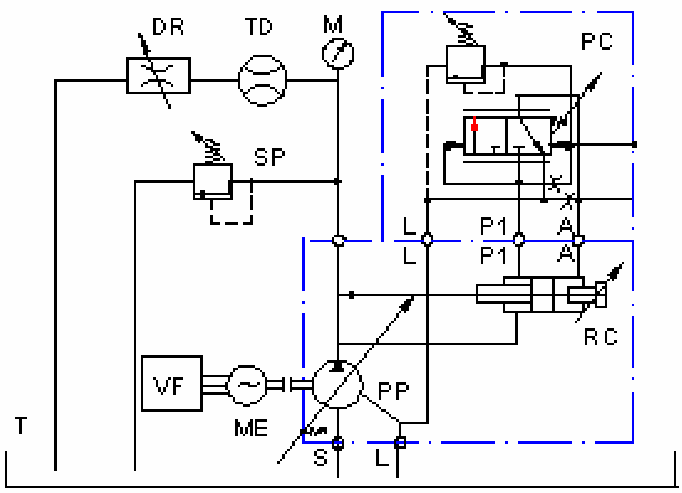

Figure 5: Scheme of testing

As it may be seen in Fig. 5, the pump PP, subjected to tests, was coupled, by means of an elastic coupling, to the ax of the electric asynchrony motor, which is supplied by network through a frequency inverter VF, which allows the variation of the electric motor revolution. The pump is presented graphically in a symbolic form, in detail, in Fig. 5, where are put into evidence the scheme of the displacement adjustment device RC and the scheme of the pressure compensator PC. The testing of the pump consisted in performing different flow, adjustments by means of the special device provided for modifying the pump s displacement RC, as well as other various pressure adjustments at the pressure compensator PC Were tested the adjustment of the revolution by adjusting the electric motor's supply frequency.

3.3.2 The presentation of the testing stand

The stand for testing the pumps with variable displacement, from INOE 2000 IHP, shown in Fig. 6, materializes the testing scheme from Fig. 5.

a) overall view of the stand

b) pump on the stand

c) Flow transducer, manometer, throttle and pressure limitator

d) data acquisition system for the fluid flow

Figure 6: Stand views

3.3.3 The operation mode for testing the pump

The operation performed on the testing stand consisted in the following:
After starting the pump's motor, Fig. 6b, with the throttle DR completely open for each max. pressure value set adjusted at the compensator PC, the throttle was gradually close, until the compensator passed the pump on null, flow = 0. For each pressure value desired and read on the manometer M, Fig. 6c, included in the range of pressure values, from 0 to the max set value, was noted the corresponding flow value, detected by the flow transducer TD and indicated by the electronic measurement system from Fig. 6d. The results were listed in the next tables.

3.3.4 The adjustment of the pump flow

The adjustment of the pump flow was made by readjusting the displacement of the pump, from the screw, especially provided, and by modifying the frequency of the electric current supply of the motor. The flow variation by turning on the screw of the displacement RC:
The flow variation was made at a revolution of 1000 rot/min, corresponding to a frequency read on the electric panel of 33,333 Hz, by turning on the screw adjusting displacement, this being placed on the pump body for changing the angle of inclination of the pump disk. This allowed obtaining a max flow of about 92 l/min, of some intermediary flow values and of a very low flow close to 0.
The flow variation by means of varying the supply frequency:
In addition to the initial requirements, during testing the pump, was aimed to reach a variation of the pump flow at min pressure, close to 0, at 1000 rot per min corresponding to 33,3 Hz, when the flow value was of about 90...92 l/min, as well as for a revolution of about 1500 rot/min corresponding to a frequency of 49.86 Hz, when the flow value was of 134...136 l/min.

3.3.5 The adjustment of pressure at the pressure compensator

The pump which was tested, equipped with a pressure compensator/ regulator, was subjected to special tests for proving the possibility of adjusting the pressure compensator, observing by means of different adjustments its modality of response namely the flow variation at the pressure increase In this respect were performed the following tests:
The adjustment of the max operational pressure at the compensator.

For this, was taken into account the real constructive solution which allows a number of rotations at the adjustment screw, about 9,5, for covering the entire adjustment range. After 2...3 shifts, starts the adjustment of the max. desired pressure, at which the pressure compensator tips and determines the pump to decrease the flow to almost a null one. The tipping pressure increases, when the number of shifts increased at the adjustment screw, according to the table 1, from below:

Table 1

Nr. of shifts at the adjustment screw	2,75	3,25	3,5	4,0
The tipping pressure PC bar]	20	75	100	150

Variation of the flow and pressure on pump static characteristic

In table 2 are shown the flow and pressure variations for different set values at the pressure compensator CP, till the tipping of the pump and making it have null flow.

Table 2

PRESSURE COMPENSATOR (PC) Adjustment									
ADJUSTMENT PC at 15 – 16 bar									
Pres.[bar]	5	10	12	15	**16**	-	-	-	-
Flow [l /min]	52,5	52	51	46,3	**0**	-	-	-	-
Adjustment PC at 65 – 70 bar									
Pres.[bar]	-	10	20	30	40	50	60	65	**70**
Flow [l/min]	-	52	49,7	49	48,4	47,5	47	45	**0**
Adjustment PC at 140 – 145 bar									
Pres.[bar]	-	10	20	50	80	100	120	140	**145**
Flow [l/min]	-	52	51	49,9	48,4	47,2	46	43	**0**

3.3.6 Watching noise and temperature values during operation

The testing on the stand of the pump took place during summer, at the following temperatures: the environmental temp. 33...380C; the oil temperature 54...570C and pump temperatures 33...650C.
Noise and temperature during operation
During the tests, was carefully followed the noise and found in normal limits. The temperature measured on the pump body increased up to a normal one.

3.3.7 Finding the static characteristics of the pump with pressure compensator

From the experimental measurements, performed for the 3 levels set at the pressure compensator, were detected the static characteristics of the pump with axial pistons, equipped with pressure compensator; these characteristics are represented in Fig.7 a, b, c.

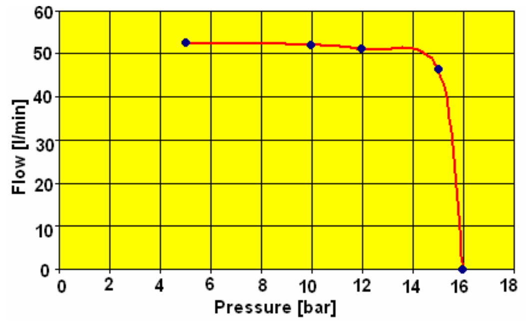

a) adjusting at 15-16 bar

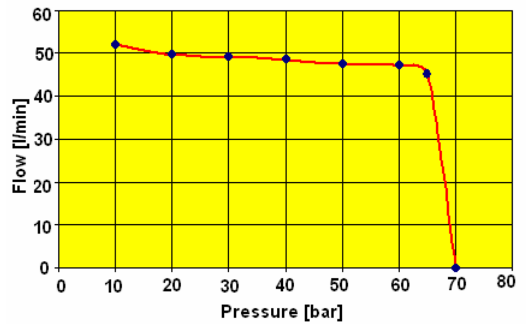

b) adjusting at 65-70 bar

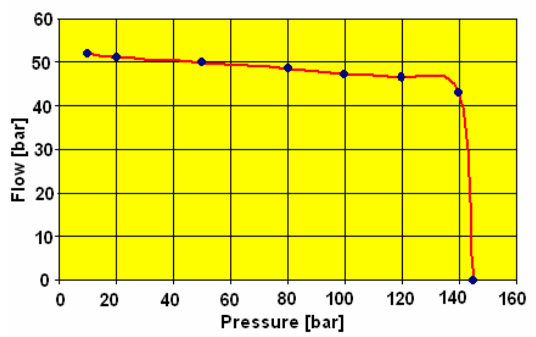

c) adjusting at 140-145 bar

Figure 7: The static characteristics of the pump with pressure compensator

4. Conclusions and remarks

From the information presented above, it may be noticed the significant role of an adequate maintenance of the hydraulic installations, for ensuring a long lifespan. This comes out from the theoretical approach from the beginning and from the real case studied in the second part. It was concluded that the tested pump has a normal behavior, having the possibility of adjusting the displacement and the pressure compensator as well, these being proven by means of the performed tests. The pump was found adequate for being assembled at the hydraulic installation with the condition of a careful assemblage and of a proper maintenance, being recommended to use good quality hydraulic oil, with the required characteristics, according to the manufacturer's recommendations.

REFERENCES

[1]. N. Vasiliu, D. Vasiliu, "Fluid Power Systems", Vol.I. Technical Publishing House, Bucharest, 2005
[2]. *** PARKER: Catalogue Industrial Hydraulics HZ11-2500/UK, March 2002
[3]. Marin V., Moscovici, Rd., Teneslav, D. "Hydraulic drive systems with automatic adjustment. Practical problems, design, execution, exploitation". Technical Publishing, Bucharest, 1981.
[4]. Drumea, P., Cristescu, C., "Tribology researches on increasing the lifetime of hydraulic components and systems". In: PROCEEDINGS of the International Scientific-Technical Conference HYDRAULICS AND PNEUMATICS-2012,16-18th of May 2012, Wroclaw, Poland.
[5] Lepadatu, I., - Experimental research focused the mechatronic positioning systems for regulating the geometrical volume of the pumps with radial pistons, Buletin Stiintific nr. 4 al UPB, 2010
[6]. ***PARKER, Senso-Control, http://www.rotec.net/pdf/senso%20control.pdf
[7]. ***HYDAC, HMG 500: http://www.hydac.com/de-en/products/measurement-display-and-analysis-tools/measuring-instruments/handheld-measuring-instruments/hmg-500.html
[8]. *** PARKER, LCM20, http://www.ezihose.com/pdfs/catalogues/LaserCM.pdf

ISSN 1454 - 8003
Proceedings of 2014 International Conference of Hydraulics and Pneumatics - HERVEX
November 5 – 7, Calimanesti-Caciulata, Romania

DRIVE INSTALLATION OF HARMONY FLOW ASSEMBLY CONNECTION WITH ONE BIG CONDENSER C_M AND ONE FRICTION RESISTANCE

Prof.dr. eng. Carmen BAL[1], assist. drd. eng. Carmen Ioana IUHOS[2], Prof. dr. eng. Nicolaie BAL[3]

[1] Technical University of Cluj Napoca, carmen.bal@dppd.utcluj.ro;

[2], Technical University of Cluj Napoca, bic-tkd@yahoo.com

[3] Technical University of Cluj Napoca, nicubal@yahoo.com.

Abstract: *In this paper we propose to analyses the alternative flow in the parallel installation including the capacity, and the friction resistance In this paper we show the caloric effect due to the displacement of the low in the friction resistance calculate. We propose to calculate the section of the friction resistance in the drive installation assembly connection with one big condenser c_m and one friction resistance, were we know the capacity and the flow and sonic pressure*.

***Keywords**:* sonic pressure, sonic flow, friction resistance, sonic condenser, temperature etc

1. Introduction

In the last time, the development of the science and the technicians are realised the big progress and the level of the general knowledge of the persons implicated in this activity are advances and probable the knowledge of the sonicity are not brake by the wrong idea or disregarded by “incompressibility of flow”

Fig. 1 The sonic installation about one friction resistance

The mathematical calculus used by the technicians of the last generation is strong and enable to once understand and the tackle creative the sonicity. This approaching by the actual technical calculus of the hydraulic system and the theory of the sonic transmissions are big, when we can affirmed the sonicity by power transmission through harmonic oscillations to the liquid colons represent a new modality by compression of the energies through the hydraulic system in the permanent regime harmonic.

To produce heat vibrations to build a sonic generator phase, this consists of a pump equipped with a moving piston and a cylinder alternative. Pump speed is given by a DC electric motor with variable speed. The cylinder leaves a pipe to a condenser (capacitive cylinder) filled with liquid steel. As fluid is preferably water, with a coefficient of elasticity than oil.

To protect the system against rust oil was used. This capacitor can be considered equivalent to a capacitor of electricity called capacitor. From the other end of the condenser leaving a pipeline that is connected to a tube of small diameter, the shape of a coil spring. Tubing (resistance of friction which acts as an electrical resistance) is linked with a second capacitor (capacitive cylinder) filled with liquid [2]. This assembly of hydraulic viewpoint is nonsense as classical hydraulic fluid compressibility is not taken into account (figure 1).

If you take into account the liquid compressibility factor can be put in motion generator through a mechanism with eccentric (or rod crank), which produces alternative movement of the piston. As a result of the reciprocating piston pulsations occur in the first cylinders. Thus the tank becomes a kind of sonic generator.

Sonic waves are forced to pass inside the friction resistance and capacitor to reach its end. Movement is possible because of compressibility energy transmission waves [2]. Alternative energy via friction resistance thin tube made sonic friction loss, such losses caused by passing electric current through ohmic resistance to electricity.

2. Experimental research about the frictional effects in the harmonic connection

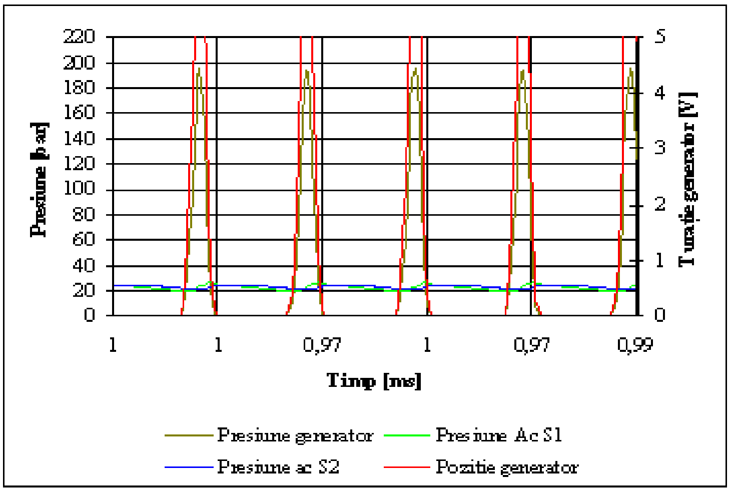

Fig. 2. The variation of the pressure in time in the case of the installation

We considered the sonic system formed by with one capacity cylinder and one friction resistance (figure 1). Is formed by sonic generators who are connecting by the friction resistance R_f. with a pipe, this resistance is connected also by a pipe to the capacity cylinder. The capacity of cylinder are V= $2405{,}282 \cdot 10^3$ mm^3 [2].

After the work of the experimental dates obtained from the three sensor place in the system, are results the primary histograms represented in the figure 2, this show the evolution of the generator pressure and also the pressure to the extremity of the capacity cylinder. Also we can see the revolution of the generator. The evolution of the pressure curve to notice the existence the phases difference by the generator pressure and the pressure of the capacity cylinder.

n = 320 rot/min **p_s = 0 Pa**

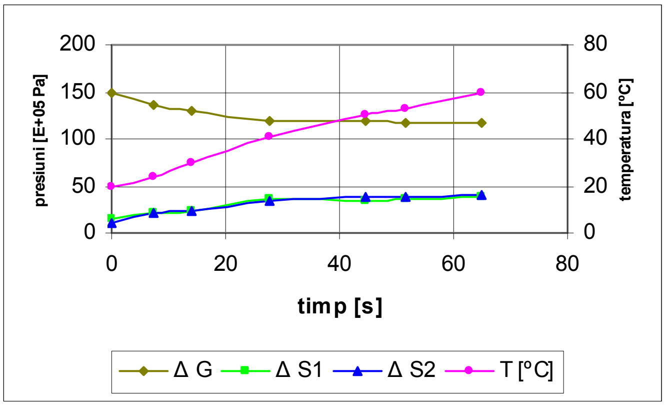

Fig. 3 Diagram of pressures and temperature variation of speed according to the static pressure of 0 Pa

For make in evidence the effects of the friction we can study the effects of the sonic pressure in the drive installation charge the system with static pressure. For same static pressure (1 bar) we obtained the diagrams for this charges.

For the first experiment we used the begin speed 320 rot/min and the static pressure by 0 Pa. After the processing the histograms we obtain the graphics presented in the Figure 3 and 4. These developments are illustrates the pressures, temperatures and the corresponding generator of turaţiilor functioning. It is observed that the pressure on start generator was 150 bar pressure that fell along the bar at 115 bar, while the pressures at the two ends of the cylinder were roughly equal to each other (10 bar) stabilized to 40 bar. The temperature curve shows its variation, which stabilized at 60ºC after 65 seconds to the start of drive installation.

ps = 0 Pa

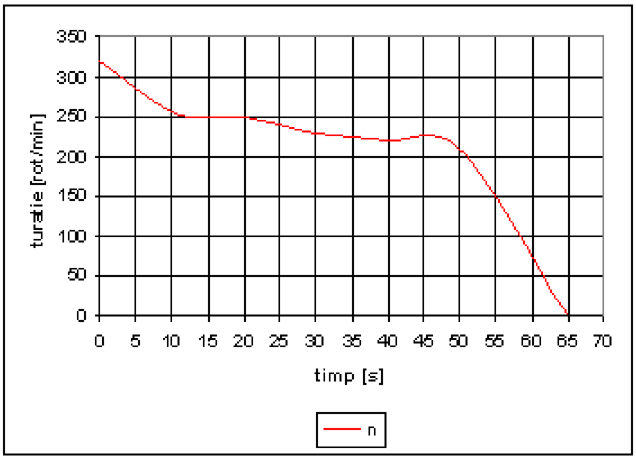

Fig. 4 The variation of revolution in time to the static pressure 0 Pa

Pressure drop across the resistance of 75 bar. Everything went normally as if it would have created a pressure in the drive installation that led off the electric motor whose speed has dropped from 320 rpm engine speed drops to 0 due to ther expansion of oil temperature, manifested by increasing $\Delta V = V_0 \cdot \alpha \cdot \Delta T$; also the viscosity decreases with increasing tempe-rature which leads to an increase in pressure in the system.

In the experimental graphics we are noted with:

ΔG – the variation of the generator pressure;

ΔS_1 – the variation of the pressure obtained by the first sensor of pressure place to the left

n = 1667 rot/min **p_s = 0,25E+05 Pa**

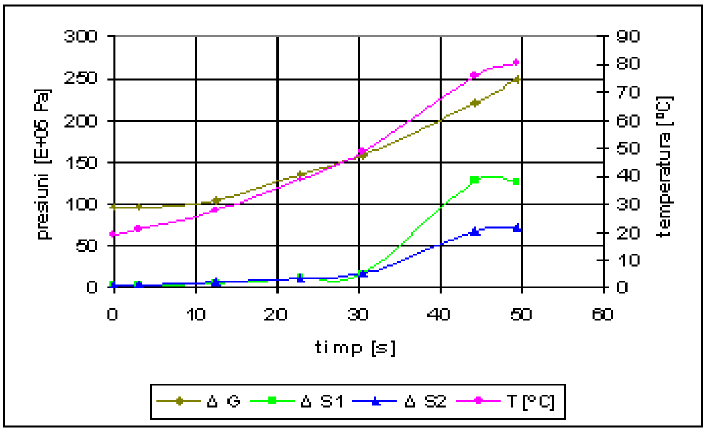

Fig. 5 Diagram of pressures and temperature variation of speed according to the static pressure of 0,25E+05 Pa

of the capacity cylinder

ΔS_2 – the variation of the pressure obtained by the right sensor of pressure placed to the capacity cylinder;

T – temperature

In Figures 5 and 6 designed for a static pressure of 0,25E+05 Pa and speed n = 1667 rpm sart. Temperature reached after 1 minutes at 75°C operation. Perceived pressure from the cylinder pressure sensors are recorded for 30 seconds at a pressure equal, then the sensor located at the end of the resistance from friction grew larger pressure difference between them reaching 50E + 05 Pa, and difference between the sensor indicates the pressure drop (from the generator and the

p_s = 0,25E+05 Pa

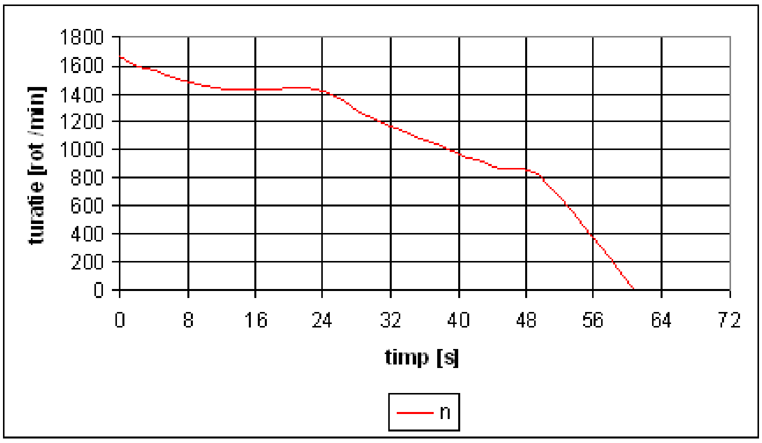

Fig. 6 The variation of revolution in time to the static pressure of 0,25E+05 Pa

cylinder end was in continuing friction resistance) reached 120 E + 05 Pa. Due to the high pressures occurring in the system occurred abruptly stopping the electric motor.
On the basis of the histogram results (from experiments) of the type shown in Figure 4 and graphs were constructed and the temperature variation of the pressure versus time and speed. Because of

n = 1667 rot/min **p_s = 0,5E+05 Pa**

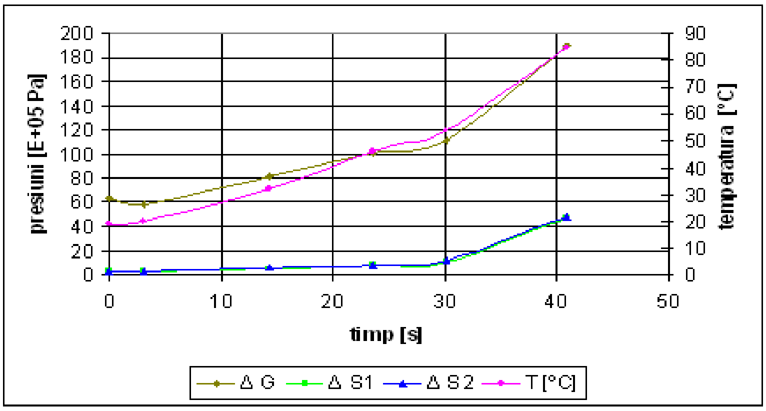

Fig. 7 Diagram of pressures and temperature variation of speed according to the static pressure of 0,5E+05 Pa

the large number of histograms obtained we plotted only in Figure 2, the rest is processed without being presented.

Figures 7 and 8 are represented by diagrams of variation of variation of pressure and temperature versus time and speed to the static pressure 0,5E+05Pa. It appears that the pressure on the condenser pressure sensors are equal and grow up to the 50E+05 Pa, while the generator pressure reached 190E + 05 Pa at the stop of the electric motor. Since starting speed was quite

p_s = 0,5E+05 Pa

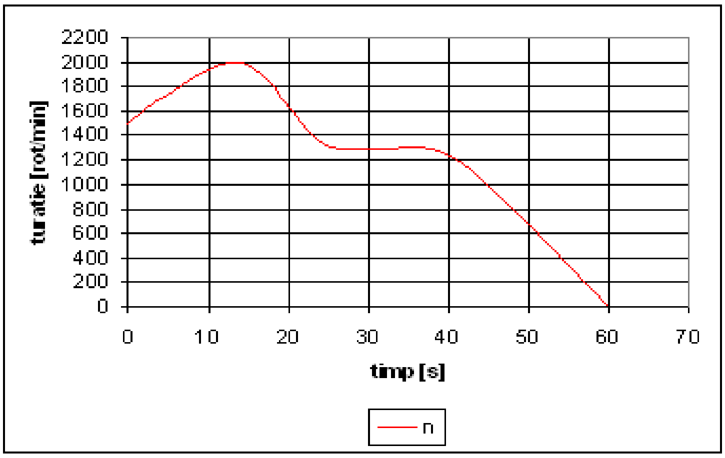

Fig. 8 The variation of revolution in time to the static pressure 0,5E+05 Pa

high - 1500 rev / min heating phenomenon of resistance due to friction leads to a rapid increase in its surface temperature reached after 40 seconds at 85 °C.

3. Conclusions

Analyzing charts above we can draw the following conclusions:

- The greatest influence on increasing pressure and the temperature in the system has the higher speed so that it is higher to start the fastest growing pressures and temperature resistance friction;
- The static pressure in the system to a lesser extent affect the temperature rise;
- As the electric motor stops after a short period of operation is not recommended for making the stand consists of a friction resistance and a cylinder.

REFERENCES

[1] Constantinescu, G., (1985), *The theory of the sonicity*, Bucureşti, Ed.Academiei.
[2] Carmen Bal, (2007)**,** *Caloric effect in the circuits by harmonic flow***,** Cluj Napoca, Ed. ALMA MATER.
[3] Carmen Bal, (2006), *Research and contributions about the drive systems with the harmonic flow*, The doctoral thesis Technical University of Cluj Napoca.
[4] Pop I. Ioan**,** Carmen Bal, Marcu Lucian ş.a**.,** (2007), *The sonicity applications. Experimental results*, Iaşi**,** Ed. Performantica.

ISSN 1454 - 8003
Proceedings of 2014 International Conference of Hydraulics and Pneumatics - HERVEX
November 5 – 7, Calimanesti-Caciulata, Romania

ELECTROMECHANICAL CONVERTERS USED IN HYDRAULIC EQUIPMENT

Radu RADOI[1], Ioana ILIE[1], Gabriela MATACHE[1]

[1] INOE 2000 – IHP, Bucharest; radoi.ihp@fluidas.ro; Ilie.ihp@fluidas.ro; fluidas@fluidas.ro

Abstract:
Electromechanical converters are the linking elements between electronics and hydraulics. Proportional to the electrical current as the input variable, they produce force and displacement as the output variable. In hydraulics those equipment are used to direct drive valve slides and to clog holes. Assembly consisting of an electromechanical converter and a hydraulic flow control device is named electro-hydraulic amplifier. This paper present the main electromechanical converters used in hydraulics from the structural and functional point of view.

***Keywords**: torque motor, proportional valve, solenoid, hydraulic, actuation, servo-jet, jet pipe*

1. Introduction

Electromechanically converters transform an electric signal in displacement of a plunger for solenoids or displacement of a lappet for torque motor. Assembly consisting of an electromechanical converter and a hydraulic flow control device is called electro-hydraulic amplifier. They are called amplifiers due to the ratio value between hydraulic power and electric power is the order of $10^3 \div 10^6$. There are many electro-hydraulic devices that used electromechanically converters like: electro-valves, directional control valves, directional proportional control valves, proportional valves, servo-valves, proportional throttles, flow controls.

2. Electromechanically converters

ON/OFF solenoids

In solenoids, electromagnetic energy is transformed into mechanical energy in order to perform the movement of the spool held in the hydraulic valve. Basically, solenoids are made up of a *coil,* a copper insulated conductor wound in a spiral on a sleeve inside which a cylindrical *core* made of ductile iron slides. The excitation resulting from the voltage connected to the coil ends trigger a magnetic field that moves the core axially. The element air or oil between the core and the coil, depending of constructive form, is called *“gap”*.

Figure 1 ON/OFF solenoid

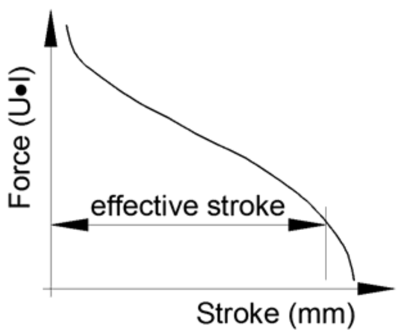

Figure 2 ON /OFF solenoid force/movement characteristic

For the CA electromagnets used in on/off control valves the initial power (UI) is high and decreases progressively towards the end of the plunger stroke (Figure no.2)

Force-controlled solenoid

Solenoid with particulary defined force/current relationship over a very short stroke are called forece controlled solenoid. The solenoid force is controlled by the change in current I in the force controlled solenoid without the armature of the solenoid performing a measurable stroke. The force proportional electromagnets are used particularly for pilot operated proportional directional and pressure control valve, single stage or two stage directional control valves.

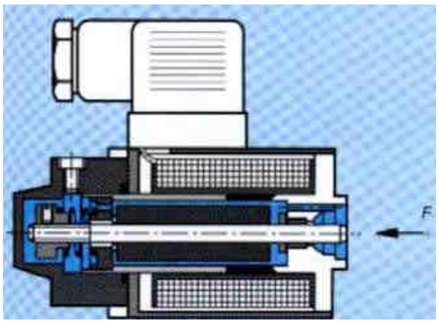

Figure 3 Force-controlled proportional solenoid

When the coil is crossed by a voltage between the mobile core and the leg appears a force of attraction whose value is proportional to the command current (Figure 4). The force-current relationship has a threshold and a hysteresis. The magnetic circuit contains a magnetic barrier (made by brass or aluminum) that forces the lines of magnetic flux to travel axially movable core, limiting the magnetic dissipation. The inner of the electromagnet are in the oil bath ensuring lubrication and cooling too. One or more channels inside the mobile core and the leg provide oil circulation within the sleeve. Spool and sleeve are located inside the electromagnet. The sleeve is made of magnetic material to concentrate the magnetic field in the space between it and the moving core.

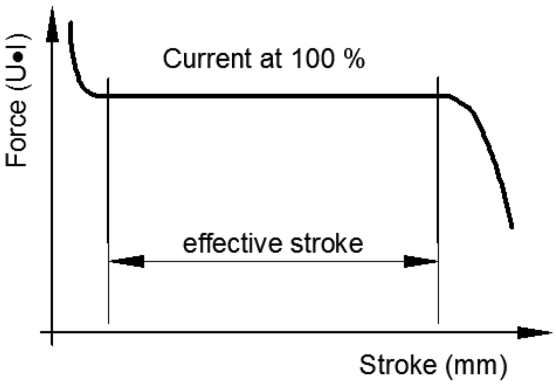

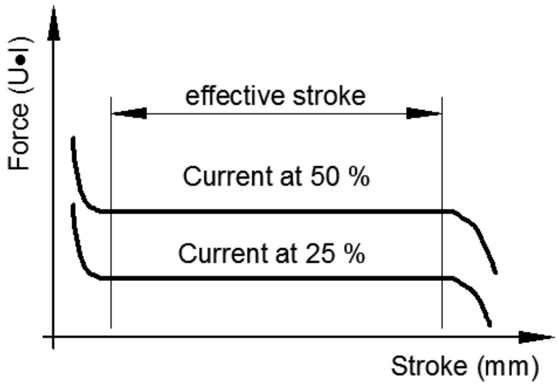

Figure 4 Force-stroke characteristic of force-controlled solenoid

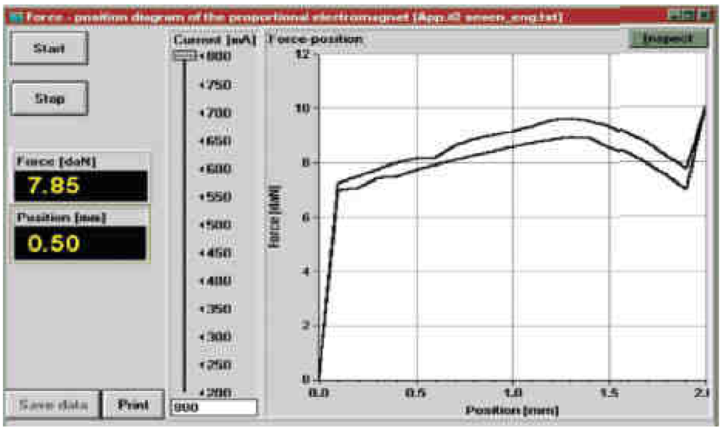

Figure 5   Aplication software for force-stroke characteristic determination

Stroke –Controlled Solenoid

Solenoids with comparatively linear stroke/current relationship over a reasonably long stroke lenght are called Stroke –Controlled Solenoids. The position of the armature is controlled by a closed –loop control circuit an maintained irrespective of the counter pressure. With such a type of solenoid, the spools of proportional directional, flow as well as pressure control valves can be directly operated and be controlled, in any stroke position. The stroke of solenoid is between 3 and 5 mm depending of size. In conjunction with the electrical feedback, the hysteresis and the repetition error of the solenoid are maintained with very light tolerances.

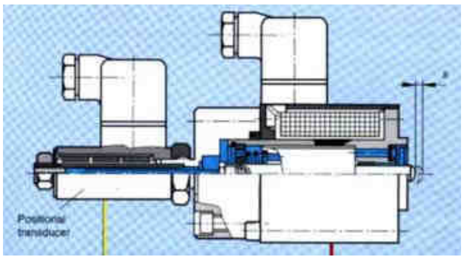

Figure 6 Stroke-controlled proportional solenoid

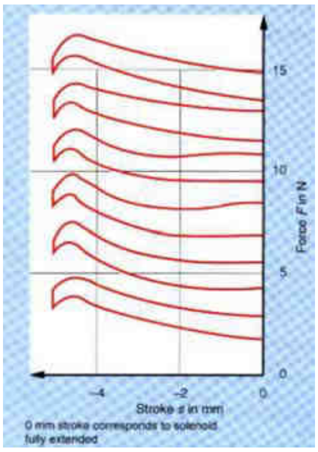

Figure 7 Characteristic curve, stroke-controlled solenoid

ISSN 1454 - 8003
Proceedings of 2014 International Conference of Hydraulics and Pneumatics - HERVEX
November 5 – 7, Calimanesti-Caciulata, Romania

Voice coil actuators

The actuator consists of a cylindrical coil that is free to move axially in an air gap. The air gap is formed between a cylindrical center pole and a permanent magnet that surrounds it. A soft iron shell houses both the magnet and the pole.

By applying a voltage across the terminals causes the voice coil actuators moving part, magnet or coil, to travel in a given direction. Reversing the polarity of the applied voltage will change the direction of the moving magnet or coil. The generated force is proportional to the flux crossing the coil and the current that flows through this coil.

Figure 8 Voice coil actuators produced by the Mönninghoff company

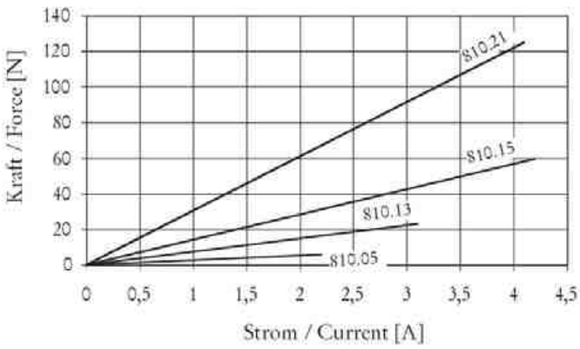

Figure 9 Force/Current chart of the actuator

Voice coil actuators provide high force and acceleration capabilities along with high-speed linear position control.

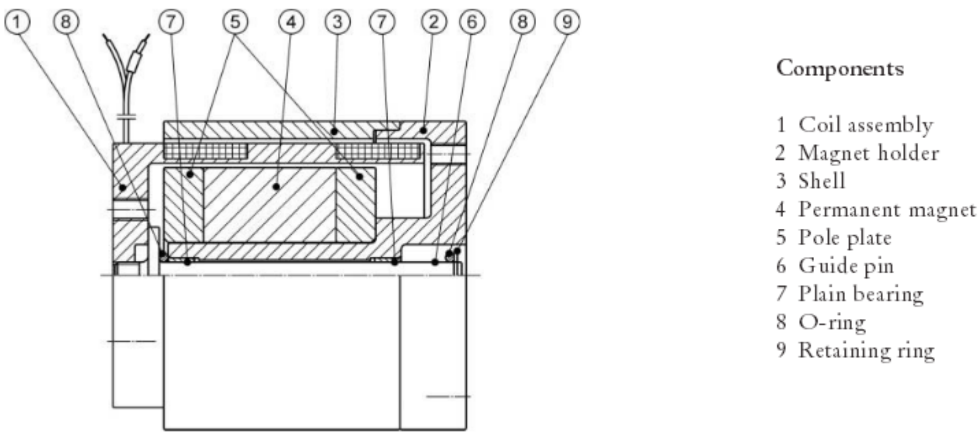

Figure 10 Actuator componets

Torque motor for servo-valves

The torque motor (Figure 11) converts a small current (mA) into a proportional, mechanical movement. The torque motor is hermetically sealed from the hydraulic device. An armature made of soft magnetic materials is mounted on a thin flexible tube, which acts as a spring, a seal for the pressure medium, and carries the flapper-jet. The flapper-jet physically belongs to the torque motor, but functionally to the hydraulic amplifier.
The torque motor is a motor excited by a permanent magnet. Using adjustable pole screws, the gap between armature and pole screw can be adjusted and hence the motor characteristic optimized.
The two coils on the armature, which can be connected in series or parallel, magnetize the armature. As a result, a torque is exerted on the tube acting as a return spring. The torque is proportional to the pilot current and null when the pilot current is zero. As a result, the tube returns the armature and consequently the flapper plate to the center.

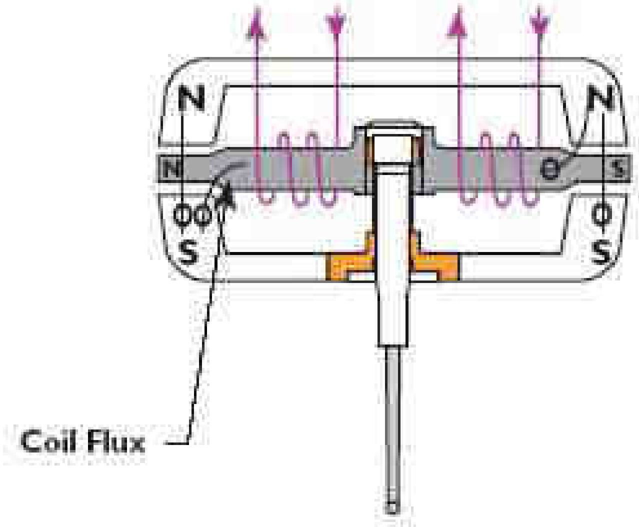

Figure 11

Servo jet converter

In a jet pipe converter (Figure 12), the flow is directed through a jet projector, which is a tube with a nozzle on the end. The flow exiting the jet projector nozzle is directed toward a receiver. The receiver has a hole into which fluid from the nozzle is directed. Inside the receiver, the hole branch out into two passages. Each passage is connected to an end of the main spool. The occurrence of control current in coils creates a magnetic field in opposition to the two ends of the mobile armature located between the two coils, which drives the jet projector to the one hole of jet receiver, depending of the command current sense. Once the force motor is actuated in one direction or the other, the angle of the jet pipe is changed, thus directing the flow toward one edge of the receiver. The flow from the nozzle is thus directed more toward one receiver line than the other line, creating a higher pressure in one of the lines (Figure 13). This higher pressure then acts upon that line to one spool end, shifting the main spool. The displaced spool then connects system pressure to one of the working ports while, at the same time, the opposite working port is connected to tank. The angle of the jet pipe is proportional to the in put current applied to the force motor. The pressure in one receiver line rises proportionally to the angle of the jet pipe, and the resulting spool displacement is proportional to the rise in pressure in the adjacent routes.

Figure 12 Moog Servo-jet converter

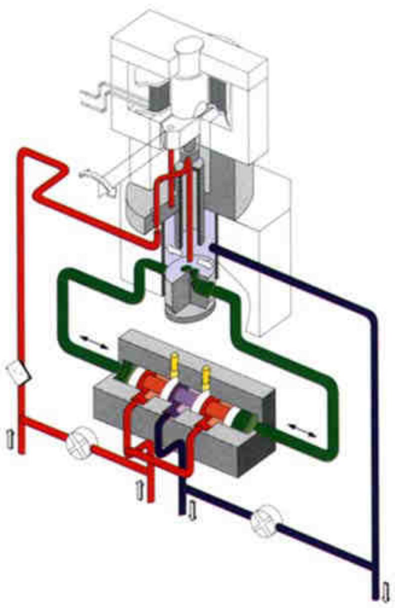

Figure 13 Hydraulic circuit in a Moog Servo-jet servo valve

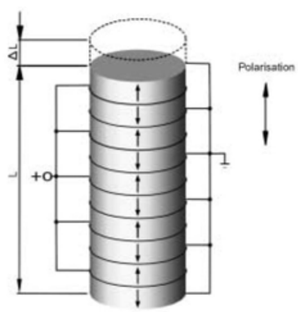

Figure 14

Piezoceramic actuator

Inverse piezoelectric effect is the development of a mechanical deformation when an electric field is applied to the piezoceramic element (Figure 14).

Piezoelectric materials have a high energy density at low volumes and masses, respond well to high frequencies, their response time is of the order of microseconds.

Piezoelectric elements produce a more linear response than electrostrictive or magnetostrictive materials. However, they do not produce large strokes, the maximum relative deformation of 0.1%, may be 0.15% for some compositions.

In recent years there have been made various types of piezoelectric elements: multilayer piezoelectric elements, piezo-ceramic elements, MLA (Multilayer Piezo Ceramics for Actuators), Parallel Prestress actuator (PPA), piezoelectric actuators APA (Amplified Piezo Actuators), relaxor ferroelectric single crystals (PZN-PT şi PMN-PT), PLZT compositions, etc. Among them, PZN-PT materials are distinguished by relative deformation that can exceed 1%, the energy density of strain is 5 times higher than that of conventional piezoelectric materials.

MLA actuators provide a relative deformation of 0.1% (1μm/mm) at typical voltage of 150V. The relative elongation of a piezoelectric element is $\frac{\Delta L}{L} = E \cdot d_{33}$, where E is the electric field strength [V/m], d_{33} is the piezoelectric coefficient of the material [m/V], for the case when the direction of electric field is longitudinal (direction 3) and the deformation is that measured also on direction 3 (longitudinal).

From the standpoint of the response time, a piezoelectric actuator can perform its nominal movement in approximately 1/3 from the period of its resonance frequency

Resonance frequency is calculated as $f_0 = \frac{1}{2\pi}\sqrt{\frac{k_T}{m_{ef}}}$ where k_T is the rigidity of the piezoelectric actuator [N/m], m_{ef} is the effective mass (approx. 1/3 of the mass of the piezoelectric element plus the mass of connection elements).

The firm CSA Engineering (USA) recently made a prototype of piezoelectric servo valve with direct drive (Figure15).

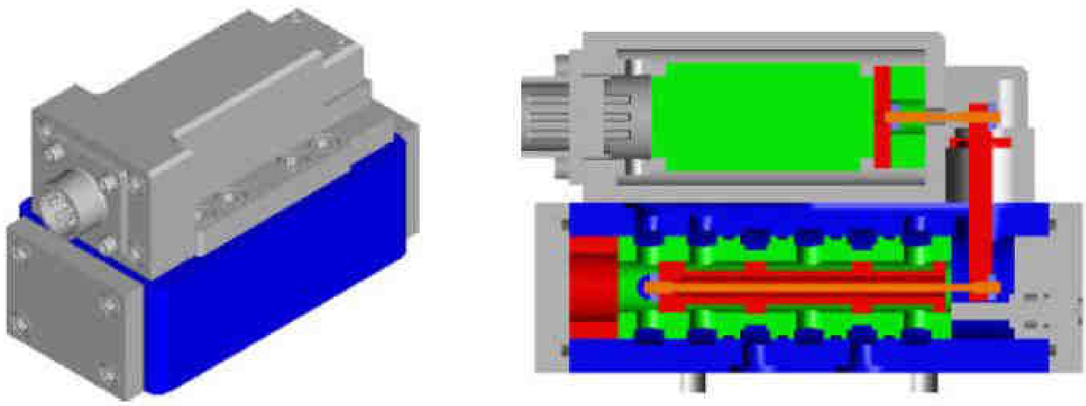

Figure 15

The amplification ratio of the lever arm is 5, so that at the nominal race of piezoelectric stack of 60 μm, the maximum displacement of spool is 0.3 mm. The piezoelectric element is stack type with composition PLZT, with dimensions 40 x 20 x 20mm, capacity of 3.5 μF.

3. Conclusions

Is ascertained that exist a diversity of models of converters, each with different characteristics. Some provide a greater force, other precision, better linearity and switching frequency, other higher stroke , good repeatability and low hysteresis. Each type finds its applicability in a certain type of hydraulic equipment for command or adjustment such as: directional valves, proportional directional valves, proportional valves, throttle valves, flow regulators or servo valves.

REFERENCES

[1] H. Dorr, R. Ewald, J. Hutter, D. Kretz, F Liedhegener, A. Smith, “Hydraulik Trainer Vol. II – Proportional and Servo Valve Technology”, Rexroth GmbH, 1986
[2] Hubertus Murrenhoff, “Trends in Valve Development”, O + P Ölhydraulik und Pneumatik, 46 (2003) Nr. 4
[3] Don DeRose, “Fluid Power Journal”, March/April 2003
[4] Moog’s Pilotstufen Trainer – Microsoft Power Point Show
[5] http://www.moog.com/literature/ICD/ProportionalServoValveTechnolog-fpjarticle.pdf

ISSN 1454 - 8003
Proceedings of 2014 International Conference of Hydraulics and Pneumatics - HERVEX
November 5 – 7, Calimanesti-Caciulata, Romania

A FUNDAMENTAL STUDY OF SUPERCAPACITIVE CELLS

Alexandru RIZOIU[1], Stanica ENACHE[1], Mihai VARLAM[1], Paul SVASTA[2]

[1] National Center for Hydrogen and Fuel Cell, INC-DTCI ICSI Rm. Valcea, Romania, alexandru.rizoiu@icsi.ro

[2] University Politehnica of Bucharest, UPB-CETTI Bucharest, Romania, paul.svasta@cetti.ro

Abstract: *In this work, we carry out detailed investigations on the energy storage capability of a commercially available 10F/2.5V Suntan supercapacitor. For that, we make use of dedicated measurement methods and techniques: i.e., cyclic voltammetry, chronoamperometry, chronovoltametry and open circuit voltage. From cyclic voltammetry measurements, we show that the dependence of capacity on the applied voltage is linear. By using chronoamperometry and chronovoltametry, we determine the time dependence of the transient currents and voltages, together with the equivalent series resistance (ESR). Open circuit voltages monitored over a long period of time suggests strongly that the leakage currents are mediated by two charge redistribution mechanisms with kinetics defined by rate constants that differ by one order of magnitude.*

Keywords*: supercapacitors; high – power rechargeable batteries; electrochemical impedance spectroscopy*

1. Introduction

Electrical double-layer capacitors (EDLC) are electrochemicalcapacitors [1]. They are often referred in literature as supercapacitors or ultracapacitors. Supercapacitors do not have conventional solid dielectrics. Their capacitance is given by the electrostatic storage of electrical energy by separation of charge in a Helmholtz double layer at the interface between the surface of a conducting electrode and an electrolytic solution combined with reversibleredox reactions that involve adsorption/desorption phenomena occurring mainly at the highly porous electrode-electrolyte interface [2]. In essence, a supracapacitor is either in the form of a half electrolytic cell or twosimilar ones, separated by an insulator to circumvent internal charge recombination.

EDLCs exhibit high energy storage capabilities with the possibility to deliver it in short time. From mobile to stationary applications, the supercapacitors bridge the gap between conventional capacitors and rechargeable batteries. They store the most energy per unit volume or mass (energy density) and support up to 6500F/2.5V, which is up to 10000 times that of electrolytic capacitors.

Fabrication of supercapacitive cells involves state-of-the-art deposition methods which combine solid-state routes with wet-chemical ones to obtain highly porous media (i.e., with active areas of hundreds of m2/g) for an increased energy storage capacity. That can be obtained by spray pyrolysis of carbon suspensions on sputtered metallic electrodes to also ensure low equivalent series resistance (ESR) values.

From an application point of view, the supercapacitors are especially attractive for energy buffer applications [3]. For instance, in order to prevent energy shortfall in fuel cells and wind turbines, the supercapacitive cells can be used as back-up power systems during transient operation. For automotive applications, the supercapacitive cells can be connected in parallel to the battery in hybrid electric vehicles in order to provide the energy burst, either for engine start-up or regenerative breaking [4]. Transient power applications are very specific on the amount of power delivered in a given time domain and for that a better understanding of the supercapacitor is important.

Transient power applications are very specific on the amount of power delivered in a given time domain. In order to match that performance, it is, however, highly desirable to have a detail investigation of the supercapacitive components subjected to various operational modes [5].

For that, we make use of a commercially available supercapacitive cell (i.e., 10F/2.5V from Suntan) in conjunction with a potentiostat/galvanostat system to determine the I-V characteristics, the time dependent charging and discharging voltages and currents, the corresponding ESR values, as well as the open circuit voltage, which gives an impression on the internal leakage currents.

2. Experimental

A. Introduction

In this work, we use a supercapacitor that has been pulled out of production recently, due the technological fabrication issues related to component manufacturing protocols. The main characteristics of the supercapacitor are given in Table.1.

Table 1: Characteristics of Suntan 10F/2.5V supercapacitors

Operating temperature	Rated voltage	Surge voltage	Rated capacity	ESR 1kHz (MΩ)	Capacitance tolerance
-40°C;+70°C	2.5 V	3.0 V	10 F	35	-20%; + 80%

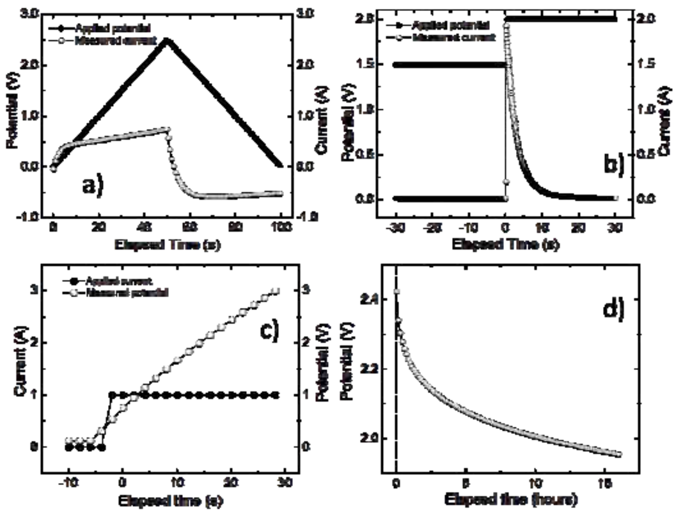

Fig. 1 Measurement techniques involved in characterization of supercapacitive cells. In a), the cyclic I-V curves are obtained upon a voltage sweep up to a desired voltage (e.g., charging regime, from 0V to 2.5V) and down (i.e., discharging regime, from 2.5V to 0V), with a given sweep rate (i.e., 50 mV/s), whereas the current is measured continuously. The time resolved potential and current step methods involved by the amperometry and chronovoltametry techniques are shown in b) and c), respectively. The time evolution of open circuit voltage (OVC) associated to internal charge recombination phenomena is indicated in d), for a spercapacitive cell charged at ~2.5V.

Starting from these specifications, we established the characterization protocols in order to assess the compliance of Suntan supercapacitors to the manufacturer performance values. For that, we make use of devoted electrochemical impedance spectroscopy methods, such as I-V measurements, chronoamperometry and chronovoltametry methods, as well as open circuit voltage (OCV) determination. Next, we describe each investigation method in part, with emphasis on the information they provide.

B. Cyclic I-V characterizations

Cyclic voltammetry (i.e., or I-V characterization) relates an applied voltage to the faradaic charge transfer phenomena occurring in an electrolytic cell that yields to a measurable current. In our case, we have used slow voltage sweeps (i.e., with a sweep rate of 50 mV/s) between the working and the reference electrodes connected to a potentiostat / galvanostat system (Princeton Parstat 2273 Model), whereas the resulted current is measured between the sensing and the counter electrodes. The connections are made such as the supercapacive cell is directly polarized in charging mode; i.e., the working and sensing electrodes are connected at the positive electrode. A typical time dependent cyclic voltammetry experiment is shown in Fig. 1a).

From the applied voltage and the measured current, one may directly determine the amount of charge that passed through the electrolytic cell. That is by the time integral of the measured electrical current:

$$Q = \int I(t)dt \qquad (1)$$

In this work, we investigate the charging and discharging regimes by two-step cyclic voltammetry (i.e., as shown for the applied voltage in Fig. 1), between 0V and 0.5, 1.0, 1.5, 2.0, 2.5 and 3.0V, for both direct and reversed polarizations, respectively. We carry out three charging cycles for each applied potential, starting with the supercapacitor in a fully discharged state.

C. Chronoamperometry

We use this method to carry out transient charging/discharging experiments at constant voltage, whereas the current is continuously recorded. At the moment of time t=0, the potential is raised/decreased by 0.5V and the corresponding charging/discharging current is monitored. For this experiment, we allowed a 30s delay prior applying a potential step. Then the potential step is applied and the corresponding charging/discharging current is monitored for the next 30s, which is sufficient time for current to decay to zero value. In Fig.1 b), we show the time dependent characteristics for the applied voltage and the measured current, respectively.

For this study, the charging and discharging currents are measured directly on the supercapacitor electrodes, without making use of an external resistive load capable to withstand peak-currents as high as 10A when, for instance, applying a potential step of 3V. Therefore, in order to prevent irreversible damage from high discharge currents running across both the supercapacitor and the potentiostat bridge (i.e., whose current is limited to 2A), we have limited the applied voltage step to 0.5V.

D. Chronovoltametry

This investigation method applies to transient phenomena occurring upon application of a current step excitation, whereas the resulted voltage is recorded in time. Due to surge voltage limitations, the overcharging potential is set to 3V. Initially, the supercapacitor is fully discharged by short-circuiting the electrodes for 5 minutes. Then the circuit is closed and the voltage is monitored for 10s at 0A (i.e., in Fig. 1c). At $t = 0$, a current step is applied and the voltage is measured continuously at a constant sampling rate of 0.5Hz. In order to observe the supercapacitive behavior in both burst and steady operating modes, we have conducted a series of charging experiments at high (i.e., for $0.5<I(A)<1.0$) and low (i.e., for $0.5<I(mA)<25$) currents, respectively. For comparison, the time required to charge the supercapacitor up to a potential of 3V by applying a constant current of 1A is 30s, whereas for an applied current of 25mA it takes nearly one hour. This study is essential to evaluate the energy storage capacity of the supercapacitor when operating in fast or slow charging modes; i.e., for instance, when in conjunction with a fuel cell as a back-up fuse or as an energy scavenger connected to a peltier element.

E. Open circuit voltage (OCV)

Different from the other measuring techniques, the open circuit voltage (OCV) method allows to measure the potential of a supercapacitor without involving an external electronic load (i.e., in Fig. 1d). From that, one can understand the behavior of the supercapacitor in a circuit over a long period of time in which the system is on standby and the internal space charge recombination phenomena correlated to current leakage are monitored.

ISSN 1454 - 8003
Proceedings of 2014 International Conference of Hydraulics and Pneumatics - HERVEX
November 5 – 7, Calimanesti-Caciulata, Romania

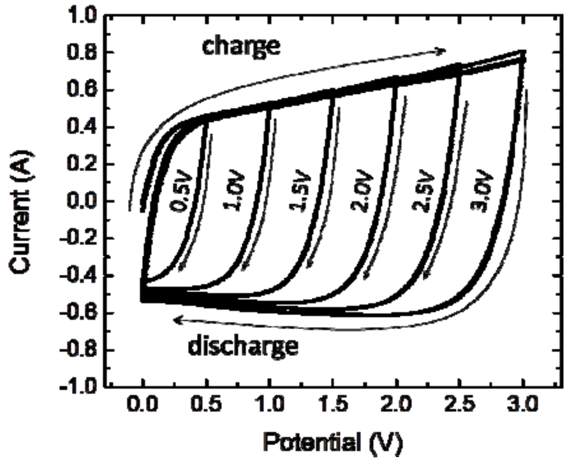

Fig. 2 Typical I-V charging/discharging curves of a supercapacitive cell upon two-step potential sweeps, from 0V to 3V and in reverse, in steps of 0.5V, respectively.

The experiment was conducted on the same supercapacitive cell charged at different potentials; i.e., 1.0V, 1.5V, 2.0V, 2.5V and 3.0V.

3. Results and discussion

A. Cyclic I-V characterizations

In Fig. 2, we show the I-V curves corresponding to the charging/discharging cycles obtained by sweeping the voltage at a rate of 50mV/s, between 0V and 0.5, 1.0, 1.5, 2.0, 2.5 and 3.0V, respectively. For each maximum applied voltage, we carry out three consecutive charging/discharging cycles, with the difference that the first charge is carried out on a fully discharged supercapacitor. That is obtained by short-circuiting the supercapacitor leads for 5 minutes. The subsequent charging/discharging cycles followed without restoring the fully discharged state.

At first site, one should point out the charging/discharging curves in Fig. 2 exhibit rather similar features. At low potentials, the current increases abruptly with increasing voltage, between 0V and 0.5V. Further increase of the applied potential results in a linear increase of the measured current, which is a typical characteristic for supercapacitors with an important internal resistance component. Upon discharging, the current decreases sharply first to a negative value. That is followed by a slight increase of the measured current, up to a non-zero value at 0V. This may be correlated to some remnant charge that is resilient to discharging in reversed polarization. It is, however, worth it to point out that this feature is exhibited by all I-V characteristics in Fig. 2, independent of the maximum applied voltage.

Moreover, the first charging cycle is very different from the subsequent ones in the sense that they all fall on top of each other, in a closed loop. As one shall see, the effect of remnant charge and the equivalent residual capacitance can be determined directly from the data in Fig. 2.

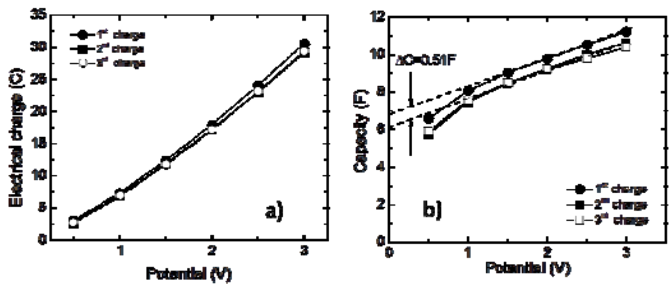

Fig. 3 The potential dependence of the stored electrical charge and the corresponding capacity for a Suntan 10F/2.5V supercapacitor, determined from the I-V characteristics in Fig. 2, measured upon 3 consecutive charging cycles.

By using (1), one may calculate the total electrical charge stored by supracapacitor upon charging at a constant sweep rate of 50 mV/s, from 0V up to the potential values from Fig. 2. The results are shown in Fig. 3 a).

From that, the equivalent capacity can be obtained by dividing the obtained electrical charge to the corresponding value of the maximum charging potential (i.e., $C=Q/V$). The results obtained for the first, second and third charging regimes are shown in Fig. 3 b), as a function of the maximum applied potential, respectively.

In other to understand the non-linear dependence of the electrical charge on the applied voltage in Fig. 3 a), one should consider that, however, the internal structure of the supercapacitor is somewhat affected by the continuous accumulation of charge upon applying a direct potential. On a macroscopic scale, the *extra* charge stored by supercapacitor may be viewed as a result of an increased *effective* dielectric constant associated to the constituent porous media. On a microscopic scale, this may be related to an increased active area as a result of electric field penetration inside the porous electrodes, resulting in an *extra* capacitive component. The net result is, nevertheless, that more electrical charge is stored at a given charging potential, resulting in a non-linear behavior, such as that depicted in Fig. 3 a).

In Fig. 3 b), we show a typical capacitance characteristic as a function of the charging voltage, as determined from measurements on a 10F/2.5V Suntan supercapacitor, upon three successive charging cycles. The data indicate that the working point of 10F/2.5V is in accordance with the specification provided by manufacturer for our supercapacitor (i.e., in Table 1). One should note that, however, the capacitance data for the first charge lay well above those obtained from the subsequent ones, which also fall on top of each other. Nevertheless, the explicit dependence of the capacity as a function of the maximum applied voltage is linear, for voltages higher than 1.5V. Therefore, the capacitance can be modeled as a function of voltage by using:

$$C(V) = C_0 + kV \qquad (2)$$

where C_0 is the value of capacity at zero voltage and k the voltage dependent capacity (i.e., in F/V).

By using (2), a fit to the data in Fig. 3 b) yields k = 1.33 F/V for the voltage dependent capacitance, whose value is independent of charging cycle.

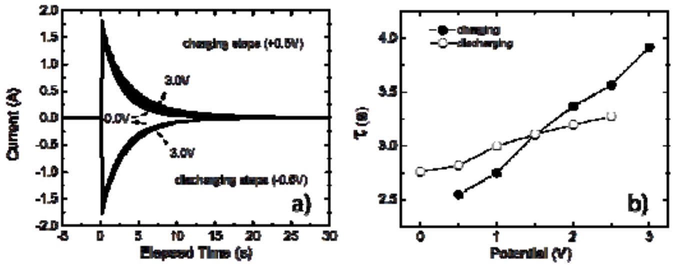

Fig. 4 Time dependence of the electrical current measured on a 10F/2.5V Suntan supercapacitor, upon charging /discharging at constant voltages, between 0V and 3V, in steps of +0.5/-0.5V, respectively (in a). The characteristic decay time τ determined from fit to the corresponding data in a) by using (3) is shown in b), as a function of the applied potential.

The values for C_0, corresponding to the firstand the subsequent charging regimes, are 6.8F and 6.3F, respectively. From that, an estimate for the equivalent residual capacity resulted from the charging sequence used in this work is of about 0.51F. This value is nearly 5% of the capacity value of 10F at 2.5V, in accordance with the capacitive tolerances provided by manufacturer (i.e., ± 20% at 25^0C).

B.Chronoamperometry

In Fig. 4a), we show the current charging curves measured upon increasing the applied potential in steps of +0.5V, from 0V to 3V. Together with that, we show the corresponding discharging curves, when the potential step is decreased in steps of 0.5V, from 3.0V to 0V. Both the charging and the discharging regimes are somewhat similar, in the sense that the corresponding electrical currents decrease in an exponential fashion on a time scale not larger than 30s, from the moment t=0s when the potential step is applied. At first site, one may note that the characteristic decay time

ISSN 1454 - 8003
Proceedings of 2014 International Conference of Hydraulics and Pneumatics - HERVEX
November 5 – 7, Calimanesti-Caciulata, Romania

for the measured current is different for the charging regime compared to the discharging one. In order to emphasize that, we fit all current curves to the exponential decay relation:

$$I(t) = I_0 \exp(-t/\tau) \quad (3)$$

where I_0 is the value for current at $t=0s$ and τ the characteristic decay time (in s).

In Fig. 4b), we show the potential dependence of the characteristic decay time τ obtained from fits to the corresponding electrical current data in Fig. 4a). The data suggest that there are two specific regimes, delineated at the potential value of 1.5V. For voltages below 1.5V, the supercapacitor charges slower than it discharges, at constant applied potential. This corresponds to the upper most current curves in Fig. 4a). This is different for voltages above 1.5V, where the charging time constant is larger in comparison to the discharging one. However, there is a crossover between the charging and discharging regimes (i.e., at 1.5V), where the corresponding values of τ are identical. This aspect is especially important for high power applications, since different charging and discharging time constants require power integrated components capable to withstand relatively high electrical currents that otherwise would result in irreversible damage of the integrated electronics.

The values of τ in Fig. 4b), corresponding to the charging and the discharging regimes, fall on straight lines, respectively.

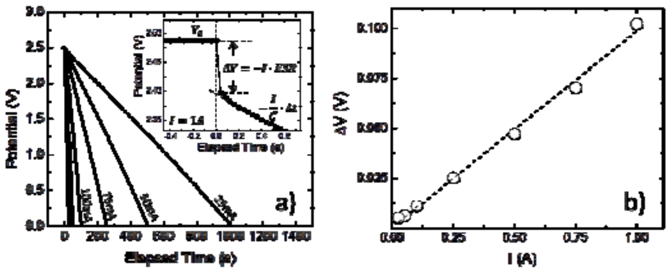

Fig. 5 Time dependence of the electrical current measured on a 10F/2.5V Suntan supercapacitor, upon charging/discharging at constant voltages, between 0V and 3V, in steps of +0.5/-0.5V, respectively (in a). The characteristic decay time τ determined from fit to the corresponding data in a) by using (3) is shown in b), as a function of the applied potential.

The slopes determined from linear fits to data have the values of 0.6s/V for the charging regime and 0.2s/V for the discharging one. In order to understand these features, we make use of the fact that the value for the characteristic decay time τ is given by:

$$\tau(V) = RC(V) \quad (4)$$

where C(V) is the potential dependent capacity whose dependence on the applied voltage is linear (i.e., in 2), whereas R is the resistance accounting for ohmic losses upon charging and discharging, respectively. From that, the explicit dependence of τ on V is linear:

$$\tau(V) = \tau_0 + \alpha V \quad (5)$$

where τ_0 = RC_0 and $\alpha = Rk$, with C_0 and *k* from (2). For the charging regime, we have found that $\alpha = 0.6$s/V and that the value of *k* is 1.33 F/V. From that, the value for R is 0.38Ω.

C. Chronovoltametry

For chronovoltametry measurements, we first charge the capacitor up to a potential of 2.5V and then measure the discharge voltage upon applying a constant current (in reversed polarization), with values between 25mA and 1A. The results are shown in Fig. 5 a). First, one should note that all discharge curves in Fig.5 a) are linear as a function of time. In the inset, we specify the explicit contributions to the measured voltage, as measured upon discharging at 1A. This feature can be expressed in the following form:

$$V(\Delta t) = V_0 - \frac{I}{C}\Delta t - I \cdot ESR \quad (6)$$

where *ESR* is the equivalent series resistance, *I* the discharge current, whereas V_0 (i.e., ~2.5V)and *C* (i.e., ~10F) are the potential and the capacitance at *t = 0s*, respectively.

The sudden drop in potential shown in the inset of Fig. 5a) is associated with the equivalent series resistance of our supercapacitor. This feature is often involved in determining the pure ohmic losses in supercapacitive cells and for proton conducting membranes in fuell cells. In literature, this is referred as the current interrupt technique. However, a fit to the data shown in Fig. 5b), yield the ESR value of (98.6±1.6)mΩ.

For constant current charging experiments, the supercapacitor is first discharged by short-circuiting the supercapacior leads for 5 minutes and then followed by the application of a current step.

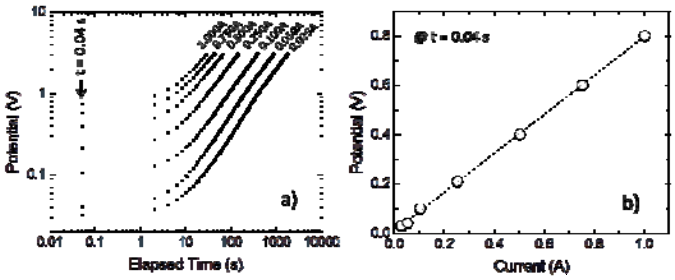

Fig. 6 Double logarithmic representation of the charging potential as a function of time, upon applying a current step on a 10F/2.5V Suntan supracapacitor (in a). In b), we show the potential values measured with a 40ms delay from the moment t = 0s, when the current step is applied.

The data indicate that the energy dissipation is purely ohmic, corresponding to an ESR value of 0.7Ω.

In all experiments, the voltage is limited to the surge potential value (i.e., at 3V). The results are shown in Fig. 6a), in double-logarithmic scale. At a low time scale (i.e., for t<2s), the measured voltage is independent of time. For this specific time scale, the relation between the measured voltage and the applied current is linear, as shown in Fig. 6b). This corresponds to a ESR value of 0.7Ω, which is by a factor 7 higher than that obtained from the constant current discharge measurements, in Fig. 5 (i.e., ~98 mΩ). Since this cannot be correlated to the much lower electrical resistance value of the connecting leads (i.e., 2mΩ), the different ESR values obtained from charging and discharging experiments can only be understood in terms of charge transfer over a potential barrier at the interface between the metallic electrodes and the porous media. However, one should note that for t > 10s, *all* potential curves in Fig. 6a) fall on top of each other. This indicates that, at a large time scale, the charging mechanism is independent on the applied current value.

D. Open circuit voltage (OCV)

In Fig.7, we show the time decay of the open circuit voltage and the corresponding leakage currents, as measured on our supercapacitor. The leakage current values are between 40μA and 60 μA and show an overall slight decrease by 10% over which may be due to temperature drop overnight (i.e., for t > 8 hours), in the sense that the ionic conductivity of the electrolyte increases with increasing temperature, leading to increased leakage currents. From this point of view, it is, nevertheless, worth it to investigate the OCV behavior as a function of temperature.

We look now in more detail at the explicit time dependence of OCV from Fig. 7a). First we note that a fit to the data by using single exponential decay function leads to rather high residual values, whereas a function expressed as a sum of three exponentials is more than suffieicient to parametrize the dependence of OVC as a funcgtion of time. The best fit, however, is obtained by using the following expression:

$$OVC(t) = A_0 + A_1 e^{-t/\tau_1} + A_2 e^{-t/\tau_2} \qquad (7)$$

where A0 is the OVC value at t=0, A_1 and A_2 the amplitude of the exponential functions whose decay constants are given by τ1 and τ2, respectively. The results obtained from fits to data by using (7) are shown in Fig. 8.

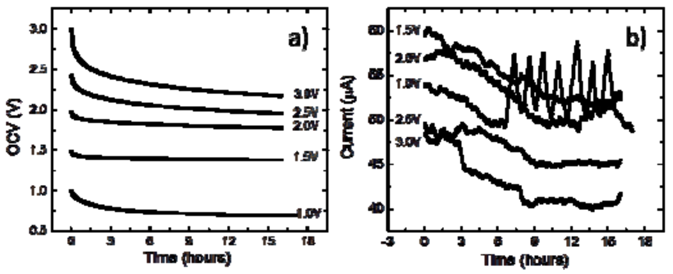

Fig. 7 The decay of the open circuit voltage (OCV) in a) and the corresponding leakage currents in b), as measured on a 10F/2.5V Suntan supercapacitor initially charged at the indicated potentials.

In Fig. 8a), the potential dependence of the exponential amplitudes indicates that the two exponentials in (7) have almost identical contributions to OCV. They also show a slight increase with increasing the charge voltage which is a typical feature observed in over-charged supercapacitors.

However, these contributions are well separated over the measurement time scale. This is shown in Fig. 8b), where the corresponding decay constants are different by one order of magnitude.

The fact that the OVC decay over time is described by two exponential functions with decay constants that differ by one order of magnitude is consistent with the presence of two distinct mechanisms associated to charge redistribution in our supercapacitor. At a large time scale (i.e., defined by τ_1, in Fig. 8b), the OVC decay may be related to the ionic transport in electrolyte, as is results from the leakage current drift to lower values in Fig. 7b), for $t > 8$ hours. At a microscopic scale, the correspondent for that is the rearrangement of the ionic species within the Helmoltz double layer that would results in space-charge fluctuations around an equilibrium value. This is, however, accompanied by charge transfer from electrolyte to the porous electrodes, whose kinetics is faster (i.e., given by τ_2, in Fig. 8b) since it is related to pure electronic species.

However, these contributions are well separated over the measurement time scale. This is shown in Fig. 8b), where the corresponding decay constants are different by one order of magnitude.

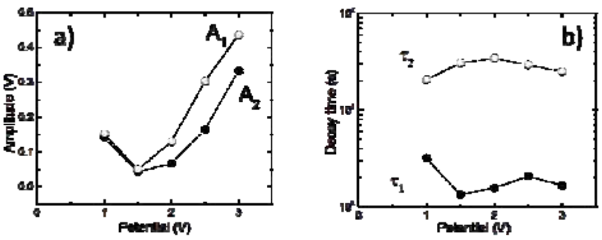

Fig. 8 Voltage dependence of the amplitude (in a) and the corresponding decay time (in b) obtained from fits to the OCV data by using the double exponential decay function (i.e., from 7)

4. Conclusions

In this paper, we present a detailed study on the fundamental properties of a 10F/2.5V Suntan supercapacitor. For that, we have made use of dedicated characterizations, such as I-V measurements, chronovoltametry, amperometry and open circuit voltage monitoring, for different charging and discharging cycles at various currents and voltages, respectively.

From I-V characterizations, we show that the explicit dependence of capacity as a function of the charging potential is linear. However, we have evidence that the Suntan supercapacitors 5% more energy upon the first charge cycle than during the subsequent ones. This may be related to some remnant charge that is resilient to a complete discharge of the supercapacitor. However, the obtained results are within the specification provided by manufacturer (i.e., 10F/2.5V) in their data sheet.

Chronoamperometry and chronovoltametry investigations indicate that the supercapacitor behaves differently upon charging and discharging at constant voltage and current, respectively.

The chronoamperometry indicate that the current decays rapidly upon applying a charging/discharging potential step. Here we show that the characteristic decay time of the measured current increases linearly with increasing potential, in a fashion given by the well know relation: $\tau = RC$, with C the potential dependent capacity determined from I-V measurements. On the other hand, the discharge potential determined by current interrupt method exhibit [6] a linear dependence on time. From that, we are able to determine the equivalent resistance value of (98.6±1.6) mΩ, which is in reasonable agreement with the ESR values reported for Suntan supercapacitors. However, the charging experiments at constant current show a different behavior for the measured voltage; i.e., the explicit dependence of the voltage as a function of time is somewhat reminiscent to an exponential growth, which is often observed in dielectric capacitors.

Finally, the open circuit voltage (OCV) decay monitored over a large period of time (i.e., up to 16 hours) reveals two competing mechanisms with characteristic decay constants that differ by one order of magnitude. They are associated to charge redistribution at the interface between the solution electrolyte and the porous media. At a large time scale, the drift of OVC to lower values is mediated by the kinetic transport of ionic species which may rearrange within the Helmolthz double layer. The overall charge transfer associated to that denotes the second factor responsible to the OVC decay, whose kinetics is faster. It is, however, worth it to look in some more detail at this feature since the supercapacitors are not especially suited for prolonged storage of energy, but for delivering it at fast rate (i.e., in transient operation mode).

REFERENCES

[1] P. Svasta, A. Vasile, C. Ionescu, V. Golumbeanu, “Condensatoare”, Cavallioti, Bucharest 2010;
[2] Lee Hee-Young s.a., “ Metal oxide electrode for supercapacitor and manufacturing method thereof” Pat SUA Nr.6339 528 B1, decl. 28Feb. 2000, publ. 15 Jan 2002;
[3] Conway, B. E. (1999). Electrochemical Supercapacitors: Scientific Fundamentals and Technological Applications. New York, Kluwer-Plenum;
[4] Burke, A. (2000). "Ultracapacitors: why, how, and where is the technology." Journal of Power Sources 91(1): 37-50.
[5] R. Kötz, S. Müller, M. Bärtschi, B. Schnyder, P. Dietrich, F. N. Büchi, A. Tsukada, G. G. Scherer, P. Rodatz, O. Garcia1, P. Barrade, V. Hermann, R. Gallay, “Supercapacitors for peak power demand in fuel-cell driven cars”
[6] F. Richer, C-A Schiller , N.Wagner, “Current interrupt technique measuring low impedances at high frequencies”, Electrochemical applications 2002

ISSN 1454 - 8003
Proceedings of 2014 International Conference of Hydraulics and Pneumatics - HERVEX
November 5 – 7, Calimanesti-Caciulata, Romania

REMOTE CONTROL OF A PNEUMATIC DEVICE

Mihai AVRAM[1], Victor CONSTANTIN[2]

[1] Politehnica University of Bucharest, mavram02@yahoo.com

[2]Politehnica University of Bucharest, victor_florin.constantin@yahoo.com

Abstract: *Pneumatic positioning systems have a series of advantages, especially when it comes to working in environments with a lot of noise, vibrations and especially with hazardous materials. Consequently, it is sometimes necessary to control them from a distance, or, as is the case with highly automated devices that only interact with the system periodically. Working with compressed air presents a series of natural advantages. Among these we can mention the large power/weight ratio of pneumatic actuators, easy and affordable install and maintenance as well as being clean working systems. However, due to working with compressed air, there are a series of issues, such as static and transient nonlinear behaviour, mostly due to the high compressibility of air. However, a lot can be done in terms of making the already-existing systems easier to control, as well as more user friendly. One way to do that is to allow for remote control of such systems. Since pneumatics are usually used for simple automation tasks, there is no need for permanent supervision. This paper presents such a low cost and easy to implement and maintain system. This system is also in line with the recent development of the Internet of Things.*

Keywords*: pneumatic, LabVIEW, Internet, GSM, DAQ, microcontroller, Internet of Things*

1. Introduction

The need for remote control of applications appears in the conditions of work in hazardous environments (high risk of explosion environments with hazardous chemical agents to humans, extreme temperatures). The economic aspect is also not to be ignored: such a system makes it possible to concentrate qualified personnel in one location so that a smaller team of people can manage multiple tasks simultaneously.

Among the main advantages of working with compressed air, are included: high power / weight ratio of this type of actuator, easy installation and maintenance and clean operation that is recommended to be used in sterile environments. This is due to the used working environment (usually air). Its use brings itself but after a number of disadvantages, which include strong nonlinear static and dynamic nature of the actuators and the compressibility of the working environment. In this way pneumatic often loses ground to electrical drives particularly from the perspective of their use in precision actuators.

The system is intended as a modular one, so that its purpose can be changed with minimal interference. The schematic diagram of the control system reflects this. Evolution of the system can be pursued through a video camera, all through software developed in LabVIEW software.

The system will allow modification of the functional parameters of the system locally (changing supply pressure and clamping force) and remotely (Internet or GSM) via a server-client architecture (changing the direction of rotation, the start / stop system , the angular velocity of the device), as well as monitoring specific parameters (supply pressure in the active chamber of the mechanical hand, the angle of rotation).

Control signals obtained from the computer will be transmitted through a data acquisition board or microcontroller board to a control circuit, which is the one that performs the actual control of the device.

The end result is intended to be a proper SCADA architecture, given that any operation can be stopped at any time and also, the system can be implemented over a very large number of stations.

ISSN 1454 - 8003
Proceedings of 2014 International Conference of Hydraulics and Pneumatics - HERVEX
November 5 – 7, Calimanesti-Caciulata, Romania

2. Schematic of the system

The hardware structure of the system is comprised of the following (figure 1):

- Server PC – The application is responsible for sending and receiving signals to and from the data acquisition board, as well as capturing and sending images to a client PC, through a FTP client;
- Client PC – This application is responsible for receiving and preseting the data to a user, as well as transmitting the user's input towards the Server PC and onto the controlled system;
- DAQ board or microcontroller board – used to interface the Server PC with the system that is being monitored;
- USB Webcam – Offers video feedback from the system. The camera is mounted on a X-Y system actuated using Servo RC motors;
- Controlled system – As an example, the system is a pneumatic gripper, along with a three phase pneumatic stepper.

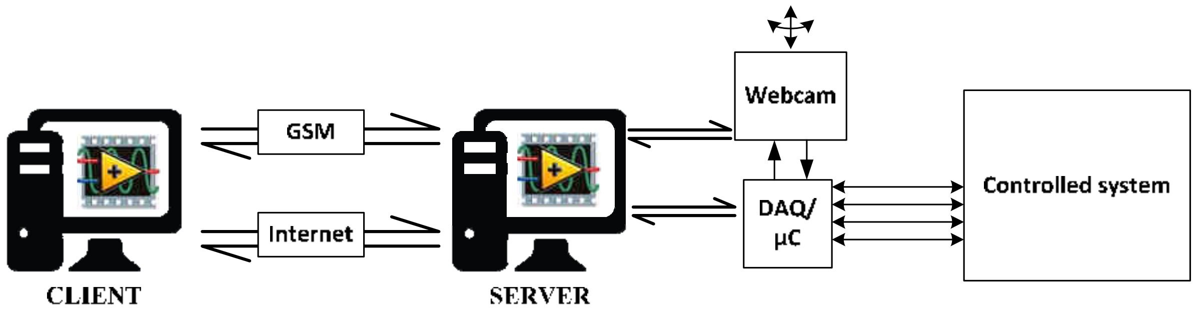

Figure 1 – Basic schematic of the system

The system works by allowing a remote user to connect to the server system by means of the TCP/IP protocol. The virtual instrument implemented on both server and client side is created using LabVIEW. The server PC can be connected to either a data acquisition board or a microcontroller break-out board (such as Arduino, Microchip's Explorer board, etc). For this paper, the system is implemented using a Arduino board. This was selected in order to keep the overall cost of the system low[3]. The system also allows for backup usage of the GSM protocol. This is to be used only if there are issues with the Server PC. Since the GSM module is connected directly to the microcontroller board, it will circumvent any issues that might occur at PC level.

3. Working principle of the monitored system

The device chosen to exemplify a possible use for this system is a pneumatic gripper[1] attached to the shaft of a pneumatic three phase stepper motor. The basic schematic of this system is presented in figure 2.

At the base of pneumatic stepper motor sits a cam mechanism, which, unlike the classic case of the movement, the cam drives the cam follower and not vice versa. The cam is formed by a succession of identical portions of ascent-descent, so that it has the form of a gear. The system involves the use of two or more tappets, one of which is always indexed. The cams are actually the rods of the pneumatic cylinders.

The system, as cam be observed in figure 2 is comprised of the following elements:

- Gripper mechanism – contains the piston, cam and tappets used to actuate the gripper. As can be observed, once pressure is removed from the gripper, the fingers are brought back into position by a spring;
- Rotary coupling, used to deliver air to the gripper;
- Stepper motor.

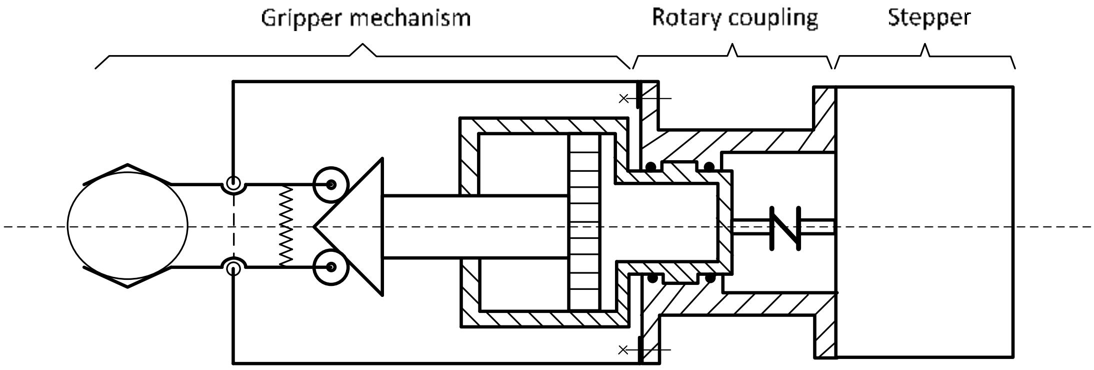

Figura 2 – Pneumatic gripper basic schematic

The control system is composed of 4 5/2 pneumatic way valves, three (D1, D2 and D3) to control the 3 roller cam that compose the pneumatic stepper motor and one (DP) way valve for the gripper. The system is fitted with a pressure switch P confirming that the pressure inside the gripper's piston chamber is high enough to actuate it. Schematic diagram is shown in Figure 3.

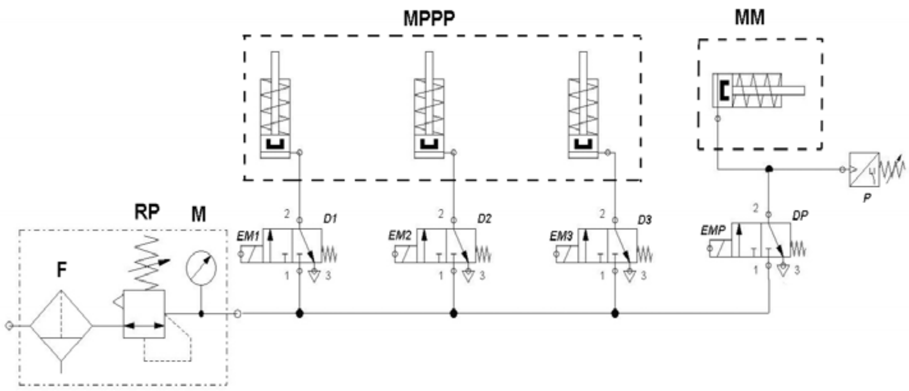

Figure 3 – Basic schematic of the device

Driving the electromagnets included with the way valves is done by using a general purpose Darlington driver, the ULN2803A, along with optocouplers used to protect the microcontroller board.

4. Working principle of the monitoring system

The system works in client-server mode, where the server is continuously connected to the monitored system and issuing commands to it. Also, the server controls a two servo RC motor mechanism that allows a webcam to be directed at different parts of the monitored system. When a client connects to the server, it is given, based on the monitored system, options to issue commands to the said device. The client is fed snapshots from the device through a known port of a FTP server.

Also, in parralel with Internet mode, the system works in GSM mode, where text messages can be sent to the device from a mobile device allowing the device to be controlled, or stopped in case of connectivity loss. Also, the device can be configured to send updates through the SMS service to a specified number at certain intervals of time. Figure 4 shows the breadboarded view of the circuit. A read-made GSM module has been used for this function. A note could be made in that the GSM module also allows data connection through the GPRS protocol that could be used as another backup for faster connectivity to the system. A breadboarded view of the system is presented in figure 4.

The front panel of the client application built to run the system is shown in figure 5. As can be observed it has controls adapted to the device that needs to be monitored, as well as a video window that shows the latest image received from the client. The system adapts itself to lower transfer speeds and only shows the latest image received.

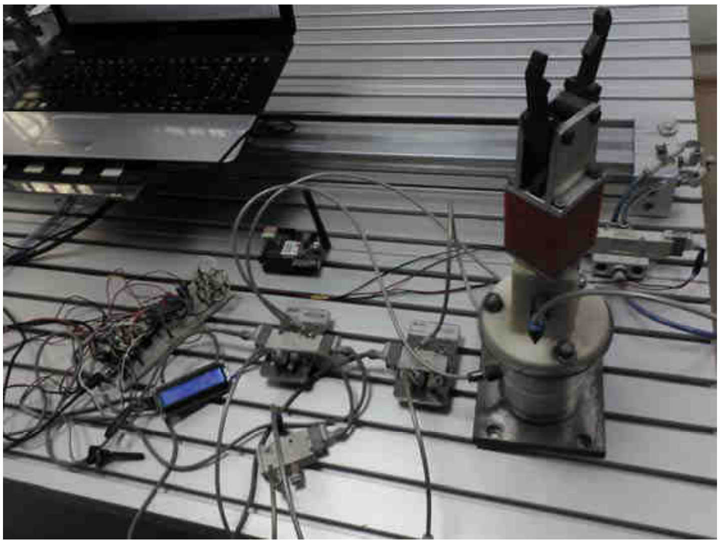

Figure 4 – Breadboarded view of the system

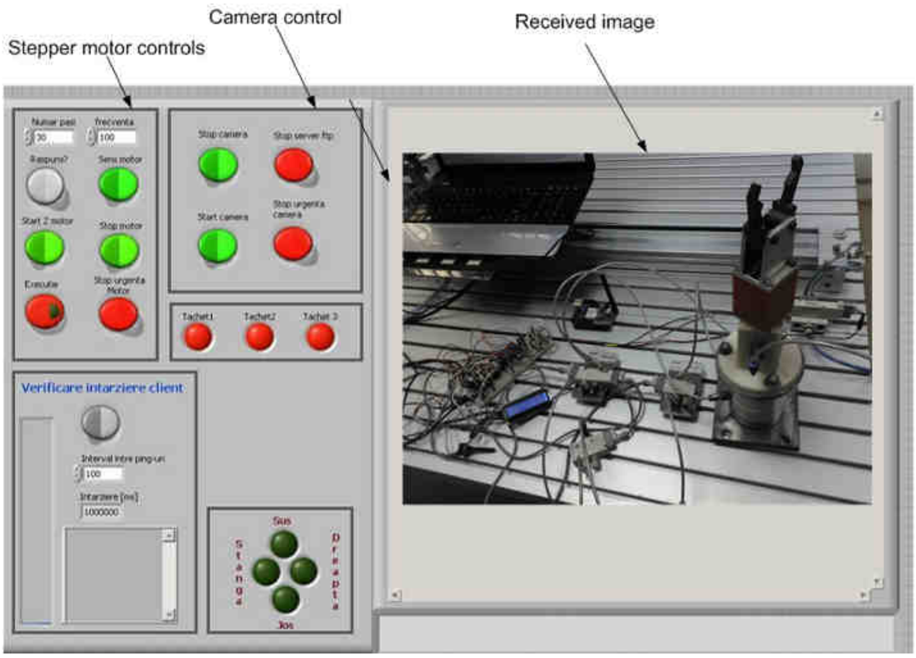

Figure 5– Client side application front panel

Figure 6 shows the server-side screen of the application. This allows for the device to be controlled from the server's side, as well as the client. However, the server's commands will cancel out the latest command received from the client. This application also shows the latest image grabbed from the camera. Depending on the response time from the client, only a certain number of images will be transferred, to reduce delay. Also, if connectivity from the client is lost without confirmation of connection closure, the system will automatically switch to GSM mode and call a preprogrammed number in order to ask for further commands.

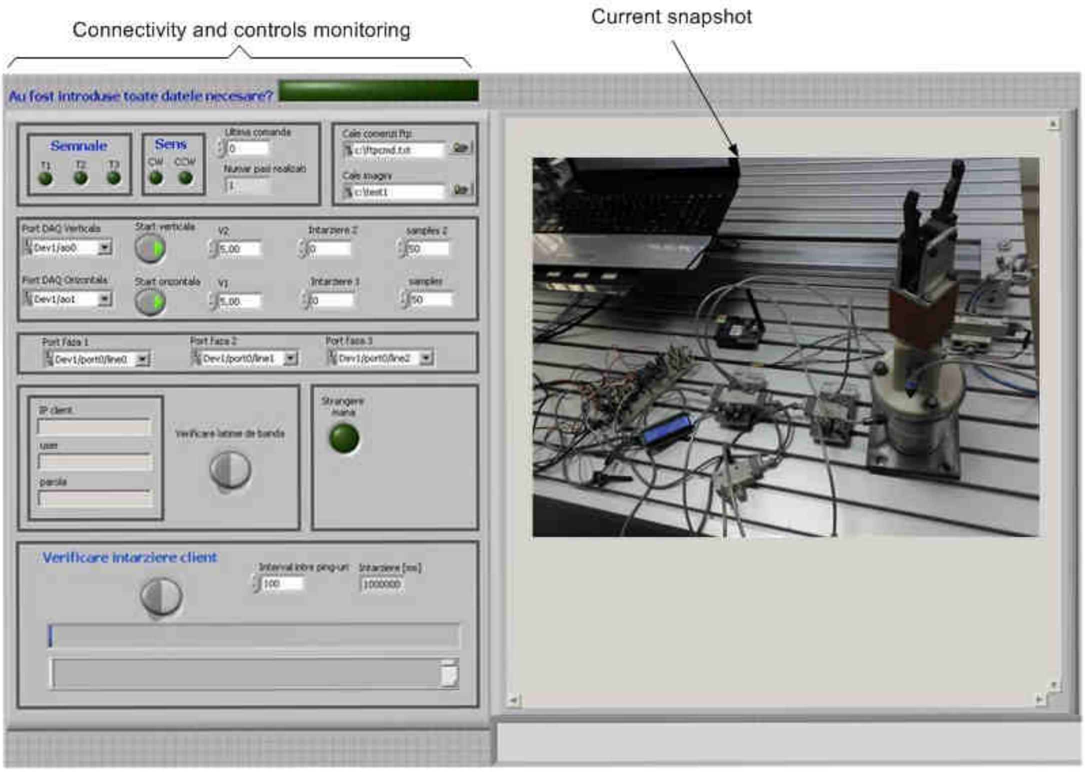

Figure 6 – Server side application front panel

5. Conclusions

The proposed system has been tested and has proven to work as intended. Due to its modular characteristics it can be easily adapted to most devices or systems and can be extended to cover many such devices. Also, through its dual Internet and GSM connectivity, the system has much great redundancy at a much lower cost than that of commercial systems.

The work falls in line with the recent trend of including devices in general purpose networks, or what is commonly known as the Internet of Things. The system can be extended to work with other software, such as Matlab's Simulink, and could allow for further use as a conduit in hardware in the loop systems.

REFERENCES

[1] Traian, DEMIAN, Valeriu, BANU, Micromotoare pneumatice liniare si rotative, Editura Tehnica, Bucuresti, 1984.
[2] Janos Gyeviki, Jozsef Sarosi, LabVIEW based position control for a pneumatic cylinder, ANNALS OF FACULTY ENGINEERING HUNEDOARA – INTERNATIONAL JOURNAL OF ENGINEERING. Tome VIII (Year 2010). Fascicule 1 (ISSN 1584 – 2665)
[3] Banzi, M. (n.d.). Getting started with Arduino. 1st ed.
[4] Mike, MEYERS, Manualul Network+ pentru administrarea si depanarea retelelor, Editura Rosetti Educational, Bucuresti, 2006
[5] CCNA Exploration 4.0 1,2,3,4, Cisco Systems, Inc.
[6] Radulescu, Tudor, QoS in retelele IP multimedia, Editura Albastra, 2008

ISSN 1454 - 8003
Proceedings of 2014 International Conference of Hydraulics and Pneumatics - HERVEX
November 5 – 7, Calimanesti-Caciulata, Romania

ALTERNATIVE FLOW DRIVEN HYDRAULIC BIPHASIC ROTARY MOTOR

Lucian MARCU[1], Daniel BANYAI[2]

[1] Technical University of Cluj-Napoca, Lucian.Marcu@termo.utcluj.ro

[2] Technical University of Cluj-Napoca

Abstract: *The paper presents a concept of hydraulic alternative flow driven biphasic rotary motor, designed using the principles of alternative flows transmissions combined with gear reducers. The functioning of the converter are based on the bidirectional displacement of a predefined volume of hydraulic oil through the connection pipes between the alternating flow and pressure energy generator and the motor. The rotation motion of the main shaft is obtained from the pistons translation movements using a series of drawn cup roller clutches and gears.*

Keywords*: alternative flow, hydraulic motor.*

1. General aspects regarding hydraulic alternative flow driven systems

Along the time was developed a series of rotary hydraulic motors providing great stability of movement in a wide range of variation of the output values (from 1 to 3000 rev/min) and a good ratio between active torque and moment of inertia. Also, in the case of heavy loads at low speed, was designed "slow" running motors that work stable at low speeds and provide high torque. [1], [3]

The conventional solutions of hydraulic systems imply a unidirectional flow of the fluid through pipes between the energy converters, hydraulic pumps and motors (actuators).

The hydraulic transmission using alternating flows is based on the bidirectional displacement of a predefined (finite) volume of hydraulic oil through the connection pipes between a hydraulic generator and a hydraulic motor. [4]

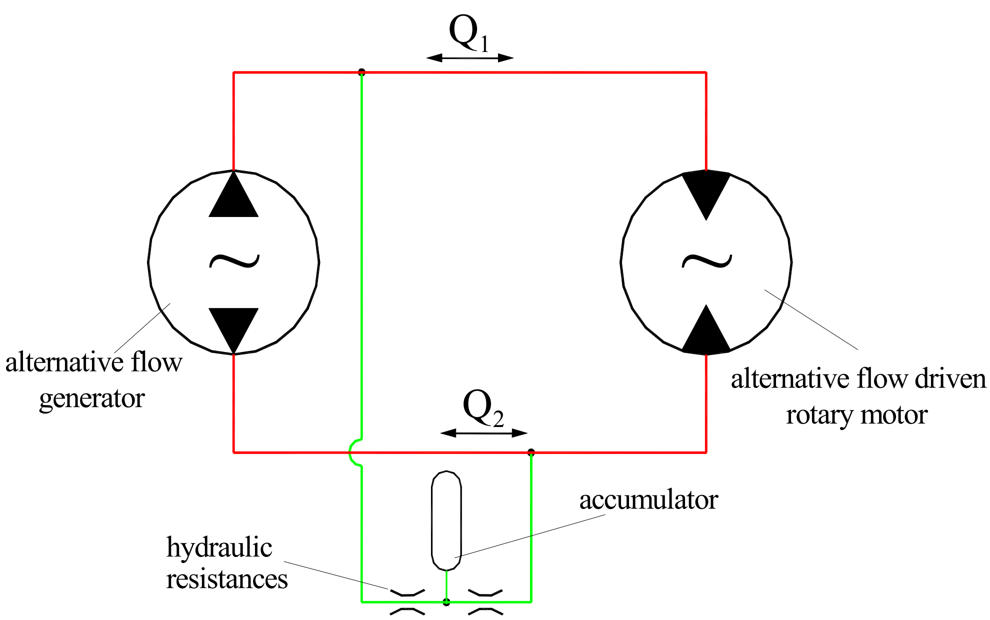

Figure 1. Functioning schema of the alternative flow driven hydraulic transmission

An alternating flow driven hydraulic transmission, as figure 1 shows, consists in a alternating flows and pressures generator and a motor, the connection between them being realized with a number of pipes equal with the number of phases, the pipes being filled with fluid at a certain (pre-established) pressure. During the functioning of the system the pressure and the flow within each pipe varies in a sinusoidal way, around an average value.

In order to have a proper functioning it is compulsory that this average pressure from each pipe to have the same value and to have a constant value in time. Therefore, to obtain the correct functionality we create from the beginning either a pressure in each phase, higher than the amplitude maximum value, or this pressure is modifying itself during the functioning.

This result is obtained by using both a series of hydraulic resistances rigorously calculated which interconnect all the phases and a hydraulic accumulator connected to them in a single point.

The resistances must eliminate the maximum average pressure rising value in one second when the diminution of the flow amplitude from a phase does not exceeds 1%. [5]

The accumulator presence makes the pressure in a connection to be all the time approximately constant, it being able to take over the oil surplus from the dilatations and in the same time to complete the eventually oil loses.

2. The construction of the hydraulic alternative flow driven biphasic rotary motor

In figure 2 is presented the principle schema of the hydraulic alternative flow driven rotary motor, in which the main components are: 1 and 5 - gear rack conversion mechanism, 2 - drawn cup roller clutch, 4 - output shaft and 3 - gear transmission. [4]

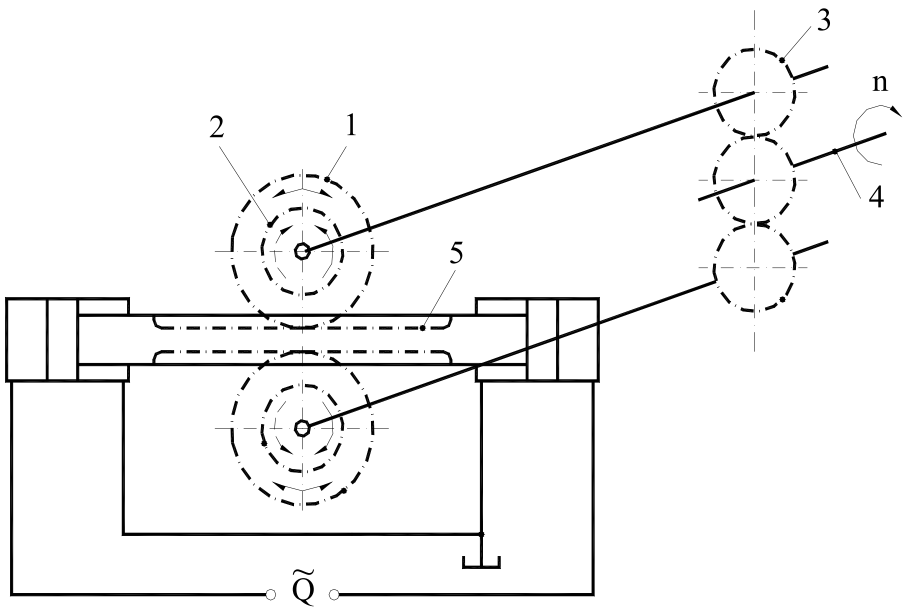

Figure 2. Functioning schema of the alternative flow driven hydraulic converter [4]

According with the functioning schema presented in figure 1, combined with mechanical and CAD principles and development facilities [2], was designed a prototype of an biphasic alternative flow driven hydraulic rotary motor, figures 3, 4 and 5, which provide a continuously torque conversion in a wide range of values, depending on the alternative flow provided by an specific generator.

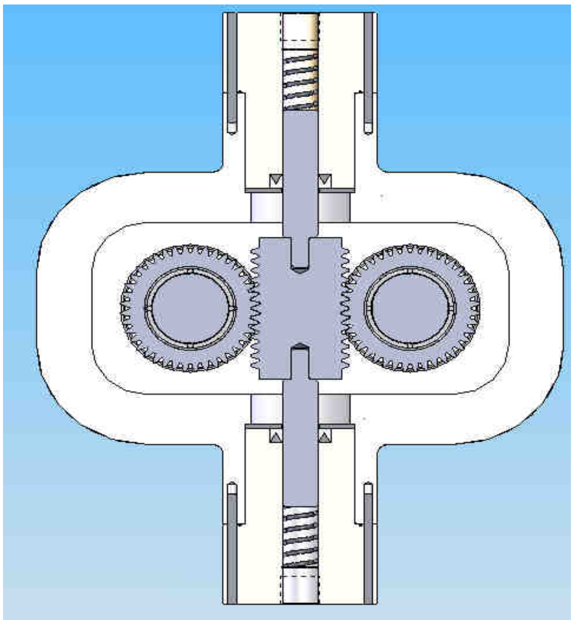

Figure 3. The conversion mechanism of the alternative flow driven hydraulic motor

In the hydraulic motor shown in Figure 3 the harmonic motion of the rack, produced by the two-phase flow supplied by the generator, drived by phase pistons, is converted in rotational motion due to the one-way clutches antagonist acting on the gears.

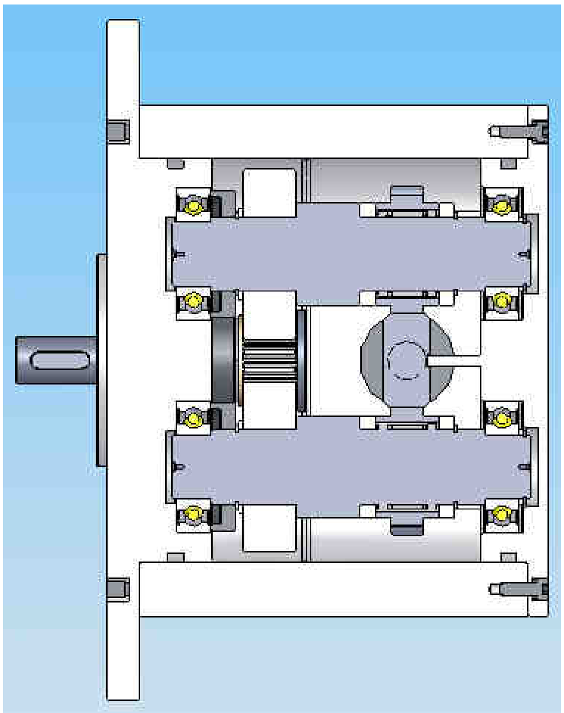

Figure 4. Gear transmission of the alternative flow driven hydraulic converter

The rack meshing with two wheels mounted on the two one-way clutches, so as to allow rotation of the output shaft in the same direction. The output shaft will rotate continuously due to the unidirectional movement of the two intermediary shafts, transmitted by the cylindrical gears, as figures 4 and 5 shows.

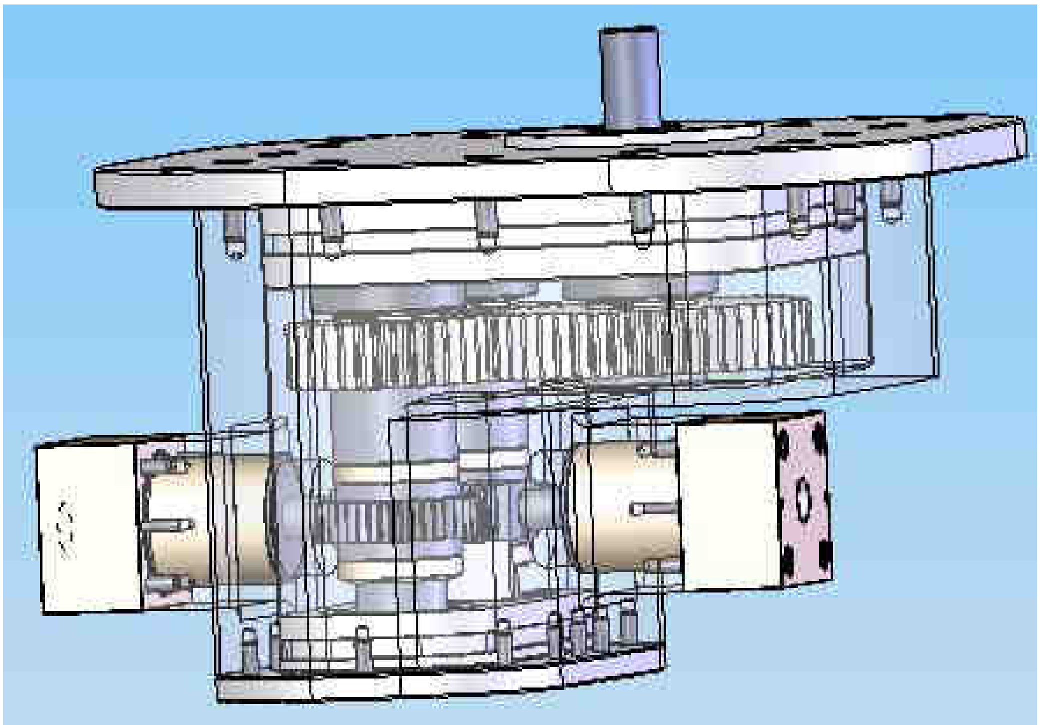

Figure 5. Three-dimensional representation of alternative flow driven hydraulic converter

3. Conclusions

The use of small linear hydraulic motor is possible only in association with devices for converting the oscillation movement of the pistons into a rotary motion of a shaft, and coupling of this is usually required for transmitting the wheel movement to the output shaft.

If is considered a hydraulic system in which every working volume of an alternating motor is connected independently, by a phase pipe, with the corresponding working volume of an generator, then any modification of the volume of the generator will produce an alternative flow and pressure transmitted along the phase line to the motor.

The pressure amplitude in each phase is dependent of flow amplitude needed by the motor as of other factors like: the liquid elasticity from a phase, the liquid inertia from that phase, the hydraulic loses between motor and generator, the motor load.

REFERENCES

[1] Banyai, D., Vaida, L., Năşcuţiu, L., Opruţa, D., Giurgea, C., Marcu, I.L., "Synoptic view of the latest trends in hydraulic actuation", Buletinul Institutului Politehnic din Iași, Tom. LVI (LX), Fasc.1, Secția Construcţii de Maşini, 2010, ISSN 1011-2855, pp.148-155.
[2] Curta, R.T., Steopan, M., "New Feature Based Design Software Development", 2012 IEEE International Conference on Automation, Quality and Testing, Robotics (AQTR 2012), May 2012, Cluj-Napoca, Romania, ISBN 978-1-4673-0703-1.
[3] Grama, L., Banyai, D., Vaida, L. "Experimental testing of a low speed hydraulic motor with axial pistons", Hidraulica Magazine, No. 3, 2013, ISSN 2343 – 7707, pp. 64-73.
[4] Pop, I., "Sonic theory treatise" (in romanian), Performantica Publishing House, Iasi, 2006.
[5] Saceanu, V. "In improvements in the functioning of the state-of-the-art multiphase sonic transmissions, by using hydraulic resistances between the phases as well as hydraulic accumulators", Scientific bulletin of the "Politehnica" University of Timisoara, Transaction of Mechanics, Tom 49 (63), Special Issue, October 2004, ISSN 1224-6077, pp. 531-536.

ISSN 1454 - 8003
Proceedings of 2014 International Conference of Hydraulics and Pneumatics - HERVEX
November 5 – 7, Calimanesti-Caciulata, Romania

AN OVERVIEW OF NOVEL DESIGNS FOR HYDRAULIC PISTON UNITS

Katharina Schrank, Dirk Schulze Schencking, Christian Schleihs, Hubertus Murrenhoff

RWTH Aachen University, Institute for Fluid Power Drives and Controls, Germany,
post@ifas.rwth-aachen.de

Abstract: *In fluid power systems, displacement units are the key component for a continuous operation. Depending on the requirements of the application different designs have been developed so far each having design dependent advantages but also restrictions in operation. The applicability and efficiency of the components highly depend on their working principle as it determines the location and type of energy losses as well as the operation range.*

In this paper, the design and operating principle of the most commonly used hydraulic displacement unit, the axial piston machine is discussed and difficulties are pointed out. Starting from this, an overview of optimization approaches for this pump design is given. Finally, two new designs for piston pumps are introduced and feasible operating ranges and efficiencies of the new designs are discussed. This is essential for future industrial developments regarding new components.

Keywords*: piston units, innovative pump designs, optimization of axial piston units, tribological contacts*

1. Introduction

Fluid power systems are widely used in applications where a high power density is needed as for example in mobile machinery like excavators or cranes or in stationary industries such as in a forming press. In fluid power systems the power is transferred by a pressure fluid, often mineral based oil. This pressure fluid is additionally used to remove heat from the components and to lubricate the system. Besides a high power density and good lubricity the use of hydraulic systems has more advantages. The controllability of the system is good as well as the simply implementable overload protection with hydraulically operating pressure relief valves. In addition, fluid power can be easily used to realize linear movements with robust cylinders.

The main goal of hydraulic systems is the transmission of power from a power generating machine like for example an internal combustion engine to a work performing user like the cylinders in an excavator. Mostly, the power is provided rotationally by a rotating shaft. This movement has to be converted into hydraulic power with the help of a displacement pump. The power is then transmitted with the help of the fluid via pipes and tubes. The power transmission can be controlled by the pump in primary controlled systems, by valves or other resistors in conductive controlled systems or by the motor in secondary controlled systems. Depending on the design of the system different requirements arise for the displacement unit. In secondary controlled systems the motor has to be adjustable in order to control the system.

Because of the important role of displacement units in hydraulic systems, different working principles have been developed so far and some effort has been conducted to improve them. The different displacement units can be classified by the displacement principle into piston units, gear and vane machines. Piston units can further be subdivided into axial piston machines with a wobble plate, a swash plate or bend-axis design. Radial piston machines can be designed with internal or external support or as inline-piston machines. Gear machines can be realized as internal or external gear machines or orbit motors. Radial piston and vane machines can also be designed as single stroke or multiple stroke units. An overview of the different working principles as well as their advantages and disadvantages can be found in [1] and [2].

2. Design of Standard Axial Piston Units

The most often used displacement units in high performance operations at middle and high pressures are swash plate machines because of their good and fast adjustability and large operation range. The main characteristic feature of a swash plate pump is the power feed through. The cylinder block is directly connected to the driving shaft. The pistons move inside the cylinder block linearly and are supported by slippers on the stationary swash plate. A lift-off of the slippers from the swash plate has to be prevented by slipper hold-down devices or by springs in the piston chamber. The angle of the swash plate can be fixed or adjustable so that units with a fixed or variable displacement volume can be realized. The layout of this unit can be found schematically in Figure 1.

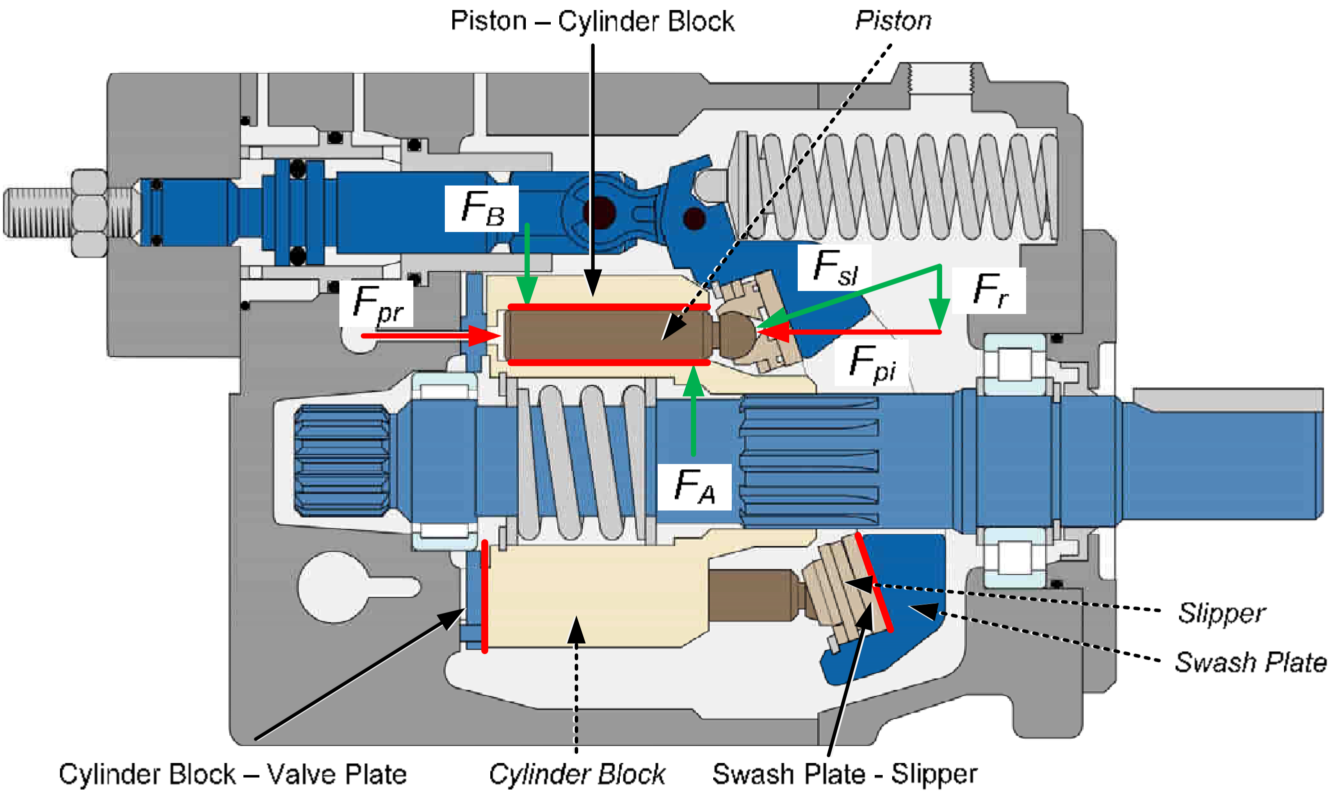

Figure 1 Schematic design of a swash plate machine including forces and tribological contacts [Parker]

Due to the relative movement between piston and cylinder block, the pistons suck fluid from the low pressure side inside the displacement chambers during half of the rotation. During the second rotation half the fluid is pressed into the high pressure line. The delivery volumes of each piston chamber superpose to an overall flow rate. The pulsation of this flow rate therefore depends on the number of pistons. Mostly units with seven or nine pistons are used. The reversing process is commonly realized by the use of a stationary valve plate on the back of the cylinder block.

Caused by the design of swash plate units lateral forces are acting on the pistons. The force based on the pressure of the fluid F_{pr}, that acts on the piston, points in direction of the piston's axis. On the back side of the piston the sliding contact between slipper and swash plate can only support forces normal to the surface F_{sl}. The resulting force F_r is therefore acting on the piston and has to be countered by the two forces F_A and F_B. These transversal forces lead to high stresses in the piston guide. Especially with large swivel angles and low rotation speeds the piston's lubrication condition deteriorates. In addition to this tribological contact between piston and cylinder block, two other contacts are of interest in swash plate machines. As a result of the cylinder block rotation and the stationary valve plate this contact is relevant as well as the contact between the stationary swash plate and the moving slippers. These contacts are lubricated by the pressure fluid that has to be delivered by the pump. Therefore when the lubricating film is too thick, too much leakage is produced in the unit resulting in a low volumetric efficiency. Vice versa, when the lubricating film is too low, solid-body contact can result, inducing friction and leading to low hydro-mechanical efficiency. The overall efficiency is the product of volumetric efficiency and hydro-mechanical efficiency and in consequence these contacts are the key features for efficiency improvements in swash plate units.

3. Optimization of Piston Units

As shown before, three main tribological contacts exist that affect the operating performance and efficiency of swash plate axial piston units. When regarding the contact between piston and cylinder block in detail, different features for optimization can be found for the described working principle. On the one hand the lubricating film depends on the contour of the piston, respectively the contour of the bore inside the cylinder block. On the other hand it depends on the material of the two components. Some research has been done dealing with optimizing the contours, the use of new materials or coating of pistons and bushings to improve overall efficiency [3], [4], [5].

The optimization of the geometry of piston and bushing, concerning i.e. gap width, contour and cylinder length was investigated in [3] by the use of a new three dimensional simulation program. The code solves the Reynolds Equation in the lubricating film and results in information about the film thickness and pressure distribution. Therewith the range of solid-body contact and fully developed lubrication film is calculated, resulting in knowledge of friction forces, volumetric and mechanical losses and overall efficiency. Figure 2 shows the total losses as a function of guidance length and gap height of over 250 single simulation runs.

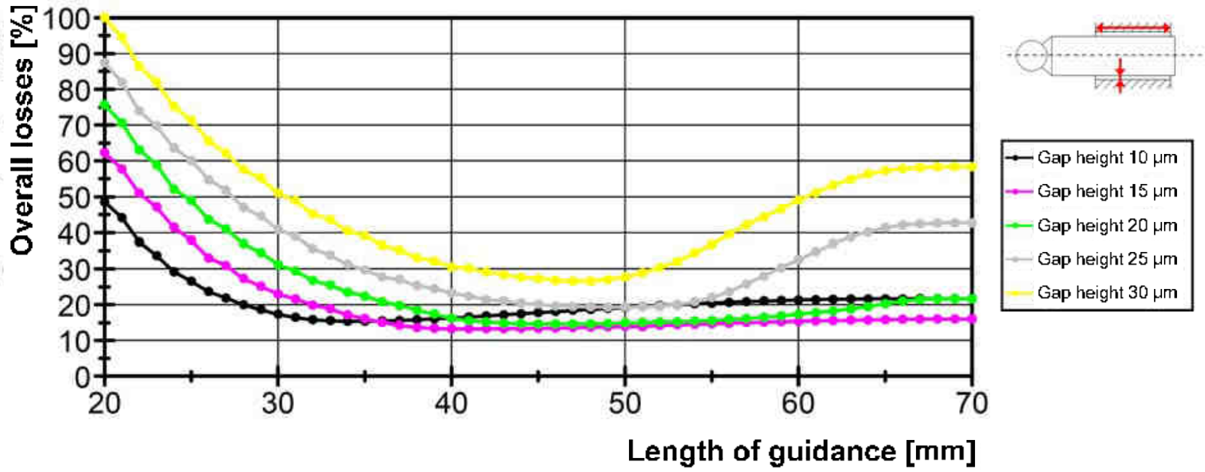

Figure 2 Simulated losses dependent on the length of guidance and gap height [3]

The total losses combine the losses due to axial and tangential friction as well as to leakage. Friction forces are small when mixed friction does not occur. Therefore the length of guidance of the piston should have a reasonable length, since the overall losses decrease by increasing guidance length. By further increasing this length the losses increase again as the area where viscous friction appears enlarges. For higher gap width the leakage losses increase resulting in higher total losses. From Figure 2 it can be seen that the losses can be drastically reduced by choosing the optimal length of guidance and gap height.

In addition, the front contour of the cylinder has an influence on the losses. In Figure 3 the simulation results of the front contour variation with the parameters contour length and radius are shown. Basis for these simulations was the optimized guidance length and gap height from Figure 2. The overall losses are shown in relation to the maximum of the total losses from Figure 2.

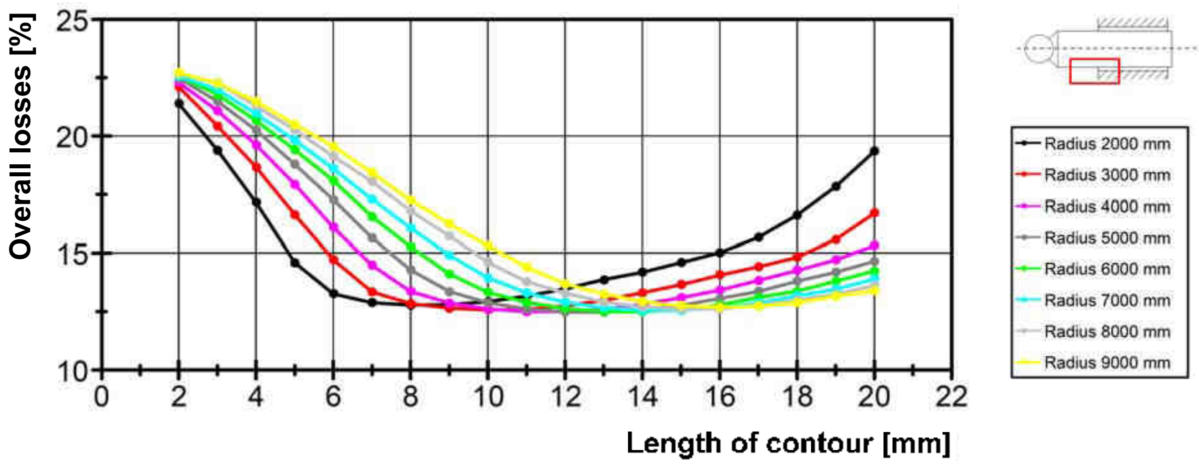

Figure 3 Simulated losses dependent on length and radius of front contour of the cylinder [3]

The front contour has a large influence on friction losses as well as on leakage losses. A small radius leads to an increase in leakage losses such as an increase in the contour length. To decrease axial and tangential friction forces an optimum between the radius and the length of the contour can be found. Nevertheless, the optimization of the front contour only achieves a fraction of the improvements obtained by the guidance length and gap height optimization. [3]

In [4] measurements of a pump with standard components and a pump with optimized components are performed. The pump with standard components consists of steel pistons that are guided in brass bushings. Standard cylinder roller bearings are used. The pistons of the improved combination are made out of 31CrMoV9 steel and are coated with zirconium carbide ZrC_g. The cylinder block does not contain bushings and is made from Ck45 steel. Coated roller bearings are used. The measured overall efficiency is shown in Figure 4 for the two configurations.

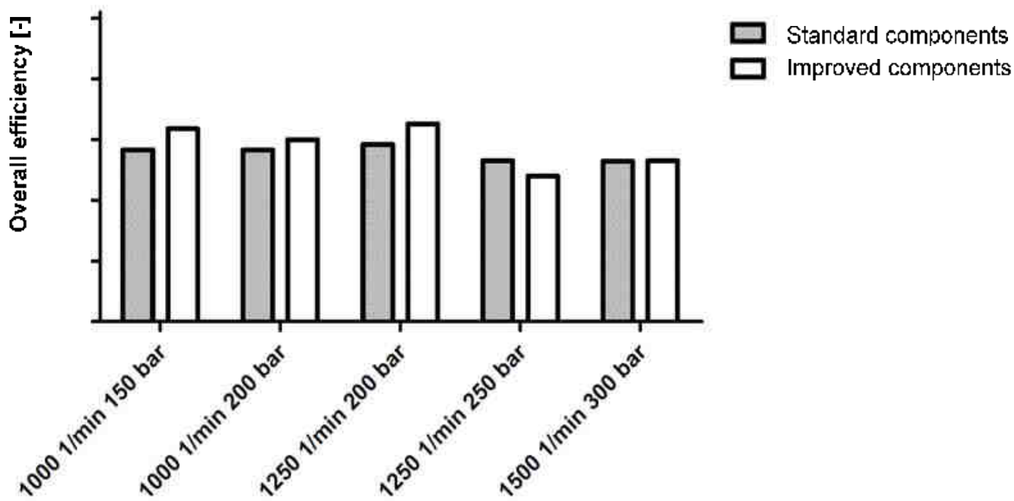

Figure 4 Overall efficiency measured with standard components and improved materials [4]

It can be seen that the overall efficiency increases with the improvements in material combinations. The volumetric efficiency was found to be constant between the two configurations. Therefore it can be said that the improvements are directly linked to an improved hydro-mechanical efficiency due to the materials used. This is also confirmed by the decrease of improvement at higher rotational speeds.

In addition to the efforts to optimize the tribological contact between piston and cylinder block, research is dealing with the contact between valve plate and cylinder block. In [5] a simplified simulation model based on the Reynolds equation to simulate the lubricating film is presented. Here, the hydrostatic pressure of the lubricating film, the gap height, the hydrodynamic pressure build up as well as solid and viscous friction are calculated. In typically used swash plate units, the contact between cylinder block and valve plate is compensated between 80 and 95% of the acting forces. This results in solid friction at low rotational speed because the hydrodynamic pressure is not build up yet. At higher speeds the contact reaches its fully compensated stage. In Figure 5 the simulated friction torque is shown for two different simulation set-ups, one with a compensation of 80% and one with a compensation of 99%. The total friction is calculated as the sum of viscous and solid friction torques.

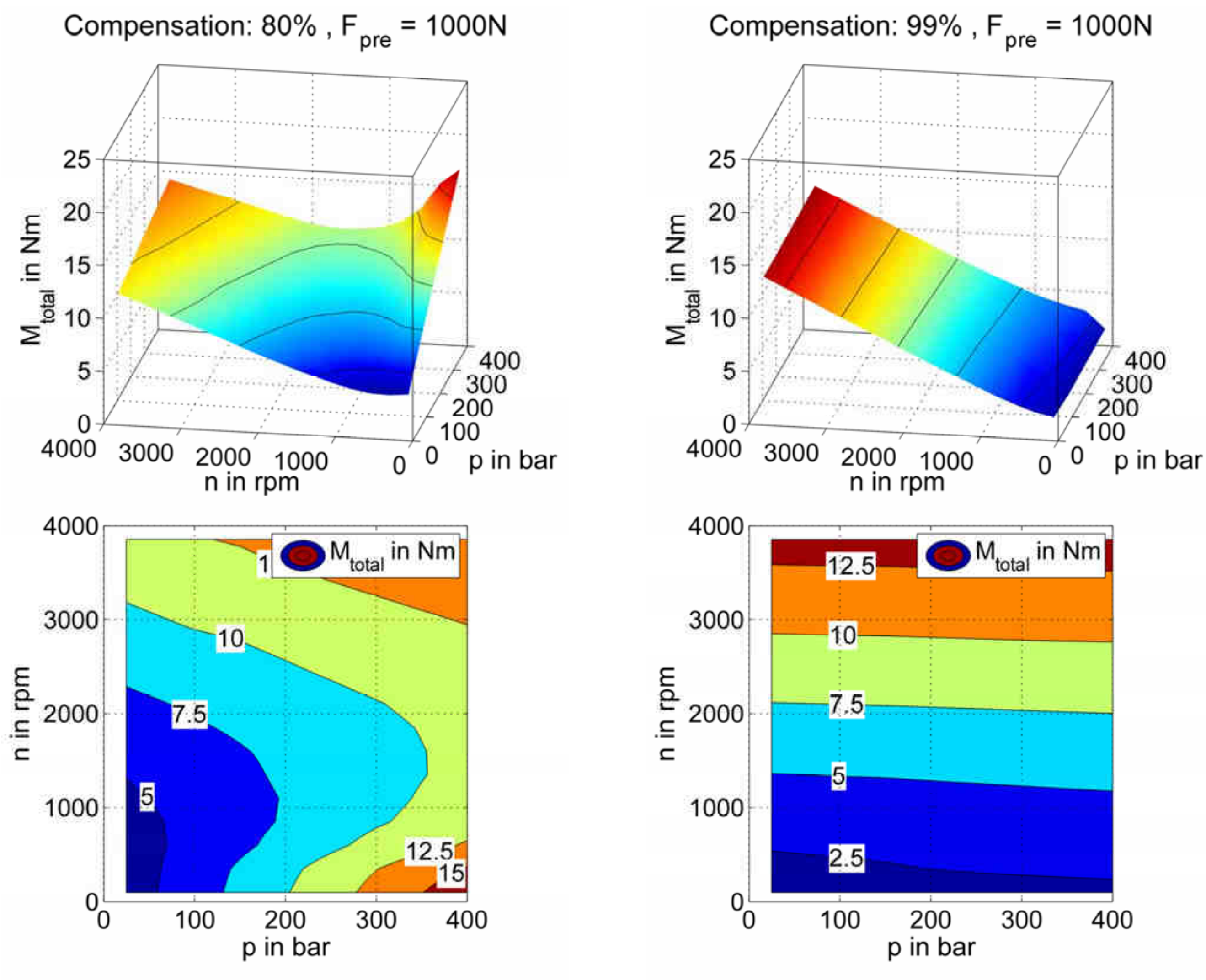

Figure 5 Simulated friction of the cylinder block – valve plate contact [5]

With a lower compensation level the stribeck curve is seen and solid body contact occurs at lower rotational speeds. Therefore the use of components parameterized in this way would not be possible for the use in high pressure applications at low speed. In contrast the compensation of

99% shows high viscous friction torques at high rotational speeds. In addition to the compensation, the influence of the pretension can also be investigated. Therefore it is possible to find an optimum between compensation and pretension dependent on the application.

4. New Designs of Piston Units

In the past decades a lot of optimization efforts have focused on specific effects as mentioned before, but only a few new innovative concepts have been elaborated. Two promising concepts are presented in this chapter.

In the field of radial piston units a machine with two axial spherical valve plates called RAC has been invented by Dr. Berbuer in Aachen, Germany. The most obvious difference to standard radial piston units is the pair of spherical valve plates that substitute the common control journal. The axial valve plates provide large flow channels, an ample passage for the drive shaft, and a power feed trough. A cross section of the whole unit is depicted on the right side of Figure 6 with a close up of the rotational group on the left.

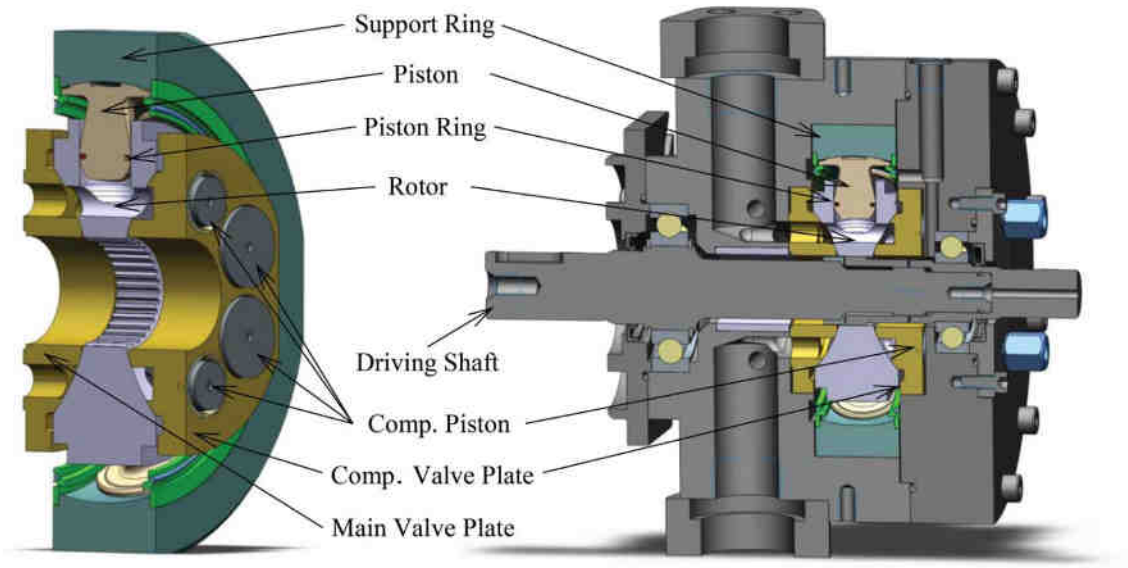

Figure 6 Design of the RAC [6]

Due to the spherical shape of the valve plates the rotor is supported in axial as well as in radial direction. This enables a complete hydrostatic bearing of the rotor. To ensure a tight gap between the valve plates and the rotor the plate's functions are separated. The main valve plate is responsible for commutation and is fixed in the housing. To adjust the gap height between rotor and valve plates a compensation plate with an axial degree of freedom is applied. On the rear side of this plate eight compensation pistons are integrated. Four of them are connected to high and four to low pressure. Therewith the compensation pistons can counterbalance the pressure forces acting on the contact zone between rotor and plates. With this setup the driving shaft and also the bearings are decoupled from hydraulic loads. A further advantage of avoiding a control journal are the enlarged flow cross section for fluid through the large valve plate kidneys with the result of decreased pressure losses and higher suction flow.

Another main difference to common radial piston units are the one piece tilted pistons and the special sealing technology. Figure 7 illustrates the principle of direct torque generation due to an unbalanced pressure area inside of the piston chamber.

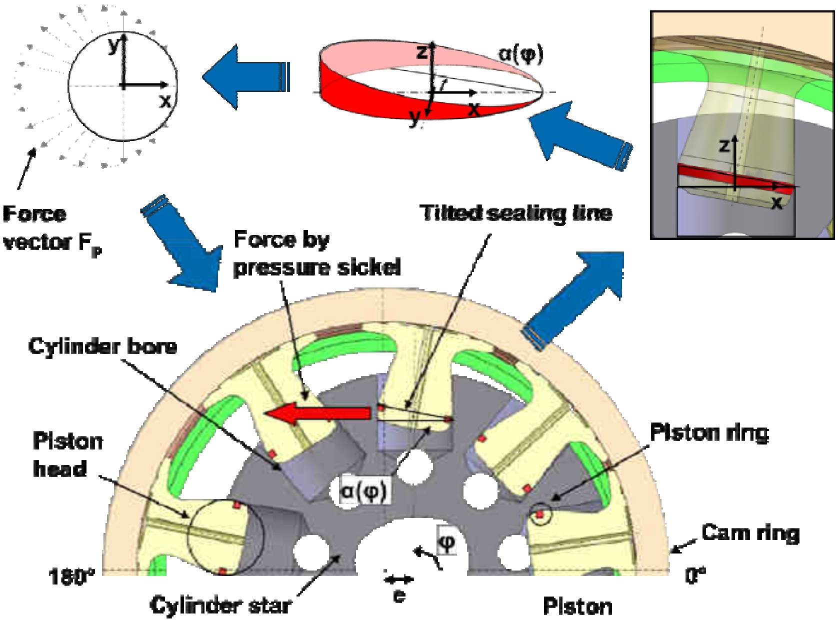

Figure 7 Direct torque generation of the RAC

While rotating the shaft, the pistons need to tilt in the bore to balance the eccentricity. Therewith a wedge shaped segment arises delimited by the tilted sealing line of the piston ring and the cylindrical segment of the remaining chamber. Pressure is applied to the surface of the resulting wedge which leads to an asymmetric force vector field. The total amount of forces is unequal to zero and directed in tangential direction. This force generated by the pressure sickle induces the torque directly to the rotor while avoiding transversal forces on the piston. Therewith hydro-mechanical losses are lower and independent of pressure and rotational speed. To reduce the mixed friction especially in low speed application the piston has a fully compensated slipper. In difference to common units the degree of relief is considerably larger than one. As shown in Figure 8 the slipper forces F_S are larger than the piston forces F_P. To prevent the piston to lift off the support ring and causing huge leackage a laminar resistor is installed inside the piston body.

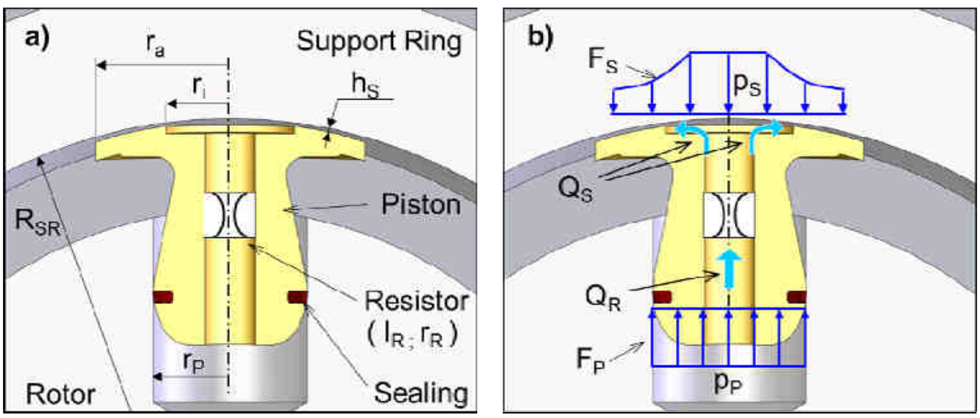

Figure 8 Detailed view of the pistons including their compensation [6]

The combination of the spherical valve plates and the tilting pistons with a fully hydrostatically compensated piston slipper results in an entirely hydrostatically supported rotational group. This predestines the RAC for motor mode and also for use with poorly lubricating fluids. In addition to motor mode it is also applicable for pump mode operation. Advantageous is also the limited number of parts which will result in lower production costs.

Another unit that has been invented during the last decade is the Floating Cup (FC) developed by Dr. Achten, INNAS BV, Netherlands. The principle of the FC is based on an axial piston unit but the kinematic concept is inverted. As can be seen in Figure 9 the pistons are joined with the rotor. To enable the elliptical track of piston movement in relation to the swash plate each piston has its own cylinder, called cup supported by the barrel plate. The bottom of the cups is hydrostatically compensated and takes over the function of a piston slipper. In difference to common axial piston units the valve plate is integrated into the swash plate which also contains the flow channels (Figure 10).

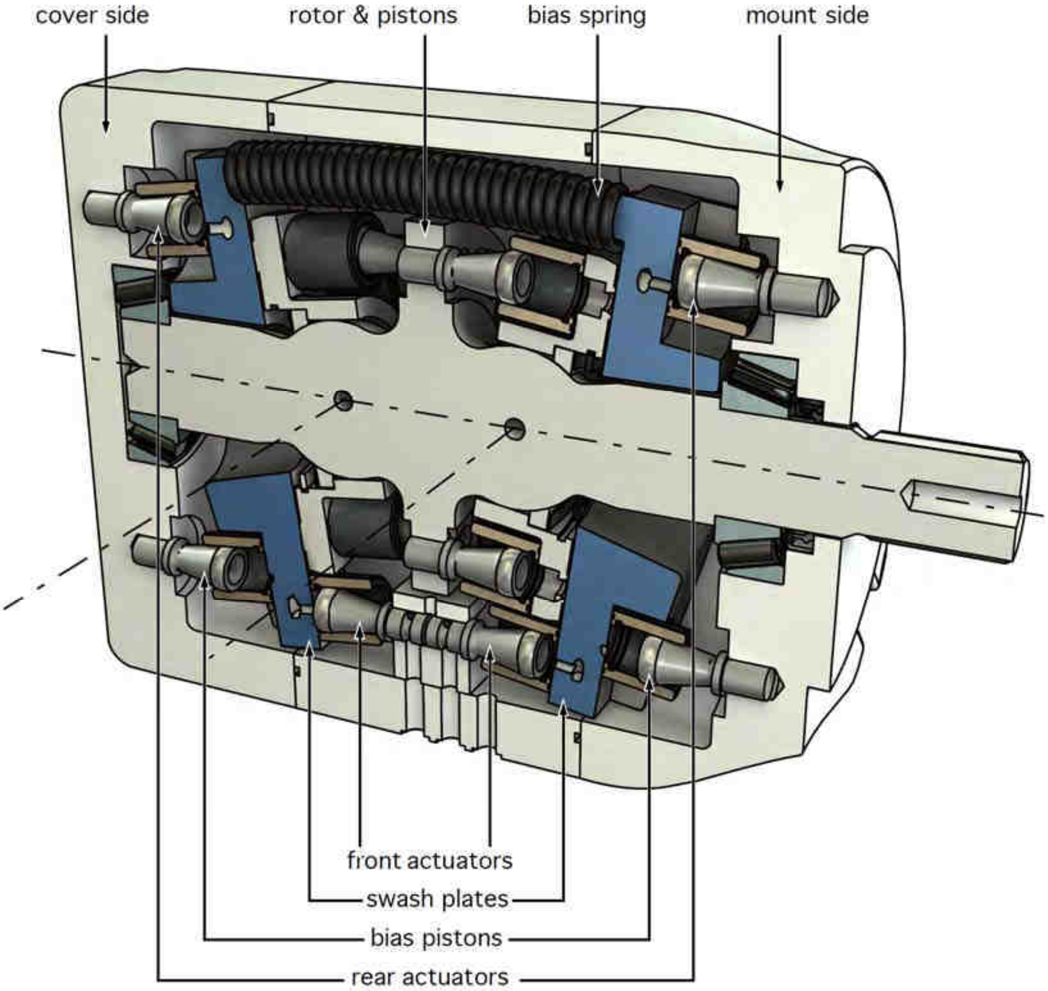

Figure 9 Design of the Floating Cup unit [9]

To reduce the shaft bearing's load the power train is designed symmetrically. Thus the axial piston forces are compensated and the bearings only need to support the radial piston forces. In addition, the number of displacement chambers is doubled resulting in a significant reduction of pressure pulsation and a compact design.

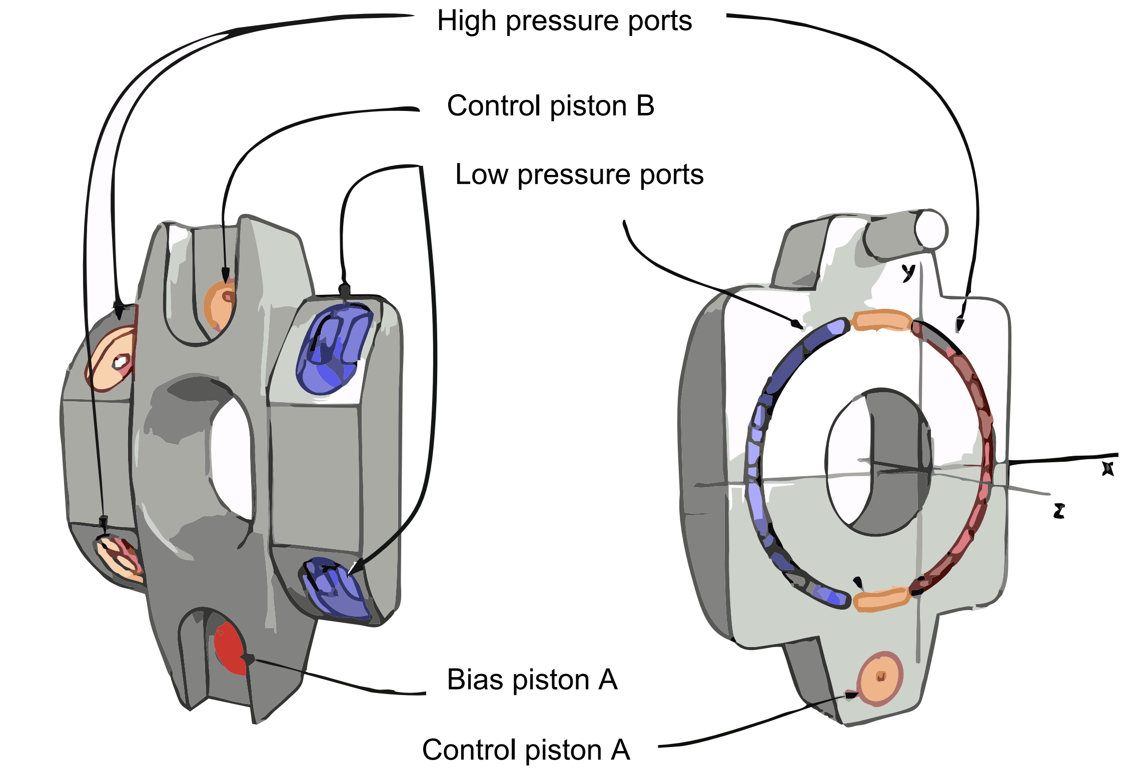

Figure 10 Swash plate of a Floating Cup unit [10]

The principle of torque generation is depicted in Figure 11. The spherically shaped piston head assures a sealing line perpendicular to the rotational axis of the cup. This leads to a transverse force at the pistons head. Due to the solid body junction, the transverse forces are supported by the rotor which generates a torque on the shaft.

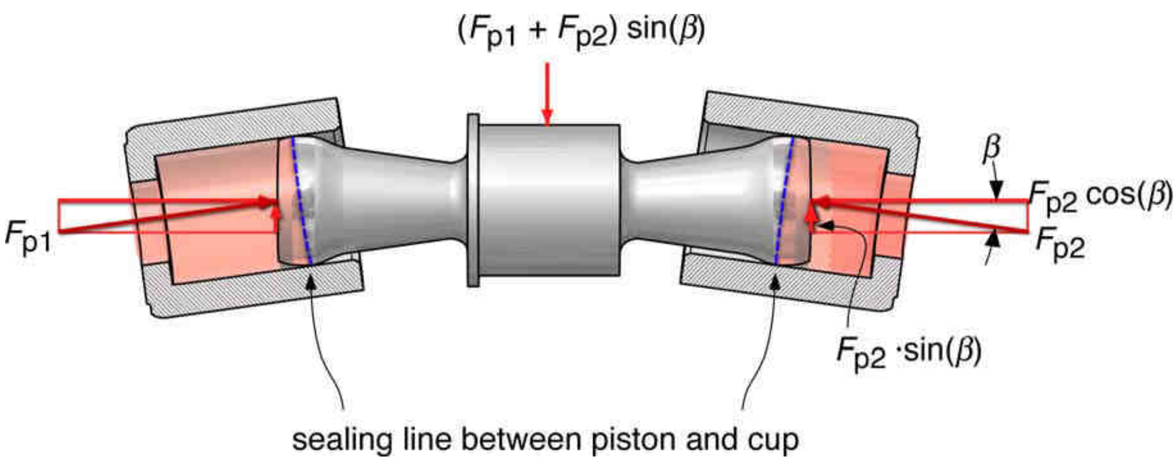

Figure 11 Direct torque generation of the Floating Cup Unit [7]

Similar to the RAC concept the torque is induced without transmitting a force via a critical tribological contact. Idealized no friction forces develop between piston and cylinder. Therewith hydro-mechanical losses are lower and independent of pressure and rotational speed. Efficiency measurements have shown overall efficiencies of about 96% in pump operation and 97% in motor operation [8].

5. Conclusions

Due to a restricted availability of usable energy, the efficiency of power transmission constantly gains importance. In hydraulic transmission the conversion of power from mechanical energy to hydraulic energy and vice versa plays a significant role.

In this paper the basic principle of an axial piston unit in swash plate design was shown and difficult tribological contacts were pointed out. Selected solutions for optimizing these contacts were presented resulting in an improved efficiency of this commonly used unit. Afterwards, two novel principles were discussed that meet some of the future challenges.

As a conclusion it can be stated that in the last decades a lot of effort has been focused on the optimization of specific parts and parameters of displacement units. Among other things this is based on the increasing computational power resulting in more complex and accurate simulation tools. Besides the optimization of existing units it is also important to search for new designs to meet the challenges of the future.

REFERENCES

[1] H. Murrenhoff, “Fundamentals of Fluid Power – Part 1: Hydraulics”, Lecture Notes, Shaker, Aachen, Germany, 2014
[2] J. Ivantysyn, M. Ivantysynova, “Hydrostatic pumps and motors”, Academia books international, New Delhi, India, 2001
[3] S. Gels, „Einsatz konturierter und beschichteter Kolben-Buchse-Paare in Axialkolbenmaschinen in Schrägscheibenbauweise“, Dissertation, RWTH Aachen University, Germany, 2011
[4] C. Enekes, “Ausgewählte Maßnahmen zur Effizienzsteigerung von Axialkolbenmaschinen“, Dissertation, RWTH Aachen University, Germany, 2012
[5] S. Wegner, S. Gels, H. Murrenhoff, “Simulation of the tribological contact cylinder block / valve plate and influence of geometry and operating points on the friction torque in axial piston machines”, Proceedings of the 9. International Fluid Power Conference, IFK2014, Aachen, Germany, 2014
[6] D. Schulze Schencking, J. Berbuer, H. Murrenhoff, “Systematic influence of hydrostatic displacement unit efficiency in operating range”, Proceedings of the 9. International Fluid Power Conference, Aachen, Germany, 2014
[7] P. Achten, “Power density of the floating cup axial piston principle”, Proceedings of the 2004 ASME International Mechanical Engineering Congress and Exposition”, Anaheim, USA, 2004
[8] P. Achten, “Efficiency measurements of the hydrid motor/pump”, Proceedings of the 12th Scandinavian International Conference on Fluid Power, Tampere, Finland, 2011
[9] P. Achten, “Swash plate oscillation in a variable displacement floating cup pump”, Proceedings of the 13th Scandinavian International Conference on Fluid Power, SICFP2013, Sweden, 2013
[10] P. Achten, “Design of a variable displacement Floating Cup”, Proceedings of the of the 9th Scandinavian International Conference on Fluid Power, SICFP´05, Sweden, 2005

ISSN 1454 - 8003
Proceedings of 2014 International Conference of Hydraulics and Pneumatics - HERVEX
November 5 – 7, Calimanesti-Caciulata, Romania

ELASTOPLASTIC PROPERTIES AND DEFINITION OF POROSITY CHARACTERISTICS COMPOSITE IRON-NICKEL COATINGS

Vasile JAVGUREANU[1], Pavel GORDELENCO[2]

[1] Technical University of Moldova, v_javgureanu@yahoo.com

[2] Technical University of Moldova, pavel_gr@mail.utm.md

Abstract: *This paper presents the elastic-plastic properties (he, hp; h; Ae; Ap; A; H; Hh; Hd, P) and define the parameters (Pcr; Hhcr; Hdcr) beginning of brittle fracture of iron-nickel composite coatings. First established experimentally that with the beginning of brittle fracture (Pcr = P), the work expended in elastic (Ae), plastic (Ap) and elastic-plastic (A) deformation significantly increases the load on the diamond spherical indenter (Pcr = P) and indentation depth (hp; h) decreases with increasing current density (DK) and a decrease in the electrolysis temperature (T). Critical load indentation (Pcr), not restored critical hardness (Hhcr) or the critical stress can be taken as a criterion for assessing the propensity of iron-nickel composite coatings to brittle fracture.*

Keywords*: elastoplastic, deformation, failure, galvanic, electrolytic, iron-nickel coatings.*

1. Introduction

The electro deposition of iron-nickel coatings are included in a large number of foreign particles significantly affect the structure of sediments, and consequently on their physic-mechanical properties. A high internal stress coating depends on the electro crystallization sediments. These features are the main reason for defining the properties of the coatings such as hardness, porosity, brittleness, fatigue strength of coatings [1].

Under the influence of internal stresses in the coatings appears porosity, which can be divided into three groups:
1) macro pores occur depending on coating structure which is influenced by the conditions of the electrolysis;
2) micro pores arise depending on the coating structure which is influenced by the conditions of the electrolysis;
3) pores type channel (grid cracks) arising from the presence of large internal stresses.

In all cases an increase of internal stresses in the coatings leads to an increase in porosity [1]. Formation of pores in the coating type channel promotes higher wear resistance of coatings with their work in conditions of lubrication lack.

Electrolysis conditions have significant impact on the density of the coating [1]. This is due to the change in porosity sediments. Perhaps that is why there are significant changes in elastic properties of coatings.

Ratio H_h/H is virtually independent of the nature of the distribution of pressure in the track, and is determined only by the average pressure, normalized to reduced contact modulus.

Analysis of elastic deformations in print followed by calculating the ratio of the reduced and unreduced hardness is important for the study and development of pilot test methods of the kinetic hardness and micro hardness. Attitude H_h/H - important experimental parameter, and its deviation from the calculated value can characterize such a necessary indicator for materials and hardening of the surface layers and coatings, as porosity. Analysis of this relationship is considered in a number of papers [2] which also find the displacement of two elastic bodies in contact (one of them is the indenter) the applied load is distributed over the area of the plastic print.

To estimate the porosity of the surface layers of the material proposed method assesses the degree of porosity of the material on his seal indentation. The seal appears to change the height of the roller around the indentation and leads a decrease in the ratio H_h/H. Hence for quantifying and seals need to measure both hardnesses (H_h - unrestored hardness, H - restored hardness). In the absence of material porosity ratio H_h/H in the first approximation should be constant.

Due to the high localization of the area of plastic deformation test with continuous registration process parameters indentation of a spherical indenter can give more information than a tension test at preserving its main advantage as a non-destructive method and express control of material properties.

One of the defining characteristics of the coating powder materials is their porosity (**ρ**), estimated as the general level, as well as the nature of the pore size distribution. The latter is very important because the pores which concentrate stress, remove the plastic properties of the material.

Influence of porosity on the indentation process depends on the size of the print. If the pore size and the distance between them is greater than the print size, the probability of entering the pores in the print zone, and hence the local fluctuation of density of the material subordinating static laws. If the print size appreciably larger than the distance between the pores, the fingerprint is stored in the average area density of the material depends on the total porosity of the material.

The total porosity of the indentation determines the change in the elastic modulus E and the ratio H_h/H.

The porosity of the material is determined by the formula:

$$\rho = 2(1-\kappa);$$

where:
k - coefficient taking into accounts the degree of compaction of the material;

$$\kappa = \left(\frac{H_h}{H}\right)^{0,5};$$

where:
H_h - unrestored hardness;
H - restored hardness.

E value and H_h/H depend on the form of pores. Tapered pore according M.Krivoglaz give a lower modulus of elasticity E. In addition, they are easier to heal under the imprint area of the plastic, since spherical pores healing requires a higher degree of hydrostatic compression. In connection with these pores are easily compacted flattened and therefore have a low ratio whiter H_h/H and higher strain hardening coefficient.

In the paper, elastic-plastic properties and porosity characteristics of iron-nickel composite coatings obtained from the electrolysis of 4 [1, pp. 59]. The samples used in the rollers of diameter 30 mm, thickness 0.5 mm and the coating length of 100 mm, which were processed under optimal grinding.

Physical and mechanical properties were determined at the facility for the study of the hardness of materials in macro volume equipped with an inductive sensor and a differential amplifier allows you to record chart indentation diamond spherical indenter and indentation recovery after removal of the load [1].

ISSN 1454 - 8003
Proceedings of 2014 International Conference of Hydraulics and Pneumatics - HERVEX
November 5 – 7, Calimanesti-Caciulata, Romania

2. Discussion of the experimental study.

These studies have shown that the investigated physical and mechanical properties of iron-nickel composite coatings varie with the electrolysis conditions (tables 1 and 2).

With increasing current density (Дк) of 5×10^{-4} to 80×10^{-4} kA/m^2 electrolysis at constant temperature (40^{0}C), plastic (h_p) component of the indentation depth ratio H_h/H ratio which takes into account the degree of compaction (k), elastic modulus (E) decrease, respectively, from 0.866 to 0.650 (micrometers), from 0.433 to 0.325 (micrometers) and from 0.658 to 0.570 (micrometers), from 21000 to 17500 (N/mm^2), and the elastic component (h_e) indentation depth and density of iron-nickel coatings increase accordingly from 1.134 to 1.350 (micrometers), and from 0.684 to 0.800 (micrometers). The total depth of the indentation in this case was constant, and was 2 micrometers (N). Work expended in elastic (A_e), plastic (A_p), the total deformation (A) recovered hardness (N), unrestored hardness (H_h), indentation load spherical diamond indenter (P) are the extreme value with changes in current density (Дк) from 5x10^{-4} to 80x10^{-4} kA/m^2 electrolysis at constant temperature (40^{0}C).

These studies have shown that with increasing current density of 5×10^{-4} to 50×10^{-4} kA/m^2 electrolysis at a constant temperature (40^{0}C) the work expended in elastic deformation of the coating increases from 17.2×10^{-3} to 23.5×10^{-3} (N·mm), the work expended in plastic deformation of coatings increased from 13.2×10^{-3} to 13.8×10^{-3} (N·mm), the total work spent on elastoplastic deformation of coatings increased from 30.4×10^{-3} to 37.3×10^{-3} (N·mm). With further increase in current density from 50x10^{-4} to 80×10^{-4} kA/m^2 electrolysis at a constant temperature (40^{0}C), the work spent on the elastic deformation of the coating increases from 23.5×10^{-3} to 18.8×10^{-3} (N mm), the work expended in plastic deformation

Table 1.

Elastoplastic properties and porosity of the iron-nickel composite coatings

Electrolysis conditions		Elastoplastic properties						H, N/мм^2	H_h, N/мм^2	H_h/H	E, N/мм^2	P, N	k	ρ
Дк, ×10^{-4} кА/м^2	T, ^{0}C	h_e, μм	A_e, N·мм	h_p, μм	A_p, N·мм	h, μм	A, N·мм							
5	40	1,134	0,01723	0,866	0,01316	2	0,03040	8385	3630	0,433	21000	45,6	0,658	0,684
10	40	1,150	0,01767	0,850	0,01351	2	0,03073	8636	3670	0,425	20500	46,1	0,652	0,696
20	40	1,172	0,01863	0,828	0,01357	2	0,03180	9173	3800	0,414	19800	47,7	0,643	0,714
30	40	1,210	0,02017	0,790	0,01361	2	0,0333	10081	3980	0,395	19500	50,0	0,628	0,744
40	40	1,240	0,02137	0,760	0,01369	2	0,0347	10839	4120	0,380	19300	51.7	0,616	0,768
50	40	1,260	0,02356	0,740	0,01384	2	0,03740	12065	4470	0,370	18800	56,1	0,608	0,784
60	40	1,280	0,02020	0,720	0,01212	2	0,0337	11173	4020	0,360	18000	50,5	0,600	0,800
70	40	1,350	0,01577	0,650	0,00904	2	0,0278	10221	3320	0,325	17500	41,7	0,570	0,860

Table 2.

Elastoplastic properties and porosity of the iron-nickel composite coatings.

Electrolysis conditions		Elastoplastic properties						H,	H_h,	H_h/H	E,	P,	k	ρ
Дк, ×10^{-4} кА/м^2	T, ^{0}C	h_e, μм	A_e, N·мм	h_p, μм	A_p, N·мм	h, μм	A, N·мм	N/мм^2	N/мм^2		N/мм^2	N		
50	20	1,520	0,02113	0,480	0,00667	2	0,02780	13854	3320	0,240	17100	41,7	0,49	1,02
50	40	1,260	0,02356	0,740	0,01384	2	0,03740	12065	4470	0.370	18800	56,1	0,608	0,784
50	60	1,028	0,01563	0,972	0,01377	2	0,03040	7475	3630	0,486	20500	45,6	0,697	0,606

decreased from 13.8×10^{-3} to 9.0×10^{-3} (N mm), the total work spent on the elastic-plastic deformation of the coating decreased from 37.3×10^{-3} to 27.8×10^{-3} (N·mm). From the results of research can be seen that the work expended in elastic (A_e), plastic (A_p) and elastic-plastic (A) deformation of iron - nickel coatings have extreme character with a change of the current density (Дк) at a constant temperature electrolysis (T).

Character of change of reconstituted (N), unreduced (H_h) hardness and indentation load (P) on a spherical diamond indenter at a depth of 2 micrometers, with increasing the current density from 5×10^{-4} to 80×10^{-4} kA/m^2, electrolysis at a constant temperature (40ºC) has an extreme character (table 1).

With increasing current density from 5×10^{-4} to 50×10^{-4} kA/m^2, electrolysis at a constant temperature (40ºC), restored the hardness (N) increased from 8385 to 12065 (N/mm^2) are not restored hardness ($H_П$) increased from 3630 to 4470 (N/mm^2), indentation load on the diamond spherical indenter increased from 45.6 to 56.1 (N). With further increase of the current density from 50×10^{-4} to 80×10^{-4} (kA/m^2), at a constant temperature electrolysis (40ºC) restored the hardness (N) decreased from 12065 to 10221 (N/mm^2), hardness is not restored (H_h) decreased from 4470 to 3320 (N/mm^2) and the indentation load on the diamond spherical indenter (P) decreased from 56.1 to 41.7 (N), Table 1.

With increasing temperature electrolysis (T, Table 2) at a constant current density (50×10^{-4} kA/m^2), from 20 to 60°C the plastic component ($h_П$), the depth of indentation ratio H_h/H, the modulus of elasticity E, and the power factor takes K into account to seal correspondingly increased from 0,480 to 0,972 micrometers, from 0.24 to 0.486, from 17100 to 2050 (N/mm^2), and from 0.490 to 0.697, and the elastic component (h_e) indentation depth recovered hardness (N) and the porosity of the coatings (ρ) decreased respectively from 1.520 to 1.028 (μm) from 13854 to 7475 (N/mm^2) and from 1.02 to 0.606.

Nature of the change work expended in elastic (A_e), plastic (A_p) and elastic-plastic deformation of iron-nickel coatings with temperature electrolysis from 20 to 60ºC at a constant current density (50×10^{-4} kA/m^2) has an extreme character. With increasing temperature electrolysis from 20 to 40ºC at a constant current density (5×10^{-4} kA/m^2), the work expended in elastic (A_e), plastic (A_p) and elastic-plastic deformation (A), respectively, increased from 21,1×10^{-3} to 23,5×10^{-3} (N/mm^2), from 6,7×10^{-3} to 14,8×10^{-3} (N mm) and of 27,8×10^{-3} to 38,3×10^{-3} (N mm). With further increase of the temperature of the cell from 40 to 60ºC at a constant current density (50×10^{-4} kA/m^2), the work expended in elastic (A_e), plastic (A_p) and elastic-plastic deformation (A) iron - nickel coatings decreased respectively by 23,5×10^{-3} to 15,6×10^{-3} (N mm), from 14,8×10^{-3} to 13,8×10^{-3} (N mm) and of 38,3×10^{-3} to 29,4×10^{-3} (N mm).

Nature of the change is not reduced hardness (H_h) and the indentation load diamond spherical indenter, at a depth of 2 micrometers, with an increase in temperature of the cell from 20 to 40ºC at a constant current density (50×10^{-4} kA/m^2) not restored hardness increased from 3320 to 4470 N/mm and the indentation load (P) of the spherical diamond indenter is increased from 41.7 to 56.1 (N). With further increase of the temperature of the cell from 40 to 60ºC at a constant current density (50×10^{-4} kA/m^2) unrestored hardness (H_h) decreased from 4470 to 3630 (N/mm^2), and indentation load diamond spherical indenter decreased from 56.1 to 45.6 (N).

Studies have shown that the unreduced hardness (H_h), the work expended in elastic (A_e), plastic (A), elastic-plastic deformation, the load on the diamond spherical indenter (P, for h = 2 micrometers) have extreme character changes in the conditions of electrolysis (Дк, T) for the study of iron - nickel coatings and coincide with the earlier recommendations in terms of ensuring their optimum durability.

It is shown experimentally (Table 1 and 2) that the ratio H_h/H, the coefficient *k* - taking into account the degree of compaction and the modulus of elasticity (E) decreases with increasing current density (Дк) and low temperature (T). With increasing current density (Дк) and a decrease in the electrolysis temperature (T) increases the porosity of the material (ρ, Tables 1 and 2). This proves that the electrolysis conditions (Дк, T) have a significant effect on the density and porosity of iron - nickel coatings, which are in good agreement with the existing literature data.

3. Conclusion

It was established experimentally that the reconstructed hardness (N), unrestored hardness (H_h), the work expended in elastic (A_e), plastic (A_p) elastic-plastic deformation (A) and the load on the diamond spherical indenter (P, for h=2 micrometers) have the extreme nature of changes in the conditions of electrolysis (Дк,T) for the study of iron - nickel composite coatings.

First determined experimentally, taking into account the power factor of the seal material (k) and the porosity of the material (ρ) with the change in the conditions of electrolysis (Дк, T) iron - nickel composite coatings.

It has been established that the increase of the current density (Дк) and a decrease in temperature (T) of the electrolysis for the iron - nickel composite coatings factor takes into account the degree of compaction (k) decreases, while the porosity of the coatings (ρ) increases.

Extreme values of the reduced hardness (N), unreduced hardness (H_h), the work expended in elastic (A_e), plastic (A_p) elastic-plastic deformation (A), the load on the diamond spherical indenter (P) coincide with those obtained recommendations for iron - nickel composite coatings in terms of ensuring their optimum durability.

The method of measuring the hardness in the macro - the most amount reasonably and accurately determine physical - mechanical characteristics (H, H_h, A_e, A_p, A, P, H_h/H, E, K, ρ) iron - nickel composite coatings.

Physical - mechanical characteristics (A_e, A_p, A, H, H_h, P) composite iron - nickel coatings have good wear rate correlation with these coatings.

REFERENCES

[1] S. Bulychev, V. Alekhin, “Ispytaniye materialov nepreryvnym vdavlivaniyem indentora", Moskva. Mashinostroyeniye, pp.224, 1990 (in Russian).
[2] V. Gologan, V. Azhder, V. Zhavguryanu, “Povysheniye dolgovechnosti detaley mashin iznosostoykimi pokrytiyami", Kishinev, Izd-vo Shtiintsa, pp.112, 1979 (in Russian).
[3] M.P. Markovets, “Opredeleniye mekhanicheskikh svoystv materialov po tverdosti", Moskva , Mashinostroyeniye , pp.191, 1979 (in Russian).
[4] V.Javgureanu, V.Ajder, V.Ceban, S.Pavlova, “The correlation of restored and unrestored microhardness of. Wear-proof iron plating", International Scientific Conference TMCR. Chisinau, pp.412-415, 2003.
[5] V.Javgureanu, P.Gordelenco, M.Elita, “The work of deforming wear -proof iron-nikel plating in microsquelging", The Annals of University Dunărea de Jos of Galați, Fascicle VIII, Tribology, Romania, pp.65-68, 2004.
[6] V.Javgureanu, P.Gordelenco, M.Elita, “Relationship of the restored and unrestored microharedbess of the cromium coating", The Annals of University Dunărea de Jos of Galați, Fascicle VIII, Tribology, Romania, pp.48-51, 2004.
[7] V.Javgureanu, P.Gordelenco, M.Elita, “Le rapport de la microdurete restauree et non restauree des convertures de crome", International Scientific Conference TMCR, Chisinau, pp.166-169, 2005.
[8] V.N.Zhavguryanu, P.A.Godelenko, “Sootnosheniye vosstanovlennoi i nevostanovlenoy mikrotverdosti khromovykh pokrytiy", Mezhdunarodnaya NTK "Mashinostroyeniye i tekhnosfera XXI veka", Sevastopol', 2005. (in Russian).

ISSN 1454 - 8003
Proceedings of 2014 International Conference of Hydraulics and Pneumatics - HERVEX
November 5 – 7, Calimanesti-Caciulata, Romania

NEW DIRECTIONS REGARDING FINDING THE OPTIMAL HYDRAULIC SOLUTION

Leonard-Stefan BOGHIAN[1], Boris PLAHTEANU[2], Constantin CHIRITA[3]

[1] "Gheorghe Asachi" Technical University of Iasi, stefboghi@yahoo.com

[2] "Gheorghe Asachi" Technical University of Iasi, plahteanu@yahoo.com

[3] SC Hydramold SRL, constantin.chirita@hydramold.com

Abstract: *This paper is on finding the optimal hydraulic solution in terms of the ratio benefit / cost, in relation to user requirements in reaching this solution by differentiating specific hydraulic parameters in 6 categories, so that user requirements can be accurately achieved.*

Keywords*: (Arial, 11pt, Italic, Justified) parameters, hydraulic equipment, optimal solution*

1. Introduction

It is imperative that when you have to choose between one or the other hydraulic equipment, the decision to be taken in relation to the specific needs of the user. For this purpose, we have identified six types of parameters, by means of which the utility of each solution can be determined. In addition, this approach facilitates decision making using the computer.

2. Parameters of type I

Within these parameters, the user must define a range, within which, as the parameter value will be greater than the utility of the product will increase. If we note:

- Si_{min} - the lower limit of the range; if the value of the parameter is below this limit, the equipment is inadequate (product P1 in Figure 1), because there is no utility for the client;
- Si_{max} - the upper end of the range; a value that exceeds this limit adds no utility to the customer, but an additional cost (product P3 in Figure 1).

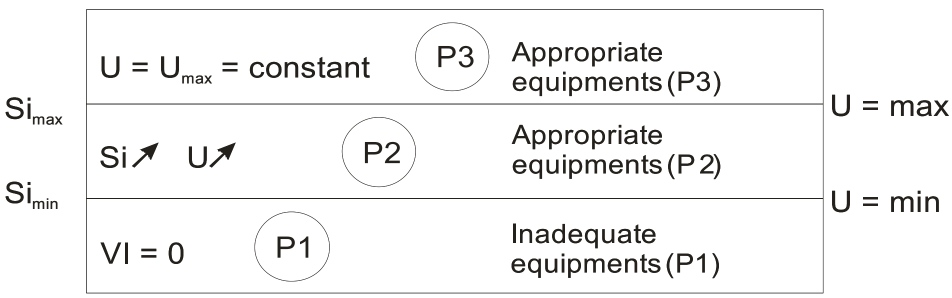

Fig. 1. The utility limits of the parameter of type I

The product searched by the user is in the area between the limits Si_{min} and Si_{max}; between these limits increasing the value of the parameter entails a proportional variation of utility (U).
For instance, we assign the limits Si_{min}=700 bar and Si_{max}=850 bar for the pressure parameter of the high pressure hydraulic source.

3. Parameters of type II

This parameter can be configured, as in the previous case, by introducing the two values:

- Si_{max}, which distinguishes between appropriate and inadequate products (Figure 2) and
- Si_{min}, which is the limit of utility to the user.

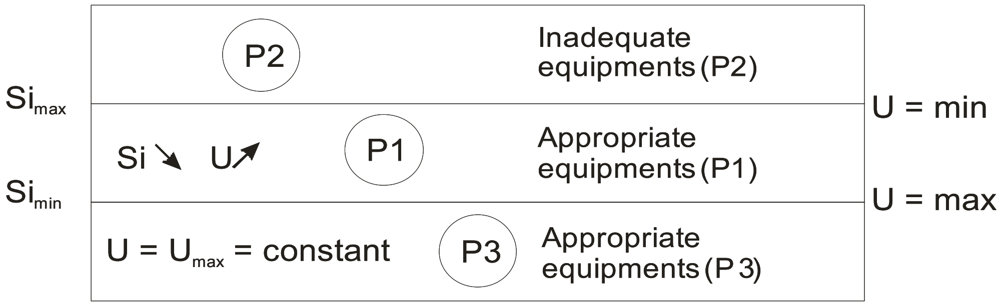

Fig. 2. The utility limits of the parameter of type II

If the value of the parameter (Si) is upper than Si_{max}, the equipment is inadequate. If the values (Si) are lower than Si_{max}, the utility of the product is inversely proportional to Si until Si is equal to Si_{min}. If the values (Si) are lower than Si_{min} the utility of the product no longer increases.
For instance, we assign the utility limits Si_{min}=10 kg şi Si_{max}=40 kg for the weight parameter.

4. Parameters of type III

This type of parameter is expressed as a range whose length is desired to be as long as possible. A length of the range exceeding certain utility limits will no loner increase the utility but it will generate additional costs. Thus, the client has to set the following four values:

- Si_{1min} and Si_{1max} (figure 3) are the limits within a variation of the inferior limit of the range of the parameter p_i determines an inversely proportional variation of the utility; a value lower than Si_{1min} implies no increase of utility; he is not interested to pay for it. A value higher than Si_{1max} leads to an inadequate product;
- Si_{2min} şi Si_{2max} are the limits within a variation of the superior limit of the range of parameter p_i produces a proportional variation of the product utility. A value lower than Si_{2min} means that the product is inadequate and a value higher than Si_{2max} means no additional utility for the user.

The ideal equipment for the user is the one for which the values of the parameter p_i are equal to the limits Si_{1min} and Si_{2max}.
An example of this type of parameter is the range of temperature of the high pressure hydraulic sources, for which the user sets the following utility limits: Si_{1min} =-30°C; Si_{1max} = -10°C; Si_{2min} = 40°C and Si_{2max} = 60°C.

5. Parameters of type IV

The product utility, considering this type of parameter, is delimited by the consumer through two values (figure 4):

- for the product to be adequate, the inferior limit of the range of the parameter p_i must be higher than Si_{1min} ;
- for the product to be adequate, the superior limit of the range of the parameter p_i must be lower than Si_{2max}.

The utility will be proportional with the inferior limit Si_1 and inversely proportional with the superior limit Si_2.

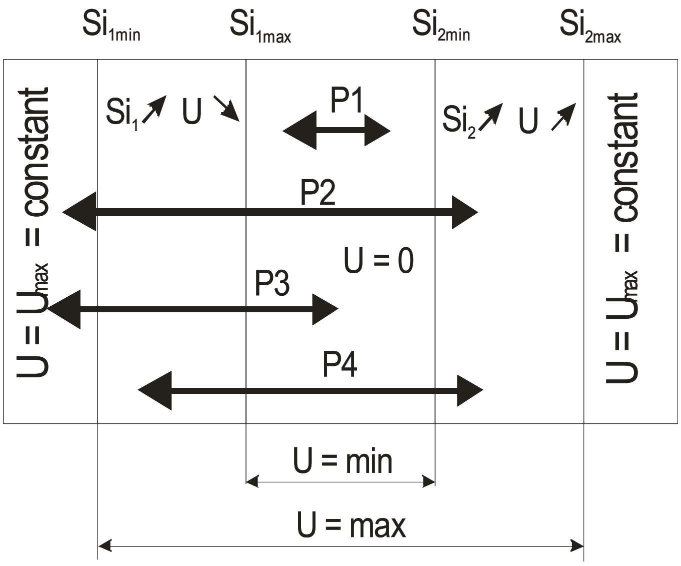

Fig. 3. The utility limits of the parameter of type III

An example of this type of parameter is the elastic deformation of a sealing element for which are set the following limits: Si_{1min} =0.05 si Si_{2max} = 0.15 mm.

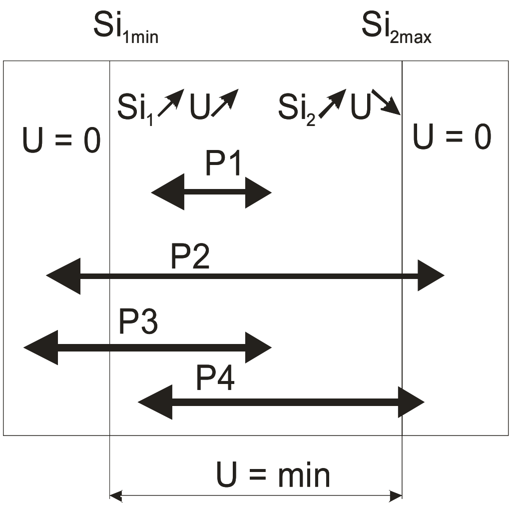

Appropriate equipments(P1);
Inadequate equipments(P2, P3 si P4)

Fig. 4. The utility limits of the parameter of type IV

6. Parameters of type V

This is a "yes/no" type of parameter. The user only has to choose between the values "yes" or "no". The parameter only filters the appropriate equipments from the inadequate equipments. There is no variable function of utility.
An example of this type of parameter is the possibility to start under full load of a high pressure hydraulic source, by assigning the values "yes" or "no".

7. Parameters of type VI

The last type of parameters is expressed by a set of discrete values and the user will choose among them. The user has to assign utility coefficients to the selected criteria.
An example of this type of parameter of an electrical power hydraulic source is the supply voltage and the values are: 110 V, 220 V and 380 V.

The figure 5 is an example of setting the utility limits of the parameter of type III using a software application.

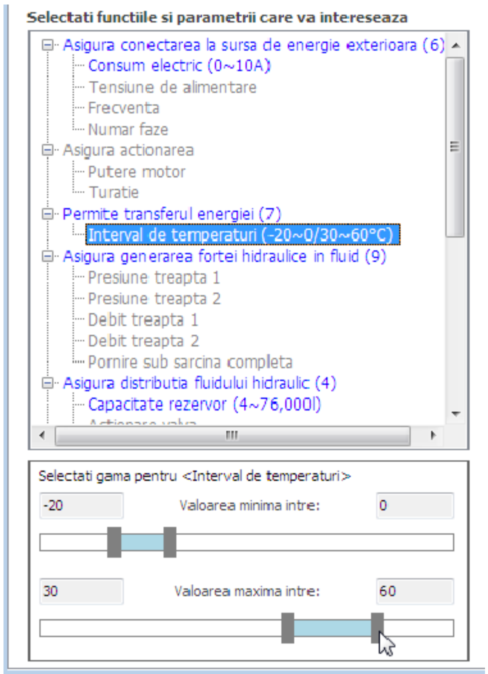

Fig. 5. Example of setting the utility limits of the parameter of type III using the computer

8. Conclusions

By differentiating specific parameters of hydraulic equipments, were obtained 6 types of parameters, through which the user requirements are accurately achieved, so when the user has to choose a hydraulic equipment, he will receive the optimal solution in terms of ratio utility/cost.

REFERENCES

[1] B. Plahteanu, "Ingineria valorii şi performanţa în creaţia tehnică ", Performantica Publishing House, Iaşi, 1999
[2] L.Ş.Boghian, "Un nou program informatic creat pentru facilitarea căutării soluţiilor tehnice performante în acţionarea hidraulică de înaltă presiune", Vol. INVENTICA 2014, THE 18-th INTERNATIONAL CONFERENCE "INVENTICA 2014", Performantica Publishing House, Iaşi, 2014, ISSN1844-7880; pp. 500-505

ISSN 1454 - 8003
Proceedings of 2014 International Conference of Hydraulics and Pneumatics - HERVEX
November 5 – 7, Calimanesti-Caciulata, Romania

INFLUENCE OF VOLUME HEAT TREATMENT ON BRONZE RESISTANCE AMPCO M4 TO CAVITATION EROSION

Lavinia Madalina MICU[1], Ilare BORDEASU[1], Mircea O. POPOVICIU[1], C-tin BORDEASU[1], Dorin BORDEASU[1], Laura Cornelia SALCIANU[1], Octavian Victor OANCA[1]
[1]„Politehnica" University of Timisoara, Romania

Abstract: *The first observations of the destructive effects of cavitation have been made on marine propellers. As a result, researchers and shipbuilders requested materials, techniques that treated materials propellers, which confer resistance to cavitation erosion. Such a technique, very well mastered, is the volumetric heat treatment due to the knowledge of all the factors that define it. This paper presents the effect of treatment on behaviour and resistance type CuNiAlFeMn bronze (symbolized AMPCO M4) to cavitation erosion caused by vibrating piezoelectric crystal vibrating device T2 cavity found in the laboratory of U.P Timişoara. The resistance created by the application of this treatment is carried out based on the characteristic curves of erosion MDE (t) and MDER (t), compared with the material condition of the material delivered and CuNiAl III RNR standard, the reference for the ships propellers Romania. Comparison with state material delivered with the standard shows that the treatment you get a large increase in resistance due to increasing hardness of the surface layer exposed to cavitation.*

Keywords*: cavitation erosion, the average depth of penetration of erosion, erosion rate, hardness, heat treatment volume, AMPCO bronze M4*

1. Introduction

One way to increase the cavitation erosion resistance of materials used frequently requested for cavitation, is the application of heat treatments. How marine propellers, are highly stressed parts category to cavitation, the use of such treatments in order to increase their lifetime is a beneficial solution obviously if the size propellers allow. One such treatment is the volume, as it provides a significant increase of all mechanical resistance characteristics [4], which according to previous studies, helps increase resistance to attack destructive cavitation. Home ownership, indicated by Garcia and Hammitt [5], [6], with a direct effect on the resistance to cavitation erosion is hardness of attacked surface. Following these guidelines , the paper presents the results of research conducted on specimens of bronze AMPCO M4 [12], heat treated volume, which gives a substantial increase in microhardness.

2. Heat treatment

The heat treatment applied is the same as that applied to the alloy CuNiAlMn - AMPCO M4 (the diagram of Fig. 1)

- Heated to 860 ^{0}C (40 min.) - Maintenance 20 min. - Cooling water, followed by
- Heating 480 ^{0}C (40 min.) - Maintenance 60 min. - Air cooling

ISSN 1454 - 8003
Proceedings of 2014 International Conference of Hydraulics and Pneumatics - HERVEX
November 5 – 7, Calimanesti-Caciulata, Romania

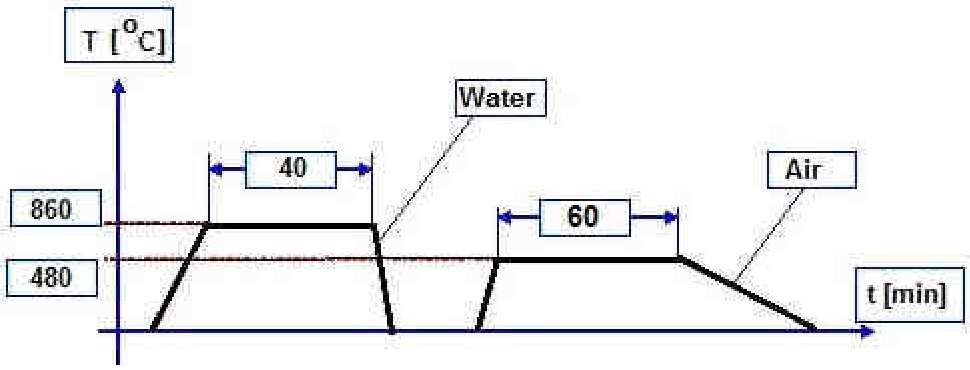

Fig.1. ***Heat treatment Ciclograma***

Measurements of hardness, 8-point, Table 1 shows the extent of growth obtained by the heat treatment of the surface exposed to cavitation. Also in this table have been introduced and hardness values measured in untreated sample surface to highlight the effect of applied heat treatment.

Table 1: HARDNESS HV3

CuNiAlMn- AMPCO M4 HEAT TREATED			CuNiAlMn-AMPCO M4 WITHOUT HEAT TRATMENT		
Depth [μm]	HV3	average HV3	Depth [μm]	HV3	average HV3
133,5	310		138	292	
134,5	305		139	288	
135	305		139	288	
135	305	303	139	288	
135,5	301		139	288	
136,5	296		140	284	282.5
136,5	296		140	284	
			142	276	
			143	272	
			145	265	

It is observed that the heat treatment was obtained a growth of 7.44% average hardness HV3.

3. Experiment results

Cavities were prepared and tested three samples, as determined in the laboratory procedure provided consistent with the requirements of ASTM Standard G32-2010 [9], [11].
The tests were carried out in the piezoelectric crystal vibrator device T2 [9]. The method used is the standard, subject to the requirements in ASTM G32-2010.
Using statistical method specified in the previous chapters, the purpose of certification accuracy research, the repeatability of the results and how the cavitation erosion was built band dispersion, Fig. 2 and maximum values were determined cumulative mean depth of erosion at the completion of the test, regression curves and standard error (sxy), Table 2

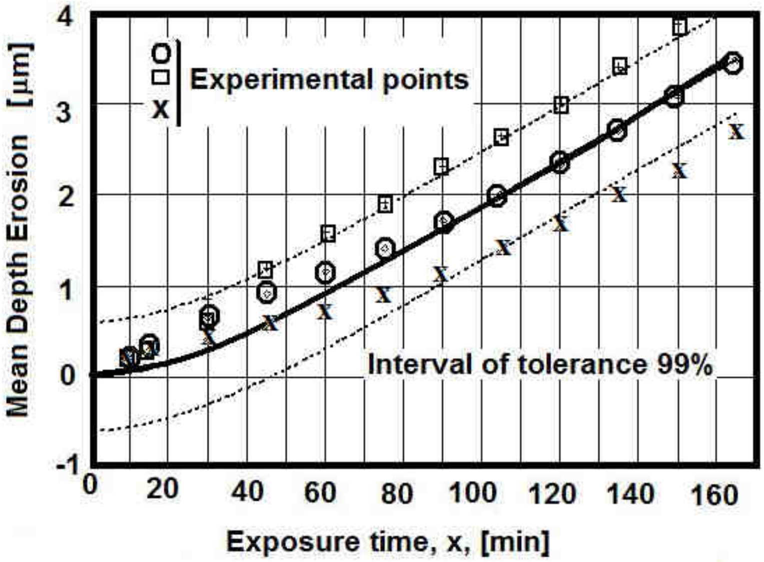

Fig. 2 ***Band dispersion***

Fig.2 is noted that the band of dispersion in this case is reduced, which show a similar behavior of the three tested samples. Differences are natural and tape errors.

Table 2: Values of statistical parameters

Average depth of penetration of erosion after 165 minutes of attack	3,478
Maximum value according to the polynomial	4,072
The minimum value according to the polynomial regression	2,884
Standard error of estimation (sxy)	0,198

The low standard deviation below 0.2, show the effect of heat treatment on the structure and properties of the surface exposed to cavitation, in particular by increasing the hardness HV3; erosion being made uniformly and almost identical in the three samples.

4. Specific curves and characteristic parameters of cavitation erosion

Both diagrams in Figure 3 show that the approximation/mediation points experimental analytical curves is very well done, the duration of the cavitation attack.
Photos taken at three times features illustrate a very good resistance to cavitation vibrating of attacked surface

ISSN 1454 - 8003
Proceedings of 2014 International Conference of Hydraulics and Pneumatics - HERVEX
November 5 – 7, Calimanesti-Caciulata, Romania

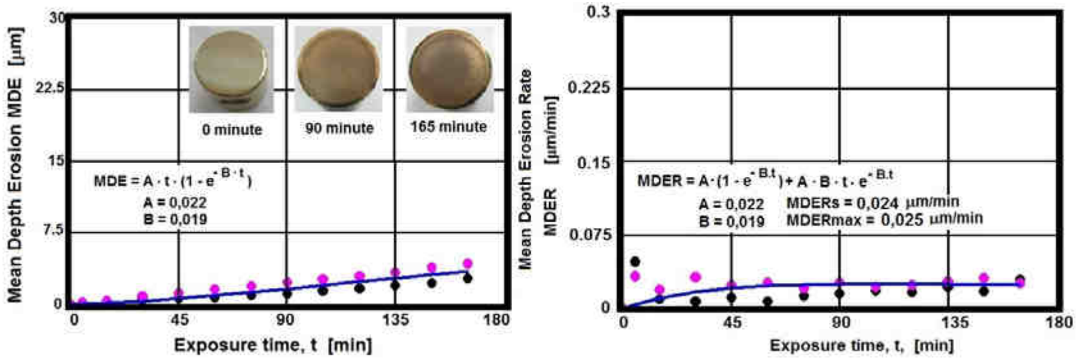

a) b)

Fig.3 ***The specific curves of evolution and resistance to cavitation behavior:***
a) Evolution of the mean depth of erosion during attack
b) Evolution of the average speed of penetration of erosion attack duration

5. Analysis of experimental results

The evolution of the curve approximation and the arrangement of data points, to this, that the material alloy CuNiAlMn - AMPCO M4, the attacked area, uniformity and hardness is almost constant (see Table 1) in all three samples, resulting in a behavior, and resistance almost identical. The small differences observed on the diagram in Fig.3.b, the velocities of the three samples in the range 0-30 minutes, insignificant, taking more than how to clean and wash the surfaces of samples after heat treatment and polishing.
The layout of the experimental points, an approximation curve in Fig3.b, between 30-90 minutes for one of the samples (black dots) shows the resistance created by the treatment, the surface exhibited higher, the impact and shock waves with microjets,i s something more higher than the other two. But this mode of evolution of behavior is part of a complex manifestation of the answer, one and the same material [4], [5], [7], [10]
How averaging data points of the two curves analytical approximation shows that the energy consumed during cavitation, almost equally distributed deformation, cracks, breaks and expulsions. Thanks to this behavior, the difference between the maximum erosion rate of penetration (0.025 μ m/min) and tends to stabilize (0.024 μ m/min) is totally insignificant. Difference between analytical curves and experimental points for the duration of cavitation attack show increased resistance to cavitation gained bronze that the beneficial effect of the applied treatment.
As with the untreated alloy, the development of specific reaction curve approximation suggests very good material erosion resistance to cavitation.

6. Influence on the resistance to cavitation treatment of investigated bronzes.

In this chapter evaluates the behavior and strength bronzes CuNiAlMn - AMPCO M45 and M4 , by comparing the characteristic curves and cavitation erosion of the main parameters: cumulative average penetration depth erosion, MDE, after 165 minutes of attack and cavitation erosion resistance, defined by parameter 1/MDER where MDER is value toward which the permeation rate to stabilize erosion. Evaluation is done by comparison with standard materials OH12NDL characteristic curves (Russian brand, Kaplan turbine blades used in casting the Iron Gates I and II [1], [2] and taken as reference in manufacturing hydraulic turbine blades and rotors in Romania , due to cavitation erosion resistance good [3] and naval bronze CuNiAl III RNR (with excellent resistance to cavitation erosion [2], [3], [8] and recommended by the RNR and former Institute ICEPRONAV in manufacturing marine propellers).

However, comparing between them, bronzes resistances corresponding states investigated using MDE and 1/MDER parameter values at the end of the attack.

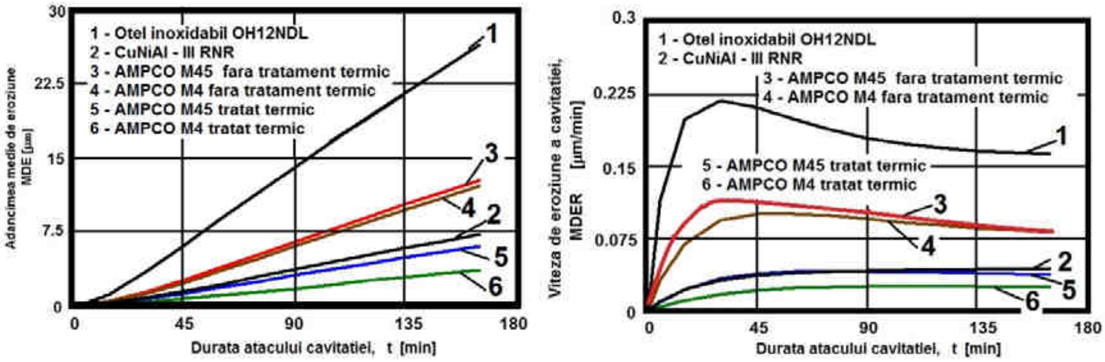

a) b)

Fig.4 ***The specific curves to the evolution behavior and resistance to cavitation:***
a) Evolution of the mean depth of erosion during attack
b) Evolution of the average speed of penetration of erosion attack duration

In figure 4 are highlighted behaviors and strengths of the two bronzes, the conditions of delivery (curves 3 and 4) and heat treated (curves 5 and 6). Comparison with standard steel OH12NDL, curve 1, shows that, regardless of status, bronzes CuNiAlMn - AMPCO M4 and M45 have very good behavior and resistance.
Developments curves MDER (t) with low maximum stability and trends close to the maximum values, specific strength steels and behaviors increased cavitation erosion [2], [9]. After MDER parameter values of the stabilization against OH12NDL steel, bronze resistance AMPCO M4 is about 2 times higher, and the delivered state about 6.8 times bigger heat-treated condition.
Comparing the value toward which tends to stabilize erosion penetration rate (parameter MDER) CuNiAl alloy III RNR, fig. 4b ($\cong$ 0.046 μm/min), curve 2, shows that the state delivered bronze (AMPCO M4) have a resistance of less than about 1.8 times. However, thermal, vibratory cavitation erosion resistance increases over traditional strength alloy used in casting marine propellers, CuNiAl III RNR from about 2 times for AMPCO M4.

7. Conclusions

The small size of the error band certify the performance of the experiment, all three samples .
Almost identical behavior of the three samples show homogeneity achieved by heat treatment, surface attacked structure.
The low standard deviation obtained from the statistical analysis shows that the thermal treatment of the alloy CuNiAlMn - AMPCO M4 were obtained which led to microhardness uniform behavior throughout the cavitation attack.
Form experimental curves approximation points , layout data points to curve approximation and reduced dispersion of the points corresponding to the three samples proves that the use of heat treatment for AMPCO bronze CuNiAlMn - M4 is beneficial and recommended if practical conditions and size of ship propeller permit. This heat treatment leads to behavior and resistance to cavitation erosion surface subject -specific material very good resistance to cavitation vibrators.

REFERENCES

[1] Anton I., Cavitatia, Vol II, Editura Academiei RSR, Bucuresti, 1985
[2] Bordeaşu I., Eroziunea cavitaţională a materialelor, Editura Politehnica, Timişoara, 2006
[3] Bordeaşu I., Teză de doctorat : Eroziunea cavitaţională asupra materialelor utilizate în construcţia maşinilor hidraulice şi elicelor navale. Efecte de scară, Timişoara, 1997
[4] Franc J.P., ş.a., La Cavitation, Mecanismes phisiques et aspects industriels, Press Universitaires de GRENOBLE, 1995
[5] Garcia R., Hammitt F. G., Nystrom R.E., Corelation of cavitation damage with other material and fluid properties, Erosion by Cavitation or Impingement, ASTM, STP 408 Atlantic City, 1960

[6] Hammitt F.G., Cavitation and Multiphase Flow Phenomena, McGraw Hill International Book Company, 1980
[7] Hattori S., Kitagawa T., Analysis of cavitation erosion resistance of cast iron and nonferrous metals based on database and comparison with carbon steel data, Wear, Volume 269, Issues 5-6, 19 July 2010, Pp. 443-448, 2010
[8] Mânzână M.E., Studii și cercetări experimentale privind modificările structurale produse prin cavitație-eroziune în diferite materiale metalice, Teza de doctorat, Bucuresti, 2012
[9] Oanca O., (2014) Tehnici de optimizare a rezistenţei la eroziunea prin cavitaţie a unor aliaje CuAlNiFeMn destinate execuţiei elicelor navale, *Teza de doctorat*, Timișoara
[10] Xiao-ya Li, Y.-g.Y., Zhen-min Xu, Hian-guo Li, Cavitation erosion behavior of nickel-aluminum bronze weldment. Transactions of Nonferrous Metals Society of China, Vol.13: p. 1317-1324, 2003
[11] *** (2010). Standard method of vibratory cavitation erosion test, ASTM, Standard G32-10
[12] *** http://www.ampcometal.com/common/datasheets/en/AM4_EX_E.pdf

ISSN 1454 - 8003
Proceedings of 2014 International Conference of Hydraulics and Pneumatics - HERVEX
November 5 – 7, Calimanesti-Caciulata, Romania

CASE STUDY 1: PLATE HEAT EXCHANGER WITH GASKET

Oana GIURGIU[1], Angela PLESA[2], Dan OPRUTA[3]

[1] Technical University of Cluj Napoca, Department of Mechanical Engineering, Oana.Giurgiu@termo.utcluj.ro

[2] Technical University of Cluj-Napoca, Department of Mechanical Engineering, Angela.Plesa@termo.utcluj.ro

[3] Technical University of Cluj-Napoca, Department of Mechanical Engineering, Dan.Opruţa@termo.utcluj.ro

Abstract: *This paper present a part of a complex research program based on optimization and design of plates for heat exchangers and shows the results of experimental research conducted on a plate heat exchanger with gaskets stand. Experimental analysis helps to determine the performance of the heat exchanger under imposed condition; in this case the mass flow rate and temperature (inlet and outlet for both circuits) were controlled.*

Keywords: *plate heat exchanger, experimental,*

1. Introduction

Heat exchangers are key components of many products available in the marketplace, and their application are important in an extremely wide range of industrial processes. The effective design of heat exchangers can have substantial impact on industrial process efficiency and their relevance to the problem of conservation of energy resources. [1 - 3]

Figure 1. Plate heat exchanger under study [4]

The objectives of study aims to optimize plates, in order to obtain a more efficient heat exchanger for which the values of heat transfer coefficient to be high and for pressure drops to be low.

It is known that corrugated channel geometry improve thermal performance by increasing the heat transfer surface and true turbulence occurrence in the flow. [1 - 3]

The V channel arrangement offers many areas of narrowing flow path that provides an increase of turbulence.

The advantage of plate heat exchangers that use V - shapes channels is that they may operate at higher pressures for smaller plate thickness.

Based on this consideration the present study is conducted on plate heat exchanger with gaskets having sinusoidal V - shaped channels. For this part of the experimental program was used a plate heat exchanger that has 9 plates which, after assembly, formed eight flow channels: 4 for the hot agent and 4 for the cold agent; circulation is in counter flow, each agent having a single pass through the device, as is shown in

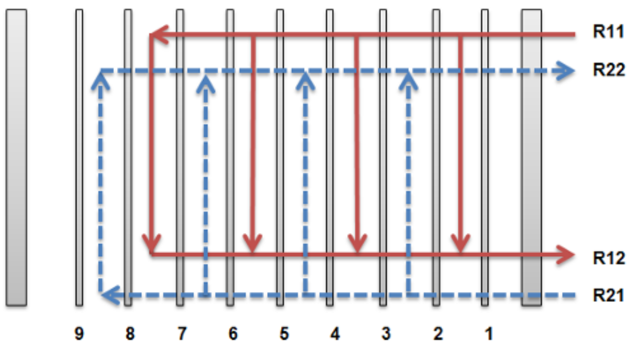

Figure 2. Internal configuration of the tested device[4]

figure 2.

The plate, presented in figure 3, that was used in the device has the follow parameters presented in table 1:

Figure 3. Plate model [5]

Table 1 Plates parameters [4]

Nr. crt.	Parameter	Symbols	U.M.	Plate model TK
1.	Corrugated angle	β	°	30
2.	Active length of the plate	L	mm	220
3.	Active width of the plate	l	mm	190
4.	Height of wavy channel	H_0	mm	2.5
5.	Crimping step	p	mm	10

The measurements on TK heat exchanger were conducted maintained constant values for the following parameters: temperature of the working agents' (t_{11}, t_{21}) and volume flow rate of hot agent $\dot{v}_1$. Along measurements were conducted, it decreased the output temperature of the hot agent (t_{12}) and increased the output temperature of the cold agent (t_{22}), marking the heating of cold agent. Also, was establish the gradually increasing of volume flow rate for cold agent between (1.6 ... 2.3) m^3/h with up to 0.1 for a set of measurements.

Table 2 Measured values for TK heat exchanger at $\dot{v}_1$=0.5 m^3/h [4]

Nr. crt.	t_{11} [°C]	t_{12} [°C]	Δt_1	$\dot{v}_1$ [m^3/h]	p_{11} [bar]	p_{12} [bar]	t_{21} [°C]	t_{22} [°C]	Δt_2	$\dot{v}_2$ [m^3/h]	p_{21} [bar]	p_{22} [bar]
1	67.1	35.37	31.73	0.5	1.25	1.21	7.8	17.23	9.43	1.6	2.13	2.03
2	67.1	35.1	32	0.5	1.25	1.21	7.8	16.76	8.96	1.7	1.85	1.69
3	67.1	34.85	32.25	0.5	1.25	1.21	7.8	16.33	8.53	1.8	1.63	1.42
4	67.1	34.64	32.46	0.5	1.25	1.21	7.8	15.94	8.14	1.9	1.39	1.1
5	67.1	34.33	32.77	0.5	1.25	1.21	7.8	15.61	7.81	2	1.25	0.9
6	67.1	34.16	32.94	0.5	1.25	1.21	7.8	15.28	7.48	2.1	0.88	0.49
7	67.1	34.02	33.08	0.5	1.25	1.21	7.8	14.98	7.18	2.2	0.84	0.44
8	67.1	33.93	33.17	0.5	1.25	1.21	7.8	14.69	6.89	2.3	0.83	0.42

Table 3 Measured values for TK heat exchanger at $\dot{v}_1$=0.707 m^3/h [4]

Nr. crt.	t_{11} [°C]	t_{12} [°C]	Δt_1	$\dot{v}_1$ [m^3/h]	p_{11} [bar]	p_{12} [bar]	t_{21} [°C]	t_{22} [°C]	Δt_2	$\dot{v}_2$ [m^3/h]	p_{21} [bar]	p_{22} [bar]
1	67.1	42.73	24.37	0.707	1.02	0.97	7.8	18.08	10.28	1.6	2.13	2.03
2	67.1	42.61	24.49	0.707	1.02	0.97	7.8	17.54	9.74	1.7	1.85	1.69
3	67.1	42.45	24.65	0.707	1.02	0.97	7.8	17.08	9.28	1.8	1.63	1.42
4	67.1	42.36	24.74	0.707	1.02	0.97	7.8	16.63	8.83	1.9	1.39	1.1
5	67.1	42.22	24.88	0.707	1.02	0.97	7.8	16.24	8.44	2	1.25	0.9
6	67.1	42.09	25.01	0.707	1.02	0.97	7.8	15.89	8.09	2.1	0.88	0.49
7	67.1	41.93	25.17	0.707	1.02	0.97	7.8	15.58	7.78	2.2	0.84	0.44
8	67.1	41.84	25.26	0.707	1.02	0.97	7.8	15.28	7.48	2.3	0.83	0.42

Tabelul 4 Measured values for TK heat exchanger at $\dot{v}_1$=**0**.9m^3/h [4]

Nr. crt.	t_{11} [°C]	t_{12} [°C]	Δt_1	$\dot{v}_1$ [m^3/h]	p_{11} [bar]	p_{12} [bar]	t_{21} [°C]	t_{22} [°C]	Δt_2	$\dot{v}_2$ [m^3/h]	p_{21} [bar]	p_{22} [bar]
1	67.1	47.15	19.95	0.9	0.9	0.79	7.8	18.51	10.71	1.6	2.13	2.03
2	67.1	47.04	20.06	0.9	0.9	0.79	7.8	17.95	10.15	1.7	1.85	1.69
3	67.1	46.95	20.15	0.9	0.9	0.79	7.8	17.44	9.64	1.8	1.63	1.42
4	67.1	46.88	20.22	0.9	0.9	0.79	7.8	16.98	9.18	1.9	1.39	1.1
5	67.1	46.75	20.35	0.9	0.9	0.79	7.8	16.58	8.78	2	1.25	0.9
6	67.1	46.64	20.46	0.9	0.9	0.79	7.8	16.21	8.41	2.1	0.88	0.49
7	67.1	46.53	20.57	0.9	0.9	0.79	7.8	15.87	8.07	2.2	0.84	0.44
8	67.1	46.48	20.62	0.9	0.9	0.79	7.8	15.54	7.74	2.3	0.83	0.42

Tabelul 5 Measured values for TK heat exchanger at $\dot{v}_1$=1.2 m^3/h [4]

Nr. crt.	t_{11} [°C]	t_{12} [°C]	Δt_1	$\dot{v}_1$ [m^3/h]	p_{11} [bar]	p_{12} [bar]	t_{21} [°C]	t_{22} [°C]	Δt_2	$\dot{v}_2$ [m^3/h]	p_{21} [bar]	p_{22} [bar]
1	67.1	51.41	15.69	1.2	0.87	0.57	7.8	19.03	11.23	1.6	2.13	2.03
2	67.1	51.29	15.81	1.2	0.87	0.57	7.8	18.46	10.66	1.7	1.85	1.69
3	67.1	51.21	15.89	1.2	0.87	0.57	7.8	17.93	10.13	1.8	1.63	1.42
4	67.1	51.15	15.95	1.2	0.87	0.57	7.8	17.44	9.64	1.9	1.39	1.1
5	67.1	51.07	16.03	1.2	0.87	0.57	7.8	17.01	9.21	2	1.25	0.9
6	67.1	51.02	16.08	1.2	0.87	0.57	7.8	16.61	8.81	2.1	0.88	0.49
7	67.1	50.92	16.18	1.2	0.87	0.57	7.8	16.26	8.46	2.2	0.84	0.44
8	67.1	50.87	16.23	1.2	0.87	0.57	7.8	15.92	8.12	2.3	0.83	0.42

The data obtained after testing plate heat exchanger type TK, presented in the tables 2-5 served to calculate mass flow rates of the two working agents ($\dot{m}_1$, $\dot{m}_2$) heat fluxes ($\dot{Q}_1$, $\dot{Q}_2$) and thermal efficiency (η) of the device.

2. Experimental data processing

The measured values presented in tables 2 – 5 allow calculating average temperature and average pressure, as is shown in relation (1) and (2).

$$t_{m1} = \frac{t_{11}+t_{12}}{2}, [°C] \qquad t_{m2} = \frac{t_{21}+t_{22}}{2}, [°C] \tag{1}$$

$$p_{m1} = \frac{p_{11}+p_{12}}{2}, [bar] \qquad p_{m2} = \frac{p_{21}+p_{22}}{2}, [bar] \tag{2}$$

For this value, using EES (Engineering Equation Solver [117]) software, were calculated thermo physics parameters: specific heat, density, thermal conductivity, kinematic viscosity and Prandtl numbers, using relation (3 -7):

cp1= CP(Water, T= tm1,P= pm1), [J/kgK]; cp2= CP(Water,T= tm2,P= pm2), [J/kgK] (3)

ρ1=DENSITY(Water,T=Tm1,P=Pm1), [kg/m3]; ρ2=DENSITY(Water,T=Tm2,P=Pm2), [kg/m3] (4)

ISSN 1454 - 8003
Proceedings of 2014 International Conference of Hydraulics and Pneumatics - HERVEX
November 5 – 7, Calimanesti-Caciulata, Romania

λ_1=CONDUCTIVITY(Water,T=Tm1,P=Pm1), [W/m K] ; (5)

λ_2= CONDUCTIVITY (Water,T=Tm2,P=Pm2), [W/m K]

(6)

ν_{1cm}=VISCOSITY(Water,T=Tm1,P=Pm1), [m^2/s];
ν_{2cm}=VISCOSITY(Water,T=Tm2,P=Pm2), [m^2/s]

(7)

Pr_1=PRANDTL(Water,T=Tm1,P=Pm1), [-]

Pr_2=PRANDTL(Water,T=Tm2,P=Pm2), [-]

Mass flow rate for the two agents was determine from volume flow rate using relation (8)

$$\dot{m}_1 = \frac{\rho_1 \dot{V}_1}{3600}, [kg/s] \qquad \dot{m}_2 = \frac{\rho_2 \dot{V}_2}{3600}, [kg/s] \tag{8}$$

Relations (9) permit to calculate the heat flux for both, hot and cold, agents:

$$\dot{Q}_1 = \dot{m}_1\, c_{p1}(t_{11} - t_{12}) \quad [W] \qquad \dot{Q}_2 = \dot{m}_2\, c_{p2}(t_{22} - t_{21}) \quad [W] \tag{9}$$

Thermal efficiency is given by the ratio between heat flux accepted by the cold agent and heat flux given by the hot agent, as shown in relation 10:

$$\eta = \frac{\dot{Q}_2}{\dot{Q}_1} 100 \qquad [\%] \tag{10}$$

Table 6 presents the calculated values of the heat fluxes for both agents and thermal efficiency of the device for all cases studied. The imposed conditions were keeping constant the inlet temperature of both agents (t_{11}, t_{21}) and volume flow rate for the hot temperature ($\dot{V}_1$).

Table 6 Calculated values [4]

Nr. crt	$\dot{V}_1$=0.5 m^3/h			$\dot{V}_1$=0.707 m^3/h			$\dot{V}_1$=0.9 m^3/h			$\dot{V}_1$=1.2 m^3/h		
	$\dot{Q}_1$ [W]	$\dot{Q}_2$ [W]	η [%]	$\dot{Q}_1$ [W]	$\dot{Q}_2$ [W]	η [%]	$\dot{Q}_1$ [W]	$\dot{Q}_2$ [W]	η [%]	$\dot{Q}_1$ [W]	$\dot{Q}_2$ [W]	η [%]
1	18197	17531	96.34	19728	19108	96.86	20538	19906	96.93	21515	20871	97.01
2	18355	17699	96.43	19826	19238	97.03	20652	20046	97.07	21680	21052	97.1
3	18497	17842	96.46	19956	19399	97.21	20745	20161	97.19	21790	21184	97.22
4	18618	17974	96.54	20029	19495	97.33	20817	20256	97.31	21873	21290	97.33
5	18797	18154	96.58	20143	19616	97.38	20951	20406	97.39	21983	21413	97.41
6	18896	18258	96.62	20249	19745	97.51	21065	20525	97.43	22052	21499	97.49
7	18977	18361	96.76	20380	19893	97.61	21179	20636	97.44	22190	21640	97.52
8	19029	18421	96.81	20453	19997	97.77	21231	20691	97.46	22258	21716	97.56

As the hot agent transfer heat, it is taken quickly to the beginning of the transfer due to the large temperature difference between the working agents and then gradually decreases due to the reduction of heat pick-up ability of the cold agent, according to the results shown in Table 6. For the four values of the mass flow, it is noted that the heat flux taken up by the cold agent records maximum values for all types of heat exchangers tested at low temperature difference (Δt2).

Measurements that were done, show an increase in thermal efficiency with increasing mass flow of secondary heating agent, its values being in the range (96.5 ... 97.8)%, which highlights the effectiveness of these devices.

3. Performance number

The determination of flow regime involves calculating the Reynolds number and is determined by the relation $Re = \frac{w d_{ech}}{\nu}, [-]$, in which the hydraulic equivalent diameter is the most difficult to determine due to the complex geometry. For this reason, the author used SolidWorks design program to determine the area (Ss) and the wet perimeter (Ps) for the flow cross-section. In figure 5.17 are presented the three cross-sections through a flow channel of the heat exchanger.

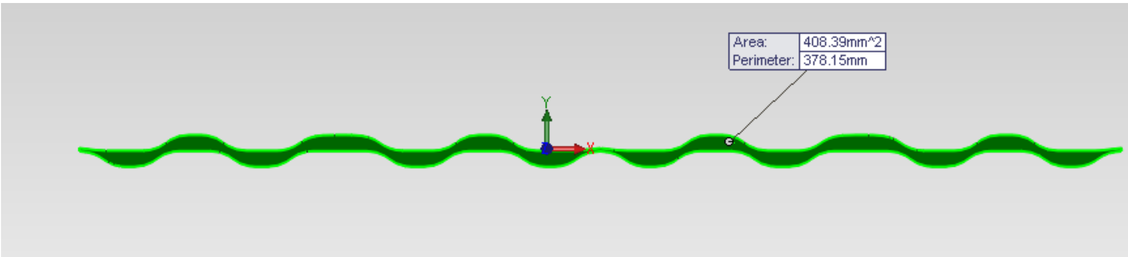

Figure 4. Determining the hidraulyc diameter for TK model (β= 30°) [4]

It resulted the following: S_S=408.39 x 10^{-6} m; P_S=378.15 x 10^{-3} m; d_{ech}=0.0043 m. Conditions for liquid flow is delimited by the Reynolds number.

According to the values obtained for Reynolds number, ranging from 3000 to 10000 (Re> 10,000) the flow regime is laminar to transient, with values in the range (3581 ... 7695). Graphs presented in figure 5 show performance close to the 4 sets of measurements made, this due to close velocities flow.

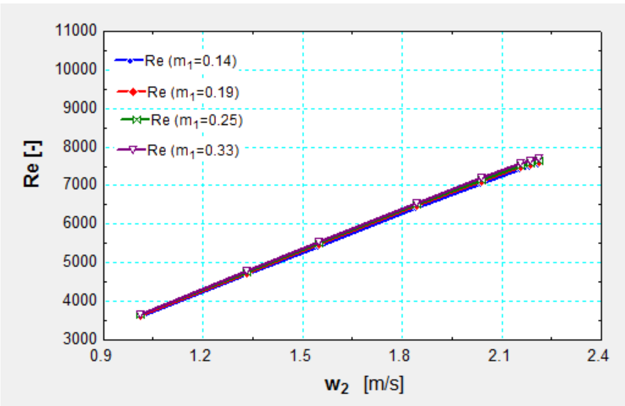

Figure 5. Re= f(w_2)

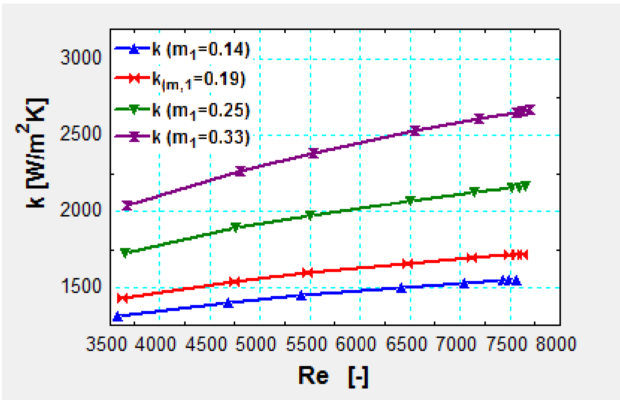

Figure 6. k= f(Re)

According to the chart presented in figure 6, for each test performed, there is a proportional increase of overall heat transfer coefficient with the increase of mass flow reflected in Reynolds criterion.

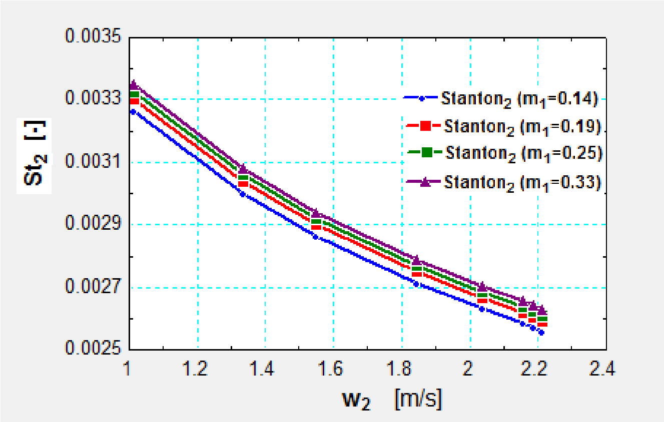

Figure 7. St= f(w_2)

For increasing values of the flow rate through the channel is recorded the increasing of Reynolds number, leading to a decrease in Stanton number. This means that an intense heat transfer with high speed flow values will record low values for Stanton number, which is confirmed by the graphic in Figure 7.

4. Conclusions

From the analysis we can draw the following conclusions:

- heat flow over the heating prmar is directly proportional to the temperature difference between the temperature of primary heat agent input and output, so its variation is continuously increasing.
- for the four values of mass flow, is observed that heat flux taken up by the secondary agent register maximum values for all four tests conducted at low temperature differences (Δt2);
- measurements on all heat exchangers equipment indicates an increase in thermal efficiency with increasing mass flow of secondary heating agent, its values being in the range (96.4 ... 97.8)%, which highlights the effectiveness of these devices;
- according to the values obtained for Reynolds number ranging from 3000 to 10000, laminar flow regime is transient ·
- overall coefficient of heat exchange for plate configurations tested, increases with increasing mass flow for registered agent with values between 1310 and 2777 W / m^2K; ·
- according to the results obtained for the Stanton number, its variation depending on the mass flow of the secondary agent is very small;.

REFERENCES

[1] Plesa A., Grieb C. F., Nagi M., Utilaje termice. Schimbatoare de caldura cu placi, Mediamira, Cluj-Napoca, 2008
[2] Zhu J., Zhang W., Optimization design of plate heat exchangers (PHE) for geothermal district heating systems, 2004, 33, p. 337-347
[3] Rush T.A., Newell T.A., Jacobi A.M., An experimental study of flow and heat transfer in sinusoidal wavy passages, Int. J. Heat Mass Transfer, 1999, 42, p. 1545–1553
[4] Irimies Giurgiu Oana, "Cercetări privind studiul curgerii fluidelor prin canalele schimbătoarelor de căldură cu plăci în vederea creşterii performanţelor termodinamice ale acestora", PhD thesis, UTC-N, Cluj – Napoca, 2014
[5] http://www.sondex.ro/

ISSN 1454 - 8003
Proceedings of 2014 International Conference of Hydraulics and Pneumatics - HERVEX
November 5 – 7, Calimanesti-Caciulata, Romania

ELASTOPLASTIC PROPERTIES AND TENDENCY OF IRON-NICKEL COMPOSITE COATINGS TO BRITTLE FRACTURE

Vasile JAVGUREANU[1], Pavel GORDELENCO[2]

[1] Technical University of Moldova, v_javgureanu@yahoo.com

[2] Technical University of Moldova, pavel_gr@mail.utm.md

Abstract: *This paper presents the study of elastic-plastic properties (he, hp; h; Ae; Ap; A; H; Hh; Hh/H, E, P), taking into account the degree of compaction coefficient (K) and porosity (ρ) composite coatings of iron- specific method macro indentation. First experimentally determined coefficients taking into account the degree of compaction (K) and porosity (ρ) iron-nickel coatings with changing conditions of electrolysis (DK, T). It has been established that the increase of the current density (DK) and a decrease in temperature (T) of the electrolysis of iron-nickel coatings for, taking into account the power factor of the seal (K) coatings decreases and the porosity (ρ) increases coatings.*

Keywords: *elastoplastic, deformation, failure, galvanic, electrolytic, iron-nickel composite coatings.*

1. Introduction

Nickel-iron composite coatings are used to harden and restore parts of machines in the industry in order to increase their longevity. Electro deposition conditions have a significant impact on physical and mechanical properties of the coatings. Knowledge of the physical and mechanical characteristics of composite iron-nickel coatings is needed to make informed choices of deposition process conditions, depending on the operating conditions of remanufactured parts, as well as to perform strength calculations.

2. The common information.

Actual problems of study of physical and mechanical properties of materials on surface and subsurface layers are related to the fact that the deformations are associated with all modern methods of treatment, hardening and metal compounds.

Importance of determining the elastoplastic characteristics (h_e, h_p, h), the work required for deformation (A_e, A_p is, A), unrestored and dynamic hardness (H_h, H_d), modulus of elasticity (E) coatings, the critical load indentation diamond spherical indenter in which begins the process of brittle fracture (P_{cr}), the ratio of non-reduced and dynamic hardness to elastic modulus (H_h/E, H_d/E), yield strength (σ_b), the true tensile strength (S_b), tensile strength (σ_v), toughness (α_H), the degree of material deformation in the contact zone (Ψ) is invaluable.

An important parameter of iron-nickel composite coatings is their fragility. This property is undesirable because increase in brittleness affects such important characteristic as wear [2].

It is known that the fragility of coatings depends on substrate pretreatment conditions and electroplating. It can be caused by the inclusion of hydrogen coating, surface active agents (surfactants), metals and other foreign particles.

To determine the brittleness of sediments, a method based on bending of the plate is mainly used. Occurrence of a crack in the sediments and the bending angle of the plate, coating brittleness is evaluated. [2] In this case, the test results can depend on the nature of the material and thickness of the substrate plate. Moreover, using this method, researchers have information on the relative brittleness of coatings, excluding the applied voltage necessary for the formation of cracks in the coating. To this end, an attempt was made to use the indentation method [1-4] which allows to determine tension stress.

Electro deposition conditions have a significant effect on the fragility of coatings: with the increase of their stiffness (increased current density, decreasing the temperature of the electrolyte) it is significantly increased. The electrolyte composition may differently affect the properties of the coatings considered.

In the paper, elasto-plastic properties and their tendency to brittle fracture of iron-nickel composite coatings obtained from electrolyte 4 [2, p.59] are shown. The samples used in the rollers 30mm in diameter, thickness 0.5mm and length of 100mm, which were treated under optimal grinding. Physical and mechanical properties were determined at the facility for the study of the hardness of materials in macro volume equipped with an inductive sensor and a differential amplifier that can record chart indentation diamond spherical indenter and indentation recovery after unloading.

The dynamic hardness (Hd) was determined as the ratio of the total of (A) consumed for elastoplastic deformation of the deformable volume indentation (V) under load, in all investigated iron-nickel composite coating. Coatings on the plastic deformation associated with the preparation of destruction is spent working (A_p).

Currently, theoretical and experimental issues associated with the assessment of the properties of brittle materials indentation of a spherical indenter, are well developed [1-4].

Studies carried out in [2] showed that when a spherical indentation gradually increase in load on the indenter can reach a critical state in which the circumferential cracks are formed, approximately coinciding with the indentation diameter of coatings obtained under all conditions of electrolysis [2]. However, the critical condition occurs when the elastoplastic deformation, due to a small residual strain covering major difficulties in measuring the diameter of the indentation, so its boundaries are fixed on the contact patch. Furthermore, in this case before a continuous ring-cracks appear, new random direction cracks occur [2].

In scratching the critical load was recorded with cracks perpendicular to the direction of movement of the indenter. As with spherical indentation, brittle fracture occurred in the presence of plastic deformation. Due to fracture coatings formed during the test as new individual crack located at different angles to the direction of movement of the indenter [2].

Analysis of the results showed that in spite of the plastic deformation of the coating for all the studied sediments as under static indentation and scratching critical load varies as the radius of the sphere. With increasing current density, the critical state occurs at lower loads [2].

For comparison of theoretical and experimental values of the ratio of the critical load at slip (P_{cr}) to the critical load under static indentation (P_{st}) a formula was used, derived from the condition that the critical stress upon the occurrence of damage in case of static and dynamic indentation:

$$\frac{Pcr}{Pst} = \frac{1}{(1 + 3Af)^3}$$

where: P_{cr} and P_{st} - critical load, respectively, scratching and static indentation.

f - the coefficient of friction between the indenter and the sample scratching.

To determine the values of A used the expression:

$$A = \frac{3\pi \cdot (4+\mu)}{8 \cdot (1-2\mu)}$$

where : μ - Poisson's ratio of coatings.

Studies have shown that using macro indentation selection of load and the diameter of the sphere is possible to determine the physical and mechanical properties of the coatings.

Despite the valuable information that can be detected by indentation with its use have difficulties associated with determining the diameter of the indentation and the onset of brittle fracture, which affects the plastic deformation of elastic coatings by immersion of the indenter. Besides hardness measurement method based on determination of the diameter of the impression, does not allow to obtain information about the nature of elastic materials. Therefore, to study the hardness of the coatings was used in macro volume hardness TCS -1 allows you to record chart indentation diamond spherical indenter and indentation recovery after unloading. Synthetic diamond indenter with spherical radius 1mm was used.

By measuring the physical and mechanical properties of iron coatings with different loads on the indenter (P) established that the Primer loads (up to P_{cr}) ratio: $\frac{P}{\pi \cdot D \cdot h}$ is a constant value. With further increase in load, this value rises sharply, indicating a deviation from the mechanical similarity. On Regularities are strongly influenced by the conditions of electrolysis. With increasing current density violation original patterns occurs at lower loads on the indenter [2].

Study of features (h_e) elastic and plastic (h_p) strain coatings showed that responsible for the results obtained is the changing nature of the elastic deformation depending on the loading conditions. Regardless of the conditions for obtaining coatings with increasing load on the indenter elastic deformation component coatings first increases sharply and then it rises slightly [2].

The main reason that causes the violation of the law of the mechanical similarity is associated with the beginning of brittle fracture surfaces.

Comparing this critical loads with their values determined from observations form a ring crack, it can be argued that the onset of brittle fracture coatings can be determined much more accurately by measuring the depth of the indentation and the critical load (P_{cr}) as to form an annular crack growth is possible source of cracks and the formation of new, behind which is difficult to observe. The critical stress can be taken as a criterion for evaluating the tendency to brittle fracture coatings.

3. Discussion of experimental studies.

Studies have shown that the elastic-plastic properties and susceptibility to brittle fracture of iron-nickel composite coatings vary with the electrolysis conditions (Table 1-4).

With increasing current density (Дк) of 5×10^{-4} to 80×10^{-4} kA/m^2 electrolysis at a constant temperature (40^{0}C), plastic indentation depth (h_p) and the critical load indentation (P_{cr}) for spherical diamond indenter is reduced accordingly from 2,598 to 0,0892 (μm) and 350 to 210 (N), and the elastic component of the indentation depth (h_e) is increased from 3,402 to 4,050 (μm), total indentation depth (N) of 6,0 (μm). Work expended in elastic (A_e), plastic (A_p), elastoplastic deformation (A) not restored (H_h), dynamic (H_d) hardness iron - nickel coatings, indentation load on the diamond spherical indenter (P) are the extreme value with changes in density current (Дк) from 5×10^{-4} to 80×10^{-4} kA/m^2 electrolysis at constant temperature (40^{0}C), table 1. Elastoplastic property iron-nickel coatings and their susceptibility to brittle fracture (Tables 1 and 2) were determined for a single indentation depth (h=6.0 μm) by a known procedure (2).

Studies have shown that with increasing current density from $5×10^{-4}$ to $50×10^{-4}$ kA/m^2 electrolysis at a constant temperature (40^{0}C), the work spent on the elastic deformation of coatings increased from $168.6×10^{-3}$ to $226×10^{-3}$, (N×mm), the work expended in plastic deformation (Ap) coatings increased from $128.8×10^{-3}$ to $132.8×10^{-3}$ (N×mm), the work spent on the elastic-plastic deformation (A) coating increased from $297.4×10^{-3}$ to $358.8×10^{-3}$ (N×mm), unrestored coating hardness (Hh) coatings increased from 3930 to 4760 (N/mm^2), dynamic hardness (Hd) coatings increased from 2636 to 3181 (N/mm^2) and the indentation load on the diamond spherical indenter (P) increased from 148.7 to 179.4 (N).

Table 1.

Elastoplastic properties of iron-nickel composite coatings and their tendency to brittle fracture.

Electrolysis conditions		H_h,	H_d,	Elastoplastic properties						P,	P_{cr},
Дк, $×10^{-4}$ кА/m^2	T, ^{0}C	N /mm^2	N /mm^2	h_e, µm	A_e, N·mm	h_p, µm	A_p, N·mm	h, µm	A, N·mm	N	N
5	40	3930	2636	3,402	0,1686	2,598	0,1288	6,0	0,2974	148,7	350
10	40	3970	2652	3,450	0,1720	2,550	0,1272	6,0	0,2992	149,6	340
20	40	4120	2752	3,516	0,1819	2,484	0,1285	6,0	0,3104	155,2	320
30	40	4280	2860	3,630	0,1952	2,370	0,1274	6,0	0,3226	161,3	300
40	40	4440	2966	3,720	0,2075	2,280	0,1227	6,0	0,3202	167,3	280
50	40	4760	3181	3,780	0,2260	2,220	0,1328	6,0	0,3588	179,4	265
60	40	4320	2886	3,840	0,2084	2,160	0,1172	6,0	0,3256	162,8	245
80	40	3640	2432	4,050	0,1851	1,950	0,0892	6,0	0,2743	137,2	210

Table 2.

Elastoplastic properties of iron-nickel composite coatings and their tendency to brittle fracture.

Electrolysis conditions		H_h,	H_d,	Elastoplastic properties						P,	P_{cr},
Дк, $×10^{-4}$ кА/m^2	T, ^{0}C	N/mm^2	N/mm^2	h_e, µm	A_e, N·mm	h_p, µm	A_p, N·mm	h, µm	A, N·mm	N	N
50	20	3640	2432	4,560	0,2088	1,440	0,0659	6,0	0,2747	137,2	210
50	40	4760	3181	3,780	0,2260	2,220	0,1328	6,0	0,3588	179,5	265
50	60	3930	27636	3,084	0,1529	2,916	0,1446	6,0	0,2975	148,7	320

With increasing current density (Дк) from $50×10^{-4}$ to $80×10^{-4}$ KA/m^2, electrolysis at a constant temperature (40^{0}C) the work expended on elastic (A_e) deforming coatings decreased from $185.1×10^{-3}$ to $226×10^{-3}$ (N×mm), the work expended in plastic deformation coatings (A_p) decreased from $132,8×10^{-3}$ to $89,2×10^{-3}$ (N×mm), the work spent on elastoplastic deformation (A) coatings decreased from $358,8×10^{-3}$ to $274,3×10^{-3}$ (N×mm), unrestored coating hardness (H_h) decreased from 4760 to 3640 (N/mm^2), dynamic coating hardness (H_d) decreased from 3181 to 2432 (N/mm^2) and the indentation load on the diamond spherical indenter (P) decreased from 179.4 to 137,2 (N). From the results of the study (Table 1) shows that the work expended in elastic (A_e), plastic (A_p) elastic-plastic (A) deforming coatings unrestored (H_h), dynamic (H_d) hardness and load dented the diamond spherical indenter (P) monitoring the density of current (Дк) at a constant temperature of electrolysis (T) have extreme values (Table 1).

With increasing temperature electrolysis (T) from 20 to 60ºC (Table 2), at a constant current density (Дк) =50×10^{-4} kA/m^2 critical load indentation ($P_{cr.}$) On diamond spherical indenter characterizes the beginning of brittle fracture of iron-nickel coatings plastic component (h_p) and the depth of the indentation work spent on plastic deformation of coatings (A_p) respectively increased from 210 to 320 (N/mm^2), from 1.44 to 2.916 (micrometers) and from 65.9×10^{-3} to 144.6×10^{-3} (N×mm), and elastic component (h_e) indentation depth decreased from 4.56 to 3.084 (micrometers).

Nature of the change work expended in elastic (A_e), elastoplastic deformation (A) coatings, unrestored (H_h), dynamic (H_d) coating hardness and load indentation (P) on the diamond spherical indenter at a depth of 6.0 micrometers are also extreme. With increasing temperature electrolysis (T) from 20 to 40ºC, at a constant current density (Дк) 50×10^{-4} kA/m^2 work spent on the elastic deformation of the coating increased to 208,8×10^{-3}, 226,0×10^{-3} (N×mm), the work expended elastoplastic deformation (A) increased from 274,7×10^{-3} to 358,8×10^{-3} (N×mm), unrestored hardness (H_h) coatings increased from 3640 to 4760 (N/mm^2), the dynamic hardness of the coatings increased from 2432 to 3181 (N/mm^2) and the indentation load (P) the diamond spherical indenter increased from 137.2 to 179.5 (N). With further increase of the temperature (T) of the cell from 40 to 60ºC, at a constant current density (Дк) 50×10^{-4} kA/m^2 work expended elastic deformation of coatings (A_e) decreased from 226.0×10^{-3} to 152.9×10^{-3} (N×mm), the work expended on the elastic-plastic deformation of the coating decreased from 358.8×10^{-3} to 297.5×10^{-3} (N×mm), unrestored coating hardness (H_h) decreased from 4760 to 3930 (N/mm^2) dynamic coating hardness (H_d) decreased from 3181 to 2636 (N/mm^2) and indentation load (P) on the diamond spherical indenter decreased from 179.5 to 148.7 (N), Table 2.

Study of the influence of the current density (Дк) and the electrolysis temperature (T), the tendency of iron-nickel coatings and brittle fracture, showed that an increase in current density (Дк) of 5×10^{-4} to 80×10^{-4} (kA/m^2) at a constant temperature electrolysis (40ºC), the critical load for pressing the spherical diamond indenter is reduced from 350 to 210 (N), indicating an increase in iron-nickel coatings tendency to brittle fracture. With increasing temperature, the electrolysis of from 20 to 60ºC, at a constant current density (Дк) 50×10^{-4} kA/m^2, the critical load for pressing the spherical diamond indenter (P) is increased from 210 to 320 (N) that indicates a decrease tendency of iron-nickel coatings to brittle fracture.

Is of great interest to determine the beginning of the brittle fracture of composite iron - nickel coatings in the indentation test. For most of the theoretical strength of materials review Tmax, significantly greater than the theoretical shear strength G max [1]. This is due to the fact that the sliding connection between the atoms, a plane perpendicular to the sliding periodically reversed. Degree of recovery of these relations define a measure of material ductility. Unrestored appearance bond equivalent of a new elementary surface on which creation is spent working, the measured surface energy [1].

On the plastic deformation associated with the preparation of destruction, work is expended. From this point of view, consider the change elasto-plastic properties of composite coatings when iron-early brittle fracture (P_{cp}, Tables 3 and 4).

With increasing current density (Дк) of 5×10^{-4} to 80×10^{-4} kA/m^2 electrolysis at a constant temperature (40ºC), the critical load (P_{cr}), elastoplastic properties (h_e; h_p; h; A_e; A_p; A) decreases, respectively, from 350 to 210 (N), from 7.15 to 5.6 (micrometers), from 3.95 to 1.8 (micrometers) from 11.1 to 7.4 (micrometers) from 834×10^{-3} to 392×10^{-3} (N×mm) from to 461×10^{-3} 126×10^{-3} (N×mm) from 1295×10^{-3} to 518×10^{-3} (N×mm). The volume of prints (V) under load also decreased from 38.47×10^{-5} to 17.13×10^{-5} (mm^3). The results demonstrate that the process of brittle fracture of iron-nickel coatings began. Work spent on plastic deformation and total iron- coating indentation significantly higher (respectively 126×10^{-3}, 461×10^{-3}, 518×10^{-3}, 1295×10^{-3} (N×mm) than in the previous case (Table 1 and 2), respectively, 89.2×10^{-3} - 128,8×10^{-3} and 274,3×10^{-3}, 358,8×10^{-3}

(N×mm). This proves that the total plastic deformation and iron-nickel coatings spent significantly more work (A_p; A), which is associated with the preparation of brittle fracture surfaces.

Table 3.

Elastoplastic properties of composite iron-nickel coatings on reaching a critical state.

Electrolysis conditions		$P_{кр}$,	$H_{hкр}$,	Elastoplastic properties						V,	H_{dcr},	H_{hcr} /E	H_{dcr} /E
$Д_к$, $\times10^{-4}$ кА/м^2	T, ^{0}C	N	N/мм^2	h_e, μм	A_e, N·мм	h_p, μм	A_p, N·мм	h, μм	A, N·мм	$\times10^{-5}$ мм^3	N/мм^2		
5	40	350	5021	7,15	0,834	3,95	0,461	11,1	1,295	38,47	3366	0,0239	0,0162
10	40	340	5013	6,8	0,771	4,0	0,453	10,8	1,224	36,45	3360	0,0245	0,0164
20	40	320	5045	6,68	0,713	3,42	0,365	10,1	1,078	31,87	3382	0,0255	0,0171
30	40	300	5082	6,1	0,610	3,30	0,330	9,4	0,94	27,61	3405	0,0261	0,0175
40	40	280	5124	5,83	0,544	2,87	0,268	8,7	0,812	23,66	3432	0,0265	0,0178
50	40	265	5480	5,33	0,471	2,37	0,209	7,7	0,68	18,55	3666	0,0291	0,0195
60	40	245	5133	5,41	0,442	2,19	0,179	7,6	0,62	18,08	3431	0,0285	0,0191
80	40	210	4519	5,6	0,392	1,8	0,126	7,4	0,518	17,13	3024	0,258	0,0173

Table 4.

Elastoplastic properties of iron-nickel composite coatings achieve the critical state

Electrolysis conditions		P_{cr}, N	H_{hcr}, N/мм^2	Elastoplastic properties						V, $\times10^{-5}$ мм^3	H_{dcr}, N/мм^2	H_{hcr} /E	H_{dcr} /E
$Д_к$, $\times10^{-4}$ кА/м^2	T, ^{0}C			h_e, μм	A_e, N·мм	h_p, μм	A_p, N·мм	h, μм	A, N·мм				
50	20	210	3843	6,6	0,462	2,1	0,147	8,7	0,609	23,65	2574	0,0225	0,0151
50	40	265	5480	5,33	0,471	2,37	0,209	7,7	0,680	18,55	3666	0,0291	0,0195
50	60	320	4549	6,03	0,643	5,17	0,551	11,2	1,194	39,17	3051	0,0222	0,0149

With increasing current density (Дк) of 5×10^{-4} to 4, 80×10^{-4} kA/m^2, electrolysis at a constant temperature (40° C), unrestored critical hardness (voltage), the critical dynamic hardness (H_{dcr}) ratio H_{hcr}/E and H_{dcr}/E have extreme nature (Tables 3 and 4). Since the beginning to achieve brittle fracture composite iron - nickel coatings, the critical load is changed from 350 to 210 (N) and the overall penetration depth was varied from 11,1 to 7,4 (μm).

Studies have shown that with increasing current density (Дк) of 5×10^{-4} to 50×10^{-4} (kA/m^2), at a constant temperature electrolysis (40°C), unrestored critical hardness (N) increased from 5021 to 5480 (N/mm^2), the critical dynamic hardness increased from 3366 to 3666 (N/mm^2), and the ratio H_{hcr}/E and H_{dcr}/E respectively increased from 0.0239 to 0.0291 and from 0.0162 to 0.0195. With further increase of the current density from 50×10^{-4} to 80×10^{-4}(kA/m^2), at a constant temperature electrolysis (40°C) unrestored critical hardness (N) decreased from 5480 to 4519 (N/mm^2), the critical dynamic hardness (H_{dcr}) decreased from 3666 to 3024 (N/mm^2) and the ratio and correspondingly decreased from 0.0291 to 0.0258 and from 0.0195 to 0.0173.

With increasing temperature electrolysis of 20 to 60°C (Table 4) with a constant current density (Дк= 50×10^{-4} kA/m^2), the critical load (P_{cr}) characterizes the beginning of brittle fracture coatings elastoplastic properties (h_e; h_p; h; A_e; A_p; A) increases, respectively, from 5.33 to 6.6 (micrometers), from 8.7 to 11.2 (micrometers), from 462×10^{-3} to 643×10^{-3} (N×mm), from 147×10^{-3} to 551×10^{-3} (N×mm) and from 609×10^{-3} to 1194×10^{-3} (N×mm).

With increasing temperature, the cell from 20 to 40°C at a constant current density 50×10^{-4} kA/m^2 unrestored critical hardness (N) increased from 3843 to 5480 (N/mm^2), the critical dynamic hardness (H_{dcr}) increased from 2574 to 3666 (N/mm^2), the ratio H_{hcr}/E and H_{dcr}/E increased respectively from 0.0225 to 0.0291 and from 0.0151 to 0.0195, while the volume of indentation under load (V) decreased from 23.65×10^{-5} to 18.55×10^{-5} (mm^3).

With further increase of the temperature of the cell from 40 to 60°C at a constant current density (Дк=50×10^{-4} kA/m^2), unrestored (H_{hcr}) critical hardness (N) decreased from 5480 to 4549 (N/mm^2), the critical dynamic hardness (H_{dcr}) decreased from 3666 to 3051 (N/mm^2), and the ratio decreased, respectively, from 0.0291 to 0.0222 and from 0.0195 to 0.0149, while the volume of indentation load (V) increased from 18.55×10^{-5} to 39.17×10^{-5} (mm^3). In this case the results obtained confirm the brittle fracture start composite iron - nickel coatings (Table 4). With increasing temperature, the electrolysis of from 20 to 60°C, at constant current density (D_k=50×10^{-4} kA/m^2) coatings tendency to brittle fracture is reduced, since the critical load (P_{cr}), which begins when a brittle fracture of the coating increases from 210 to 320 (N). This is confirmed by the fact that the work spent on plastic (A_p) and elastic-plastic deformation of iron - nickel coatings (Table 4) constitute $147\times10^{-3}\div551\times10^{-3}$ (N×mm) and $609\times10^{-3}\div1194\times10^{-3}$ (N×mm) and significantly higher than in the previous case (Table 2) respectively $65{,}9\times10^{-3}\div144{,}6\times10^{-3}$ (N×mm) and $27479\times10^{-3}\div358{,}8\times10^{-3}$ (N×mm). This proves that a higher amount of plastic (A_p) and elastoplastic work associated with the preparation of the beginning of brittle fracture of composite iron - nickel coatings.

Comparing the experimental data it can be argued that the onset of brittle fracture of composite iron - nickel coatings can be determined as much by measuring the depth of the elastic-plastic indentation (N) diamond spherical indenter, elastoplastic characteristics (h_e; h_p; h; A_e; A_p; A), the critical load, the beginning of brittle fracture (P_{cr}), the critical stress (H_{hcr}; H_{dcr}) iron-nickel coatings. The critical stress can be taken as a criterion for assessing the tendency to brittle fracture coatings.

Study of the influence of electrolysis conditions (Дк, T) coatings on the tendency to brittle fracture showed that the critical state of coatings occurs at higher current densities (Дк) and lower temperature electrolysis (T).

Studies have shown that the maximal values of elastoplastic characteristics (A_e; A_p ; A; H_h; H_d; P; Tables 1 and 2), iron-nickel coatings can be selected to produce coatings obtained under different conditions of the electrolysis (Дк, T) in terms of their maximum durability. It will significantly reduce the time of the experiments, increasing the amount of research that will significantly extend the effective use of iron-nickel coatings industry.

4. Conclusions

Experimentally found that hardness unrestored (H_h), dynamic hardness (H_d), the work expended on elastic (A_e), plastic (A_p), elastoplastic (A) deformation and load spherical diamond indenter (P at h = 6,0 μm) have to change the nature extreme conditions of electrolysis (Дк, T) for iron-nickel coatings studied, with the proviso that $P<P_{cr}$.

Experimentally established the beginning of brittle fracture of iron-nickel coatings on critical load indentation (P_{cr}) and unreduced critical hardness (H_{hcr}), changes in the conditions of electrolysis

(Дк, T), the critical load indentation (P_{cr}) diamond spherical indenter and the critical stress (hardness H_{hcr}) can be taken as a criterion for assessing the tendency to brittle fracture coatings.

For the first time experimentally shown that with the beginning of brittle fracture of iron-nickel coatings at $P = P_{cr}$, the work expended on elastic (A_e), plastic (A_p), elastoplastic deformation (A), the load on the diamond spherical indenter ($P = P_{cr}$) and the indentation depth (h_p; h) decreases with increasing current density (Дк) and reduction temperature of electrolysis (T).

For the first time experimentally shown that with the beginning of brittle fracture of iron-nickel coatings at $P = P_{cr}$ work expended on elastic (A_e), plastic (A_p) and elastic-plastic (A) deformation significantly increases in value than in ($P<P_{cr}$). This proves that the increase of the work spent on the elastic (A_e), plastic (A_p) and elastic-plastic (A) deformation associated with the preparation of the start of the brittle fracture of iron-nickel coatings.

It is found that with increasing current density (Дк) and decreasing temperature electrolysis (T) increases the propensity of iron-nickel coating to brittle fracture.

For the first time experimentally shown that unrestored critical hardness (voltage, H_{dcr}), the critical dynamic hardness (H_{hcr}), ratio H_{hcr}/E and H_{dcr}/E have extreme character changes in the conditions of electrolysis (Дк, T) for the study of iron - nickel coatings. Extreme values and H_{hcr} H_{dcr}, relations H_{hcr}/E and H_{dcr}/E coincide with our earlier recommendations for iron - nickel coatings in terms of ensuring their optimum durability.

Extreme values unreduced hardness (H_h), dynamic hardness (H_d), the work expended in elastic (A_e), plastic (A_p) elastic-plastic deformation (A) and the indentation load on the diamond spherical indenter (P) coincide with our earlier recommendations for iron- nickel coatings in terms of ensuring their optimum durability.

REFERENCES

[1] S. Bulychev, V. Alekhin, “Ispytaniye materialov nepreryvnym vdavlivaniyem indentora”, Moskva. Mashinostroyeniye, pp.224, 1990 (in Russian).
[2] V. Gologan, V. Azhder, V. Zhavguryanu, “Povysheniye dolgovechnosti detaley mashin iznosostoykimi pokrytiyami”, Kishinev, Izd-vo Shtiintsa, pp.112, 1979 (in Russian).
[3] M.P. Markovets, “Determination of mechanical properties of materials for hardness“. Moscow, Mechanical Engineering, 1979, pp.191. (in Russian).
[4] V.K. Grigorovich, “Hardness and microhardness of metals“. Moscow, Publishing House" Science, 1976, pp.230 (in Russian).
[5] V.Javgureanu, V.Ajder, V.Ceban, S.Pavlova, “The correlation of restored and unrestored microhardness of. wear-proof iron plating”, International Scientific Conference TMCR. Chisinau, pp.412-415, 2003.
[6] V.Javgureanu, P.Gordelenco, M.Elita, “The work of deforming wear-proof iron-nikel plating in microsquelging”, The Annals of University Dunărea de Jos of Galați, Fascicle VIII, Tribology, Romania, pp.65-68, 2004.
[7] V.Javgureanu, P.Gordelenco, M.Elita, “Relationship of the restored and unrestored microharedbess of the cromium coating”, The Annals of University Dunărea de Jos of Galați, Fascicle VIII, Tribology, Romania, pp.48-51, 2004.
[8] V.Javgureanu, P.Gordelenco M.Elita, “Le rapport de la microdurete restauree et non restauree des convertures de crome”, International Scientific Conference TMCR, Chisinau, pp.166-169, 2005.
[9] V.Zhavguryanu, P.Godelenko, “Sootnosheniye vosstanovlennoi i nevostanovlenoy mikrotverdosti khromovykh pokrytiy”, Mezhdunarodnaya NTK "Mashinostroyeniye i tekhnosfera XXI veka", Sevastopol', 2005. (in Russian).
[10] V.Zhavguryanu, “Issledovaniye raboty deformatsii iznosostoykikh gal'vanicheskikh pokrytiy pri mikrovdavlivanii”, Mezhdunarodnaya NTK Novyye protsessy i ikh modeli v resurso i energosberegayushchikh tekhnologiy, Odessa, pp.7-8, 2003 (in Russian).

ISSN 1454 - 8003
Proceedings of 2014 International Conference of Hydraulics and Pneumatics - HERVEX
November 5 – 7, Calimanesti-Caciulata, Romania

HYDRAULIC SYSTEMS OF DRILLING MACHINES AND EQUIPMENT DESIGNED IN KOMAG

Piotr ROJEK[1]

[1]ITG KOMAG, projek@komag.eu

Abstract: *Hydraulic systems of drilling machines for underground and surface mining industry, designed in KOMAG, are presented. Main functions as well as principle of operation of main subassemblies of drilling machines are described. Advantages of energy-saving load sensing system, enabling control of working medium flow regardless of load of a machine are discussed.*

Keywords*: mining industry, drilling technology, drilling rig, hydraulics, load sensing*

1. Introduction

Drill rigs are used in many branches of industry, such as underground and surface mining, building engineering as well as in extraction of crude oil, of natural gas, mineral water and drinking water.

In Poland design-and-research work on drilling rigs are carried out from many years in many scientific-and-research centres, including KOMAG Institute of Mining Technology. KOMAG's solutions are closely related with the coal industry and thus most of solutions are intended to be used in undergrounds of mining plants. Small-diameter cigar-shaped drill rigs or cutter-head (on carriage) drill rigs, in a form of quasi-stationary devices or self-propelled machines, are used in hard coal mines. Drill rigs of different types and in different configurations are used in many mining operations, starting from drilling the blasting holes and ending with drainage holes [1]. Drill rigs designed at KOMAG are also used in the rock mining industry and more and more often in the building engineering.

Solutions of drill rigs developed at KOMAG differ in design and functionality, and they meet the users' needs. Increase of effectiveness of drilling operations through optimisation of technological processes is one of basic requirements of the users. Optimisation includes two directions. The first is searching for optimal force pressing the drilling column to the hole's bottom, depending on speed and torque of drilling column and parameters of cleaning the hole's bottom from drillings. The second is increasing the effectiveness through minimization of time of each stage of drilling process. Both methods aim at proper arrangement of hydraulic system. Manufacture profitability of drill rigs, besides the problem their effectiveness, affects significantly the design of drill rig i.e. its hydraulic system.

The following two types of hydraulic systems were used in drill rigs in the recent years:

- simple one with throttling control,
- based on Load Sensing system.

Systems with throttling control are mainly used in simple and cheap devices. Drill rigs equipped with Load Sensing system are the devices of more complex design.

Taking onto account mechanical design and place of use of drill rig, KOMAG's designs can be divided into the following three main types:

- quasi-stationary small-diameter drill rigs,
- drilling jumbos for underground mining industry,
- surface geological-and-engineering drill rigs.

2. Quasi-stationary small-diameter drill rigs

Quasi-stationary small-diameter drill rigs are designed for geological-and-exploration drilling as well as for drilling dewatering, degassing and preceding holes in rocks of different hardness. Three drill rigs of power from 3 to 7.5 kW, installed on sprags or sledges, create the type- series [2].

Fig. 1 WMD 150 small-dimension drill rig [5]

WMD-150 drill rig manufactured by ZMUW Engineering Sp. z o.o. is the example of small-diameter drill rig of low power (Fig. 1). The drill rig has modular design and consists of the following sub-assemblies:

- gear with turntable,
- clamping head,
- supporting head,
- hydraulic cylinders,
- sprag or sledge,
- hydraulic system,
- clamping device.

ISSN 1454 - 8003
Proceedings of 2014 International Conference of Hydraulics and Pneumatics - HERVEX
November 5 – 7, Calimanesti-Caciulata, Romania

Drive gear of drill rig (Fig. 2) consists of gearbox body (in which toothed gear was installed) and turntable body. Due to rotational installation of turntable body on gearbox body, it is possible to obtain required direction of drilling (0÷360°). Hydraulic gear pump and electric motor of power 7.5 kW are fixed to the gearbox body [2].

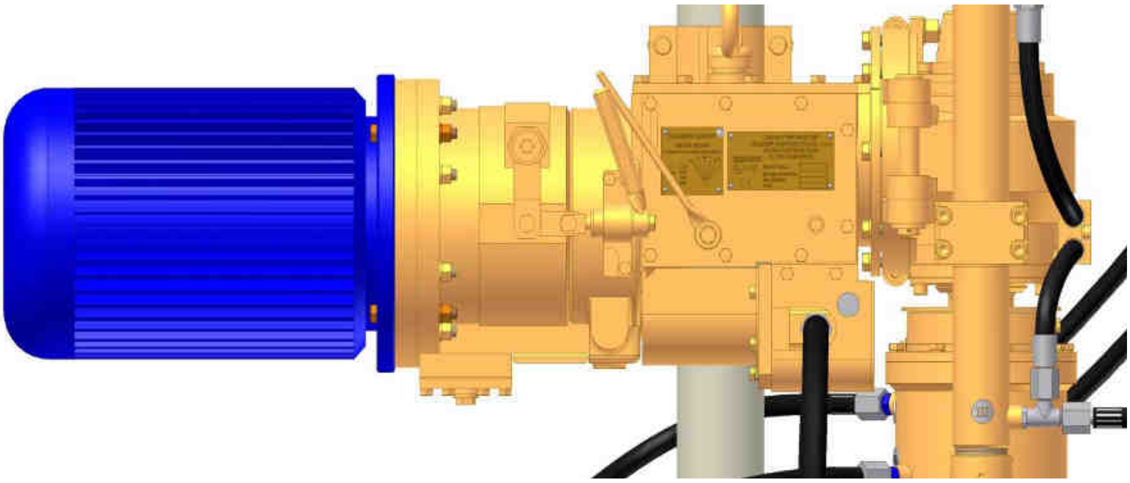

Fig. 2 Drive gear [5]

WMD – 150 drill rig is equipped with supporting head designed to disassemble and to support the drilling hose. Two hydraulic cylinders were used to set the clamping head spindle in to-and-fro motion and to press the drilling hose.

WMD - 150 drill rig can be installed on one of two types of sprags or on the walls. The first type is a tripod spaced between floor and roof.

The sprag is attached to the gearbox body. It enables moving the drill rig up and down to fix its position at the required height. The length of sprags can be changed from 1900 mm to 4400 mm.

ISSN 1454 - 8003
Proceedings of 2014 International Conference of Hydraulics and Pneumatics - HERVEX
November 5 – 7, Calimanesti-Caciulata, Romania

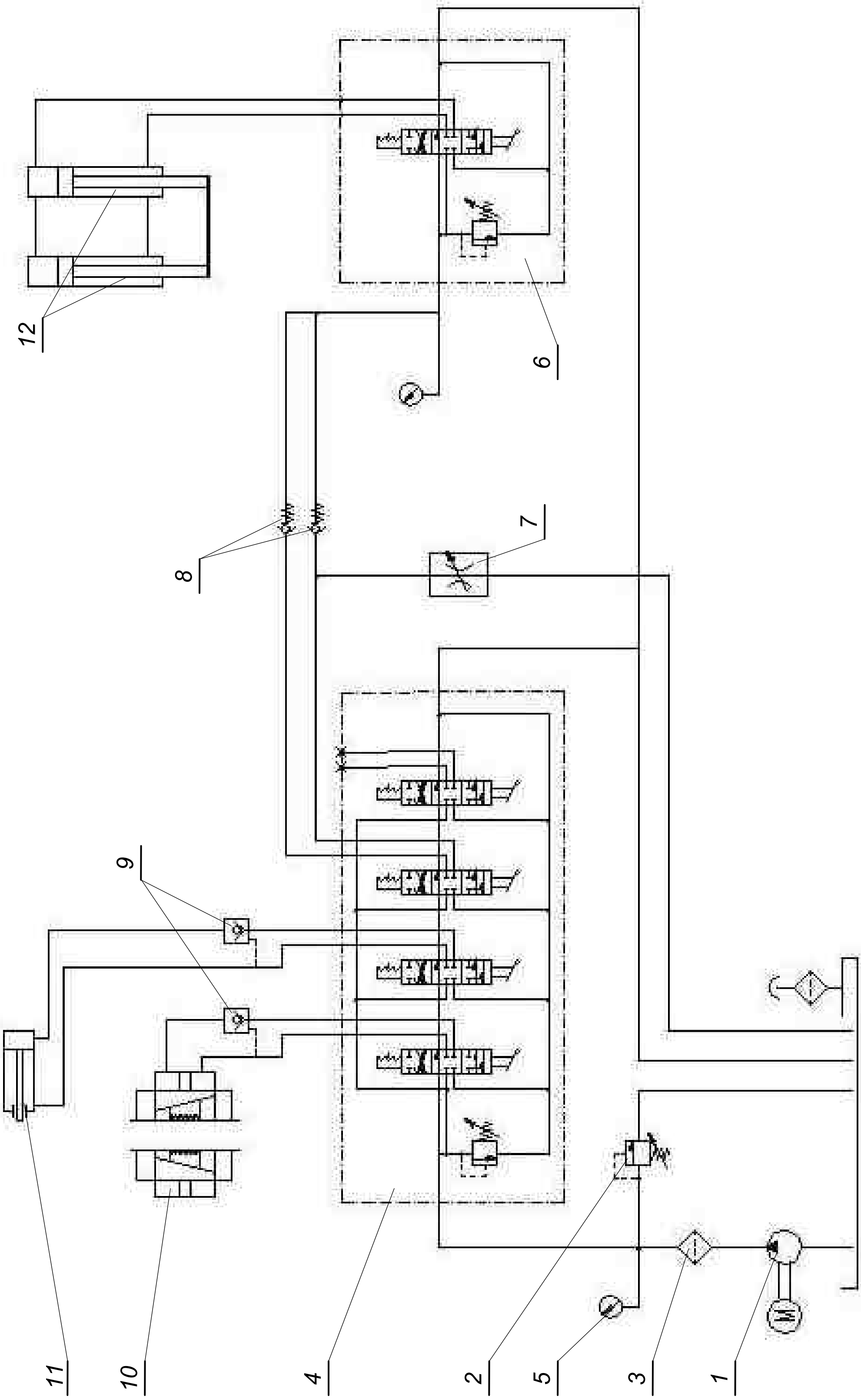

Fig. 3 Hydraulic diagram of WMD – 150 drilling rig [5]
1 – Gear pump, 2 – Overflow valve, 3 – pressure filter, 4 – Block of distributors, 5 - Manometer, 6 - distributor, 7 – Throttling valve, 8 – Check valves, 9 – Controlled check valves. 10 – Clamping head, 11 – Supporting head, 12 – Pressing cylinders

The drill rig was equipped with hydraulic system with throttle control (Fig. 3). The oil is sucked from the tank by the pump (1) attached to the gear body and pumped through the filter to the block of four-section distributor (4). Manometer (5) showing the pressure in the whole system is installed in a pumping line. The block of four-section distributor (4) deflects the lever of each section and directs oil to the receivers. Section III of distributor is responsible for the stroke of pressing cylinders (12). Operational strokes and manoeuvring strokes are possible. Deflecting the lever of section III of the distributor the oil feeds the slide distributor. Moving the lever backwards causes feeding the block distributor as well. However, throttle valve (7) was installed ahead of check valve (8). Due to this, part of oil is directed to the tank. Control of amount of liquid flowing through the throttle enables control of force of pressing cylinders. Slide distributor (6), which is responsible for movement of hydraulic cylinders, enables putting down and pulling the hose. Section I of block distributor is designed for control of clamping head (10), while section II for control of supporting head (11). Both sub-systems were equipped with controlled check valves (9) protecting against drop of pressure in the system. The fourth section is a reserve section.

3. Drilling jumbos for underground mining industry

To meet the users' expectations, KOMAG developed several solutions of drilling jumbos [3, 14, 15]. MWW-1 small-size drilling jumbo, manufactured by Zakłady Mechaniczne "BUMAR – ŁABĘDY" S.A., is one of them (Fig. 4).

Fig. 4. MWW-1 small-size drilling jumbo [10]

MWW-1 drilling jumbo consists of the following sub-assemblies:

- caterpillar chassis,
- drilling jib,
- hydraulic power pack with hydraulic equipment.

ISSN 1454 - 8003
Proceedings of 2014 International Conference of Hydraulics and Pneumatics - HERVEX
November 5 – 7, Calimanesti-Caciulata, Romania

Blasting holes can be drilled in the roadway face of width 6220 mm and height 5500 mm from one position of small-size MWW-1 drilling jumbo. It is possible to drill the blasting holes of standard diameter Φ42 mm and length up to 2250 mm [6, 7].

Hydraulic system of MWW-1 small-size drilling jumbo is a hydrostatic open system built on the basis of A11VLO piston pump with LRDS controller (marked with red frame) – Fig. 5. Adaptation of pump output to oil consumption is the pump advantage. Such solution enables to avoid energy losses associated with overflow of unused part of operational medium through the valve protecting the system.

The pump supplies the following systems:

- drive of drilling jumbo,
- drilling jib,
- supporting system of drilling jumbo.

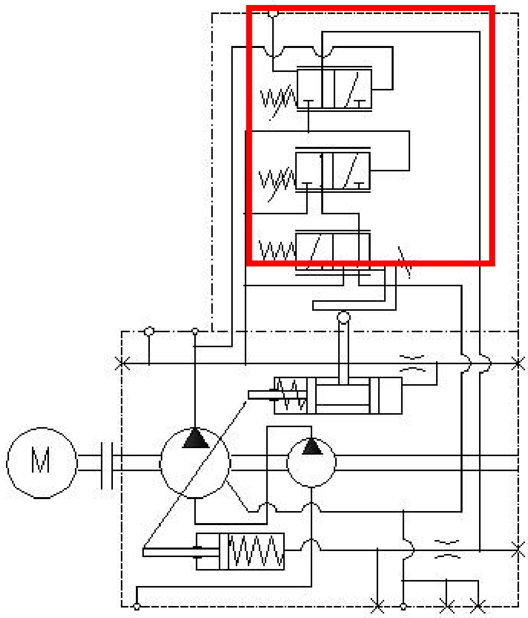

Fig. 5. Hydraulic diagram of A11VLO pump with LRDS controller [4]

Hydraulic system of a drive (Fig. 6) consists of two piston motors of constant absorption capacity, installed on planetary gears driving the caterpillars. Hydraulic motors are equipped with braking valves, which protect the MWW-1 drilling jumbo against uncontrolled movement. Additionally, the gears are equipped with disc parking brakes, which are released by pressure of hydraulic oil from braking valves. Two pressure transmitters, which cooperate with sound signalling system started during backward drive, were used in the system (separately for each supply line of the motors). Modified hydraulic block, adapted for operation in the Load Sensing system, was used in the hydraulic system of drilling jumbo [8].

ISSN 1454 - 8003
Proceedings of 2014 International Conference of Hydraulics and Pneumatics - HERVEX
November 5 – 7, Calimanesti-Caciulata, Romania

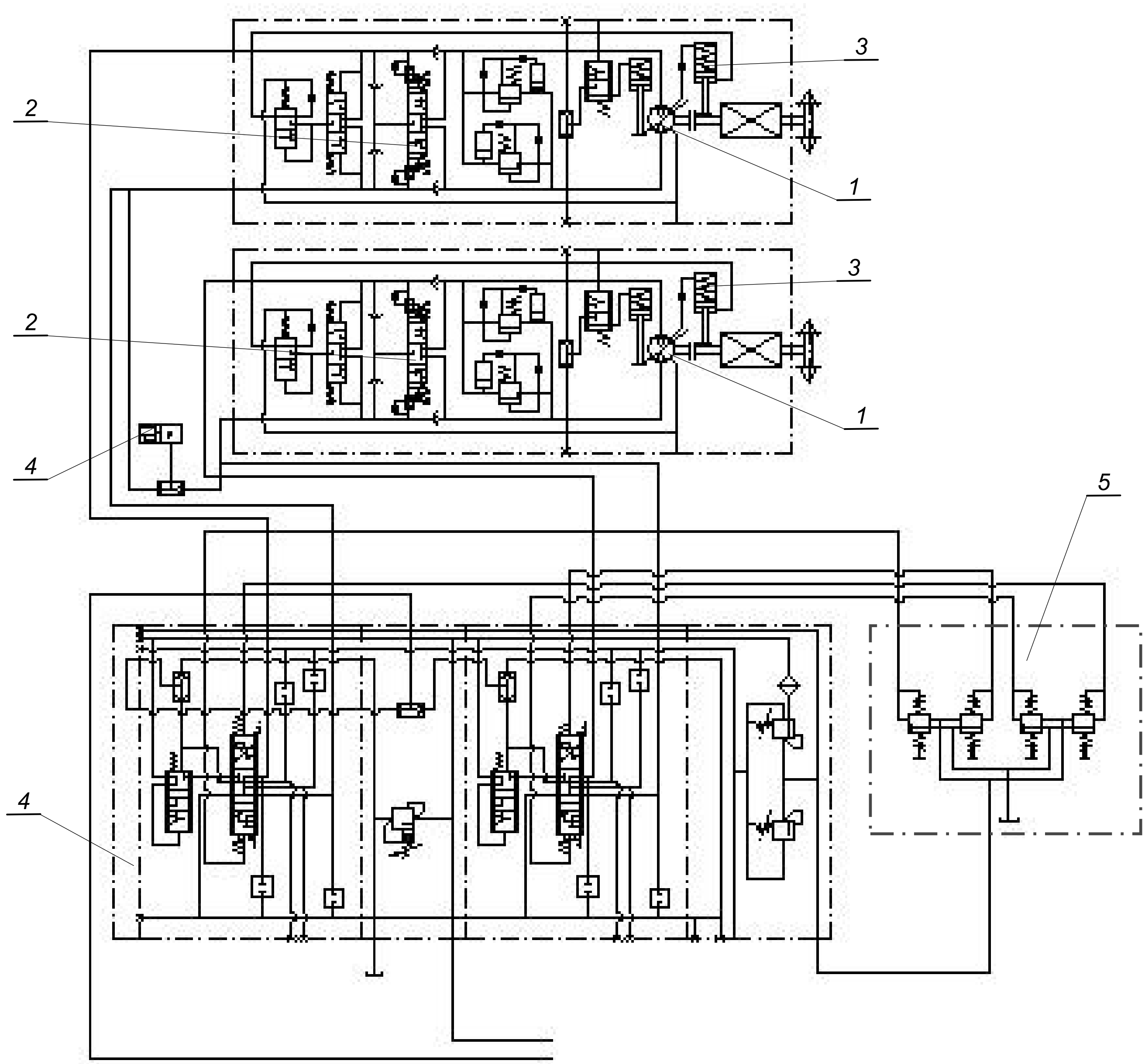

Fig. 6. Hydraulic diagram of advance drive [10]
1 – Piston motor, 2 – Braking valve, 3 – Parking brake, 4 – Hydraulic block,
5 - Manipulator, 11 – Pressure transmitter

The drilling jib system is built of actuating components (mainly hydraulic cylinders). The following two main blocks can be distinguished (Fig. 7):

- drive of drill's spindle and percussion (pos. 1),
- jib's arm drive (pos. 2).

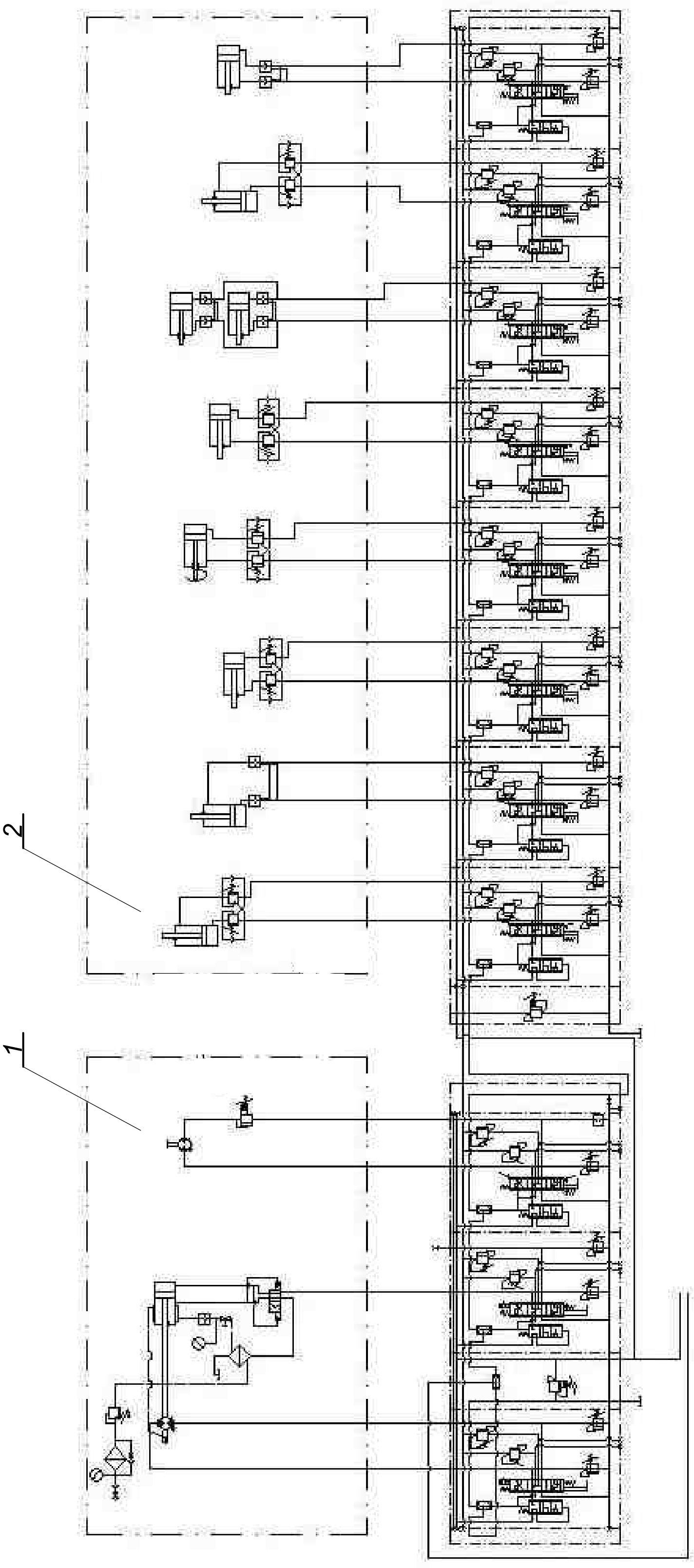

***Fig. 7.** Hydraulic diagram of MWW-1 drilling rig's jib [10]*

Hydraulic cylinders of the jib have braking valves protecting against not controlled jib arm movement and against impact of the jib weight on its speed.

Controlled check valve, which enables flow of flush water at the moment of starting the rotation of the drill, is installed in the drill's spindle drive supply system.

The car supporting system consists of distributor's block and four pairs of telescopic cylinders spreading the supports and four supporting cylinders. Each of the supporting cylinders is protected with a hydraulic lock to avoid drawing aside the supports.

Hand pump, connected hydraulically with drainage filter of the hydraulic system, was used to fill up the tank with oil. Such a solution protects against accidental contamination of the hydraulic system in a result of filling up the tank directly from a barrel or bucket. Design of the filling system ensures drainage of used oil from the tank using the same hand pump.

4. Surface geological-and-engineering drilling rigs

In many cases, quasi-stationary small-diameter drilling rigs transported on sledges are used in surface drilling. These drilling rigs have limited scope of use due to low power. In KOMAG the design of WIG-200 geological-and-engineering drilling rig was developed and ZMUW Engineering sp. z o.o. started its manufacture.

Fig .8 WIG-200 drilling rig [9]

WIG-200 drilling rig (Fig. 8) is the stationary machine, installed on a truck or pickup of load capacity below 5500 kg (Fig. 10).

It is designed for geodesic, geotechnical, construction work as well as for the work with use of state-of-the-art trench-less technologies [11]. Its versatility enables using it in many industries in a wide range. It is efficient in making boreholes for exploration of raw minerals. Its design has the following functions:

- determination of geotechnical parameters of construction base,
- making horizontal rebores under roads or railway tracks,
- reinforcement of foundation with bolts,
- stabilisation of slopes and landslides,
- filling the rock mass voids caused by previous mining operations or karst phenomena ,
- piling,
- hydrotechnical work,
- injection work.

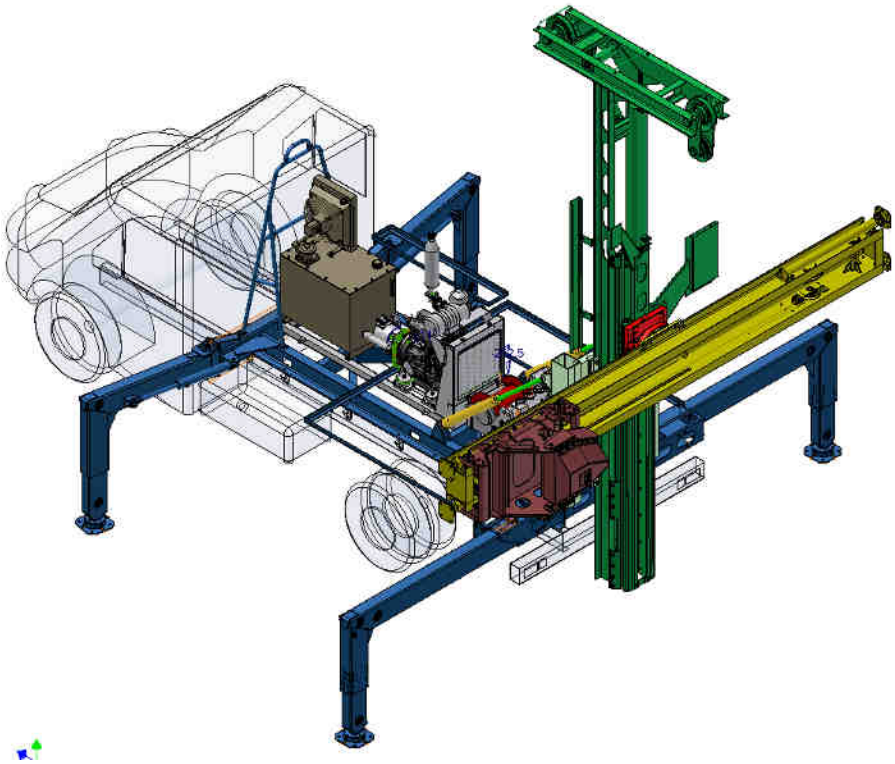

Fig. 9 WIG-200 drilling rig - 3D model (horizontal drilling) [9]

WIG-200 drilling rig consists of the following subassemblies:

- transportation car,
- adaptive frame,
- diesel hydraulic power pack,
- mechanism of drilling rig positioning,
- complete mast,
- two-gear drill,
- hoist,
- jerk-line.

Adaptation frame and supports are installed on the chassis of transportation car. Hydraulic diesel power pack, winch and jerk-line ware installed on this frame. Folded frame of the mechanism for positioning the drilling rig was fixed pivotally. Design of mechanism of drilling rig enables taking the following positions: operational and transportation. Change of position is realized through extension of cylinders installed between the frames. The mast and drill were fixed, through carriage and turntable, to the mechanism for positioning the drilling rig [13].

Use of extended carriage and turntable enables to obtain different positions of drilling. Drilling can be realized at different heights and angles. It gives wide possibilities to make the holes from one position of the drilling rig (Fig. 9).

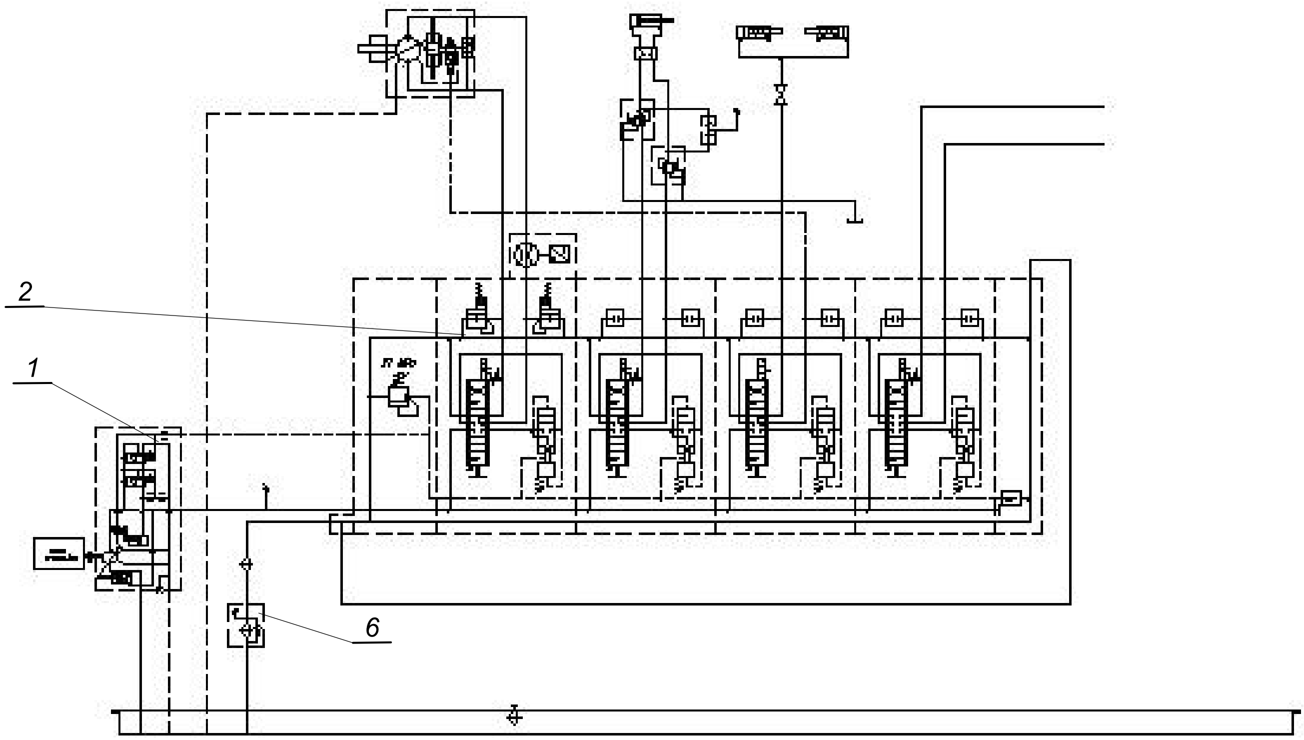

Fig. 10 Diagram of the system for control of drilling parameters (main block of distributors) of WIG-200 drilling rig [9] 1 – Pump, 2 – Block of distributors, 3 – Drill, 4 – Cylinder of advance, 5 – Cylinders of gripper, 6 – Run-off filter

Hydraulic system of WIG-200 drilling rig was designed to meet the customer requirements as regards geodetic, geotechnical and construction drilling, and to enable making the exploration and special boreholes (horizontal rebores and controlled piercing). Diagrams presented in Fig. 10, 11 and 12 show flow of operational medium through the blocks of distributors to each receiver realizing given functions. Four blocks of distributors were planned for hydraulic system. The task of the main block of distributors (pos. 2; Fig. 10) is to control the drill (pos. 3; Fig. 10) operation, i.e. its rotary speed, advance speed and pressing force of drilling column. The last section of this block is used to supply other blocks of distributors, where two blocks (pos. 1; Fig. 11) control the flow of liquid to the cylinders of front and rear supports (pos. 2, 3; Fig. 11), which are responsible for proper setting the whole drill rig to operation. The fourth block of distributors (pos. 1; Fig. 11) ensures the planned direction of drilling, positioning the supports of the mast and the maintenance of jerk-line and winch.

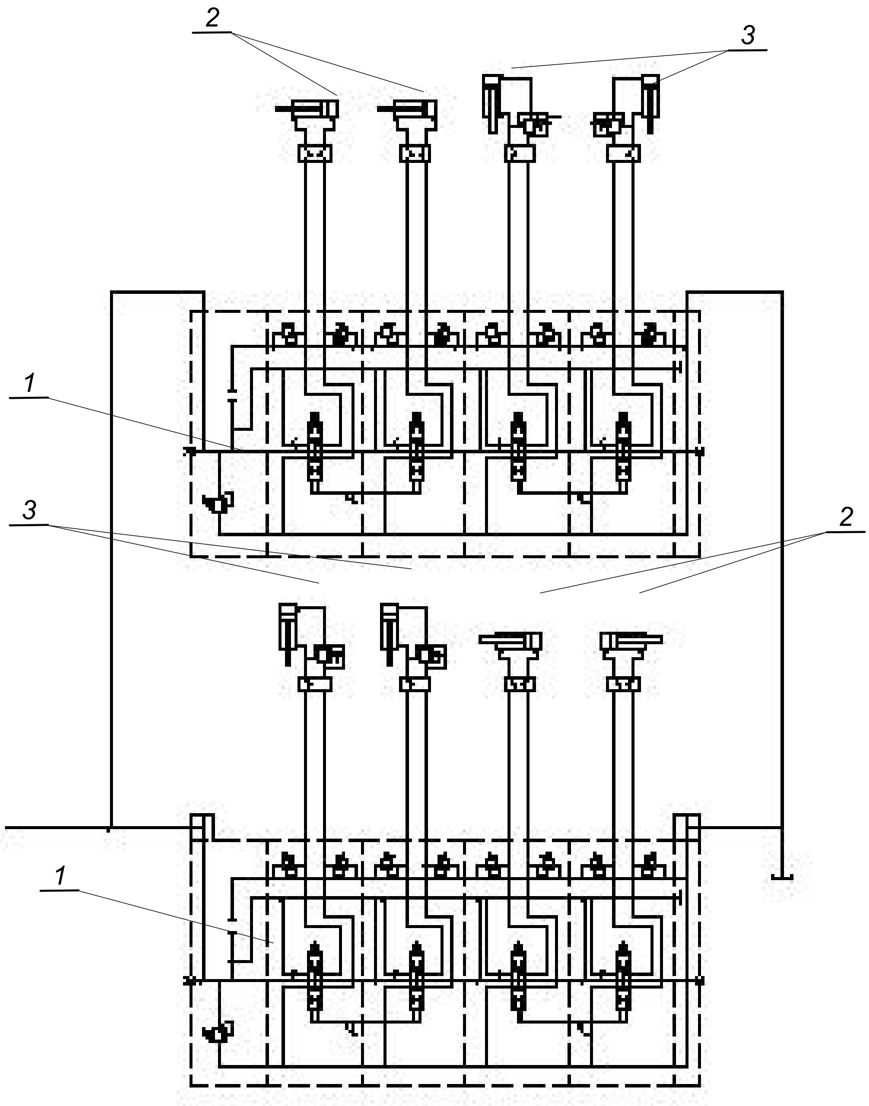

Fig. 11 Diagram of supporting system of WIG-200 drilling rig [9]
1 - Block of distributors, 2 – Cylinder for positioning of supports, 3 – Supporting cylinders

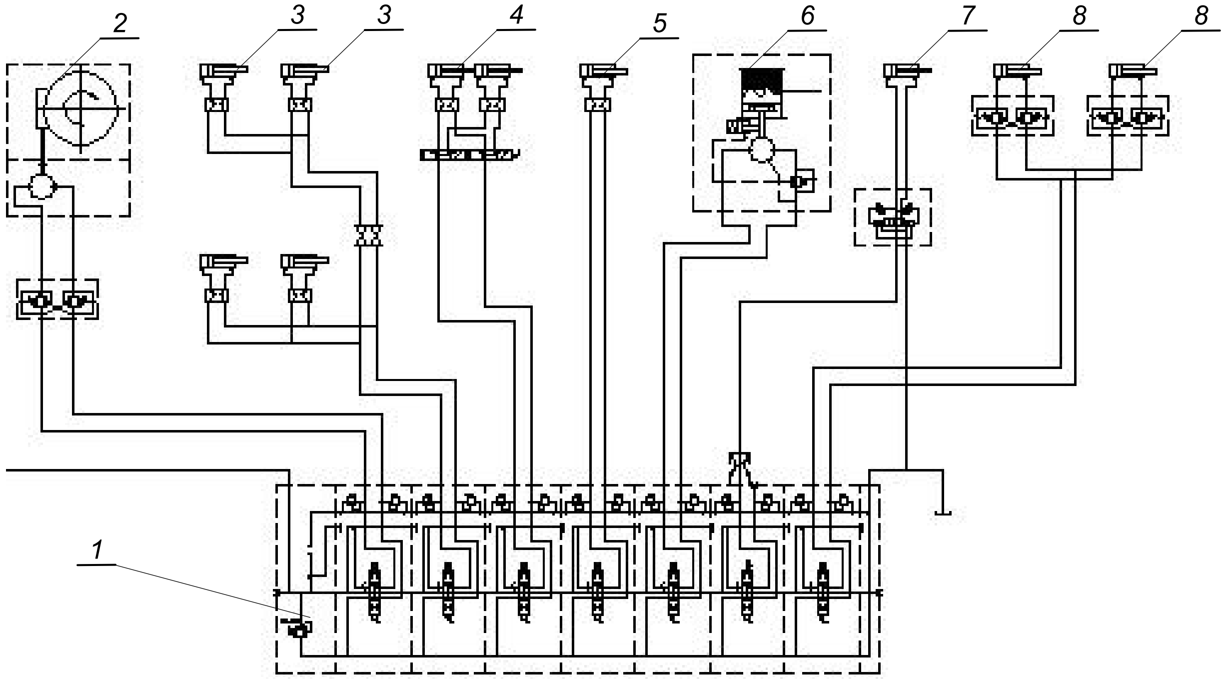

Fig. 12 Diagram of hydraulic system of mast positioning mechanism [9]
1 - Block of distributors, 2 – Hydraulic motor of turntable, 3 – Cylinders of mast supports, 4 – Carriage cylinders, 5 - Cylinder of head, 6 – Hydraulic motor of hoist, 7 – Jerk-line cylinder, 8 - Cylinders for mast extension

Pump unit, feeding (trough block of distributors) each actuating subassembly, is the main component of hydraulic system of WIG-200 drilling rig. Hydraulic diesel power pack (given in Fig. 13) consisting of the following components makes the pump unit:

- diesel engine,
- hydraulic pump,
- oil cooler,
- oil filter,
- oil tank,
- assembly frame.

High-pressure diesel engine is the main component of the power pack. It has been selected after analysis of current solutions of engines of power to 60 kW of manufacturers such as: Kubota, Deutz, Hatz, Ruggerini, Lister Peter, Briggs and Straton. Diesel engine of power 40 kW and maximal rotational speed 2700 min-1 was selected. MA10VO piston pump is integrated with the engine [12].

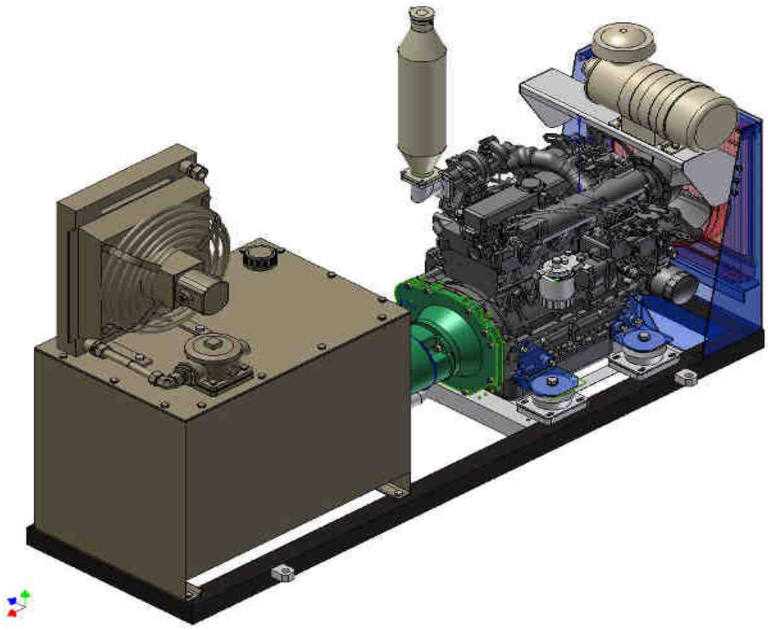

Fig. 13 Hydraulic diesel power pack [9]

Positioning mechanism is an integral part of drilling rig. The mechanism is responsible for setting the drilling rig's mast in an operational position as well as setting the drilling direction and position of boreholes. Advance of the drill is realized by a hydraulic cylinder and rope transmission. Such a solution enabled minimization of the mast size maintaining proper advance force [12].
In the drilling rig a hydraulic drill with two-gear piston motor (Fig. 14) was used. The motor meets high demands put to the drill at possibly lowest power consumption. The gear is changed hydraulically.

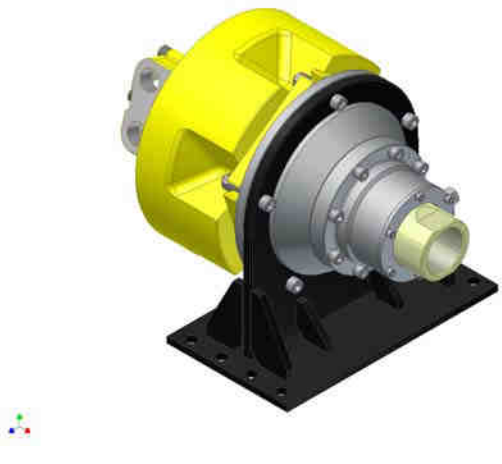

Fig. 14 Hydraulic drill [9]

4. Summary

A series of solutions of small and medium-diameter drilling rigs was developed at KOMAG. Experience in the field of drilling rigs enables to design the machines of high functionality and reliability, what has a direct impact on the increase of work safety. Only the selected KOMAG's solutions were described.

Two types of hydraulic systems have been preferred in drilling rigs so far. The first type, with throttling control, has been used in low power machines of simple use and low price. The second type (based on Load Sensing system) is used in machines of higher power, where the emphasis is put on kinematics of movement, ergonomics and functionality of control as well as energy efficiency of drilling process. Due to the use of state-of-the-art control and supply systems, drilling rigs designed at KOMAG are more innovative in comparison with the competitive products.

REFERENCES

[1] A. Bęben, „Technika wiertnicza w odkrywkowym górnictwie skalnym" Śląskie Wydawnictwo Techniczne, Katowice, 1992
[2] M. Hajduła, J. Obrączka, P. Rojek, „Nowe rozwiązanie małośrednicowej wiertnicy dołowej typu WMD 150", Conference proceedings: KOMTECH 2006 "Innowacyjne i bezpieczne systemy mechanizacyjne do eksploatacji surowców mineralnych", vol 1, Zakopane, 14 16.11.2006 p. 169 176.
[3] K. Kasperlik, E. Wyrobek, „Nowoczesna zespolona maszyna wiercąco-kotwiąco-ładująca do drążenia kamiennych wyrobisk korytarzowych i komorowych w skałach wymagających zastosowania techniki strzelniczej", Nowoczesne metody drążenia wyrobisk korytarzowych z uwzględnieniem aspektów bezpieczeństwa pracy. Conference proceedings, Szczyrk, May 1996
[4] Katalog firmy Bosch Rexroth.
[5] „Koncepcja małośrednicowej wiertnicy do wierceń dołowych i powierzchniowych", CMG KOMAG 2006, – not published
[6] K. Nieśpiałowski, P. Rojek, T. Jasiulek, T. Derda, „Układ hydrauliczny wiertnicy WIG-200", CYLINDER 2009, Badanie, konstrukcja, wytwarzanie i eksploatacja układów hydraulicznych, Instytut Techniki Górniczej KOMAG, Gliwice 2009 p. 207-217.
[7] K. Nieśpiałowski, P. Rojek., N. Rawicki, M. Kalita, „Układ hydrauliczny małogabarytowego wozu wiertniczego MWW-1", Napędy Sterow. 2008 No. 7/8 p. 76-80.
[8] K. Nieśpiałowski, P. Rojek., N. Rawicki, M. Kalita, „Układ hydrauliczny wozu wiertniczego konstrukcji CMG KOMAG", CYLINDER 2008, Badanie, konstrukcja, wytwarzanie i eksploatacja układów hydraulicznych, Centrum Mechanizacji Górnictwa KOMAG, Gliwice 2008 p. 329-341.
[9] Projekt celowy nr 04303/C.ZR8-6/2008, 2011 „Wiertnica inżyniersko geologiczna WIG 200" ITG KOMAG– not published
[10] Target project No. 6 ZR8 2006C/06772 „Małogabarytowy wóz wiertniczy" ITG KOMAG, 2009– not published
[11] P. Rojek, T. Derda, „Nowoczesne rozwiązanie wiertnicy inżyniersko-geologicznej", Masz. Gór. 2011 No. 3 p. 53-60.
[12] P. Rojek, T. Derda, „Wiertnica inżyniersko-geologiczna WIG-200", MM Magazyn Przemysłowy styczeń-luty 2011 No. 1-2(104) p. 40-41
[13] P. Rojek, T. Derda, N. Rawicki, „Nowoczesne rozwiązanie konstrukcyjne wiertnicy geologiczno-inżynierskiej typu WIG-200", KOMTECH 2011, Innowacyjne techniki i technologie dla górnictwa. Bezpieczeństwo - Efektywność - Niezawodność, Instytut Techniki Górniczej KOMAG, Gliwice 2011 p. 237-251.
[14] "Wóz wiertniczy WWS-12", Gwarectwo Mechanizacji Górnictwa POLMAG. Informator '86 Maszyny i urządzenia górnicze chodnikowe, Katowice 1986
[15] "Wóz wiertniczy WWS-1M", POLMAG Catalogue card

ISSN 1454 - 8003
Proceedings of 2014 International Conference of Hydraulics and Pneumatics - HERVEX
November 5 – 7, Calimanesti-Caciulata, Romania

CLEANING MACHINE FOR FARMS OF PHOTOVOLTAIC PANELS WITH HYDRAULIC ACTUATION SYSTEM

Radu RADOI[1], Marian BLEJAN[1], Ioana ILIE[1]

[1] INOE 2000 - IHP, Bucharest, radoi.ihp@fluidas.ro
blejan.ihp@fluidas.ro
ilie.ihp@fluidas.ro

Abstract: *The efficiency of the photovoltaic panels depend on the cleanliness of the reception surface of solar energy. As in time on this are deposited all kinds of impurities, the productive efficiency can drop even up to 50 %. It is necessary from this cause their regular cleaning. The paper presents procedures that can be used for washing and a washing machine with rotating brush developed in our country.*

Keywords*: hydraulic, pv washing, controller, rotating brush*

1. Introduction

The efficiency of the photovoltaic panels depend on the cleanliness of the reception surface of solar energy. As in time on this are deposited all kinds of impurities, the productive efficiency can drop even up to 50 %. It is necessary from this cause their regular cleaning. There are several methods of cleaning the photovoltaic panels namely:

Hand wash using mops and potable water (Figure 1)

Cleaning efficiency achieve 80-90% but costs gained per kWh by cleaning are high due to high water consumption (6,5 ÷ 12 liters/m^2) and high value of labor (4,5 ÷ 5 m^2/min) with four operators.

Figure 1

Washing with high pressure water jet (Figure 2)

In this case the cleaning efficiency achieve 70 – 80% because is missing wiping that would remove much of the residual impurities.

Costs per kWh are medium, having a high water consumption (~ 2,7 l/m^2) and medium value of labor (18 – 20 m^2/min with three operators).

Figure 2

Cleaning with compressed air jet (Figure 3)

In this case the cleaning efficiency achieve ~ 70%, and costs are at an average level for that no consume water, and productivity is comparable with wshing with pressure jet water (about 17 m^2/min with three operators).

Figure 3

Cleaning with steam under pressure (Figure 4)

In this case the efficiency is about 90% with very low costs due to low water consumption (0,5 ÷ 0,6 l/m^2) and a high productivity (23 ÷ 26 m^2/min with a single operator).

Figure 4

ISSN 1454 - 8003
Proceedings of 2014 International Conference of Hydraulics and Pneumatics - HERVEX
November 5 – 7, Calimanesti-Caciulata, Romania

Wash with water sprinklers (Figure 5)

Depends only of water and gravity with the disadvantages that have high maintenance costs, a negative impact on the safety of the electrical system and the high initial cost of infrastructure.

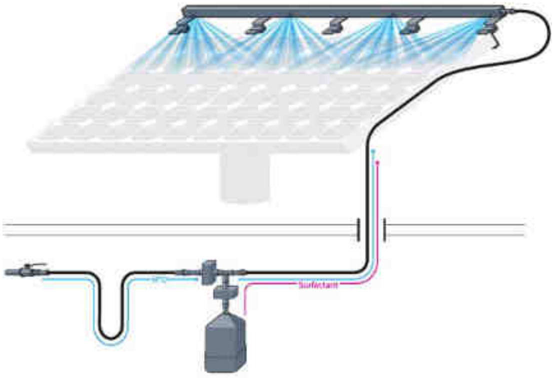

Figure 5

Cleaning systems with sliding brush mounted permanently on the string of panels (Figure 6)

It has the advantage that it does not consume water, cleaning efficiency is average, but with the disadvantages of expensive maintenance, high initial cost, and a higher degree of abrasion of the surface cleaned.

Figure 6

Comparison between systems

	Cleaning Systems					
	1. Manual	**2.Water jet**	**3.With compressed air jet**	**4.With steam jet**	**5. With sprinklers**	**6. With sliding brush**
Efficiency	80 – 90%	70 – 80%	70%	90%	70%	70%
Cost/kWh	high	average-high	average	scăzut	mediu	average
Water consumption	6,5÷12% l/m^2	2,5 ÷ 2,8 l/m^2	-	0,5÷ 0,6 l/m	6,5÷12 l/m^2	-
Labor	4÷5 m^2/min with 4 operators	18–20 m^2/min with 3 operators	15-20 m^2/min with 3 operators	22-27 m^2/min with 1 operator	-	-

Examples of cleaning machines for photovoltaic panels of some foreign companies

Figure 7 Mulag FWG700 machine

Figure 8 Bitimec machine

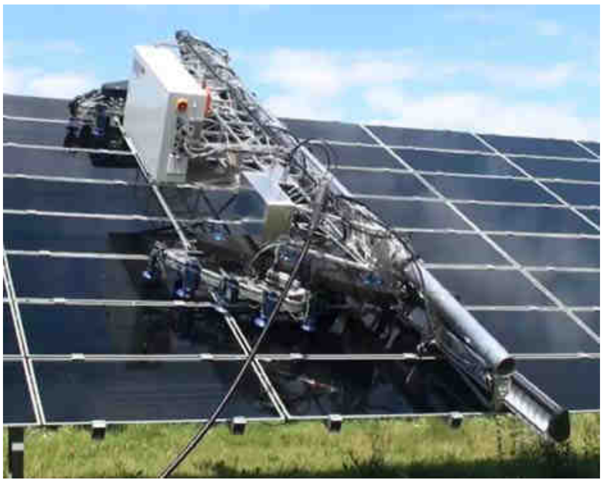

Figure 9 Gekko Serbot machine from Switzerland

3. The cleaning machine for photovoltaic panels developed in our country

Structure

The cleaning machine (Figure 10, 13) combine washing system with low pressure water jet (~2 bar) with brushing the photovoltaic panel. The mechanics and kinematics of the machine was developed by the R&D institute ICTCM Bucharest, and hydraulic drive and automation part was developed by the R&D institute INOE 2000 – IHP Bucharest. Mechanics of the cleaning machine and related peripheral systems are loaded on a Toyota Hilux utility vehicle. The mechanism incorporates a 180° rotatable pivot driven by a toothed rack - gear whell type mechanism.The toothed rack is driven left or right by a hydraulic cylinder. At the upper end of the pivot is mounted an arm that has at end a swivel support that is driven through some levers by the hydraulic cylinder **(14)**. Incination of the arm is made with the hydraulic cylinder **(2)**. Rotating of the brush is provided by hydraulic motor **(32).** On the brush holder are mounted nozzles that provide washing of the PV with waterjet. The hydraulic cylinder **(2)** performs vertical positioning of the brush to the photovoltaic panel and the hydraulic cylinder **(14)** performs positioning of the brush parallel to the panel. These cylinders must constantly correct vertical position of the brush and angular position because of irregularities of mounting of the panels and due to the irregularities of the terrain encountered on the route conducted by car along of the panels.

On the same utility vehicle is loaded water pump hydraulically driven, hydraulic station for driving hydraulic motors, the combustion engine which act the hydraulic pumps and the water tank for washing.

The heat engine that provides energy for hydraulic station is a 4.5 kW diesel engine with 2200 rev / min.

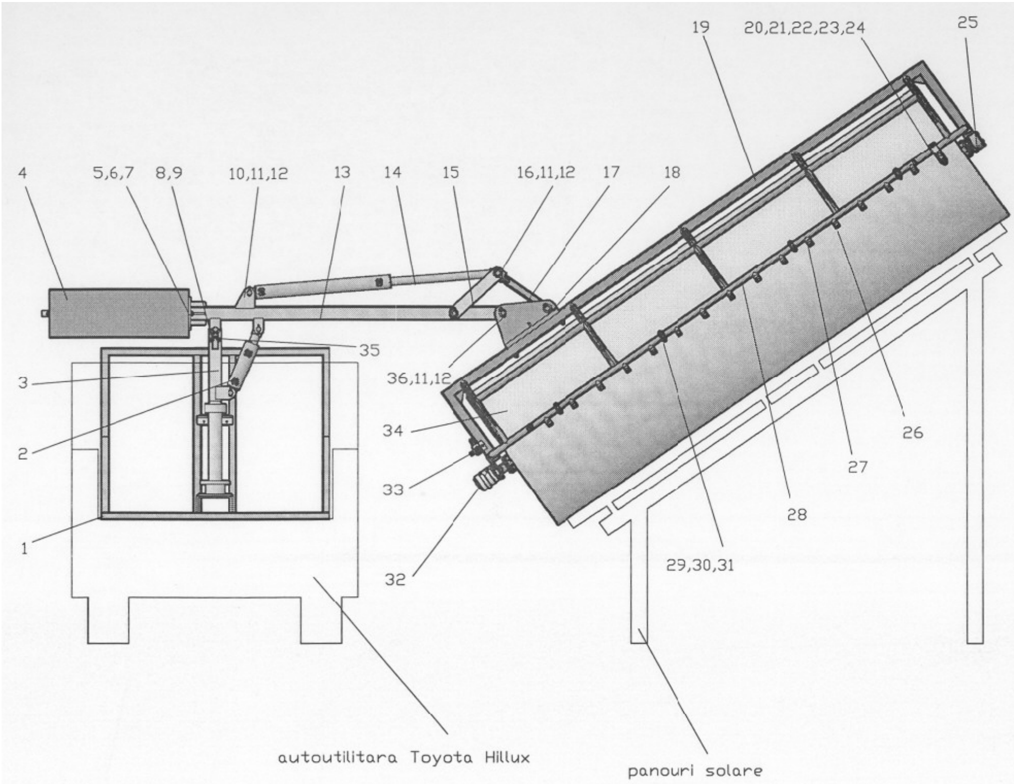

Figure 10

Hydraulic actuation scheme

Hydraulic station of which diagram is shown in the figure 11 is composed of:

- Hydraulic tank of 100 l with return filter and oil cooling system. Solenoid valve **(20.2)** turns on or off, depending on the command received from a thermostat, the coolant. Washing water circuit is used as a coolant.
- Pumping group comprising a triple pump driven by a combustion engine of 4.5 kW. The first section of the pumping unit has parameters of 14 l / min and 100 bar feed a pressure bus of which with hydraulic directional valves **10.1, 10.2** and **10.3** are supplied hydraulic cylinders **17,18** and **19** providing vertical positioning of the brush, angular motion or rotating the pivot.

The second section of the pumping group with parameters 4.5 l / min and 60 bar, act through the directional valve **(11)** the hydraulic motor for rotating the brush in direction left or direction right with speed of 125 rev / min.

The third pumping section with parameters 7,5 l/min and 50 bar, act through directional valve **(12** the hydraulic motor for water pump at a speed of 2800 rev / min.

The pressure line for the first pumping section is provided with a hydropneumatic accumulator which is designed to store a volume of about 0.3 l of oil at the stages when its consumers do not consume oil and to restore in the system when its consumers are activated. A loop of automation based on signals from pressure switches 9.1 and 9.2 download to tank the first pumping section when pressure reaches 120 bar and connect back to the pressure line when the pressure dropped to 90 bar with directional valve (6).

For accidental situation when heat engine is defective in work field, to execute movements for folding the mechanism in marching position of the vehicle, was set a hydraulic electric pump (26) with parameters of 500 W, 2.5 l / min and 100 bar supplied from the vehicle's electrical system (12 V).

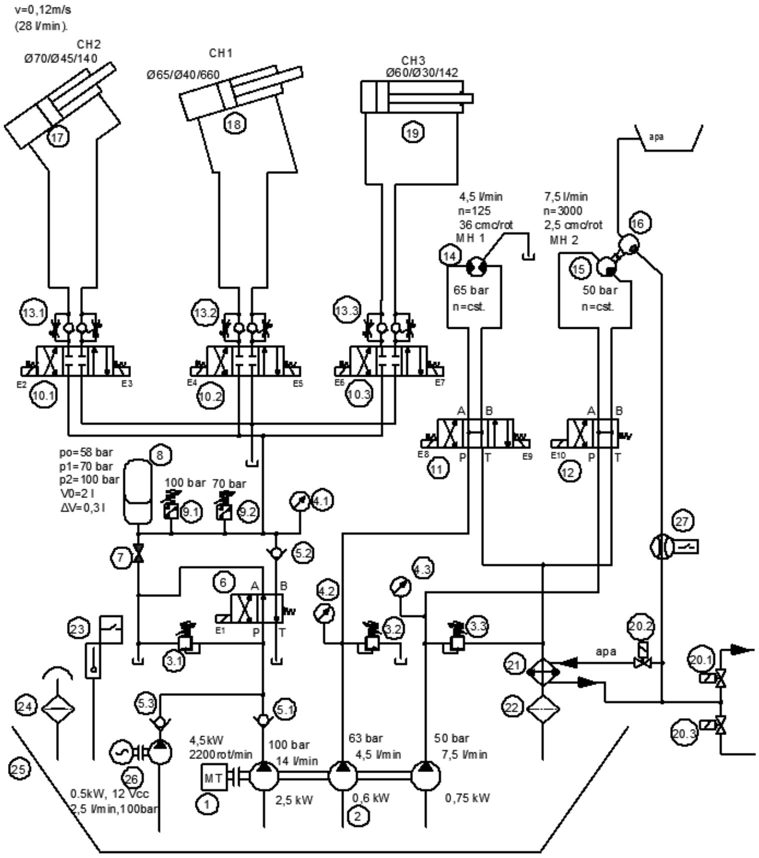

Figure 11

The automation system

Automating of the installation is based on a microcontroller unit that receives information from sensors, from contacts limiter, thermostat and the pressure switches and gives commands to the valves coils for making various movements. Electrical commands are given through high side switches. Commands received by the valves enable a mechanisms movements such as rotating column, arm tilt, brush angle adjustment and controlling valves for washing on the left side, on the right side or cooling circuit. To keep the brush in parallel with solar panels was implemented a control loop with two ultrasonic distance transducers The average distance given by the distance transducers from the ends of the brush constitutes the command for positioning the height of brush through the directional valve for arm tilt. (Figure 12).The difference of the distances given by transducers on the ends of the brush constitutes the command, in order to achieve parallelism of the brush to the solar panel, to directional valve for brush angle.

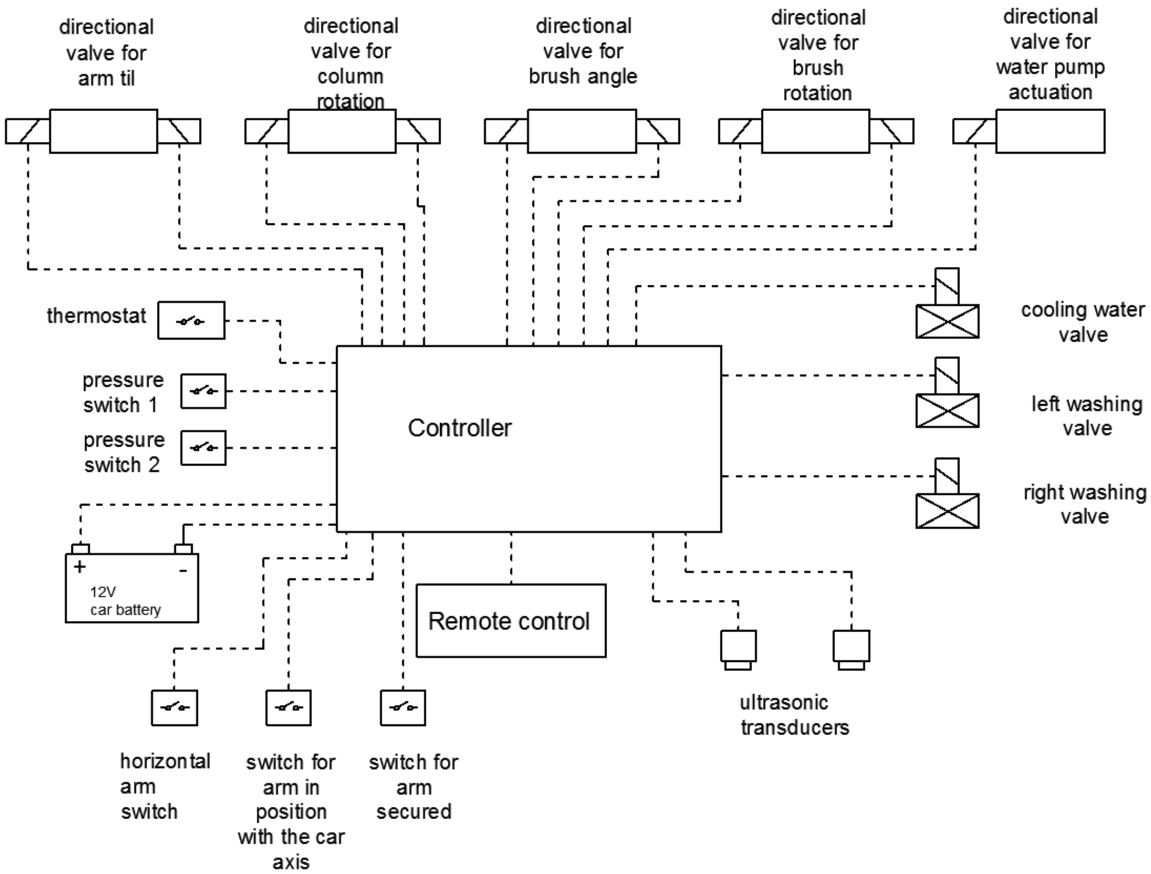

Figure 12

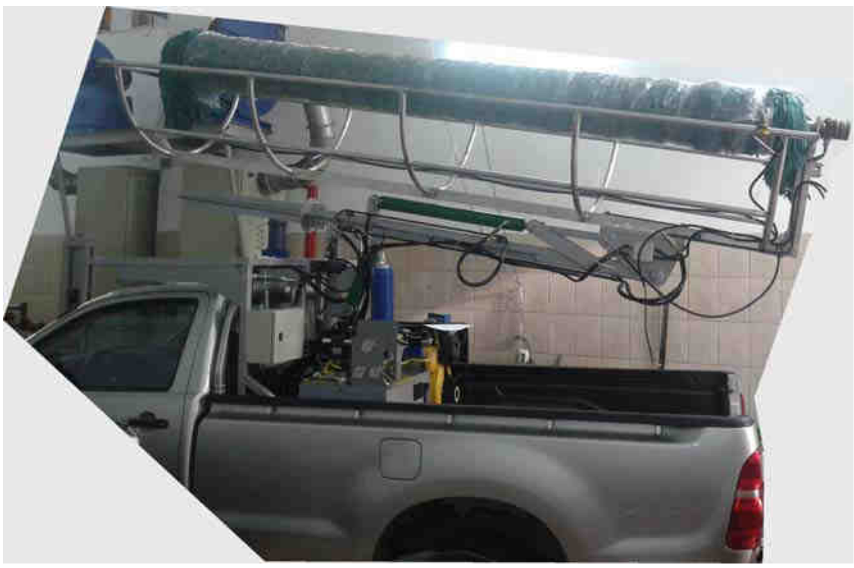

Figure 13

4. Conclusions

The project is very complex and required design in terms of kinematics, hydraulics and automation systems.

The washing machine for solar photovoltaic panels is the first of its kind being developed in the country and is in prototype stage.

Experiments are underway to carry out adjustments and determine technical performances.

REFERENCES

[1] Sami Al-Ghannam, Comparison Analysis on Different Cleaning Technologies for Photovoltaic Panels of Utility Scale Application, Saudi Aramco Study pdf, 2012
V. Marin, R. Moscovici, D. Teneslav, Sisteme hidraulice de reglare automată – Probleme practice, Editura Tehnică Bucureşti, 1981
[2] G. Rădulescu, R. Rădoi, I.Duţu, Complex systems for electrohydraulic drive mechatronic, Caciulata, Romania; 7-9 November, 2009, “Proceedings - HERVEX”, ISSN 1454-8003; pp.182-187
[3] http://www.solar-facts-and-advice.com/solar-panel-cleaning.html
[4] http://www.ipceagle.com/products/solar-panel-pure-water-cleaning-system#.VEeGzhbHRjU
[5] http://www.bitimec.com/bitimec_page.asp?IDProdotto=315
[6] http://www.saudi-sg.com/2012/files/B42.pdf

ISSN 1454 - 8003
Proceedings of 2014 International Conference of Hydraulics and Pneumatics - HERVEX
November 5 – 7, Calimanesti-Caciulata, Romania

RESEARCH ON RHEOLOGY OF CUTTING FLUIDS

Alexandru RĂDULESCU[1], Irina RĂDULESCU[2]

[1] University POLITEHNICA Bucharest, e-mail: varrav2000@yahoo.com

[2] University POLITEHNICA Bucharest, e-mail: irena_sandu@yahoo.com

Abstract: *Cutting fluids are used to reduce the negative effects of the heat and friction on both tool and work piece. The cutting fluids produce three positive effects in the process: heat removal elimination, lubrication on the chip–tool interface and chip removal. This work proposes a development of a vegetable fluid based on sulfonate castor oil, that can be used in drilling process to replace the commonly used mineral oil based emulsion. The rheological properties of the vegetable fluids (sulfonate castor oil in pure state and used through drilling process) were investigated using shear viscosity rheological measurements. Supplementary tests have been made, regarding the thermal behaviour of the lubricants.*

Keywords*: rheology, bio-degradable fluid, drilling process, thermal*

1. INTRODUCTION

Cutting fluids are used to reduce the negative effects of the heat and friction on both tool and work piece. The cutting fluids produce three positive effects in the process: heat removal elimination, lubrication on the chip–tool interface and chip removal, [1 - 3].
The use of vegetable fluids makes possible the development of a new generation of cutting fluid where high performance in machining combined with good environment compatibility could be achieved. Interest in vegetable oil-based cutting fluids is growing. Compared to mineral oil, vegetable oil can even enhance the cutting performance, extend tool life and improve the surface finishing according to some recent analysis from industry.
A sustainable environmental development is achieved considering some important factors like biodegradability and toxicity of lubricants. On the other hand, the lubricants should be stable during usage under different operating conditions [4, 5]. Cutting fluids are consisting of base fluids and additives. Mineral oil, rapeseed oil and synthetic or native esters can be used as base fluids. If biodegradability should be considered, esters and vegetable oils are more indicate to formulate cutting fluids, because they are readily biodegradable in contrast to mineral oil.
In the use vegetable oil have some problems due to inadequate oxidative stability and problems associated with use in high or low temperature observed in this oil. The problem of poor oxidative stability can be mitigated by the structural modification of vegetable oil by chemical reactions. Sulphur and ozone modifications were used in these reactions [6, 7].
Some of the substances included in the fluids composition can lead to problems to the working environment and in their disposal [8]. Cutting fluids can also affect the operator's health due to the formation of mists and smoke. These aerosols may cause dermatological and respiratory irritations [9]. Then these substances, additives, should be chosen carefully.
This work proposes a development of a vegetable fluid based on sulfonate castor oil, that can be used in drilling process to replace the commonly used mineral oil based emulsion, [10]. The rheological properties of the vegetable fluids (sulfonate castor oil in pure state and used through drilling process) were investigated using shear viscosity rheological measurements. Supplementary tests have been made, regarding the thermal behaviour of the lubricants.

2. EXPERIMENTAL PROCEDURE

The rheological measurements were performed on a Brookfield viscometer CAP2000+ equipped with four cone-and-plate geometry and using a Peltier system for controlling the temperature. The

ISSN 1454 - 8003
Proceedings of 2014 International Conference of Hydraulics and Pneumatics - HERVEX
November 5 – 7, Calimanesti-Caciulata, Romania

CAP 2000+ Series Viscometers are medium to high shear rate instruments with cone-plate geometry and integrated temperature control of the test sample material (Figure 1).
The technical parameters of the viscometer are:
- rotational speed ranges: 5 – 1000 rpm;
- temperature control of sample: 5 – 75°C;
- software for complete control and data analysis: CAPCALC32.

Figure 1: Geometry of Brookfield viscometer

The physical and chemical properties of the sulfonate castor oil are presented in Table 1, [5]. The bio-degradability of this cutting fluid is due to the large number of unsaturated ricinoelic acids from castor oil.

Table 1: Physical and chemical properties of the sulfonate castor oil, [5]

Parameter	Value
Aspect	Oily
Water content (%)	8 - 9
Colour	Chestnut
Acid number (mg KOH/g)	0.5 max.
Saponification number on dry basis (mg KOH/g)	68 - 82
pH	10.77
Flash point (^{0}C)	> 120
Pour point (^{0}C)	15 approx.
Density 20 ^{0}C (g/cm^3)	1.12
Kinematic viscosity (cP)	129
Solubility	Soluble in water

The selected vegetable oil is obtained from a plant called with the scientific name *ricinus communis* or castor-oil plant, in English. This oil was selected for its chemical stability. In order to improve the oxidative stability and others problems with use at high temperatures (like temperatures reaching during drilling processes), the castor oil were structural modified using sulfurization.
To determine the rheological model of the bio-degradable fluids, it was used a test-type "shear rate imposed", with limits of variation of (50 … 2000) s^{-1} and a reference temperature of 20 ^{0}C. The

tests were performed with a load up to 2000 s^{-1} and unloading to 50 s^{-1} in order to highlight the effects of thixotropy of lubricant.
The bio-degradable cutting fluid was tested in fresh state (emulsion with a concentration of 5% - 6%) and used state, after 500 working hours on a G20 drilling machine.

3. RESULTS AND DISCUSSIONS

The rheograms characteristics for the bio-degradable cutting fluid in fresh state and used through drilling process are presented in Figure 2.

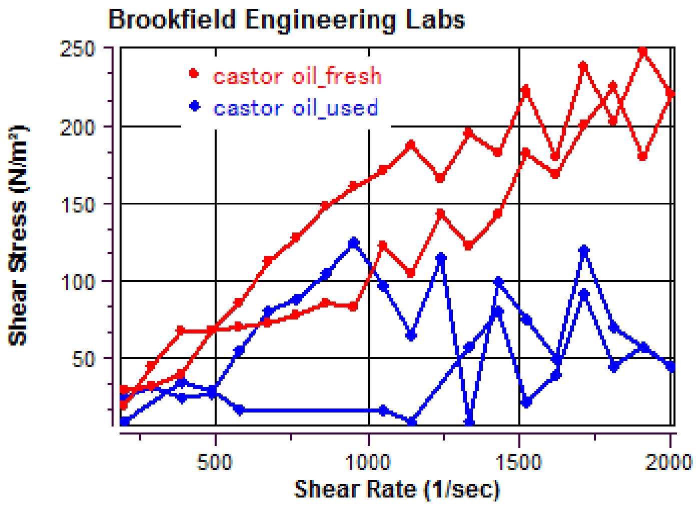

Figure 2: Rheograms for emulsion, in fresh and used state

It can be observed that in the fresh state, the emulsion is characterized by a reduced thixotropy, with small variations of the apparent viscosity versus shear rate. For the used emulsion, the thixotropic behavior increase, with large oscillations of the viscosity and a very unstable structure.
The rheological results where analyzed using regression analysis method and assuming the validity of two rheological models:

- the Newtonian model: $\tau = \eta \frac{du}{dy}$ (1)
- the power law model: $\tau = m\left(\frac{du}{dy}\right)^n$ (2),

where: τ - shear stress, η - viscosity, *m* - consistency index (which is equivalent to the Newtonian fluid viscosity), *n* - flow index (equal to 1 if the fluid is Newtonian).
The results presented in Table 2, according to the Newtonian model, show the decreasing of the viscosity for the used emulsion with almost 50 %, by comparison with fresh emulsion. If the power law model is assumed (Table 3), it can observed that the fresh fluid is characterized by a clearly Newtonian behavior (n = 1.05). For the used fluid, its behavior is non-Newtonian (n = 0.461), with a very poor correlation coefficient of the results.

Table 2: Rheological parameters of fresh and used emulsion (Newtonian model)

State	Viscosity, Pa·s	Corr. coeff.
Fresh	0.0663	0.512
Used	0.0425	0.294

Table 3: Rheological parameters of fresh and used emulsion (Power law model)

State	Consistency index, Pa·s^n	Flow index	Corr. coeff.
Fresh	0.053	1.05	0.591
Used	1.65	0.461	0.282

In order to emphasize the differences between fresh and used emulsion, two thermal tests have been made, at three different values of the shear rate: 250 s^{-1}, 500 s^{-1} and 750 s^{-1}. The results are presented in Figure 3 for the fresh emulsion and in Figure 4 for the used emulsion.

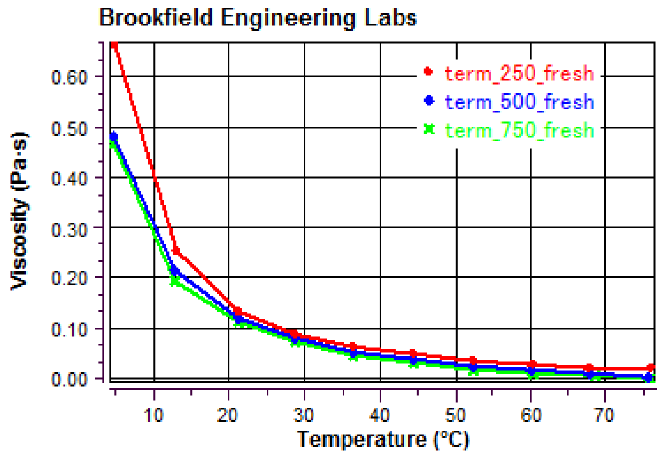

Figure 3: Variation of the viscosity with temperature for the cutting emulsion, in fresh state

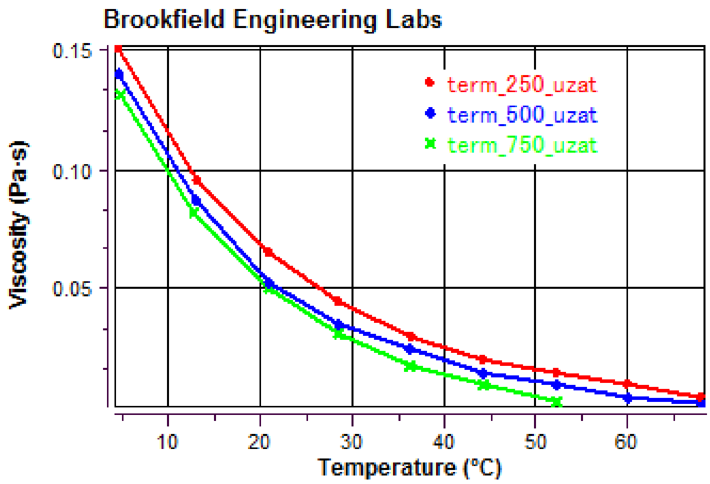

Figure 4: Variation of the viscosity with temperature for the cutting emulsion, in used state

Analyzing the Figures 3 and 4, it can be observed an important difference between fresh and used emulsion, regarding the variation of the viscosity with temperature. At low temperatures, the viscosity of the used emulsion decrease 4 times by comparison with fresh emulsion.

Also, at any temperature, the viscosity of the fresh emulsion doesn't depend on the shear rate, which emphasize the Newtonian behavior of the fluid. From this point, the used emulsion is very sensitive to the variation of the shear rate.

4. CONCLUSIONS

The bio-degradable cutting fluids, based on sulfonate castor oil, so called “green cutting fluids”, have good lubricating properties, high viscosity index, non-toxic and better bio-degradable ability.
The emulsion of sulfonate castor oil has a strong Newtonian behavior in fresh state. If the emulsion is used through drilling process, the viscosity decrease and an important thixotropy can be observed.
Therefore, the rheological methods are very useful to evaluate the wear degree of a fluid and to emphasize the life time for a concrete application.
From this study, it can be concluded that the new developed vegetable based fluids could be a promising alternative to mineral based emulsions for its use as metal working fluids, not only thanks to their environmentally friendly characteristic but also due to their technical properties.

REFERENCES

[1] Booser, R., 1994, CRC hand book of lubrication and Tribology. *CRC press Inc, BOCA RATON*.
[2] John, J., Bhattacharya, M., Raynor, P. (2004). Emulsions containing vegetable oils for cutting fluid application. *Colloids and Surfaces A: Physicochem. Eng. Aspects*, 237, 141-150.
[3] Woods, S. (2005). Going Green. *Cutting Tool Engineering* 57 (2), pp. 48-51.
[4] Cetin, M. H., Ozcelik, B., Kuram, E., & Demirbas, E. (2011). Evaluation of vegetable based cutting fluids with extreme pressure and cutting parameters in turning of AISI 304L by Taguchi method. *Journal of Cleaner Production*, *19*(17), 2049-2056.
[5] Kuram, E., Ozcelik, B., & Demirbas, E. (2013). Environmentally Friendly Machining: Vegetable Based Cutting Fluids. In *Green Manufacturing Processes and Systems* (pp. 23-47). Springer Berlin Heidelberg.
[6] Deiab, I., Raza, S. W., & Pervaiz, S. (2014). Analysis of Lubrication Strategies for Sustainable Machining during Turning of Titanium Ti-6Al-4V Alloy. *Procedia CIRP*, *17*, 766-771.
[7] Kolawole, S. K., & Odusote, J. K. (2013). Performance Evaluation of Vegetable Oil-Based Cutting Fluids in Mild Steel Machining. *Chemistry and Materials Research*, *3*(9), 35-45.
[8] Debnath, S., Reddy, M. M., & Yi, Q. S. (2014). Environmental friendly cutting fluids and cooling techniques in machining: A Review. *Journal of Cleaner Production*.
[9] Padmini, R., Krishna, P. V., & Rao, G. K. M. (2014). Performance assessment of micro and nano solid lubricant suspensions in vegetable oils during machining. *Proceedings of the Institution of Mechanical Engineers, Part B: Journal of Engineering Manufacture*, 0954405414548465.
[10] Mendoza, G., Igartua, A., Arizaga, I., Aspiazu, F. & Santiso, G. (2012). Metal Working Fluids Based on Vegetable Oils for Grinding Operations. *Journal of Mechanics Engineering and Automation* 2, 638-646

ISSN 1454 - 8003
Proceedings of 2014 International Conference of Hydraulics and Pneumatics - HERVEX
November 5 – 7, Calimanesti-Caciulata, Romania

MODELING AND SIMULATION OF HYDROSTATIC TRANSMISSIONS – DESIGN TOOL FOR AUTOMOTIVE SYSTEMS

Florin RADOI[1], Georgiana Claudia VASILIU[2]

[1] PhDs, Parker Hannifin -Romania, florin.radoi@parker.com

[2] Lecturer, PhD, University POLITEHNICA of Bucharest, vasiliu@fluid-power.pub.ro

Abstract: *The development of simulation software performances during the last two decades facilitated a very fast technological progress, and also the implementation of new advanced engineering management systems, like Concurrent Engineering. In the frame of automotive industries, Concurrent Engineering helps companies shorten the product development cycle and quickly bring products to market.*

This paper presents the conception of a hydrostatic transmission for mobile equipment, as part of the larger efforts of developing a complete vehicle. The transmission was configured, sized, simulated and optimized using high performance simulation software AMESim and Simulink.

The ability to use simulation software (like AMESim, Simulink, etc.) is a key fact in implementing CE. A team of highly qualified engineers can work in parallel to develop parts of the final product

Keywords*: Hydrostatic transmission, mobile equipment, concurrent engineering, servomechanism, hydrostatic drive.*

1. Introduction

The need for a transmission in a mobile vehicle is a consequence of the characteristics of the internal combustion engine. Engines typically operate over a range of 600 up to 7000 revolutions per minute (though this varies, and is typically less for diesel engines and especially heavy mobile equipment), while the vehicle's wheels rotate between 0 rpm and 1500 rpm (obviously less for mobile vehicle).

A transmission (or drive) is a very complex electro-mechanical-hydraulic system, whose main purpose is to transfer the power from a source (electric motor, combustion engine, etc.) to a working machine, and to adapt it to the real dynamic needs of the working machine, with high energy efficiency.

A solution widely used in heavy machinery is the **HYDROSTATIC TRANSMISSION**, which mainly consists of a variable pump connected in a closed loop with a fixed or variable hydraulic motor.

Due to high demands of performance for mobile machines, the regular hydrostatic transmissions can also be connected in series with a mechanical gearbox. This design increases the performance of the transmission, but also the costs.

For machines with engine power of 200 kW or above, the traditional solution is to use a hydrodynamic transmission (torque converter) in series with a conventional multi speed gearbox. For lower power applications, the solution is a hydrostatic transmission in series with a gearbox. This solution is shown in Fig. 2.

ISSN 1454 - 8003
Proceedings of 2014 International Conference of Hydraulics and Pneumatics - HERVEX
November 5 – 7, Calimanesti-Caciulata, Romania

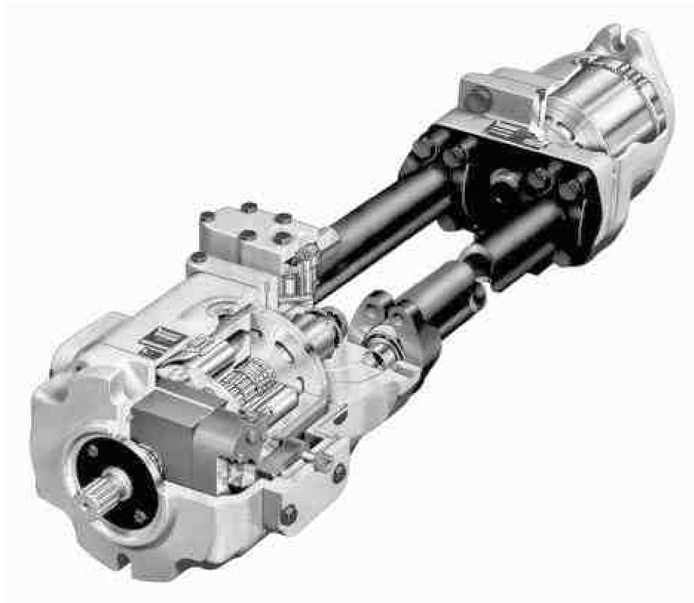

Fig. 1 Parker Gold Cup hydrostatic transmission

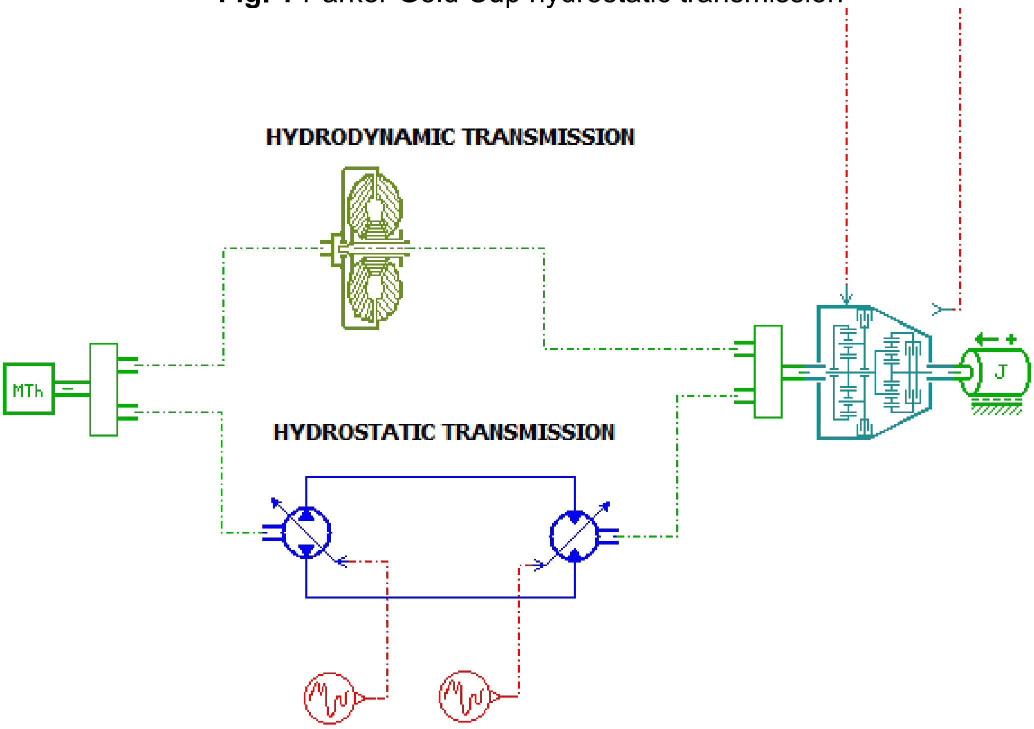

Fig. 1 Hydrodynamic / Hydrostatic transmission solution

2. Design of a Hydrostatic Transmission

Design Theme

Design the main hydrostatic transmission for a multi-purpose mobile vehicle, with the following parameters:

- Speed adjustment range: (0,125 – 1,0)*V_{max}
- Main engine: DIESEL , with: n_D (M_{Dmax}) = 1800 rpm
- Vehicle mass: 3000 kg
- Maximum ramp: $\beta_{max} = 30^0$;
  Maximum speed in maximum ramp: V_{max} (β_{max}) = 4,5 km/h
- Maximum system pressure: 320 bar
- Maximum speed of the vehicle: 30 km/h
- Dynamic radius of motor wheels: r_d = 0,3 m
- Final gear ratio: i=6

Requirements

- The transmission will equip a heavy mobile vehicle, so it will be used a “closed loop” configuration.
- For low power applications, we can use a single main pump. For medium/high power a multiple pump configuration is needed.
- In order to achieve a high Theoretical Range (TR), with V =(0,125 – 1,0) * V_{max}, a variable pump and variable motor solution is needed.
- An auxiliary hydraulic circuit for filtering, cooling, and protection against cavitation and over-pressure is needed.
- The hydraulic pilot pressure of the main pump is supplied by an auxiliary pump
- The hydraulic motors available are high speed, so a final gearbox is needed. (An option is to use a planetary gearbox and 2 motors mounted directly in the wheel hub)
- The ideal command of the transmission is presented in the next diagram.
-

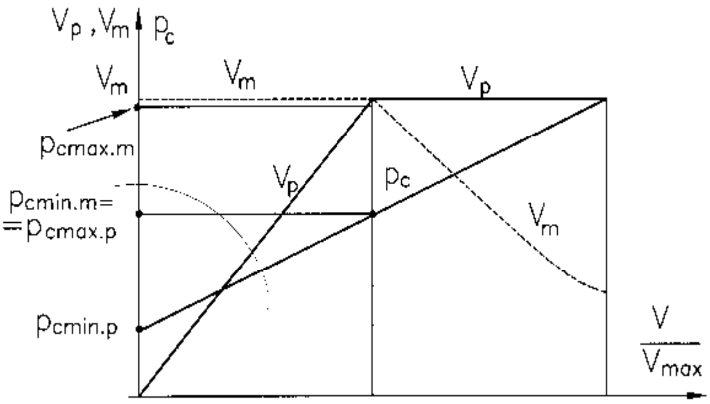

Fig.3 Ideal command sequence of a hydrostatic transmission.

The pumps displacement (*Vp*) is continuously increased up to maximum. Meanwhile the motors displacement (*Vm*) is maximum. When *Vp* reaches maximum level, *Vm* starts to decrease up to a minimum displacement of ~50% of the maximum.

3. Sizing the main components of the transmission
Sizing the motor

The main sizing condition for the hydraulic motors is to ensure the vehicle can climb the maximum ramp specified in the theme.

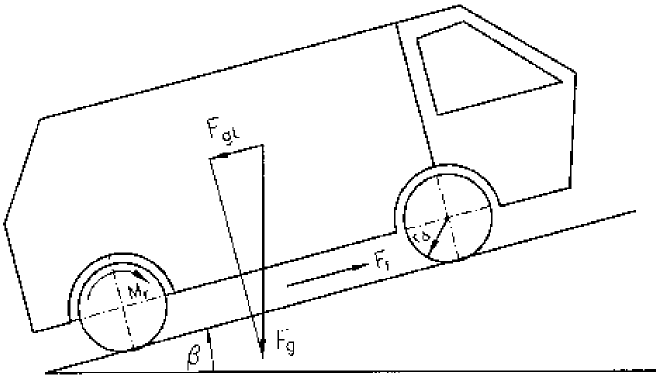

Fig.4 Force equilibrium for a vehicle climbing a ramp.

Starting from this diagram, it has been deducted the following sizing equation for the motors:

$$\mathrm{V}_{m\max} = \frac{\pi r_d mg \sin\beta_{\max}}{i\Delta p_{\max}\eta_{\max}\left(P_{\max}\right)} \tag{1}$$

Applying the initial conditions in the above equation, we achieve:

$$V_{m\ max} = 76\ cm^3/rev \tag{2}$$

For further calculus we will consider round value

$V_{m\ max}$ = 80 cm^3/rev

This is a value widely offered in the portfolio of various hydraulic equipment manufacturers.

SIZING THE PUMP

The condition for sizing the pump, is to achieve the maximum speed on flat land.

From this condition, the equation for sizing can be deducted as follows:

$$V_{p\max} = \frac{2n_{m\max}V_{m\min}}{n_D\left(M_{D\max}\right)\eta_{vm}\left(n_{m\max}\right)\eta_{vp}\left(Q_{p\max}\right)} \tag{3}$$

From the above equation, we have calculated:

$$V_{p\max} = 43{,}18\cdot 10^{-6}\ m^3/rot = 43{,}18\ cm^3/rot \tag{4}$$

For further calculus we will consider round value:

$V_{p\ max}$=45 cm^3/rev

4. AMESim model of the transmission.

The configuration of the transmission was studied starting from a basic model (only a pump and a motor connected together), up to the real model equipped with electro-hydraulic servo-pump and servo-motor. All the simulation were conducted using AMESim Rev.10 software, developed by IMAGINE company.

ISSN 1454 - 8003
Proceedings of 2014 International Conference of Hydraulics and Pneumatics - HERVEX
November 5 – 7, Calimanesti-Caciulata, Romania

The basic model of a hydrostatic drive consists of a variable pump and a motor connected in an open-loop configuration, and a safety relief valve. Such a model is also available in the library of AMESim Rev10 software. The load is simulated by an inertia connected to the motor's output.

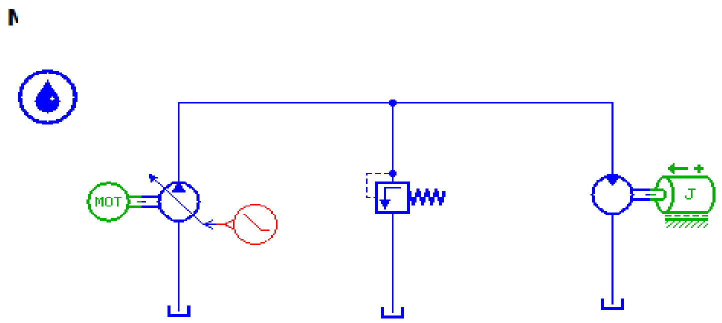

Fig.5 Basic model of a hydrostatic transmission.

This model offers basic information about the real dynamics of a transmission, but it highlights a real problem that might occur, which is ***cavitation*.**

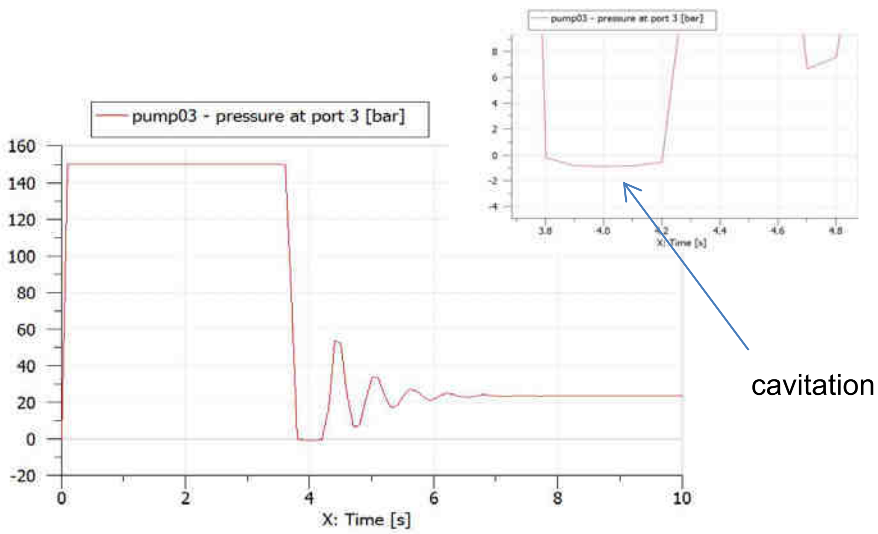

Fig.6 Pressure variation in the system, with the presence of **cavitation.**

A real hydrostatic drive has a safety block for protection against cavitation. It also features some important differences from the basic model:

- Closed loop design
- Introduction of a supercharge auxiliary pump
- Introduction of a safety block against cavitation
- Introduction of real model of the servo-pump
- Flexible hoses are used for connecting the pump and motor.

The complete model of the transmission is detailed in *Appendix A.*

Using the transmission model, the ideal command was simulated. The results are presented next.

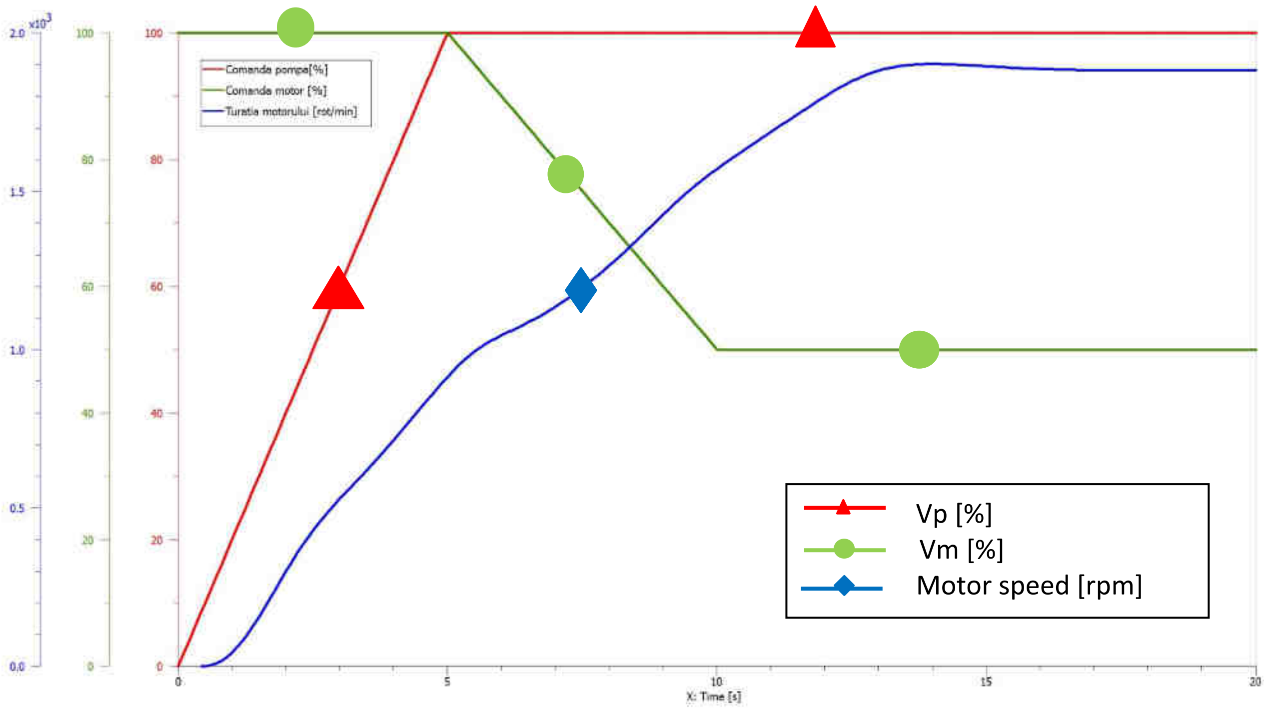

Fig.8 Transmission’s dynamics with ideal command session. Legend:

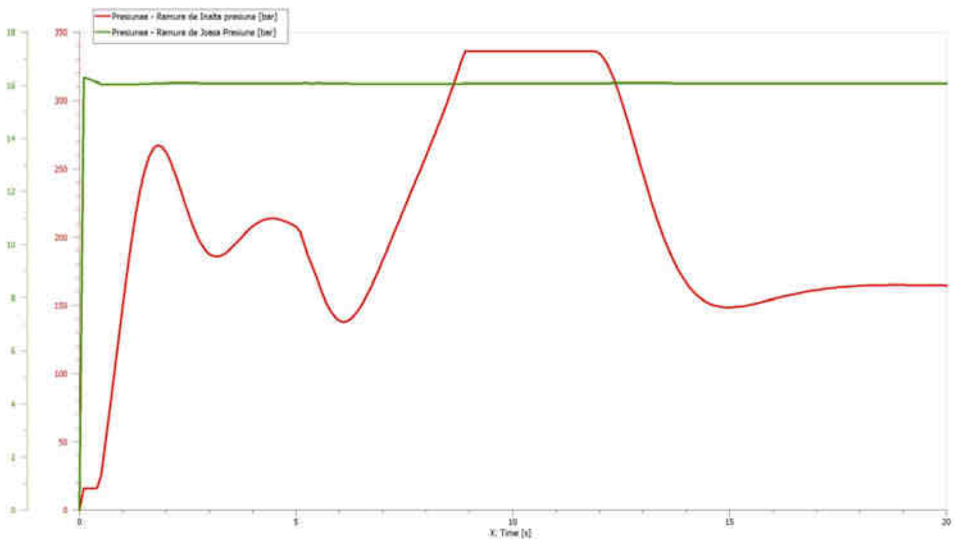

Fig.9 Pressure variation in the system.

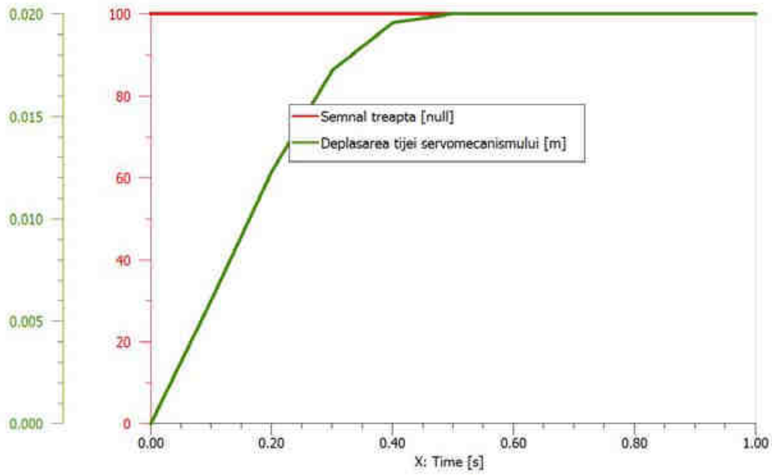

Fig.10 Pump's response to step signal.

5. Conclusions

It is a key conclusion that numerical simulation using AMESim software is a real help in engineering complex systems, offering a cost-effective tool for refining and optimizing various parameters of these systems, and also for anticipating real problems that might occur during lifetime.

Also, another big advantage of using simulation in engineering is the ability to implement Concurrent Engineering management system.

To make Concurrent Engineering a real success, all the necessary information concerning products, parts and processes, has to be available at the right time. A lot of partially-released information has to be exchanged under tightly controlled conditions. Concurrent Engineering allows users, whether in small teams or enterprise-wide groups, to access, distribute, store, and retrieve information from a variety of sources.

REFERENCES

[1] Vasiliu N., Vasiliu D. – „*Hydraulic and Pneumatic Drives. Vol.I.*", Technical Press House, Bucharest, 2005
[2] Negoita Georgiana C. – *Research of the dinamics od hydrostatic transmissions,* Ph. D. Thesis, Faculty of Power Engineering, University POLITEHNICA of Bucharest.
[3] Karl-Erik Rydberg – "Hydrostatic Drives in Heavy Mobile Machinery – New Concepts and Development Trends", Linkoping University, 1997.
[4] Johannes S., Gunnar M. – "Hydrostatic transmission for wind turbines – comparison of different configuration and their applicability", RWTH Aachen University, Institute for Fluid Power Drives and Controls
[5] Vasiliu D., 1997, *"Researches on the Servo Pumps and the Servo Motors of the Hydrostatic Transmissions"*, Ph.D. Thesis, Faculty of Power Engineering, University POLITEHNICA of Bucharest.
[6] Parker Hannifin GmbH, 2004, Catalogue HY11- 3243/UK - *Axial Piston Pump, Series PV, Variable Displacement*, Hydraulic Control Division, Kaarst, Germany.
[7] MOOG, 2010, *Electro Hydraulic Valves - Applications, Selection Guide, Technology, Terminology, Characteristics* , East Aurora, MA, U.S.A.
[8] Andreescu Cr., – *Dinamics of road vehicles. Vol I*, POLITEHNICA PRESS, Bucharest, 2010, ISBN 978-606-515-107-9

[9] Assofluid – *Hydraulics in industrial and mobile applications*. Grafiche Parole Nuove SRL, Milano, 2007
[10] PARKER – *Denison GOLD CUP Product Catalog*, HY28-2667 01/GC/NA,EU
[11] Masashi S. - „Large Capacity Hydrostatic Transmission with Variable Transmission", Mitsubishi Heavy Industries, Ltd., Nagasaki R&D Center
[12] Mitra S., Sinha B. – "Application of Concurrent Engineering in New Automobile Design", Institute Of Management, Calcutta, India

WEB references

[1] http://www.parker.com
[2] http://www.boschrexroth.com
[3] http://www.lmsintl.com/
[4] http://www.wikipedia.org

The Authors are grateful to Mr. Professor Nicolae VASILIU, from University POLITEHNICA of Bucharest for his continuous support, and for offering us access to LMS software tools extremely valuable for this paper.

The work has been funded by the Sectoral Operational Programme Human Resources Development 2007-2013 of the Ministry of European Funds through the Financial Agreement POSDRU/159/1.5/S/134398.

ISSN 1454 - 8003
Proceedings of 2014 International Conference of Hydraulics and Pneumatics - HERVEX
November 5 – 7, Calimanesti-Caciulata, Romania

APPENDIX 1 – Complete AMESim model of the transmision

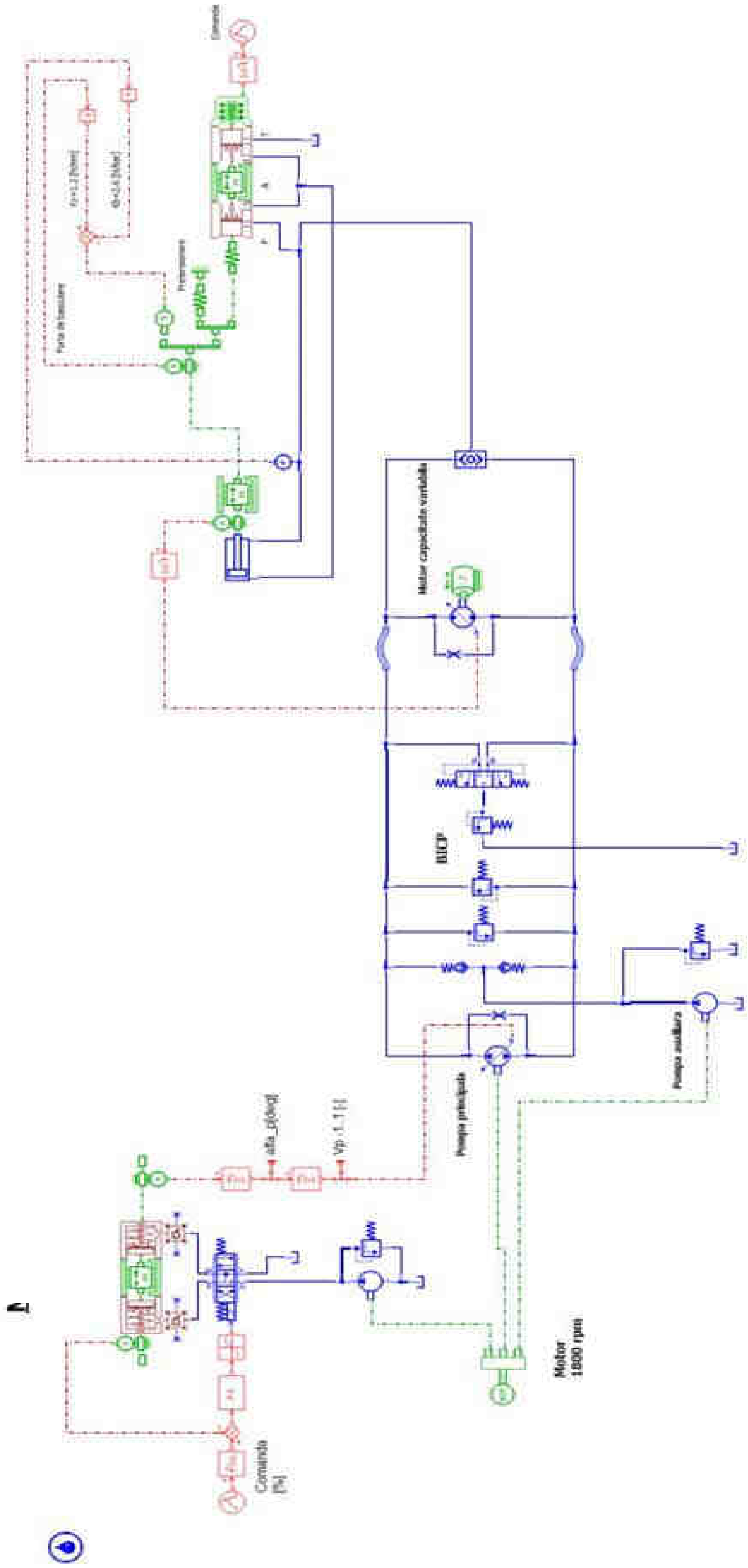

ISSN 1454 - 8003
Proceedings of 2014 International Conference of Hydraulics and Pneumatics - HERVEX
November 5 – 7, Calimanesti-Caciulata, Romania

APPENDIX 2 – AMESim model of servopump and servomotor - detail

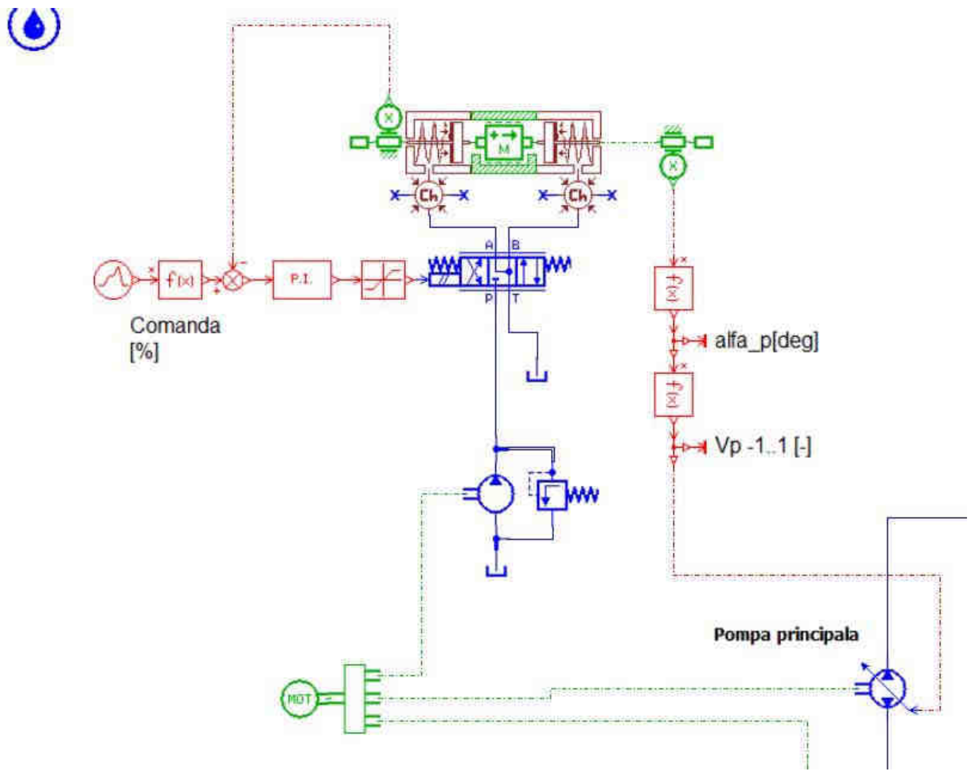

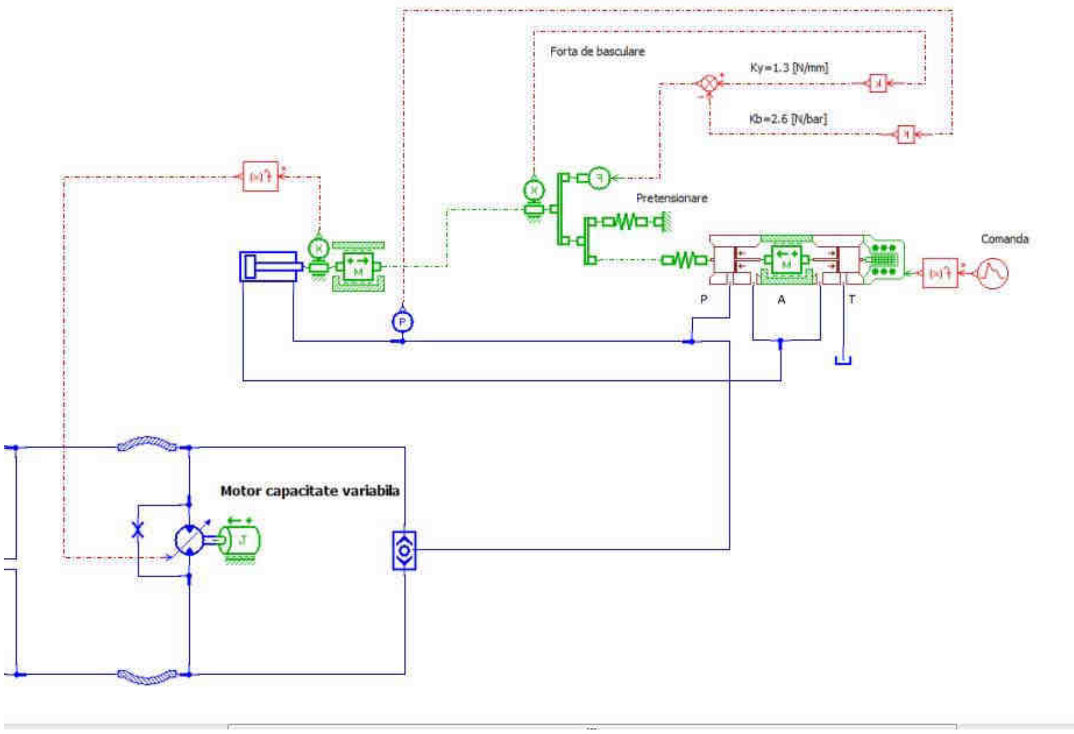

ISSN 1454 - 8003
Proceedings of 2014 International Conference of Hydraulics and Pneumatics - HERVEX
November 5 – 7, Calimanesti-Caciulata, Romania

HYDRAULIC DRIVE OF LDS LOCOMOTIVE

Krzysztof NIEŚPIAŁOWSKI[1]

[1]KOMAG Institute of Mining Technology, kniespialowski@komag.eu

Abstract: *In the Polish mining industry the rail transportation machines equipped with diesel and electric locomotives are used for transportation of materials and run-of-mine. Part of the locomotives is equipped with hydraulic supply and control systems due to specific conditions in mines. Lds locomotive is one of the underground diesel locomotives with hydrostatic drive.*
Design of the hydraulic system used in the above mentioned locomotive is presented in the paper.

Keywords: *diesel locomotive, locomotive's hydraulic system*

1. Introduction

Demand of users of the machines used in the mining industry for increase of their productivity and reduction of costs force the machines manufacturers to search for new solutions. The problem mainly regards the transportation means, which in the process of mineral production decide about their effectiveness Solutions of the hydraulic drive for Lds locomotive (with low-toxic diesel engine) which meet users requirements are given in the paper. The locomotive due to its features enables improving the transportation process as well as improving condition of work in underground workings. These features are as follows: versatility, as it can be used for transportation of machines and their components of high weight and for transportation of people as well as mobility, which increases effective working time of miners in faces and shortens time of relocation of machines and equipment as the face front [2, 3].

Well-functioning hydraulic system of the locomotive ensures its reliable and safe operation.

2. Drive of Lds locomotive

Two versions of Lds underground diesel locomotive were developed in KOMAG:

- Lds-100K-EM, to be used in ore mines and meeting the requirements of 98/37/EC Directive (Machinery Directive),
- Lds-100K-EM-A, to be used in hard coal mines and meeting additionally the requirements of 94/9/WE–ATEX Directive (with mechanical-and-hydraulic drive transmission).

Lds locomotive (Fig. 1) is designed in a modular form with two operator cabins separated with the engine compartment. In the engine compartment there is a driving unit with a control-and-actuating (hydraulic and electric) system.

The driving unit consists of a high-pressure, turbo-charged diesel engine, transmitting torque through the hydrokinetic gearbox, the gearbox and two axis gears, shafts of which are the wheels axles (Fig. 2). In the hydraulic version, the hydrokinetic and reversible gearboxes are replaced by a hydrostatic system based on piston units (pumps and motors).

Locomotive's hydraulic system ensures realization of the following functions:

- supply and lubrication of hydrokinetic gearbox,
- lubrication and control of reversible gearbox operation,

ISSN 1454 - 8003
Proceedings of 2014 International Conference of Hydraulics and Pneumatics - HERVEX
November 5 – 7, Calimanesti-Caciulata, Romania

- control of travel speed,
- manoeuvring braking and emergency-parking braking,
- activation of sanders.

In the case of dust and/or methane explosion hazard, the following systems are additionally installed in the hydraulic system:

- diesel engine start-up system,
- oil cooler fan motor’s driving system [4].

Fig. 1 Lds underground diesel locomotive [1]

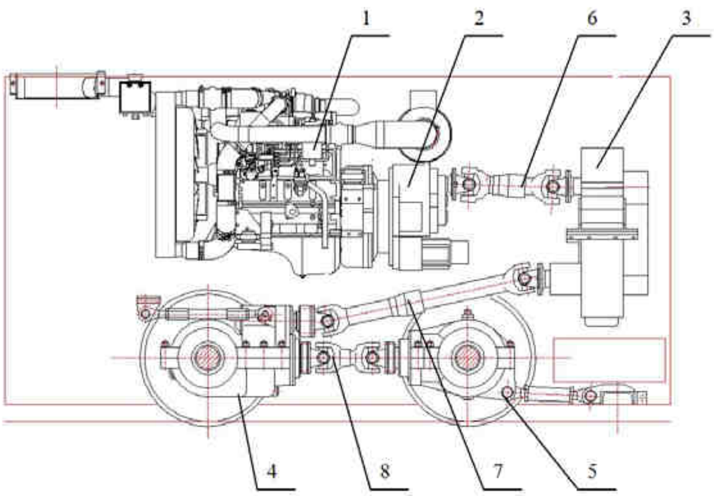

Fig. 2 Drive of Lds locomotive: 1 - high-pressure engine, 2 - hydrokinetic gearbox, 3-reversible gearbox, 4 – front axis gear, 5 – rear axis gear, 6, 7, 8 – driving shafts [1]

Lds locomotive has the following parameters:

- tractive force up to 42 kN
- power of diesel engine 81 (93) kW

- maximal speed 5 m/s
- minimal bending radius 12.5 m
- weight 12 000 kg
- distance between bumpers 6200 mm
- height from the rail head 1650 mm
- width 1100 mm ÷ 1250 mm
- track gauge 550 mm ÷ 900 mm

Driving system of Lds locomotive (presented in a form of block diagram in Fig. 3) was designed basing on the following components:

- pumping unit (ZP), made of gear pumps, where one of them cooperates directly with a hydrokinetic gearbox and the other one operates in low-pressure circuit,
- gear pump (PZ), operating in high-pressure circuit.

Pumping unit (ZP) ensures supply and lubrication of hydrokinetic gear as well as lubrication and control of reversible gear. Gear pump (PZ), operating in high-pressure circuit ensures control of travel speed, manoeuvring braking “with sensing the loading”, release of parking brake, activation of sanders and filling the hydraulic accumulator intended for emergency braking with use of manoeuvring brakes. The locomotive operating in the areas of potentially explosive atmosphere is additionally equipped with the following systems: hydraulic supply of fan oil cooler motor’s driving system from low-pressure circuit as well as the system for filling the hydraulic accumulator responsible for start-up of diesel engine. On the forcing line of each pump, installation of accurate high-pressure filter and sealed valve protected against excessive pressure increase, is planned.

Hydraulic system of Lds locomotive has the following parameters:

- output of low-pressure circuit pump $Qn = 29.5\ cm^3/rev$
- output of high-pressure circuit pump $Qw = 12.4\ cm^3/rev$
- maximal pressure in low-pressure circuit $pn = 1.7$ MPa
- maximal pressure in high-pressure circuit $pw = 16$ MPa
- filtration accuracy $\beta = 10$ µm
- working liquid HLP68 or HLP46

ISSN 1454 - 8003
Proceedings of 2014 International Conference of Hydraulics and Pneumatics - HERVEX
November 5 – 7, Calimanesti-Caciulata, Romania

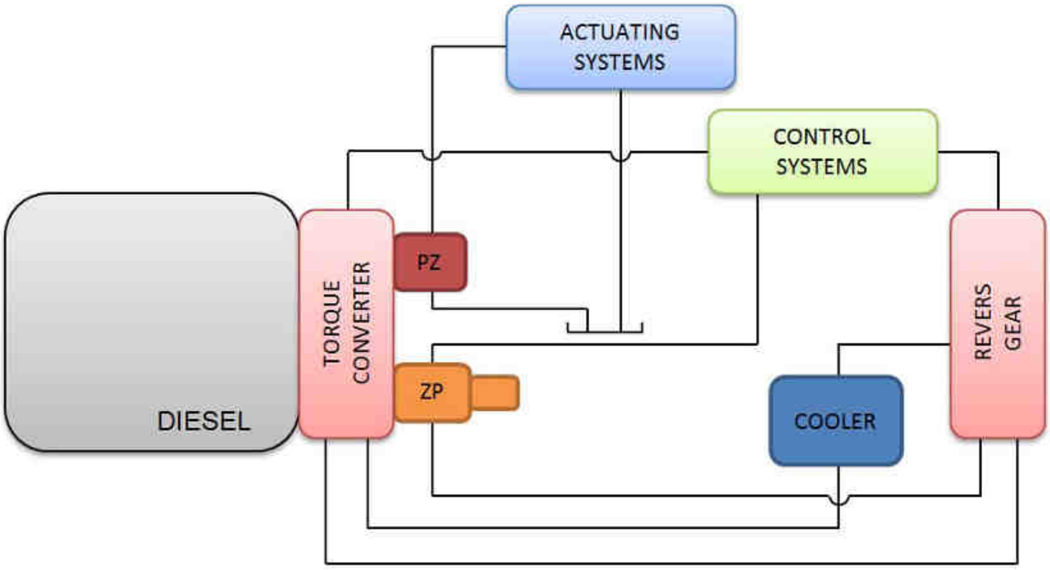

Fig. 3 Driving system of the Lds locomotive: PZ – gear pump of high-pressure circuit, ZP – pumping unit in low-pressure circuit (own source)

2.1 Lds-100K-EM locomotive

Driving system of Lds-100K-EM locomotive (Fig. 4) was developed to be used in areas, which are not threatened by explosion hazard. It is built of standard sub-assemblies, which do not require intrinsically safe design. Typical electric starter was used to start-up of diesel engine, while fan of the cooler is driven by DC motor. Rotational speed of diesel engine is controlled electro-hydraulically, and manoeuvring brake is controlled hydraulically. Due to the fact that increase of pressure of hydraulic medium activates the brake, a distributor with “M” piston was installed in the brake circuit, so in the case of electric system failure (electrically controlled standard slide valves decide about the direction of liquid flow) the operator can safely brake the locomotive. Accumulator installed in the hydraulic system also increases safety as it enables effective barking of locomotive in the case of diesel engine failure.

The system was additionally equipped with a distributor, which has to prevent against start of the locomotive without prior release of parking brake. Increase of pressure of operational medium in the parking brake system causes hydraulic reversing of parking brake, and thus oil flow to reversible gearbox through the distributor for selection of travel direction is possible.

Reversible gearbox can be also equipped with a distributor enabling use of the second gear, which allows the locomotive to move with higher speed.

ISSN 1454 - 8003
Proceedings of 2014 International Conference of Hydraulics and Pneumatics - HERVEX
November 5 – 7, Calimanesti-Caciulata, Romania

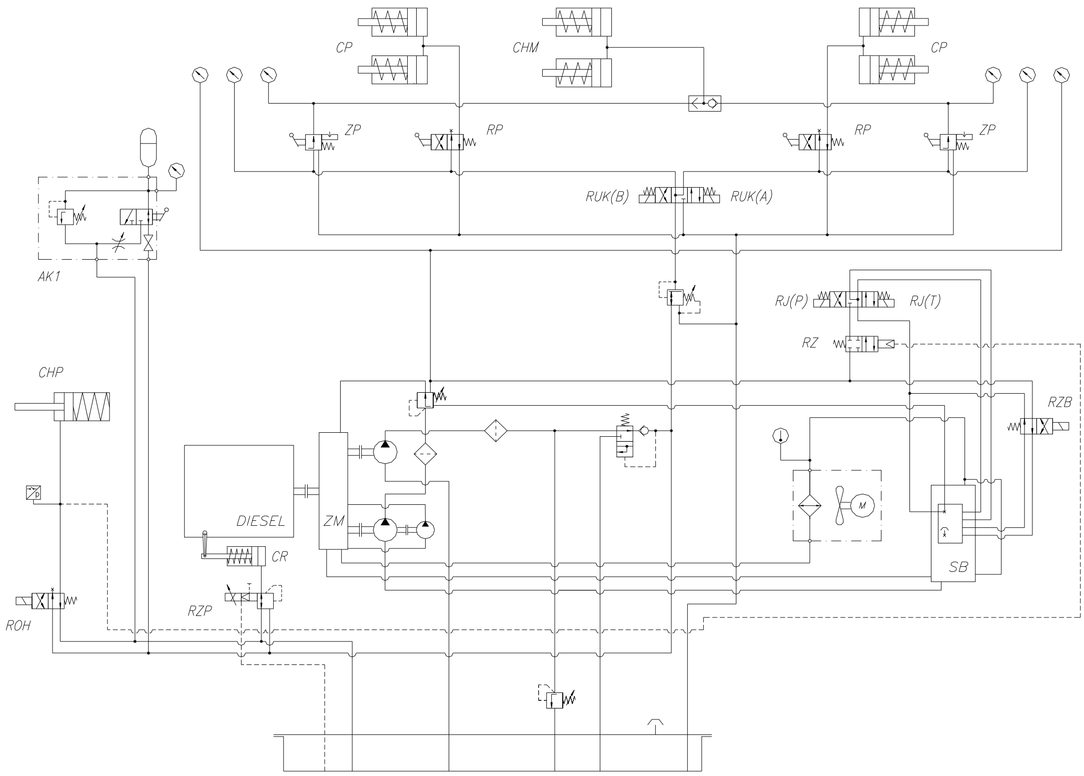

Fig. 4 Diagram of Lds-100K-EM locomotive hydraulic system: AK1-hydraulic accumulator, CHP-cylinder of parking brake, CHM-cylinders of manoeuvring brake, CP-cylinders of sanders, CR-control cylinder, ZP-manual proportional valves, RP-distributors of sanders, RUK-lever giving authority to operate the cabin, RJ-distributor for selection of travel direction, RZ-protecting distributor, RZB-distributor for gear ratio change, ROH-distributor of parking brake, RZP-reducing proportional valve, ZM-torque converter (hydrokinetic gear), SB-reversible gear [6]

2.2 Lds-100K-EM-A locomotive

Lds-100K-EM-A locomotive is designed for operation in conditions of coal dust and/or methane explosion hazard. Hydraulic system of the locomotive is presented in Fig. 5. Requirement of ATEX Directive caused that diesel engine is started up hydraulically, including opening the throttle, what enables air inflow to the inlet system, and opening the valve to make fuel flow possible.

The start-up system consists of the following components:

- hydraulic starter,
- hydraulic accumulator (with valve block and the system of control distributors) supplying the starter,
- hydraulic accumulator (with valve block and control distributor) supplying the cylinder of air inflow throttle and cylinder of fuel cut-off,
- throttle cylinder,
- fuel cut-off cylinder.

Hydraulic accumulators emptied during start-up are refilled during locomotive operation. Manual pump installed in the system enables refilling of accumulators in the case of lack of working medium, which is required for start-up and emergency release of brakes in the machine.

Requirements as regards devices operating in atmosphere threatened by explosion hazard caused that the hydraulic motor, supplied directly from low pressure system operating the torque converter and reversible gear, was used to drive the cooler's fan.

Intrinsically safe, proportional pressure reducing valve is responsible for control of rotary speed of diesel engine. However, this valve can not be supplied from high pressure pipeline. That is why, the valve reducing the pressure to the value specified in technical documentation of proportional valve, was installed just ahead of this valve.

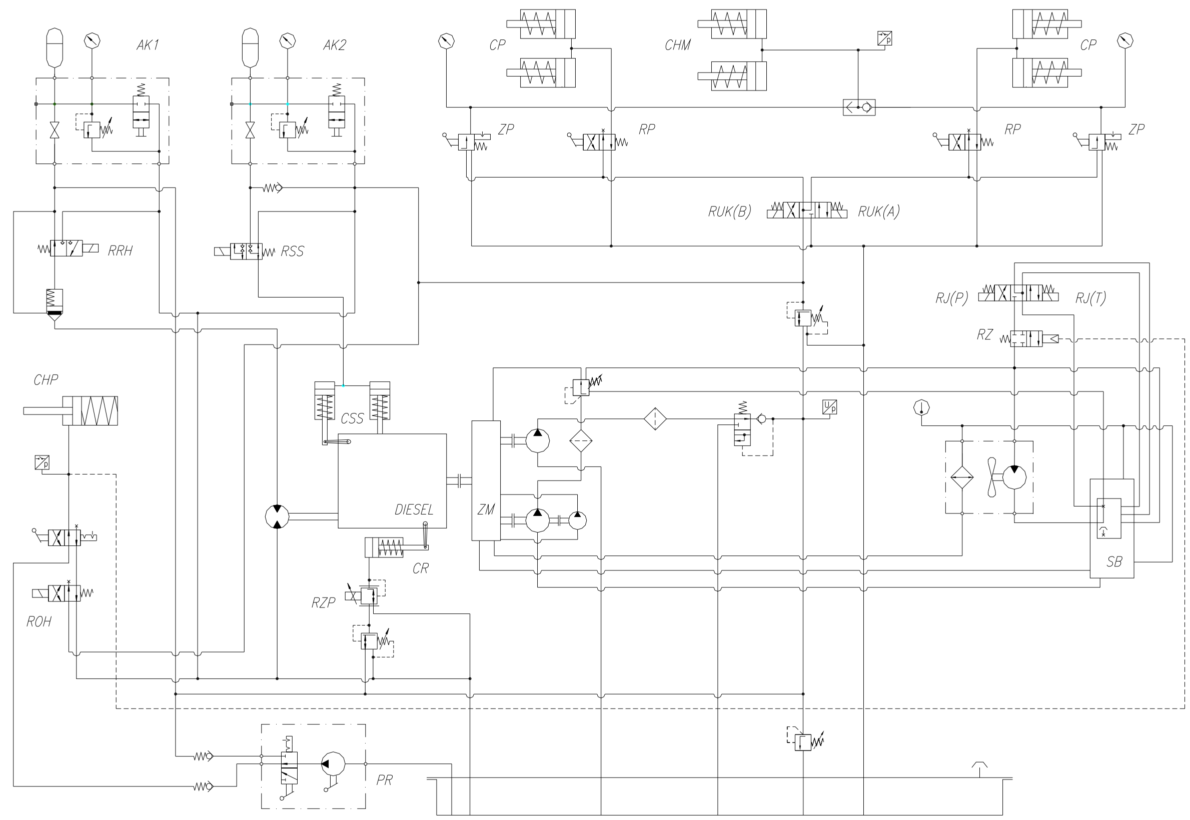

Fig. 5 Diagram of Lds-100K-EM-A locomotive hydraulic system: AK1, AK2-hydraulic accumulators, CHP-cylinder of parking brake, CHM-cylinders of manoeuvring brake, CP-cylinders of sanders, CSS-cylinder of throttle and fuel cut-off, CR-control cylinder, ZP-manual proportional valves, RP-distributors of sanders, RUK- lever giving authority to operate the cabin, RJ-distributor for selection of travel direction, RZ-protecting distributor, ROH-distributor of parking brake, RZP-reducing proportional valve, PR-manual pump, ZM-torque converter (hydrokinetic gear), SB-reversible gear [7]

2.3 Lds-100K-EM-A locomotive (with hydrostatic system)

Lds-100K-EM-A locomotive with hydrostatic system, which replaces hydrokinetic gear and reversible gear, is the next design version of the locomotive. Hydrostatic gear (pump-and-motor system) operates in a closed circuit, and hydraulic system of the locomotive ensures realization of each function as it is in the case of Lds-100K-EMA locomotive. Diagram of the hydraulic system solution is presented in Fig. 6.

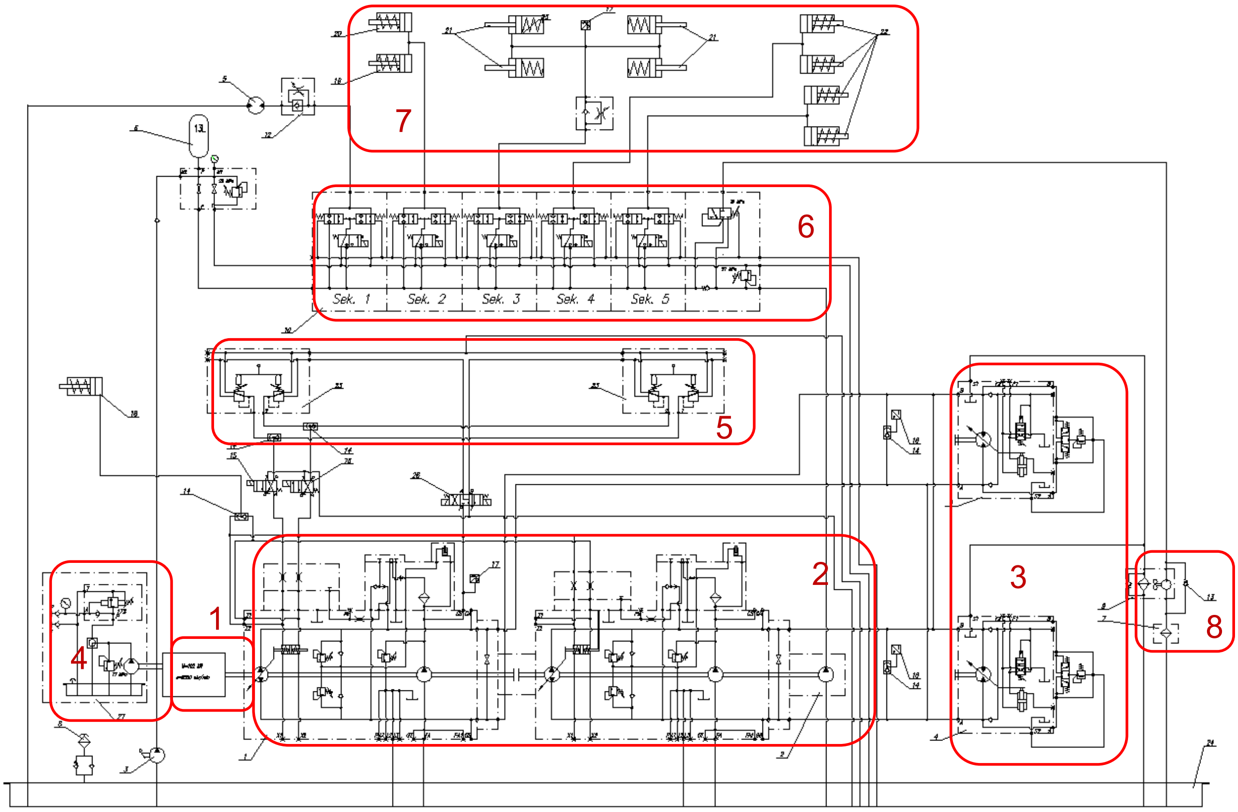

Fig. 6 Diagram of Lds-100K-EM-A locomotive hydraulic system with hydrostatic system: 1 - diesel engine, 2 - three-sectional system of pumps, 3 - system of hydraulic motors, 4 - auxiliary supply system, 5 - control system, 6 - system of distributors, 7-system of actuating devices, 8 - cooling-and-filtration system [8]

Hydraulic system of the locomotive is based on three-sectional pump system (Fig. 7), installed on the common shaft and driven by diesel engine through the coupling. Two first pump sections operate in independent closed circuits and they are used for transmission of torque from diesel engine to locomotive wheels. The third section operates in an open circuit and ensures operation of other machine systems. Integrated system of main pump and filling pump makes the first pump section. Piston pump of changeable capacity with a controller, designed for operation in closed circuit, was used as the main pump. It supplies one of hydraulic motors, which is connected with a gear of wheel set. Hydraulic motors are also equipped with controllers which, depending on the load (operational pressure), determine the maximal rotary speed. The second pump section is a copy of the first one. Both sections are equipped with make-up pumps, designed to make up oil losses and to replace oil

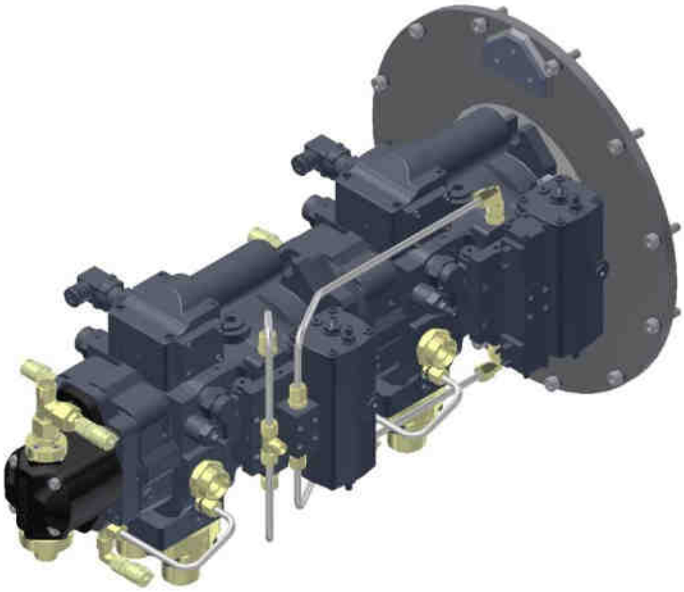

Fig. 7 Pump system with installed connectors and coupling lid [5]

in a closed circuit. Hydraulic manipulators and electro-hydraulic distributors control the pumps.

The third section of pump system is the gear pump protected by overflow valve, which ensures, among others, release of emergency-and-parking brake, activating the sanders as well as cooling and filtration of operational medium [5].

3. Summary

Development of several types of diesel locomotives, equipped with devices improving the safety, work effectiveness and ergonomics, is the result of designing and research work carried out from many years at KOMAG. Work safety and operational parameters competitive to the parameters of similar solutions were especially emphasized. Presented Lds-100K underground diesel locomotives are designed for operation in ore and hard coal mines.

REFERENCES

[1] Dobrzaniecki P., Suffner H., Budzyński Z.: Nowoczesne lokomotywy dołowe produkcji Energo-Mechanik Sp. z o.o. Transport Przemysłowy No. 3/2007
[2] Marciniak Z., Mierzwa Z., Nieśpiałowski K., Pieczora E.: Hydrauliczny układ napędu i sterowania lokomotywy podwieszanej spalinowej LPS-90. Conference proceedings: CYLINDER 2000, Dziesiąta Jubileuszowa Ogólnopolska Konferencja "Badanie, konstrukcja, wytwarzanie i eksploatacja układów hydraulicznych", Szczyrk, September 2000
[3] Nieśpiałowski K., Rojek P., Jasiulek T.: Hydraulic systems of Lds locomotives designed by KOMAG. Proceedings of the conference: Riadenie tekutinovych systemov 2008, VIII medzinarodna vedecka a odborna konferencia, Strbske Pleso (Slovakia), 2.4. - 4.4.2008
[4] NIEŚPIAŁOWSKI K.: Układy hydrauliczne maszyn i urządzeń dla przemysłu górniczego. Maszyny Górnicze 2010 No. 3-4
[5] Narrow-gauge WLP-85 surface locomotive. KOMAG statutory project
[6] KOMAG technical documentation: W23.036SH07
[7] KOMAG technical documentation: W23.037SH07
[8] KOMAG technical documentation: W23.037.06SH07

ISSN 1454 - 8003
Proceedings of 2014 International Conference of Hydraulics and Pneumatics - HERVEX
November 5 – 7, Calimanesti-Caciulata, Romania

PNEUMO-HYDRAULIC DEVICE FOR LIFTING PROVIDED WITH ENERGY RECOVERY

Teodor Costinel POPESCU[1], Catalin DUMITRESCU[2], Liliana DUMITRESCU[3]

National Institute for Optoelectronics, INOE 2000-IHP Bucharest,[1] popescu.ihp@fluidas.ro ;

[2] dumitrescu.ihp@fluidas.ro ; [3] lilianad.ihp@fluidas.ro

Abstract: *This material relates to a compact device for lifting-lowering, that contains a differential hydraulic cylinder, equipped with its own distribution system and a system for storing a part of the potential energy of the load, in the lifting phase, respectively its consumption during the lowering phase. Operation of the device provided with energy recovery is based on the change of the pressure and the volume in three closed chambers; one positioned on the central axis, using nitrogen as working fluid and the other two located outside, coaxially with the former, which use hydraulic oil as working fluid.*

Keywords: *lifting-lowering device, energy recovery, nitrogen, hydraulic oil*

1. Introduction

There is known a wide range of hydraulic cylinders, actuated by pressurized hydraulic oil, which are used in the lifting-lowering mechanisms: with single or double effect, with or without elastic return, telescopic cylinders, plunger cylinders, and so on. When lowering the load, these cylinders discharge to the tank by means of a hydraulic distributor, the entire amount of oil accumulated in the active chamber during the lifting phase, without recovering not even a little bit of the potential energy of the load.

There are also known hydraulic lifting-lowering systems that recover some of the potential energy of the lifted load. They include hydraulic cylinders and accumulators, and recovery of the potential energy is done during the lowering of the cylinder by directing the hydraulic oil to the pneumo-hydraulic accumulator. Inside the accumulator there is an elastic membrane that separates two fluid media: nitrate, which is compressed in the lowering phase of the cylinder, accumulating the potential energy and pressurized hydraulic oil which in the lifting phase, by the expansion of the nitrogen, is directed to the hydraulic cylinder.

The main disadvantages of these types of systems are:

- the distribution system of the working fluid between the supply pump, hydraulic cylinder and pneumo-hydraulic accumulator is complicated both constructively and functionally;
- the cost of the entire installation is very high, because in addition to the supply pump, hydraulic drive distributor and hydraulic cylinder, the system also includes a second hydraulic distributor, for controlling the intake / discharge of oil to / from the accumulator, a throttle valve, two pressure relays and a pneumo-hydraulic accumulator.

2. Lifting-lowering hydraulic installation provided with energy recovery

Figure 1 and Table 1 present the principle schematic diagram and the operating cyclogram for a lifting-lowering hydraulic installation that stores some of the potential energy of the load in the lowering phase of a hydraulic cylinder and reuses it in lifting phase. The installation includes an electric pump, a safety valve, four hydraulic distributors, two pressure relays, a hydropneumatic accumulator, a hydraulic cylinder and a way throttle. By means of three hydraulic distributors and the two maximum and minimum pressure relays, is ordered charge / discharge of the hydraulic accumulator and coupling / decoupling to/from the load of the fixed flow rate displacement pump. Lifting/lowering of the hydraulic cylinder rod is ordered by means of a fourth hydraulic distributor. The way throttle adjusts the descent speed of the cylinder rod.

ISSN 1454 - 8003
Proceedings of 2014 International Conference of Hydraulics and Pneumatics - HERVEX
November 5 – 7, Calimanesti-Caciulata, Romania

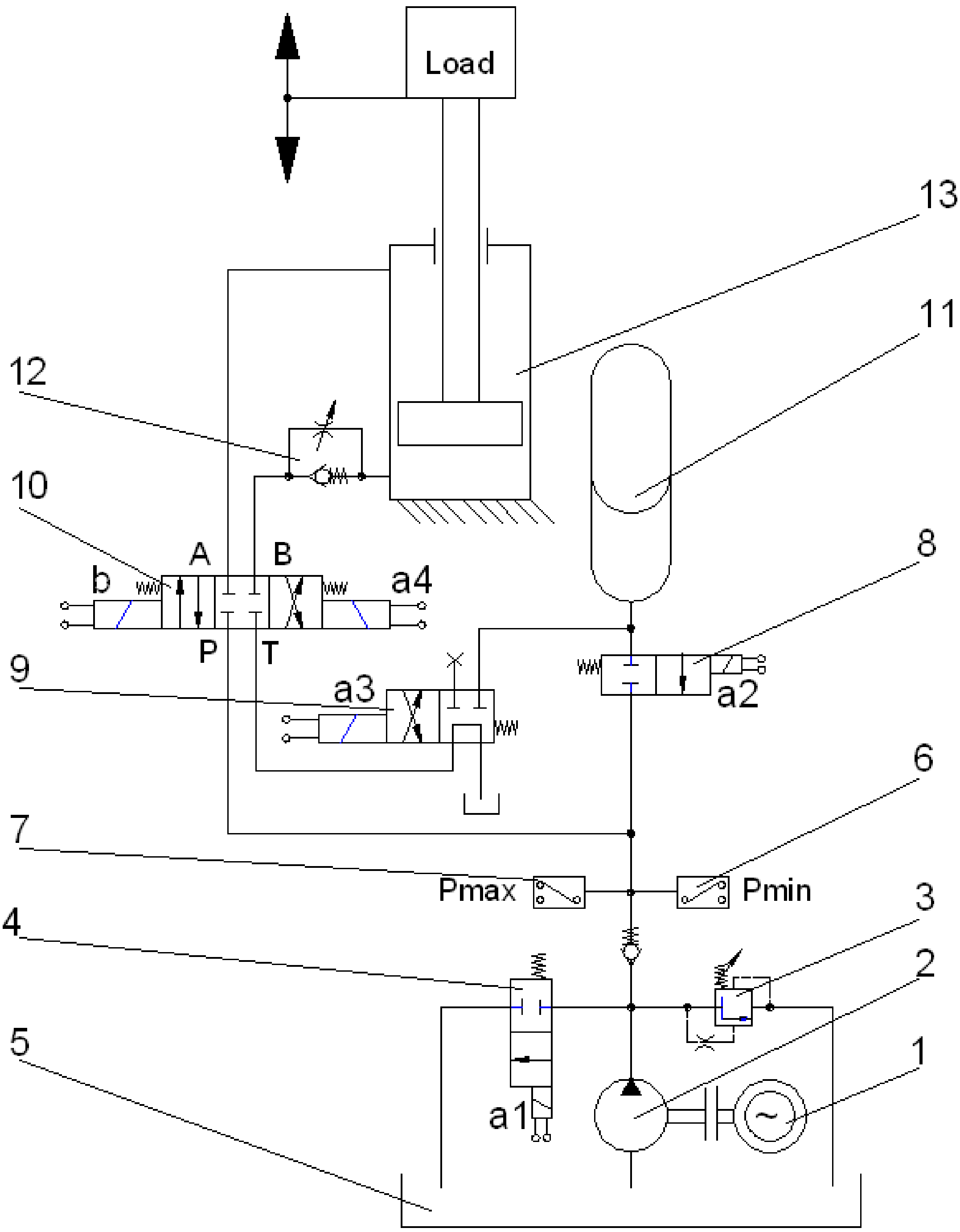

Fig.1. The lifting-lowering hydraulic installation provided with energy recovery - Principle diagram: 1- constant speed electric motor; 2-fixed displacement pump; 3-safety valve; 4- electric drive 2/2 hydraulic distributor; 5-oil tank; 6-minimum pressure relay; 7-maximum pressure relay; 8- electric drive 2/2 hydraulic distributor; 9- electric drive 4/2 hydraulic distributor; 10- electric drive 4/3 hydraulic distributor; 11-hydropneumatic accumulator; 12-way throttle; 13-double acting hydraulic cylinder.

Table 1 The lifting-lowering hydraulic installation provided with energy recovery – functioning cyclogram:

Actuating of the cylinder	**Condition of the electromagnets**					**Condition of the relays**		**Observations**
	a1	a2	a3	a4	b	Pmax	Pmin	
Lifting	-	+	-	+	-	-	-	AHP discharge
Lowering	-	-	+	-	+	-	-	AHP charge
Maintaining position	+	+	-	-	-	+	-	Decoupling pump
	-	+	-	-	-	-	+	Coupling pump

Caption: ”**+**” = the electromagnet has closed / closed relay contact; ”**- ”** = the electromagnet has opened / opened relay contact

3. Importance of the hydropneumatic lifting device provided with energy recovery

The importance of this device is to recover some of the accumulated potential energy and reuse it for lifting some loads, only by means of the lifting hydraulic cylinder, thus substantially simplifying the hydraulic drive installation which comprises, apart from the device, only the oil tank, supply pump and control pilot of the distribution system, embedded in the device.
The lifting device provided with energy recovery removes the disadvantages of the known hydraulic lifting installations due to its compact structure, consisting of a cylindrical sleeve closed at the top with a cap, in which slides a tubular rod, to which there is attached a piston that has an outer diameter **ØD2,** driven by pressurized hydraulic oil.
The sliding tubular rod is centered on the inside to another fixed tubular rod with an outer diameter **ØD1**, which communicates with the inside of another cylinder sleeve, positioned concentrically and outwardly from the former. Fixed volume between the two concentric cylindrical casings and the variable volume from the inside of tubular rods are charged with nitrogen pressure, through a filling valve attached to the device. Maintaining the position of the cylinder piston is made by a distribution system consisting of two unlockable check valves mounted in a body, which can be unlocked by a float plunger.
The lifting device has the following three advantages:
- cumulates simultaneously the functions of three classical hydraulic equipments: hydraulic cylinder, hydraulic distributor and pneumohydraulic accumulator;
- can store and reuse up to 60% of the energy consumed during the lifting phase of a load;
- simplifies and cheapens considerably the hydraulic supply and drive installation.

4. Structure of the hydropneumatic lifting device provided with energy recovery

The device, Fig. 2, consists of an inner cylindrical sleeve **1**, made of three welded parts, closed at the top by a cap **2**, attached by means of screws, in which there is a tubular rod **3**, to which there is attached a piston **4**, secured by a nut **5**.
The tubular rod, the piston and the nut can slide on another rod **6** with holes in the middle, fixed by another nut **7** to the cylindrical sleeve **1**.
Outwardly and concentrically from the cylindrical sleeve **1,** there is another cylindrical sleeve **8**, also made from three welded parts, to which there is fixed a valve **9**, for filling with nitrogen. This outer cylindrical sleeve is assembled in package with the cap **2** and the inner cylindrical sleeve **1**, delimiting the fixed volume **c** that through the perforated rod **6** communicates with the variable volume **d**, in the rod **3**.
On the cap **2** there is fixed the distribution system, Figure 3, consisting of a body **10** provided with two threaded holes **e** and **f** for the oil supply connections. In the body there are two unlockable check valves **11.1** and **11.2**, which can be unlocked by a piston **12**, for the purpose of entry and discharge of oil to / from the chamber **a** by means of a direct duct in the cap **2**, or to / from chamber **b** by means of a pipe connection **13**.
The cap **2** is provided with a plug **14** for the initial filling of the chamber **a** with oil.

Both tubular rod **3** and sleeve **8** are provided with threaded ends, at the ends of the assembly, for mechanical fastening within the serviced system.

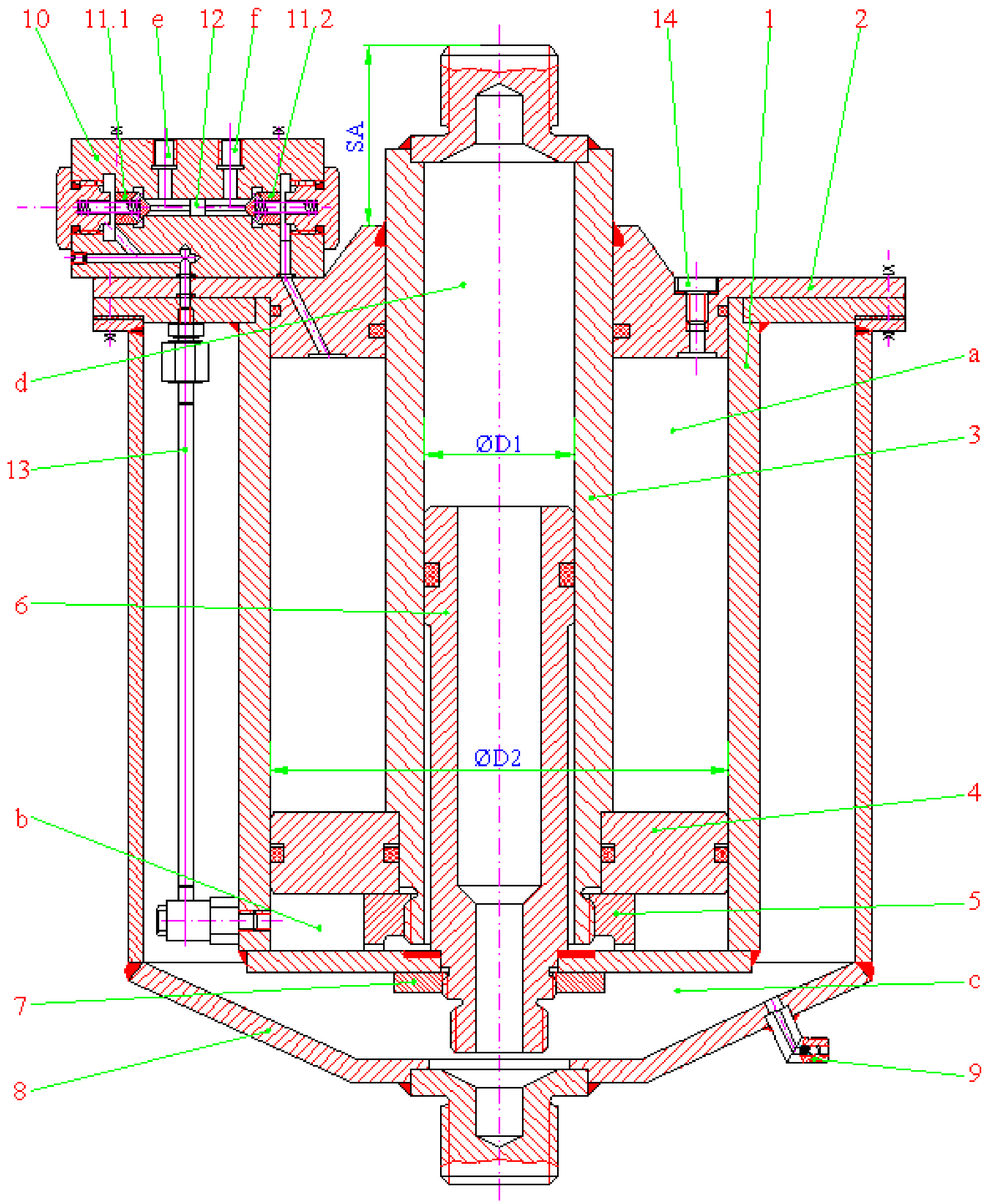

Fig. 2. Hydropneumatic lifting device provided with energy recovery

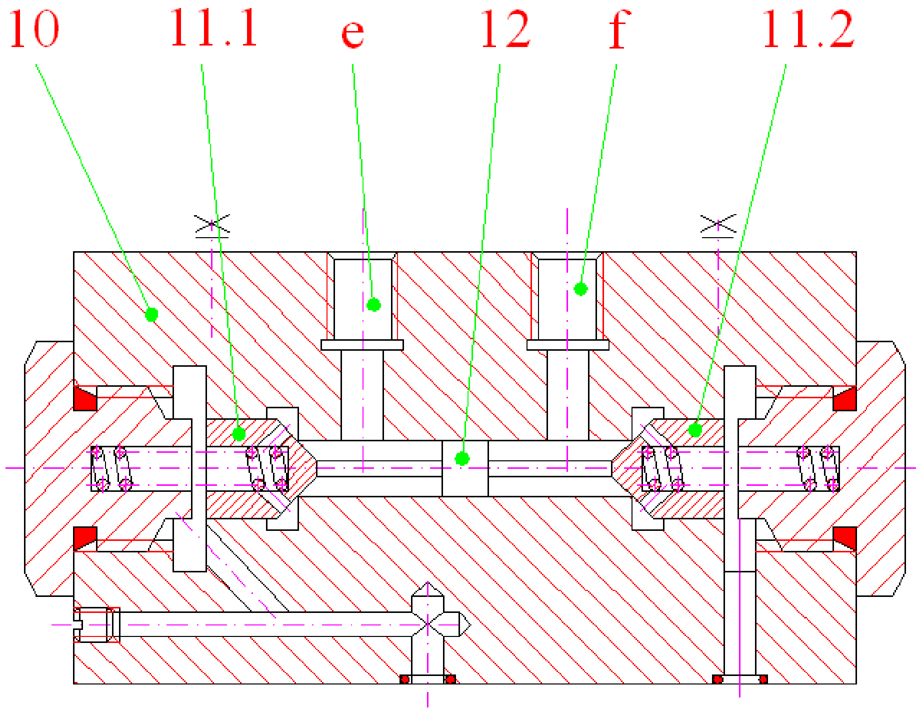

Fig. 3. Detail from the distribution system dedicated to the hydropneumatic lifting device provided with energy recovery

Before starting, the following operations are performed:
- check compliance with the mounting rate **SA**, namely if the device is assembled with the piston at the bottom of the cylinder stroke; possibly restore the mounting;
- fill with hydraulic oil the chamber **a**, through the hole of the plug **14**, after that this one is tightened securely;
- load chambers **c** and **d** with nitrogen, from an outer gas cylinder, not shown, by the valve **9,** at a prescribed charging pressure, the value of which is equal to the load that must be lifted divided by the cross-section of the cavity **d** (it is recommended that at this model of cylinder to be marked by punching the maximum pressure for filling with nitrogen and the corresponding load that it can lift, when operating with energy recovery).

5. Operation of the hydropneumatic lifting device provided with energy recovery

Operation of the device described in phases, is as follows:
Stationing on position:
The cylinder positioning at stroke ends or in any intermediate position is achieved by not driving the slide valve of a 4/3 distributor, closed center, for piloting its own distribution system, in the outside of the device. For example, when positioning the cylinder at the lower end of stroke, due to not driving the pilot slide valve, the oil from chamber **a** can not be discharged to the connection hole **f**, because the valve **11.2** being closed, the pressure of nitrogen, installed in the cavity **d** will not determine the lifting of the tubular rod **3**.
Lifting the load:
It is achieved by actuating the pilot slide valve in the sense of supplying with pressurized oil the hole **e**, which produces the opening of the valve **11.1** and oil entering into the chamber **b** through connection **13**, at the same time with unlocking valve **11.2** through the piston **12,** for discharging oil from the chamber **a**, to the hole **f**. The upward movement of the rod **3** integral with the piston **4**, so lifting of the load, is due to the pressure forces generated both by the oil pressure, installed in the chamber **b** and the nitrogen pressure in the cavity **d**. While the piston **4** performs lifting stoke, oil pressure increases because the nitrogen in the cavity **d**, which increases its volume, expands and decreases its pressure initially installed.

The decrease in the nitrogen pressure, in the lifting phase, will be the lower the more change in volume of the cavities filled with nitrogen is smaller, and for increasing the percentage of recovery of the potential energy available there will be chosen a volume as large as possible for the enclosure **c** (fixed volume), as compared to the final volume of the cavity **d** (fixed volume plus the increasing in volume).

Lowering the load:

It is achieved by actuating the pilot slide valve in the sense of supplying with pressurized oil the hole **f**, which generates the opening of the valve **11.2** and oil entering into the chamber **a**, at the same time with unlocking the valve **11.1**, through the piston **12,** for draining the oil in the chamber **b** to the hole **e**. At this stage the piston **4**, integral with the rod **3**, retracts and the load descends, and the nitrogen compresses up to the initial charging value, storing part of the potential energy, converted into addition of pressure energy that will be used in a new lifting phase, that is produced with a reduced pressure of hydraulic oil, almost equal to that required for overcoming the friction forces of the system.

6. Conclusions

- Through this material the authors test the market of those interested in producing a lifting lowering device provided with energy recovery, for which a patent application has been submitted.
- The device, playing the role of volume linear motor, is designed primarily for hydraulic lifting-lowering installations of the kind existing in auto repair shops, in hydraulic elevators, freight or for people, in installations for lifting and rolling back on line the derailed rolling stock etc. The pneumohydraulic device can lift and lower loads of various weight, but there should be properly correlated the initial pressure for charging with nitrogen.
- The device can also be used in other mechanisms, for instance those with horizontal displacement of the load, without energy recovery. In this case there should be removed the outer sleeve **8,** and the unit will work as a general purpose hydraulic cylinder.

REFERENCES

[1] N. Ionita, T.C. Popescu, C. Dumitrescu, “Cilindru hidraulic pentru ridicare“ (*Hydraulic cylinder for lifting*), Patent Application No. A/00713/09.10.2012

ISSN 1454 - 8003
Proceedings of 2014 International Conference of Hydraulics and Pneumatics - HERVEX
November 5 – 7, Calimanesti-Caciulata, Romania

VALIDATION OF POROUS HEAT EXCHANGER SIMULATION MODEL

assistant professor Petre OPRIŢOIU[1]

[1]Technical University of Cluj-Napoca, Department of MTC, E-mail: petre.opritoiu@infra.utcluj.ro

Abstract: *The continuous increase speed and performance of electronic components, while reducing their size and weight, constitutes an important feature of technical development of the last decades. This growth is often limited by the heat thereof, which should always be avoided because exceeding prescribed temperature decreases the quality, safe operation and reliability of these components.*
In the case of electronic components cooling, out of many ways and variants of existing heat transfers, the fluid single-phase forced convection heat is an effective and widely practiced method, especially due to its simplicity and economical character.
Thermal management, with the increasing and progressive miniaturization of electronic components, becomes a very important aspect and task for engineers designing electronic cooling systems. It is estimated that a power dissipation requirement in the order of 30-50 W/cm^2 is anticipated for the next years resulting in the need for the arrival of new techniques for the use in thermal application [1,4]. The working method used is the numerical simulation using FLUENT software in which the actual characteristics of porous metal indicated by the manufacturing company, Erg Materials and Aerospace [2], were introduced.
Numerical solutions use the mathematical models to describe a real phenomenon, and this description does not always present a high accuracy. The results obtained through numerical simulation program may be inaccurate and should therefore be carefully examined and validated by experimental results. This article describes the validation of the heat transfer and flow results obtained by simulation with FLUENT software.

Keywords*: simulation, pressure drop, flow features, convection coefficient, heat transfer performance.*

1. Introduction

Forced air cooling has been the preferred cooling technique in electronic equipment, given its simplicity and reliability. Requirements of permissible acoustic noise for electronic cooling restrict the use of mean air velocities above 5 m/s for many applications. Many researchers have studied various solutions to the problem such as vortex promoters and staggered chip arrangements using traditional heat sink technology obtaining 20 to 50 percent improvement; however this will still not be sufficient for the above mentioned upsurge in power dissipation requirement for years to come.
An increase in fin density in traditional heat sink technology offers this increase in heat transfer area as some researchers have already experimented with and even though the arrangement could be a ducted arrangement with free flow area this is not nearly enough for the mentioned heat dissipation requirements [1].
It is one of the objectives in this article work to validate what some researchers have already proposed, the use of metal foams for heat exchanger applications. Metal foams provide extended surface area, up to a 10 fold compared with commercially available heat sinks and, although the structure gives an increase in pressure drop, an enhanced heat transfer coefficient due to local thermal dispersion caused by eddies that are shed in the wake of the flow past the medium fibers.
As has been proven in earlier works as that of Cruz [3], the penalty of producing a slightly greater pressure drop could be traded by the enhancement of heat transfer and the reduction in weight that these highly porous mediums offer. This in contrast to traditional heat sinks as is the case for electronic cooling were the system area necessary to provide a same amount of heat dissipation is greater for a given heat flux. The goal of the research in this article is the analysis by FLUENT

numerical simulation of the heat transfer and flow process within the porous aluminum open-cell heat exchanger (fig. 1), starting from existing experimental data in the literature [3,4].

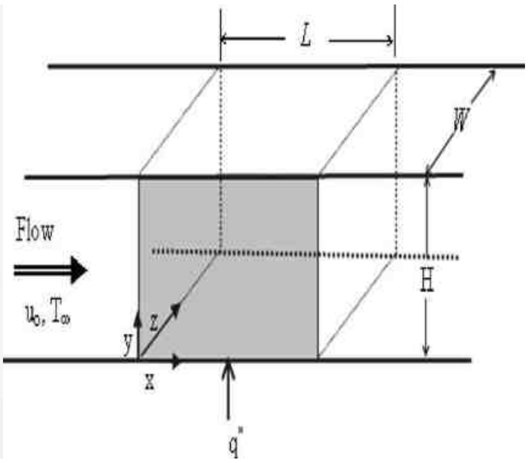

Fig. 1. Aluminum foam heat exchanger ***Fig. 2. Schematic of geometrical model [1].***

2. Theory

The final overall dimensions of the compressed foam blocks used in pressure-drop and heat transfer simulations were 250mm×100mm×50mm, with the cross-sectional area normal to the flow direction measuring 250mm×100mm. To make them functional heat exchanger, each foam was brazed in a central position to an adjoining heat spreader plate made by solid aluminum. A typical flow and heat transfer configuration is shown in fig. 2.
A heat source is bonded or joined to a thin conductive substrate on which a block of open-cell aluminum foam of length L and thickness W is attached. The foam is then placed in a channel, and cooling fluid of velocity u_0 at a temperature T_∞ is pumped through the open celled material, thereby affecting heat transfer from the hot source to the cooling fluid [1].
The analysis uses the typical parameters reported by the foam manufacturers such as the porosity (ε) and the area density (σ), defined as the ratio of the surface area of the foam to the volume (table 1).

Table 1. Metal foam properties [4].

No.	PPI	ε [-]	d_l [mm]	d_P [mm]	Size LxWxt [mm]	σ [m^2/m^3]
1	10	0.914	0.406	5.08	250.8 x 101.6 x 50.8	809.1
2	10	0.704	0.406	1.93	250.8 x 101.6 x 50.8	2053.1
3	10	0.682	0.406	1.24	250.8 x 101.6 x 50.8	3169.3
4	20	0.924	0.203	2.90	250.8 x 101.6 x 50.8	1240.2
5	20	0.774	0.203	0.89	250.8 x 101.6 x 50.8	3593.7
6	20	0.679	0.203	0.63	250.8 x 101.6 x 50.8	5104.3
7	40	0.923	0.102	1.70	250.8 x 101.6 x 50.8	1800.8
8	40	0.918	0.102	1.70	250.8 x 101.6 x 101.6	1800.8

The hydraulic diameter is determined based on the size of the compressed porous cell, of the metal filament's diameter and the porous density. Boundary layers play an important role for heat transfer. The shape of the crossing section is determined by the metal filaments and it is meant to grow the local turbulence of fluid and heat transfer when it flows into the porous metal. Turbulence intensity values and resistance coefficients of viscous and inertial type, required for running the FLUENT software for a porous medium were obtained using MATHCAD program, starting from equations specific to Brinkman's porous environment [5].

3. Validation of the Fluent simulating results – heat transfer

It validated the temperature distribution within the open-cell porous aluminum heat exchanger at different distances from the input section and the variation of the convection coefficient for different geometrical characteristics.

3.1. Temperature distribution

Comparing the values obtained by simulation with the experimental ones, relative errors resulted that were less than 5%, for most of the parameters studied, leading to the validation of simulation model developed in FLUENT by the experimental data (table 2). The temperature measurements were read from the computer screen and these were introduced in Excel pages.

Table 2.Comparison between simulation and experimental temperature data for v=5.38m/s.

Thermocouple position	x [cm]	$t_{sim2.54}$ [°C]	$t_{sim5.08}$ [°C]	$t_{sim7.62}$ [°C]	$t_{sim\ 9.52}$ [°C]	$t_{exp2.54}$ [°C]	$t_{exp5.08}$ [°C]	$t_{exp7.62}$ [°C]	$t_{exp9.52}$ [°C]	$\sigma_{2.54}$ [%]	$\sigma_{5.08}$ [%]	$\sigma_{7.62}$ [%]	$\sigma_{9.52}$ [%]
1	**Base plate**	84.85	84.85	84.85	84.85	85.00	85.00	85.00	85.00	0.17	0.17	0.17	0.17
2	0.64	40.74	50.19	56.49	56.49	53.70	53.70	58.38	64.84	24.13	6.53	3.25	12.87
3	1.27	28.14	34.44	40.74	39.85	28.53	28.53	32.06	39.51	1.36	20.71	27.07	0.86
4	1.91	21.84	28.14	31.29	31.29	24.01	24.01	26.46	28.19	9.03	17.20	18.25	10.99
5	2.54	21.84	21.84	24.99	24.99	23.11	23.11	24.39	25.07	5.49	5.49	2.46	0.31
6	3.18	21.84	21.84	21.84	21.84	22.78	22.78	23.24	23.40	4.12	4.12	6.02	6.66
7	3.81	21.84	21.84	21.84	21.84	22.61	22.61	22.78	22.89	3.40	3.40	4.12	4.58
8	4.44	21.84	21.84	21.84	21.84	22.26	22.26	22.41	22.47	1.88	1.88	2.54	2.80
9	5.08	21.84	21.84	21.84	21.84	22.12	22.12	22.35	22.40	1.26	1.26	2.28	2.50
10	6.35	21.84	21.84	21.84	21.84	22.06	22.06	22.10	22.17	0.99	0.99	1.17	1.48
11	8.89	21.84	21.84	21.84	21.84	22.04	22.04	22.06	22.09	0.90	0.90	0.99	1.13
12	13.97	21.84	21.84	21.84	21.84	22.02	22.02	22.04	22.06	0.81	0.81	0.90	0.99
13	19.05	21.84	21.84	21.84	21.84	22.01	22.01	22.01	22.02	0.77	0.77	0.77	0.81

It is clear a variation along the axis parallel to the flow direction, increasing the base temperature while we get farther away from the leading edge. This is given because the condition of constant heat flux is obtained at the lower part of the base and the temperature readings are taken at 0.25" from the lower part of the 0.5" base. The temperature grows in the flow direction reaching its maximum value at the output from the heat exchanger (fig. 3).

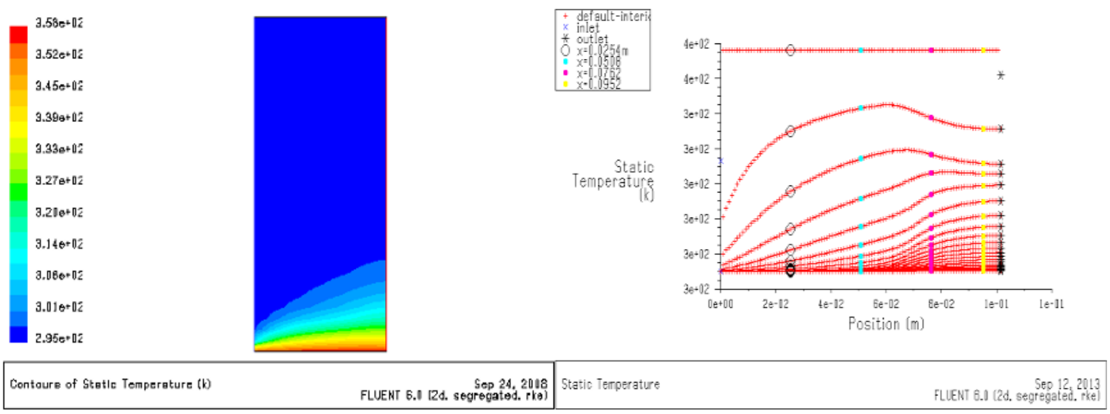

Fig. 3. Contour of static temperature and corresponding xy plot.

The temperature was plotted against distance along x direction and these plots were used to compare with the experimental data. The following graphs (fig. 4a, b, c and d) shows the data gathered for one of the simulation runs made with the 40 PPI sample at v=5.38 m/s flow velocity, at z=2.54, 5.08, 7.62 and 9.52 cm measured from the entrance.

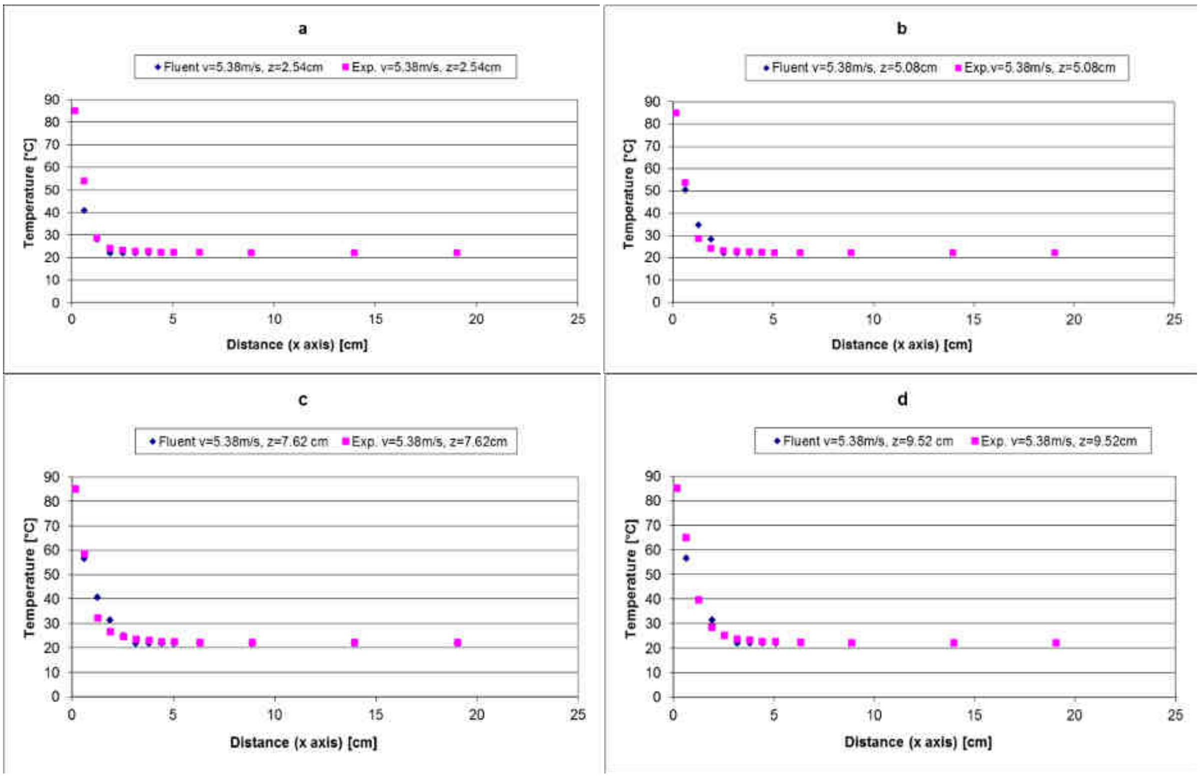

***Fig. 4.** Comparison between simulation and experimental temperature data for v=5.38m/s at z=2.54, 5.08, 7.62 and 9.52 cm measured from the entrance.*

It can be seen how the temperature distribution is modified when the distance along the z direction is increased. When the position along z axis is close to the fluid entrance of the foam, the temperature drops faster, but when the position is far from the entrance, the temperature takes a little more distance in the x direction to drop.
Research can be done on the characteristics of porous metal heat exchanger simulation with FLUENT software, because, the difference between the experimentally determined temperature and that resulting by simulation is generally acceptable (fig. 4).
Another way to analyze the temperature behavior is fixing the distance along the z direction and plotting the temperature distribution at different velocities. Figure 5 shows the temperature distribution for different velocities at one inch (2.54 cm) and three inches (9.52 cm) from the entrance.

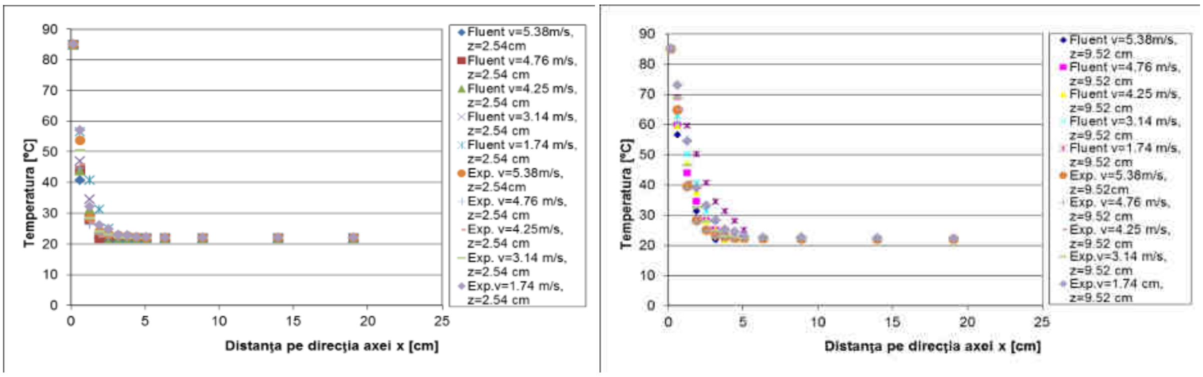

***Fig. 5.** Comparison between simulation and experimental data for different velocities at z=2.54 (a) and 9.52 (b) cm measured from the entrance.*

In the fig. 5(a) it is observed how the temperature distribution drops in a small distance when the velocity is high. For the next velocities, the temperature distribution is very similar, but it can be noticed that for v=1.74 m/s the temperature takes more distance to drop, compared to other cases. Figure 5(b) shows the temperature distributions at different velocities at a distance of 3.75 inches from the entrance. At this distance, it is more notorious that the temperature at v=3.14 m/s and v=1.74 m/s take more distance to reach ambient temperature.
The relative error is below 5% in most of the cases studied, it presents particularly low values in input section, results explained by the fact that this temperature drop is very high (table 3). Maximum relative erorr is reached for low flow velocities and at exit section (table 3 and 4).

Table 3. Relative erorr for z=2.54 cm, at different velocities.

Thermocuple location	x [m]	σ2.54[%], v=5.36m/s	σ2.54[%], v=4.97m/s	σ2.54[%], v=4.25m/s	σ2.54[%], v=3.14m/s	σ2.54[%], v=1.74m/s
1	0.18	0.17	0.17	0.17	0.17	0.17
2	0.635	24.13	1.65	4.31	6.68	0.96
3	1.27	1.36	6.99	15.85	21.27	27.16
4	1.91	9.03	5.49	11.42	3.6	19.87
5	2.54	5.49	3.4	3.38	5.92	0.92
6	3.18	4.12	1.88	0.72	2.07	4.53
7	3.81	3.4	1.26	0.72	0.68	4.49
8	4.44	1.88	0.99	0.72	0.68	1.74
9	5.08	1.26	0.95	0.72	0.68	1.41
10	6.35	0.99	0.9	0.72	0.68	1.07
11	8.9	0.9	0.81	0.72	0.68	0.83
12	13.97	0.81	0.77	0.72	0.68	0.79
13	19.05	0.77	0.72	0.72	0.68	0.76

Table 4. Relative erorr for z=9.52 cm, at different velocities.

Thermocuple location	x [m]	σ9.52[%], v=5.36m/s	σ9.52[%], v=4.76m/s	σ9.52[%], v=4.25m/s	σ9.52[%], v=3.14m/s	σ9.52[%], v=1.74m/s
1	0.18	0.17	0.17	0.17	0.17	0.17
2	0.635	12.87	1.93	8.69	9.05	5.23
3	1.27	0.86	13.02	14.72	8	9.35
4	1.91	10.99	24.18	28.53	25	28.36
5	2.54	0.31	14.41	9.15	11.5	22.96
6	3.18	6.66	8.67	4.93	12.91	21.77
7	3.81	4.58	3.38	4.21	8.34	23.74
8	4.44	2.8	2.36	3.36	5.02	14.79
9	5.08	2.5	2.5	2.5	2.5	8.02
10	6.35	1.48	1.48	1.62	1.48	3.29
11	8.9	1.13	1.13	1.17	1.13	2.93
12	13.97	0.99	0.99	0.99	0.99	2.51
13	19.05	0.81	0.81	0.77	0.81	1.77

3.2. Thermal convection coefficient and thermal resistance

Thermal convection coefficient values determined by simulation with FLUENT are also experimentally confirmed, the relative error between them is 0.54 ─ 10.23%. They depend on the flow rate, the nature of the agent flow (air or water), porosity, pore density and thickness of the heat exchanger.
The convective heat transfer is more intense near the limit surface between the solid aluminum heated board and the porous aluminum heated board, due to thermal contact resistance and low porosity in that area.

It is noticed that at the same porosity, the thermal convection coefficient is higher if the porosity density is higher, the difference between them increases with decreasing speed. Relative error is bigger if porous density decreased (fig. 6).

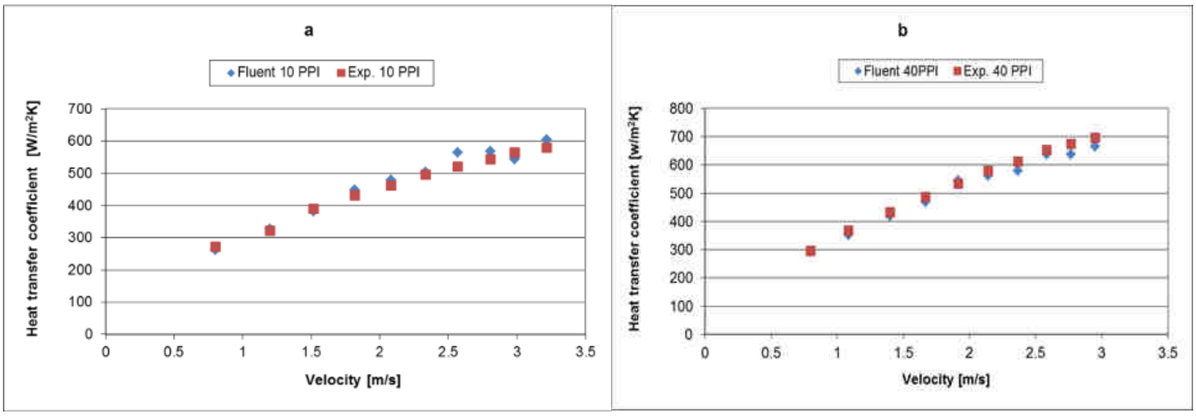

Fig. 6. Comparison between simulation and experimental heat transfer coefficient data at different velocities, for 10 and 40 porous densities and porosities ε=0.927(a) and ε=0.921(b).

At the same time, it can be observed that at the same speed and porous density, the thermal convection coefficient grows with decreasing porosity. Relative error is bigger if porosity increased (fig. 7).

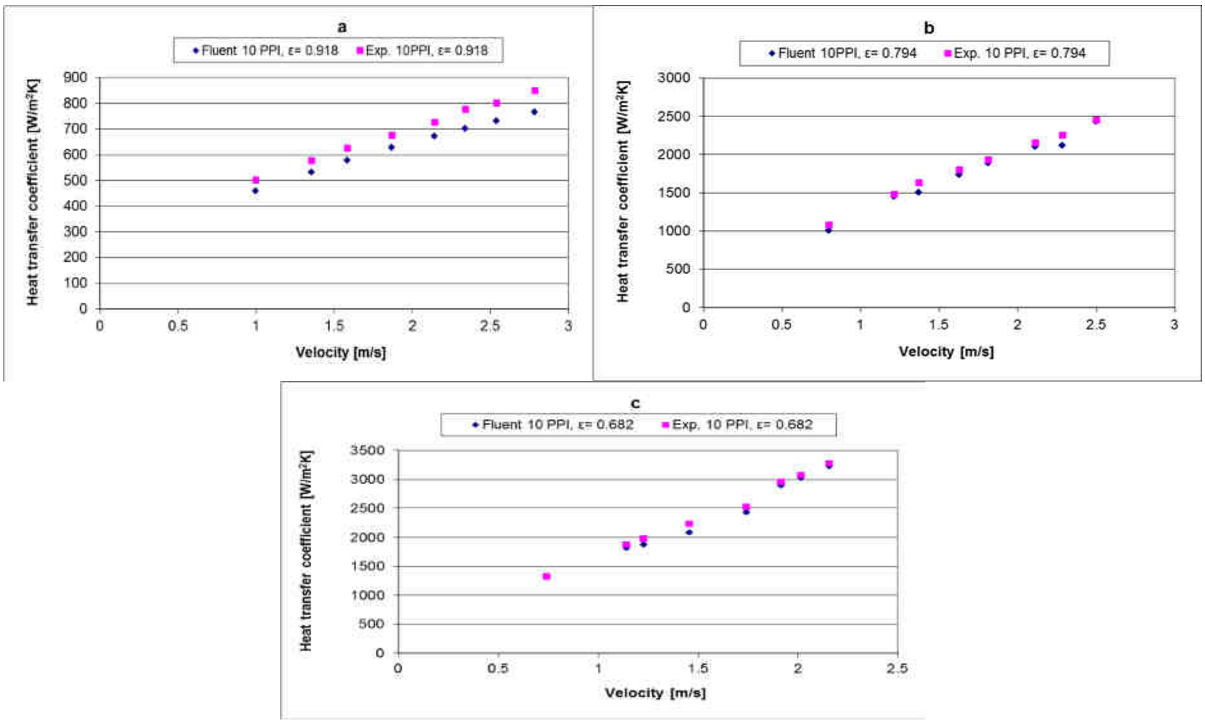

Fig. 7. Comparison between simulation and experimental heat transfer coefficient data at different velocities, for 10 PPI porous density and different porosities ε=0.918(a), ε=0.794(b) and ε=0.682(c).

Thermal resistance values are validated in which the relative error has values between 0.02 – 13.7% in case of thermal resistance, relative error is lower if the porosity has low values (fig. 8).

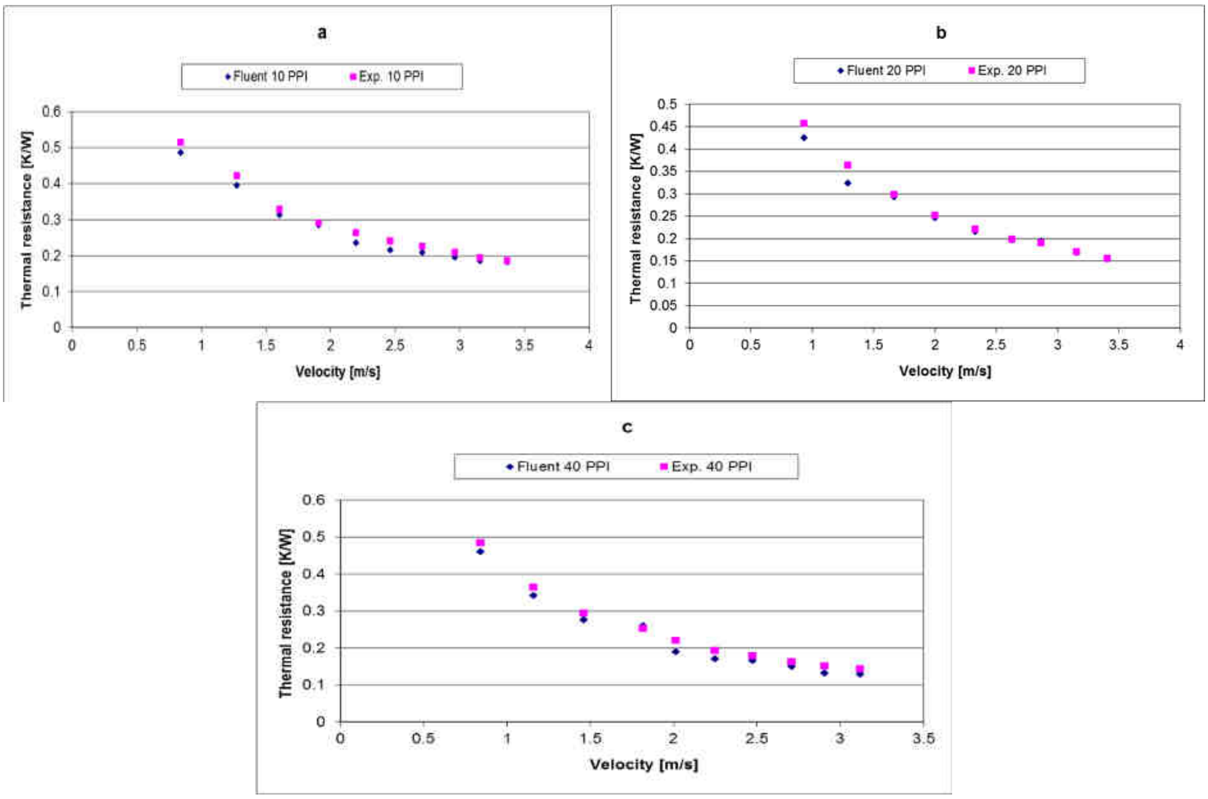

Fig. 8. Comparison between simulation and experimental thermal resistance data at different velocities, for 10(a), 20(b) and 40(c) PPI porous density and porosity ε=0.927.

4. Validation of the results specific to the porous metal flow

Validation of the flow is achieved through comparative research conducted on the distribution of pressure drop. Flow parameters are also validated, so the pressure drop calculated by simulation has a deviation of 1.31 – 8.27%, the relative error grows if the porosity has low values. The pressure drop is also influenced by the porosity, the density of porosity and the fluid velocity and thickness. At the same porous density and porosity the pressure drop is influenced by the flow rate of working agent and thickness. Relative error increased with thickness (fig. 9).

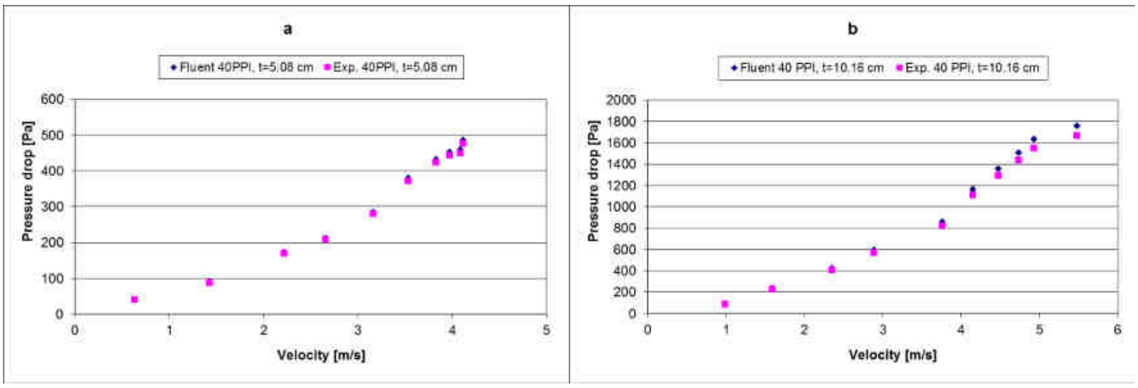

Fig. 9. Comparison between simulation and experimental pressure drop data at different velocities, for 40 PPI porous density ,porosity ε=0.927 and heat eschanger thickness t= 5.08(a) and 10.16(b).

At the same porosity and flow rate, the pressure drop increases with the porous density. Relative error increased with porous density (fig. 10).

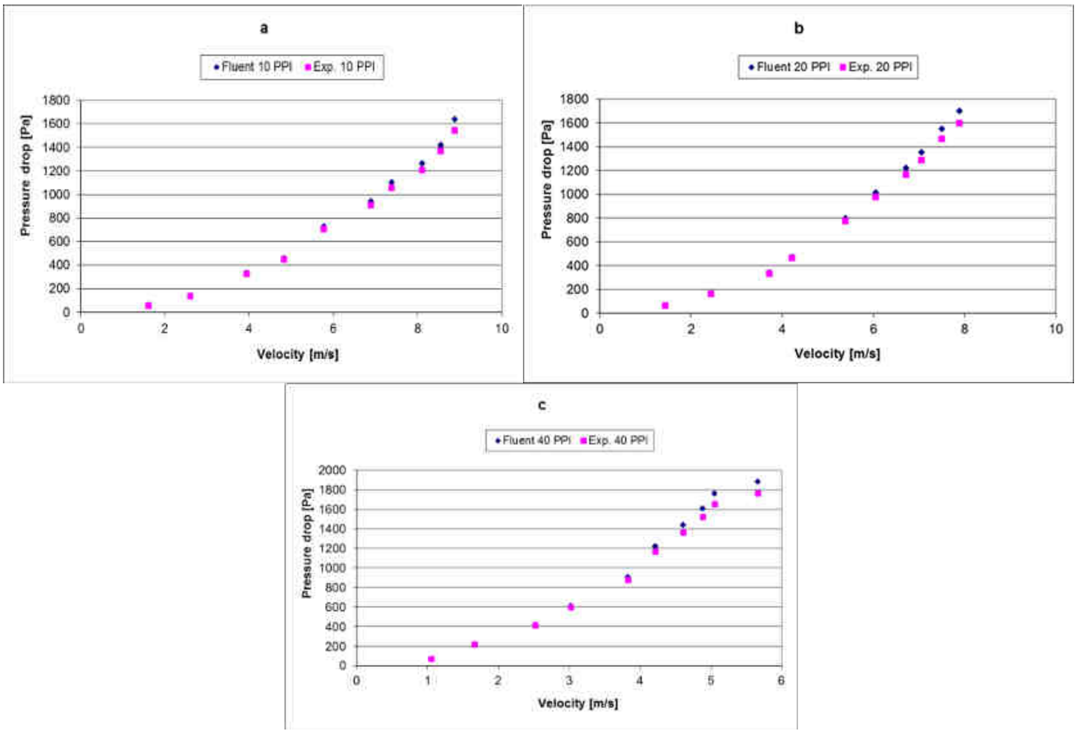

Fig. 10. Comparison between simulation and experimental pressure drop data at different velocities, for 10(a), 20(b) and 40(c) PPI porous density and porosity ε=0.927.

At the same porous density and flow rate, the pressure drop increases with decrease of the porous density. Relative error increased if porosity decreased (fig. 11).

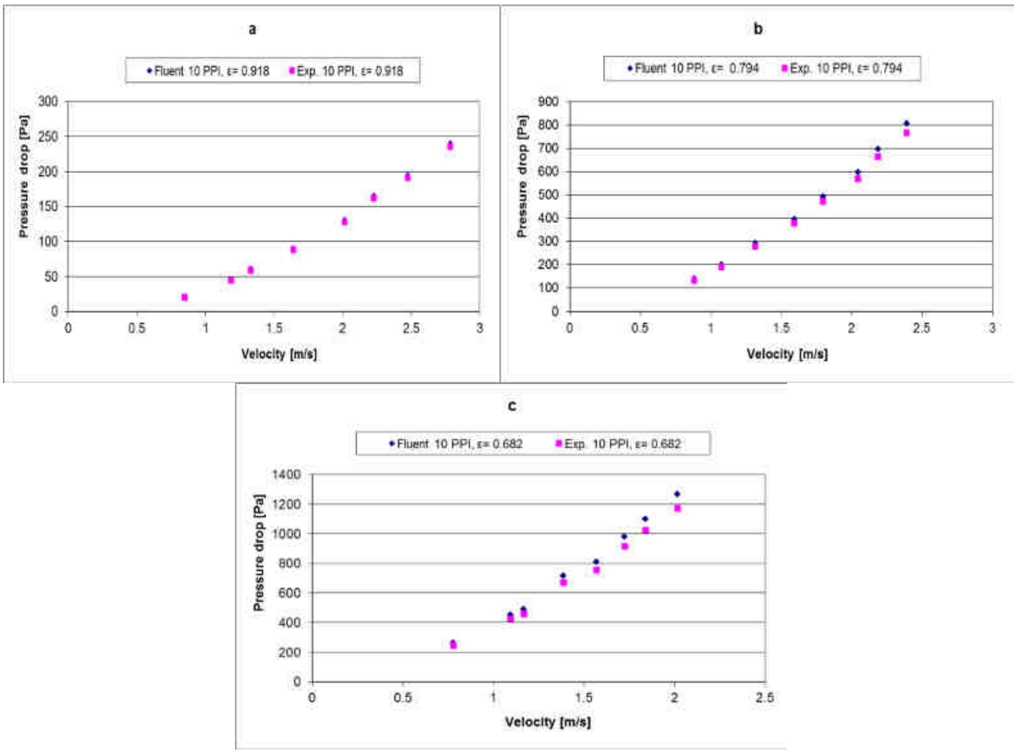

Fig. 11. Comparison between simulation and experimental pressure drop data at different velocities, for 10 PPI porous density and different porosities ε=0.918(a), ε=0.794(b) and ε=0.682(c).

It is important to obtain correct values for viscous and inertial resistance. The viscous resistance is less influenced by speed, but it depends largely on the density of porosity. When the porosity decreases, the permeability decreases and so will increase the viscous resistance, in case of similar porosity, the increment of density of porosity will lead to decrement of permeability and thus to increment of viscous resistance [6,7,8,9].
These observations are important because they show how increasing the density of porosity or decreasing the porosity leads to obstruction of air flow inside the porous metal, reducing permeability. It is also obvious the fact that an increase in density and a decrease in porosity leads to an increase the coefficient of inertia. The friction factor coefficient decreases to a constant value if the flow rate increases. Also, it is observed that its value increases if the porosity density increases or the porosity decreases.

5. Conclusions

This article describes the validation of the results obtained by simulation with FLUENT software. It validated the temperature distribution within the open-cell porous aluminum heat exchanger at different distances from the input section and the variation of the heat transfer coefficient and thermal resistance for different geometrical characteristics. Validation of the flow is achieved through comparative research conducted on the distribution of pressure drop.
Comparing the values obtained by simulation with the experimental ones, relative errors resulted that were less than 5%, for most of the parameters studied, leading to the validation of simulation model developed in FLUENT by the experimental data.

REFERENCES

[1] Nihad, D., Ruben, P., and Alvarez, H., 2006, Heat transfer analysis in metal foams with low-conductivity fluids, ASME J. of Heat Transfer, 128, pp. 784-789.
[2] Duocel Aluminum Foam Data Sheet, 1999, ERG Material and Aerospace, Oakland.
[3] Cruz, E., 2004, Modeling of heat transfer in open cell metal foams, University of Puerto Rico, Mechanical Engineering Departament.
[4] Alvarez, H., 2005, Combined flow and heat transfer characterization of open cell aluminium foams, University of Puerto Rico, Mayaguez Campus.
[5] Opritoiu, P., 2007, Fluid flow and pressure drop simulation in aluminium foam heat exchanger, Acta Tehnica Napocensis, nr.50.
[6] Opritoiu, P., 2013, Rans simulation of combined flow and heat transfer through open-cell aluminum foam heat sink, Magazine of Hydraulics, pneumatics, tribology, ecology, sensorics, mechatronics.
[7] Opritoiu, P., 2013, Modelling turbulence in open cell aluminum foam heat exchanger, Acta Tehnica Napocensis, nr.56.
[8] Lage J.L., 1998, The Fundamental Theory of flow through permeable media from Darcy to turbulence, Transport Phenomena in Porous Media, Elsevier Science, Oxford, pp.1-30.
[9] Antohe, B. V., Lage, J. L., Price, D. C., and Weber, R. M., 1997, Experimental Determination of Permeability and Inertia Coefficients of Mechanically Compressed Aluminium Porous Matrices, ASME J. Fluids Eng., 119, pp. 404-412.

ISSN 1454 - 8003
Proceedings of 2014 International Conference of Hydraulics and Pneumatics - HERVEX
November 5 – 7, Calimanesti-Caciulata, Romania

USE OF KOMAG'S TESTING INFRASTRUCTURE FOR IMPROVEMENT OF HYDRAULIC SYSTEMS' OPERATIONAL SAFETY, RELIABILITY AND ERGONOMICS

Malgorzata MALEC, Ph.D.Eng.[1]

[1] KOMAG Institute of Mining Technology, mmalec@komag.eu

Abstract: *The paper presents KOMAG's facilities for testing hydraulic systems in the aspect of safety, reliability and ergonomics. Special attention is paid to the test results required in certification processes as technical assessments of products are essential parts of conformity declarations. Detailed information about test rigs is given and some modernization activities, co-financed by the European Regional Development Fund, are described. The paper is ended with selected examples of research projects oriented onto an increase of operational safety, reliability and ergonomics in mining machines and equipment.*

1. General information about the KOMAG Institute scope of activity

KOMAG Institute of Mining Technology conducts scientific, research and development projects in the domain of mechanizing mineral winning and preparation processes in the aspect of environmental protection, work safety, ergonomics and reliability. In particular it develops mechanization systems for technological processes in the hard coal mining industry, machines and equipment for winning and processing of minerals, mechatronic systems for control, diagnostics, monitoring and visualization of production processes, technologies for using vertical and horizontal mine workings, drive systems, technologies and equipment for environmental protection as well as expert opinions [1].

In important part of the Institute's activity includes laboratory and in-situ tests of machines and equipment as regards their functionality, reliability, ergonomics, safety and environmental protection. The research and testing infrastructure enables to conduct interdisciplinary, versatile tests in five laboratories such as:

- ✓ Laboratory of Tests,
- ✓ Laboratory of Applied Tests,
- ✓ Laboratory of Material Engineering and Environment,
- ✓ Laboratory of Modelling Methods and Ergonomics,
- ✓ Laboratory of Virtual Prototyping Methods.

The Laboratory of Tests and the Laboratory of Applied Tests are oriented onto testing hydraulic and pneumatic systems.

2. Laboratory of Tests

The Laboratory of Tests is accredited by the Polish Accreditation Centre in the scope of testing powered roof support units and hydraulic executive components. It guarantees independent, unbiased and reliable performance of tests according to the Quality Management Systems meeting the requirements of the PN-EN ISO 9001:2009 and PN-EN ISO/IEC 17025:2005 Standards. So far more than 340 types of powered roof support units and about 1300 types of legs and hydraulic cylinders have been tested against orders of domestic and foreign equipment producers as well as their users. Apart from testing components of powered roof supports, playing a crucial role as regards operational safety of longwall systems, many research and development projects have been oriented onto hydraulic pipelines, friction legs, clevises, steel sprags, mesh linings and crib support.

The test rigs enable to take measurements of pressure of relative elongation with strain gauges, of displacements with inductive transducers, of force and speed, but also of quick-changing parameters and flows. The tests give a possibility of a thorough assessment of the component under testing which contributes to a safe operation of the equipment. The test results are indispensable for certification processes, because a technical assessment of the product is a part of the conformity declaration procedure. All the tests are performed by a team of experienced researchers in the laboratory conditions at the KOMAG Institute, at producers' of machines and equipment and at their users'. The measurements are taken in a parallel, multi-channel mode with high-class measurement apparati. The Laboratory of Tests closely collaborates with the Certification Unit and it is a testing back-up facility for researchers, designers, producers and users of machines and equipment.

2.1. Testing functionality of powered roof support unit

The rig for testing the functionality of powered roof support unit is shown in Fig 1. It enables to apply loading forces up to 10 MN, at inclination angles up to 90^0. The maximal distance between the floor and the artificial roof is 4 meters. The roof surface is 5x7.2 meters which makes tests of kinematic parameters of three powered roof support units of pitch 1.5 meters possible.

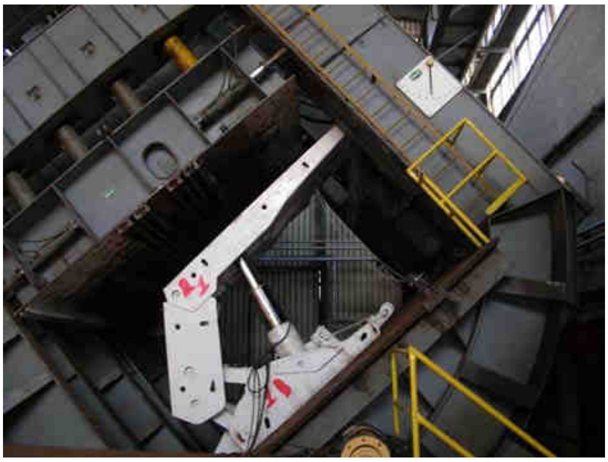

Fig.1. Rig for testing the functionality of powered roof support unit

2.2. Strength testing of powered roof support unit

The rig, shown in Fig.2, enables to apply loading forces up to 16 MN in the vertical plane and up to 4.5 MN in the horizontal plane. The maximal distance of the artificial roof from the floor is 4.8 meters. The load can be applied actively by a movement of the rig roof and passively by feeding the power hydraulic system with high pressure liquid.

Fig.2. Rig for strength testing of powered roof support unit

2.3. Testing legs and components of high pressure hydraulics

Flexibility characteristics of legs, hydraulic cylinders and a determination of their static and fatigue strength at pulsatory pressure are performed at the rig shown in Fig.3. It also enables to induce dynamic loads with a generator where explosives are used. This method of generating dynamic loads allows obtaining high speeds of load increase. It is important that the tests have no dynamic impact on the environment. The maximal load which can be obtained is 8 MN. The length of hydraulic cylinders, which can be subject to testing, should not exceed 4.8 meters.

Fig.3. Rig for dynamic testing legs and components of high pressure hydraulics

2.4. Strength testing of machinery components

Static and pulsatory tests of hydraulic components are carried out at the rig, shown in Fig.4. Legs, supports and auxiliary cylinders, subject to tensioning, compressive, bending and complex loads, are tested. The rig is equipped with two testing levels and the distance between them is 1.6 metres. The maximal static load, which can be applied to the object under testing, is 12 MN, and the maximal distance between cross-beams is 7 meters.

Fig.4. Rig for strength testing of machinery components

2.5. Testing valves

The rig shown in Fig.5, is used for testing control and protective components of hydraulic cylinders of smaller overall dimensions. Static, dynamic and pulsatory tests can be conducted here. Dynamic load of release (overflow) valves is applied by a free fall of weight on a standard hydraulic cylinder, to which a valve under testing is connected. The maximal rig load is 0.8 MN.

Fig.5. Rig for testing valves

3. Modernization of existing and a construction of new test rigs at the Laboratory of Tests

Taking advantage of the European Structural Funds, some modernization activities, aiming at up-grading the test rigs, were conducted. The scope of the modernization included as follows [2]:

- ✓ an implementation of an automatic control system for endurance tests and for monitoring the operational condition of the rig for strength testing of powered roof support units,

- ✓ an installation of highly efficient hydraulic cooling system operating in the supply – drift system of the test rigs,
- ✓ an exchange of hoses in the supply pipeline for steel mains and a replacement of plug connections with screwed connections in the systems of liquid distribution and control,
- ✓ a modernization of hydraulic and control systems of the rigs for testing powered roof support units and components of machines and equipment.

The modernization activities enabled to improve quality and reduce costs of tests which contributed to strengthening the position of the KOMAG Laboratory of Tests in the European Research Area. At present the state-of-the-art control system of test rigs allows for full monitoring of rig operation and for recording all the test cycles in the text files. The modernization resulted in a possibility of increasing the number of performed tests and it increased the test rig reliability. The gained experience was used for a further development of the control system and for a full visualization of tests conducted at other test rigs.

The next stage of the test rig modernization tasks was realized within the Regional Operational Programme of the Silesia Voivodship for 2007-2013, co-financed by the European Fund for Regional Development. The project was entitled “Extension of Laboratories of the KOMAG Institute of Mining Technology in Gliwice to carry out the tests aiming at increasing a safe use of products”. The costs of technical documentation, indispensable for the project application, were covered by KOMAG. The documentation included the following tasks:

- ✓ a modernization of the hydraulic system of the rig for testing functionality and kinematics of powered roof support units,
- ✓ a modernization of the control system of the rig for testing functionality and kinematics of powered roof support units,
- ✓ a modernization of the rig for testing hydraulic props,
- ✓ a modernization of the rig for testing steel sprags.

One of the essential project objectives aimed at an implementation of an information platform for e-Laboratory incorporating three KOMAG accredited laboratories: the Laboratory of Tests, the Laboratory of Applied Tests and the Laboratory of Material Engineering and Environment.

The modernization of the rig for testing functionality and kinematics of powered roof support units was oriented onto mechanical components of the rig roof, enabling to change a support system of the unit subject to testing. The components of the rig hydraulic system were exchanged and the hydraulic cylinders of the rig rotation, roof advance and interlocking mechanisms were up-graded. The plug connections of STECKO type were eliminated and they were replaced by screwed connections. Due to such changes reasons of down-time due to failures of connecting elements, caused by a pressure surge of the medium in the hydraulic system, were eliminated.

3.1. Testing legs and sprags

The rig, shown in Fig. 6, enables to perform tests of hydraulic legs according to the harmonized standard PN-EN 1804-2+A1:2012. Its technical specification is as follows:

- ✓ maximal static compressive force – 3.3 MN,
- ✓ maximal static tensile force – 2.5 MN,

- ✓ maximal compressive force at changing load – 1.8 MN,
- ✓ maximal tensile force at changing load – 1.4 MN,
- ✓ maximal length of the leg – 1.7 metres.

The rig, shown in Fig. 7, is used for testing sprags made of sections: V25, V29, V32 and V36 for conformity with the requirements of the standard PN-G-15000-7. Its technical specification is given below:

- ✓ static compressive and tensile force – max 0.15 MN,
- ✓ maximal sprag length – 2.0 metres.

The rig is equipped with two dynamometers of extensometer type. Their measurement scope reaches 200 kN and 6000 kN for measuring applied load. A high pressure pump of WAP HDP 22 type, of pressure 62 MPa was installed for supplying both test rigs.

Fig. 6. Test rig for legs

Fig.7. Test rig for sprags

ISSN 1454 - 8003
Proceedings of 2014 International Conference of Hydraulics and Pneumatics - HERVEX
November 5 – 7, Calimanesti-Caciulata, Romania

3.2. Modernization of control systems for test rigs

Control desks, shown in Fig. 8 and 9, are used for monitoring and visualization of testing processes conducted at the rigs.

Fig.8. Control desk – rig for testing functionality and kinematics of powered roof support unit

Fig.9. Control desk – rig for testing legs

KOMAG specialists elaborated the software of controllers for collecting data from the test rigs and enabling automatic testing of machinery and its components. An introduction of each rig control system to the integrated control system makes keeping of test documentation archives possible and it also facilitates a supervision of a synchronous control of several tests.

3.3. Technical infrastructure of e-Laboratory information platform

The following tasks were performed to create e-Laboratory in the Laboratory of Tests:

- ✓ an elaboration of software to store, analyze and visualize measurement data,
- ✓ a development of software to introduce and keep archives of laboratory documents as well as to send them to the clients,

- ✓ a preparation of an electronic supervision system of measurement and testing equipment in the KOMAG laboratories.

The modules of the information platform in e-Laboratory are shown in Fig. 10.

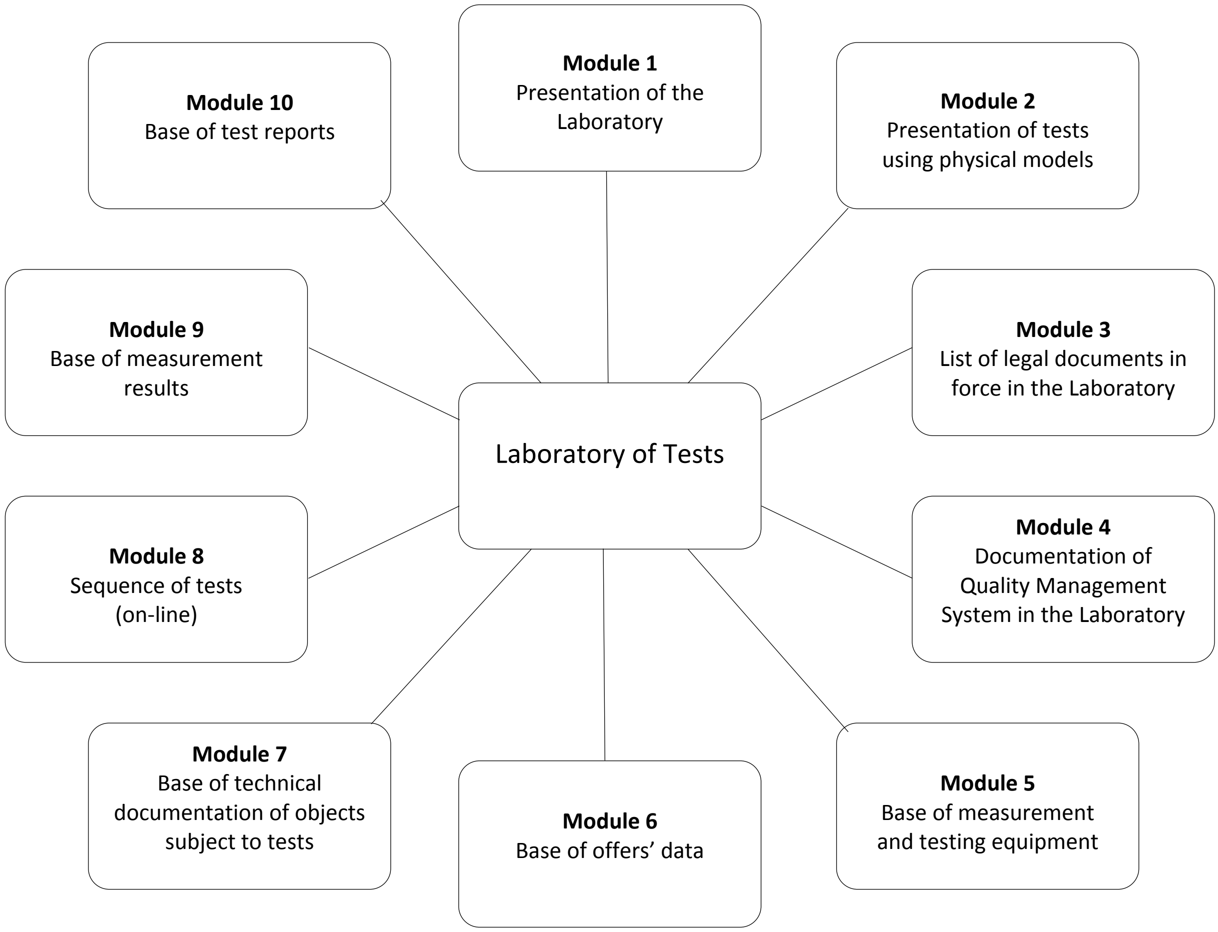

Fig. 10 Modules of e-Laboratory information platform

The developed technical infrastructure of e-laboratory information platform enables full recording, keeping archives and a dissemination of test results among internal and external clients. The system gives a possibility of digitalizing the most important areas of activity and it also meets the requirements of the Standards: PN-EN ISO/IEC 17025 and PN-EN/ISO 9001 as well as it is in accordance with the Good Practice Laboratory principles.

4. Selected examples of research projects oriented onto safety of products

Irrespective of the accredited tests conducted for a certification of products, the Laboratory of Tests performs tests of powered roof support units planned for repair. The obtained test results enable to determine the scope of indispensable repair. One of research projects entitled: "Simulation of dynamic loads in hydraulic legs during bumps", was oriented onto an analysis of pressure increase in legs. The project results confirmed a possibility and usefulness of leg testing with dynamic force generated with explosives. A method of dynamic tests, including all the disadvantageous phenomena experienced by a leg in the result of the rock burst, bumps both natural as well as resulting from the mineral winning activity, was developed. Basing on the conducted tests, elastic strain energy absorbed by a leg was determined. An analysis of damage in the powered roof support unit due to dynamic rock impact showed that hydraulic cylinders are the components which fail most often.

The research work was continued and it was oriented onto making the hydraulic cylinders more susceptible to dynamic loads.

5. Recapitulation and conclusions

- ✓ The KOMAG Institute takes an active part in shaping work safety in consecutive phases of machinery life cycle. At the designing stage a risk assessment of machinery operation in a virtual work environment is conducted. Then laboratory tests are performed.
- ✓ In the result of research projects and tests, realized at the KOMAG Laboratory of Tests, many weak points in the machinery hydraulic systems were detected. Apart from powered roof support units, the Laboratory tested pipelines, friction legs, devises and sprags. The orders were placed by domestic producers of machinery and equipment as well as by foreign clients form Belarus, Great Britain, Iran, Spain, Russia and the USA.
- ✓ New test rigs and a modernization of the existing ones and of their control systems as well as a creation of the e-Laboratory information system results from an intention of meeting the clients' needs and expectations.
- ✓ Up-graded test rigs are and will be used for conducting research projects according to the requirements of machinery producers and users.
- ✓ Activities of the KOMAG Institute, oriented onto a development of its testing infrastructure, support a realization of research and development projects. The test results enable to improve machinery safety, reliability and ergonomics. The research and testing potential is used for an increase of competitiveness of the Polish economy based on knowledge and innovations.

REFERENCES

[1] Kłeczek Z., Kozieł A., Malec M.,: Maszyny Górnicze 3-4/2010, p. 5-16.
[2] Madejczyk W., Maszyny Górnicze 3-4/2010, p. 17-23.
[3] Madejczyk W., Maszyny Górnicze 1/2014, p. 3-7.

CLOUD COMPUTING FOR HYDROPNEUMATIC DRIVES

Ioana ILIE[1], Marian BLEJAN[1], Alexandru VASILE[2]

[1] INOE 2000 – IHP, Bucharest

[2]University POLITEHNICA of Bucharest

Abstract: *Cloud computing is a modern concept in computer science, representing a distributed set of computing services, applications, access to information and data storage, without the user needing to know the physical location and configuration of the systems that provide these services. The paper refers to "Development of technologies for hydropneumatic drives using the cloud infrastructure in order to monitor their behavior when in use at the beneficiaries". Hydropneumatic equipment manufacturers, the beneficiaries of the technology proposed will use Software as a Service (SaaS), a term used for software applications that run on a "private cloud" type infrastructure.*

Keywords: *cloud computing, hydropneumatic equipment, monitoring, software*

1. Introduction

Worldwide there are studies regarding the implementation of monitoring systems for the equipment that are in use. Among these, we can mention Rolls-Royce Company that monitors jet engines used in aviation in compliance with the Measure-Acquire-Transfer-Analyze-Act principle in order to maximize their reliability and availability. Rolls Royce monitoring systems use proprietary infrastructures for data transfer, data storage and data processing [1].

The term „cloud computing" derives from a symbolic graphical representation of the Internet in the shape of a cloud ("the cloud") [2], used when the technical details of the Internet can be ignored, as shown in the fig.1. The concept and the English term were first used in practice around 2006-2007.

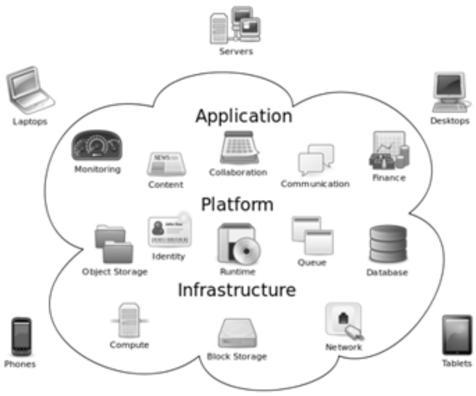

Fig. 1 Cloud computing structure

The Cloud computing essential features are on-demand services, access through the network, resource pooling, elasticity, control and optimization of resources.

Permanent user connection to the Internet has become widespread, so that now almost all available resources can be placed on the Internet and shared, sometimes between completely independent users: the programs and data are moved from the Internet to the user computer on demand, as if they are common public services such as water or electricity.

Running of computer applications online (on the Internet) and not on the workstation represents a new change of paradigm, following the one that was in the 1980s when a shift from mainframes to the client-server concept took place. If the interface made available by the cloud computing provider is of good quality, then the user is freed from the task of being an expert in the technology and infrastructure used. For example, he does not need to update the software because the software is updated centrally at the provider.

Cloud computing uses new methods of providing Internet services which can usually be sized dynamically and include virtualized resources. It is actually just a secondary possibility due to the ease with which you can now access all servers and data centers interconnected through the Internet.

Typical cloud computing providers make available, for example, standard commercial applications; the user has access to them only through a local browser because both the application and the user's own data are hosted in the cloud on the provider's server. In these circumstances, confidentiality and data access rights play a key role in the context of pervasive Internet. Often cloud providers offer additional services in a single location (page or web site) by enhancing all their offers for all their customers. The largest suppliers in this field are Microsoft, Salesforce, Skytap, HP, IBM, Amazon and Google.

Using the cloud computing structure[3], the end user is provided with the following advantages:
- on-demand self-service - the user can assign himself the computing resources (time on server and storage space in the network), the service provider intervention is not needed;
- broad network access - the capabilities offered to the user can be accessed through the network using a standard mechanism which allows the use of a variety of client terminals (phones, tablets, laptops, workstations);
- resource pooling – the computing resources offered to the user are designed to serve multiple users by dynamic allocation in correlation with the demand. The user has optimal access to resources regardless of the location from which he accesses the system.
- rapid elasticity - resources can be assigned and released quickly depending on user requirements which give the impression of unlimited resources in time and size.
- measured service - cloud systems automatically control and optimize computing resources according to the user's level, in the sense that access to resources increases accordingly with the amount the user pays to the service provider.

Models of services possible through cloud structures (fig.2) [3]:
• **Software as a Service (SaaS)** - applications and related data are stored in a data center and are provided to users on demand via the Internet (with a specialized browser). This service provides a high standard of working. It is used for collaborative applications, mobile etc., not so much for real-time applications.
• **Infrastructure as a Service (IaaS)** - a set of hardware components (servers, storage devices, networks, etc.) together with certain software components (operating systems, virtualization, clustering, etc.) are offered to users. This model provides an intermediate stage that is used for essential demands, but it is not used when multiple standards are required.
• **Platform as a Service (PaaS)** – the environments for the development and implementation of informational applications are provided to the developers.

Implementation models [4],[5]:
• **Private services - Private Cloud** – The infrastructure is available only within an organization that includes several consumers. One possible case is a retail store chain. Infrastructure may be owned, configured and used by the organization or by third parties, or combinations of these two alternatives.
• **Community Services - Community cloud** – The infrastructure is used by different entities that share some purposes. One possible example is represented by the emergency services - police, fire department, ambulance.
• **Public Services - Public cloud** – The infrastructure is open for use by the general public for academic or governmental purposes. A third party is required to physically provide the cloud infrastructure.
• **Joint Services - Hybrid cloud** – The infrastructure is a combination of private, community, and public services that retain their consistency, but are united by a technology that ensures the portability of information and of the used software applications.

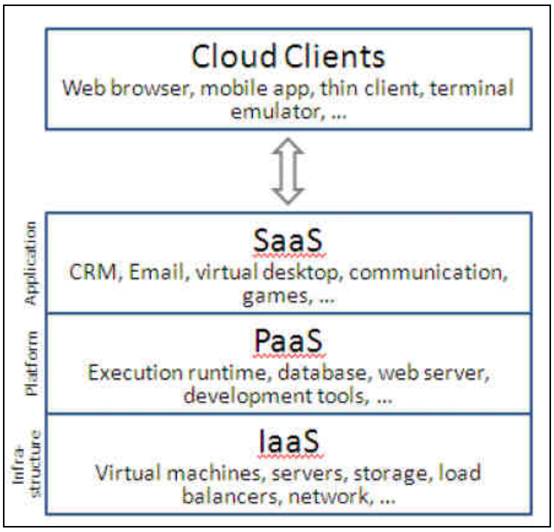

Fig. 2. Cloud structures models of services

2. Cloud computing for monitoring hydropneumatic drives

Taking into account the existing concerns presented, the project aims to develop technologies for monitoring hydropneumatic drives using the cloud computing infrastructure.
This approach offers an affordable solution for online monitoring of hydropneumatic drives that eliminates jams like:
- Slow development of equipment because those who produce them do not have enough information about their behavior in operation;
- Higher maintenance costs covered by the producer in warranty and by the user in post-warranty.

The monitoring technologies using cloud infrastructure allow online monitoring of the equipment during operation providing information that can be used to upgrade products. This information may be used by the manufacturer in the warranty period and by the beneficiary.
The technologies achieve only online monitoring, and not real time monitoring, but open the path to real time monitoring and control of equipment, solution that currently cannot be implemented because of the various cloud infrastructure limitations, mainly network latency.
These types of monitoring technologies for hydropneumatic drives that use cloud computing structures imply the online tracking of hydropneumatic drives during operation. This fact involves the synergy between the cloud computing infrastructure and the hydropneumatic drives – an original approach form the information technology point of view as well as from the hydraulic drive point of view.

The monitoring technology using cloud structures will allow continuous surveillance of the hydropneumatic drive, the requirement for on-line monitoring being Internet access. The technology will be offered to hydropneumatic equipment manufacturers/producers to be used for predictive maintenance of equipment bringing them the opportunity to improve the design and execution after analyzing operation data. Another advantage of using the proposed technologies is related to a reduction of warranty and post warranty.
The monitoring technology could be used by the end user of hydropneumatic drives giving them the opportunity to integrate the equipment in their own manufacture tracking system or energy management.
The monitoring technologies involve establishing the monitoring requirements in order to track the behavior of hydropneumatic drives for predictive maintenance applications, design and execution improving, warranty and post-warranty cost reduction, integration in production tracking systems and in energetic tracking systems. After establishing the monitoring requirements, the hydraulic drive will be equipped with the sensors and the electronic systems needed to obtain the operating parameters using the monitoring module [6].

The connection between the monitoring module and the cloud infrastructure will be done through a data network and a router (fig. 3).

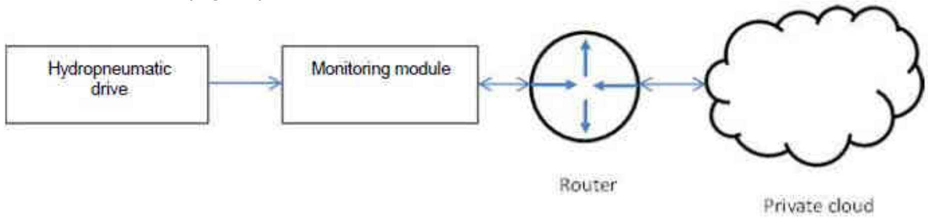

Fig.3. Block schematics of hydropneumatic monitoring solution

The cloud computing infrastructure for the hydropneumatic drive monitoring implements network features - covers the geographical area where the monitored systems are located - data storage and management functions, data processing and data presentation applications following various criteria and services.

3. Conclusions

Possible applications have three categories of beneficiaries:
- *Hydropneumatic drives users* by giving them the ability to integrate equipment in information systems;
- *Hydropneumatic drives producers* through feedback given by the data obtained by monitoring the behavior of the machine in operation and predictive maintenance;
- *Cloud-service providers* by enlarging the market with new Software as a Service (SaaS) clients in the field of hydropneumatic drive monitoring.

The benefits of introducing new measurement and control technologies are given mainly by the advantages of using computer based means in the production process with direct benefits on production quality, energy saving, automated and centralized control of the production process at a company level.

Production equipment with hydraulic drives using new informational technologies for monitoring will have superior operating performance, ability to communicate through the cloud computing infrastructure making possible their integration in informational production administration and control systems. All these perspectives offered by the new technologies developed in the frame of the project will enable a more precise and swift operation of equipment used in production. Products resulted from the use of this equipment will be of higher quality as a result of the higher precision of the hydropneumatic drives; work productivity will also improve as a result of the higher dynamic of the hydraulic drives.

REFERENCES

[1] A. Drumea, “Control of Industrial Systems Using Android–Based Devices”, Proceedings of the 36th International Spring Seminar on Electronics Technology, Alba Iulia, Romania, 8–12 May 2013; pp.405–408.
[2] http://www.rolls-royce.com/about/technology/systems_tech/monitoring_systems.jsp
[3] https://en.wikipedia.org/wiki/Cloud_computing
[4] Peter Mell and Timothy Grance, “The NIST Definition of Cloud Computing”, National Institute of Standards and Technology, U.S. Department of Commerce, September 2011, http://csrc.nist.gov/publications/nistpubs/800-145/SP800-145.pdf.
[5] Somasundaram Gnanasundaram and Alok Shrivastava, “Information Storage and Management: Storing, Managing, and Protecting Digital Information in Classic, Virtualized, and Cloud Environments”, 2nd Edition, John Wiley & Sons, May 2012, ISBN978-1-118-09483-9
[6] A. Drumea , A. Vasile , M. Comes and M. Blejan "System-on-chip signal conditioner for LVDT sensors", Proceedings of 1st IEEE Electronics System-Integration Technology Conference ESTC06, Dresden, Germany, vol. 1, pp.629 -634

ISSN 1454 - 8003
Proceedings of 2014 International Conference of Hydraulics and Pneumatics - HERVEX
November 5 – 7, Calimanesti-Caciulata, Romania

DYNAMIC PROCESSES IN AN ELECTRO-HYDRAULIC SYSTEM WITH A SERVO VALVE AND SPACE VECTOR CONTROL OF THE PUMP ELECTRIC DRIVE

Borislav GEORGIEV[1], Hristo HRISTOV[2], Ivan IVANOV[3]

[1] Technical University of Gabrovo, gborislav@gbg.bg

[2] hristo@tugab.bg

[3] ivanov201549@abv.bg

Abstract: *The present paper views a mathematical model of the dynamic processes in an electro-hydraulic system for automatic control of the speed of a hydraulic motor with vector control (SVM) of the hydraulic pump induction motor and servo valve control. The transient responses in the system are simulated with MatLab, SimHydraulic. The transients obtained from the simulation are shown in a few graphs.*

Keywords: *electro-hydraulic system; automatic control; servo valve control, space vector control.*

1. Introduction

The design of modern machines such as metal cutting machines, blow molding, injection molding machines etc., requires the use of efficient hydraulic drive systems. The throttle control, which is most often achieved through proportional and servo valves, is characterized by large energy losses and therefore should be limited. On the other hand, fast response and good regulation are the advantages of such hydraulic systems. The combined control leads to improved energy efficiency and performance boost and at the same time provides fast response and good control.

As a control strategy [4, 5, 6] used in variable frequency drives, vector control provides a feasible solution to torque/speed control of AC machines by controlling the phase currents into the machine even if it gives rise to a considerable computation burden for the processor where the control algorithms are implemented. The most noticeable merit of vector control is to get rid of machine speed dependency on power grid frequency and make it possible to reach the desired machine speed within safety and power limits.

This paper is based on a mathematical model developed to simulate dynamic processes in the electro-hydraulic system with vector control of the motor and adjustment of the hydraulic motor by means of a servo valve. This allows us to use cheaper fixed-displacement hydraulic pumps rather than the more expensive adjustable ones as the performance is maintained and the energy efficiency is improved.

2. Math model

Fig. 1 shows an electro-hydraulic system for automatically controlling the speed of the shaft of the induction motor by means of vector control (SVM) and feedback from the tachometer generator to the proportional valve. The system consists of: 1 – fixed displacement pump, 2 – servo valve, 3 – hydraulic motor, 4 – tachometer generator, 5 – block setup, 6 – inverter, 7 - induction motor, 8 – setting device.

ISSN 1454 - 8003
Proceedings of 2014 International Conference of Hydraulics and Pneumatics - HERVEX
November 5 – 7, Calimanesti-Caciulata, Romania

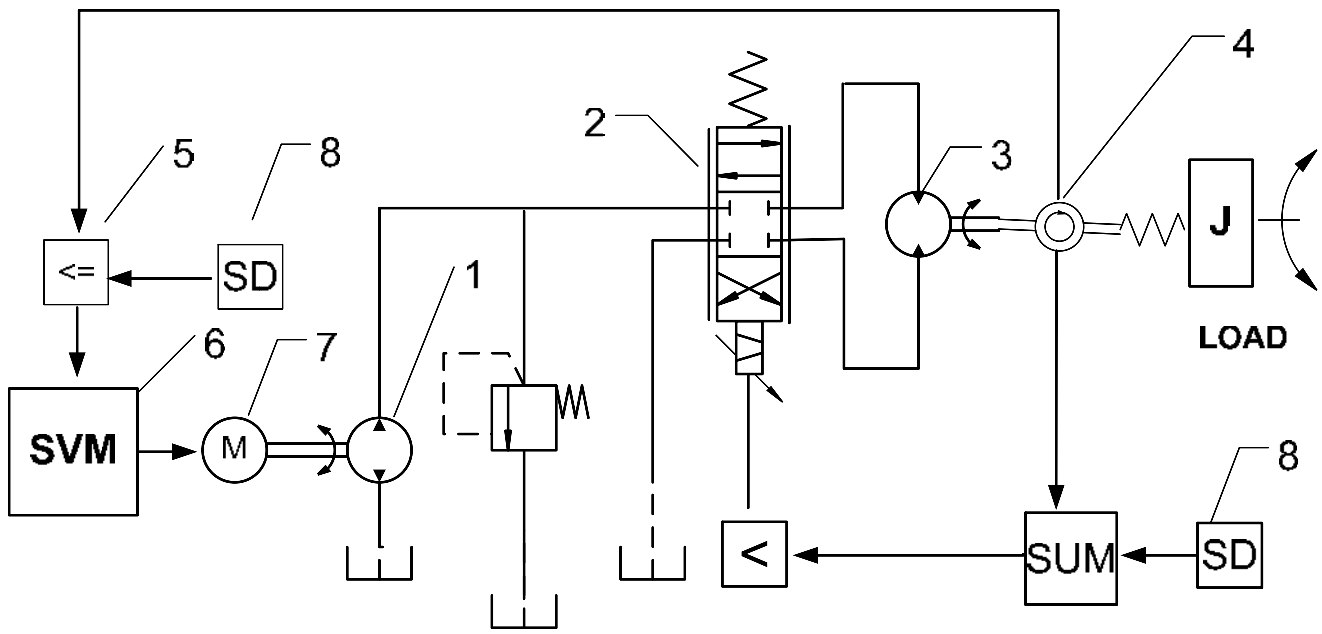

Fig. 1. Electro-hydraulic drive system.

The speed of the induction motor is adjusted by the inverter. The signal from the tachometer coupled to the shaft of the hydraulic motor is used for comparison with the set value in the block setup (See Figure 1.). The servo valve, which uses feedback from the tachometer generator forms a suitable control signal. The dynamics of the electro-hydraulic closed loop control system is described by the following equations:

2.1. Equation of the induction motor

The induction motor consists of a stator and a rotor. The stator is fixed, while the rotor rotates inside with a small air gap between them. The magnitudes of the flux linkages (Ψ_A, Ψ_B and Ψ_C) could be expressed as :

$$\Psi_{(t)} = \int \left(u_s(t) - R.i_s(t)\right)dt, \tag{1}$$

where: $u_s(t)$ is the voltage applied to each winding, R is the resistance of each winding and $i_s(t)$ is the current through each winding. If a three-phase voltage is applied onto the stator windings, the equation is as follows:

$$u_{sa}(t) = U_{pk}\sin(360f\,t + 90^0)$$

$$u_{sb}(t) = U_{pk}\sin(360f\,t + 210^0)$$

$$u_{sc}(t) = U_{pk}\sin(360f\,t + 330^0), \tag{2}$$

where U_{pk} and f are respectively the peak value and the frequency of the applied voltage. This will result in a sinusoidal flux linkage in each phase that lags the phase voltage by 90^0. If the winding resistance is ignored, then:

$$\begin{aligned}\Psi_A(t) &= \Psi_{pk}\sin(360ft)\\ \Psi_B(t) &= \Psi_{pk}\sin(360ft+120^0)\\ \Psi_C(t) &= \Psi_{pk}\sin(360ft+240^0).\end{aligned} \tag{3}$$

The magnitude of this rotating resultant flux is 1.5 times higher then the peak value of each wingding flux linkage. The rotating speed N_s of the resultant flux is referred to as a synchronous speed, calculated as follows:

$$N_s = 60\frac{f}{N_p},\ [rpm] \tag{4}$$

where f - three phase voltage frequency and N_p - number of pole pairs.

2.2. Vector control equations

The control of the stator current is achieved by controlling the stator voltage. We could say that the vector control is conceptually the same as the control of DC machines. Two important transformations [7], known as transformations of Clarke and Park, are included in the vector control system to transform the AC machine into a separately magnetized DC machine (see fig. 2.(a), (b)).

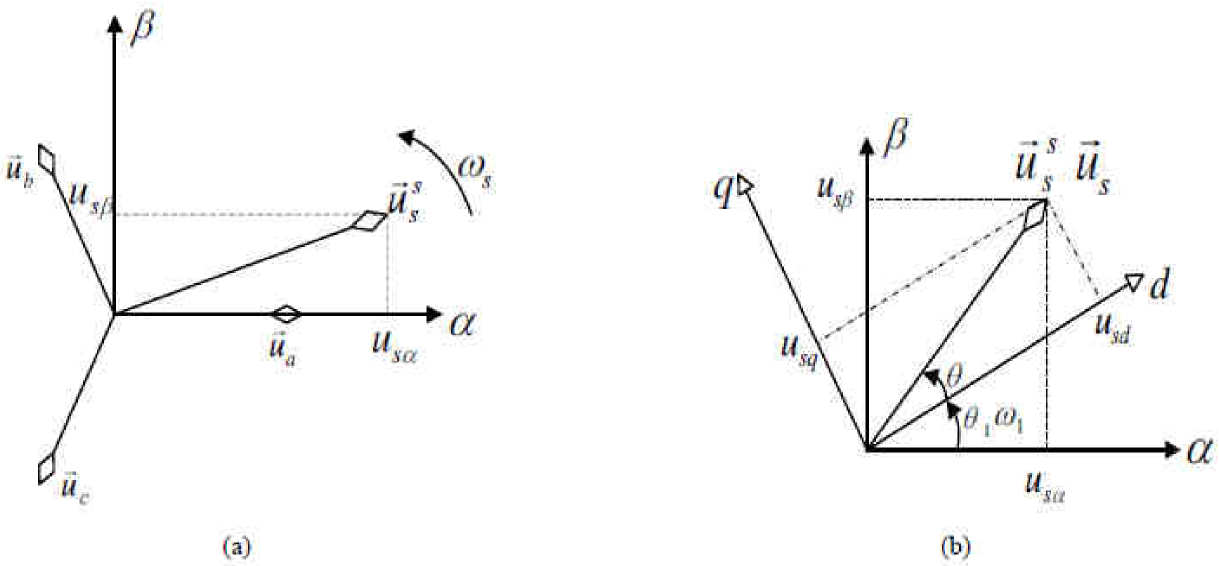

Fig. 2. Clarke and Park transformations

In the theory of vector control the process of three-phase to two-phase coordinate transformation and vice versa is called transformation and inverse transformation of Clarke and can be expressed in the form of a matrix:

$$\begin{bmatrix} u_{s\alpha} \\ u_{s\beta} \end{bmatrix} = \begin{bmatrix} \frac{2}{3} & -\frac{1}{3} & -\frac{1}{3} \\ 0 & \frac{1}{\sqrt{3}} & -\frac{1}{\sqrt{3}} \end{bmatrix} \cdot \begin{bmatrix} u_{sa} \\ u_{sb} \\ u_{sc} \end{bmatrix} \tag{5}$$

$$\begin{bmatrix} u_{sa} \\ u_{sb} \\ u_{sc} \end{bmatrix} = \begin{bmatrix} 1 & 0 \\ -\frac{1}{2} & \frac{\sqrt{3}}{2} \\ -\frac{1}{2} & -\frac{\sqrt{3}}{2} \end{bmatrix} \cdot \begin{bmatrix} u_{s\alpha} \\ u_{s\beta} \end{bmatrix} \tag{6}$$

The Clarke transformation can also be applied to other three-phase quantities, such as flux, rotor currents and so on, in order to obtain the corresponding space vectors. However the α-components and the β-components of these rotating vectors are still AC sinusoidal quantities. A new coordinate system is defined, called the dq coordinate system, which has the same origin as the $\alpha\beta$-coordinate system but it rotates with the same speed as the flux. The d-axis of the dq coordinate system coincides with the space vector of the flux. The transformation of the space vector between the two coordinates can be achieved by multiplying the vector by $e^{j\theta_1}$ or $e^{-j\theta_1}$, where θ_1 is the angle between the two coordinate system. If we take the stator voltage as an example, (fig. 2.b) the space vector of the stator voltage is referred to as $\vec{u}_s^s$ in the $\alpha\beta$ - coordinate system and as $\vec{u}_s$ in the dq - coordinate system. Figure 2(b) shows that $\vec{u}_s^s$ and $\vec{u}_s$ are transformed as:

$$\vec{u}_s^s = \left|\vec{u}_s^s\right| e^{j(\theta+\theta_1)} = \left|\vec{u}_s^s\right| e^{j\theta} e^{j\theta_1} = \vec{u}_s\, e^{j\theta_1}$$

$$\vec{u}_s = \vec{u}_s^s\, e^{-j\theta_1} \tag{7}$$

The transformation from the $\alpha\beta$ - coordinate system to the dq - coordinate system is called Park transformation while its inverse process is known as Inverse Park transformation.

If $\vec{u}_s^s$ and $\vec{u}_s$ are written in the form:

$$\vec{u}_s^s = u_{s\alpha} + ju_{s\beta}$$

$$\vec{u}_s = u_{sd} + ju_{sq}\,, \tag{8}$$

and $e^{j\theta_1}$ and $e^{-j\theta_1}$ are expanded by using Euler's formula:

$$e^{j\theta_1} = \cos\theta_1 + j\sin\theta_1$$

$$e^{-j\theta_1} = \cos\theta_1 - j\sin\theta_1\,, \tag{9}$$

Eq. (5) and Eq. (6) can be expressed in a matrix form as follows:

$$\begin{bmatrix} u_{sd} \\ u_{sq} \end{bmatrix} = \begin{bmatrix} \cos\theta_1 & \sin\theta_1 \\ -\sin\theta_1 & \cos\theta_1 \end{bmatrix} . \begin{bmatrix} u_{s\alpha} \\ u_{s\beta} \end{bmatrix} \tag{10}$$

$$\begin{bmatrix} u_{s\alpha} \\ u_{s\beta} \end{bmatrix} = \begin{bmatrix} \cos\theta_1 & -\sin\theta_1 \\ \sin\theta_1 & \cos\theta_1 \end{bmatrix} . \begin{bmatrix} u_{sd} \\ u_{sq} \end{bmatrix} .$$

2.3. Equation of the induction motor-hydraulic pump unit.

$$J\frac{d\omega_p}{dt} = M_d - M_p\,, \tag{11}$$

where, $M_d = k_d \frac{IU}{\omega_p}$ - engine torque and $M_p = \frac{q_p}{2\pi} p_p$, - moment of resistance of the hydraulic pump.

2.4. Pump flow rate equation:

$$Q_p = \frac{q_p}{2\pi}\omega_p\,, \tag{12}$$

where: q_p - pump displacement; ω_p - rotational frequency of the pump shaft.

2.5. Equations of the proportional servo valve [2]**.**

2.5.1. Flow rate equations:

$$Q_1 = \mu_1 \pi d x \sqrt{\frac{2(p_p - p_1)}{\rho}} \tag{13}$$

$$Q_2 = \mu_2 \pi d x \sqrt{\frac{2(p_2 - p_R)}{\rho}} \tag{14}$$

where:

μ_1, μ_2 - flow discharge coefficient;
d - spool diameter;
ρ - mass density of the fluid;
x - servo valve spool displacement;
p_1, p_2 -pressure of the hydraulic motor chambers.

2.5.2. Servo valve flapper rotation:

$$T_f^{\,2}\frac{d^2\varphi}{dt^2} + 2\zeta_f T_f \frac{d\varphi}{dt} + \varphi = k_i . i - k_{rx} x \tag{15}$$

where:
φ - servo valve flapper rotation;
T_f, ζ_f - servo valve flapper and damping ratio time constants;
i - input current of the servo valve;
x - servo valve spool displacement.

2.5.3. Servo valve spool displacement:

$$T_{\varphi x}\frac{dx}{dt}+x=k_{\varphi x}\varphi \tag{16}$$

where:

$T_{\varphi x}, k_{\varphi x}$ - time constant and gain of the flapper rotation.

2.6 The electro-mechanical transducer:

$$T_i\frac{di}{dt}+i=k_U U \tag{17}$$

where:

U - output voltage of PID controller;

T_i, k_U - time constant and gain of the electro-mechanical transducer.

2.7. Equation of the PID controller:

$$U=k_r U_y+\frac{1}{T_I}\int U_y dt+T_D\frac{dU_y}{dt}, \tag{18}$$

where U_y - voltage of electronic amplifier ; T_I, T_D, k_r - time constant of PID controller;

2.8. Feedback equation:

$$U_{ov}=k_{ov}\omega, \tag{19}$$

where:

U_{ov} - feedback voltage;

k_{ov} - gain of feedback;

ω - angular velocity of the shaft of the hydraulic motor.

2.9. Equation of the summing device:

$$\Delta U=U_z-U_{ov}, \tag{20}$$

where:

U_z - input voltage;

ΔU - output voltage of the summing device.

2.10. Equation of the electronic amplifier:

$$T_y\frac{dU_y}{dt}+U_y=k_y\Delta U \tag{21}$$

2.11. Hydraulic motor flow rate equation by taking into account the compressibility of fluid:

$$Q_1 = \frac{q_m}{2\pi}\omega + \frac{V_1}{B}\frac{dp_1}{dt} \tag{22}$$

$$Q_2 = \frac{q_m}{2\pi}\omega - \frac{V_2}{B}\frac{dp_2}{dt} \tag{23}$$

B - Bulk modulus of the hydraulic oil;

V_1, V_2 - pipeline fluid volumes.

If we neglect leakage and compressibility, it can be assumed that $Q_1 = Q_2 = Q$.

2.12. Hydraulic motor equations.

2.12.1. Angular velocity and moment of the shaft of the hydraulic motor:

$$\omega = \frac{2\pi}{q_m}Q \tag{24}$$

$$M_m = (p_1 - p_2)\frac{q_m}{2\pi} \tag{25}$$

2.12.2. Equation of motion of the shaft of the hydraulic motor:

$$J_m \frac{d\omega}{dt} = \frac{q_m}{2\pi}\Delta p_m - k_T\omega - M_l \tag{26}$$

where:

$\Delta p_m = p_1 - p_2$ - pressure drop ;

J_m - moment of inertia of the shaft of the hydraulic motor;

q_m - motor displacement;

k_T - friction coefficient .

2.13. Load Equation.

The rotary inertia load is described by the following equation:

$$M_l = \int_0^R (2\pi\rho L\omega r^3)dr = \pi R^2 L\rho\frac{R^2}{2}\omega = \frac{mR^2}{2}\omega = J\omega \tag{27}$$

where:

M_l - torque moment, J - inertia moment, ω - angular velocity, ρ - density,

m, R, L - mass, radius, and width of the rotary load.

2.14. Equation of the tachometer generator.

As feedback a tachometer generator with the following equation is used:

$$U_{tg} = k_{tg}.\omega \tag{28}$$

where k_{tg} – transmission rate of the tachometer generator.

When compiling the mathematical model, the leakage in the hydraulic pump and motor is ignored.

3. Modeling and simulation of the system

To simulate [8, 9, 10] the processes in the system, Matlab Simulink, Simhydraulic, SimElectronic are used. Based on the abovementioned mathematical model, a simulation model of the system is developed (fig.3). The numerical values of the most important coefficients used in the simulation are shown in table 1.

Table 1: Simulation coefficients.

q_p	20e-6	m^3/rev
η_{vP}	94	%
M_l	60	Nm
K_r	9	-
T_I	10	-
T_D	0	-
k_{tg}	0.010	$V/\min^{-1}$
fluid	N46	-
q_m	36e-6	m^3/rev
$\eta_{v,m}$	94	%

An ideal source of mechanical energy is used as a load that generates a torque proportional to the input signal. A tachometer generator, which provides feedback to the control of the proportional servo valve, is connected on the shaft of the hydraulic motor. The signal from the tachometer generator is used to compare the speed of the hydraulic motor in the setup block with the preset speed, where a suitable control signal is generated to the inverter. With the help of the PI controller the speed of the induction motor in relation to the load can be adjusted by increasing or reducing the output of the fixed hydraulic pump by adjusting the speed of the induction motor. When the load is increased until the moment where the system cannot maintain the set minimal speed of the shaft of the hydraulic motor, a signal is passed from the block setup to the inverter which regulates the speed of the electric motor.

Figure 4 shows the simulation of the hydraulic system consisting of a hydraulic pump with constant displacement, a proportional servo valve and a hydraulic motor, an ideal source of mechanical energy, speed and pressure sensors.

Figure 5 shows the transition responses of the speed of the shaft, the electric current and the electromagnetic torque of induction motor, the speed of the shaft of the hydraulic motor, the pressure in the system and the loading. Within the first second of the simulation, the speed of the hydraulic motor drops down below the set value due to the increasing load. The speed is compared with the preset value in the setup block which passes a signal for increasing the speed of the electric motor to the inverter so as to compensate for the reduced speed.

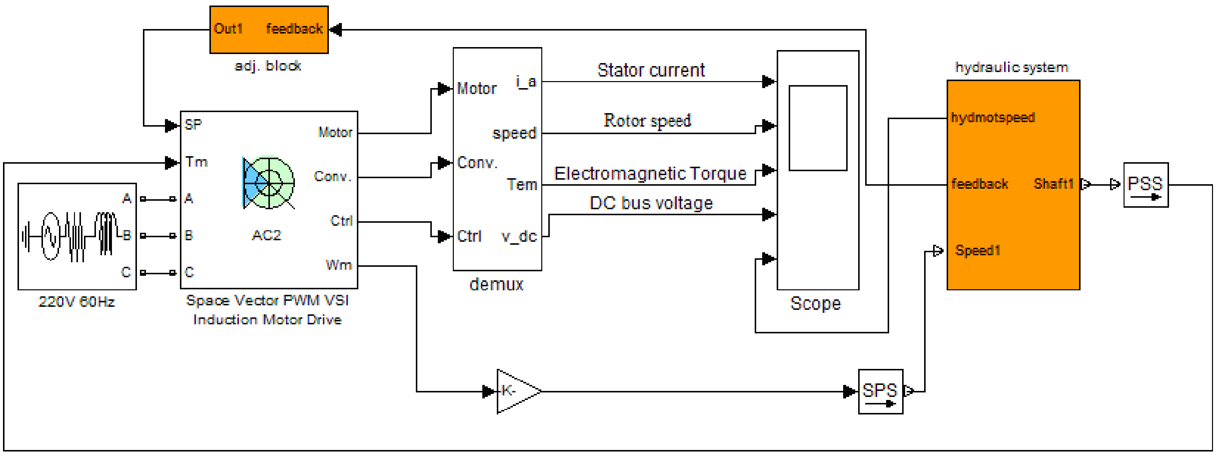

Fig. 3. Simulation model of the electro-hydraulic drive system.

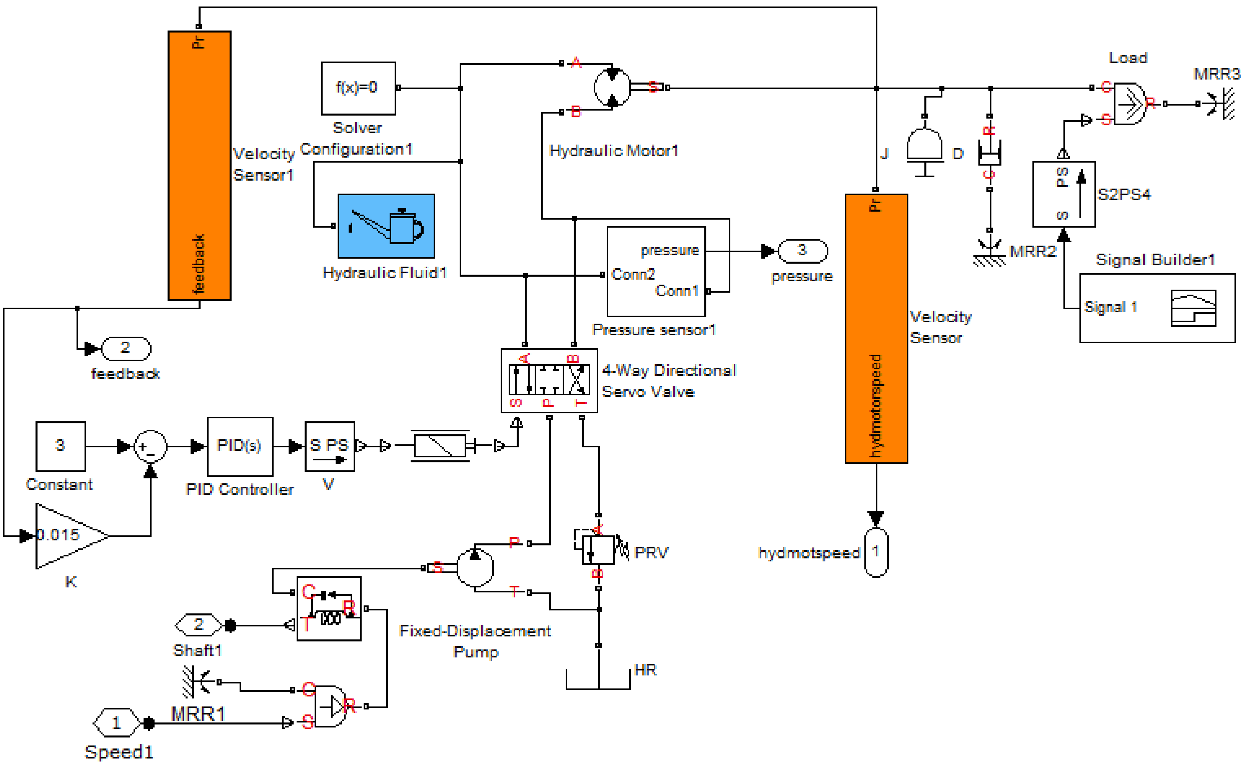

Fig. 4. Simulation model of the hydraulic subsystem.

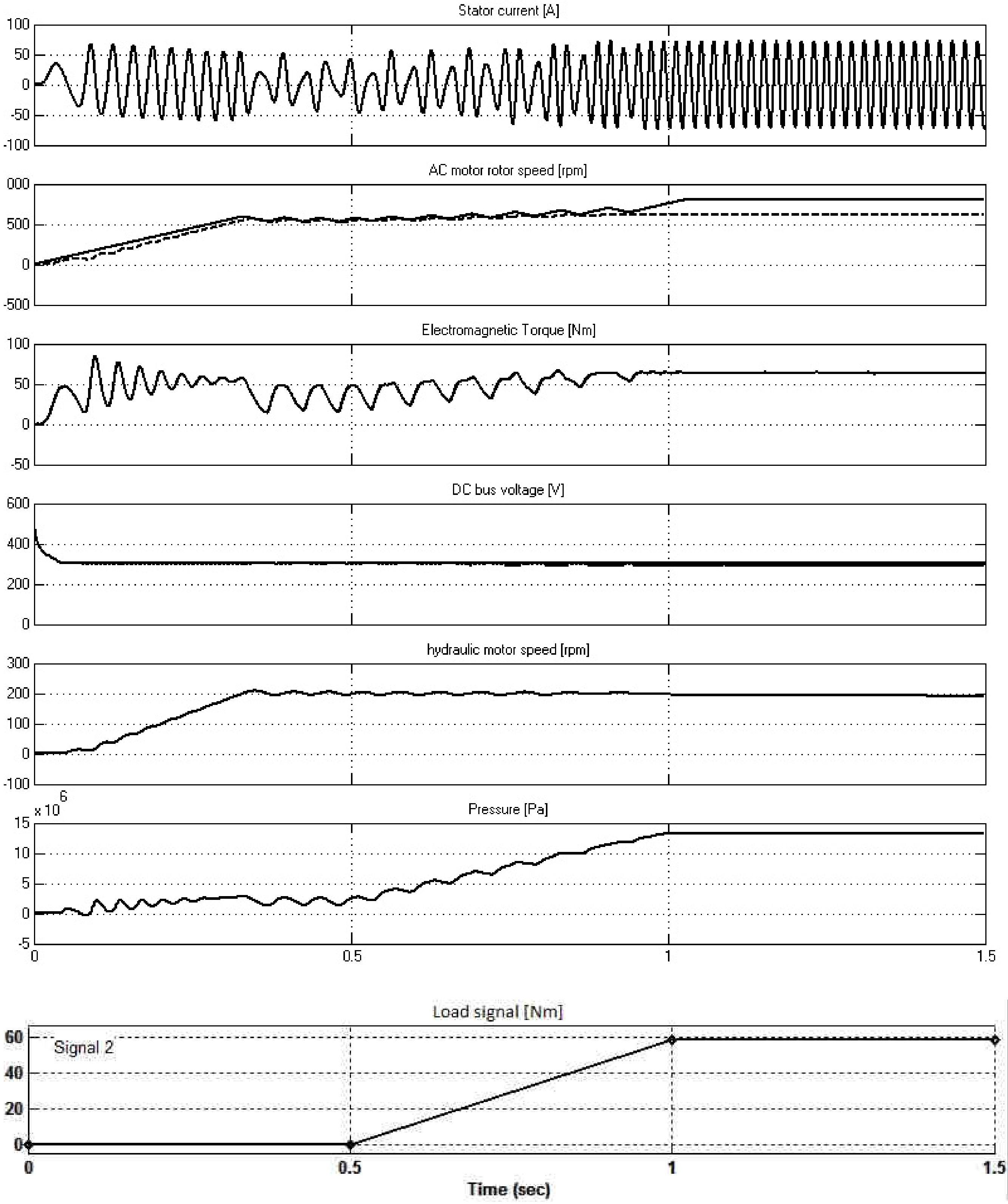

Fig. 5. Transition responses in the electro-hydraulic system.

4. Conclusions

The developed simulation model makes possible to examine the dynamic characteristics of the electro hydraulic drive system. The resulting transients allow us to analyze the system behavior and to evaluate the influence of various parameters. Upon using the signal from the tachometer generator, when necessary, an additional power could be added to the system. The results obtained from the computer simulation can be compared with those obtained from the experimental studies so as to verify and refine the model coefficients, which are theoretically difficult to calculate.

REFERENCES

[1] Ivanov P., Hristov H. et al., Dynamics of automated hydraulic and pneumatic systems, Gabrovo, 2004.
[2] Hristov H., Experimental investigation of the dynamic processes and parameters identifications in electrohydraulic power system, Technical University - Gabrovo, Bulgaria.
[3] Georgiev B., Hristov Hr., Dynamic processes modelling in electrohydraulic system with fixed hydraulic motor, Technical University – Gabrovo, Bulgaria. Unitech 2012.
4] Georgiev B., Hristov Hr., Study on dynamic processes in rotation electro-hydraulic drive system with vector control (SVM), Part I – Math model, International conference, Sliven, 2014.
[5] Georgiev B., Hristov Hr., Study on dynamic processes in rotation electro-hydraulic drive system with vector control (SVM), Part II – Modelling and simulation, International conference, Sliven, 2014.
[6] Cheng Q., Vector Control of an Induction Motor based on a DSP, Master of Science Thesis.
[7] Texas Instruments, “Clark & Park Transform” Texas Instruments, Tech. Rep., 1997.
[8] MathWorks, 2001, Introduction to MATLAB, the MathWorks, Inc.
[9] MathWorks, 2001, SIMULINK, the MathWorks, Inc.
[10] MathWorks, 2001, What is SIMULINK, the MathWorks, Inc.

"The present document has been produced with the financial assistance of the European Social Fund under Operational Programme “Human Resources Development”. The contents of this document are the sole responsibility of “Angel Kanchev” University of Ruse and can under no circumstances be regarded as reflecting the position of the European Union or the Ministry of Education and Science of Republic of Bulgaria."

Project № BG051PO001-3.3.06-0008 “Supporting Academic Development of
Scientific Personnel in Engineering and Information Science and Technologies”

ISSN 1454 - 8003
Proceedings of 2014 International Conference of Hydraulics and Pneumatics - HERVEX
November 5 – 7, Calimanesti-Caciulata, Romania

REDUCING SHOCKS DUE TO WIND ON THE PHOTOVOLTAIC TRACKERS USING THE MAGNETORHEOLOGICAL FLUID DAMPERS

Florin RAVIGAN[1], Ionel Laurentiu ALBOTEANU[2]
[1,2] University of Craiova,[1] ravigan.florin@gmail.com, [2] lalboteanu@em.ucv.ro

Abstract: *In recent years, applications that use photovoltaic systems are a continuously growing. The current trend is to optimizing these systems by ensuring functionality with maximum efficiency. Using the tracking systems for photovoltaic panels contribute to the increase energy efficiency. One of the issues that arise in these tracking systems refers to the supplementary load due to the wind. Shock and vibration may occur which lead to an unstable operations of tracking system.*
This paper presents an innovative solution to reduce the shock in tracking systems for photovoltaic panels by using the dampers with magnetorheological fluid.

Keywords: *photovoltaic, trackers, shocks, damping, smart materials*

1. Introduction

Energy issues have become the primordial in recent years due to the depletion of fossil fuel resources, their price variations and political dependence of nations they delivers [14]. Use of renewable energy resources is gaining more ground, because continuous increase in the price of fossil energy carriers and lower stocks management respectively waste resulting from nuclear energy [14].

For increasing the energy production of photovoltaic systems usually are used the tracking systems for photovoltaic panels. Wind action on PV panels lead to the emergence of important efforts, shock and vibration in solar trackers. To take these further loads, the actuators of solar trackers are usually oversized and have a supplementary consumption of energy.

To reduce the supplementary load and energy consumption is used an innovative solution based on magnetorheological fluid dampers.

2. Photovoltaic tracking system

Electricity production of a PV system depends largely on solar radiation absorbed by the photovoltaic panels. As the sun changes with the seasons and over a day, the amount of radiation available for the conversion process depends on the panel tracking.

In practice are two kinds of tracking systems: single axis and double axes tracking systems . In the case where the two orientation axes 3 types of systems can be distinguished, depending on how the axes are placed and how the two movements are entered into the system [7]: the azimuthally systems, the equatorial systems and the pseudo-equatorial systems. In this paper was considered the pseudo-equatorial system (Fig.1).

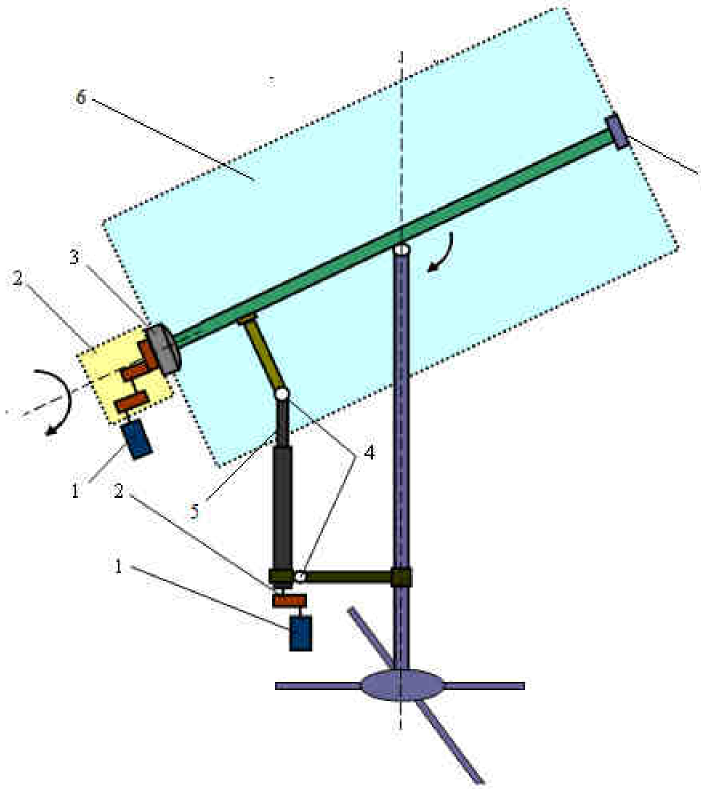

Fig. 1. Pseudo-equatorial tracker of PV panel: 1-actuators, 2- gears, 3,7- couplings, 4- joints, 5- actuator rod, 6- PV panel.

3. Wind load calculation for photovoltaic panel

Initial condition:
- lenght of PV panel: $L = 1{,}6m$;
- windt of PV panel: $l = 0{,}8m$;
- the fixing point is considered to be the center of mass of the panel, and at the same time the center of rotation for both movements;
- the tracking system is in the normal temperature (T = 20 °C) and pressure (p = 1atm);
- are neglected friction in the joints.

Wind power is given by relation:

$$P = \frac{1}{2} \cdot \rho \cdot S \cdot V^2 = F \cdot V[W] \quad (1)$$

where:
- $\rho = 1{,}293\, Kg/m^3$ - the air density in conditions of temperature and pressure given;
- S- the surface which acting the wind to normal direction;

F - wind force.

Wind power in the more disfavoured is:

$$F = \frac{P}{V} = \frac{1}{2} \cdot \rho \cdot S \cdot V^2 [N] \quad (2)$$

Consider wind speed (the worst case): $V = 30 m/s$

Surface considered is:

$$S = \frac{S_{panel}}{2} = \frac{1{,}6 \cdot 0{,}8}{2} = 0{,}64 m^2 \tag{3}$$

$$\Rightarrow F = \frac{1{,}293 \cdot 0{,}64 \cdot 900}{2} = 372{,}384 N \tag{4}$$

a) Wind force transmitted to the actuator joint North South direction:

Considering the point of application of force to the centre of mass of the panel surface covered (Fig.2), the arm force is:

$$b_V = \frac{L}{4} = \frac{1{,}6}{4} = 0{,}4 m \tag{5}$$

Torque in the vertical plane is:

$$M_V = F \cdot b_V = 372{,}348 \cdot 0{,}4 = 148{,}939 Nm \tag{6}$$

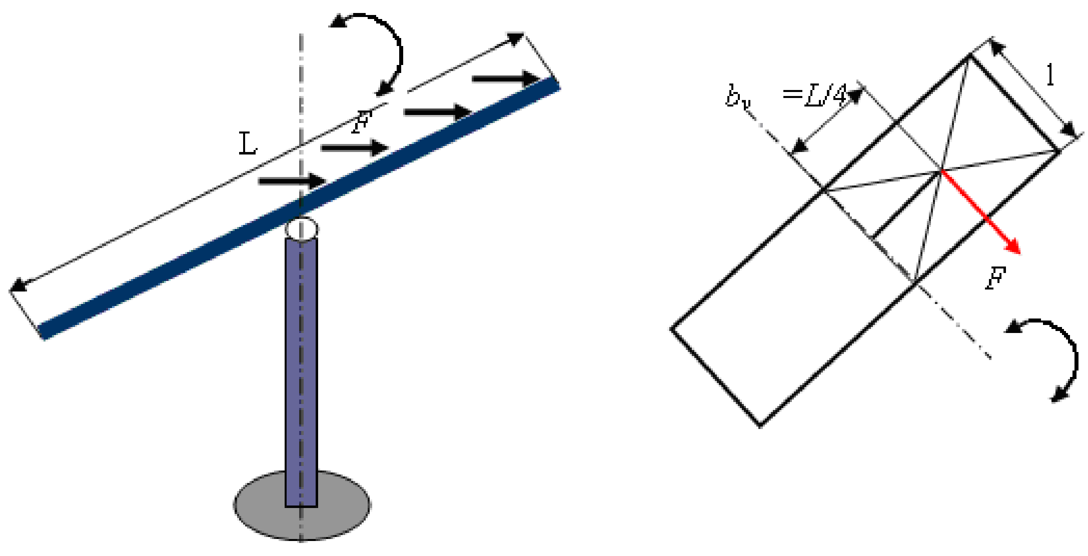

Fig. 2. Explanatory regarding to calculation of the wind force torque to South North direction

b) Wind force transmitted to the actuator joint East West direction

Consider the point of application of the wind force in the longitudinal half of the centre of mass of the panel (Fig. 3).

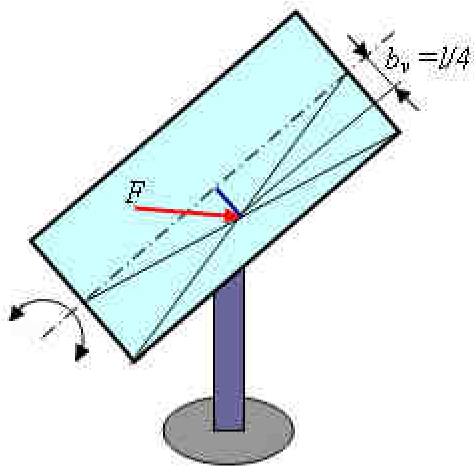

Fig. 3. Explanatory regarding to calculation of the wind force torque to East West direction

In this case the arm force is:

$$b_E = \frac{l}{4} = \frac{0,8}{4} = 0,2m \tag{7}$$

The torque after East West direction

$$M_E = F \cdot b_E = 372,384 \cdot 0,2 = 74,476 Nm \tag{8}$$

Based on these relationships can be seen as a wind force can insert in solar trackers the significant values of resistance torques

4. Semi-active shock damping systems

To mitigate impacts caused by gusts of wind, you can use semi-active damping systems. In these systems, the damping coefficient is not constant and can be controlled.

One such solution is the magnetorheological fluid dampers based. These fluids are part of smart materials are fluids that change their rheological properties in the presence of magnetic field. Rheological properties of interest for technical applications are the viscosity. Thus, the presence of magnetisable particles form chains of the magnetic field of the particles along the field lines, which changes the flow of the fluid, passing it to the state of the fluid viscous gel state. This change is carried out within a time of less than 1 ms.

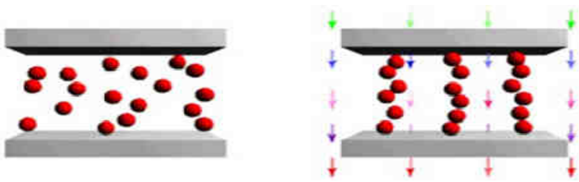

Fig.4. Magnetorheological fluid behaviour in a magnetic field

An interesting thing is that unlike magnetic fluids, magnetorheological fluids have no magnetic hysteresis.

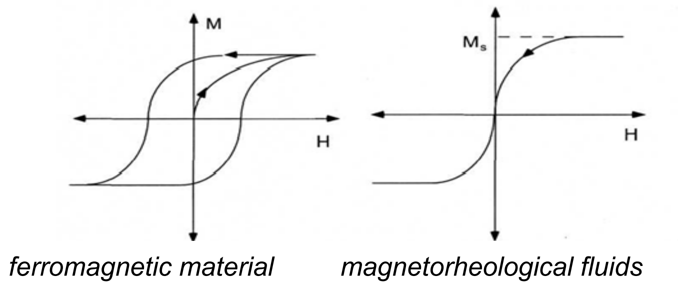

Fig.5. Hysteresis behavior in the presence of a magnetic field

A manufacturer that has established itself as world leader is Lord US company which currently produces both magnetorheological fluids and devices whose operation is based on them. Fluids are produced by the company in the form of a gray liquid and the operating temperature range of -40 - 130ºC. Lord Company products are classified into the following categories: magnetorheological fluids, magnetorheological dampers, magnetorheological brakes, magnetorheological devices dedicated controller, steer-by-wire devices. They are based on two basic structures: the structure with fixed poles (valve-stop) and the pole in relative motion (piston).

Magnetorheological dampers are devices that can be controlled damping force. This comes down to control the current through its coil, and hence the magnetic field energizing magnetorheological fluid. Structure of a magnetorheological damper knows multiple ways. One of these options is chosen by the American company in achieving Lord magnetorheological damper RD-1097-1001, a device that lends itself to taking shocks caused by gusts of wind on an adjustable structure of a photovoltaic panel and more. This embodiment is shown in figure below.

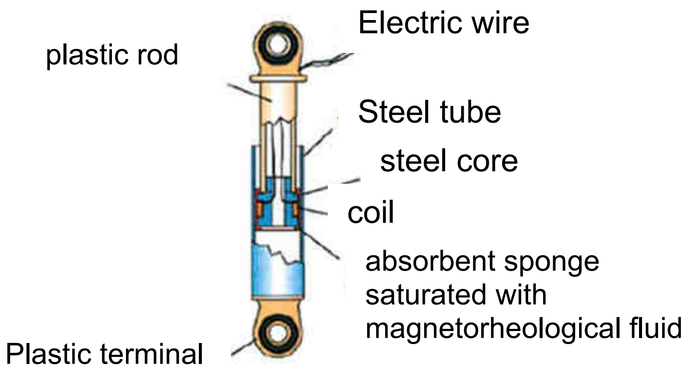

a)

b)

Fig.6. Magnetorheological damper RD-1097-1001: a) structure; b) Overview

RD-1097-1001 LORD damper [12] is a magnetorheological fluid damper controlled friction is an example of a device suitable for low force applications, suspensions for light duty applications and shock isolation. It consists of a cylindrical steel rod movable sliding damper. In this energizing coil is 50mm in length wrapped in a cloth saturated with magnetorheological fluid. Both cylinder and rod ends are mobile hub through which one can connect mechanical damper.

Friction damping is controlled by the yield stress of the magnetorheological fluid in response to the intensity of the applied magnetic field. This device has a stroke of 5.2mm, a lower response speed of 25 ms and can operate at temperatures ranging from -40 ° C to 70 ° C.

Its damping force is given by:

$$F_d = F_c \operatorname{sgn} \dot{x} + c_0 \dot{x} \tag{9}$$

Where F_c is the force of friction, the velocity of the piston and c_0 is the viscous damping coefficient. Both F_c and c_0 can be written by current and constant number of design parameters of the damper.

In order to detect the movement of the linear position transducer can be used SLS095. It is produced by Penny-Giles Controls Ltd. and is a position transducer performance characteristics. He is a resistive sensor with a linear resistance 20kΩ presents virtually infinite resolution and the operation is just as voltage divider.

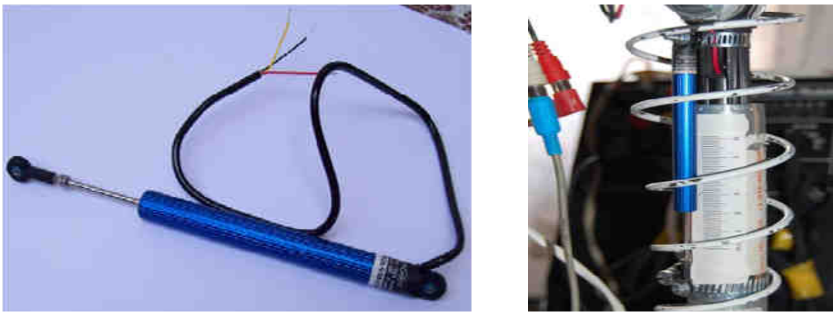

a) b)

Fig.7. The linear displacement transducer Penny-Gilles SLS095(a) mounted on damper(b)

The transducer is mounted between the fixed and the mobile element of the damper. The mathematical processing it provides in addition information and data travel speed, acceleration and shock.

Below are given some experimental data obtained using a data acquisition system Quanser 626, showing how to mitigate forces that require the movable damper. It is noted that the displacement of the damper rod is smaller as the current applied increases.

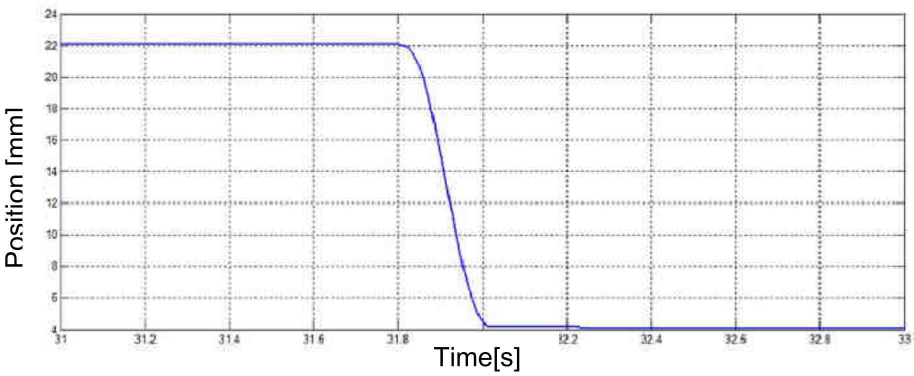

Fig.8 Moving the damper rod to a force of 20N and supply voltage 2V

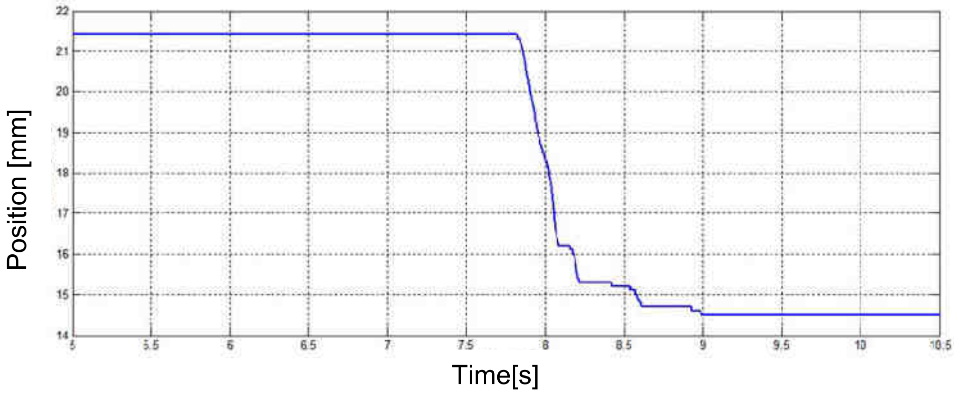

Fig.9. Moving the damper rod to a force of 20N and supply voltage 4V

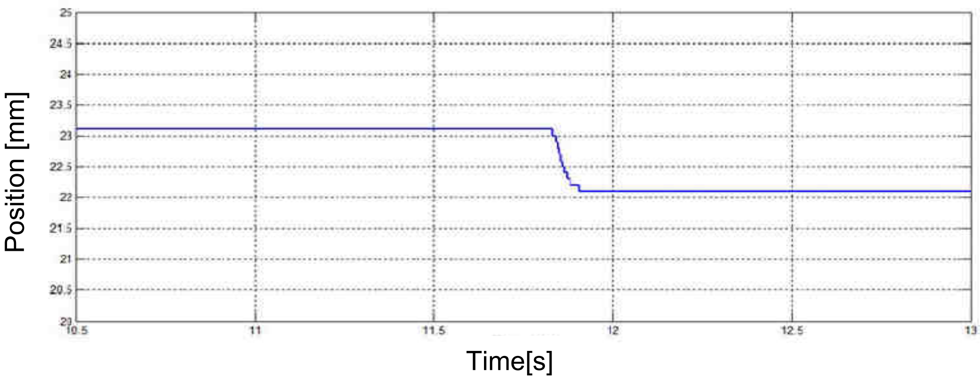

Fig.10. Moving the damper rod to a force of 20N and supply voltage 10V

Damper control can be applied proportional control movement. The microprocessor evaluates the information from the analogue displacement sensor, and as the command value increases to increase the shock absorber. The coefficient of proportionality is adjusted so that the damping device to take the shock.

Also, you can use a command-based look-up table or using PI algorithms.

The voltage applied to the coil of the damper is in the form of pulse width modulated, following which the current does not exceed the maximum value required by the manufacturer. In this way, the control is limited to prescribing the duty cycle of a PWM signal.

5. Conclusions

In conclusion, the performances of shock mitigation devices based on magnetorheological fluids can be a solution to protect tracking systems for photovoltaic panels and more. Used in conjunction with the operating system may obtain an active damping system to which the control loops are relatively simple and easily implemented using a general purpose microcontroller.

Acknowledgment

This work was partially supported by the grant number 29C/2014, awarded in the internal grant competition of the University of Craiova.

REFERENCES

[1] I.L. Alboteanu, G. Manolea, F. Ravigan, "Positioning systems for solar panels placed in isolated areas", Annals of the University of Craiova, Electrical Engineering series, No. 30, 2006, ISSN 1832-3804, pp.163-168.
[2] I. L. Alboteanu, F. Ravigan, S. Degeratu, C. Sulea, "Aspects of designing the tracking systems for photovoltaic panels with low concentration of solar radiation" Computational problems in Engineering II, 2014, Springer-Verlag,in press.
[3] I. L. Alboteanu, Advanced stand-alone photovoltaic system, Craiova, "Universitaria", Publisher, 2013.
[4] S. Barkaszi,C. O'Brien "Wind load calculation for PV array", Solar American Board for Codes and Standards Report, BEW Engineering, June 2010.
[5] G. Ciuprina, D. Loan, I. Munteanu, "Use of intelligent-particle swarm optimization in electromagneticsȚ, IEEE Trans. Magn. 38, 1037–1040, 2002
[7] M. Comşiţ, "Specific orientation mechanisms of solar energy conversion systems", PhD thesis, Transilvania University of Brasov, 2007
[8] Ivanescu, Mircea, și alții, și alții. Sisteme neconventionale pentru conducerea robotilor. Craiova, Universitaria, 2003.
[9] B.F. Spencer Jr., S.J. Dyke, M.K. Sian, J.D. Carlson, Phenomenological model for magnetorheological dampers, J. Eng. Mech. (March) (1997) 230–238
[10] F. Ravigan, A. Petrisor, N. Boteanu, C. Vladu – The Controlled Damping of Vibrations for Robotics. Buletin of the Transilvania University of Brasov.The 4th International Conference of Robotics. Brasov 2008.
[11] Lai, C.Y. și Liao, W.H.- Vibration Control of a Suspension System via a Magnetorheological Fluid Damper. 2002, Journal of Vibration and Control, 8(4):527–547.
[12] **** RD-1097-1001 Lord Damper. Technical Datasheet.
[13] **** "Minimum Design Loads for Buildings and Other Structures (7-05)", American Society of Civil Engineers (ASCE), 2006.
[14] ***** http://europa.eu/pol/ener/flipbook/ro/files/energy_ro.pdf

ISSN 1454 - 8003
Proceedings of 2014 International Conference of Hydraulics and Pneumatics - HERVEX
November 5 – 7, Calimanesti-Caciulata, Romania

IMPROVING THE ENERGY CONVERSION EFFICIENCY OF COUNTER ROTATING WIND TURBINES BY USING INNOVATIVE GENERATORS

Mihail POPESCU[1], Sergiu NICOLAIE[1], Gabriela OPRINA[1], Radu CÎRNARU[1], Andreea MITULEȚ[1], Rareș CHIHAIA[1], Radu MIREA[1]

[1] National Institute for R&D in Electrical Engineering ICPE-CA, mihail.popescu@icpe-ca.ro, sergiu.nicolaie@icpe-ca.ro, gabriela.oprina@icpe-ca.ro, radu.cirnaru@icpe-ca.ro, andreea.mitulet@icpe-ca.ro, rares.chihaia@icpe-ca.ro, radu.mirea@icpe-ca.ro

Abstract: *The paper presents solutions for improving the efficiency of the wind energy conversion into electricity by using counter rotating wind turbine systems and permanent magnets electric generators. The innovative design of the generators allows obtaining an increased speed and eliminates the speed multiplier. This design leads to an improved efficiency on the entire energy conversion system. The electric machine has both rotating armatures, each of them being entrained by a wind rotor. One rotor rotates clockwise, while the other counterclockwise. There are presented the results obtained for testing a generator with mobile armatures used for undertaking the movement provided by a counter rotating horizontal axis wind turbine (CRHAWT) system and elements of designing a model of counter rotating vertical axis wind turbine (CRVAWT) system.*

Keywords*: electric generator, mobile armature, wind turbine, slotless armature, permanent magnets, conversion efficiency*

1. Introduction

Nowadays, when fossil fuel reserves are harder to find and request for electricity grows by the day, it was passed to the promotion and development of renewable energy sources. Within the last two decades have been patented, studied and promoted a series of solutions and systems for converting the kinetic energy of wind into electricity. Beside the investigations regarding the performance of single wind turbines, several researches related to tandem wind turbines and counter rotating wind turbines were performed in order to increase the degree of conversion of the wind stream into power. Thus, several solutions of electric generators able to summarize the movement of the two rotors were investigated. The solution with one generator for each rotor was approached in [1], the solution with one generator coupled to the rotors through a differential planetary system in [2] and the one with single permanent magnets generator, with kinematic coupling of the rotors in [3]. Some researches focussed on investigating the optimum distance between the two rotors [2], [4] while others on predicting the increase in annual energy production as compared to the energy produced by a single rotor turbine of same type. Most of the researches approach the influence of several parameters on the aerodynamic performance of the wind turbine system. Moreover, the research is performed both numerically and experimentally.

The main goal of the research presented in this paper was to increase the efficiency of mechanical energy conversion into electrical energy, and increasing the global power coefficient of the wind turbine systems. This paper presents the results obtained for testing a generator with mobile armatures used for undertaking the movement provided by a counter rotating horizontal axis wind turbine (CRHAWT) system and elements of designing a model of counter rotating vertical axis wind turbine (CRVAWT) system.

2. Stages in the development of wind generators

One of the solutions for increasing the conversion efficiency consisted in the use of mechanical speed multipliers (figure 1). The mechanical movement of rotation provided by the wind motor is multiplied by a toothed gear driveline, and then the mechanical energy is provided at the end of a machine's shaft that converts it into electricity. This solution was actually the first solution used, since it allowed the use of electric machines and existing mechanical and electrical parts which were commercialized on the market. In this way, the cost of construction and putting into operation was reduced. Another advantage of this solution consists in the reduced overall size of the electric conversion machine; but it led to yield diminishing since a share of the rotation mechanical power is consumed in the speed multiplier. A different disadvantage of this solution is that increases the overall weight that needs to be lifted and mounted inside the nacelle.

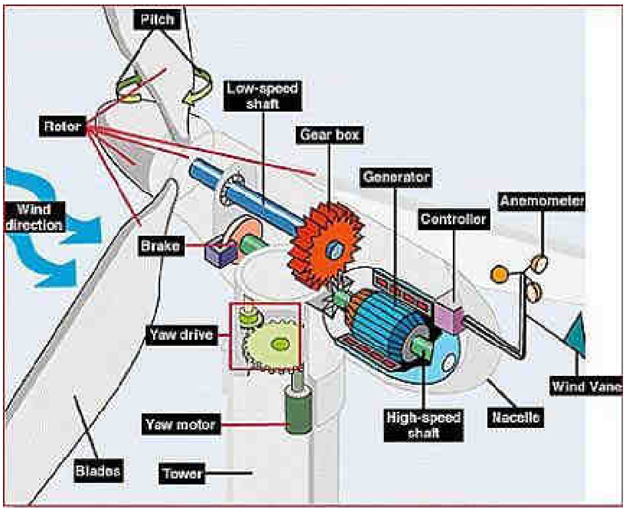

Fig. 1. Wind turbine with gearbox

The second solution consisted in using the so-called Pseudo Direct Drives (PDD), a hybrid solution promoted by MAGNOMATICS [5]. This is a combination of a reducer / multiplier and a permanent magnet synchronous generator. From the functional point of view, this solution is similar to the previous one, but its cost is very high, since it uses a large amount of permanent magnets. Also, the difficulties of manufacturing the mechanical parts are high.

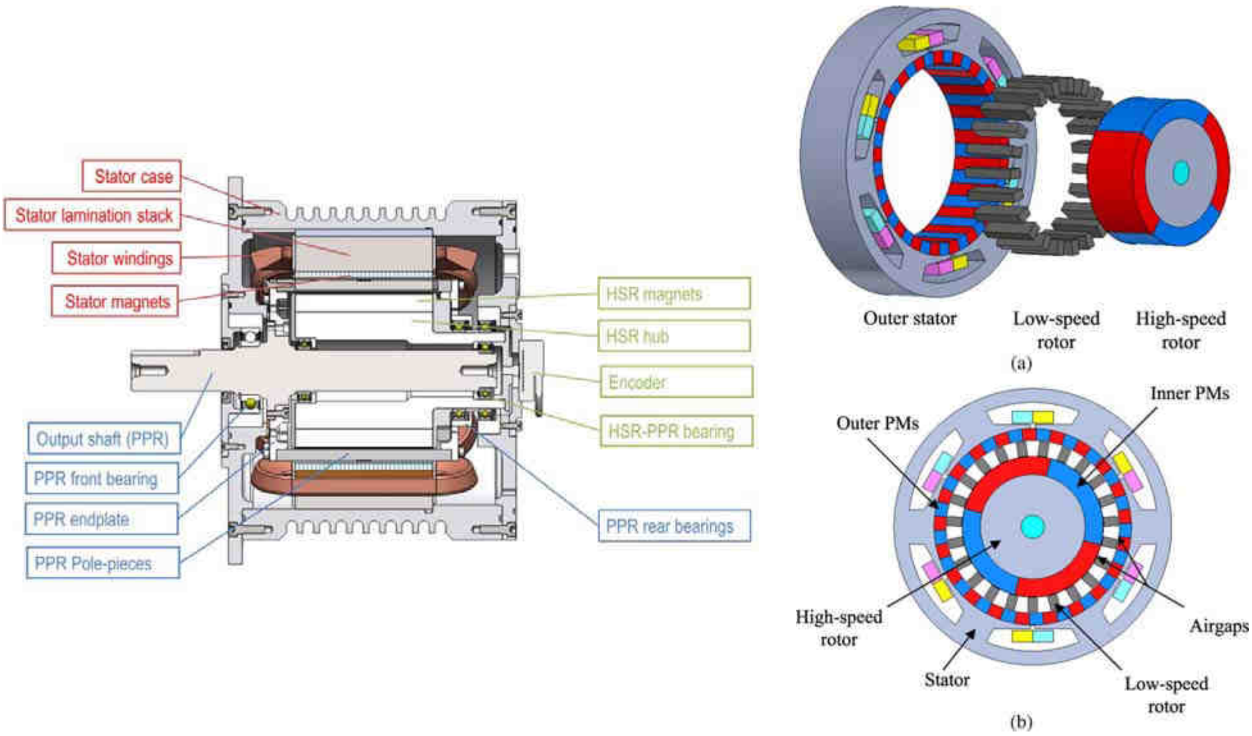

Fig. 2. Longitudinal section view and perspective view of a PDD [5]

3. Theory

The theoretical maximum power that can be extracted from the wind using a single rotor is 59% according to Betz' theory. The remaining energy is lost in the wake behind the rotor, where the vortex rotates in opposite direction of the blades rotation. By using two wind turbines with the same diameter there could be extracted 64% of the available energy [4], [6], [7], which means an increase of up to 30% compared to existing conversion systems. This additional energy input is due to the fact that the turbulences produced by the blades of the front rotor push the rear blades into the opposite direction. The behaviour of equipment with counter rotating armatures is similar to systems provided with speed multipliers. The lack of the speed multiplier determines an increase of the global yield of the wind turbine. The performance of a wind turbine is mainly described by the power coefficient variation depending on the turbine speed, respectively the $c_P = c_P(\lambda)$ characteristic. The increase of the maximum theoretical power coefficient is indicated in some studies depending on the diameter ratio of the two rotors. For 1:1 ratio the global power coefficient of the wind turbine system is $c_{Pglobal}$ = 0.615, while for a different ratio $c_{Pglobal}$ = 0.64 can be obtained.

The power coefficient is given by the following equation:

$$c_p = \frac{P}{0{,}5\,\rho\, v_1^3\, A} \qquad (1)$$

where P [W] is the theoretical power output of the wind turbine; ρ - the air density, in kg/m^3; A - the surface described by the turbine rotor, perpendicular onto the wind direction, in m^2; v_1 - the air velocity when entering the turbine, in m/s.

4. Manufacturing elements of the CRHAWT system's generator and its testing results

For the envisaged application, namely for capturing the motion of a wind turbine system having two counter rotating rotors, there has been manufactured a three-phase synchronous electric generator with counter rotating armatures, having the power of 1.6 kW, 3×24 V, at 750 rpm. This solution was chosen due to its advantages: the use of two rotating armatures leads to decreased overall size of the generator, increased rotational speed and no losses due to movement transmission. The paper presents some of the technical data regarding the developed solution and thorough details are described in a patent application [8].

The armature stator package has been winded according to the imposed parameters, the generated power being accessible via a slip ring system at the terminal block. The permanent magnets have been fitted up on the surface of the rotor cage, in specially designed locations. The rotating motion from the two blades systems is undertaken through two different coaxial axes: the first one fixed by using a flange to the electric machine shield, while the second one is actually the original shaft, but with a longer length, obtained by mechanical processing. In order to achieve the independent rotation of the two armatures, inducer and induced, the assembly was mounted in a larger case.

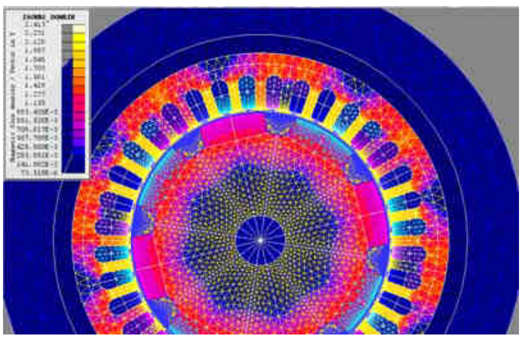

Fig. 3. Cross-section distribution of the magnetic field inside the generator

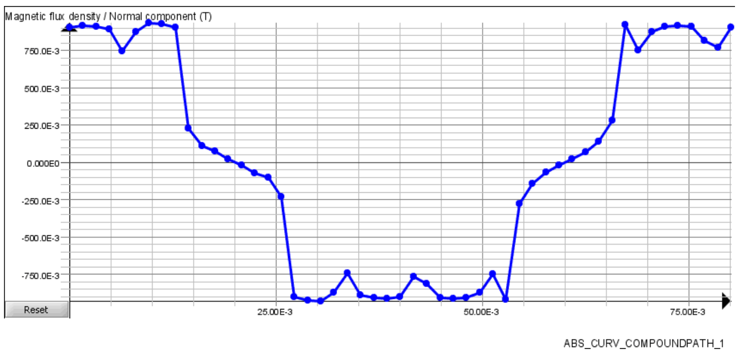

Fig. 4. Magnetic flux density in the air gap

ISSN 1454 - 8003
Proceedings of 2014 International Conference of Hydraulics and Pneumatics - HERVEX
November 5 – 7, Calimanesti-Caciulata, Romania

A Flux/2D modelling was performed for the generator geometry in order to determine the magnetic field distribution in different components. For a better visualization of the distribution, it was chosen to numerically analyze the cross-section. The inductive magnetic field structure is shown in Figure 3.

Fig. 5. Manufactured wind generator mounted in the case

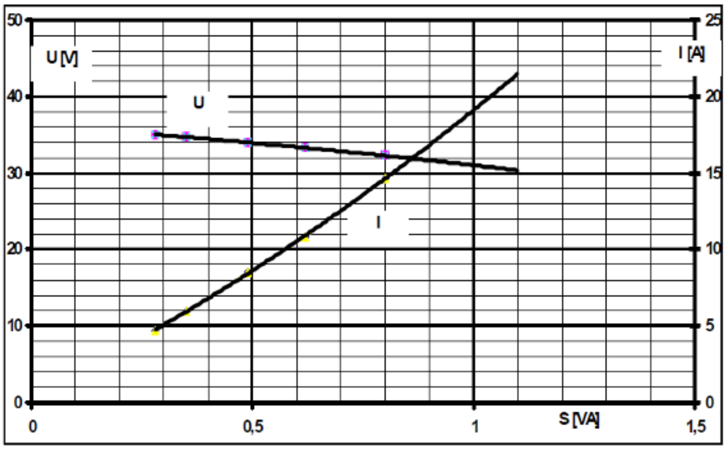

Fig. 6. Current and voltage load working characteristics of the generator

The generator was tested on a specialized bench of ICPE-CA, equipped with measurement devices and with a data acquisition system. Details regarding the test bench, testing procedure and the mechanical and electrical characteristics of the electric generator are given in [9].

As it can be noticed in figure 6, the tension drop as difference between load and no load operation of the generator is

$$\Delta U = \frac{U_0 - U_n}{U_n}100 = \frac{37-24}{24}100 = 30\%,$$

and the maximum discharged current is 30 A for load operation.

After determining the operational parameters of the designed and manufactured generator (figure 5) in order to achieve its proposed purpose, to the generator were assembled the two rotors with a diameter ratio 1:1.08.

Fig. 7. Mounting process of the rotors and the counter rotating wind turbine system

Figure 7 shows the mounting process of the two wind rotors on the cased generator and the entire assembly of the wind turbine system (permanent magnet synchronous generator with mobile armatures, front rotor and rear rotor). The entire assembly will be tested in a wind tunnel in order to determine the overall performance of the system for different wind velocities.

5. Manufacturing elements of the CRVAWT system

Based on the gained experience, a versatile wind conversion system has been designed which can be easily mounted on light poles or on the roofs of apartment buildings. In this way, energy can be provided for indoor or outdoor public lightening systems.

In order to investigate the performance of the proposed solution of permanent magnets generator with mobile armatures for VAWT systems, a model of such a system was designed. In this case, the two rotors have the same diameter (ratio 1:1) and are of H-Darrieus type.

Having in mind that the supporting structure of a wind turbine holds a significant share of the total manufacturing cost, in order to reduce the overall cost, there was chosen to design a turbine able to be mounted on already existing structures. To reduce the influences given by the adjacently operation of the two turbines and to obtain a higher velocity of the upcoming wind, an aerodynamic profile (a deflector) was used to separate the rotors (figure 8). The inner of the central deflector was used for placing the electric generator; this option leads to simplifying the mechanic construction.

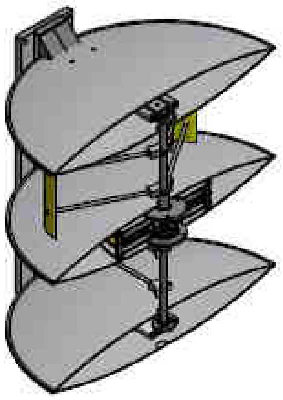

Fig. 8. Cross section of the CRVAWT system, showing the positioning of the deflectors

Fig. 9. The exploded scheme of the electric generator of the CRVAWT system

The use of permanent magnets allows the manufacturing of a light and small size synchronous generator. Since the hanging couple plays an important role in wind turbines' operation, it was decided to use a slot less armature construction (figure 9), thus allowing purely electric adding up the movement provided by the two turbines. Therefore, the version of two rotors equipped with permanent magnets and a twin fixed stator was chosen (a single slot less armature and two stator windings placed on both sides). This eliminates the collector and the brushes that would have been required for the rotation of the winding.

6. Conclusions

The paper presents innovative solutions to increase the energy conversion efficiency from wind stream to electricity, by using counter rotating wind turbines. The solutions are based on the use of a synchronous permanent magnets generator having mobile armatures (both the inducer and the induced), each of them being connected to a wind rotor, either horizontal or vertical. One rotor is rotating in clockwise direction and the other in counter-clockwise direction.

There has been analyzed the performance of a 1.6 kW permanent magnets generator with mobile armatures suitable for HAWT systems, on a specialised electric machineries testing bench. Each armature is entrained by a wind rotor of different diameter, with the ratio 1:1.08. For this generator was determined the tension drop between load and no load operation and the maximum discharged current: 30% and 30 A respectively for load operation. Also, using Flux/2D software it was determined the inductive magnetic field distribution inside the generator. From the calculation and the cross-section distribution map shown in Figure 3, it is found that the maximum magnetic saturation does not exceed 1.7 Tesla in the stator teeth and the air gap magnetic flux density has a value of 0.8 Tesla.

Another research was focussed on designing a model of VAWT counter rotating system of 100 W, with the diameter ratio 1:1. Beside the use of the developed generator a single slotless armature and two stator windings placed on both sides, a particular feature of this system consists in using a set of deflectors in order to increase the wind speed in the rotors/blades area. In order to rotate in opposite directions, the blades of the two rotors are positioned “in the mirror”.

The present study highlights that the investigation of counter rotating wind turbine (CRWT) systems is complex, since different components have to be characterized, both individually and while operating as an integrated system. To get a further insight in the field of CRWT, more investigations have to be performed.

Although in the use of counter rotating wind turbines some technical issues arise, the numerous researches performed in this field show that they are becoming more and more attractive in the global challenge to increase the energy obtained from renewable energy sources. Even if some progress has been registered in this domain, there are still some issues to be investigated in order to better characterize the performance of the entire CRWT system.

ACKNOWLEDGMENT

The research has been carried out with the support of the Executive Unit for Financing Higher Education, Research, Development and Innovation (UEFISCDI), PNCDI II program – Joint Applied Research Projects, Contract no. 39/2012, *Power Generation System which Uses a Double - Effect Wind Turbine in Order to Ensure the Energy Autonomy in Specific Applications*.

REFERENCES

[1] Y. Debleser and Jeumont Industrie, “Wind turbine with counter rotating rotors”, US Patent No. 6504260, 2003.

[2] S.N. Jung, T.-S. No, K.-W. Ryu, “Aerodynamic performance prediction of a 30 kW counter-rotating wind turbine system”, Renewable Energy, vol. 30, 2005, pp.631-644.

[3] C. Shinn and Kowintec, “Over–drive gear device”, US Patent No. 5222924, 1993.

[4] P.S. Kumar, A. Abraham, R.J. Bensingh, S. Ilangovan, “Computational and experimental analysis of counter-rotating wind turbine system”, Journal of Scientific & Industrial Research, vol. 72, May 2013, pp. 300-306.

[5] D. Lattimer, “Highly integrated and efficient lightweight direct drives for electric vehicles”, European Conference on Nanoelectronics and Embedded Systems for Electric Mobility, eMobility - eMotion, 25-26 September 2013, Toulouse, France.

[6] S. Lee, H. Kim, S. Lee, “Analysis of aerodynamic characteristics on a counter-rotating wind turbine”, Current Applied Physics, vol.10, 2010, pp. 339-342.

[7] W.Z. Shen, V.A.K. Zakkam, J.N. Sorensen and K. Appa, “Analysis of counter-rotating wind turbines”, The Science of Making Torque from Wind, IOP Publishing, Journal of Physics: Conference Series, vol. 75, 012003, doi:10.1088/1742-6596/75/1/012003, 2007.

[8] G.M. Mihaiescu, M. Popescu, S. Nicolaie, G. Oprina, I. Chirita, N. Tanase, R. Chihaia, A. Mitulet, “Hidroagregat de conversie a energiei hidraulice extrase din cursurile de apă curgătoare (*Hydro power unit used for hydraulic energy conversion extracted from water streams*)”, Patent application registration no. A/00865/23.11.2012.

[9] M. Popescu, G. Oprina, A. Mitulet, S. Nicolaie, R. Chihaia, A. Nedelcu, M. Mihaiescu, M. Miu, D. Marin, „Aspects Regarding the Application of Electric Generators to Wind Energy Conversion Using Counter Rotating Turbines”, THE 8th International Symposium on Advanced Topics in Electrical Engineering, May 23-25, 2013, Bucharest, Romania, ISSN: 2068-7966, ISBN: 978-1-4673-5978-8, IEEE Catalog Number CFP1314P-CDR.

ISSN 1454 - 8003
Proceedings of 2014 International Conference of Hydraulics and Pneumatics - HERVEX
November 5 – 7, Calimanesti-Caciulata, Romania

STRUCTURE OF A HYDRAULICALLY ACTUATED AXIS

Adrian MIREA[1], Petrin DRUMEA[2], Gabriela MATACHE[2]

[1] ROMFLUID S.A., Bucharest, adrianmirea@romfluid.ro

[2] INOE 2000-IHP, Bucharest, ihp@fluidas.ro; fluidas@fluidas.ro

Abstract:*This article makes an analysis, in terms of structure and functioning, upon a hydraulically actuated axis based on which there has been achieved a mathematical model of ensemble. The analysis was completed by creating a hydraulic axis which has been the subject of the PhD thesis entitled Theoretical and Experimental Research on the Dynamic Behavior of Intelligent Hydraulically Actuated Axes and has been tested in the Servo technique Laboratory of INOE 2000 –Hydraulics and Pneumatics Research Institute.*

1. Introduction

The hydraulically actuated axis has a structure specific to position control systems, being made up of:
- Cylinder type linear motor, with bilateral rod, with displacement / stroke "y", whose rod also generates movement of mobile part of the stroke transducer which corresponding to displacement "y" supplies voltage "U".
- Two amplification stages servo-valve, as shown in Figure 1, comprises: torque motor (I), preamplifier (II), nozzle - clack valve type, and power amplifier (III) which, supplied with flow from a constant flow hydraulic pump of pressure p_0, distributes to the linear motor chambers flow rates set to pressures p_1 and p_2;
- Servo-controller (IV), for drive and control, in the structure of which there is a proportional regulator with the purpose to compare instantaneous voltage, given by the stroke transducer "U", with control voltage U_0, strictly proportional to the current *i* - for supply of the torque motor windings.

The main criterion for the classification of such units is the response speed/time, directly dependent on the nature and type of flow distribution / flow control equipment.

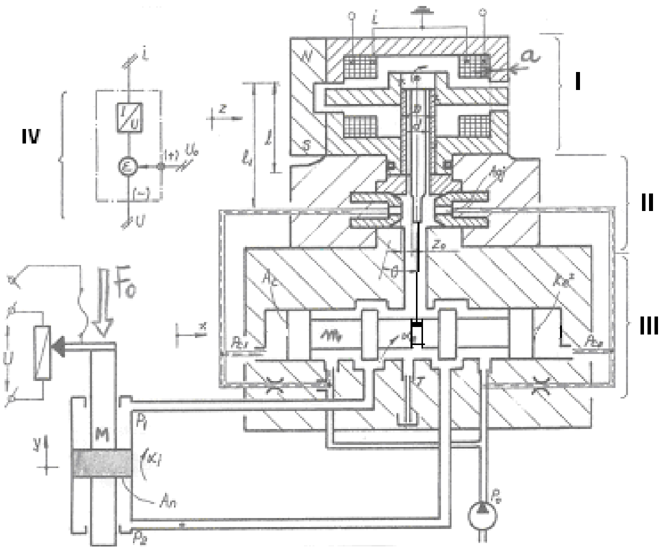

Fig.1

Table1

TYPE OF UNIT	TYPE OF ELEMENT	TRANSFER FUNCTION	TYPE OF DEVICE
SLOW	Proportional	$W(s)=k_{\xi}=\left.\frac{\partial x}{\partial t}\right\|_{t=0}$	Proportional directional control valve
NORMAL	Retarder- order I	$W(s)=\frac{k_{xi}}{T_{SV}\cdot s+1}$	Two-stage servo-valve
FAST	Retarder- order II	$W(s)=\frac{K_{xi}}{\left(\frac{s}{\omega}\right)^2+2D\left(\frac{s}{\omega}\right)+1}$	Three-stage servo-valve

2. Structure and functioning of a hydraulic axis

Classical structure of a hydraulic axis which aims to implement intelligence is shown in Figure 2. Operation of the unit is correlated with the aim of obtaining a high-precision positioning "y", via a control voltage U_0 – input into the system.

By adjusting the voltage $U_0(y_0)$ of the servo-controller (SC) through the control potentiometer and converting it into current, there is supplied the electric stage of the torque motor from the servo-valve (SW) which causes rotation by the angle θ and accordingly displacement "z" of the clack valve, figure 1, of the preamplifier. Thus there is adjusted the control pressure p_c of the amplifier sliding valve whose movement is "x". Displacement "x" adjusts the feed rate of the cylinder (CH), which produces a displacement thereof by "y". Displacement of the cylinder (CH) piston is strictly monitored by the displacement transducer (TD) which sends to the servo-controller (SC) a voltage U(y) continuously compared with the set / adjusted one $U_0(y_0)$. (SC) includes a module for calculating and amplifying the tracking error and a Dither signal generator.

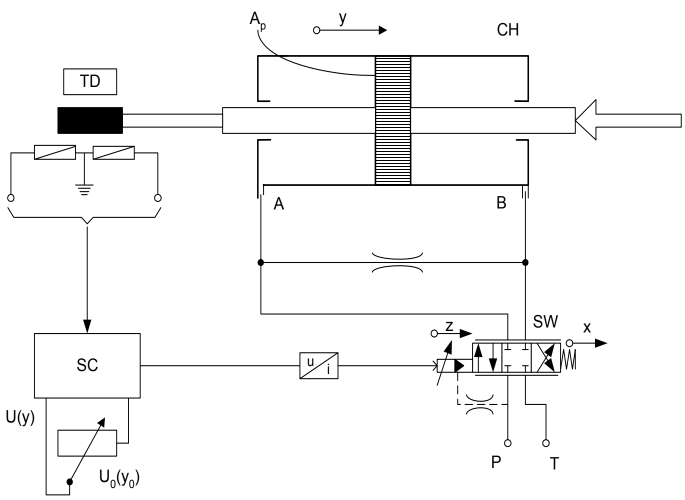

Fig. 2 Hydraulic axis – hydraulic diagram

CH: hydraulic cylinder;
TD: displacement transducer;
SW: servo-valve;

SC: servo-controller;
U(y): transducer voltage;
x: displacement of sliding valve;
y: motor / piston stroke displacement;
z: displacement of preamplifier clack valve.

3. The basic equations of the mathematical model for the hydraulic axis

- Flow rate through the servo-valve:

$$Q_{SV}(x,p) = k_{Qx} x \sqrt{1 - |x| \frac{P_A - P_B}{p}}$$, k_{Qx} - amplification factor (1)

- Equation of displacement of the sliding valve

$$\frac{1}{\omega_0^2}\ddot{x} + \frac{2 \cdot \xi}{\omega_0}\dot{x} + x = k_{xi} \cdot i \, , \qquad (2)$$

ω_0 - natural pulsation of the system, ξ - damping factor, k_{xi} - amplification factor;
- Equation of continuity of flows servo-valve - cylinder:

$$Q_{SV} = A_p \cdot \dot{y} + k_1 \cdot p + \frac{A_p^2}{R_H} \cdot \dot{p} \quad , \qquad (3)$$

A_p - area of the cylinder piston, R_H - hydraulic rigidity of the motor, k_1 - laminar flow coefficient;
- Equation of piston displacement in the hydraulic cylinder:

$$\ddot{y} + f_v \cdot \dot{y} + \omega_1^2 \cdot y = a_1 \cdot p + a_0 \quad , \qquad (4)$$

f_v - fluid viscous friction coefficient, ω_1 - natural pulsation at a hydraulic cylinder;
- Equation specific to the position transducer:

$$U = k_T \cdot y \, , \qquad (5)$$

k_T – transducer constant;
- Equation of electronic comparator:

$$\varepsilon = U_0 - U(y) \, , \qquad (6)$$

ε - setting error;

- Equation of power converter

$$i = k_{i\varepsilon} \cdot \varepsilon \, , \qquad (7)$$

$k_{i\varepsilon}$ - conversion factor.
Integration of the system consisting of the basic equations can be done:

- directly, with the linearized flow equation as:

$$Q_{SV} = k_{Qx} \cdot x - k_{op} \cdot p \, ;$$

- numerically, non-linear form, for different control voltages $U_0(t)$.

The integration of such a system has led to the following conclusions:
- choosing a higher power servo-valves ensures a faster response; transitional regime is non-periodic, and time constant $T_{ar} \sim 4 \cdot 10^{-2}$ s;
- sudden variation of force in the cylinder rod causes a negligible "slip" of the mechanical system (for instance - increasing from 0 ... 30 MPa in response to a step signal of a small amplitude leads to a temporary reduction of stroke of $5 \cdot 10^{-6}$ m for a stroke of $2 \cdot 10^{-3}$ m);
- at the same time constant response speed depends on the servo-valve size;
- at small inertial masses driven into moving instability issues do not occur.

ISSN 1454 - 8003
Proceedings of 2014 International Conference of Hydraulics and Pneumatics - HERVEX
November 5 – 7, Calimanesti-Caciulata, Romania

4. The transfer function of the device on an axis

$$H(s) = \frac{A_n \cdot k_Q^{II} \cdot H_{SV}(s)}{A_n \cdot k_T \cdot k_Q^{II} \cdot H_{SV} + \left[\left(\frac{W_n}{4E} \cdot s + \alpha_n\right) \cdot A(y) + A_n^2 \cdot s\right]} \tag{8}$$

If $\mathrm{H_{SV}} = \frac{\mathrm{k_0}}{1 + \mathrm{T_0} \cdot \mathrm{s}}$ equation (4.38) gets

$$H(s) = \frac{k_0 \cdot k_Q^{II} \cdot A_N}{A_n \cdot k_0 \cdot k_Q^{II} \cdot k_T + (1 + T_0 \cdot s)\left[\left(\frac{W_n}{4E} \cdot s + \alpha_n\right) \cdot \overline{A}(y) + A_n^2 \cdot s\right]} \tag{9}$$

In equation (9) the characteristic polynomial is of degree 4, in which case it can be analytically determined the optimum point of operation and the stability range.

5. Evaluation data of the system

Considering: E – the modulus of the fluid elasticity; M - the equivalent mass of the mobile assembly, y_{max} - maximum displacement stroke; A_n - section of the cylinder piston - Figure 3, shall be determined the characteristics of the servo-valve and the positioning accuracy of the system

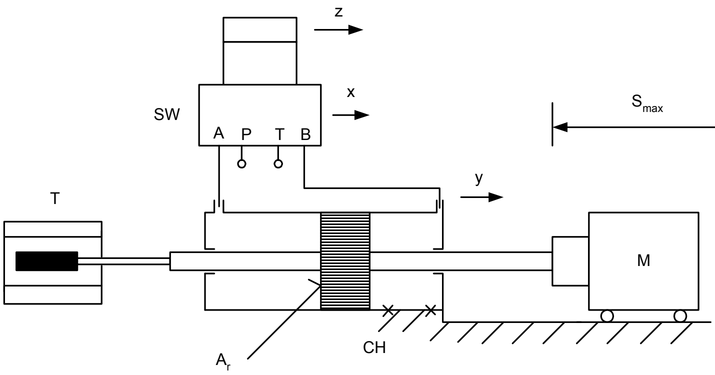

Fig. 3

Calculation of parameters:

- Own pulsation of the mobile assembly (ω_L) and the frequency (f_L):

$$\omega_L = \sqrt{\frac{4E \cdot A_n}{s_{max} \cdot M}} \text{ and } f_L = \frac{\omega_L}{2 \cdot \pi} \tag{10}$$

- Optimum amplification factor of the system (k_{Vop}) and time constant (T_S):

$$k_{Vop} = \frac{1}{3}\omega_L \text{ si } \mathrm{T_s} = \frac{1}{k_{Vop}} \tag{11}$$

- Possible acceleration time (T_B) and the total acceleration time (T_{tot}):

$$T_B = 5 \cdot T_S \quad \text{si} \quad \mathrm{T_{tot}} = 5 \cdot T_B \tag{12}$$

- Maximum speed of the system (Figure 4):

$$V = \frac{S_{max}}{T_{tot} - T} \tag{13}$$

- Flow required and the servo-valve pulsation (ω_v)

$$Q = A_n \cdot V \tag{14}$$

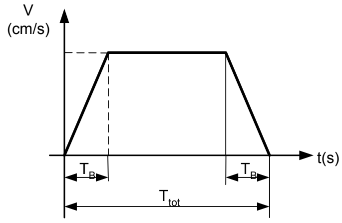

Fig. 4

There is selected a servo-valve with rated flow $Q_N \geq Q$ at Δp = 70 bar.
According to the diagram in Figure 5 for Q_N = 75 l/min, and sinusoidal control signal of amplitude 25% of the maximum amplitude (the curve marked with x), at a phase shift (φ- 90^0) and the frequency f_v there results the pulsation $\omega_V = 2 \cdot \pi \cdot f_v$

- Critical pulsation of the system (ω_{cr}), optimal amplification coefficient (k_{Vop})

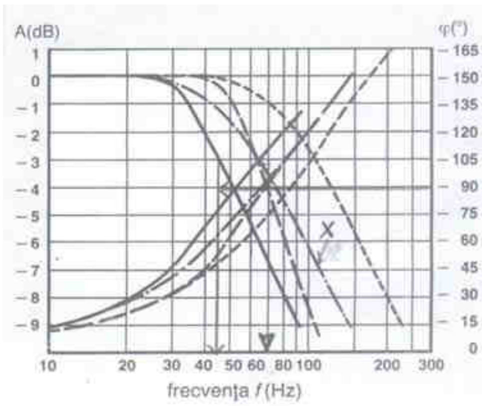

Fig. 5 The frequency characteristic

$\omega_{cr} = \dfrac{\omega_L \cdot \omega_V}{\omega_L + \omega_V}$ and $k_{Vop} = \dfrac{1}{3}\omega_{cr}$ (15)

- Servo-valve time constant (T_{SW}) and the maximum acceleration time (T_{BV})

$T_{SW} = \dfrac{1}{k_{Vop}}$ and $T_{BV} = 5 \cdot T_{SW}$ (16)

- maximum possible speed

$$v_{\max} = \frac{S_{\max}}{7 \cdot T_{BW}} \qquad (17)$$

- Maximum positioning error of the linear motor

$$\Delta S = \pm 0{,}05 \frac{v_{\max}}{k_{Vop}} \qquad (18)$$

For the numerically actual case:

$E = 1{,}66 \cdot 10^9 \left(\dfrac{kg}{m \cdot s^2} \right)$; $\mathrm{M} = 1000\,\mathrm{kg}; \mathrm{s}_{\max} = 0{,}1\,\mathrm{m}; \mathrm{A_n} = 1{,}96 \cdot 10^{-3}\,\mathrm{m}^2$ (corresponding to a linear hydraulic motor with bilateral rod, 70 mm piston diameter and 49 mm rod diameter) there results the flow required for servo-valve $Q \cong 1{,}225 \cdot 10^{-3} \dfrac{m^3}{s}$ (73 l/min) S.

There is selected a servo-valve with rated flow Q_n = 75 l/min at Δp = 70 bar. As in Figure 5, for Q_N=75 l/min and sinusoidal control signal of amplitude 25% of the maximum amplitude, the frequency which is reached at a phase shift φ - 90^0 , is: f_v = 70 Hz.

REFERENCES

[1]. Oprean A., Ispas C., Ciobanu E., Dorin Al. – Actionări şi automatizări hidraulice. Modelare, Simulare, Incercare/ *Automation and Fluid Power. Modeling, Simulation, Testing*. Technical Publishing House, Bucharest 1989;
[2]. Alexandrescu, N – Mechatronic Positioning System with Hydraulic Actuation - Proc International Conference on Multidisciplinary Desing in Engineering, Montreal, Canada, 2001;
[3]. Drumea, P., Matache, G., Rădulescu, G., - Echipamente mecatronice cu structură hidraulică/ *Mechatronic equipment with hydraulic structure* - HERVEX 1999 Confrence Proceedings;
[4]. Mircea Comes, Andrei Drumea, Adrian Mirea, Alexandru Marin, Servo-hydraulic actuator as a mechatronic system, MTM 2001, Romania;
[5]. Drumea, P., Comes, M., Mirea, A., Blejan, M. – Positioning systems tuning interface using proportional hydraulic drivers – The 4TH International Symposium For Informatics And Tehnology In Electronic Modules Domain, Bucharest, September 22 – 24, 1998;
[6]. P. Drumea, A. Mirea, A. Marin, P.Svasta - Quality control management for electro-hydraulic equipment with top dynamic performances– HRTC 2000 – The international Workshop 2000, March 13-14, 2000;
[7]. Adrian Mirea; Gabriel Rădulescu, Gabriela Matache – Cercetări teoretice asupra unităţilor de translaţie pe o axă / *Theoretical research on parallel displacement units on an axis*, International Symposium of Hydraulics, Pneumatics, Seals, Precision Mechanics, Tools, Devices and Specific electronic equipment, Mechatronics –HERVEX 2006;
[8]. *** - MOOG Catalogues.

ISSN 1454 - 8003
Proceedings of 2014 International Conference of Hydraulics and Pneumatics - HERVEX
November 5 – 7, Calimanesti-Caciulata, Romania

MODELLING AND VERIFICATION OF HYDRAULIC SYSTEMS INSIDE MECHANIZED HOUSING

Zygmunt DOMAGAŁA[1], Krzysztof KĘDZIA[1]

[1] Wroclaw University of Technology, Mechanical Faculty, Chair of Hydraulic Machines and Systems, zygmunt.domagala@pwr.edu.pl, krzysztof.kedzia@pwr.edu.pl.

Abstract: *The occurrence of dynamic phenomena in the form of shock (subsidence) is a consequence of mining exploitation and poses a threat to the safety of miners working as well as machines in the mine. The result of the mining activity is a violation of the balance of the rock mass, which leads to the release of energy accumulated in it. In paper was presented simulation model and results of the simulation. Then the results were compared with experimental data received during real tests on the hydraulic press.*

Keywords*: Simulation model, hydraulic props, relief valve.*

1. Introduction

An important reason for the occurrence of dangerous dynamic phenomena in the rock mass are technical factors, as the system operation or the stress concentration caused by the impact of exploitation, parameters of mining process such as the length and height of the walls and the speed of mining operations.

The second group of factors determining the seismic activity of the rock mass are the organizational factors directly related to the erroneous actions of man. In this group of factors can be distinguished: incorrect procedures of mining operations and do not take preventive measures that could prevent the threats.

Mining subsidence resulting in rock layers that lie above the excavation. This leads to cracking the sandstones. After crossing the stress border, the rock is breaking up. This type of processes occurring in rock mass layers trigger dynamic phenomena in the subsurface. Fig. 1. shows a diagram of disturbed rock mass occurring over exploited deposits [4].

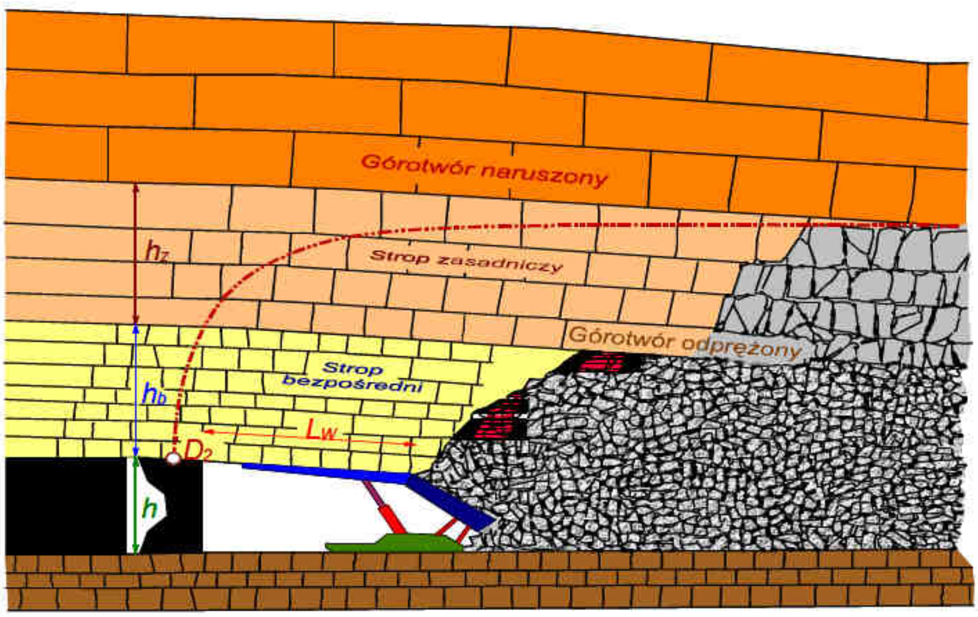

Figure 1. Schematic of disturbed rock mass occurring over exploited deposits [9]

Housing is an important component of mechanized longwall system. Valid choice affects the good state of maintenance of the excavation ceiling that determines the safety and effectiveness of operation [9].

Exploitation of coal mostly carried out by caving, so for this kind of exploatation, there are the largest number of different types of housing [8]. In the paper authors analyzed the dynamic phenomena occurring in hydraulic props of mechanized housing, which is shown in Figure 2.

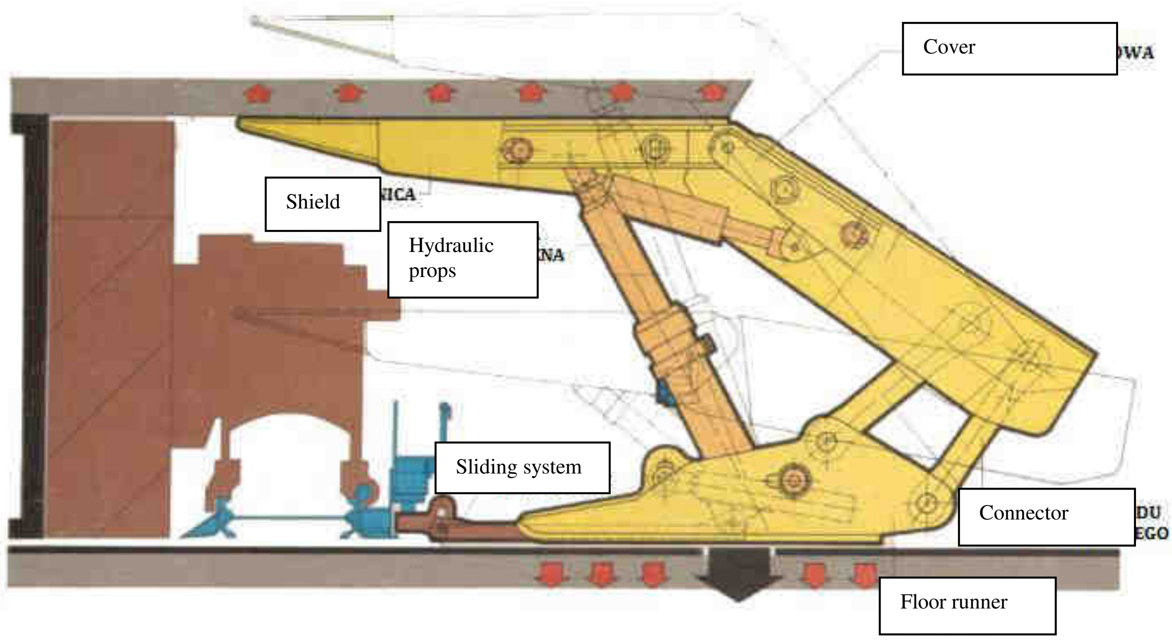

Figure 2. Mechanized housing.

Double telescopic stands (hydraulic props) are typically used in enclosed excavations of variable height of the deck.

This paper presents an analytical method for determining the hydraulic props load based on discrete mathematical model. The model was verified during experimental tests carried out on a hydraulic press at Stalowa Wola Ironworks.

2. Mathematical model

A mathematical model was build assuming a discrete distribution of mass and elasticity, with limitations of the MATLAB Simulink software. The hydraulic system of mechanized longwall consists of many components (actuators, pipes, pumps, tank, valve block). In order to simplify the mathematical model and simulation the number of circuit elements was reduced. Schematic of the reduced hydraulic system is shown in Figure 3.

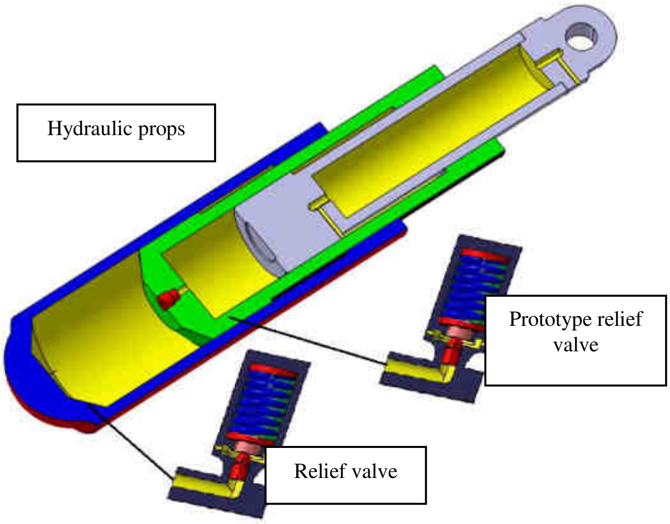

Figure 3. Simplified diagram of the modeled system - the idea [source: own]

The hydraulic cylinder is equipped with overflow valve with prototype disc spring in second stage.

2.1. Simplification assumptions

Creating a mathematical model was possible by the adoption of simplifying assumptions, allowing the representation of a real object with the required accuracy.

The following assumptions:

- sink side pressure is constant,
- modulus of elasticity, density and viscosity did not change during operation of the system,
- the force of gravity does not affect the operation of the system,
- hydraulic components are non-deformable,
- relief valve springs have linear characteristics,
- mass and elasticity parameters are as concentrated parameters,
- dry friction that occurs between the moving surfaces was omitted,
- there is no cavitations in the system,
- spring elements weight of hydraulic props is defined as 40% of the total spring weight.
-

2.2. The mathematical model of the hydraulic props

The nomenclature which was used in mathematical equations are shown below on Figure 4.

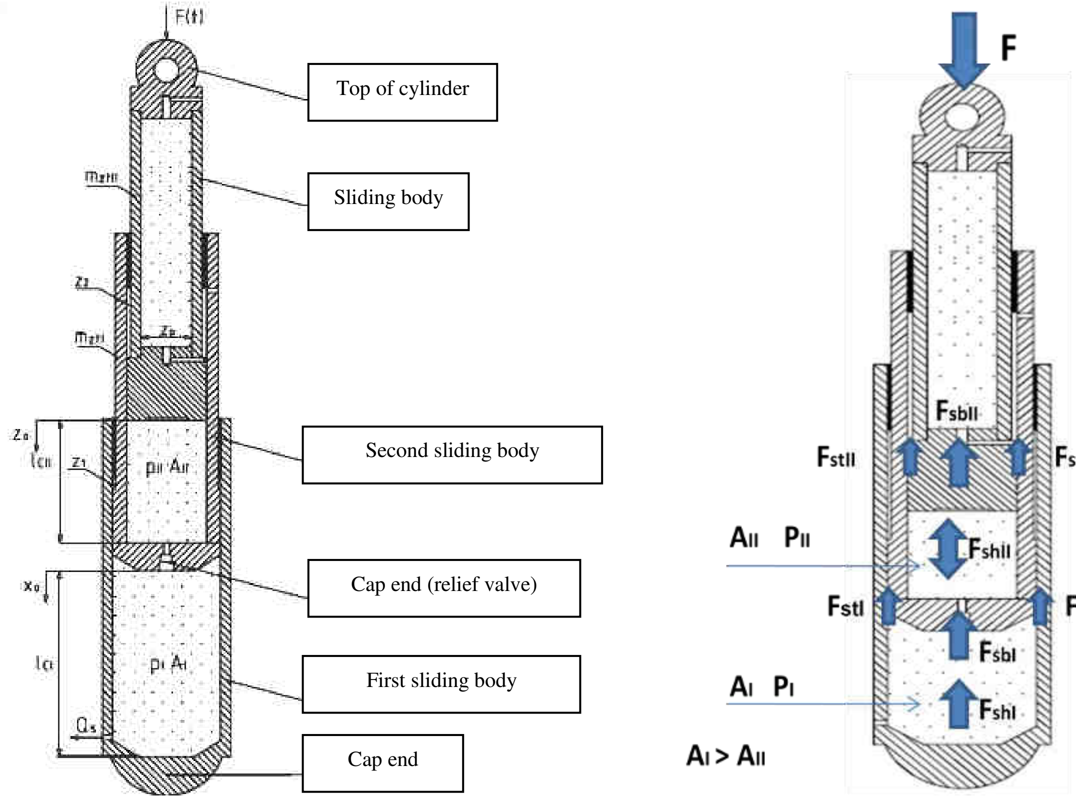

Fig. 4. Hydraulic props [source: own]

- **The equations of the forces acting on the hydraulic props**

The equations of the forces acting on the hydraulic props:

$$F(t) - F_{sbII} - F_{stII} - F_{shII} = 0 \quad (1)$$

$$P_{II}(A_{II} - A_d) - F_{sbI} - F_{stI} - F_{shI} = 0 \quad (2)$$

where:
F_{sb} – inertia force of the stand,
F_{st} – viscous friction force,
F_{sh} – the force exerted by the pressure on the piston surface,
F(t) – the force of the rock mass.

Equations (1) and (2) are considered for the following initial conditions:

$$x = x_{gr}, \quad \frac{dx}{dt} = 0, \quad \frac{d^2x}{dt^2} = 0, \quad z = 0, \quad \frac{dz}{dt} = 0, \quad \frac{d^2z}{dt^2} = 0$$

and for the following boundary conditions:

$$x = x_{gr}, \quad \frac{dx}{dt} = 0, \quad \frac{d^2x}{dt^2} = 0, \quad z = z_{gr}, \quad \frac{dz}{dt} = 0, \quad \frac{d^2z}{dt^2} = 0$$

- **The equation of forces acting on the overflow valve plug I**

Figure 5 shows schema of overflow valve with nomenclature used to create the mathematical model.

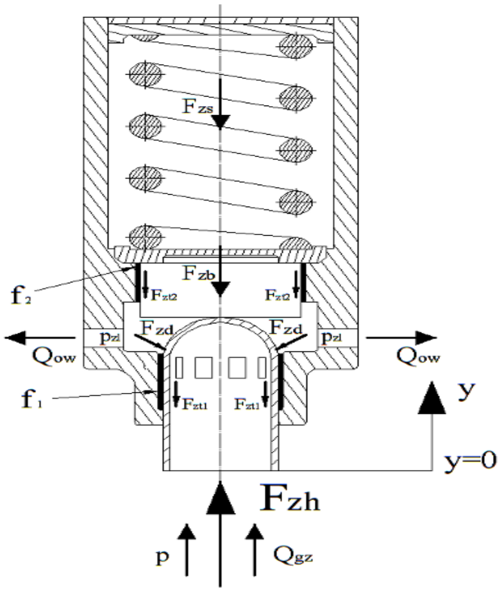

Figure 5. Diagram of the overflow valve [source: own]

The equation of forces acting on the overflow valve plug is:

$$F_{zh} - F_{zb} - F_{zt} - F_{zs} - F_{zd} = 0 \tag{3}$$

where:
F_{zh} - the force exerted by the pressure on the overflow valve plug,
F_{zb} – inertia force,
F_{zt} - viscous friction force,
F_{zs} - force from the deflection of the spring,
F_{zd} - hydrodynamic force.

These equations are considered for the following initial conditions:

$$y = 0,\ \frac{dy}{dt} = 0,\ \frac{d^2y}{dt^2} = 0$$

and for the following boundary conditions:

$$y = y_{gr},\ \frac{dy}{dt} = 0,\ \frac{d^2y}{dt^2} = 0$$

- **Flow equation through the under valve plug chamber**

$$\mathrm{Q_{gz}} - \mathrm{Q_{cp}} - \mathrm{Q_{gp}} - \mathrm{Q_{w}} = 0 \tag{4}$$

where:

Q_{gz} – the intensity of the stream flowing through the valve plug,
Q_{cp} – flow due to compressibility of fluid in the under- valve plug chamber,
Q_{gp} – flow due to displacement of the valve plug,
Q_{w} – flow rate through the under valve plug chamber.

Along with the movement of the valve plug surfaces of the openings through the fluid flows is changed. The relationship is shown in equation 5. It illustrates the variation of the surface as a function of displacement of the valve plug "y".

$$A_{0g} = \frac{r_1^2}{2}\left[arccos\left(\frac{2(r_1-y)^2}{r_1^2}-1\right)-\sin\left(arccos\left(\frac{2(r_1-y)^2}{r_1}-1\right)\right)\right] \tag{5}$$

where: r_1 - radius of the orifice in the valve plug.

- **The equation of forces acting on the valve plug of the second prototype relief valve II.**

The equations of forces and flow rates for the second overflow valve of the prototype are the same, except that the relief valve plate spring characteristics is shown in Figure 6.

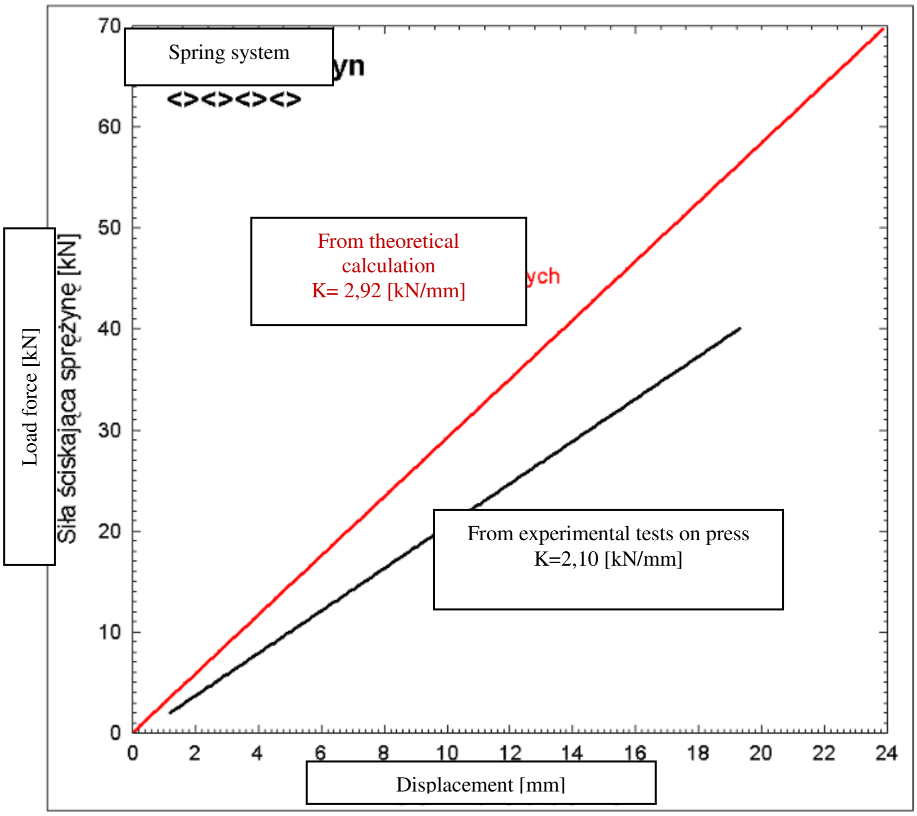

Figure 6. The spring stiffness determined theoretically and experimentally measured [source: own]

- **The equation of flow ratio in modeled system**

Figure 7 shows a schematic of the modeled hydraulic system with accepted symbols:

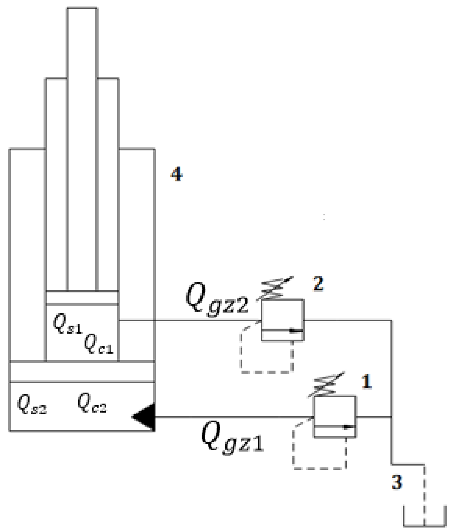

Figure 7 Schematic of the modeled system, with marked flow rates [source: own]

$$Q_{s1} - Q_{gz1} - Q_{c1} - Q_{g1} = 0 \quad (6)$$

$$Q_{s2} - Q_{gz2} - Q_{c2} - Q_{g2} = 0 \quad (7)$$

where:

Q_s – liquid flow caused by the movement props rod,

Q_c – liquid flow caused by the compressibility under the props piston,

Q_g – liquid flow ratio due to displacement of the valve plug,

Q_{gz} – the flow ratio through the valve plug.

3. Simulation model

Simulation studies were made in Matlab Simulink software. This program allows to perform numerical calculations, algorithms testing, modeling, simulations and making data analysis and visualization.

3.1. Block diagram of the hydraulic system

Designed subsystems (fig. 8) could be a components of other simulation research. It could be achieved due to greater transparency of created simulation models.

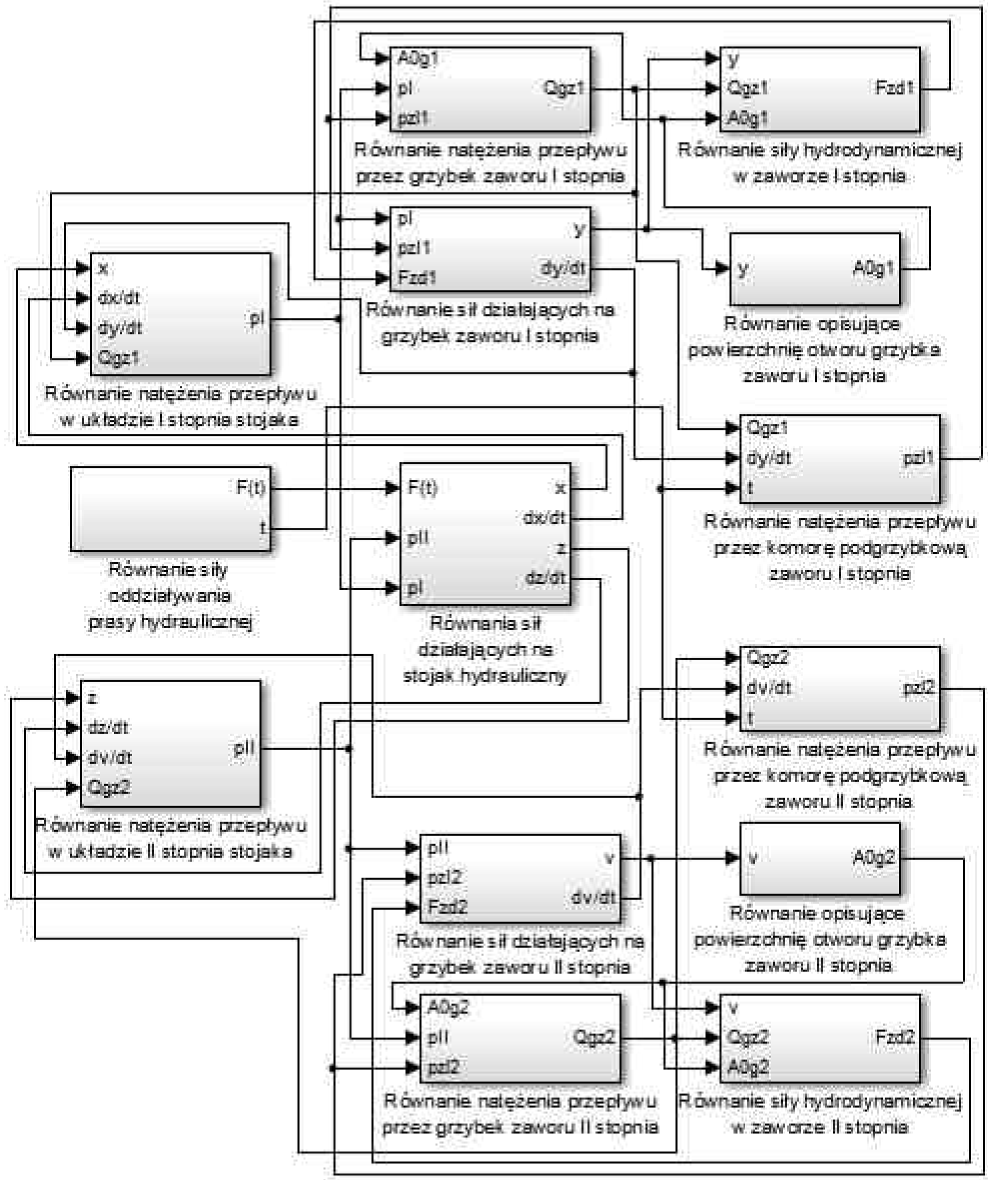

Figure 8. Block diagram of the hydraulic system [source: own]

4. Experimental test stand.

The simulation model was validated on base of experimental tests conducted in HSW Stalowa Wola.

The purpose of the comparison was:
- operation of the overflow valve in the conditions in which it is located,
- determine the flow ratio (throughput) of the valve,
- determine the pressure opening and closing of the valve.

Research program included a test of compression process of stands for different speeds. Compression process of stands necessitated of opening external hydraulic relief valve.

The test stand consisted of three systems:
- mechanical system of forging press (adapted for the purposes) ,
- hydraulic venting and positioning control system
- measuring system.

For the compression process of props was used forging press used in HSW Stalowa Wola for crushing and forging steel ingots.

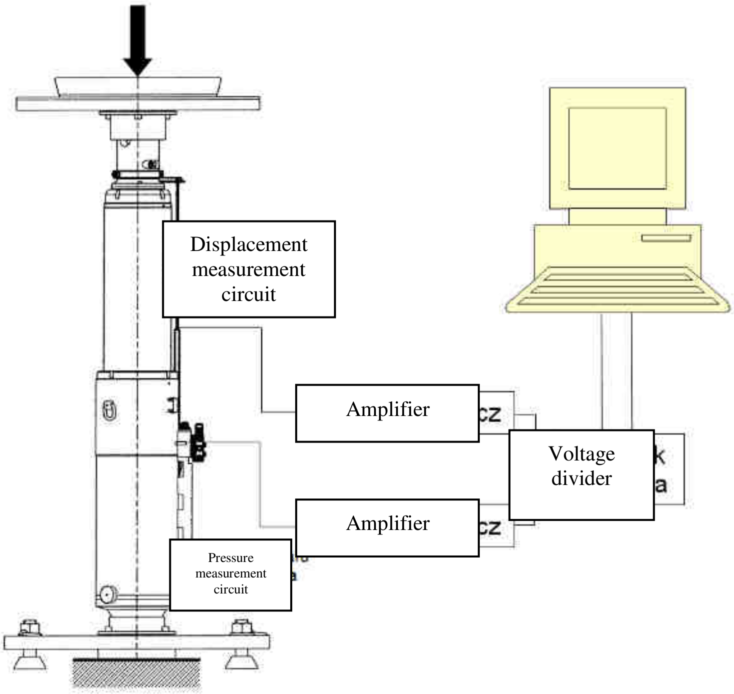

Figure 9. Schematic of the measurement system used to verify telescopic cylinders [3] [4]

Measurements of the stand was conducted for speed of 10%, 20%, 30%, 40%, 50%, 60%, 70%, 80%, 90 % and 100% of its maximum capabilities.

5. Verification of the mathematical model

To determine the accuracy of the model, authors compared received results with experimental ones contained in the paper [4]. For the relief valve was performed three trials measuring:

- the first (valve opening pressure of the second stage - try 31),
- the second (valve opening pressure of the second stage - try 45),
- the third (valve opening pressure of the second stage: the sample 39).

As a result, it was possible to examine the accuracy of the mathematical model and the created simulation model for various input parameters. Below are charts describing the course of the change in the operating system, and discussion of the results.

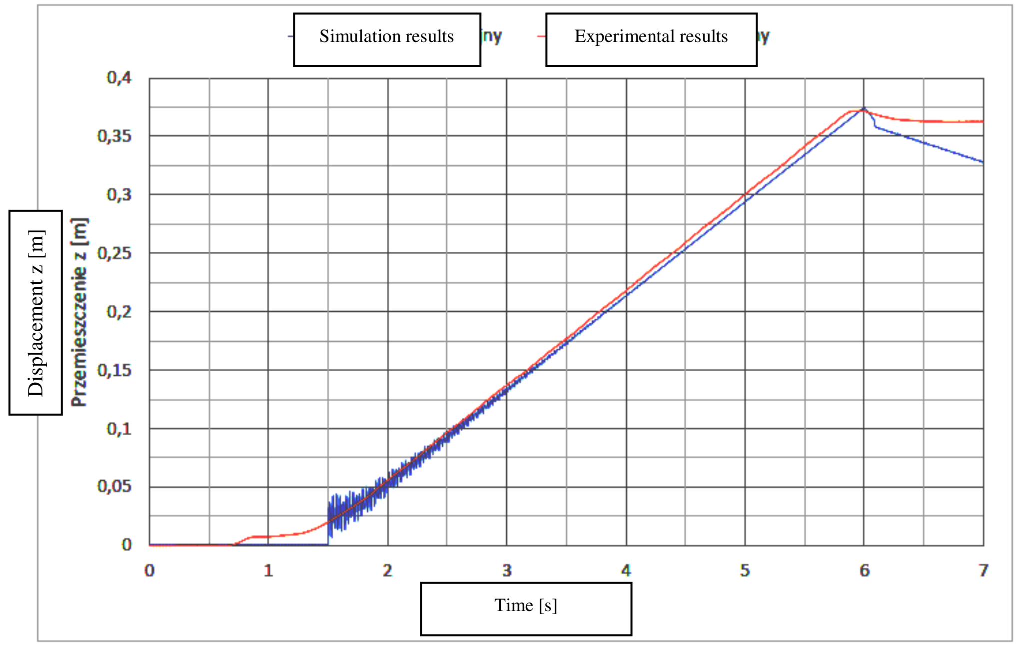

Figure 10. Displacement of second sliding body of hydraulic props - for the sample 31 [source: own]

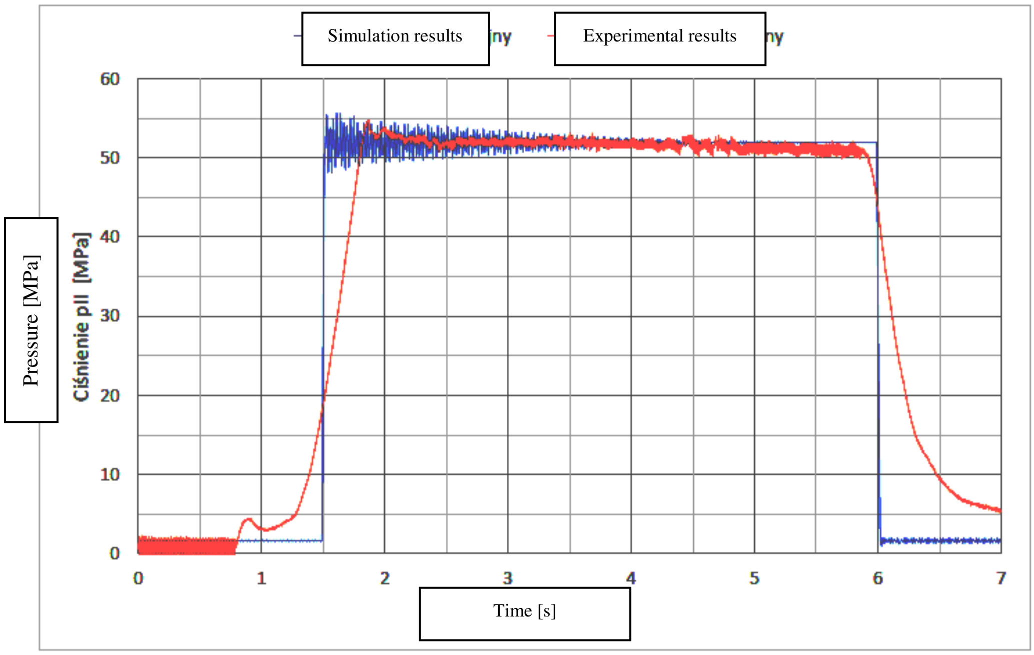

Figure 11. The pressure profile in the second sliding body of hydraulic props- the sample 31 [source: own]

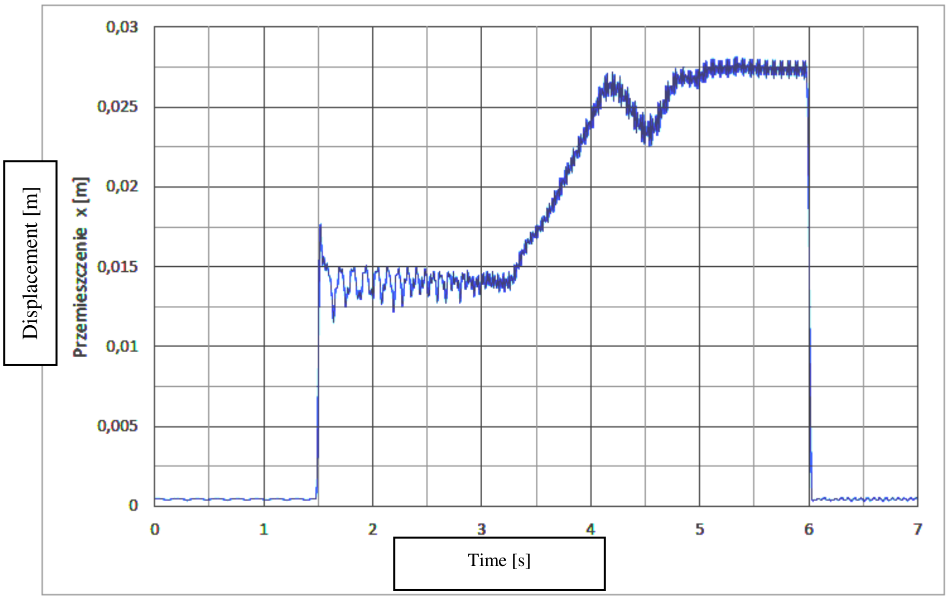

Figure 12. Displacement of first sliding body of hydraulic props- for the sample 31 [source: own]

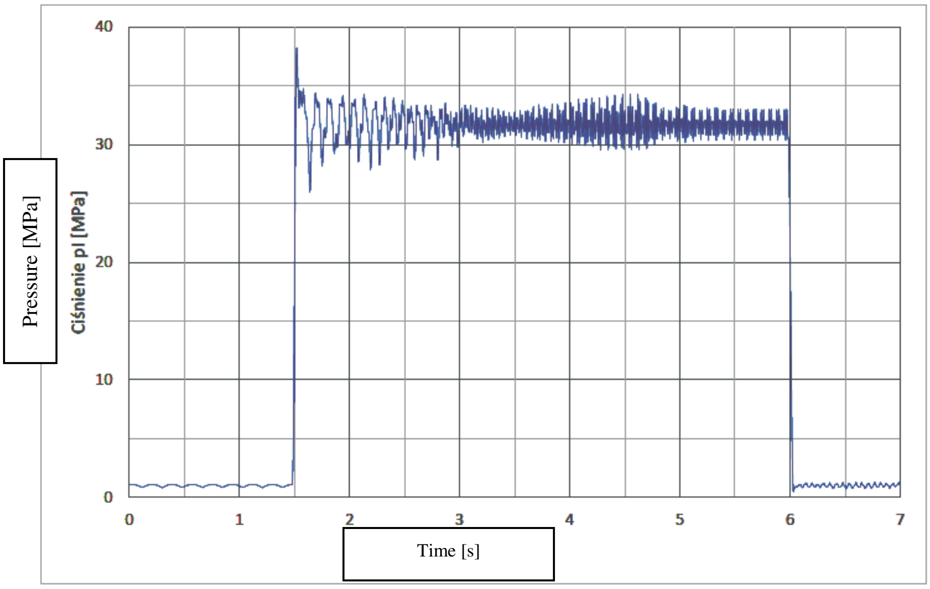

Figure 13. The pressure profile in the first sliding body of hydraulic props- for the sample 31 [source: own]

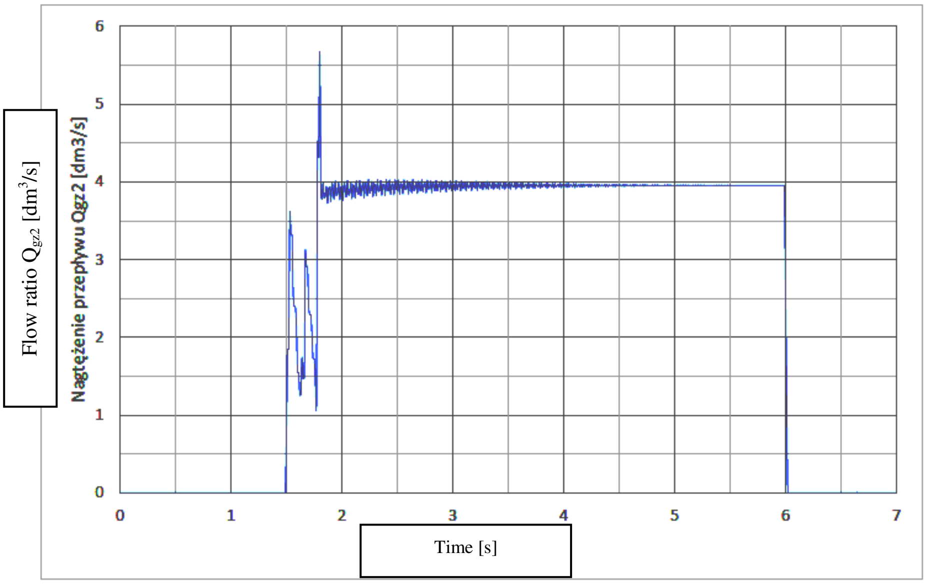

Figure 14. The flow rate through valve disk of second sliding body of hydraulic props- the sample 31

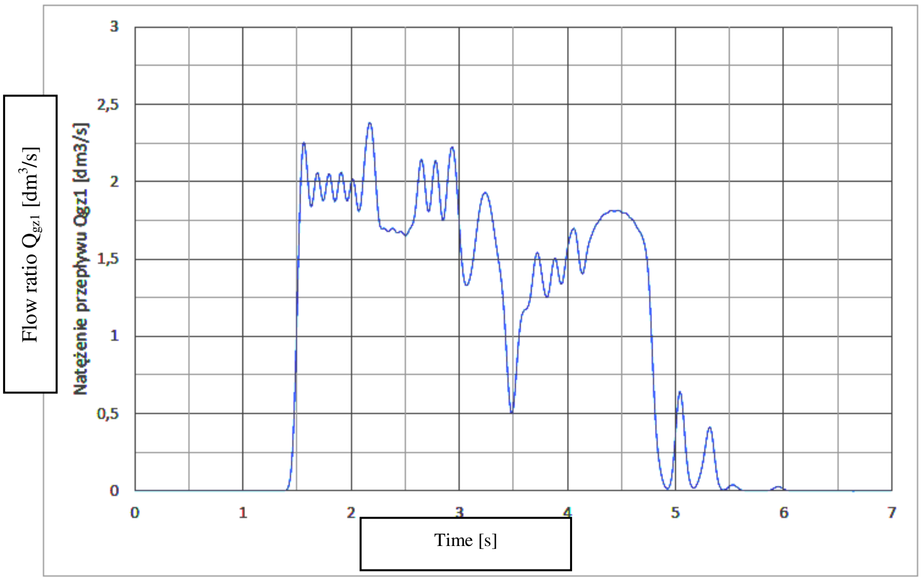

Figure 15. The flow rate through the valve disk of first sliding body of hyd. props- the sample 31 [source: own]

The figures from 10 to 15 shows the changes of the three simulation parameters (displacements, pressure and flow rate through the overflow valve) for hydraulic props. Figure 10 and Figure 11 include both: simulation as well as experimental results obtained for test no 31. Comparison of these waveforms allows the assessment of the correctness of the used mathematical as well as simulation models of the hydraulic system.

Carried out a comparative analysis of simulation results with experimental results showed compliance of displacement and pressure waveforms of second sliding body of hydraulic props.

The biggest discrepancies occurred on the beginning and at the end of simulation. The main reason for these discrepancies was simplification assumptions of the force acting to hydraulic props. In simulation model the load force was increased very fast, which is inconsistent with its actual course.

Therefore, the model was modified. In this approach the load is a series of linear loads. The results of the simulation are shown in Figure 16.

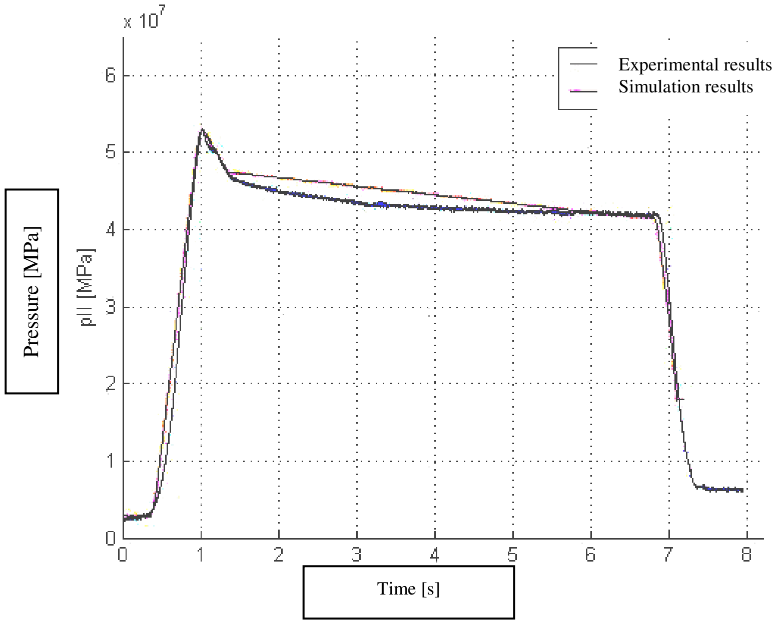

Figure. 16. The pressure profile in the second sliding body of hydraulic props- for the sample 41 [source: own]

The more accurate model of load improved the accuracy of received results.

6. Conclusions

The proposed method for determining the dynamic phenomena in the hydraulic props equipped with relief valves can get results similar to the experimental tests results. Tests by using presses is much cheaper and more convenient to use. It can also be used to assess the suitability of different construction props designed to absorb dynamic loads in different operational conditions.

REFERENCES

[1] Domagała Z.: Modelowanie i symulacja zjawisk zachodzących w zmechanizowanej obudowie ścianowej. Maszyny Górnicze. 2009, nr 4

[2] Domagała Z., Prokopowicz J.: Analiza zjawisk dynamicznych zachodzących w hydraulicznej podporze górniczej w warunkach gwałtownego zaciśnięcia wyrobiska. Górnictwo Odkrywkowe. 2010,

[3] Domagała Z., Marianowski J. Modelowanie i weryfikacja zjawisk dynamicznych zachodzących w teleskopowych stojakach hydraulicznych", „Badanie, konstrukcja, wytwarzanie i eksploatacja układów hydraulicznych, Gliwice 2013

[4] Kalukiewicz A., Marianowski J., Kipczak P.: Przeprowadzenie badań stanowiskowych stojaka do upodatniowej obudowy dużej podporności. AGH Kraków czerwiec 2010. Umowa 5.5.130.900/TK/54/10 [niepublikowane].

[5] Kalukiewicz A., Marianowski J., Kipczak P.: Wykorzystanie prasy kuźniczej do badań stojaków obudowy zmechanizowanej o dużej podporności. KOMTECH 2010 Innowacyjne techniki i technologie dla górnictwa. Bezpieczeństwo – Efektywność – Niezawodność. Monografia. Instytut Techniki Górniczej KOMAG Gliwice 2010, s.405- 414.

[6] Marianowski J.: Siła hydrodynamiczna w charakterystyce zaworu ciśnieniowego. Hydraulika i Pneumatyka. 2011 R. 31 nr 2 s. 12–15.

[7] Marianowski J.: Gdzie ukryła się siła hydrodynamiczna w charakterystyce zaworu ciśnieniowego. Badanie, konstrukcja, wytwarzanie i eksploatacja układów hydraulicznych. Praca zbiorowa. Monografia. Gliwice : Instytut Techniki Górniczej KOMAG, 2010 CYLINDER 2010 s.111–122.
[8] Stoiński K.: Obudowy górnicze w warunkach zagrożenia wstrząsami górotworu, Wydawnictwa GIG, Katowice 2000.
[9] Jaszczuk M., Ścianowe systemy mechanizacyjne, „Śląsk” Wydawnictwo Naukowe, Katowice 2007
[10] Stryczek S.: Napęd hydrostatyczny Tom 1,2 WNT Warszawa 1995.
[11] Domagała Zygmunt, Kędzia Krzysztof, Prokopowicz Jarosław, Popczyk Zygmunt: Simulation of dynamic phenomena in hydraulic prop for wall lining. Hervex 2009, Calimanesti - Caciulata, 18-20 November 2009.

ISSN 1454 - 8003
Proceedings of 2014 International Conference of Hydraulics and Pneumatics - HERVEX
November 5 – 7, Calimanesti-Caciulata, Romania

USING REAL TIME SIMULATION FOR OFF-LINE TESTING OF ELECTRO HYDRAULIC FORCE CONTROL SYSTEM

Ph.D. eng. Dragos Daniel ION-GUTA[1]

[1] INCAS - The National Institute of Aerospace Research “ELIE CARAFOLI”, Bucharest, Romania

Abstract: *Using the methods of real time simulation of the processes the scientists and technical designers may shorten the period of development of the applications from various fields. These methods offer the possibility of optimization of the functional systems depending on the criteria of performance imposed. The present paper presents a generic application of real time simulation of the electro hydraulic servomechanisms. This was developed for determining rapidly the dynamic characteristics of the studied servo systems.*

Keywords*: HIL, real time simulation, electrohydraulic servomechanisms*

1. Real time systems

Real time simulation of the systems is very well applied in the area of complex applications, where some phenomena are still not theoretically well grounded or where the degree of complexity of the mathematical models is very high. Benefiting from the means of process identification and the power of computers, researchers can shorten the application development period in several domains, by generating a solution that is close enough to reality starting from the design phase.
Introducing computers in supervising and leading processes determination the change of the technological systems. The high degree of flexibility they offer allows the
“software optimization” of the systems. In this context, the opportunity of using hybrid simulators is highlighted, one part mathematical models and another part – physical system. This concept appears in technical literature as “hardware in the loop - HIL”.
Using Industrial Computers in order to Control Automatic Processes Adjustment Systems
The thorough knowledge of the hardware components specific to the real time systems leads to the efficient use of soft and hard resources. Although as far as programming is concerned, they prefer developing programs without going to details regarding the machine they run on, in the field of real time systems this cannot be achieved.

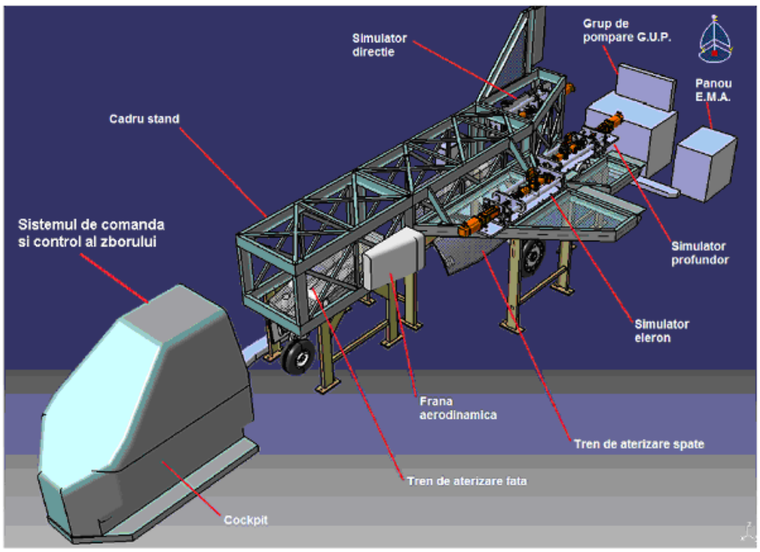

Fig.1. HIL (hardware in the loop) Iron-Bird test platform
Autopilot testing in the virtual environment

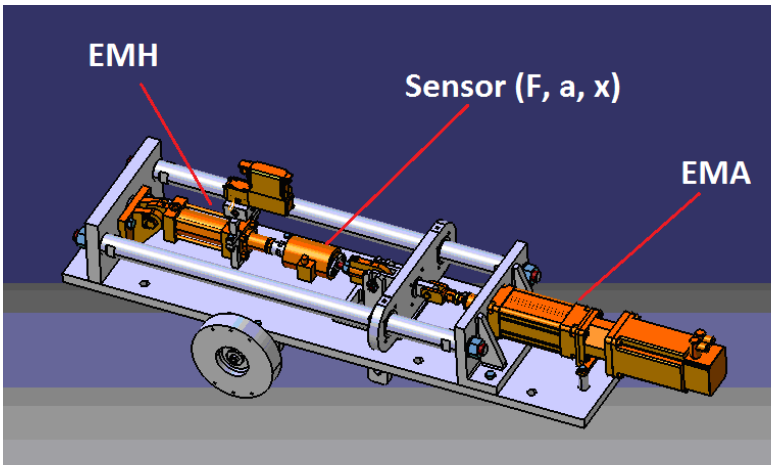

Fig.2. The system testing and its first implementation will be conducted on the real time Bird Iron flight simulation bench - available in the laboratories of the Systems Department of INCAS (Fig. 1.)

Real Time Simulation of the Automatic Adjustment Systems

Currently, it is hard to imagine the analysis of a complex dynamic system without benefiting from the possibility to shape/simulate that system. Shaping and simulating dynamic systems are highly used techniques in the computer assisted analysis of the systems, representing at the same time an important step in the process of calculus system assisted conception.
The numerical simulation of the dynamic systems represents the process that leads to obtaining, with the help of the numeric calculator, information regarding the behavior in time of the systems' characteristic sizes.
Real time simulation of the systems represents the capacity of some calculus systems to perform numerical simulation in very short time intervals.
Real time simulation of the automatic adjustment systems usually implies simulating the command mode in order to test its functionality and performances. Also, it is a way to identify the possible situation when some malfunctions may occur. Another important aspect of the RT simulations is the possibility to simulate the subsystems. Thus, one may create hybrid simulation networks that include real subsystems and real time simulated subsystems.

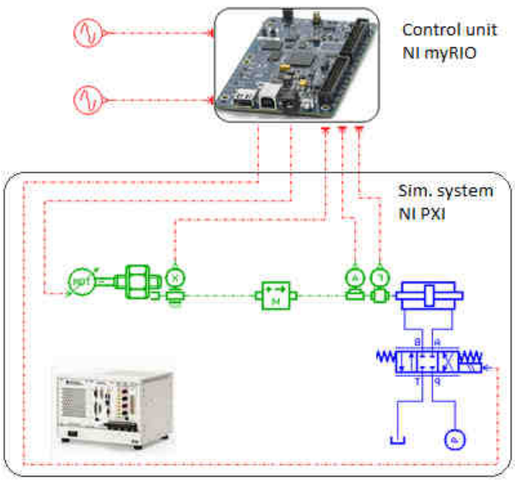

Fig.3. RT sim

Figure 3 shows a RT simulation application of an electro-hydraulic process. In this application, the operation system, electro-hydraulic component, was mathematically adjusted in real time with an advanced simulation language, and as part of the command the industrial controller was used. This means of adjustment/simulation of the system allowed both online tuning of the regulator, without using the due subsystem, and easy change of the electro-hydraulic subsystem features, in order to optimize it.

2. Modern architectures of the real time process simulation systems

In order to develop real time simulation applications, one may choose the necessary hardware and software components out of a large range offered by specialized companies. Among these offers, we may highlight the IPG-Automotive, PXI National-Instruments and Adwin systems.
IPG_Automotice offers a series of services and equipments for hardware in the loop simulations, especially for the automotive area. With the help of the real time simulation systems they offer, one may proceed to complex simulations regarding the dynamic behavior of automobiles, motorcycles and trucks. IPG-Automotive offers solutions for performing analyzed systems simulations, performing tests as well as technical support. For RT simulations, IPG-Automotive recommends the “CarMaker/HIL” component. This helps to perform both simulation typical to the automobile components and simulation of electronic control units systems (ECU)
PXI defines a robust calculus platform for the measurement and automation applications. The PXI modular tools benefits from the advantages of the PCI (Peripheral Component Interconnect) high speed thoroughfare, which represents the de facto standard that leads the PC design, both hardware and software. Consequently, the PXI users can benefit from all the PCI advantages within an architecture that adds mechanical, electrical and software features, suitable for measurement applications, data acquisition and industrial automation. Entirely based on an open industrial standard, the PXI modular instrumentation represent an efficient solution, as it combines the high speed electrical architecture of the PCI with an industrial high reliable case, synchronizing functions, incorporated temporization and full inter-use with
Compact PCI. The reduced size of the PXI system is ideal for a large variety of portable 2 desk or rack applications for testing, measuring, data collection and industrial automation.

The PXI Real Time Controllers

The real time option of the well known LabVIEW graphic development environment expands its possibilities of creating real time incorporated systems that use smart measurement tools form the National Instruments. These include the inserting acquisition boards with own microprocessor, the PXI controllers and the FieldPoint network modules family. The PXI controllers of the Real-Time series are different form the usual ones, because they have a hard drive with Run Time LabVIEW engine, running thus, instead of Windows, a real time operating system. The Real-Time controllers may run along with Windows, the two environments having the possibility to communicate.
The Adwin systems are process controllers designed for data acquisition and fast automation applications. The applications developed by means of the ADwin systems are real time executed. The values of the acquisitioned signals and the events measured by these applications can be processed in certain periods of time. The ADwin systems have analogical and digital input/output (I/O) modules, a local processor,
SHARC RISC or DSP and local memory. All the ADwin equipments have a local processing unit and memory. An ADwin equipment has one of the three 32 bits RISC processors that are compatible with the cards. The specialized processing unit ensures the calculus and processing power for the high speed real time applications. As powerful the equipment is due to its architecture, the easy to program it is. The software used in programming this equipment is ADbasic.

ISSN 1454 - 8003
Proceedings of 2014 International Conference of Hydraulics and Pneumatics - HERVEX
November 5 – 7, Calimanesti-Caciulata, Romania

3. The real time simulation of the electro-hydraulic adjustment systems

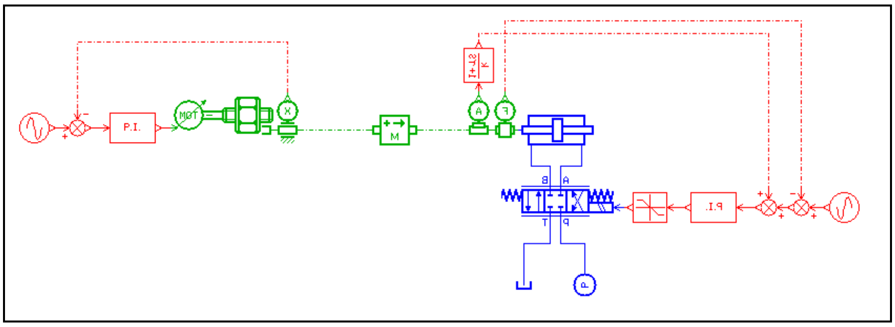

Fig. 4. Electro hydraulic force control system

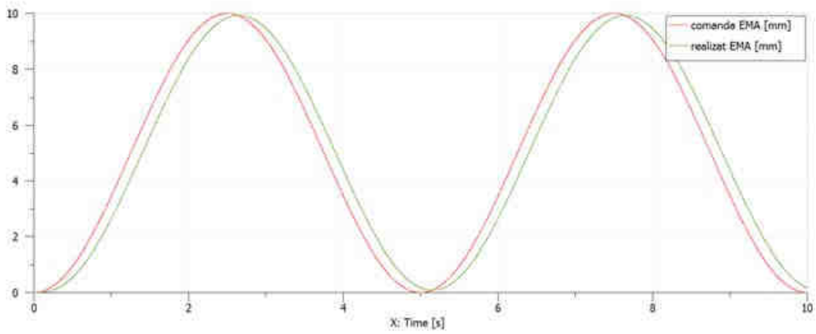

Fig. 5. Comanda / realizat pozitie EMA

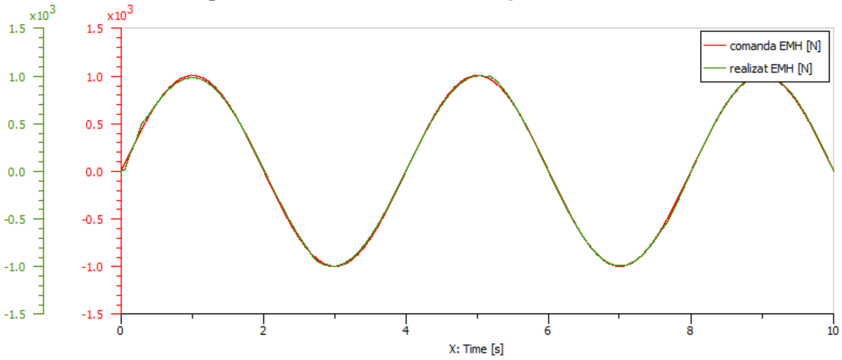

Fig. 6. Comanda / realizat forta EMH

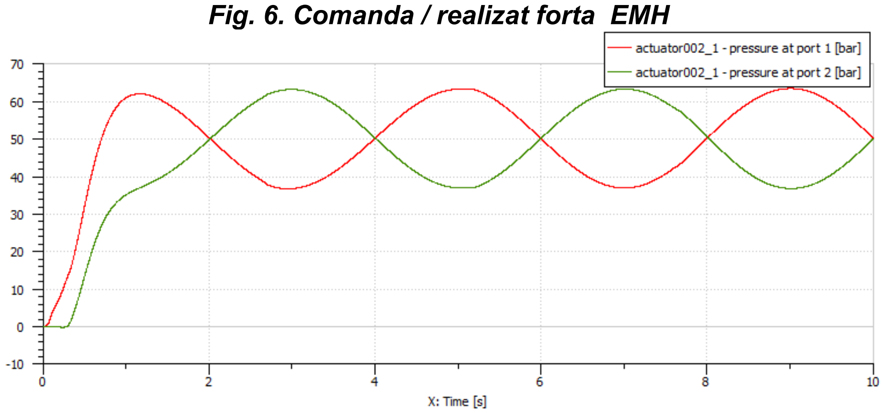

Fig. 7. Presiune PA / PB motor hidraulic liniar EMH

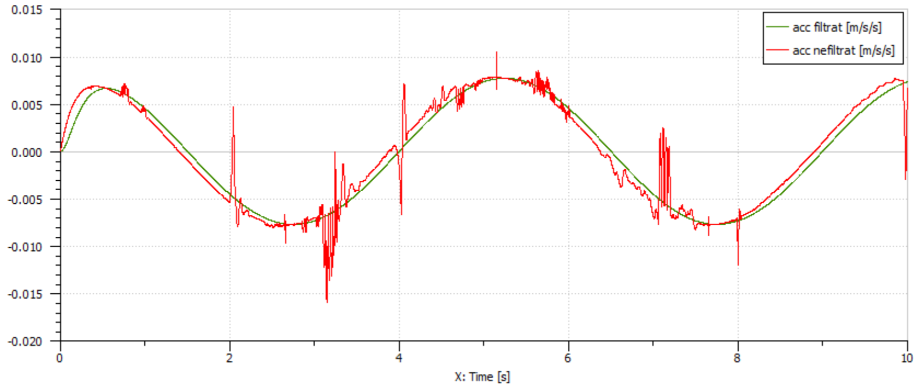

Fig. 8. Semnal acceleratie filtrat/nefiltrat

Mathematical model of an electrohydraulic servomechanism with position response(fig. 3) comprises the following equations:

- Equation of slide valve displacement

$$\frac{x(s)}{i(s)} = \frac{K_{xi}}{(s/\omega_n)^2 + 2s\zeta/\omega_n + 1}$$

- Equation of position transducer

$$\mathrm{U_T} = \mathrm{K_T y}$$

- Equation of electronic comparator

$$\varepsilon = U_0 - U_T$$

- Continuity equation of subsystem directional control valve-hydraulic cylinder

$$Q_{SV} = A_p \dot{y} + K_l P + \frac{A_p^2}{R_h}\dot{P}$$

- Equation of current generator of proportional compensator

$$\varepsilon = U_0 - U_T$$

- Motion equation of hydraulic cylinder's piston

$$m_c \ddot{y} = F_p - F_a - F_e - F_f$$

$$F_p = A_p P$$

$$F_a = K_f \cdot v$$

$$F_e = 2(K_{e1} + K_{e2})(y + y_{0e}) = 2K_e(y + y_{0e})$$

- Characteristic of directional control valve

$$Q_{SV}(x,p) = c_d A(x)\sqrt{\frac{p_S - signx \cdot P}{\rho}}$$

The simulated model of the system was implemented by means of the Real Time Toolbox in LabVIEW. This component of LabVIEW language allows runnind simulation with real time constrains. The constraint were imposed by control module (developed also with LabVIEW on PXI machine). The objective of these attempts was to validate the simulated model, with the purpose of using it to develop an “embedded” simulator of the electro hydraulic control system. This simulator's utility derives from the necessity to give preliminary control law coefficients.

4. Conclusions

The use of the virtual instrumentary allows the fast acquirement of the information of interest regarding the dynamic of the hydraulic regulation systems, the automation of the study process and the optimization of the processes on the groundwork of the performance criteria required. Real time simulation of the analyzed system presents obvious advantages. One may test, with a low level of risk, different ways of adjustment and control. Although tuning on site is inevitable, the real time analysis process allows the decrease of the time necessary for tests and tuning in the real process. The decrease of time necessary for achieving these objectives leads to minimizing costs and, at the same time, decreasing the possibility of physical damage of test equipment.

REFERENCES

[1] Experimental identification of electrohydraulic servomechanism with virtual instruments technique, Ion Guta Dragos, Catalin Dumitrescu, Ioan Lepadatu, Corneliu Cristescu, Hidraulica nr.3 / 2010, ISSN 1453-7303, pag.49-56.
[2] Utilizarea sistemelor de actionare electrohidraulice la executia amenajarilor hidroelectrice, UPB Teodor Costinel POPESCU, Dragos Daniel ION GUTA, Constantin CALINOIU, U.P.B. Dorin Pavel 2010.
[3] Research on the stability of electrohydraulic servomechanisms developed with electrohydraulic amplifiers of variable area gradient, Dragos Daniel Ion Guta, Ioan Lepadatu, Teodor Costinel Popescu, Catalin Dumitrescu, The fifth international conference on optimization of the robots and manipulators - OPTIROB 2010, ISBN 978-981-08-5840-7, pag.141-145.

ISSN 1454 - 8003
Proceedings of 2014 International Conference of Hydraulics and Pneumatics - HERVEX
November 5 – 7, Calimanesti-Caciulata, Romania

SELF-ORGANIZING, COMPLEX COMMUNICATION SYSTEM

Krzysztof STANKIEWICZ[1]

[1]Institute of Mining Technology KOMAG, kstankiewicz@komag.eu

Abstract: *In industry, we can meet complex communication systems for transmission of visual, voice and digital data from monitoring or control systems. Concept of self-organization methods allowing transformation of complex data-transmission structures into single virtual traffic routes, which are reliable communication media, is presented. Systems based on the similar techniques have high tolerance to interferences as well as enable dynamic and spontaneous changes in hardware and software to adapt quickly to changing conditions.*

Keywords*: automation, artificial intelligence methods, swarm algorithms.*

1. Introduction

From the half of last century, the methods and technologies of artificial intelligence were used especially in automatics and control of machines and processes, mainly for their optimisation, recognition of reference standards, machine learning, modelling, prediction, adaptation, etc. Artificial intelligence often enables effective, autonomous control and automation of the processes, which were previously related strictly to human activities. It is especially important in the aspect of complexity of models going beyond human perception, mainly in the aspect of work safety. Solutions with use of artificial intelligence enable partial or total withdrawal of people from especially dangerous areas, as well as early detection of hazards and to warn about them.

Mining industry is especially hazardous branch of industry. Artificial intelligence can be used in the mining industry, among others, in diagnostics of sub-assemblies and components wear [11] as well as in diagnostics of control systems of machines and mechanization systems [3, 7, 8, 12, 17, 18]. Implementations enabling intelligent adaptation of machines to changeable mining conditions are known. Future mining of thin seams of high methane concentration, threatened by bumps and thermal hazards, forces the designers to develop more and more autonomous systems, in which the role of man will be limited only to supervision.

Implementations of routing protocols based on technologies and methods of artificial intelligence are more and more often met in the mining communication systems. The implementations are most frequent in wireless voice communication, what has a direct impact on work safety. Effective routing is especially important in the case of networks built in mesh topology with implemented Ad Hoc mechanism. Wireless network for monitoring the pressure in hydraulic legs of powered roof supports or monitoring the temperature of rollers of belt conveyor is the example of such structure [16].

Ad Hoc network is an assemblage of mobile wireless devices creating dynamically the temporary network infrastructure without central administration spot. Quite often, these are multihopping structures, where on the sections between the nodes very low throughput can occur, and communication can be realized only in one direction. The nodes in such network are not only the receivers of information, but they can also play a role of devices transferring the data to other nodes [13, 15]. Initial studies on Ad Hoc networks were carried out on using such solutions in the army. However, increasing need of communication between devices, which are out of the range of transmitters of the backbone network, resulted in establishing the Mobile Ad Hoc Networking (MANET) and Network Mobility (NEMO) groups within the IETF organization. Testing and standardization of IP routing protocols as regards their use in topologies of both static and dynamic character, built of different types of hardware using the wireless communication, is the task of both groups [9, 15].

There are many problems associated with structurally composed networks of dynamically variable configuration, which should be solved. The most important problems are as follows [10, 15]:

- mobility – dynamically changing positions of nodes. Unknown number of nodes in a given network,
- multihopping – route from the source to the target goes through several nodes. Number of hops can change in short time,
- self-organization – Ad Hoc network shall independently determine its configuration parameters such as routing, position and supply control,
- energy saving – many devices creating Ad Hoc networks have supply source of limited energy. Use of protocols optimized as regards energy consumption enables to extend time of operation of these devices,
- scalability – character of Ad Hoc network enables dynamic creation of networks, which can have many nodes,
- safety – due to the character, Ad Hoc networks are one of network environments most vulnerable to network attacks.

2. Routing protocols in Ad Hoc network

Routing protocols have to ensure the route for data packages from the source node to the target node. However, taking into account the previously mentioned limitations of Ad Hoc network, realization of this task is of much greater technological challenge. There are many different routing protocols that can be implemented in mobile Ad Hoc networks. Existing solutions can be classified as follows [2, 10]:

- proactive protocols – in each node the possibly newest information about the routes to other nodes is stored. The routes are stored in routing tables, which are updated regularly. The protocols in this category are not recommended for large environments with dynamically changing topology,
- reactive protocols – known also as the routing protocols on-demand. This is the class of protocols, in which the route is determined at the time, when the source node needs to send packages to the specified target. The network is overrun with special packages of route demand starting from the closest nodes neighbouring the source. After completing the routing procedure the route is maintained until the end of its use,
- hybrid protocols – these protocols combine the properties of proactive and reactive protocols. In the majority of protocols from this group, the action consists in dividing the network into smaller fragments, and the nodes keep tables of routes for those isolated areas. Additionally, in the literature we can find two more protocol categories i.e. geographical protocols and energy efficient ones. They use broadcasting system specified by geocast and transmission through multipath channel [4, 15].

Basing on the method of data delivery, the routing protocols in Ad Hoc networks can be classified in the following way:

- unicast routing protocols – protocols transferring information to a single target place from a single source,
- multicast routing protocols – protocols transferring information to a group of receivers at the same time with use of the selected, effective strategy for using the network structure [9, 15].

3. Routing in the wireless networks

Wireless networks, in which the nodes are not limited by the physical infrastructure, enable more flexible communication. There are two categories of mobile wireless networks [14]:

- infrastructured networks,
- infrastructureless networks.

The first version of those networks consists of the stationary base and mobile stations as well as of wireless end stations. The base stations are fixed to a normal cable network acting as gates and access points for mobile points. Mobile hosts, which are in the range of operation of at least one base station, communicate through it with other stations and other mobile hosts to exchange information. Fig. 1 shows the network with full infrastructure, where BS is the base station and R are the access routers. The route between A and B hosts can be as follows: A-BS1-R1-R3-BS2-B, and between A and C hosts: A-BS1-C [20]

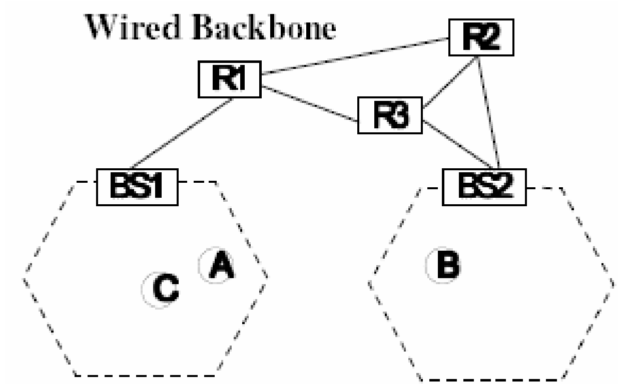

Fig. 1 Example of wireless network [20]

Infrastructureless networks or mobile wireless Ad Hoc (MANET) networks are first of all the networks in which routing is mainly based on multihop transmission. It means that not all stations can be within their range, thus it can happen that transmission will require the use of intermediary nodes, transferring information from sender to the receiver [20]. The idea of mobile Ad Hoc network means decentralized wireless network, which enables transmitting data packages, where the mobile stations can play a role both the end client and the router. Thus, each station apart of running the application can intermediate in transferring any network movement. The feature differentiating such networks from traditional ones is that none additional network infrastructure is required for communication. There is no central network management and none of the stations has strictly defined position. Such nodes can change localization, they are dynamic [20]. Fig. 2 shows the example of MANET network. The circle around each digit, which represents the node of network, determines it maximal range of transmission. Routing between the nodes 1 and 2 e.g. 1-3-4-2 or 1-5-2 is possible [20].

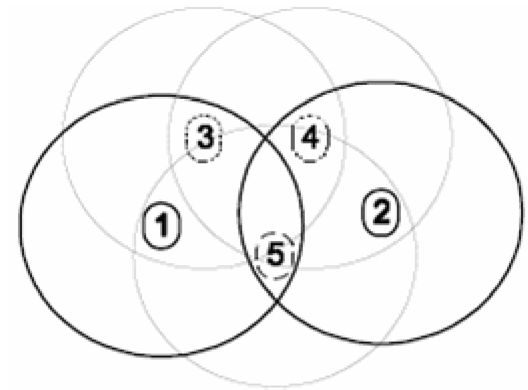

Fig. 2 Ad Hoc network with marked nodes range [20]

Ad Hoc networks can be implemented in different fields. It is worth to mention the military service (lack of central management system), rescue actions or the sensor networks/applications. However, the most important of all is that for each type of application, depending on usage, there are different requirements regarding routing protocol. For example in applications used by army, low detection and low interception rate are important, despite the problems with network that may arise at any moment. In the sensor applications low consumption of energy is important and during recue actions, fail-safety and possibility of realization of certain services on the previously set level, are important [6]. All applications in Ad Hoc networks have some specific features, differentiating them from the others as well as they have some requirements regarding the algorithms realizing the routing. High traffic intensity that can cause network congestion as well as frequent link change causing hosts inundating with the control packets, what in result cause unwanted charge of links, are not desired. In addition, mobility increases communication requirements. In addition, reducing of energy consumption is a huge challenge as in the MANET networks the devices are supplied from battery cells [6].

Traditional unicast and multicast routing protocols base on static or almost static network topology where in routing tables all possible target routes are stored. Routing protocols in mobile networks such as MobileIP [5], are intended for radio communication, considering a single-hop, in which transferring of information about routing depend on cable network. Thus, the MANET networks require their own algorithms realizing the routing, taking into account all previously mentioned needs [20]. As the nodes in mobile networks change their position, also topology of such network changes and it can happen quickly and unexpectedly. What's more, there are limits regarding network throughput and consumption of energy from battery cells [6]. Thus, traditional routing protocols are very limited, so completely different algorithms with correct exchange of data between the nodes in Ad Hoc network, have been developed.

4. Concept of self-organizing communication network

Concept of self-organizing structure bases on one of the artificial intelligence technologies known as intelligence of swarm [1], which is direct implementation of the phenomena and behaviour observed in nature among organisms living in flocks. The system structures developed by a man (regardless of the actual implementation), using this technology have a significant adaptive capacity and high operational reliability. In 1987, during the SIGGRAPH conference, the programmer Craig Reynolds, in the paper entitled "*Flocks, Herds, and Schools: A Distributed Behavioral Model",* suggested three basic rules of self-organization based on observed groups of animals, that is [19]:

- collision avoidance – control eliminating local concentration of individuals. Collision avoidance enables the individual to keep minimal required separation of effects specific for its function in relation to other individuals from the local group and in the result it prevents against accumulation of hardware or decision structures. From the other side use of only the collision avoidance would cause structural separation of the group without possibility re-centering. Thus, incorporation of the opposite centering principle is required,

- flock centering – actions towards average behaviour of local group of individuals. Flock centering makes the individual possible to group with other local individuals and prevents against decomposition of the structures. However, the introduction of this principle is still not sufficient. There may be an undesirable effect of uncoordinated actions of individuals, due to the lack of common direction. There is therefore a need to add the principle of velocity matching.

- velocity matching – actions towards average objective of local group of individuals. Velocity matching enables the individual to adapt its actions to other individuals from its local group. This prevents against the system instability, which can be described as: "I have to be the most consistent with action of X, but at the same time if I am successful I need to carry out activities divergent to X". In this situation we have the unstable system. Velocity matching, which requires individual to mimic the direction of neighbours and at the same time to meet requirements flock centering and collision avoidance, is the solution..

Referring to the suggested communication system, the coefficient determining transmission priority W_p i.e. effectiveness of data transmission to main transceiver stations should be assigned to each data frame passing through MTU (Measure Transmission Unit). This coefficient bases on data propagation time and number of hops of transmitted frames with the measurements data. Moreover, the following communication rules should be assigned to each data frame:

1. matching the transmission path with data frames from neighbouring MTUs,

2. trying to occupy the place in the path between data frames from MTU, which are within the transmission range,

3. not competing for primacy in transmission with frames of higher priority,

4. avoiding transmission by the units marked as damaged,

5. can leave the present connection, when the coefficient of transmission priority of MTU group falls or the main transceiver station was found.

Use of these simple rules causes that MTU group, which makes the transmission connection, creates the structure of reliable transmission path by itself, neglecting the damaged units – just like living creatures do, able to separate into two independent groups, when meeting the obstacle, to omit the obstacle and to join again. Frame of data can be defined by the following four additional values:

- own, unique identification number for MTU,

- X and Y coordinates defining the position they occupy in the structure of the communication path,

- priority coefficient W_p of the communication path, where the given frame is its element,

- speed of transmission for dimension X and Y, i.e. vX i vY.

Other frames that are within the range of MTU transmission, i.e. such ones, which are in a sufficiently small distance d and at the same time are in the field of vision determined by virtual angle r, are the neighbours of the fames having the number of given MTU. To check if the given frame *e* of coordinates *e.X* and *e.Y* respectively, is the neighbour of MTU *b* of coordinates *b.X* and *b.Y*, first we have to check if the element is in a sufficiently small distant, that is:

$$\sqrt{(e.X - b.X)^2 + (e.Y - b.Y)^2} < d \tag{4.1}$$

If inequality is not satisfied then the following rules are not to be verified as the given frame from MTU *e* is for sure not a neighbour of frames from MTU *b*. If inequality is satisfied, we should check if the frame is within the virtual angle of field of vision *r* by determination of angle r_1, under which the frame moves virtually:

$$r_1 = \arctan\left(\frac{b.vY}{b.vX}\right) \tag{4.2}$$

as well as virtual angle r_2 of the section connecting the frame MTU *b* with the frame MTU *e*:

$$r_2 = \arctan\left(\frac{e.Y - b.Y}{e.X - b.X}\right) \tag{4.3}$$

assuming that $b.vX \neq 0$ and $e.X - b.X \neq 0$. Then the absolute value of angle difference is calculated and the following inequality is verified:

$$|r_1 - r_2| < r \tag{4.4}$$

If inequality is satisfied, the frames are from the neighbouring MTU. Subsequently, the first rule is applied - each frame adjusts its path to the frames from the neighboring MTU. We should calculate average speed v_{avg} of all frames from the neighbouring MTU (separately for *vX* component and *vY* component) and then we should modify speed of frame transmission, taking into account priority coefficient of the path, current speed and average value calculated according to the following formula:

$$\begin{aligned} b.vX &= b.vX + \left(W_p \cdot \left(vX_{avg} - b.vX\right)\right) \\ b.vY &= b.vY + \left(W_p \cdot \left(vY_{avg} - b.vY\right)\right) \end{aligned} \tag{4.5}$$

To use the second rule, we should calculate the average number of frame hops in the transmission path d_{avg}, in relation to the frames from the neighbouring MTU, and then to modify transmission speed of the frame in relation to the neighbouring frames. Formula (4.6) is the result of using theorem of triangles similarity. It uses the position of the frame in the transmission path, speed of which is modified *b* as well as the neighbour position *e*:

$$
\begin{aligned}
d &= \sqrt{(e.X - b.X)^2 + (e.Y - b.Y)^2} \\
b.vX &= b.vX + \frac{(e.X - b.X)\cdot\left(d - d_{avg}\right)}{d} \\
b.vY &= b.vY + \frac{(e.Y - b.Y)\cdot\left(d - d_{avg}\right)}{d}
\end{aligned}
\tag{4.6}
$$

From the third rule, it results that in a situation, when the frame in the path of lower priority coefficient tries to transmit data, competing with the frame of higher transmission priority it should resign from doing that modifying its speed. In the formula (4.7), theorem of triangles similarity was also used. Let *b* be the frame of lower priority competing with the frame of neighbouring MTU of higher priority *e*. Referring to the above rule the following formula should be used:

$$
\begin{aligned}
d &= \sqrt{(e.X - b.X)^2 + (e.Y - b.Y)^2} \\
b.vX &= b.vX + \left(\frac{\left(e.X - b.X\right)\cdot d_{\min}}{d} - \left(e.X - b.X\right)\right) \\
b.vY &= b.vY + \left(\frac{\left(e.Y - b.Y\right)\cdot d_{\min}}{d} - \left(e.Y - b.Y\right)\right)
\end{aligned}
\tag{4.7}
$$

where d_{min} is the given minimal number of hops in the transmission path, which should not be exceeded by the transmitted frame.

Two last rules are entered to the system modifying the fourth rule, basing on relationships (4.7). It should be emphasized that each frame can move with the maximal speed imposed by the physical system. In the simulations, this speed should be limited and additionally we should use:

- limitations resulting from MTU in emergency or start up states (elements, which should be omitted by frames, creating transmission paths)
- attractors, in a form of main transceiver stations.

5. Summary

The method of self-organization of the communication network enables implementing the state-of-the-art and effective monitoring and control technology in underground workings, especially as regards diagnostics, monitoring and protection of machines, in which the subassemblies, equipped with the proper electronic system, can be treated as the elements of measuring swarm. It is especially important as regards work of people in underground workings, where effective evacuation of people exposed to hazards is very difficult and strongly depends on reliable communication system.

When estimating the costs of implementation of the suggested solution, we can assume that cost of manufacture of MTU electronic system designed for diagnostics of basic operational parameters of the machine in the large-scale production as well as its installation should not exceed 3 USD per single element. Cost of software programme and main transmission station (anti-explosion design) in amount of 3000 USD should be added. In the case of implementation of the solution on the machine where we need about 1000 subassemblies the investment costs should not exceed 6000 USD, what seems to be a reasonable price relating to the effective, self-organizing monitoring, increase of operational safety and elimination of unwanted breakdowns.

REFERENCES

[1] Arabshahi P., Gray A., Kassabalidis, I., Das A., Narayanan S., Sharkawi M., El Marks R. J.: Adaptive routing in wireless communication networks using swarm intelligence, AIAA 19th Annual Satellite Communications System Conference Toulouse, France 2001, p. 1-9
[2] Basagni S., Conti M., Giordano S., Stojmenovic I.: Mobile Ad Hoc Networking, IEEE Press, New Jersey 2004.
[3] Bombor J.: Artificial Intelligence in Pniówek mine! Miners not needed any more?, http://www.dziennikzachodni.pl/artykul/586769,sztuczna-inteligencja-w-kopalni-pniowek-gornicy-niepotrzebni,id,t.html#czytaj_dalej
[4] Boukerche A.: Alhorithms and Protocols for Wireless and Mobile Ad Hoc Networks, Wiley, Ottawa 2009.
[5] Feeney L.M.: A Taxonomy for Routing Protocols in Mobile Ad Hoc Networks, SICS Technical Report T99/07, October 1999.
[6] Ilyas M.: The Handbook of Ad Hoc Wireless Networks, Florida Atlantic University, Florida, 2003
[7] Jasiulek D., Rogala-Rojek J., Stankiewicz K.: The applicability of artificial intelligence techniques in control and diagnostics of mining machinery. KOMTECH 2011. Monograph. ITG KOMAG, Gliwice 2011. p. 45-54,
[8] Lodewijks, G. (2004). Strategies for automated maintenance of belt conveyor systems. Bulk Solids Handling, 24(1), p. 16-22.
[9] Misra S., Misra S. C., Woungang I.: Guide to Wireless Ad Hoc Networks, Springer-Verlag, London 2009
[10] Mohapatra P., Krishnamurthy S. V.: Ad Hoc networks (Technologies and Protocols), Springer, 2005.
[11] Mróz J., Szczygielska M., Broja A., Felka D.: The detection of faults and sources of fires on belt conveyors, KOMTECH 2011, Monograph, ITG KOMAG, p. 149-160,
[12] Prostański D., Jonak J.: An application of neural networks in the research process of mining using conical rotary bits. Monograph, CMG KOMAG, Gliwice 2003, p. 156-164
[13] Sarkar S. K., Basavaraju T. G., Puttamadappa C.: Ad Hoc Mobile Wireless Networks Principles, Protocols, and Applications, Taylor & Francis Group, 2007
[14] Słoczyński J.: Untypical routing algorithms, Lodz University of Technology, Łódź 2004
[15] Smolarek A., Malinowski T.: Routing protocols in ad hoc networks. Teleinformatics Systems and Networks Conference 2012, Proceedings, WWSI, Warszawa 2012, p. 47-60
[16] Stankiewicz K.: The concept of self-organization method for complex communication system implemented in mine, Monograph, KOMTECH 2012, ITG KOMAG, Gliwice 2012 p. 329-338
[17] Szymański Z.: An application of artificial intelligence methods to control, monitoring and diagnostics of mining transport machines. International Conference KOMTECH 2000, Szczyrk, November 2000, KOMAG, Gliwice 2000, p. 1-8
[18] Szymański Z.: An application of artificial intelligence methods to control of systems of horizontal and vertical transport machines, Driving and Control nr 12/2007, p. 114-120
[19] www.algorytmy.org, 2012,
[20] Zhu Y.: Pro Active Connection Maintenance in AODV and MAODV by Yufang Zhu, Department of Systems and Computer Engineering, Carleton University, Ottawa, September 2002.

ISSN 1454 - 8003
Proceedings of 2014 International Conference of Hydraulics and Pneumatics - HERVEX
November 5 – 7, Calimanesti-Caciulata, Romania

OVERVIEW CONCERNING THE USE OF ACOUSTIC EMISSION AND MODERN METHOD OF DIAGNOSIS OF GEARBOXES

Nicolae Florin ROTARU[1], Liviu Ioan VAIDA[2]

[1] Technical University of Cluj-Napoca, nicolae.rotaru@termo.utcluj.ro

[2] Technical University of Cluj-Napoca, liviu.vaida@termo.utcluj.ro

Abstract: *This paper describes principles and applications of an adaptive order tracking diagnosis technique for fault diagnosis in rotating machinery. The use of mechanical vibration and acoustic emission signals for fault diagnosis in rotating machinery has grown significantly due to advances in the progress of digital signal processing algorithms and implementation techniques. The conventional diagnosis technology using acoustic and vibration signals already exists in the form of techniques applying the time and frequency domain of signals, and analyzing the difference of signals in the spectrum.*

Keywords: *mechanical vibration, acoustic emission*

1. Introduction

Vibration and acoustic emission signals are often used for fault signal diagnosis in mechanical systems since they often carry dynamic information from mechanical elements. These mechanical signals normally consist of a combination of the fundamental frequency with a narrowband frequency component and the harmonics. Most of these are related to the revolutions of the rotating system since the energy of sound or vibration is increased when a mechanical element is damaged or worn.

2. Acoustic emission

In general, conditions of rotating machineries such aselectric fans, compressors and engines can be monitored by measuring their acoustic emission or vibration signals. These signals normally consist of a combination of a basic frequency with discrete or narrowband frequency components and the harmonics thereof, most of which are related to the revolution of the machinery. Noise in emission and vibration are increase when there are signs in machinery damage. Conventional Fast Fourier transform (FFT) (Fig. 1) fault technique is used to observe the amplitude difference in frequency domain for damage diagnosis.

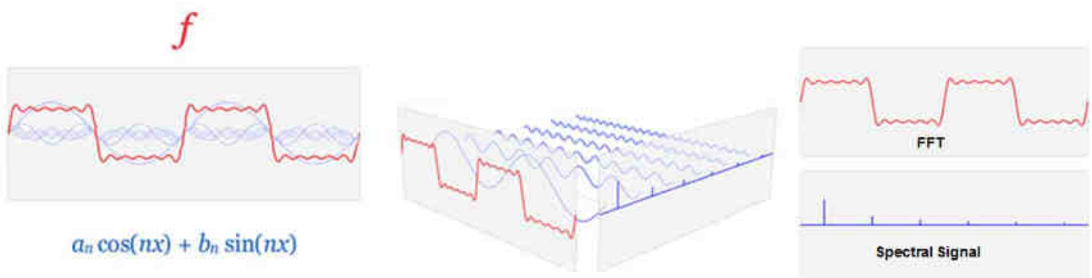

Fig. 1 Fast Fourier transform (FFT)

Some of the conventional techniques used for fault signal diagnosis include power spectra in time domain or frequency domain, and they can provide an effective technique for machinery diagnosis provided that there is the assumption that the signals are stationary. However, the conventional methods are not always effective for application under certain critical conditions such as using a fixed sampling frequency for fast Fourier transform (FFT) analysis and rapid changes of the shaft speed. The FFT represents a signal using a family of complex exponents with infinite time duration. Therefore, FFT is useful in identifying harmonic signals. However, due to its constant time and frequency resolutions, it is less effective for analysis of transitory signals. In recent years, some new techniques for fault signal diagnosis with non-stationary signals have been proposed, e.g. order tracking technique, wavelet analysis and adaptive wavelet filter. Among these new techniques, wavelet analysis has particular advantages for characterizing signals at different localization levels in time as well as signal processing, image processing, pattern recognition, seismology, machine fault diagnosis, etc. In the field of mechanical fault diagnosis, wavelet analysis has been used in gear diagnosis, rolling bearing diagnosis and compressor diagnosis. In 1995, Wang and McFadden proposed an orthogonal wavelet technique to disclose abnormal transients generated by early gear damage from gearbox casing vibration signals

In general, acoustic emission and vibration analysis are two main centers of fault detection and diagnosis systems in machine condition monitoring.

In this paper, vibration signals established as the way of recording required dataset because of the ease of measurement and the rich contents of information. To analyze raw vibration signals, a simultaneous time–frequency analysis method which maps one-dimensional signals into a two dimensional space of time and frequency was applied because of non-stationarity of vibration signals. Wavelet analysis, the most popular one for analyzing the non-stationary signals, overcomes the drawbacks of other techniques by means of analytical functions that are local in both time and frequency (Fig.2).

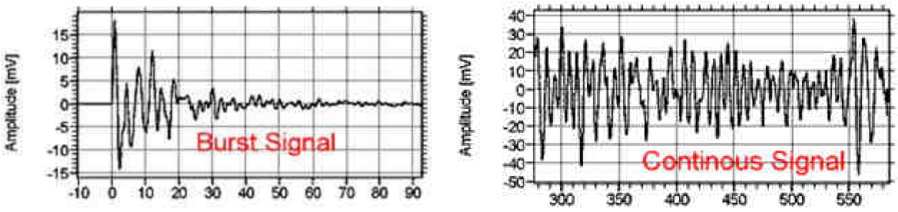

Fig.2 Signals

The prior research demonstrates the wavelet transform as the most reliable technique for gear condition monitoring and a capable technique to recognize the incipient failures and to identify different types of faults simultaneously. The most indispensable challenge in wavelet analysis is the selection of the mother wavelet function as well as the decomposition level of signal (Fig.3).

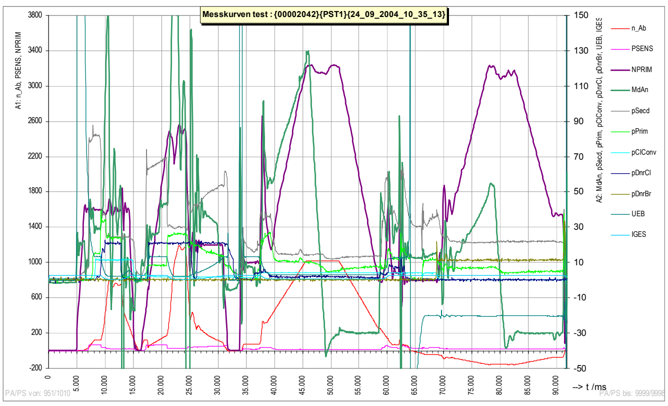

Fig.3 Gearbox Acoustic emission signals

2. Modern method of diagnostics for the gearboxes

The analysis on vibration behaviour of the gearboxes is a method increasingly prevalent due to high informational content that it offers. Limits concerning the possibilities of using this method are determined by the high costs imposed by the acquisition system of measurement values.

The oscillatory analysis plans to achieve three components:

- Observation- this component aims to monitor temporal wear indicators (anomalies);
- Control status- this component assesses the machine state by analysing the wear indicators (anomalies)
- Wear diagnosis (for the anomalies)- this component locates and describes faults using the analyse of some observation indicators

Figure 4 presents the general strategy for the body wave analysis used for the establishment of faults.

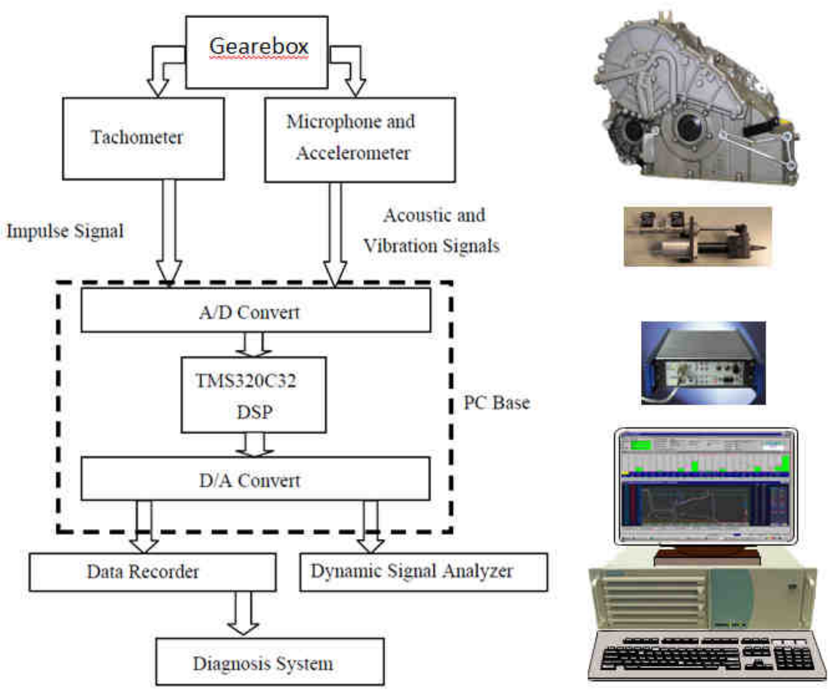

Fig.4 A model for the wave analysis strategy for establish the causes of faults

Using a piezoelectric acceleration sensor or one of acoustic emission applied on the gearbox, the casing fluctuations can be collected and recorded; then they turns in electrical temporal signals. These signals contain information that can be recovered by a frequency- analyzer.

The next important step is to find out the peak amplitude evolution in the frequency spectrum. In this way can be associate with the mechanical causes which determinated the signals (fig.5)

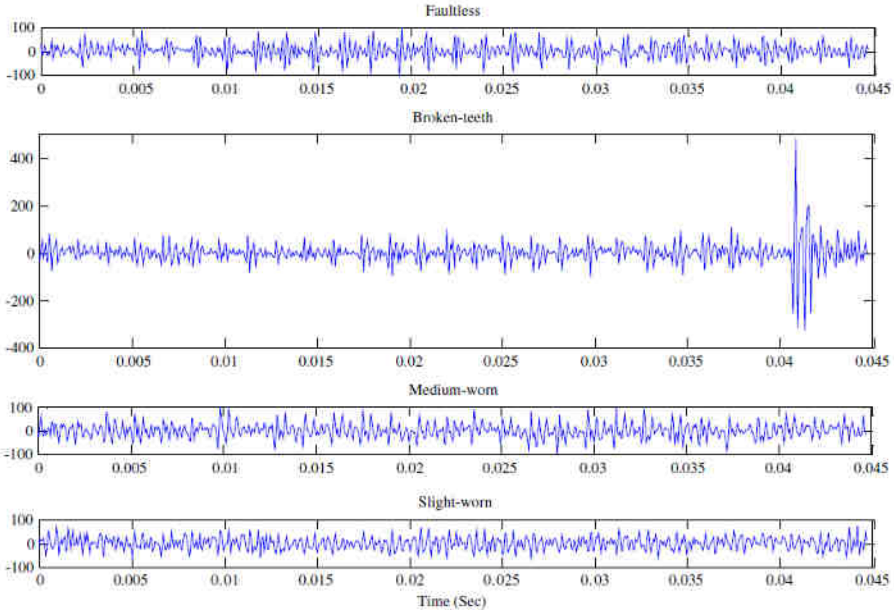

Fig.5 Synchronized vibration signals of gearbox conditions recorded during one revolution of input shaft

The appreciation of the vehicle state is resulting from qualitative interpretation of measurements comparatively with the determined frequency spectrum of a new gearbox without abnormal wear or without functional abnormalities.

The control operation of the gearbox must be done in relation to a reference value, which if it's modified outside preset limits, it is absolutely normal to intervene to prevent the extension of the fault that caused the change in this value (fig.6).

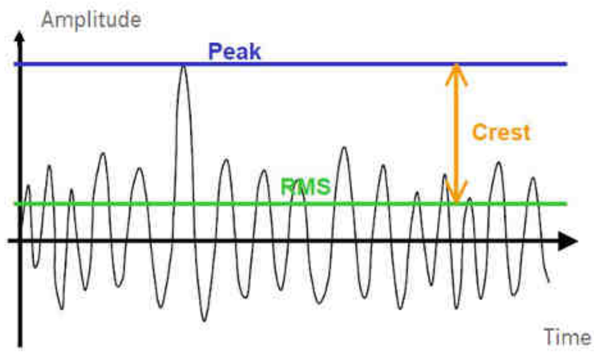

Fig.6 Reference value representation

Root-mean-square (RMS) is the cheapest and the most commonly used mathematical method for evaluating the average level of a signal oscillating.

This method can be calculated using the below formula:

$$U_{RMS} = \sqrt{\frac{\int_0^t u^2(t)dt}{t}} \tag{1}$$

This formula reflects a constant signal level that produces the same effect as the original signal, in the same conditions.

If we analyze the U_{RMS} in relation to o functional parameter (speed for example) we can make judgements on the state of gearbox at a time.

Such analysis system can be introduced to control the quality of the gearbox directly at the manufacturer. This avoids the measurement of working parameters, lifting curves, operations that require extensive work and measurement equipment.

The “oscillatory” component of a gearbox, in relation to the load speed which is then compared with the obtained allure from a reference gearbox, can give some appreciations about the gearbox tried.

Verifying the quality of gearbox using this method, reduces the test costs. The product is guaranteed because of it.

If the analysis of body wave limits on this fact, we will have a good appreciation or a bad one. If the result is “bad”, it is necessary to make an additional diagnosis. Thus, we can determine the fault.

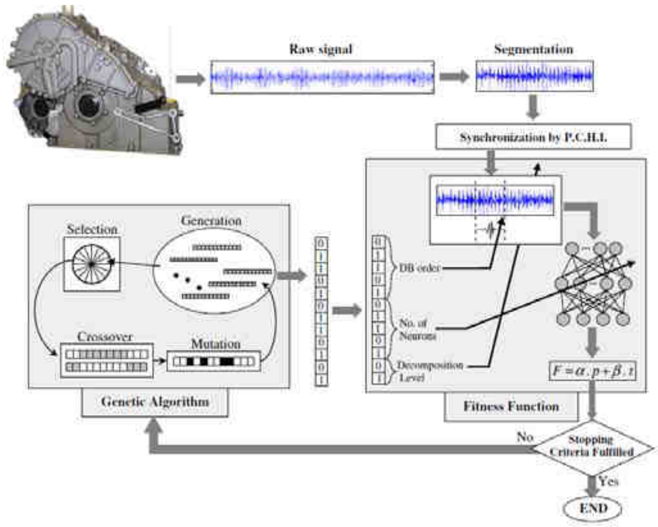

Fig. 7 Schematic of the entire proposed algorithm.

The additional diagnosis valorifies the information which is contained in the representation of the frequency function u (t) or AE which describes the wave process.

After an incorrect operation occurs, the diagnosis system must allow, based on a previously established method, accurate determination for the abnormalities of gearbox.

Based on this information we can take a decision concerning the moment when we must intervene to repair it (the replacement of components or the repair for some deviation of form)

The diagnostic method must show the next evolution abnormalities and also she must show the measures to be taken to slow the anomalies.

The only difficulty in this method is the possibility that from all the information about the body wave analysis and acoustic emission, you have to be able to discern the essential information.

In that case, the most effective solution is to provide a database that contains the frequency spectrum (fig.8) for the progressive development of abnormalities.

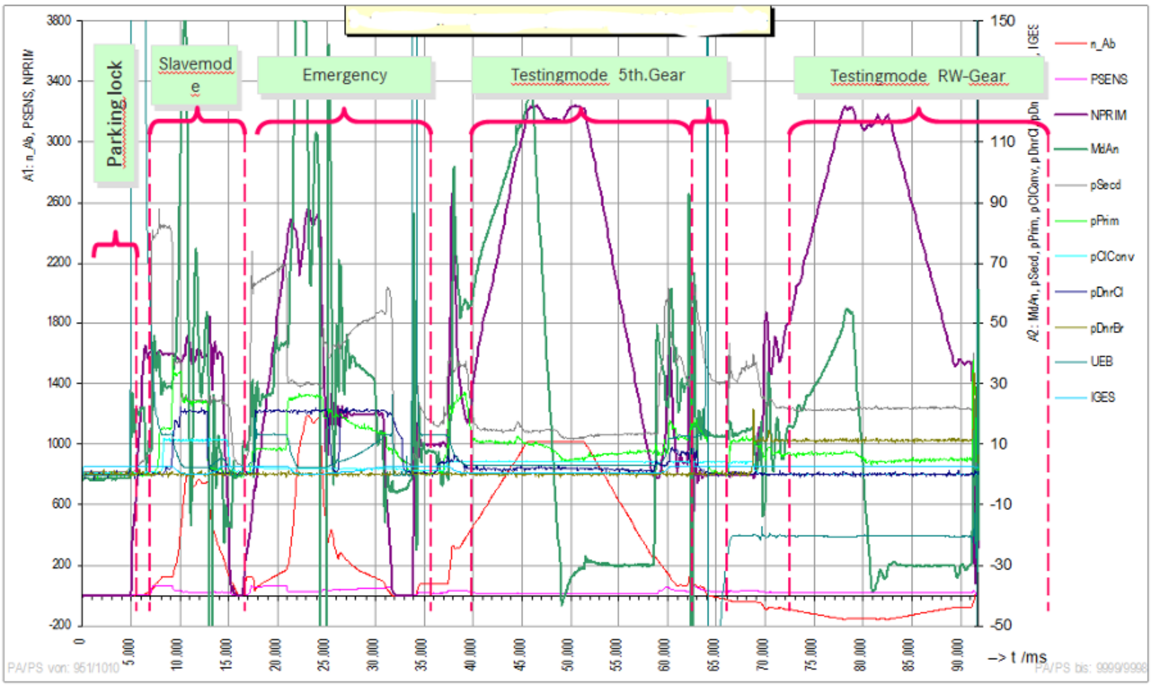

Fig. 8 The frequency spectrum

The condition for the practical use of this method is related to the existence of a database stored. Thus, it contains any possible abnormalities

3. Conclusions

Most fault diagnosis techniques are used to prevent early faults in a mechanical system. The condition of monitoring and fault diagnosis technique are used to prevent the defects of the mechanical system. The RMS method, the FFT method and the DWT method of the neutral network are useful to detect and classify the gearboxes in many stages of failure. With this method, the features of sound emission signal at different resolution levels are extracted by multi-resolution analysis without losing its original properties.

REFERENCES

[1] A. Potolea, “ Posibilitati si realizari in diagnoza pompelor cu pistoane axiale“, Cluj-Napoca 2002, PhD thesis;
[2] Jian-Da Wu, Jien Chen, “ Continuous wavelet transform technique for fault signal diagnosis of internal combustion engines“, NDT&E International 39 (2006) 304–311, www.elsevier.com/locate/ndteint
[3] J. Rafie , A. Harifi , “A novel technique for selecting mother wavelet function using an intelligent fault diagnosis system”, Expert Systems with Applications 36 (2009) 4862–4875
[4] A. Darabont, I.Iorga, M.Ciodaru, “Masurarea zgomotului si a vibratilor in tehnica”, Editura Tehnica, Bucuresti, 1983.
[5] L. Deacu, L. Kerekes, “Studiu privind utilizarea fenomenului de emisie acustica in aplicatii industriale”, UTCN, Cluj Napoca, 1997.
[6] L. Deacu, s.a., “Tendinte noi in tehnica proportionala”, Hidraulica, Cluj Napoca, 1998
[7] L. Dragos,“Principile mecanicii analitice”, Editura Tehnica, Bucuresti, 1976
[8] www.elsevier.com

ISSN 1454 - 8003
Proceedings of 2014 International Conference of Hydraulics and Pneumatics - HERVEX
November 5 – 7, Calimanesti-Caciulata, Romania

RESEARCH REGARDING THE EVO HP – 7.0 ENERGY EFFICIENT HYDRAULIC PUMP UNIT FOR OIL AND GAS EXTRACTION

Dragoş-Florin CHITARIU[1], Constantin CHIRIŢĂ[2], Adrian HANGANU[3], Cătălin DUMITRAŞ[4]

[1] The Technical University "Gheorghe Asachi" of Iaşi, Prof Dr. Doc. D. Mangeron Street 67, Iaşi, Romania, chitariudragos@gmail.com

[2] S.C. Hydramold S.R.L., Calea Chisinaului, 23, Iaşi, Romania; constantin.chirita@hydramold.com

[3] S.C. Hydramold S.R.L., Calea Chisinaului, 23, Iaşi, Romania; adrian.hanganu@hydramold.com

[4] The Technical University "Gheorghe Asachi" of Iaşi, Prof Dr. Doc. D. Mangeron Street 67, Iaşi, Romania, dumitrascata@yahoo.com

Abstract: *This paper presents research on the conception and design of an oil and gas hydraulic pump unit. There are presented avantages and results of research on hydraulic schematics and the proposed work cycle, of the hydraulic pump unit that canoperate with higher energy efficiency compared to conventional pumping units.*

Keywords: *hydraulic pump unit, oil, gas.*

1. Introduction

Usually lifting fluid is conducted through a extraction equipment, surface equipment that use a conventional crank-balanced, beam-balanced system. This beam balanced unit is driven by a prime mover that causes a long sucker-rod string to rise and fall in the well. The prime mover provedes power to the system and the gear reducer reduces the speed of the prime mover to a suitable pumping speed. The beam balanced unit tranforms the rotation movement from the gear reducer into a reciprocating motion of the rod string. The sucker rod oscilation activates a downhole pump to lift the oil through the tubing to the surface [1], [2].

A hydraulic pump unit uses a hydraulic cylinder to lift the rod between a upper and lower rod positions. The hydraulic pump that is powered by the prime mover. The hydraulic cylinder can be installed on the blowout preventer. The polished rod is connected to the rod of the hydraulic cylinder directly by means of a conventionally pipe coupling (flange, etc.) or through an intermediate coupon (intermediate pole).

2. Hydraulic pump unit operation

The upward stroke operation is performed hydraulic and the downward stroke is performed under the action of the sucker-rod weight. On the downward stroke the hydraulic piston is used to control the downward speed.

The hydraulic pump unit can flexibly adapt cycle speed and the cylinder stroke to suit current pumping conditions [3], [4]. The raising and lowering speeds can be set separately, making for greater efficiency and productivity. The hydraulic control equipment that comands the operation of the hydraulic cylinder can flexibly adapt cycle speed and the cylinder stroke to suit current pumping conditions.

Fig. 1 presents a work cycle conventional mechanical pump drive units, where the work cycle has a sinusoidal shape and can be modified only by mechanical interventions on the pumping unit [5]. Also, in Fig. 1 is shown a work cycle of a hydraulic pumping unit that can be changed by remote control from the hydraulic panel. On the hydraulic pump work cycle, the lifting and the lowering speeds can be modified and, also, the pause time on the end of the cycle.

When compared with the mechanical pump drive (conventional crank-balanced, beam-balanced system), the hydraulic pump unit is much lighter and occupies considerably less space, too.

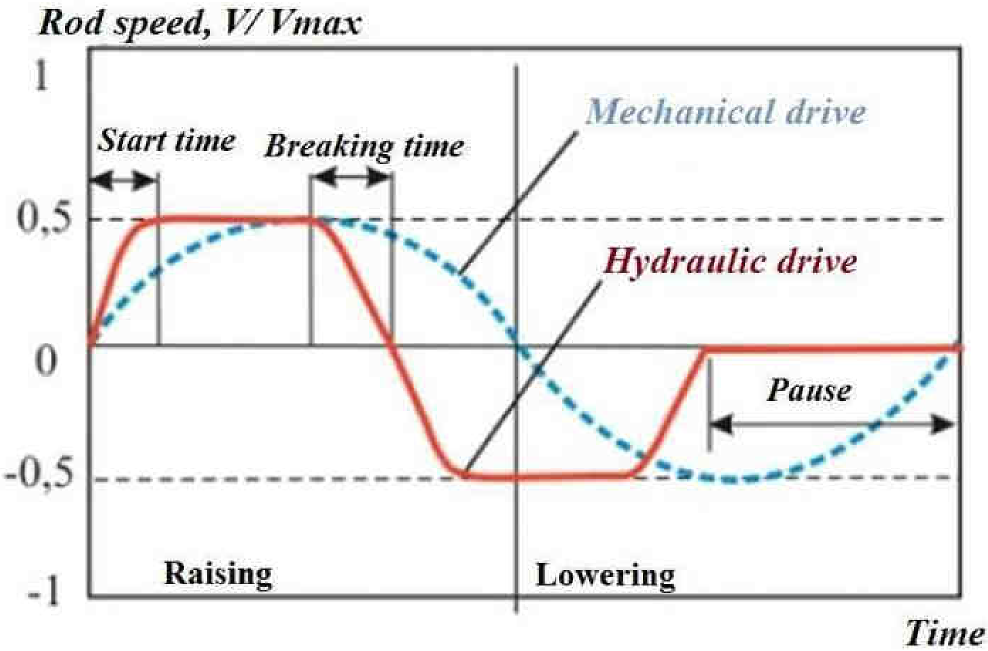

Fig. 1. Work cycle for the hydraulic pump unit and mechanical pump unit [3] [4]

The smaller dimensions and weight simplifies transportation and installation. What's more, it requires no foundation, since the hydraulic cylinder is attached directly to the casing or stufing box and in some cases on a special frame. Also, the hydraulic power unit can be installed outside area that can the subject to explosion hazard.

The command system for the hydraulic pump unit has the capability of protection against overloads of the down hole pump. If, for example, sand should enter the borehole, the hydraulic pump unit will function at a lower pumping speed that allows the evacuation of the sand. After that it will resume the normal operation. This reduces the wear of the down hole pump and prevents the possible damages. In contrast an mechanical systems can over load the pumping system and in such situations often result in the string breaking, followed by complex and expensive repairs [6] [7], [8].

Controlling the operation of the hydraulic pump unit is performed through the control panel. This allows control and hydraulic control unit operation as well, and displaying its functional parameters.

Through the control panel can be act upon the hydraulic parameters of operation of hydraulic panel for: changing the rate (number of cycles / minute), the speed of the upward then downward stroke, the force developed by hydraulic cylinder on the upward stroke and the downward stroke. It has to be mentioned that the change of stroke length with the hydraulic unit can be made via hydraulic control, but with the mechanical pump it has to make by manually adjustments [8], [9].

Setting/ control/ optimization can be performed automatically or remotely by operator intervention. By optimizing in real time the productivity can be increase, in some wells at the end of service life.

2. Hydraulic pump unit proposed by Hydramold

The hydraulic pump unit proposed by Hydramold EVO HP – 7.0 is presented in fig. 2 and fig 3. The hydraulic pump unit is composed by the frame 1, hydraulic panel 2, hoses 3, coupling 4, 5, 7 displacement transducer 6. Hydramold EVO HP – 7.0 hydraulic pump unit is designed to lift 7t of fluid.

The hydraulic panel optimizes energy consumption by summation of the flows discharged by a fixed displacement pump and one with variable displacement, by automation of the work cycle, energy recovery and adjusting of the hydraulic energy of pumping unit, depending on the oil deposit that is exploited.

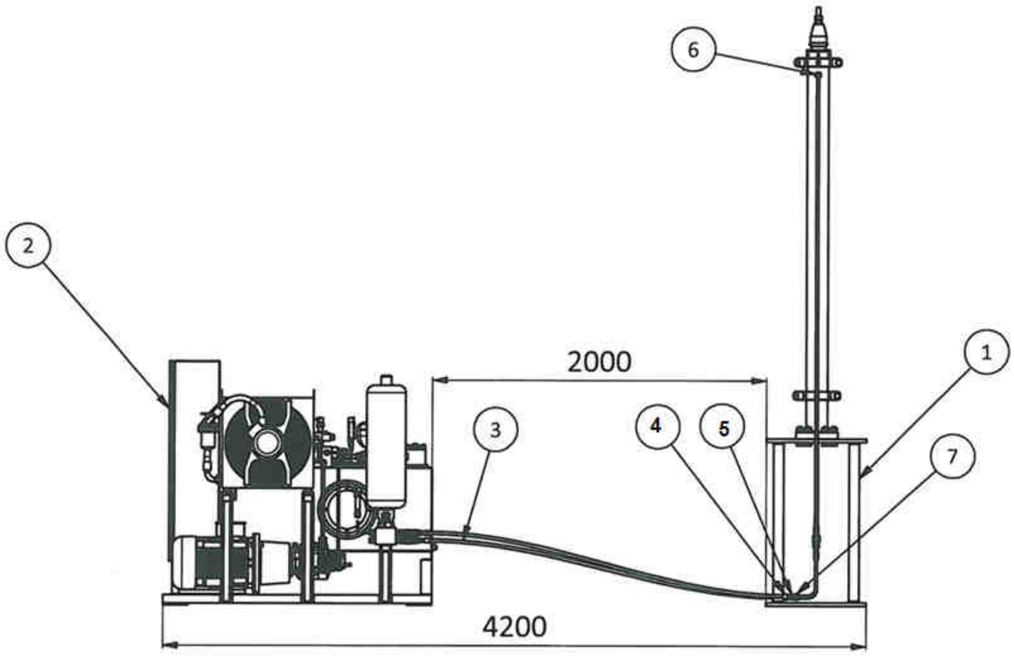

Fig. 2. View of the proposed Hydramold's hydraulic pump unit EVO HP – 7.0 [10], [11]

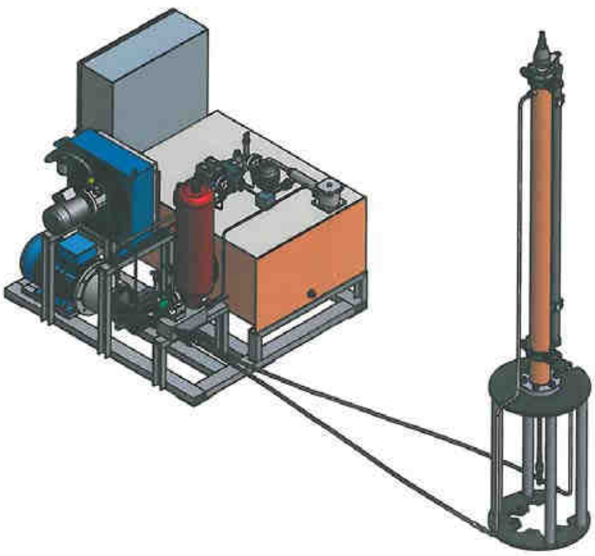

Fig. 3. View of the proposed Hydramold's hydraulic pump unit EVO HP – 7.0 [10], [11]

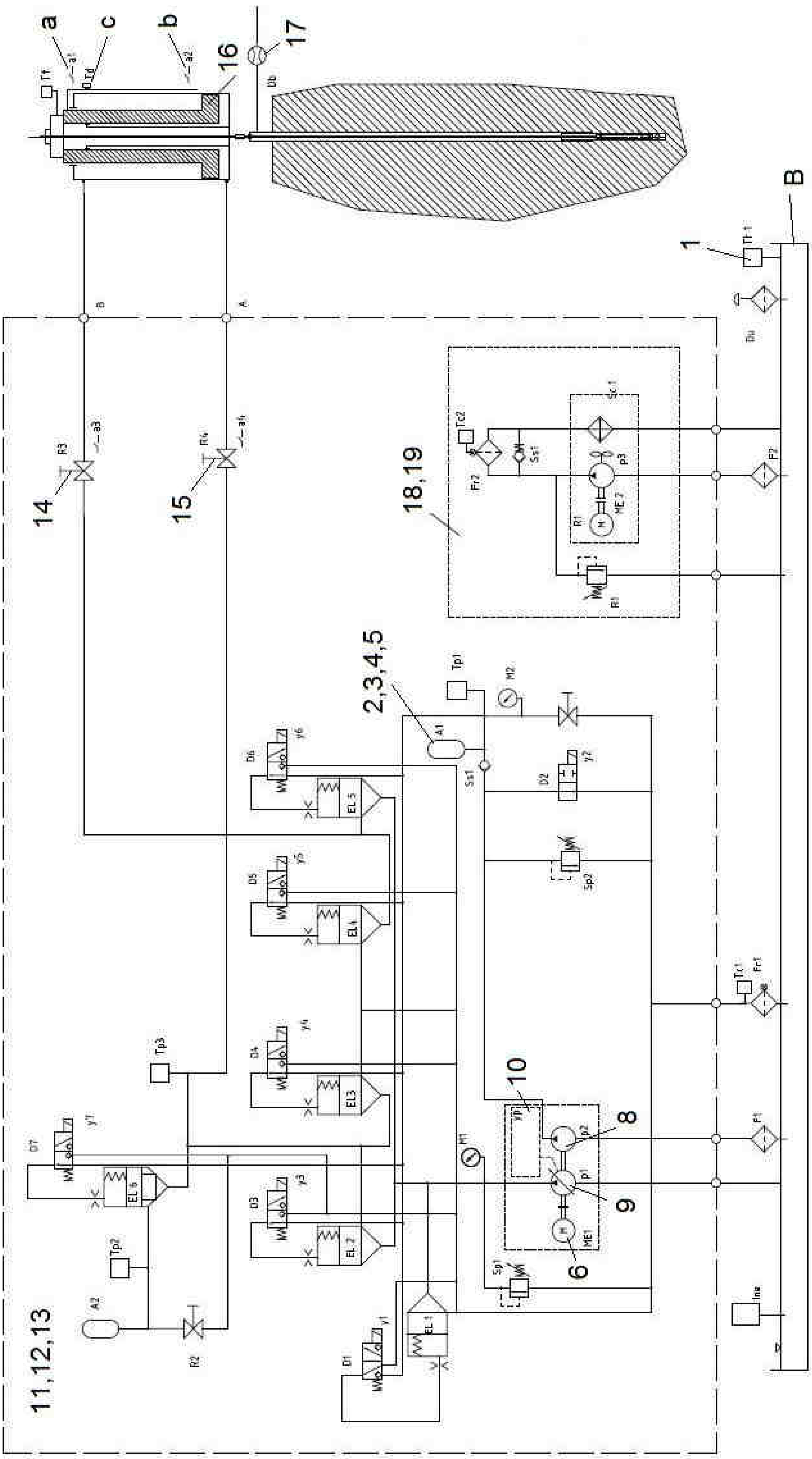

Fig. 4. Hydraulic Schematics of Hydramold's hydraulic pump unit EVO HP – 7.0 [10], [11]

In the initial state consumer connection valves are closed to allow the fixed displacement pump to charge the pilot circuit. For operating the lifting of the cylinder the two valves are opened and the fixed displacement and variable pump accumulate the required flow rate depending on technological imposed speed of the cylinder. After confirmation of the upward stroke, the downward stroke of the cylinder is performed, under the load of the weight of the sucker rods. During the downward stroke the energy recovery takes place with the loading of the high pressure hydraulic accumulator. At confirmation of the downward stroke, the hydraulic energy accumulated in the hydraulic accumulator is released and, at the set pressure, the fixed displacement and variable pump ensures the required flow to continue the lifting stroke. The cycle repeats. A flow transducer mounted on the oil line allows the assessment of flow discharged to the oil network of pipelines and adjunst the proportional adjustment of the varible displacement pump. The hydraulic schematics includes temperature monitoring system, heating and cooling of the hydraulic fluid and filter system hydraulic system with hydraulic fluid monitoring clogging and purity.

The hydraulic schematics of Hydramold's hydraulic pump unit EVO HP – 7.0, presented in fig. 4, contains an hydraulic panel with the following components: tank temperature sensor 1, pilot circuit 2 with hydraulic accumulator, hydraulic block 3 for the comand and control apparatus 4 and pressure 5. All of the mentioned elemente are mounted on a frame along the electric motor 6, jointed by its flange 7, coupled, also, with the set of fixed and variable displacement pumps 8, 9. The variable displacement pump is fitted with proportional control pilot circuit 10. The pumps are mounted on the same shaft of the electric motor, via elastic coupling. The hydraulic block 11 is equipped with a hydraulic accumulator 12, for the storage of recovered hydraulic energy, equipped with control apparatus 13 and valves 14 and 15, connecting circuits are completed under hydraulic scheme to allow operation on work cycle, for the operation of the hydraulic cylinder 16 of the pump unit. The flow transducer 17 is mounted on the oil colllection pipe.

The displacement transducers are mounted on the cylinder 16 allows adjustment of the pumping unit cadence by proportional to the piloting circuit 10. An hydraulic oil cooler and a filtration system, not shown, ensure normal operating parameters for the hydraulic oil.

The hydraulic cylinder is fixed a flange on frame. The hydraulic cylinder rod is protected from the elemets by a telescopic bellow. Between the hydraulic cylinder rod and the polished rod is mounted an force transducer that can be used along side with the displacement transducer to monitor the cylinder operation and to plot the dynamogram, for the down hole pump eficiency estimation. Also, it allows monitoring of friction between the tubing column and sucker rods and of the plunger pump. Two proximity sensors are mounted on an exterior tube, which sends information to the command and control electronic system in order to protect from failure of both the hydraulic cylinder and pump unit.

3. Conclusions

The Hydramold's hydraulic pump unit EVO HP – 7.0 can provide superior operating condition over the conventional mechanical pumps mainly through greater flexibility efficiency and productivity provided by the electronic systems of remote monitoring and control.

Compared to the mechanical pumps the hydraulic pump unit it can offer instantaneous change of the operating parameter for better exploitation of the well such as: instantaneous change of rate; change of speed lift; change stroke, working cycle control by acting on working time and rest; automation prevents damage by measuring the operating parameters of the unit and the working parameters intervention to prevent damage.

One of the disavantages of these type of pump units is represented by novelty of the technical solution compared to classical solutions known and standardized

The Hydramold's hydraulic pump unit EVO HP – 7.0 can provide low energy consumtion in operation by using hydraulic recovery system. Electronic systems of remote monitoring and control of the hydraulic pump unit can offer an intellectualization of oil extraction process.

REFERENCES

[1] Takács G. "Sucker-Rod Pumping Manual", PennWell Books, Tulsa Oklahoma, 2003.
[2] Hyne N.; Hyne J., "Dictionary of Petroleum Exploration", Drilling & Production, Pennwell Books, 1991.
[3] ***, New technologies at Lukoil: The "Geyser" Hydraulic Rod Pump, ROGTEC Magazine – Russian Oil & Gas Technologies Magazine, p. 86-91, 5.09.2011.
[4] http://www.psm-impex.com
[5] http://www.petrolsigaze.com/category/dictionar-tehnic-petrol-gaze/
[6] ***, Petro Hydraulic Lift System, L.L.C.,HYDRAULIC OIL WELL PUMPING, Patent N0.: US 7,762,321 B2, 2010;
[7] ***, Petro Hydraulic Lift System, L.L.C., HYDRAULIC OIL WELL PUMPING, Patent Application, US 2014/0196907 A1, 2014;
[8] T. Leon Brown, RECIPROCATED PUMP SYSTEM FOR USE IN OIL WELLS, Patent Application, US 2008/0135259 A1, 2008.
[9] Michael A. Fesi, Willard J. Lapeyrouse, Houma, Kenneth H. Vincent, HYDRAULIC OIL WELL PUMPING APPARATUS, US 2009/0194291 A1, 2009.
[10] ***, Hydramold, Cerere de brevet de invenţie „Cilindru hidraulic pentru unitate de pompare ţiţei", A/00851/15.11.2013
[11] ***, Hydramold, Cerere de brevet de invenţie „Grup hidraulic pentru unitate de pompare ţiţei ", A/00852/15.11.2013

ISSN 1454 - 8003
Proceedings of 2014 International Conference of Hydraulics and Pneumatics - HERVEX
November 5 – 7, Calimanesti-Caciulata, Romania

OPTIMIZATION OF THE CAVITATIONAL OPERATION REGIMES OF THE HYDRAULIC AXIAL TURBINES FROM IRON GATES I

PhD. Std. Eng. Adrian Ion SIMEDRU

[1] Hidroelectrica Serv “Iron Gates” Subsidiary of Reparation

Abstract: *The article investigates the operation of hydraulic turbines from the hydro-power plant Iron Gates I. Here during the time it was observed a difference between the non-cavitational prediction and the cavitational effects on the Kaplan axial hydraulic turbines. For explaining and avoiding in the future this contradiction and optimizing of hydraulic turbines operation it was studied closer the implied phenomena.*

In the operating point of the monitoring moment there are assumed from process monitoring measured parameters: the active and reactive power, upstream and downstream water levels (after the intake trash rake and at the outlet of the turbine draft tube), wicket gate and runner opening blades, the differential pressure in the spiral chamber and the hydrounit speed.

So, there was established the characteristic curves obtained on analytic basis and similitude and compared with the curves measured experimentally on the hydraulic machines from the power plant. The cavitational coefficient of the machine and the cavitational coefficient of the equipment in function of the system parameters between them especially the suction head, the runner and wicket gates blades angles of opening.

The solution proposed is a method of determining the operating turbine parameters and of the cavitation, by reducing the error caused by the similitude phenomenon, using an accurate estimation of the turbine operating parameters according to the universal diagram of the turbine.

The numerical obtained values permit the necessary correlation through a complex function which is able to reduce or eliminate the unwished effects of the cavitation phenomena on the hydraulic turbines of the Iron Gates power plant.

Keywords*: turbines, cavitational effects, operating point, measured parameters, error, similitude, operating parameters, “calculated” parameters, cavitational coefficient, correlation, correction coefficient.*

1. Introduction

To optimize the operation of hydraulic axial turbine must be eliminated differences between operating parameters and cavitation calculated using data from the model or diagram of operation to those measured during operation of a turbine.

Cavitation is normally defined as the formation of bubbles filled with vapour, gas or their mixture and its colapse.

Cavitation is the main obstacle to development of high performance hydraulic turbines. Cavitation erosion occurs, affecting performance hydraulic machines, noises, vibrations and oscillations of the whole system.

Iron Gates I Power Plant is functioning from 1971 and is located on the Danube at the 942,450 km upstream from Drobeta Turnu Severin town. Considering the long time of the hydrounit operation, and the volume of the reparation in the last years, it was actual the problem of refurbishment units for preparing the next cycle of 30 years in exploitation.

To combat cavitation, appropriate measures should be carefully considered and balanced throughout the planning of hydro schemes, machine selection and parametric design, machine (hydrodynamic) design and material selection, mechanical design, determination of machine setting level (the turbine cavitation number) and machine repair. The suction head is one of the main parameters which determines the cavitation phenomenon. If we correctly measure the suction head parameter of the axial turbine of great power we can find the real cavitation of the turbine.

Hydro units operating at variable falls due limited retention or lack thereof, the fall is basically dependent on flow. Turbine at rates higher than inflow causes power reduction by reducing failure and control under certain conditions required for the protection against flooding of land upstream of the dam can generate energy losses by dumping. Hydro works actually fall under the variable is set to H = cst combinatorial relationship. Several values are approximate and then fall for other operating points. If we evaluate properly the cavitation phenomenon and the operating parameters, the hydraulic turbine can avoid the unfavorable regimes in order to obtain optimized operation and to reduce the cavitation phenomenon.

Nomenclature:

P_A	MW	Active power
P_C	MW	Generator power
φ	^{0}	Wicket gates opening
β	^{0}	Runner blades opening
Q	m^3/s	Flow
n_m	rot/min	Model speed
H_T	m	Turbine head
H_S	m	Turbine suction head
H_{St}	m	Static head
p	pascals	Pressure
P_V	pascals	Vapour pressure of water
P_{at}	pascals	Atmosphere pressure
S_{P1}		Intake section of the prototype turbine
S_{P2}		Outlet section of the prototype turbine
ρ	kg/m^3	Density of water
v	m/s	Water speed
$k_{W\,3M}$, $k_{V\,3M}$	-	Speed coefficients of the model
η	%	Efficiency
σ_{inst}	-	Plant cavitation coefficient
σ_T	-	Turbine cavitation coefficient
η_{TaM}	%	Draft tube efficiency
$\gamma_P = \rho_P g_P$	N/m^3	Specific weight of the water

Subscripts:

M	model
p	Prototype
T	turbine
m	measured
c	calculated

2. The axial hydraulic turbine operation with cavitation

At the axial turbine with great discharges if it is considered only the difference from blade axis to downstream level at the draft tube outlet. It is not real because results lower than the concordant value from the exploitation diagram.

To optimize the hydraulic axial turbine it must eliminate the differences between the operating and cavitation parameters resulted from the model data otherwise from the exploitation diagram with the measured parameters in the turbine operation.

Coefficient of cavitation in hydraulics σ is a dimensionless size that characterizes the phenomenon of cavitation from such a point M of the fluid flow.

$$\sigma = \sigma_{inst} - \sigma_T = \frac{\Delta p}{1/2\rho \cdot v^2} \cong \frac{p_M - p_V}{\rho \cdot g \cdot H_T} \qquad (1)$$

Cavitation occurs when the pressure of a point is equal to the vapor pressure: $p_M = p_V \Rightarrow \sigma_{inst} = \sigma_T = \sigma_{crt}$

To avoid the cavitation is necessary that in every points of the hydraulic layout the pressure must be greater than the vapor pressure:

$p_M > p_V \Rightarrow \sigma_{inst} > \sigma_T$.

where σ_T is obtained from statistical formulae (average formula) and:

$$\sigma_{inst} = \frac{\frac{p_{at} - p_v}{\rho \cdot g} - H_S}{H_T} \qquad (2)$$

In Table 1 we have a selection of data recorded at different angles of the wicket gates and runner opening from unit 6 in the period January 2007 - June 2008, where there was the great cavitational erosions:

Table 1

φ [°]	β [°]	η_{11} [%]	Q_{11} [m³/s]	n_{11} [rot/min]	$\sigma_{11\ 0,5}$ [-]	η_T [%]	H_{STm} [m]	Q_{Tm} [m³/ s]	P_{Cm} [MW]	η_G [%]	$\sigma_{inst\ pm}$ [-]	$\sigma_{P\ 0,5}$ [-]	H_S [m]
27,53	-3,84	91,18	0,75	125,05	0.188	94,13	28,73	368	97,12	98,24	0,678	0,207	-9,36
30,00	-1,60	91,34	0,86	127,22	0.238	94,30	27,66	415	104,39	98,40	0,733	0,262	-10,16
32,03	0,26	91,47	0,95	128,92	0.271	94,43	26,90	454	112,54	98,41	0,764	0,298	-10,45
34,08	3,94	91,89	1,09	125,26	0.313	94,90	28,44	536	139,19	98,59	0,700	0,344	-9,80
36,00	6,60	91,97	1,22	126,29	0.342	94,98	28,05	593	151,57	98,65	0,721	0,376	-10,10
38,00	8,07	91,82	1,32	129,77	0.388	94,84	26,56	627	151,41	98,61	0,786	0,427	-10,76
40,00	12,45	91,40	1,50	124,74	0.475	94,49	28,66	740	190,90	98,71	0,687	0,523	-9,57
42,00	12,67	91,10	1,58	129,35	0.514	94,17	26,64	753	179,65	98,69	0,791	0,565	-10,96
44,00	14,19	90,62	1,71	131,41	0.588	93,67	25,74	802	181,78	98,69	0,815	0,647	-10,88
46,18	16,67	89,78	1,87	129,58	0.679	92,86	26,43	887	192,70	98,69	0,813	0,747	-11,37

Where: H_T formula is obtained from producer documentation.

The cavitation phenomenon is examined with the cavitation coefficient $\sigma_{inst} = \sigma_{0,5}$ on the universal cavitational diagram which is from the model tests at Astro laboratory.

So with the measured parameters. the similitude formulae there are determined the double unitary parameters η_{11} Q_{11}, and then with the universal characteristic of the model (obtained from producer documentation) the cavitation coefficient $\sigma_{11\ 0.5}$. In fig 1 the universal cavitational diagram is presented.

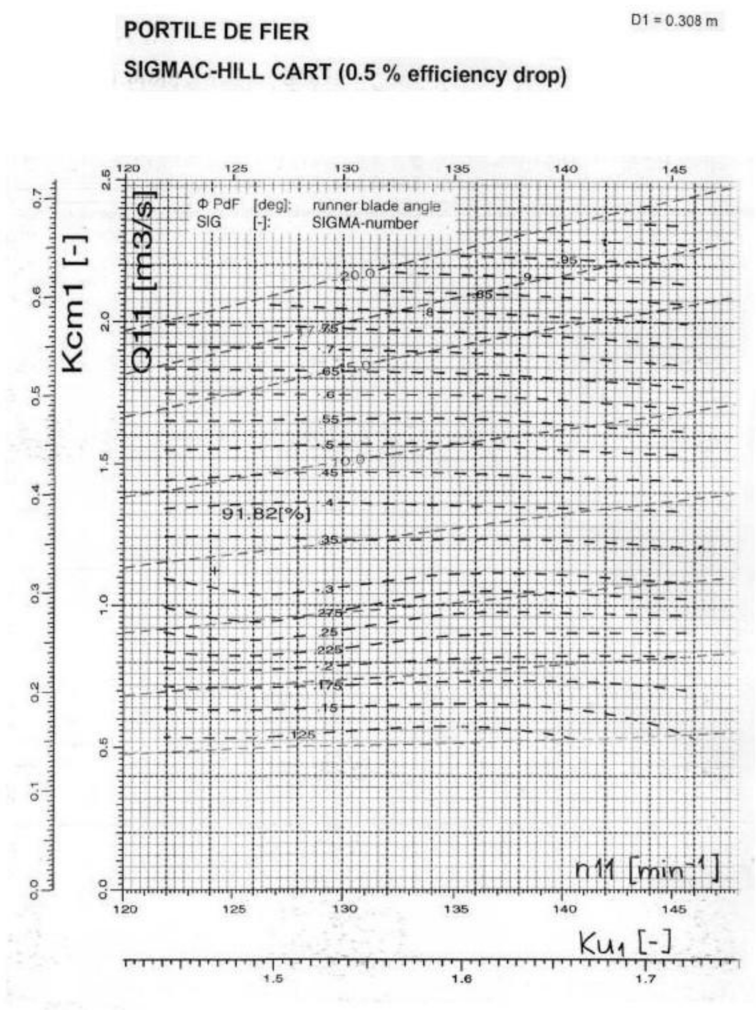

Fig. 1

To evaluate the cavitation coefficient $\sigma_M = \sigma_{0,5}$ from the diagram it is used the parameter Q_{11} depending on the parameter n_{11} and for the prototype cavitation coefficient it is used the transposition formula:

$$\sigma_T = \sigma_M \times k_{P\max 3M} k_{W3M}^2 \left(\frac{\eta_{hT}}{\eta_{hM}} - 1 \right) + \eta_{Ta\,M} k_{v3M}^2 \left(\frac{\eta_{hT}^2}{\eta_{hM}^2} - 1 \right) \qquad (3)$$

Where: $k_{p\max 3M} = \frac{w_{\max M}^2}{w_{3M}^2 - 1}$ – maximum speed coefficient of the model

$k_{P\max 3M} \cong 0,3$, $\eta_{Ta} \cong 0,8$.

$$k_{w3M} = \frac{w_{3M}}{\sqrt{2gH_M}}$$

$$k_{v3M} = \frac{v_{3M}}{\sqrt{2gH_M}}$$

$$k_{u1M} = \frac{D_M \pi\, n_M}{60(2g_M H_M)^{1/2}}$$ - tangential speed coefficient (4)

ISSN 1454 - 8003
Proceedings of 2014 International Conference of Hydraulics and Pneumatics - HERVEX
November 5 – 7, Calimanesti-Caciulata, Romania

Considering: $k_{w3M}^2 = k_{vm\ 1M}^2 + k_{u\ 1M}^2$

The parameters Q_{11m} si n_{11m} corresponding to the measured parameters there was evaluated with the similitude formulas, after the model parameters are determined.

For the efficiency value η_{11m} corresponding to the parameters Q_{11m} si n_{11m} it is obtained by the iteration method.

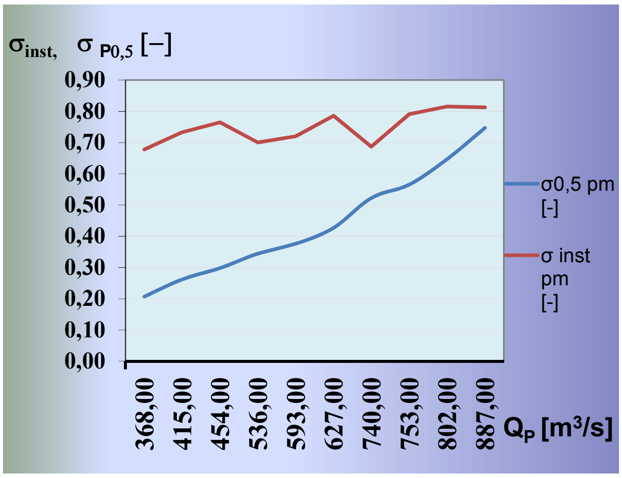

Fig. 2

It noticed that the coefficient values $\sigma_{P\ 0,5}$ is greater for greater flows and in conclusion there are worst cavitation conditions.

3. The determination of the "calculated" parameters of the axial hydraulic turbine

On the universal characteristic Fig. 3 of the turbine resulted from stand tests, the corresponding point of the industrial turbine operating point is defined by values "β_P" = "β_M" and "φ_P" = "φ_M" of the model and there are determined with Lagrange interpolation.the universal model parameters.

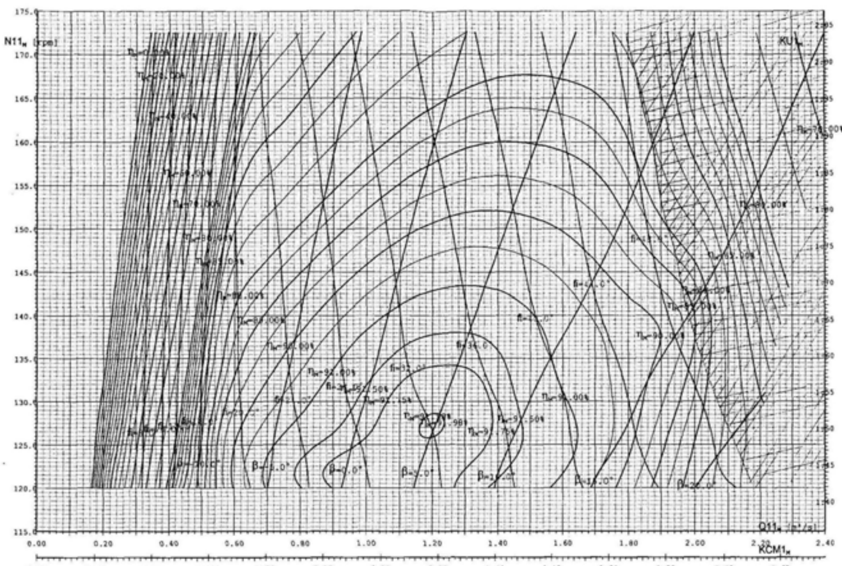

Fig. 3. Universal characteristic of the turbine model at the Iron Gates I turbines

Then the model parameters are obtained from the universal model parameters by the similitude formulae and model stand tests conditions. In the table 2 there are shown a selection of the operating model parameters in accordance with the wicket gates and runner blades opening of the registered parameters at the industrial turbine operation:

Table 2

φ [°]	β [°]	n_{11c} [rot/min]	Q_{11c} [m^3/s]	$\sigma_{11\ 0,5}$ [-]	Q_M [m^3/s]	n_M [rot/min]	η_M [%]	H_m [m]	P_M [kw]
27,53	-3,84	144	0,88	0.219	0,278	1.554,32	89,63	11,05	27,28
30	-1,60	143	0,99	0.263	0,312	1.542,41	90,4	11,03	30,95
32,03	0,26	142,5	1,092	0.296	0,344	1.535,87	90,81	11,02	34,28
34,08	3,94	136,5	1,22	0.342	0,384	1.469,68	91,79	10,99	38,68
36,00	6,60	137	1,36	0.405	0,428	1.473,20	91,53	10,96	42,95
38	8,07	135	1,47	0.45	0,463	1.450,10	91,33	10,94	46,27
40	12,45	127	1,62	0.531	0,510	1.361,95	91,08	10,90	50,76
42	12,67	129	1,71	0.581	0,538	1.381,94	90,68	10,88	53,28
44	14,19	131,5	1,79	0.628	0,563	1.407,33	90,29	10,85	55,46
46,18	16,67	129	1,93	0.717	0,607	1.378,04	89,14	10,81	58,90

In accordance with the model parameters obtained previously, the prototype turbine parameters are obtained by transposition with similitude formulae and some conditions of the model stand tests, in order to be compared with the measured parameters from the turbine operation. In the table 3 it is shown a selection of the prototype "calculated" data obtained from the model parameters in accordance with wicket gate and runner blades opening recorded from the turbine in operation:

Table 3

φ_p [°]	β_P [°]	Q_P [m^3/s]	η_T [%]	H_T [m]	P_{Cc} [MW]	H_S [m]	$\sigma_{cP\ 0,5}$ [-]	$\sigma_{inst\ P}$ [-]
27,53	-3,84	374,34	92,58	21,50	72,95	-9,36	0,241	0,914
30	-1,60	424,22	93,36	21,81	84,55	-10,16	0,289	0,935
32,03	0,26	469,75	93,77	21,96	94,71	-10,45	0,326	0,941
34,08	3,94	548,21	94,80	23,93	121,76	-9,80	0,376	0,832
36	6,60	609,36	94,54	23,76	133,97	-10,10	0,446	0,852
38	8,07	668,88	94,35	24,46	151,12	-10,76	0,495	0,855
40	12,45	784,44	94,17	27,62	199,72	-9,57	0,584	0,714
42	12,67	815,79	93,75	26,77	200,43	-10,96	0,639	0,790
44	14,19	838,31	93,34	25,76	197,35	-10,88	0,691	0,819
46,18	16,67	922,65	92,22	26,75	222,84	-11,37	0,789	0,811

The figure 4 represents the variation of the turbine and unit cavitation coefficient with the "calculated" flow of the prototype turbine.

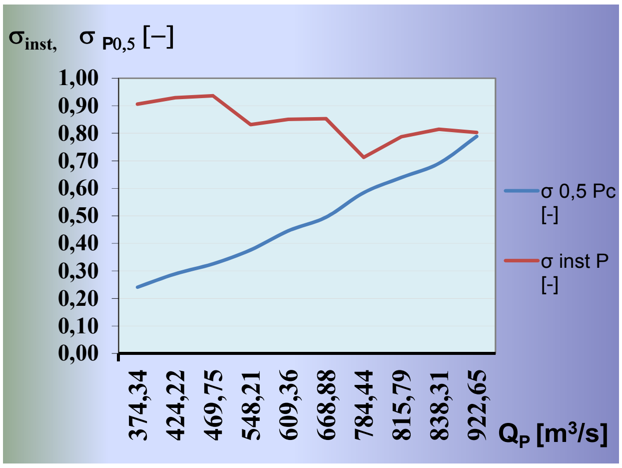

Fig. 4

4. The necessary corrections for the optimum operation of the axial hydraulic turbine

In order to study and optimize the turbine operation and to reduce the cavitation effect, there are evaluated the ″calculated″ parameters by the method described above for different measured parameters at H_{St} = cst. Then with the corresponding angle of the runner and wicket gates openings results from universal diagram of the model the double unitary parameters and then with the similitude formulas, the model parameters result.

In order to eliminate the errors between the “calculated” and measured parameters, the similitude formulas must be in corresponding with the measured parameters at the turbine operation which are the static head and the active power.

It is considered the turbine head formula included in the producer documentation:

$$H_{Tc} = H_{STm} + \frac{\alpha_1 Q_{Tc}^{\ 2}}{2gS_{P1}^{\ 2}} - \frac{\alpha_2 Q_{Tc}^{\ 2}}{2gS_{P2}^{\ 2}} \tag{5}$$

With the similitude formulas and the turbine head formula there are obtained the next formulas which evaluate the prototype turbine parameters:

$$Q_{Tc} = \frac{D_P}{D_M} \times \sqrt[3]{\frac{P_{A_m} \times D_P \times Q_M^{\ 2}}{g \times D_M \times H_M \times \eta_M \times \eta_G}} \tag{6}$$

Then it is evaluated the efficiency η_{Tc} with the next formula, which eliminates the errors from the statistical formulas in the world.

$$\eta_{Tc} = \left(\frac{n_P \times D_P}{n_M \times D_M}\right)^2 \times \eta_M \times \frac{H_M}{H_{ST_m} + \frac{\alpha_1 Q_{Tc}^{\ 2}}{2gS_{P1}^{\ 2}} - \frac{\alpha_2 Q_{Tc}^{\ 2}}{2gS_{P2}^{\ 2}}} \tag{7}$$

It is obtained the formula for the turbine power:

$$P_{Tc} = \gamma_P \cdot H_{Tc} \cdot Q_{Tc} \cdot \eta_{Tc} \cdot 10^{-6} = 998{,}3 \cdot 9{,}8066 \cdot H_{Tc} \cdot Q_{Tc} \cdot \eta_{Tc} \cdot 10^{-6} \ \text{[MW]} \tag{8}$$

From the documentation of the producer results the active power:

$$P_A = P_{Tc} \times \eta_G \tag{9}$$

The efficiency η_G is evaluated with the formula recommended by the producer.

With the parameters registered from the hydrounits for several years, there are obtained a data base in order to draw the real exploitation diagram of the turbine. If it is used the the Lagrange polynom for the registered parameters at H_{STm} = ct. to obtaind intermediate operating parameters.

In the table 4 there are presented the measured parametrs at H_{STm} = 25,77 m

Table 4

φ_p [°]	β_P [°]	η_{11} [%]	Q_{11} [m^3/s]	n_{11} [rot/min]	$\sigma_{0,511}$ [-]	P_{Cm} [MW]	Q_{Tm} [m^3/s]	η_G [%]	η_T [%]	$\sigma_{0,5\,P}$ [-]	$\sigma_{inst\,P}$ [-]
27,1	-2,1	91,5	0,76	123,49	0,207	108,80	395	98,40	94,64	0,228	0,654
29,5	-0,1	91,65	0,86	123,91	0,257	118,99	437	98,49	94,73	0,283	0,681
31,4	1,9	91,78	0,95	124,45	0,288	127,31	487	98,52	94,82	0,317	0,700
32,9	3,9	91,92	1,06	124,54	0,316	140,37	535	98,58	94,90	0,348	0,684
34,6	5,9	91,96	1,14	125,73	0,338	151,88	583	98,64	94,93	0,372	0,703
36,3	7,9	91,9	1,26	128,08	0,349	162,81	611	98,72	94,89	0,384	0,685
38,2	9,7	91,81	1,32	129,76	0,391	168,24	649	98,68	94,84	0,430	0,730
40,1	11,4	91,58	1,38	130,43	0,441	177,86	701	98,63	94,69	0,485	0,730
42,2	13,0	91,18	1,49	131,55	0,5	181,09	744	98,71	94,44	0,550	0,763
44,0	14,2	90,62	1,55	131,47	0,588	181,78	802	98,69	94,09	0,647	0,815
44,2	14,4	90,54	1,67	133,25	0,598	187,16	818	98,64	94,03	0,658	0,807
46,2	15,6	90,30	1,80	136,80	0,633	184,78	825	98,65	93,88	0,696	0,869

The figure 5 represents the variation of the turbine and unit cavitation coefficient with the measured flow of the prototype turbine at. H_{STm} = 25,77 m.

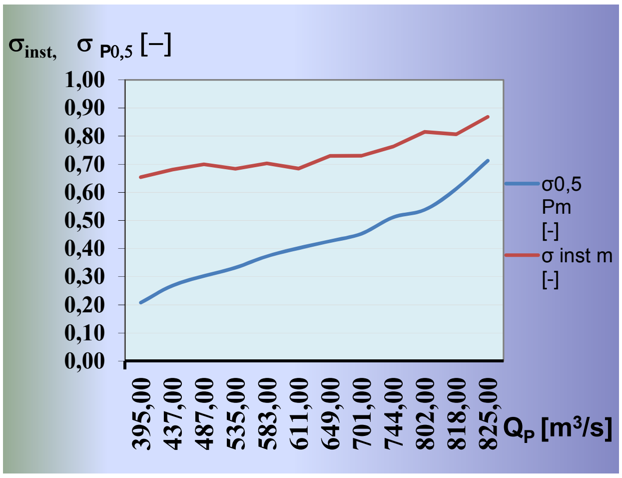

Fig. 5

In the table 5 there are presented the ″calculated″ parametrs at H_{STm} = 25,77 m with the method specifed previously.

Table 5.

φ_P [°]	β_P [°]	Q_P [m³/s]	η_P [%]	Q_{Tc} [m³/s]	η_{Tc} [%]	P_{Cc} [MW]	H_S [m]	$\sigma_{c\,0,5\,P}$ [-]	$\sigma_{inst\,c}$ [-]	ds [-]
27,1	-2,1	419,26	94,26	431,42	82,39	94,35	-9,18	0,253	0,750	1,12
29,5	-0,1	466,00	94,59	476,35	84,40	105,64	-9,56	0,303	0,764	1,10
31,4	1,9	512,79	94,82	518,88	85,68	116,10	-9,85	0,336	0,774	1,11
32,9	3,9	559,67	94,91	568,05	85,05	126,70	-9,56	0,374	0,763	1,08
34,6	5,9	606,63	94,88	615,40	86,10	138,08	-9,86	0,436	0,775	1,09
36,3	7,9	653,68	94,84	662,10	84,98	147,56	-9,59	0,459	0,764	1,06
38,2	9,7	700,85	94,38	702,37	87,22	158,16	-10,23	0,512	0,791	1,07
40,1	11,4	748,13	94,03	748,29	87,52	168,44	-10,11	0,570	0,787	1,05
42,2	13,0	795,53	93,73	785,13	90,36	179,26	-10,28	0,633	0,795	1,04
44,0	14,2	838,31	93,32	815,30	93,38	188,78	-10,88	0,690	0,820	1,06
44,2	14,4	843,08	93,28	826,49	92,33	190,25	-10,86	0,701	0,820	1,05
46,2	15,6	890,77	92,71	855,57	95,94	200,06	-11,51	0,770	0,846	1,04

The figure 6 represents the variation of the turbine and unit cavitation coefficient with the “calculated” flow of the prototype turbine at $H_{STm} = 25{,}77$ m. It is observed that there are lower cavitation condition for the calculated parameters as against the measured parameters.

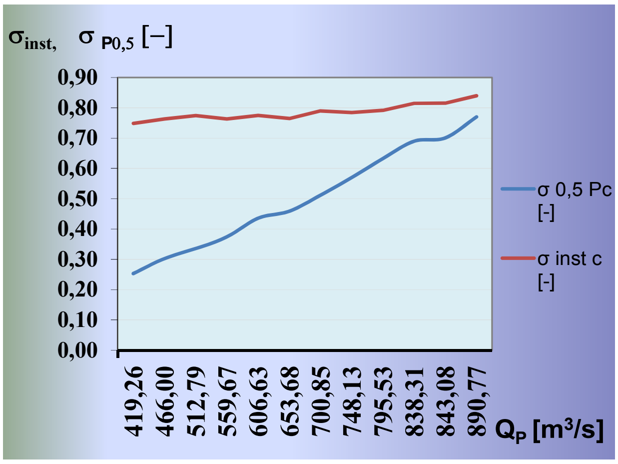

Fig. 6

It is considered in the table 5 “ds” as a coefficient of supplementary correction of the scale effect, which results from a great number of measurements achieved on the turbine exploitation.

It is observed in the figures 5 and 6, that there are lower cavitation condition for the ″calculated″ parameters as against the measured parameters.

In order to obtain from “calculated” parameters the real values correspondence to the measured parameters it is essential the supplementary coefficient of scale effect:

$$\eta_T = ds / \eta_{Tc} \; ; Q_T = ds \times Q_{Tc} \; ; P_T = (ds)^{2/3} \times P_{Tc} \tag{10}$$

5. Conclusions

Studying the parameters of cavitation in turbine operation with internationally known formulae, there are observed some substantial differences between data resulting from the calculation by universal diagram and those obtained from the measured parameters.

Comparing the diagrams translated from model to prototype with the corresponding diagram of the measured data, it is shown that for the situation, the turbine operates in lower conditions in terms of cavitation.

Hence we need to use a correction coefficient of the "calculated" parameters in accordance with the cavitation erosion phenomenon observed and found to comply with the existing reality and with the parameters measured in turbine operation at the Iron Gates I hydro-power plant.

It is recommended to determine the real exploitation diagram using a correction coefficient of an accurate assessment of the operating parameters at the turbine, which will reflect the reality by reducing the error caused by the phenomenon of similitude. If there are reduced the differences between the measured parameters and the "calculated" prototype parameters, the cavitation phenomenon is minimized.

REFERENCES

[1] Li S.C., (2000), Cavitation of Hydraulic Machinery, Imperial College Press, London.
Knapp R. T., Daily J. W., Hammit F. G., (1997), Cavitation, McGrawHill Book Company, New York.
[2] Bărglăzan M., (1999), Turbine hidraulice şi transmisii hidrodinamice, Ed. Politehnica, Timişoara.
[3] Simedru Adrian I, Bărglăzan Mircea, (2006), The Cavitation Problems Of The Axial Hydraulic Turbines Maintenance, HERVEX - Salonul international de hidraulica si pneumatica, sisteme de etansare, mecanica fina, scule, dispozitive si echipamente electronice specifice, mecatronica, editat de INOE – Institutul de Cercetări pentru Hidraulică și Pneumatică, Camera de Comerț și Industrie Vâlcea.
[4] Anton I., (1979), Turbine hidraulice, Ed. Facla Timisoara.
[5] Anton I., (2002), Energetic and cavitational scale-up effects in hydraulic turbines, Ed. Orizonturi Universitare Timisoara.

ISSN 1454 - 8003
Proceedings of 2014 International Conference of Hydraulics and Pneumatics - HERVEX
November 5 – 7, Calimanesti-Caciulata, Romania

MUST SEPARATION INTO NEW TYPE OF HYDROCYCLONE

Petru-Marian CÂRLESCU[1], Ioan ȚENU[1], Radu ROSCA[1]

[1] Department of Pedotechnics, Faculty of Agriculture, "Ion Ionescu de la Brad" University of Agricultural Sciences and Veterinary Medicine Iasi, pcarlescu@yahoo.com

Abstract: *A new type of hydrocyclone to separate must fine particles and achieve good quality wine, is designed. The hydrocyclone separating the particles from the liquid at the bottom thereof, and the liquid is discharged from the top of it. In this paper, computational fluid dynamics (CFD) and experimental study on separation efficiency of particles larger than 100 µm has been used. CFD simulations were performed with FLUENT software, by coupling the Reynolds stress model (RSM) for must flow with discrete phase model (DPM) to track the trajectory of particles to be separated by hydrocyclone. The using of RSM is useful because of the high degree of anisotropy in the must flow. The dynamics of solid particles is analyzed by using the stochastic Lagrangian model by DPM, considering phases continuous interaction. The testing of the hydrocyclone on stand allows the adjustment of flow rates and determine the must turbidity both at inlet and outlet of the hydrocyclone. The experimental values of separation efficiency are correlated with values obtained by CFD simulation for flow rate of 0.0508 kg/s. A decrease of separation efficiency in the hydrocyclone is distinguished, both experimentally and by simulation, with decreasing of particle diameter to 100 µm, for all hydrocyclone flow rates.*

Keywords: *hydrocyclone, must fine particles, Computational Fluid Dynamics (CFD), separation efficiency.*

1. Introduction

The high quality of a wine is determined by the high quality of a must. A quality must implies a cleaning phase. The existing particles into must are of organic and inorganic nature, depending on grape's contamination and the obtained process. The separation of these particles is done now by sedimentation or filtration. Both sedimentation and filtration present several disadvantages in terms of time and continuity of the separation process. Wine industry is looking for solutions for solid particles separation during must production and final stage wine clarify as well. The operation of hydrocyclones into processing plants lead to the removal of particles with sizes up to 100 µm. The amount of deposit in the form of organic and inorganic particles from wine is about 5% for gravity flow of the must. The type of pressing can reach up to 6% hydraulic presses and 15% for continuous presses. The smaller particles can be removed by subsequent filtering, if the wine technology required. Usually, it avoids the separation of particles smaller than 100 µm, since the yeast cells (5 -10 µm) could be separated, being useful in fermentation process. The advantages of separation by hydrocyclones consist in the short time separation, quality separation and the function in continuous condition. New design hydrocyclones can be developed, as a result of support provided by CFD simulations. Compared with an usual hydrocyclon, the studied hydrocyclon has a modified geometry and functions with only one outlet pipe, which stabilizes the air-core from inside the pipe and doesn't affect the separation process at the purging pipe.

In the past, many efforts have been made to experimentally study the flowing into a hydrocyclone, by using high-speed shooting of anisole droplets moving through a hydrocyclone and determine the velocities of liquid flow [1]. More recently, a number of researchers reported their measurements using laser Doppler velocimetry (LDV) and electrical impedance tomography [2,3]. Proposed experimental methods are expensive and difficult to apply technically, being limited to a liquid dispersed. In the view of these shortcomings, in the past two decades, various efforts have been made to develop a CFD model. Boysan developed one of the first CFD models and showed that the standard k-ε turbulence model was inadequate to simulate flows in a hydrocyclone, because led to excessive turbulence viscosities and unrealistic tangential velocities

[4]. A number of studies suggest that RSM can improve the accuracy of numerical solutions [5,6]. So far, many studies have been focused on the analysis of fluid flow into hydrocyclone and a few researchers have studied the movement of solid particles [7,8,9]. Wang published an experimental investigation, using a high-speed motion analyzer (HSMA) system to track the trajectories of solid particles and lately studied the dynamic of solid particles using stochastic Lagrangian model [10]. Medronho, performed studies on the movement of organic particles into a hydrocyclone, by supervise the separation of microorganisms and mammalian cells [11]. The simulations were performed at different working pressures, in order to obtain the trajectory of starch particles of different sizes [12].

In this paper, CFD simulations were performed with mathematical models, with the purpose to increase the separation efficiency. The results consider flow simulation and particle trajectory into hydrocyclone. The proposed hydrocyclone was simulated by coupling the Reynolds stress model for must flow with discrete phase model to follow the trajectory of the particles to be separated. The hydrocyclone testing was conducted by using an experimental pilot plant with which the particle separation efficiency must be determined for various conditions.

2. Numerical Methods

The hydrocyclone geometry for CFD simulation is displayed in Fig. 1. The dimensions of the hydrocyclon used in simulation are shown in Table 1.

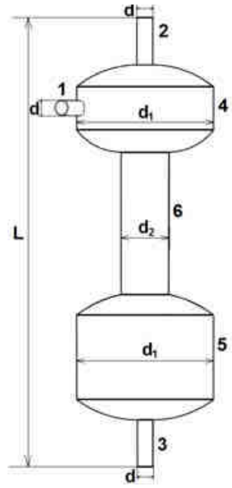

Fig. 1. Hydrocyclone geometry (1 - inlet pipe, 2 - outlet pipe, 3 – bottom purging pipe, 4 - top body; 5 - bottom sedimentation body; 6 - middle body).

Table 1 Hydrocyclone dimensions used in simulation and experiment.

d (m)	*d_1 (m)*	*d_2 (m)*	*L(m)*
0.0172	0.1612	0.056	0.536

The hydrocyclone discretization was realized in the Gambit v. 2.2.30 software with tetrahedral type mesh. A mesh density of 4,036,398 cells was optimal for good simulation and reasonable computational time. Any further increase in cell number did not result in any change in the predicted velocity profiles, indicating that the finest grid was sufficiently fine for mesh-independent flow predictions. The number of cells near the wall was10, distributed over a distance of 5 mm and the first near-wall node is placed in the direct vicinity of the wall at $y^+ \approx 1$, where the low-Reynold number approach is adequate. The near-wall mesh is fine enough to be able to resolve the viscous sublayer by applying standard wall function in the Reynolds stress model. The quality of the mesh is described by criterion CES “cell equivolume skew” which is a nondimensional parameter calculated using the volume deviation method. A value of 0 indicates a best case equilateral cell and a value of 1 indicates a completely degenerate cell. Degenerate cells (slivers) are characterized by nodes that are nearly coplanar. The CES parameter evaluated for the hydrocyclone tetrahedral meshing is 0.8 for less than 0.1% of total cells.

The precise description of the must flow into a hydrocyclone by simplified relationships is more difficult to capture when velocity and pressure gradients are large on radial direction. To characterize the turbulent flow that arises as must rotation inside hydrocyclone, a properly turbulence model is necessary to be applied. RSM describes with good accuracy the anisotropic turbulence. The choosing of the Reynolds stress model proved to be a suitable turbulence flow model in a hydrocyclone, although it is a model that requires higher computational resources than other simplified models of turbulence [13,14].

The mathematical model which can simulate particles trajectory of discrete phase with the FLUENT software in a liquid-solid mixture is achieved by integrating the force balance on a particle [15]. The dispersion of particles due to turbulence can be predicted using the stochastic tracking model, which includes the effect of instantaneous turbulent velocity fluctuations on the particle trajectory.

The force balance between flotability and drag forces in a Lagrangian reference frame can be written as:

$$\frac{d\vec{u}_p}{dt} = F_D\left(\vec{u} - \vec{u}_p\right) + \frac{\vec{g}\left(\rho_p - \rho\right)}{\rho_p} \tag{1}$$

were $F_D\left(u - u_p\right)$ is the drag force per unit particle mass and

$$F_D = \frac{18\mu}{\rho_p {d_p}^2} \frac{C_D \, \mathrm{Re}}{24} \tag{2}$$

where u is the velocity of liquid phase, u_p velocity of the particle, μ the dynamic viscosity, ρ fluid density, ρ_p particle density, d_p particle diameter, C_D sedimentation coefficient.

Re is the relative Reynolds number, which is defined as

$$\mathrm{Re} = \frac{\rho d_p \left| u_p - u \right|}{\mu} \tag{3}$$

Coupling between discrete phase (particles) and continuous phase (must) in FLUENT is done with an algorithm where the continuous phase has an effect on discrete phase and discrete phase does not influence the continuous phase. The first step aims the solving of the continuous phase flow until it reaches the stability of the solution, then it resolve the discrete phase model.

The necessary boundary conditions for hydrocyclone simulation are given in the inlet region of homogeneous must-particle mixture and for the two outlets of the liquid and solids respectively.

The inlet velocity of the must and particles are considered equal and constant values for simulation. Uniform velocity boundary conditions were used at the inlet, based on the flow rates. Hydrocyclone works with pipe purging closed but it is opened when purging. The bottom purging pipe remains open for a short time.

CFD simulations were performed with the bottom purging pipe closed. The outlet used pressure outlet boundary condition. The outlet must is moving under absolute pressure 1 atm therefore the gauge pressure at overflow or underflow are zero.

Flow rate values, in hydrocyclone for must and particles are shown as Table 2.

Table 2 Parameters in the simulation and experiment.

Flowrate (kg/s)	0.395	0.538	0.586
Must Flowrate (kg/s)	0.358	0.488	0.531
Particle flowrate (kg/s)	0,0372	0,0508	0,0553
Particle density (kg/m^3)		1130	
Must density (kg/m^3)		1085	
Must viscosity (Pa ·s)		0.0018	

Separation of solids in the must assumes the knowledge of the type and structure of existing particles must. The particles separated into hydrocyclone are considered spherical with different sizes and listed in Table 3. For small size of microbial suspensions, colloids and other solids, rejection electrical charges occur into hydrocyclone and separation is achieved by other methods (eg filtration, gluing). The separation of dispersed particles must up at 100 μm occur as a result of a centrifugal and gravitational force field.

Experimentally, the sedimentation of a mixture of must and particles was performed into a cylinder at 20 °C and it has been found that only particles with a diameter larger than 500 μm were deposited, while for the mixture water-particles, at the same temperature, the deposited particles have a diameter larger than 200 μm, because of lower viscosity.

Table 3 Particles of the must composition.

Origin	*Diameter (μm)*	*Observations*
organic and anorganic	100	particles macroscopically
	200	particles decanted in water at 20 °C
	500	particles decanted in must at 20 °C
	2000	grape seeds

Grad-efficiency curves are CFD obtained by means of a stochastic particle tracking technique. The results of the experimental study and CFD simulations for three different flow rates are shown as Fig. 10.

The grade efficiency E_G is defined as ratio between the mass fraction of solids recovered in the purging pipe F_s and total mass of injected particles M_T.

$$E_G = \frac{F_s}{M_T} \cdot 100 \tag{4}$$

For calculating the grade efficiency E_G, a given mass flow rate of each of the aforementioned particles was injected into the hydrocyclone, and the particle trajectories were calculated. FLUENT could then calculate and report the mass flow rate of trapped and escaped particles, which were the particles reaching the purging and overflow, respectively. Based on these mass flow rates, the total efficiency could be calculated. A similar procedure was adopted for grade efficiency calculations, but using mass flow rates of particles of the same size. Experimentally, the separation efficiency is obtained by measuring the turbidity of the must at the inlet and outlet of hydrocyclone. By doing the wight difference, the number of particles of a certain diameter collected in the bottom purging pipe is obtained.Particles were considered spherical and the diameter distribution was obtained statistically by microscopic measurements.

In this paper, simulations were conducted using the discretisation of all conservation equations with the upwinding discretisation and the SIMPLE pressure-velocity coupling algorithm, which coupling continuity and momentum equations. For pressure discretisation, the PRESTO (pressure staggering options) scheme was applied.

The convergence of the solution through steady solver was achieved by applying under-relaxation coefficients of 0.35 and 0.5 for viscous turbulence equations. The convergence criterion used for all variables was imposed to 0,0001. Using RSM convergence is much more difficult to achieve. Flow simulation must and motion of particles into hydrocyclone is calculated with TYAN workstation (2xCPU-Intel Xeon 3.33 GHz, RAM - 16 GB DDR3).

3. Experiments

All devices for experiment, including pump, tanks, agitator, pressure gauge, flowmeter recorder and hydrociclon separator are shown as Fig. 2 a and Fig. 2 b. Must-particle mixture to be separated is continuously stirred in tank 1 and sent through the pump 3 to the hydrocyclone. The solid particles separated by the hydrocyclone were collected in the tank 6, and the clarified must was collected in the tank 9. The must turbidity is monitored both at the inlet and outlet of the hydrocyclone with glass cylinders 2 and 7. The evaluation of separation efficiency was done by collecting and measuring the turbidity of must samples at the inlet and outlet of the hydrocyclone.

The operating pressure and flow rates at the outlets experiment and CFD simulation are shown as Table 4.

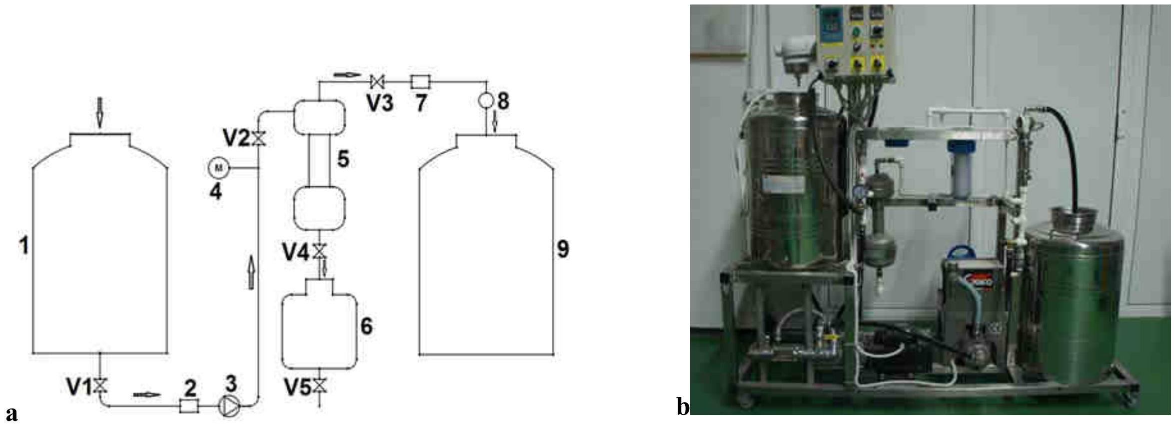

Fig. 2. Schematic diagram (**a**) and the experimental pilot plant (**b**) (1 – feeding tank, 2 – glass cylinder, 3– pump, 4 – pressure gauge, 5 – hydrociclon, 6 – purging tank, 7 – glass cylinder, 8 – flowmeter recorder, 9 – tank, V1-V5 – gate valves).

Table 4 Parameters in the experiment and CFD simulation.

Operating pressure (bar)	1.1	1.8	2.1
Experimentally Outlet flowrate (kg/s)	0.361	0.497	0.568
Simulated Outlet flowrate (kg/s)	0.374	0.511	0.552

4. Results and Discussion

The results of the processing are evidenced by the pathlines and the tracks of the particles of various sizes. The final objective is to identify the size and evolution of separated particle from the inlet to the outlet of the hydrocyclone in connection with the turbulence of must into hydrocyclone.

After stabilizing the flow in the bottom sedimentation body of the hydrocyclone, the pathlines focus to the top for a flow rate of 0.488 kg/s, and for a flow rate of 0.358 kg/s or 0.531 kg/s the pathlines reach to the purging pipe, Fig. 3.

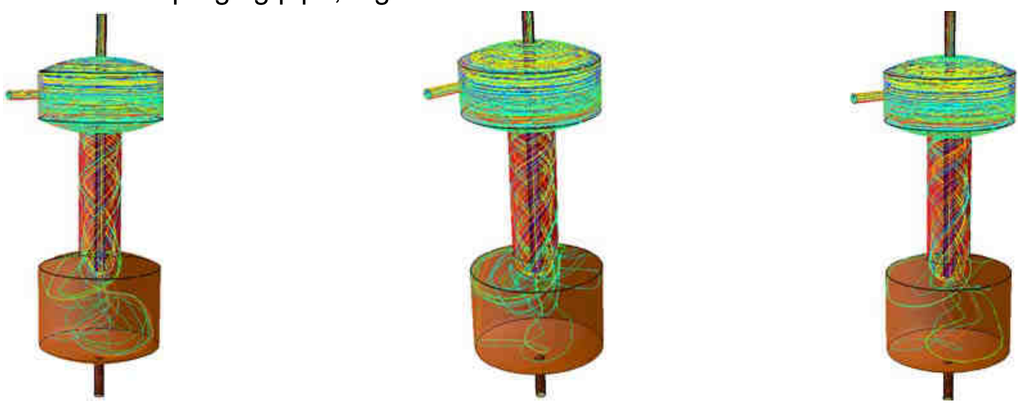

a **b** **c**

Fig.3. Pathlines tracks for three must flow rates (**a-** Q_1= 0,358 kg/s, **b-** Q_2= 0,488 kg/s, **c-** Q_3= 0,531 kg/s).

By analyzing particles trajectory inside the hydrocyclone according to their size the separation efficiency could be calculated, for the particle flow rates of Q_{P1}, Q_{P2} and Q_{P3} respectively.

The trajectories of particles of 2000 μm obtained by simulation are minimal, Fig. 4. All the particles injected through inlet pipe is found in the bottom purging pipe and no particle is discharged from the hydrocyclone with must, so with a separation efficiency of 100% for the three flow rates.

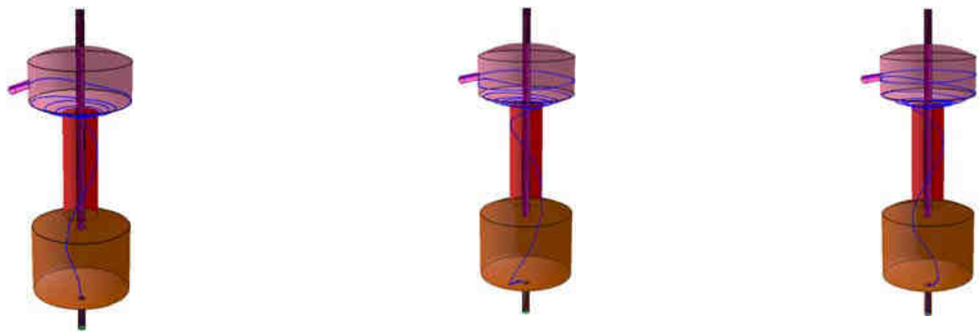

a **b** **c**

Fig. 4. The tracks for the three particle flow rates with d_p = 2000 μm (**a-** Q_{P1}= 0,0372 kg/s, **b-** Q_{P2}= 0,0508 kg/s, **c-** Q_{P3}= 0,0553 kg/s).

The particles of 500 μm injected through inlet pipe hydrocyclone shall be deposited in the bottom purging pipe, while some leave hydrocyclone along with the must. At this diameter of particles, the separation efficiency is of 51%, 58% and 42% for Q_{P1}, Q_{P2} and Q_{P3} respectively.

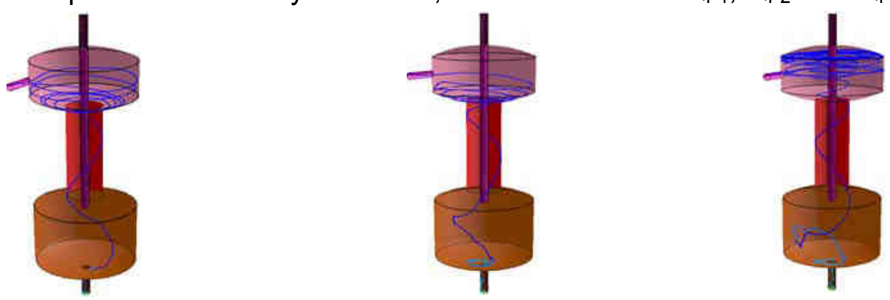

a **b** **c**

Fig. 5. The tracks for the three particle flow rates with d_p = 500 μm (**a-** Q_{P1}= 0,0372 kg/s, **b-** Q_{P2}= 0,0508 kg/s, **c-** Q_{P3}= 0,0553 kg/s).

The trajectory of the particles is circular, following the profile of top cylindrical body, as a result of centrifugal forces and by the downward movement; the particles trajectory became sinuous at the bottom sedimentation body of the hydrocyclone, Fig. 5.

The particles that leave the hydrocyclone are involved by the must through the central outlet pipe, Fig. 6. At Q_{P1} flow rate, the particle is driven till the middle of bottom sedimentation body of hydrocyclon, then is discharged from the hydrocyclone; for Q_{p3} flow rate, particle trajectory approaches to the external of central pipe, being driven by the must through the outlet pipe.

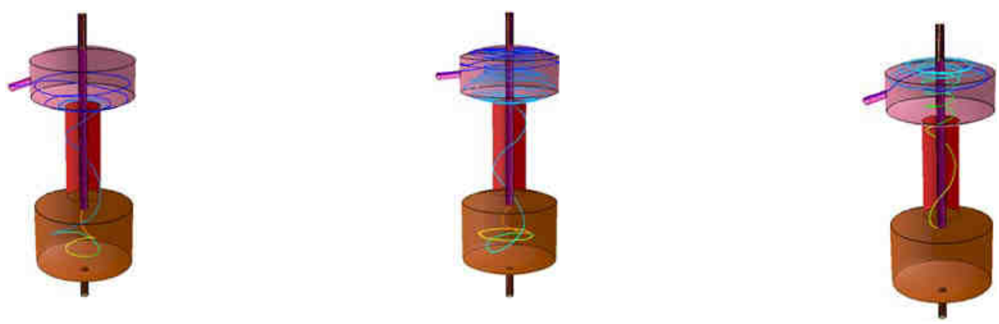

a **b** **c**

Fig. 6. The tracks for the three particle flow rates with d_p = 500 μm (**a-** Q_{P1}= 0,0372 kg/s, **b-** Q_{P2}= 0,0508 kg/s, **c-** Q_{P3}= 0,0553 kg/s).

ISSN 1454 - 8003
Proceedings of 2014 International Conference of Hydraulics and Pneumatics - HERVEX
November 5 – 7, Calimanesti-Caciulata, Romania

The trajectory of the particles with the diameter of 200 μm becomes sinuous, these being lighter, compared to the 500 μm particles. The separation efficiency is of 20%, 24.2% and 15.7% for the three particle flow rates Q_{P1}, Q_{P2} and Q_{P3} respectively. For all the three types of the simulated particle flow rates, an emphasis of particle movement is in the body top arises and the trajectory length in the bottom sedimentation body is minimal for Q_{P2}, average for Q_{P1} and maximum for Q_{P3}. Finally, for all three particle flow rates, the particles come to be collected into the purging pipe, Fig. 7.

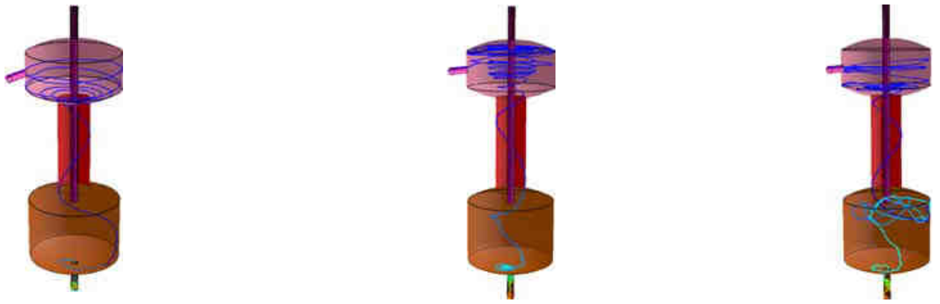

a b c

Fig. 7. The tracks for the three particle flow rates with d_p = 200 μm (**a-** Q_{P1}= 0,0372 kg/s, **b-** Q_{P2}= 0,0508 kg/s, **c-** Q_{P3}= 0,0553 kg/s).

Other particles are carried by must, and discharged from the hydrocyclone through the outlet pipe, Fig. 8.

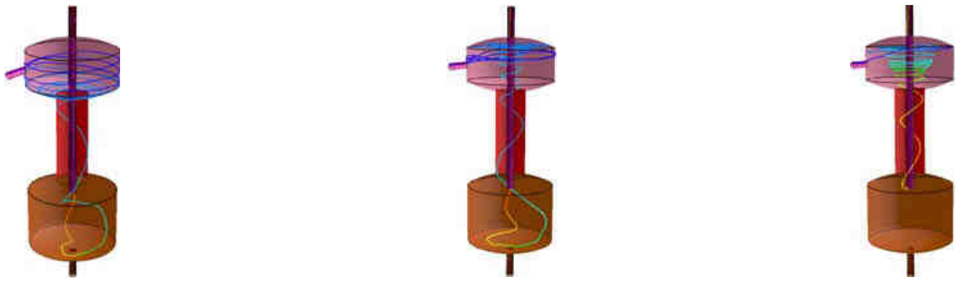

a b c

Fig. 8. The tracks for the three particle flow rates with d_p = 200 μm (**a-** Q_{P1}= 0,0372 kg/s, **b-** Q_{P2}= 0,0508 kg/s, **c-** Q_{P3}= 0,0553 kg/s).

Both Q_{P1} and Q_{P2} particle reaching into the sedimentation body touches the bottom wall losing kinetic energy but not enough to not be driven by the must through the outlet pipe. There is a high probability that some of the particles to be entrained by the must to remain as a deposit on the bottom of the sedimentation body. At the particle flow rate Q_{p3} particle trajectory is similar to the previous case.

Particles with the diameter of 100 μm are carried by must to the outside of the hydrocyclone and only a small fraction is collected at the bottom of the hydrocyclone. The separation efficiency is of 2.4%, 4.28% and 0% for the three particle flow rates Q_{P1}, Q_{P2} and Q_{P3} respectively. As the particles reach the bottom wall and by the friction lose of the necessary energy of motion, the separation efficiency is higher for Q_{P2}, compared with the other particle flow rates, Fig. 9. For Q_{P1} flow rate, the particle has a sinuous trajectory and is very close to reach the bottom wall of the sedimentation body; for Q_{P3} flow rate, the particle adheres to the central pipe of hydrocyclone, being quickly discharged along with must.

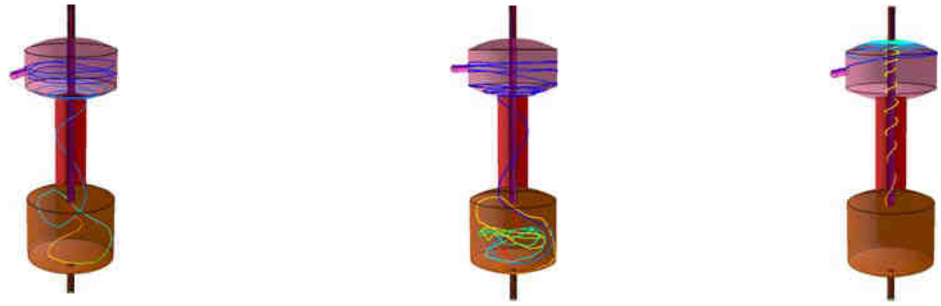

a b c

Fig. 9. The tracks for the three particle flow rates with d_p = 100 μm (**a-** Q_{P1}= 0,0372 kg/s, **b-** Q_{P2}= 0,0508 kg/s, **c-** Q_{P3}= 0,0553 kg/s).

For smaller than 100 μm dimensions, which are close to the size of yeast cells (~ 10 μm) as a result of the viscosity of the must and electrical phenomena that occur, the particles tend to remain in suspension, and finally to be carried by the must through the outlet pipe.

By analyzing the flow field of must and the particles trajectory from sedimentation body of hydrocyclon (Fig. 3, 6, 8, 9) an intensive circulation on vertical axis of outlet pipe has been observed. This circulation of both must and particles explains the delivery of small dimensional particles to outlet pipe. The circulation decreases near to purging pipe making possible the sedimentation of particles with larger size than 200 μm, Fig. 4, 5, 7.

The graphical representations of the separation efficiency for different particle diameters consider the ratio of Eq. (4), Fig. 10.

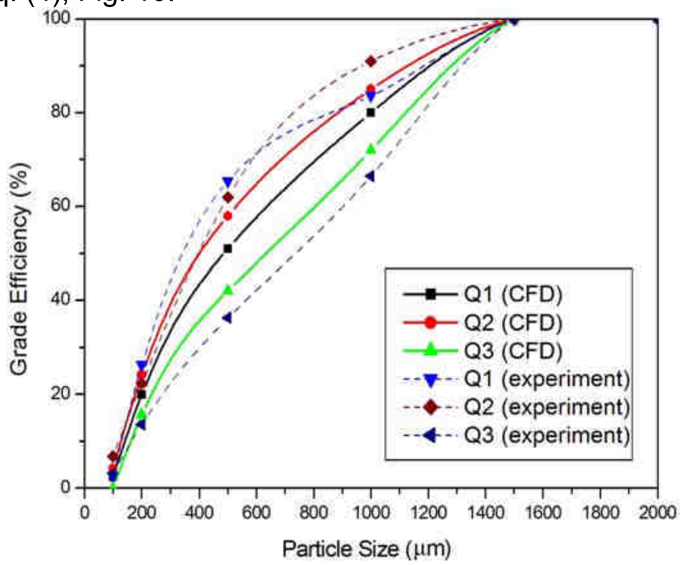

Fig.10. Graphic separation efficiency for various particle diameters injected into hydrocyclone

Both the experimental and CFD simulations give a separation efficiency of 100% for particle diameter larger than 1500 μm, and for the diameters equal or smaller than 100 μm the separation efficiency is less than 6.8%.

The standard deviation is minimal for Q_{p2} particle flow rate and the separation efficiency obtained by CFD simulation is close to the experimental values.

5. Conclusions

A hydrocyclone with new geometry that works continuously has been studied. The constructive purpose targeted the separation of particles from a must. The mathematical modelling and CFD (Computational Fluid Dynamic) simulation of the flow of a mixture in the proposed hydrocyclone showed the pathlines trajectories of the fluid and solid particles.

The CFD simulation, useful for optimizing the structural and functional characteristics of hydrocyclone, used RSM (Reynolds Stress Model) for simulation of must flow and DPM (Discrete Particle Model) for simulation of particle trajectory inside the hydrocyclone. For the hydrocyclon simulation, three different flow rates of must and solids input were introduced.

As a result of simulation of must flow into hydrocyclone, an intensive circulation into sedimentation body on vertical axis of outlet pipe has been observed, which induces a sinuous trajectory of particles in this region. The circulation decreases near to purging pipe making possible the sedimentation of particles with larger size than 200 µm. The new geometry of the hydrocyclone allows the coexistence of higher centrifugal forces at the top body without affecting the separation of particles from the must in the bottom body.

The turbidity of the must for different flow rates was experimentally determined at both inlet and outlet from the hydrocyclone. For these flow rates, the best separation was performed by CFD simulation, while the diameter of the particles remained in the must at the outlet of the hydrocyclone was smaller than 100 µm.

The comparison of experimental and simulated data for the three flow rates showed a good correlation for a must feed flow rate of 0.488 kg/s and 0.0508 kg/s of particle feed flow rate respectively.

REFERENCES

[1] S. R. Knowles, D. R. Woods, and Ia. Feuerste, “Velocity distribution within a hydrocyclone operating without an air core.” 1973, *Can. J. Chem. Eng.*, 51, pp. 263-271.
[2] K. T. Hsieh, and R. K. Rajamani (1991). “Mathematical-model of the hydrocyclone based on physics of fluid-flow.”1991, *AIChE J.*, 37, pp.735-746.
[3] G. Q. Dai, W. M Chen, J. M. Li, and L. Y. Chu, “Experimental study of solid-liquid two-phase flow in a hydrocyclone.” 1999, *Chem. Eng. J.*, 74, pp. 211-216.
[4] F.Boysan, W. H. Ayers, and J. Swithenbank, “Fundamental mathematical-modelling approach to cyclone design.” 1982, *Trans. Inst. Chem. Eng.*, 60, pp. 222-230.
[5] M. Sommerfeld, and C. A. Ho, “Numerical calculation of particle transport in turbulent wall bounded flows.“ 2003, *Powder Technol.*,131, pp.1- 6.
[6] J. C. Cullivan, R. A. Williams, T. Dyakowski, and C. R. Cross, “New understanding of a hydrocyclone flow field and separation mechanism from computational fluid dynamics.“ 2004, *Miner. Eng.*, 17, pp. 651-660.
[7] KT.Hsieh, “Phenomenological model of the hydrocyclone.”, 1988, PhD Thesis, The University of Utah, USA.
[8] K.J. Hwang, W.S. Hsueh, and Y. Nagase, “Mechanism of particle separation in small hydrocyclone.” 2008 Dry Technol., 26, pp.1002- 1010.
[9] Y.Qiang, L. Wen-jie, M. Liang, and W.Hua-lin, “CFD study on separation enhancement of mini-hydrocyclone by particulate arrangement.” 2013, Separation and Purification Technology, 102, pp.15-25.
[10]Z. B. Wang, L.Y. Chu, W.M. Chen, and S.G. Wang, “Experimental investigation of the motion trajectory of solid particles inside the hydrocyclone by a Lagrange method.” 2008, J. Chem. Eng., 138, pp.1–9.
[11]R. A. Medronho, J. Schuetze, and W. D. Deckwer, “Numerical Simulation of Hydrocyclones for Cell Separation.” 2005, Lat Am Appl Res., 35, pp.1-8.
[12]C. Y. Hsu, J. S. Wu, and R. M. Wu, “Separation and Tracks in a Hydrocyclone Particles” 2011, Tamkang Journal of Science and Engineering, 14(1),pp. 65-70.
[13]B. Wang, and A. B. Yu, “Numerical Study of the Gas-Liquid-Solid Flow in Hydrocyclones with Different Configuration of Vortex Finder.” 2008, J. Chem Eng., 135, pp.33-42.
[14] P. Xu, Z. Wu, A. S. Mujumdar, and A. B. Yu, “Innovative Hydrocyclone Inlet Designs to Reduce Erosion-Induced Wear in Mineral Dewatering Processes.” 2009, Drying Tech., 27,pp. 201-211.
[15] Fluent 6.3, 2006, “Fluent user’s guide.” Ansys Inc.USA.

ISSN 1454 - 8003
Proceedings of 2014 International Conference of Hydraulics and Pneumatics - HERVEX
November 5 – 7, Calimanesti-Caciulata, Romania

FLOATING MICRO HYDROPOWER PLANTS FOR RIVER WATER KINETIC ENERGY CONVERSION

Ion BOSTAN[1], Valeriu DULGHERU[1], Viorel BOSTAN[1]

[1] Technical University of Moldova, utmrectorat@gmail.com. [2]dulgheru@mail.utm.md.

[3]viorel_bostan@mail.utm.md

Abstract: *International research confirms that the emission of greenhouse gases is substantially lower in the case of hydropower compared to that generated by burning fossil fuels. The analysis of the constructive diversion of micro hydroelectric power plants, examined previously, does not satisfy completely from the point of view of water kinetic energy conversion efficiency. In order to increase the conversion factor of water kinetic energy (Betz coefficient), a number of structural diagrams of floatable micro hydro power plants has been developed and patented. The micro hydropower plants comprise a rotor with vertical axis and vertical blades with hydrodynamic profile in normal section. The blades are connected by an orientation mechanism towards the water streams direction.*

Keywords*: hydraulic kinetic energy, rotor with hydrodynamic blades.*

1. Introduction

The inevitable increase of global energy consumption and the risk of a major environmental impact and climate change as a result of burning fossil fuels opens wide prospects for the exploitation of renewable energies. Hydropower, as a renewable energy source, will have an important role in the future. International research confirms that the emission of greenhouse gases is substantially lower in the case of hydropower compared to that generated by burning fossil fuels. From the economical point of view, the utilisation of half of the feasible potential can reduce the emission of greenhouse gases by about 13%; also it can substantially reduce emissions of sulphur dioxide (main cause of acid rains) and nitrogen oxides.

Hydraulic energy is the oldest form of renewable energy used by man and has become one of the most currently used renewable energy sources, being also one of the best, cheap and clean energy sources. Hydraulic energy as a renewable energy source can be captured in two extra power forms:

– potential energy (of the natural water fall);

– kinetic energy (of the water stream running).

Both extra power forms can be captured at different dimensional scales.

To avoid the construction of dams, it is possible to use the river kinetic energy by utilizing water flow turbines. This type of turbines can be mounted easily and are simple in operation. Their maintenance costs are rather convenient. The section of Prut River is equivalent to 60 m^2 and its mean velocity in the zones of exploration is (1-1,3) m/s, which is equivalent to approximately (30-65) kW [1,2,3] of theoretical energy. Taking into account the fact that the turbine can occupy only a part of the riverbed, the generated energy could be much smaller. The analysis of the constructive diversion of micro hydroelectric power plants, examined previously, does not satisfy completely from the point of view of water kinetic energy conversion efficiency. The maximum depth of blade's immersion is

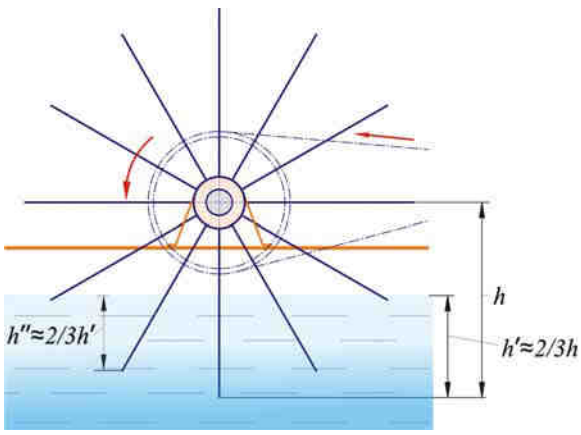

Figure 1. Conceptual diagram of the water wheel with rectilinear profile of blades.

about 2/3 of the blade height *h* in a classical hydraulic wheel with horizontal axle (Fig. 1). Thus, only this surface of the blade participates at the transformation of water kinetic energy into mechanical one. As well, the preceding blade covers approximately 2/3 of the blade surface plunged into the water to the utmost *(h''≈ 2/3h')*, that reduces sensitively the water stream pressure on the blade. The blade, following the one that is plunged into the water to its utmost, is covered completely by it and practically does not participate in the water kinetic energy conversion. Therefore the efficiency of such hydraulic wheels is small.

Insistent searches of authors have lead to the design and licensing of some advanced technical solutions for outflow micro hydroelectric power plants. They are based on the hydrodynamic effect, generated by the hydrodynamic profile of blades and by the optimal blades' orientation towards water streams with account of energy conversion at each rotation phase of the turbine rotor (Fig. 2). To achieve this, it was necessary to carry out considerable multicriteria theoretical research on the selection of the optimal hydrodynamic profile of blades and the design of the orientation mechanism of blades towards the water streams.

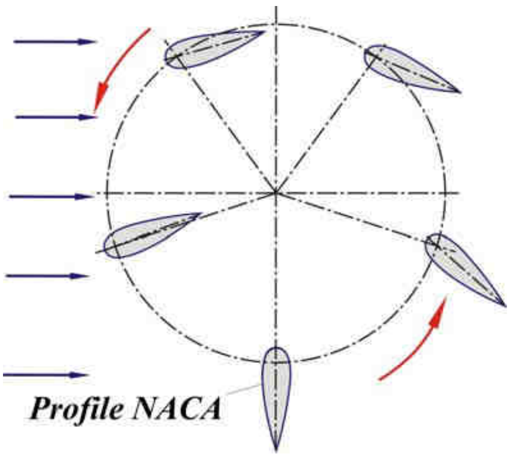

Figure 2. Conceptual diagram of the water rotor with hydrodynamic profile of blades with its orientation towards the water streams.

The main advantages of these types of micro hydroelectric power plants are:

- reduced impact on the environment;
- civil engineering works are not necessary;
- the river does not change its natural stream;
- possibility to produce floating turbines by utilizing local knowledge.

Another important advantage is the fact that it is possible to install a series of micro hydro power plants at small distances (about 30-50 m) along the river course. The influence of turbulence caused by the neighboring plants is excluded.

The conceptual development of the plant structures with hydrodynamic profile of the blades was performed on the basis of three conceptual diagrams:

- Micro hydropower plant with pintle and blades fixed on the vertical axles anchored by steel structure;
- floatable micro hydro power plant with pintle and blades fixed on the vertical axles;
- floatable micro hydro power plant with horizontal axis and blades fixed on the horizontal axles.

In order to increase the conversion factor of water kinetic energy (Betz coefficient), a number of structural diagrams of floatable micro hydro power plants has been developed and patented [6-12]. The micro hydropower plants comprise a rotor with vertical axis and vertical blades with hydrodynamic profile in normal section. The blades are connected by an orientation mechanism towards the water streams direction. The rotational motion of the rotor with vertical axis is multiplied by a mechanical transmissions system and is transmitted to an electric generator or to a hydraulic pump. The mentioned nodes are fixed on a platform installed on floating bodies. The platform is connected to the shore by a hinged metal truss and by a stress relieving cable.

The selection of the optimal blades hydrodynamic profile is very important for functional optimization of micro hydro power plants. It will allow increasing the conversion factor (Betz coefficient) due to the hydrodynamic buoyant force. As well, conversion increase is achieved by ensuring the optimal position of blades towards the water streams at various phases of rotor revolution, employing an orientation mechanism of blades. Thus, practically all blades (even those blades which move against the water currents) participate in the generation of the summary torque. Moving in the water currents direction, for torque generation the blades use both the hydrodynamic forces and the water pressure exercised on the blade surfaces. Moving against the water currents direction the blades use only the hydrodynamic lift force for torque generation. Due to the fact that the relative velocity of blades concerning the water currents is twice bigger, practically, at their motion against the water currents, the hydrodynamic lift force is relatively big, and the generated torque is commensurable to the one generated by the water pressure. This effect makes the basis of 12 patented technical solutions.

2. Theoretical justification of the hydrodynamic profile selection of the blade in normal section

Consider the symmetrical profile of the blade placed in a uniform water stream with velocity $\vec{V}_\infty$ (Fig. 3) [1,2]. In the fixing point *O′* of the symmetrical blade with lever *OO′* let consider three coordinate systems, namely: the *O′xy* system with axis *O′y* oriented in the direction of the velocity vector $\vec{V}_\infty$, and axis *O′x* normal to this direction; the *O′x′y′* system with axis *O′y′* oriented along the lever direction *O′O,* and axis *O′x′* normal to this direction, and finally the *O′x″y″* system with axis *O′x″* oriented along the profile's chord toward the trailing edge and axis *O′y″* normal to this direction. Points *A* and *B* correspond to the trailing and the leading edges, respectively. The angle of attack α is the angle between the profile's chord *AB* and the direction of the velocity vector $\vec{V}_\infty$, and the positioning angle *φ* is the angle formed by the velocity vector direction and lever *O′O.*

The hydrodynamic force $\vec{F}$ has its components in directions *O′x* and *O′y,* named the lift and drag forces, respectively given by:

$$F_L = \frac{1}{2} C_L \rho V_\infty^2 S_p, \tag{1}$$

$$F_D = \frac{1}{2} C_D \rho V_\infty^2 S_p, \tag{2}$$

where *ρ* is the fluid density, V_∞ is the flow velocity, $S_p=ch$ (*c* is the length of chord *AB*, and *h* is the blade height) represents the lateral surface area of the blade, and C_L and C_D are dimensionless hydrodynamic coefficients, called the lift coefficient and drag coefficient. The hydrodynamic coefficients C_L and C_D are functions of the angle of attack *α*, the Reynolds number Re and the hydrodynamic shape of the blade profile. The components of the hydrodynamic force in the coordinate system *O′x′y′* are

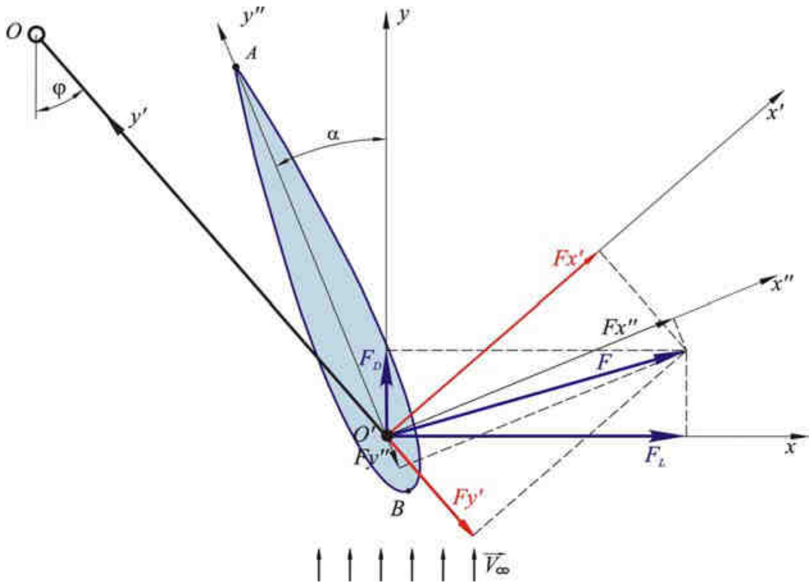

Figure 3. Hydrodynamic profile blade.

$$\begin{aligned} F_{x'} &= -F_L \sin\varphi + F_D \cos\varphi, \\ F_{y'} &= F_L \cos\varphi + F_D \sin\varphi. \end{aligned} \tag{3}$$

The torque developed by blade *i* at the rotor spindle *OO′* is

$$T_{r,i} = F_{x'} \cdot |OO'|, \tag{4}$$

and the total torque developed by all blades is

$$T_{r\Sigma} = \sum_{i=1}^{Npal} T_{ri}, \tag{5}$$

where *Npal* is the number of rotor blades.

Generally, the hydrodynamic force does not have application point in the origin of the blade axes system *O′* so that it produces a resultant moment. The produced moment is determined with respect to a certain reference point. As a reference point there is considered the point located at distance ¼ of the chord length measured from the leading edge *B*. The moment, called the pitching moment, is computed according to formula

$$M = \frac{1}{2} C_M \rho V_\infty^2 c S_p, \tag{6}$$

where C_M is the hydrodynamic moment coefficient.
The shape of the hydrodynamic profile is chosen from the library of NACA 4 digits aerodynamic profiles. The standard NACA 4 digit profiles are characterized by three shape parameters measured in percents of the chord's length: maximum value of camber C_{max}, location of the maximum camber $x_{C,max}$ and maximum thickness G_{max} . For example, the NACA 5416 profile has a 5% maximum camber located at 40% from the leading edge and has a maximum thickness of 16%. The profile coordinates are obtained by combining the camber line and the distribution of thickness. Since the considered blades will have a symmetric shape, the camber is null (C_{max}=0, $x_{C,max}$=0) and the camber line will coincide with *x*-axis

3. Micro hydropower plant with hydrodynamic rotor for river water kinetic energy conversion into mechanical energy

This model of hydro power plant is designed to convert river water kinetic energy into mechanical energy used to pump water into irrigation and sewerage systems, and supply industrial water etc. with the flow rate $Q = 40\ m^3/h$ at the height pumping $H = (10 – 15)\ m$.

Static description of the microhydro power plant. The blades 1 (fig. 4) are connected to the hydrodynamic rotor 2 by roller friction bearings to ensure their orientation under a certain entering angle α. The hydrodynamic rotor 2 is mounted on the input shaft of the planetary multiplier 3 through an auxiliary shaft, which is fixed on the bearings. The belt pulleys of the transmission 4 are mounted on the output shaft of the planetary multiplier - the big one, and the small one - on the input shaft of the centrifugal pump 5. The hydrodynamic rotor 2 and blades 1, the multiplier 3, the centrifugal pump 5 and guides 6 are mounted on the spatial housing 7, installed on the pontoons 8.

Functioning principle. The river flowing water with the energy potential dependent on the flow velocity drives the hydrodynamic profile blades 1 (fig. 5), oriented continuously by the entering angle α, and revolving in their relative movement in relation to the rotor through the bearings mounted in body 5. The micro hydropower rotor 2 comprises three blades oriented at an entering angle α, which is dependent on the water flow velocity. In the areas of blades 1 location, inefficient from the point of view of river kinetic energy conversion, under hydrodynamic forces the blades 1 are repositioned at an angle of 90^o to the currents of water or are carried by the water

ISSN 1454 - 8003

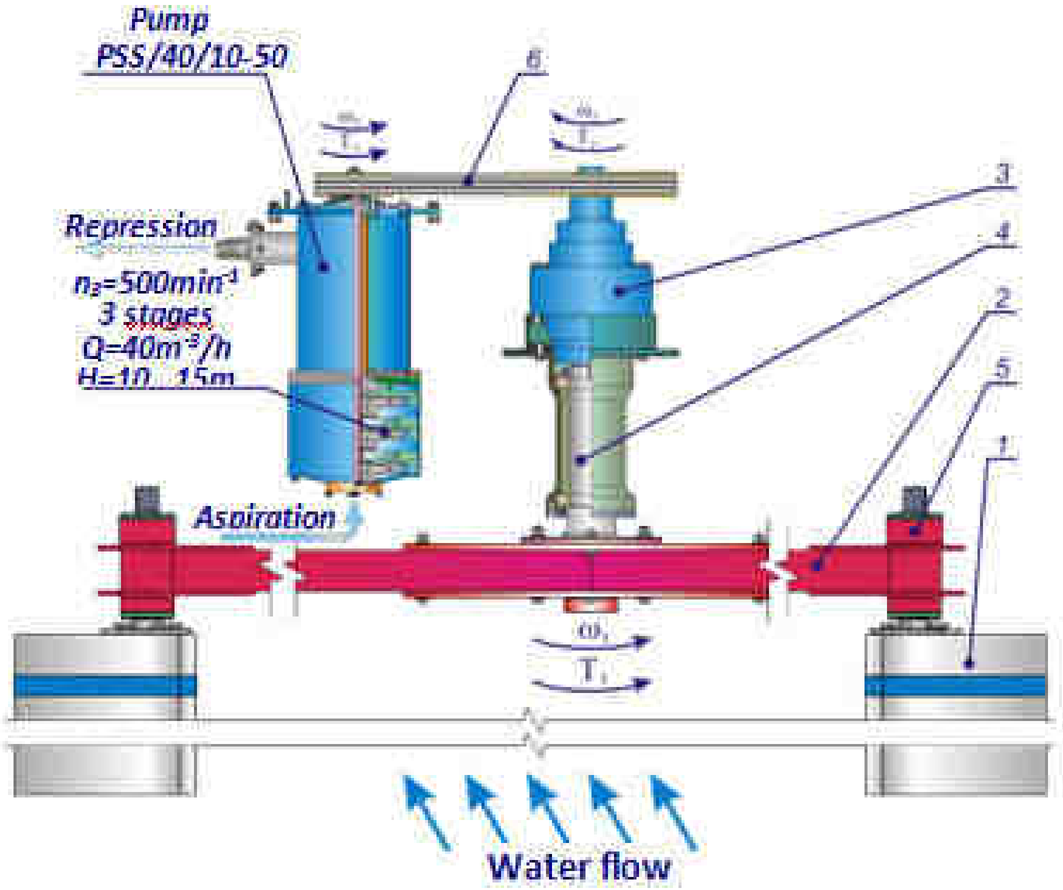

Figure 5. Kinematics of micro hydropower plant MHCF D4x1,5 M.

unhampered to the angle α ***= 0.*** Thus, the respective positioning of blades allows the increase of water kinetic energy rate converted into useful energy. As result, the water currents transmit a part of their kinetic energy to the blades 1, stressing them under the hydrodynamic forces and reporting rotational motion with angular frequency ω_1 and torque T_1 to the rotor 2. The summary torque T_1 , developed by the hydrodynamic forces and applied to the 3-blade rotor shaft at water flow velocities 1.3, 1.6 and 1.8 m/s and at the entering angle of blades $\alpha = 18^o$, is presented in fig. 6.

For rotor diameter *D = 4 m*, the submerged height of blades *h=1,4 m* and length of blade chord *l = 1,3 m,* the torque is: T_1 ***= 11938 Nm*** for water flow velocity *V = 1,3 m/s;* T_1 ***= 18084 Nm*** for *V = 1,3 m/s;* T_1 ***= 22887 Nm*** for *V = 1,8 m/s.* The calculations of kinematics and lifting capacity of all constructive elements as well as of all functional and energy parameters of micro hydropower plant have been carried out for the torque value T_1 ***= 18084 Nm.***

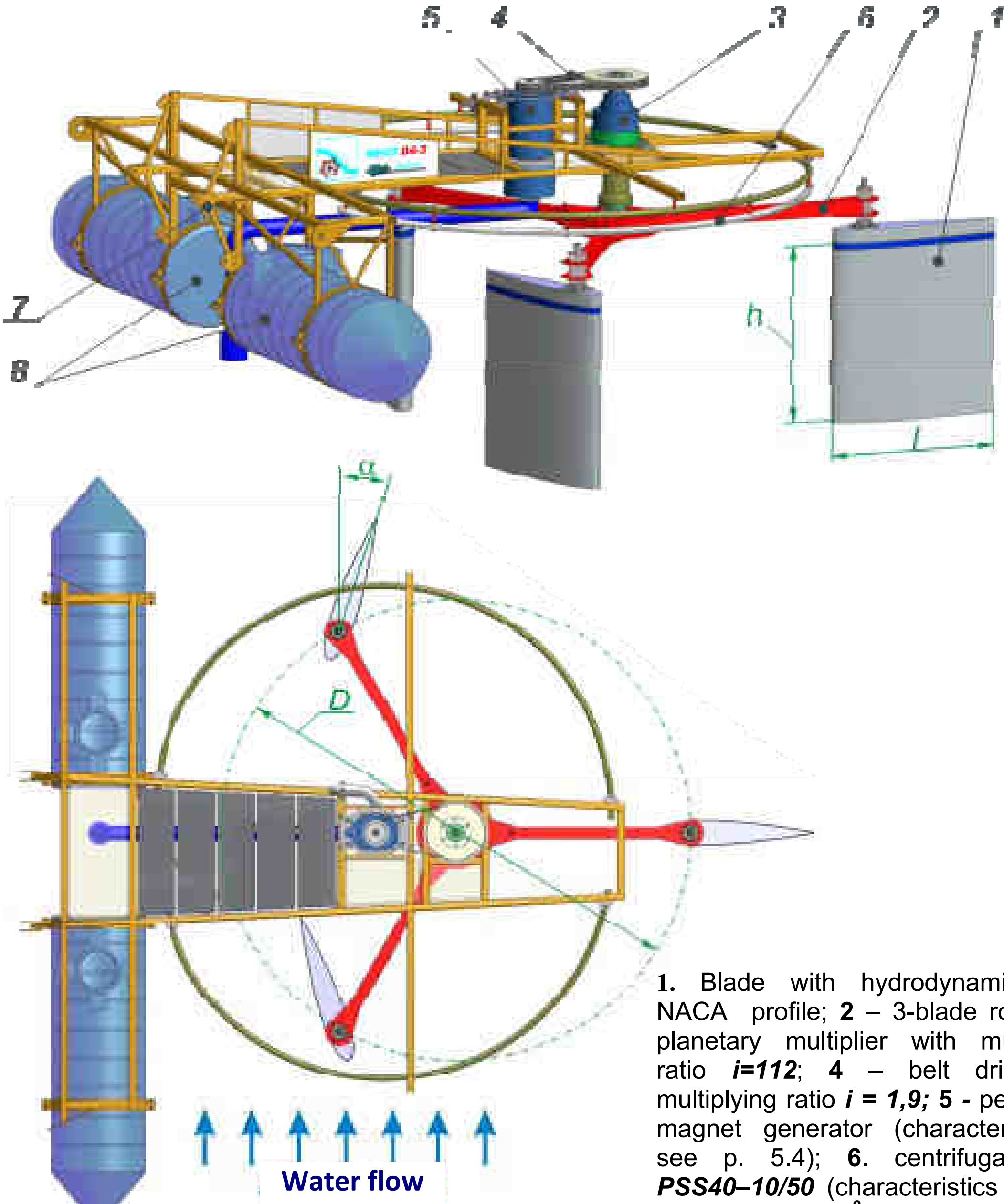

1. Blade with hydrodynamic 0016 NACA profile; **2** – 3-blade rotor; **3** – planetary multiplier with multiplying ratio ***i=112***; **4** – belt drive with multiplying ratio ***i = 1,9; 5 -*** permanent magnet generator (characteristics – see p. 5.4); **6.** centrifugal pump ***PSS40–10/50*** (characteristics – pump flow rate ***Q=40m³/h*** at pumping height ***(10...15)m***; 7 –plastic pontoons; 8 – guide; 9 – spatial housing .

Figure 4. Micro hydropower plant with hydrodynamic rotor for river kinetic energy conversion into mechanical energy for water pumping (flow rate Q = 40m³/h, pumping height H = 10...15 m).

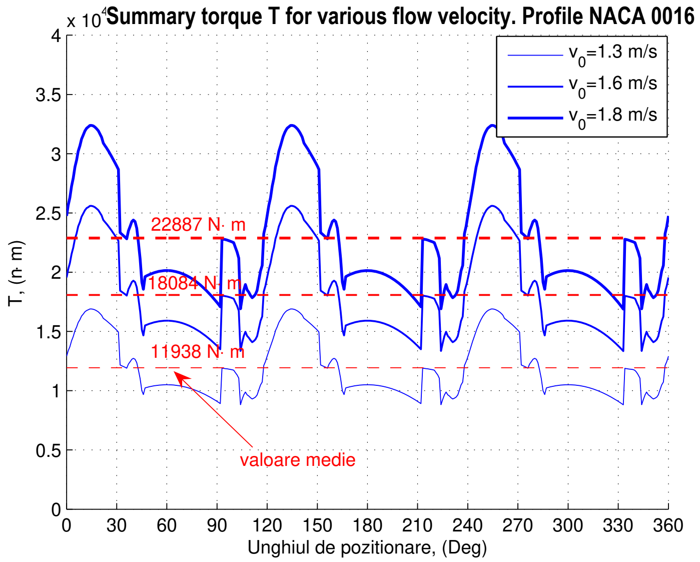

Blades positioning angle, Deg

Figure 6. Torque T_1 at the hydrodynamic rotor shaft with NACA 0016 profile blades.

Rotor 2, rigidly coupled by means of auxiliary shaft with the input shaft of the multiplier 3, transmits rotational motion to the last with angular frequency ω_1 and torque T_1. The multiplier reproduces the rotor 2 revolutions up to $n_2 = \frac{30\omega_1}{\pi} \cdot i_1 (min^{-1})$, where i_1 represents the multiplying ratio of the multiplier (***i_1=112)***. Rotational motion at angular frequency $\omega_2 = \frac{\pi n_2}{30} (s^{-1})$ is transmitted from the multiplier input shaft via a transmission belt 4 of the centrifugal pump input shaft with multiplying ratio ***i_1 = 2,25***. As result, the input shaft of the centrifugal pump swivels with angular frequency $\omega_3 = \omega_1 \cdot i_1 \cdot i_2$ (s^{-1}) and is stressed at torque:

$$T_3 = \frac{T_1 \cdot \eta_1 \cdot \eta_2 \eta_r}{i_1 \cdot i_2}, (Nm),$$

where: η_1 is the multiplier mechanical efficiency (***η_1 = 0,9)***;

η_2 - is belt transmission mechanical efficiency (***η_1 = 0,95)***;

η_r - mechanical efficiency of hydrodynamic rotor bearings (***η_1 = 0,99).***

According to the experimental research the mechanical efficiency of centrifugal pump is ***η_1 = 0,72*** at rated speed frequency

$$n_3 = \frac{30\omega_3}{\pi} = 500\, min^{-1}.$$

The mechanical efficiency of the micro hydropower plant with hydrodynamic rotor for river water kinetic energy conversion into mechanical energy, with account of all mechanical losses in the linkage (at the hydraulic pump shaft) is: $\eta_\Sigma = \eta_1 \eta_2 \eta_3 \eta_r = 0,9 \cdot 0,95 \cdot 0,99 = 0,846.$

a,b

Figure 7. a) Industrial prototype of micro-hydro power plant for river water kinetic energy conversion; b) Testing on the Prut river [1].

Accordingly, the micro hydropower plant (MHCF D4x1,5 M) ensures the transformation into useful energy of 84,6% of the kinetic energy potential of the flowing water transmitted to the hydrodynamic rotor.
On the basis of the conceptual diagram designed above, technical documentation was developed and industrial prototype of micro-hydro power plant for river water kinetic energy conversion into electrical and mechanical energy was manufactured (fig. 6,a) and installed for testing on the Prut river. Thus, micro-hydro power plant MHCF D4x1,5 ME provides conversion of up to 73,6% and 67% of useful energy for electricity production and for water pumping from the energy potential of flowing water entrapped by the hydrodynamic rotor.

Figure 8. Industrial prototype of micro-hydro power plant with modular blades [4].

Conclusions

The micro hydropower plants for river water kinetic energy conversion has the following advantages:
- Exclusion of dam construction and of the negative impact on the environment, implicitly;
- Lowest cost;
- Simplicity of construction and operation;
- Increased reliability at dynamic overload in operating conditions;
- Resistant composite materials, including conditions of high humidity;
- Automatic adjustment of the micro hydropower plant platform position in conditions of water level changing.

REFERENCES

[1] I. Bostan, A. Gheorghe, V., Dulgheru, I. Sobor, V. Bostan, A Sochirean. Resilient Energy Systems. Renewables: Wind, Solar, Hydro. Springer, VIII, 507 p. 2012. ISBN 978-94-007-4188-1

[2] I.Bostan, V.Dulgheru, V.Bostan, R.Ciupercă. Antologia invenţiilor. Sisteme de conversie a energiilor regenerabile: fundamente teoretice, concepte constructive, aspecte tehnologice, descrieri de invenţii. Vol. 3. Ch.: Ed. BONS Offices. 2009, 458p. ISBN 978-9975-80-283-3.

[3] I.Bostan, V. Dulgheru, V. Bostan [et al]. Hydropower serving rural consumers. Chişinău: Bons Offices, 2013. – 52 p.

[4] I.Bostan, V.Dulgheru, I.Sobor, V.Bostan, A.Sochirean. Sisteme de conversie a energiilor regenerabile. Univ.Tehn. a Moldovei.- Ch.: Ed. „Tehnica-Info” SRL, (Tipografia BONS Offices). 2007.- 592 p. ISBN 978-9975-63-076-4.

[5] I.Bostan, V.Dulgheru, V.Bostan, A.Sochireanu, N.Trifan, I.Dicusara, O.Ciobanu, R.Ciobanu. A micro/hydropower station for the conversion of flowing water kinetic energy. Environmental Engineering and Management Journal, Universitatea Transilvania din Braşov, România, 10-12 Noiembrie, 2011, (pag 1033-1040). IF 1,435.

[6] I. Bostan, V. Dulgheru, V. Bostan, O. Ciobanu, A. Sochireanu, V. Gladîş. Patent 601Y (MD). Cl. Int. F03B7/00, F03B13/00. Floating hydraulic station / BOPI nr. 2/2013.

[7] I. Bostan, A. Gheorghe, V. Dulgheru, , A. Sochireanu, O. Ciobanu, R. Ciobanu. Patent 3846 (MD), CIB F 03 B 13/00; F 03 B 7/00; F 03 B 13/18; F 03 B 13/22; F 03 B 17/06 Hydraulic station with horizontal axle / UTM – Nr. 2008 0064. Decl. 5.03.2008; Publ. BOPI – 2009. - Nr. 2.

[8] V.Bostan, V.Dulgheru, A.Sochireanu, O.Ciobanu, R.Ciobanu. Patent 3845 (MD), CIB F 03 B 13/00; F 03 B 7/00; F 03 B 13/10; ; F 03 B 13/22; ; F 03 B 17/06 Hydraulic station / UTM – Nr. 2008 0063 Decl. 5.03.2008; Publ. BOPI – 2009. - Nr. 2.

[9] I. Bostan, V. Dulgheru, A. Sochireanu, O. Ciobanu, R. Ciobanu, I. Dicusară. Patent 3104 (MD), CIB F 03 B 7/00: F 16 H 1/00. Hydraulic station = UTM - Nr. 2005 0273. Decl. 15.09.2005; Publ. BOPI – 2006. - Nr. 7.

[10] I.Bostan, V.Dulgheru, V.Bostan, O.Ciobanu, A.Sochireanu. Patent No. 2991(MD), CIB F03 B 7/00. Hydro Power Plant / T.U.M. – No. 2005 0136 ; Decl. 16. 05. 2005; Publ. BOPI, 2006.- No.2.

[11] I.Bostan, V.Dulgheru, A.Sochireanu, V.Bostan, O.Ciobanu, R.Ciobanu Patent No. 2992 (MD), CIB F03 B 7/00. Hydraulic Plant / U.T.M. – No. 2005 0270; Decl 15.09.2005 ; Publ. BOPI – 2006.- No.2.

[12] I.Bostan, V.Dulgheru, V.Bostan, R.Ciupercă Patent No. 2981 (MD), CIB B63 B 35/44: E02 B 17/00. Hydraulic Plant / U.T.M. – No.2005 0274; Decl. 15. 09. 2005; Publ. BOPI 2006.- No.2.

ISSN 1454 - 8003
Proceedings of 2014 International Conference of Hydraulics and Pneumatics - HERVEX
November 5 – 7, Calimanesti-Caciulata, Romania

INJECTION DEVICES USED FOR CROP FERTIGATION

Gheorghe SOVAIALA[1], Gabriela MATACHE[1],
Sava ANGHEL[1], Ioan PAVEL[1], Ana-Maria POPESCU[1]

[1]INOE 2000-IHP, Bucharest

Abstract: *Compared to the situation where irrigation and fertilization take place as distinct sequences in agricultural technological processes, fertigation has several advantages arising from the following considerations:*
- it replaces the classical system for administration of chemical fertilizers;
- it facilitates quick access of fertilizing substances to the root system of plants, in due time, for better use of them;
- it significantly reduces losses of active ingredient caused by evaporation, gravitational drainage or percolation beneath the root of plants, under the influence of unfavorable climatic factors (high temperatures associated with strong winds, downpour rain);
- it reduces the degree of injury of plants caused by direct contact of fertilizers with the aboveground parts of plants;
- it reduces irrigation water consumption.
Injection devices component of fertigation equipment are intended for introducing the primary solution into the water passing through the main pipeline of the irrigation facility, in order to obtain the fertilizing solution, administered to plants through specific distribution devices (drip equipment, micro sprinklers, sprinklers).

Keywords: *fertigation, injection devices*

1. Material and methods

Basically the fertigation equipment includes the device for primary solution injection into the irrigation water, container for the preparation of the primary solution, devices for measuring and adjusting the working parameters, elements for hydraulic connection between pieces of equipment. Choosing the proper fertigation equipment is equally important as selecting the proper nutrients. Selecting them incorrectly can damage parts of the irrigation facility, affects the efficient functioning of the irrigation system or reduces the effectiveness of nutrients.
Injection of fertilizers into the irrigation water is done through:

- differential pressure;
- vacuum;
- pumping.

2. The device for injecting fertilizers through differential pressure

The operating principle is simple, using for dosing hydraulic energy of water in the main supply pipeline of the installation.
This device allows introducing liquid fertilizers into the irrigation water within the pressurized pipeline. Maximum working pressure is 6 bar.
The device, Figure 1, consists of pipeline *1*, equipped with two couplings *2* by which it is connected between two water supply pipelines of the sprinkler irrigation facility.
Pipeline *1* is equipped with a pipe closer *3*, allowing modification of the section, thereby creating a pressure drop in the main pipeline, behind it. On the device pipeline there are also mounted the tap valves *4* (for water intake) and *5* (for fertilizer injection). The water inlet pipe is connected to the metal tank *8* through hose *6*, provided with nozzle *7*; inside the tank there is a sealed rubber bag *9*, inside which enters a stub type holed funnel *10*, which is in connection with the fertilizer supply connecting pipe *11*. The supply connecting pipe is connected by a control chamber *12*, made of

transparent material, and a hose *13* to the tap valve *5*, by which fertilizers reach the irrigation pipe. At the bottom of the tank there is the tap valve *14*, serving to water draining and ventilation.
When using this device there can be distinguished two distinct phases, namely: filling the tank with fertilizer and adding it in the irrigation pipeline.
For filling tap valves *4* and *5* are closed, tap valve *14* for ventilation is opened and filler cap *15* is removed. Then pour 50 liters of liquid fertilizer which enters through the holed stub *10* in the rubber bag *9*. The bag being elastic, it expands, pushes air out and thus occupies the whole space inside the tank. After that, the cap is installed, tap valve *14* is closed and tap valves *5* and *4* are opened in turn.

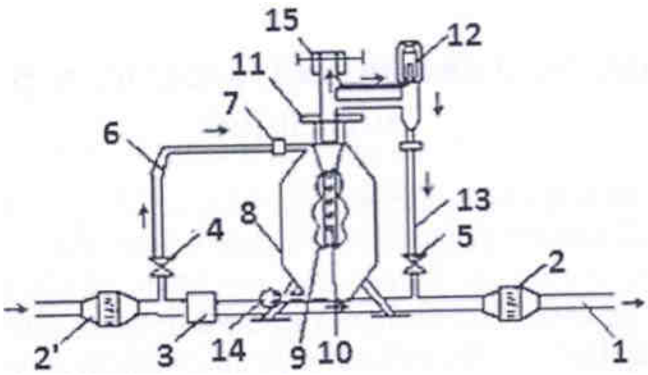

Fig. 1. Schematic diagram of the device for injecting liquid fertilizer through differential pressure

Pipe closer *3* generates a loss of pressure on the water supply main circuit of the installation, determining the penetration of part of that through hose *6* and nozzle *7* between the inner wall of the tank *8* and the outer wall of the rubber bag *9*. Due to the pressure that water exerts on the rubber bag, the liquid fertilizer inside is pushed up through the holed stub, then along control chamber *12*, hose *13* and tap valve *5* in the irrigation pipeline, behind the pipe closer, where the pressure is lower and allows the fertilizer to flow on. Mixing between fertilizer and water is done in the pipeline before reaching the sprinklers. On a new supply of the tank it is necessary to close the tap valves *4* and *5*, open tap valve *14* and then remove the filler cap *15*. Adjustment of the various flow rates is made both by substitution of the eight nozzles the device is equipped with and by changing the pipe closer on the device pipe. Thus there can be obtained flow rates between 5 and 200 l/h, making possible for a tank to get empty in a time range between 10 h and 15 min.

Advantages

- Increased reliability because it has no moving parts;
- Acquisition costs are low;
- It works by hydraulic energy existing in the network;
- The risk of container corrosion is reduced;
- It allows mixing more compatible fertilizers in order to be injected.

Disadvantages

- Injection dose is not constant;
- The injection flow rate is high, and the duration of fertigation is reduced;
- Difficult handling when moving to a new watering position;
- There is a risk of environmental pollution because of high injection flow rates;
- One must observe severely the work safety rules.

ISSN 1454 - 8003
Proceedings of 2014 International Conference of Hydraulics and Pneumatics - HERVEX
November 5 – 7, Calimanesti-Caciulata, Romania

3. The device for injecting fertilizers through a vacuum

Injection by a vacuum is based on the principle of Venturi tube, and the device is called a Venturi injector.
Venturi type liquid fertilizer injectors operate based on the Venturi effect, shown in Figure. 2, according to which, in flowing of a liquid under pressure through a given section, with sudden narrowing and progressive expansion, the suctioning phenomenon occurs. VENTURI injectors, made in the limits 3/4″- 2″, require operating pressures higher than 4.5 bar, ratio of primary solution flow and fertilizing solution flow being 1/ 5- 1/ 50 for the model 3/4″ and 1/ 5- 1/ 100 for the model 2″. Fertilizing solution flow rates achieved, depending on the dimension types (3/4″- 2″), range between 193-2640 l/h.
Venturi fertilizer dispensers require no external power source, operating based on a minimum pressure difference between the input segment and the output one. Absorption of fertilizing solution depends on the type of fertilizer, input pressure and water flow.

Fig. 2 The operating principle of a Venturi type injector

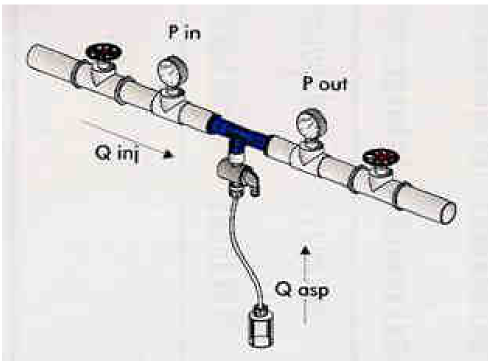

*Connecting a Venturi injector
to the main pipeline*

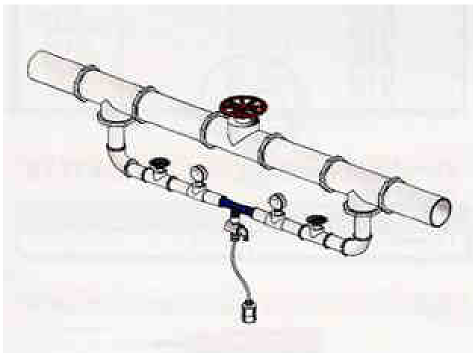

*Connecting a Venturi injector
to the secondary pipeline*

Fig. 3 Way of connecting Venturi injectors to the irrigation facilities

Venturi injectors can be installed either on the main pipeline of the irrigation facility (full flow) for structural sizes 3/4" and 1" or on a circuit parallel to that (by-pass), for structural sizes 1 ¼”, 1 ½” and 2”, Figure 3.

Flow of the primary solution injected is proportional to the flow of irrigation water transiting the injector body.
The advantage of connecting the injector to the main pipeline of the irrigation facility is represented by achieving a relatively high flow rate of primary solution injected for small structural sizes (3/4" and 1"). The disadvantage of this technical solution for connection is represented by loss of hydraulic load created in the injector body, with consequences on dimensioning the distribution network of the irrigation facility.
Connecting the injector on by-pass eliminates the disadvantage of creating a loss of hydraulic load on the main pipeline of the irrigation facility, instead occurring the disadvantage of primary solution injected flow rates lower, compared with the full-flow connection version, for the same injector dimension type.
To achieve various injection rates, on the system circuit respectively the injector circuit, two vanes are installed, Figure 4.
Absorption of fertilizer is made from an open container in which the primary solution is prepared, and the injection is done behind the vane located on the water supply circuit of the facility.
Injection dose is very sensitive to pressure variation and it can be stabilized by means of a pressure regulator that will achieve a constant pressure along the facility circuit.

Advantages
Venturi injector is constructively simple, purchasing it does not require large investment, and has high reliability in operation. It makes a good proportionality of the injector / facility flow rates, and the injection dose is constant.

Disadvantages
Pressure loss along the circuit of the facility is about 1 bar, thus flow and work capacity of the facility reduces. This situation is specific to installations with large diameters and high flow rates, on which Venturi injectors cannot be used; there is a risk of absorption of air at the completion of injection or the risk of nozzle clogging because of impurities that settle out in the fertigation process; quantitative adjustment of the fertilising solution injected is difficult to do, and therefore it is not suitable for automation.

	
50 mm PVC control head with 30 L fertilizer tank Connecting the injector on the main pipeline of the irrigation facility	50 mm PVC control head with 3/4" injector Connecting the injector on by-pass

Fig.4 Structure of assembly 50 mm PVC control head, for the two versions for connecting the Venturi injector to the irrigation facility

Figure 5 presents the flow rates of the primary solution injected, in l/h, for common structural sizes of Venturi injector.

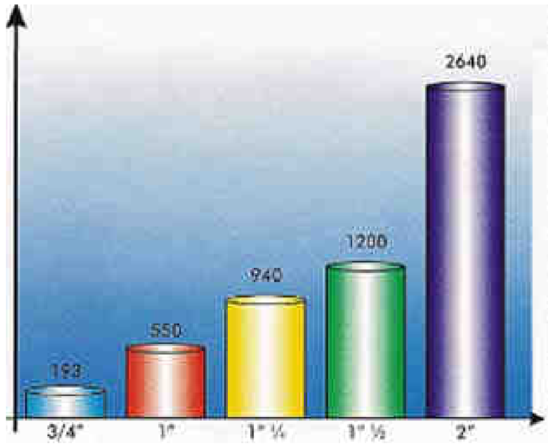

***Fig. 5** Flow rates of the primary solution injected, l/h, achieved by Venturi injectors*

4. Devices for injecting fertilizers by pumping

The devices for injecting by pumping make injection under pressure with a very good accuracy, and therefore are called dosing pumps / volumetric injectors. They can be hydraulically, pneumatically or electrically driven.

Hydraulic dosing pumps operate with hydraulic energy in the network, and they can be membrane or differential piston pumps. These pumps, depending on the direction of making the active stroke, are classified into simple effect or double effect pumps. Depending on the installation position as compared to the main circuit of the irrigation facility, the pumps are installed in series, on the main supply circuit (full flow) or in a circuit parallel with it (by-pass).

a. The device for injecting fertilizers by pumping provided with differential piston

Highest performance differential piston dosing pump is the pump DOSATRON- France, Figure 6. The pump can be placed both on the main circuit of the irrigation facility (full flow) and on a circuit parallel with it (by-pass), Figure 7, and it uses as drive fluid the irrigation water transiting its supply pipeline. Water works on the pump mobile assembly, consisting of the motion piston and dosing piston, which move together.

The operating principle of DOSATRON differential piston pump is shown in Figure 8.

Changing direction of movement of the mobile assembly of the pump is driven by the tilting mechanism, located on the motion piston, which by actuating some valves allow water intake, acting as driving fluid, below or above the piston.

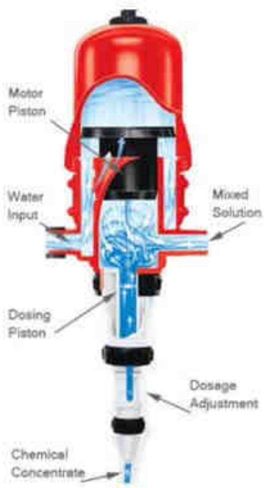

***Fig. 6** Schematic of DOSATRON differential piston dosing pump*

***Fig. 7** Circuit diagram on the by-pass of DOSATRON differential piston dosing pump*

The dosing piston is equipped with a sliding sleeve type translational seal, which in upward stroke sits in the lower seat, ensures sealing against the dosing cylinder and generates depression required for valve raising up from the seat, access of primary solution under the piston and driving of the volume of primary solution above, existing within it from the previous stroke, inside the primary solution-dive fluid mixture chamber (cylinder of the motion piston).
In downward stroke, the sealing cup of dosing piston sits in the upper seat of the piston, which places on its seat the primary solution inlet valve, and allows access of the primary solution amount already introduced into the dosing cylinder at the previous stroke, above it, through the longitudinal slots on the external generators.
By continuously varying the volume of mixture chamber, in order to reduce it, fertilizer solution is injected through the discharge port of the pump into the irrigation facility.


Fig. 8 The operating principle of DOSATRON differential piston dosing pump

DOSATRON equipment is designed so that the volume of fertilizer solution injected always be strictly proportional to the volume of water entering the unit, regardless of variations in flow or pressure that may arise in the main pipeline. High dosing precision of the DOSATRON equipment eliminates the risk of crop over-fertilizing, thus contributing to the protection of plants, consumer and environmental health.
Concentration of fertilizing solution can be set from the outside, aligning the hole on the adjustment sleeve to the desired indication on the scale, Figure 9.
The amount of primary solution injected is proportional to the amount of water acting as driving fluid that enters the DOSATRON pump, i.e., adjustment to 1% = 1: 100 = 1 volume of primary solution (concentrated) + 100 volumes of water.

Fig. 9 Setting the concentration of fertilizing solution and the amount of primary solution injected

b. The device for injecting fertilizers by pumping provided with membrane

Membrane injection device (A) designed at IHP Bucharest, Figure 10, is connected through quick couplers to the section of pipe (B), integral part of the fertigation equipment; this section allows connecting the equipment to the hydraulic circuit of the irrigation facility. Feeding the equipment with primary solution (supplied in a liquid state by the manufacturer or prepared from solid water-soluble fertilizers) will be done from the tank with liquid fertilizer (D).

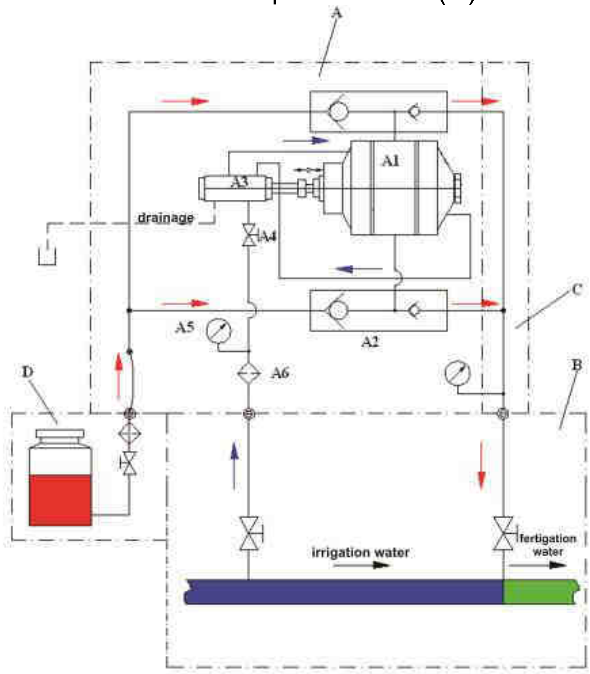

Fig. 10 Structure of a fertigation equipment provided with membrane dosing pump

A- equipment for continuous injection of primary solution; B- section for branching the fertigation equipment to the irrigation facility; C- system for monitoring the injecting process; D- fertilizer container with related accessories

By opening the tap valves on these circuits, pressurized water will enter one of the ways of the directional control valve (A3.1), into one of the drive chambers of the membrane hydraulic amplifier, Figure 11.

The drive fluid (water taken from the main hydraulic circuit of the irrigation facility) passes through the pressure filter and reaches the hydraulic 5/2 (5 ways and 2 positions) directional control valve. When the slide valve of the directional control valve ranks right connection is established between the joints P and A, feeding the left drive chamber of the pump A1 and the left chamber of the inverter, which causes displacement of the pump mobile assembly to the right, i.e. between the joints B and Drainage, allowing water discharge from the right drive chamber of the pump and the right chamber of the inverter. During this stroke, from the left injection chamber, by compressing the corresponding membrane, there is performed the process of injecting primary solution through the lower branch of the block of valves A2. The injection pressure places on seat the valves on the left-lower branch, on the right-upper branch and opens the valve on the right-lower branch, thus achieving the primary solution injection into the main hydraulic circuit of the irrigation facility.

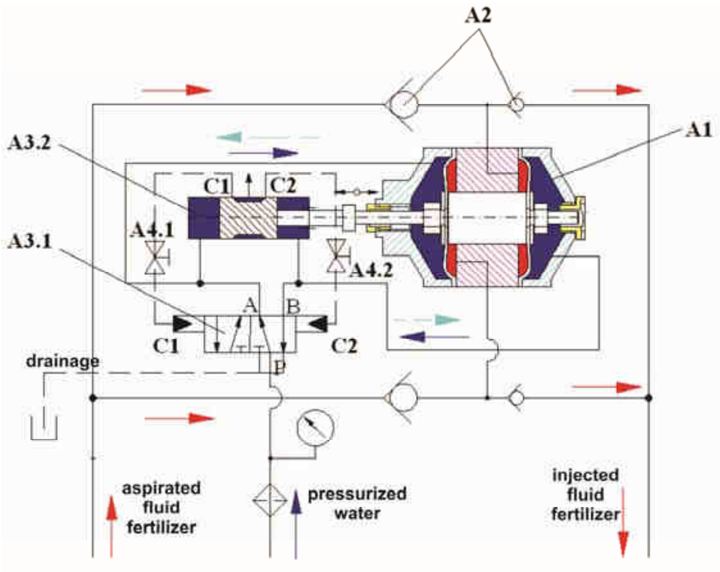

Fig. 11 The principle of operation of the dosing device
A1- double diaphragm pump (hydraulic amplifier); A2- check valves unit of injection circuit; A3.1- directional control valve for actuation of driving chambers; A3.2- hydraulic direction inverter; A4.1, A4.2- miniaturized tap valves, C1, C2 driving (piloting) chambers of directional control valve for actuation

At the same time, in the right injection chamber depression is created, causing access of primary solution through the upper branch of the block of valves (left valve opened, right valve on the seat). When releasing the hole C1 in the inverter body, there is established connection with the control of the hydraulic directional control valve, causing switching of the slide valve to the opposite position.
Double membrane pump, Figure 12, can be assimilated to a hydraulic amplifier with two identical sections, separated by a central disk (4). Cloth insertion rubber membranes (3) have the shape of disks with a central hole. They are fixed between pump external caps (2, 6) and front sides of the disk, on the outer contour, respectively between front sides of the spool (5) and special design nuts, on the inner contour. The membranes separate drive chambers of the hydraulic amplifier (located on the outer side) from the injection chambers (located on the inner side).
The connection between the drive chambers and the external hydraulic circuit for the working fluid is made through the holes into the caps, and the connection between the injection chambers and the external circuit for primary solution intake-discharge is made through the holes into the central disk.
Reversing the movement of the pump mobile assembly is made using a hydraulic inverter, whose slide valve is integral with it. The difference between the active surfaces of the membranes, which are in contact with the drive fluid (the irrigation water) on the outside and with the primary solution on the inside, generates overpressure needed to perform the injection process.

ISSN 1454 - 8003
Proceedings of 2014 International Conference of Hydraulics and Pneumatics - HERVEX
November 5 – 7, Calimanesti-Caciulata, Romania

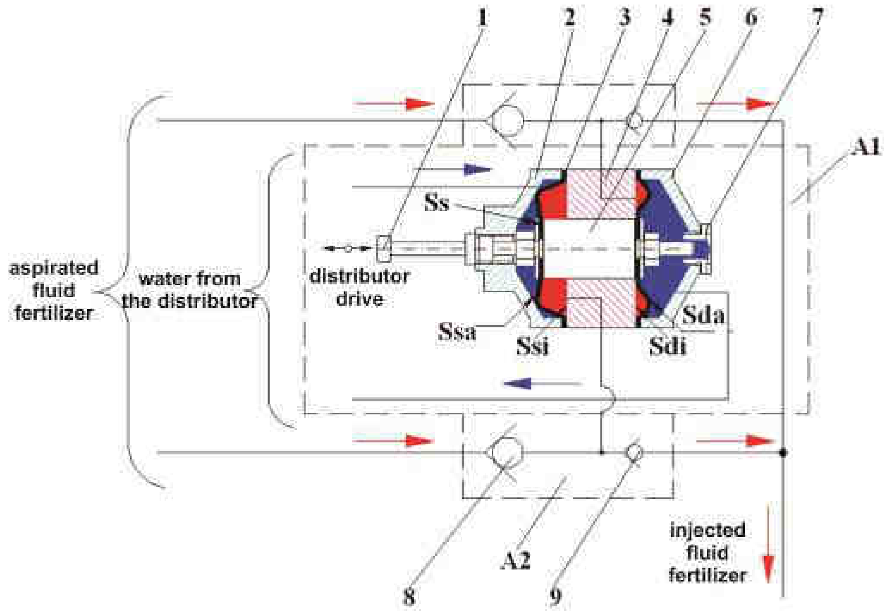

Fig.12 Hydraulic schematic diagram of the multiplier:
1- axial drive rod, 2- left cap, 3 -membrane, 4- case, 5- slide valve, 6- right cap, 7- plug, 8- intake valve, 9- discharge valve

- Ssa, Sda – circular surfaces, left and right, on which water acts;
- Ssi, Sdi – circular surfaces, left and right, on which fluid fertilizer acts;
- Ss –circular surface of slide valve.

5. Results and discussions

The injection device component of the fertigation equipment designed under a project in the field coordinated by IHP Bucharest will be of type membrane hydraulic drive (switching of the directional control valve spool will be made hydraulically) double pump;
The injection device uses as a working (drive) fluid the irrigation water, taken from the same pipe wherein is injected the primary solution, which combined with the irrigation water forms the fertilizer solution; compared with the membrane pumps produced by renowned companies in the field: VERDER AIR, DEBEM, TUV, TAPFLO, injectors developed under the project do not require electricity or compressed air, which ensures their autonomous operation at any point of the irrigation enclosure;
Injection pressure is achieved on the principle of difference between the active surfaces of drive chambers and injection chambers, and it can be determined very precisely, depending on the hydraulic parameters of the irrigation facility with which it is working in an aggregate, as early as the design of the device;
Primary substance injected flow can be adjusted in a very wide range, by changing the flow supplying the drive chambers, changing frequency of the central axis (integral with the membranes that separate the drive and injection chambers) of the pump;
The fertigation equipment will be installed in parallel with the main circuit of the irrigation facility (by-pass system) through two quick couplings, for taking the water used as drive fluid, respectively for injecting the primary solution; this mounting system does not introduce load loss in the irrigation facility pipeline;
By using in the manufacturing of parts cheap materials (polyamides, elastomers), resistant to corrosive action of fertilizing substances, it will be possible to charge sale prices attractive to potential buyers;

Fertigation equipment can be designed and manufactured in a wide size range, in accordance with the requirements on the concentration of the primary solution, injected flow (relatively high for fertilizing substances on nitrogen, phosphorus and potassium, and very low for micronutrients).

REFERENCES

[1] Ilie BIOLAN, Ion SERBU, Gheorghe SOVAIALA, Florica MARDARE, Tehnici si tehnologii de fertirigare a culturilor agricole / *Techniques and technologies for agricultural crops fertigation*, A.G.I.R. Publishing House, ISBN: 978-973-720-344-1, 2010;

[2] Mihai AVRAM, Actionari Hidraulice si Pneumatice. Echipamente si sisteme clasice si mecatronice/ *Fluid Power. Classical and mechatronic equipment and systems*, Academic Publishing House, Bucharest, ISBN 973-7787-40-4, 2005;

[3] Ilie BIOLAN, Gheorghe ŞOVĂIALA, Sava ANGHEL, Ştefan ALEXANDRESCU, Constantin NICOLESCU, Daniel BUCUR, Studies regarding the technique used for applying fertirrigation on agricultural crops, Ion Ionescu de la Brad University of Agricultural Sciences and Veterinary Medicine, Faculty of Agriculture, Scientific Papers - Agronomy Series, Vol. 53/2010 (quotated B+CNCSIS and reviewed by CAB International - Anglia), ISSN 1454 - 7414, 6 pages * Paper presented in Section II: Soil, water and environmental protection and published in Conference Proceedings and on CD-ROM ;

[4] Gheorghe ŞOVĂIALA, Ilie BIOLAN, Sava ANGHEL, Ştefan ALEXANDRESCU, Constantin NICOLESCU, Daniel BUCUR, Equipment for 338application of fertirrigation at horticultural crops, COMEFIM 10, The 10-th International Conference on Mechatronics and Precision Engineering, Bucharest 19-21 May 2011, http://www.comefim10.pub.ro, MCT 2/2011-Mecatronica Review No. 2/2011, pp. 75-79 ;

[5] Injectors for fertilizers – Agro Pataki , *www.agropataki.ro/webshop/sisteme-de-irigat-profesionale/.../ro*

[6] **Dosatron** - Agro Pataki - *www.agropataki.ro/produse/irigatii_pentru_agricultura/dosatron/ro.*

ISSN 1454 - 8003
Proceedings of 2014 International Conference of Hydraulics and Pneumatics - HERVEX
November 5 – 7, Calimanesti-Caciulata, Romania

AIR POLLUTION MONITORING IN URBAN SITES: NON-METHANE VOLATILE ORGANIC COMPOUNDS

Melinda-Haydee KOVACS[1], Mirela MICLEAN[1], Lacrimiora SENILA[1], Emoke Dalma KOVACS[2]

[1] INCD-INOE 2000, Research Institute for Analytical Instrumentation, melinda.kovacs@icia.ro

[2] Babes-Bolyai University, Chemistry and Chemical Engineering Faculty, dalma_kovacs2005@yahoo.com

Abstract: *Volatile Organic Compounds (VOCs) play an important role in the chemistry of air pollution at the local, regional, and global level. The main anthropogenic sources of VOCs in urban areas are vehicle- and industrial related. In this paper are presented the main VOCs detected in different locations from an urban area using passive samplers. VOCs detected in the highest amount were benzene, MTBE, acetylene, isobutylene and 1-pentene with their corresponding average concentration 26.11, 18.45, 16.04, 14.72, and 11.15* $\mu g \cdot m^{-3}$*, respectively. The total concentration of VOCs in the monitored sites varies between 29.18 – 167.55* $\mu g \cdot m^{-3}$*. Daily-diurnal variation was observed in most cases of VOCs detected during this study.*

Keywords*: volatile organic compounds (VOCs), passive sampling, urban area*

1. Introduction

Air pollution monitoring it is currently widely performed with attention to a set of problems caused by chemical contaminants like volatile organic compounds (VOCs). VOCs are an important group of air pollutants emitted from anthropogenic and biogenic sources into the troposphere [1].

Their importance are given by *(i.)* their impacts on human health; and *(ii.)* their important role that play in the chemistry of the troposphere – they condition the concentration of the OH radical, the production of organic acids, the regional formation of photochemical oxidants, etc. [2, 3]. In troposphere, these chemical contaminants undergo to a number of physical and chemical processes leading to their transformation or their removal from the atmosphere. These chemical processes that lead to their degradation are the photolysis, the reaction with the hydroxyl radical OH at daytime, the reaction with NO_3^* at night, the reaction with O_3 and the reaction with Cl^+ in coastal and maritime areas [3, 4]. Also, mixing processes, which are closely related to meteorological conditions, tend to redistribute pollutants through advective and convective transport in both the regional and non-regional scales [4]. Therefore, VOCs concentrations vary across time and space.

Over the past two decades, there was an increasing interest in determining the ambient concentration of VOCs and their spatial distribution in urban environments. They led to the identification of the main source of VOCs which are: vehicle exhaust gases, gasoline evaporation, residential heating, solvent usage in industrial processes and in domestic uses and the industrial emissions [5].

The United Nations estimate that over 600 million people are exposed to harmful levels of traffic-generated air pollutants in urban areas. Air pollution and its impact on human health have become issues of increasing public concern during the last decades, since the pollution prevention concept emerged many years ago [6].

In urban areas, industry and motor vehicles are the main source of air pollutants such as particulate matter, CO, NO_x, non-methane hydrocarbons (NMHCs) and derived ozone in the atmosphere. Due to the oil shortage and the resulting high price of oil, light-duty diesel vehicles (LDDVs) have become popular based on their lower fuel consumption and durability [7]. Despite advances in emission control technologies, for diesel and gasoline engines, vehicle pollution is still an important issue. In addition, VOCs and NO_x are regarded as the precursors of ozone formation via complex photochemical reactions. Therefore, there is a need to characterize the emission rates of volatile organic species under different driving conditions for these vehicles as well from different industrial activities.

2. Methods

VOCs sampling: The VOCs sampling was performed during 2013. The air samples were collected by passive method using Radiello cartridges activated with charcoal (RAD130 from Supelco, Bellefonte, PA, USA), which were placed in urban area. Samples were collected in duplicate, each time. The air samples were transported in the laboratory, where they were kept in refrigerator (4 °C at dark) and analyzed within 48 hours from sampling.

Chemical analysis of VOCs: VOCs mix standard containing 50 components (49149-U) at 1000 $\mu g \cdot L^{-1}$ in methanol:water (97:3) was purchased from Supelco (Bellefonte, PA, USA). Carbon disulfide (CS_2) (Chromasolv for HPLC, ≥ 99.9 %) was purchased from Sigma-Aldrich (St. Louis, MO, USA). The VOCs absorbed on the active charcoal were eluted with 2 mL CS_2 through dynamic condition, over 30 minutes. 1 mL of supernatant was injected in the GC-MS system provided with a split/splitless injection port (Thermo Electron Corporation, USA). TR-5 MS non polar capillary column (5 % diphenyl – 95 % dimethyl polysiloxane, Thermo Electron Corporation, USA) with 30 m length x 0.25 mm. I.D., x 1 μm film thickness was used for chromatographic separation of VOCs. Oven temperature was set as follows: 40 °C (hold constant fro 7 min) followed by a heating at 100 °C with a rate of 7 $°C \cdot min^{-1}$, after which the temperatures was raised continuously till 280 °C with a rate of 10 $°C \cdot min^{-1}$. This final temperature (280 °C) was maintained for 3 minutes. Full scan mode was used during GC-MS analysis. Chromatographic and mass spectrometric data were recorded and processes using the XCalibur software (Thermo Electron Corporation, USA).

3. Results and discussions

In urban areas, motor vehicles are the main source of air pollutants such as non-methane hydrocarbons, NO_x, CO, particulate matter and derived ozone in the atmosphere [8]. In general were more than 35 species of VOCs that was detected in atmosphere. Among the most abundant trace VOCs the following five non-methane VOCs were detected: benzene, MTBE, acetylene, isobutylene and 1-pentene.Their corresponding average, minimum and maximum concentrations are presented in Table 1. Low value of VOCs was detected usually in residential areas located on the edge of town away from the main traffic arteries.

Table 1. Average value of main volatile organic compounds detected.

Compound	Average ($\mu g \cdot m^{-3}$)	Min. ($\mu g \cdot m^{-3}$)	Max. ($\mu g \cdot m^{-3}$)	Compound	Average ($\mu g \cdot m^{-3}$)	Min. ($\mu g \cdot m^{-3}$)	Max. ($\mu g \cdot m^{-3}$)
MTBE	18.45	2.11	43.05	o-xylene	7.59	2.05	19.99
Isobutane	10.55	1.59	19.05	Toluene	6.25	2.44	16.98
Acetylene	16.04	5.06	34.02	n-heptane	5.66	1.28	9.15
Isobutylene	14.72	2.81	28.66	2.3-dimethylbutane	3.98	2.05	17.14
1-pentene	11.15	4.06	32.82	Isoprene	4.95	1.25	16.22
Benzene	26.11	1.28	56.42	2-methylpentene	2.33	1.25	8.11
Ethylbenzene	10.11	6.18	27.15	1.2.4-trimethylbenzene	4.08	2.11	19.25

An obvious seasonal cycle as well during phase of day variation (night-day) was observed in the time series plot. Daily cycle variation of main VOCs based on their average, minimum and maximum value is presented in Table 2. Also it was observed that concentrations of anthropogenic emitting hydrocarbons were relatively high in winter and lower in summer while concentration of biogenic isoprene was reverse.

Table 2. Daily cycle variation of volatile organic compounds.

Compound	Night time (21^{00} – 7^{00})			Day time (7^{00} – 21^{00})		
	Average ($\mu g \cdot m^{-3}$)	Min. ($\mu g \cdot m^{-3}$)	Max. ($\mu g \cdot m^{-3}$)	Average ($\mu g \cdot m^{-3}$)	Min. ($\mu g \cdot m^{-3}$)	Max. ($\mu g \cdot m^{-3}$)
MTBE	7.61	2.11	17.11	29.32	5.66	43.05
Isobutane	2.82	1.59	5.01	16.22	5.12	19.05
Acetylene	4.81	5.06	13.55	21.07	7.11	34.02
Isobutylene	5.05	2.81	6.05	22.59	8.01	28.86
1-pentene	4.08	4.06	7.75	15.27	6.22	32.82
Benzene	5.18	1.28	10.18	33.21	7.59	56.42
Ethylbenzene	7.11	6.18	12.05	25.41	11.51	27.15
o-xylene	3.81	2.05	6.81	21.05	13.08	19.99
Toluene	2.91	2.44	6.66	15.24	6.57	16.98
n-heptane	3.88	1.28	7.15	10.94	5.91	9.15
2.3-dimethylbutane	4.06	2.05	8.02	18.06	4.63	17.14
Isoprene	2.91	1.25	5.49	13.44	3.84	16.22
2-methylpentene	2.22	1.25	3.19	9.55	4.82	8.11
1.2.4-trimethylbenzene	2.98	2.11	5.99	16.33	6.22	19.25

4. Conclusions

The concentrations of ambient VOCs at 28 sites in an urban area were quantified using a passive sampling technique. Highest amount were detected in case of benzene, MTBE, acetylene, isobutylene and 1-pentene. The total concentration of VOCs in the monitored sites varies between 29.18 – 167.55 $\mu g \cdot m^{-3}$. Daily-diurnal variation was observed in most cases of VOCs detected during this study.

REFERENCES

[1] K.H.Chang, T.F.Chen, and H.C.Huang, “Estimation of biogenic volatile organic compounds emissions in subtropical island-Taiwan”, Science of the Total Environment, 346, pp. 184-199, 2005.
[2] C.C.Chang, C.H.Lai, C.H.Wang, Y.Liu, M.Shao, Y.Zhang, and J.L.Wang, “Variability of ozone depleting substances as an indicator of emission in the Pearl River Delta, China”, Atmospheric Environment, 42, pp. 6973-6981, 2008.
[3] S.A.Montzka, J.H.Butler, R.C.Myers, T.M.Thompson, T.H.Swanson, A.D.Clarke, L.T.Lock, and J.W.Elkins, “Decline in the tropospheric abundance of halogen from halocarbons: implications for stratospheric ozone depletion”, Science, 272, pp. 1318-1322, 1996.
[4] C.Cai, C.Hogrefe, P.Katsafados, G.Kallos, M.Beauharnois, J.J.Schwab, X.Ren, W.H.Brune, X.Zhou, Y.He, and K.L.Demerjian, “Performance evaluation of air quality forecast modeling system for a summer and winter season – photochemical oxidants and their precursors”, Atmospheric Environment, 42, pp. 8585-8599, 2008.
[5] N.Kwangsam, “Determination of VOC source signature of vehicle exhaust in a traffic tunnel”, Journal of Environmental Management, 81, pp. 392-398, 2006.
[6] EPA, “National Air Quality and Emission Trends Report”, EPA 454/K-03-001, U.S.Environmental Protection Agency, Office of Air Quality Planning and Standards, Research Triangle Park, NC, 2002.
[7] Y.Pang, M.Fuentes, and P.Rieger, “Trends in emissions of volatile organic compounds (VOCs) from light-duty gasoline vehicles tested on chassis dynamometers in Southern California”, Atmospheric Environment, 83, pp. 127-135, 2014.
[8] B.Pekey, H.Yilmaz, “The use of passive sampling and monitoring spatial trends of volatile organic compounds (VOCs) at an industrial city of Turkey”, Microchemical Journal, 97, pp. 213-219, 2011.

ISSN 1454 - 8003
Proceedings of 2014 International Conference of Hydraulics and Pneumatics - HERVEX
November 5 – 7, Calimanesti-Caciulata, Romania

CLEAN TECHNOLOGIES FOR ENERGY RECOVERY IN HYDRAULIC DRIVE SYSTEMS USED FOR INCREASING ENERGY EFFICIENCY OF MACHINERY AND EQUIPMENT

PhD. Eng. Corneliu CRISTESCU[1], PhD. Eng. Catalin DUMITRESCU[1], PhD. Eng. Radu RADOI[1], Dipl. Eng. Liliana DUMITRESCU[1]

[1]Hydraulics and Pneumatics Research Institute, INOE 2000-IHP, Bucharest, ROMANIA
cristescu.ihp@fluidas.ro

Abstract: *The paper presents a new trend in the development of the hydraulic drive systems, which aims to develop and implement devices and systems for recovery of kinetic or potential energy, which remains available after achieving useful mechanical work, in different equipments with hydraulic driving, in order to increase energy efficiency. There are shown some aspects regarding the thermo-hydraulic hybrid motor vehicles and, in brief, there is presented a Romanian version of a thermo-hydraulic hybrid motor vehicle, conceived in mechatronics conception.*
In the final part, there are presented some experimental models, which demonstrate the possibility to recover the kinetic and potential energy, and also the posibility to quantify the recovered energy, by calculation of the energy recovery coefficient. There are presented some graphical results which clearly show the phases of the energy recovery concept: capture, storage and reuse of the recovered energy. The results confirm the technology and the technical solutions adopted for kinetic energy recovery.

Keywords*: energy efficiency, energy recovery, hydrostatic drives, applied research*

1. Introduction

In view of the depletion of fossil fuel resources, a direction for immediate action is to save available energy by increasing the energy efficiency of machinery, equipment and technological systems, in order to reduce energy consumption by means of a new and clean technology, the energy recovery one, leading to a substantial increase in energy efficiency and decrease of harmful emissions, with beneficial effects on the environment. [1].
Usually when operating machinery, equipment and technological systems, most part of the installed power is used during start / acceleration in order to gain a kinetic or potential energy useful for their functioning. After consumption of the active phase of the work cycle and after the useful mechanical work is done, in these systems a certain amount of available energy remains unused, energy which, before resuming the next work cycle, is removed from the system by conventional, dissipative methods, ie by braking, when energy is irretrievably lost in the atmosphere and sometimes with a negative impact on the environment.
For engineers, the technical problem to be solved is to recover such available energy and then reuse it in the active phase of the next work cycle, to improve energy efficiency of drive systems in machines, equipment and technological systems [2]. Therefore, in the last decade, engineers have taken a number of actions to identify these situations, to design and develop technical solutions for the newly developed equipment, and also for the existing ones, through which part of this available energy can be captured, stored and then reused in the next work cycle, in order to increase energy efficiency of drive systems.
Below, there are presented some theoretical and experimental results obtained by Hydraulics and Pneumatics Research Institute, INOE 2000-IHP Bucharest, on the development and implementation of some hydraulic energy recovery systems, to demonstrate the viability and feasibility of technical solutions chosen, in order to highlight improved energy efficiency in mobile and industrial fluid power systems.

2. Kinetic energy recovery at motor vehicle braking

Increased development of road transport has a strong impact on the environment and global warming of the planet. To reduce fuel consumption and limit gas emission, manufacturers have developed less polluting motor vehicles.
As it is known, during the braking phase, the kinetic energy of the motor vehicle, accumulated during the acceleration phase, is converted into heat, which is normally and irretrievably wasted / lost to the atmosphere.
The technical problem solved by the engineers was to design and implement an energy recovery system, in order to capture, convert and store the kinetic energy, and then reuse it during the start and acceleration phase.
The propulsion systems that have in addition to a conventional internal combustion engine at least another subsystem of different kind, able to provide torque to the wheels of the car and to recover some of the kinetic energy, are known as regenerative systems, and motor vehicles that use two types of energy are called hybrid motor vehicles.
The main objective of hybrid systems consists in recovering kinetic energy from road motor vehicles, during the braking phase, reducing fuel consumption and pollution, thus increasing the energy efficiency of motor vehicles [1].
There are a lot of technical solutions for hybrid propulsion systems that can recover kinetic energy from a motor vehicle, but the most common are the thermo-electric system and the thermo-hydraulic system.
The Romanian system, shown in Figure 1, belongs to the latter type. [2]. To recover kinetic energy there has been adopted the technical solution to recover kinetic energy by hydraulic systems. In the braking phase, the kinetic energy is converted into hydrostatic energy, which is stored at a high pressure in hydro-pneumatic accumulators by a hydraulic machine operating as a pump. In the acceleration phase, the stored hydrostatic energy is converted into mechanical energy by this hydraulic machine, working now as a hydraulic motor, generating acceleration of the car [3].

2.1The conceptual model of the Romanian hydraulic system for kinetic energy recovery

The hydraulic energy recovery system has been designed to be implemented on a Romanian motor vehicle, ARO 243, Figure 1, which has a 4x4 propulsion system. In Figure 2, which presents the conceptual model, could be distinguished: diesel engine MD, gearbox CV, front gear transmission, torque and speed transducer TMR and drive shaft. There can be also noted the mechanical transmission of the hydraulic machine /hydraulic unit UH, the low-pressure tank LT and the hydrostatic energy storage system consisting of two hydro-pneumatic accumulators, Ac1 and Ac2.

Fig. 1 ***The Romanian motor vehicle ARO-243***

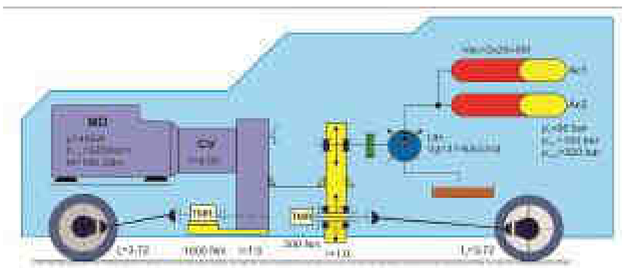

Fig. 2. ***The conceptual model of hydraulic system for kinetic energy recovery***

Hydraulic power is transmitted to the drive wheels through a torque and speed transducer (TMR) and a drive shaft. The hydraulic machine can be connected in parallel anywhere along the chain of transmission, but, generally, it is installed on the transmission shaft, between the gearbox and differential driving gear. The most important component of the energy recovery system is the variable displacement hydraulic machine UH, which is driven by a mechanical transmission and assisted by an electronic subsystem and a computerized subsystem, both interfaced with the braking and acceleration systems of the car [2].

2.2 The main physical modules of hydraulic system for kinetic energy recovery

The main modules of the system for kinetic energy recovery are shown in Figure 3:

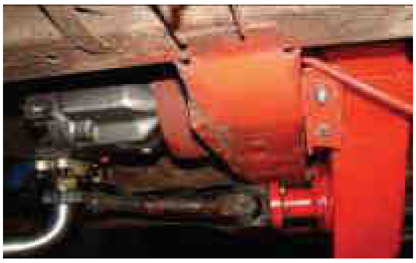

(a) Hydro-mechanical unit

(b) Hydraulic station

(c) Battery pack

Fig. 3 ***The main physical modules of hydraulic system for energy recovery*.**

3. Lifting platform provided with energy recovery system

An important category of lifting equipment is represented by hydraulic drive lifting platforms, typically used by persons with locomotor disability, for their access to public buildings (town halls, local councils, hospitals, auditoriums, museums, etc.), or to perform other lifting-lowering operations.
These devices or platforms at each upward stroke, generate the energy needed to perform the mechanical work required to lift the load, after which, when lowering the load, this accumulated potential energy is dissipated into the environment, usually by putting a brake to / throttling the fluid, which thus gets heated and other energy is required to cool this fluid. Under these conditions, the yield of equipment is low and measures are required to increase it.
The technical problem that confronts engineers is to recover at least part of this potential energy, for the purpose of reusing the recovered energy in the phases of lifting, which leads to a substantial increase in energy efficiency, respectively to decrease in energy consumption per work cycle.
To implement the hydraulic system for potential energy recovery, for the purpose of conducting experimental tests on the technical solution for energy recovery, there has been used an existing lifting platform, Figure 4, designed and developed in the Institute INOE 2000-IHP. The lifting platform provided with energy recovery system, shown in Figure 5, consists of the parts of the existing, classic, platform, whereon is implemented the module for recovery of potential energy. The system or hydraulic module for potential energy recovery complements the classic hydraulic drive installation, in order to recover the potential energy when lowering the load (the weight), by capturing, converting and storing it in hydropneumatic accumulators, followed then by reusing it in phase of load/weight lifting.
The concept of a hydraulic system for potential energy recovery is shown in Figure 6, and it has the following structure: stroke transducer (15), glycerin-filled manometer (16), accumulator safety block (17), membrane accumulator (18), a hydraulic unit (19) whereon there are mounted the hydraulic components (directional control valves, check valves etc.). The hydraulic system for potential energy recovery is currently under patenting at OSIM Bucharest.

ISSN 1454 - 8003
Proceedings of 2014 International Conference of Hydraulics and Pneumatics - HERVEX
November 5 – 7, Calimanesti-Caciulata, Romania

Fig. 4 ***The classic lifting platform***

Fig. 5 ***The platform provided with system for potential energy recovery***

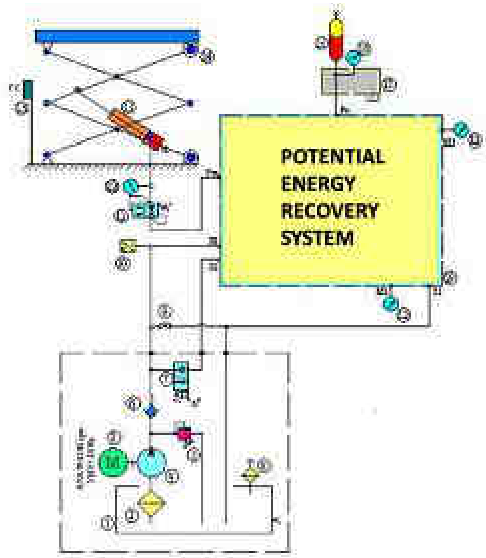

Fig. 6 ***Hydraulic diagram of the platform provided with system for potential energy recovery***

Figure 7 presents the main modules of the system for potential energy recovery.

(a) Hydraulic unit ***(b) Energy accumulator*** ***(c) Hydraulic cylinder***

Fig. 7 ***The main modules of the hydraulic system for potential energy recovery***

4. Lifting-lowering equipment provided with hydraulic drive and energy recovery system

Below, it is presented an experimental demonstrative model of the lifting-lowering equipment provided with hydraulic drive and potential energy recovery system, which has mechanisms driven by hydraulic rotary motors.

The lifting-lowering equipment designed is used in mechanical and /or repair workshops, for lifting masses / weights (tools, parts, hydraulic blocks, etc.), at various heights, by hydraulic drive, and lowering those masses / weights being made under control, through hydraulic regenerative braking, ie with recovery of potential available energy, by converting it into hydraulic energy.

The technical question put was if we can recover at least part of that potential energy, and then re-use of this recovered energy in the active lifting phases of the next work cycle, which leads to a substantial increase in energy efficiency respectively to lower energy consumption.

4.1. Presentation of the lifting-lowering equipment provided with potential energy recovery system

The lifting- lowering equipment, shown in Figure 8, consists of a welded metal structure, positioned on a movable wheeled frame, provide with a drive system of the drum / tambour from an axial piston unit / hydraulic machine, having a system of pulleys, one of which is mobile, leading to duplication of the weight lifted compared to the effort in the cable.
When lowering loads with a controlled speed rate in gravitational field, potential energy is converted by means of a cable and roller system, one roller being mobile, into kinetic rotational energy at the cable drum / tambour, and then it is transformed / converted into hydrostatic energy by means of a machine / rotary hydrostatic unit, hydrostatic energy being stored and then reused in the phases of lifting.
An important component of the lifting equipment provided with potential energy recovery is the mobile hydraulic station, Figure 9 and Figure 10, that connects with the hydraulic rotary motor actuating the cable drum by means of quick coupling hoses.

Fig. 8 ***Lifting-lowering equipment provided with potential energy recovery***

Fig. 9 ***Mobile hydraulic station (side view)***

Fig. 10 ***Mobile hydraulic station (top view)***

4.2 The module for energy recovery and re-use

When lowering the load / weight in a controlled manner, the torque produced by the drum / cable tambour and cable tangential force, operate a hydrostatic machine, now working as a pump. Thus potential energy is transformed / converted into hydrostatic energy, which is then stored in a hydropneumatic accumulator, being reused in the next work cycle. These complex functions are carried out with the module for energy recovery and re-use, Figure 11 and Figure 12, which is now in the process of patenting at OSIM Bucharest.

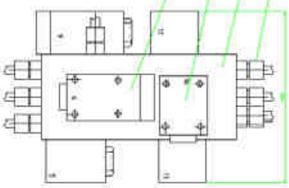

Fig. 11 ***Draft of the recovery module***

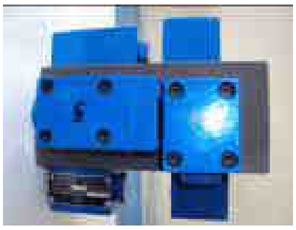

Fig. 12 ***Physical shape of the recovery module***

The mobile hydraulic station has been made starting from a standard station, on which there has been implemented the energy recovery module.

5. Demonstration model for rotational kinetic energy recovery in hydrostatic drive equipment

To develop an experimental research on the recovery of rotational kinetic energy, it was necessary to design and manufacture a demonstration model, Figure 13 and Figure 14, simulating possible technical or technological equipment, having a mechanical structure with a rotation mechanism (MROT), with a rotating mass (MR), hydraulically actuated (SHP). On the demonstration model there has been implemented a new technical solution for a rotational kinetic energy recovery system (ERHS). In order to demonstrate the possibility to recover the rotational kinetic energy, and also in order to verify the technical solution adopted, the demonstration model was subjected to a lot of tests. These tests consisted of a large variation of the main parameters, namely: variation of maximum pressure of the hydraulic system, variation of rotational masses, and also variation of the pressure of nitrogen in the accumulator, obtaining graphical variation of the main mechanical and hydraulic parameters of the system. For example, Figure 15 shows the variation of recovered energy and energy recovery coefficient. Other results are under publication [4].

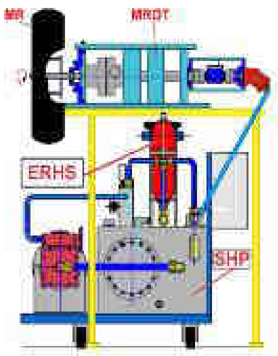

Fig. 13 ***Conceptual model***

Fig. 14 ***Physical demonstration model***

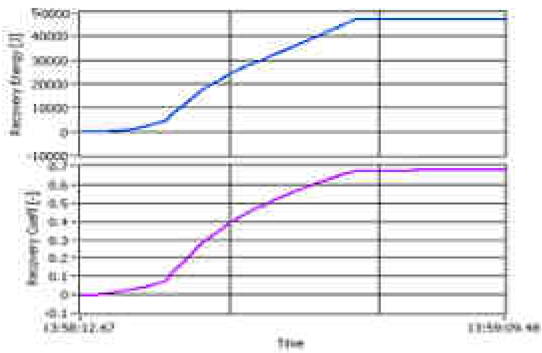

Fig. 15 ***Variation of recovered energy and energy recovery coefficient***

6. Conclusions

The paper presents experimental demonstration models that aim to demonstrate the possibility for recovery of kinetic and potential energy remaining after the completion of useful mechanical work on machines and equipment.
There are presented conceptual diagrams, the main components and also some experimental results, which allow to demonstrate the possibility for energy recovery, and also to quantify it.
The experimental results already obtained have validated the technical solutions adopted, and through experimental measurements, they have confirmed the real possibility for energy recovery with a rate of about 60%.
The technical solutions adopted can be promoted into the new technological equipment, in the design phase, and also in the existing equipment, if they can be implemented during rehabilitation.
Users of research results are the manufacturers of technological automotive and industrial equipment, hydraulically driven, who can adopt this innovative technology to obtain significant economic benefits.

REFERENCES

[1] Cristescu C, Drumea P., Dumitrescu C. - The increasing of the energy efficiency of the motor vehicles by using the hydraulic systems for kinetic energy recovering. In: Proceedings Vol. II of the 10th International Multidisciplinary Scientific Geo - Conference & EXPO - SGEM 2010, 20 - 26 June 2010, Albena Resort, Bulgaria, pp. 339- 346, ISBN 10: 954-91818-1-2, ISBN 13: 978-954-91818-1-4, Bulgaria, 2010.

[2]. Cristescu C. - Recuperarea energiei cinetice la franarea autovehiculelor (The kinetic energy recovering at the braking of the motor vehicles). Editura (Publishing House) AGIR, ISBN 978 - 973 - 720 - 219 - 2, Bucharest, Romania, 2008.

[3] Cristescu, C., Drumea, P., Ion Guta, Dr., Dumitrescu, C., Chirita, C. -Mechatronic Systems for Kinetic Energy Recovery at the Braking of Motor Vehicles, Chapter in book Advances in Mechatronics, Horacio Martínez - Alfaro (Ed.), ISBN: 978 - 953 - 307 - 373 - 6, In Tech, Croatia, 2011. Available at: http://www.intechopen.com/articles/show/title/mechatronic-systems-for-kinetic-energy-recovery-at-the-braking-of-motor-vehicles .

[4]. Cristescu, C., Dumitrescu, C., Radoi, R., Dumitrescu, L. - Echipament de ridicare-coborare cu actionare hidraulica si sistem de recuperare a energiei (Lifting - lowering equipment provided with hydraulic drive and energy recovery system). AGIR Symposium: Progresul-rezultat al cercetării (The progress- outcome of research), May 22, 2014. In: Bulletin of AGIR no. 1/2014, ISSN-L 1224-7928 (forthcoming).

ISSN 1454 - 8003
Proceedings of 2014 International Conference of Hydraulics and Pneumatics - HERVEX
November 5 – 7, Calimanesti-Caciulata, Romania

GEOSPATIALLY CONTROLED FIELD OF MIRRORS PURSUING SOLAR ENERGY

Mircea BADUT[1]

[1]A.N.C.P.I., Bucharest, Romania, m.badutz@gmail.com

Abstract: *The paper presents the key problems of continuously controlling the orientation of the hundreds/thousands mirrors which focalize the Sun's beams towards a central heat collector of a solar-thermal power plant (in the tower plant approach), and it tries to figure out solutions for the effective controlling/commanding these heliostats constituting such a mirror farm.*

1. Introduction

Even if the target of obtaining electricity directly from the sun energy motivates more and more research efforts aiming the photovoltaics designing and manufacturing, the solutions have not reached enough accessibility and efficiency. Therefore, the "traditional" conversion of solar energy into heat and then in electricity (via steam generators) – having efficiently applied technologies since 1980s – remains for long time the feasible option in the "solar" area. [1]
The first large solar systems used cylindrical-parabolic mirrors to focalize the solar heat on a long tube (a trough) sharply localized on the focal axis. The heat exchanger liquid flowing through this tubes reached temperatures up to 400º C. Lately, there are in focus those systems based on a central boiler (in top of a tower) heated by sun through the flat-mirrors constituting a mirror farm surrounding the tower (fig.) Because of intense heat concentration (such implementation requires large terrain surfaces, situated in zones where the sun radiation is high), the heat-transferring liquid temperature reaches 500 −600º C (at a pressure of 140–160 bars), justifying their costs by their high energetic efficiency. A farm producing 100 MW is typically spreading over a land of 250–300 ha, depending on the effective sun radiation [6].

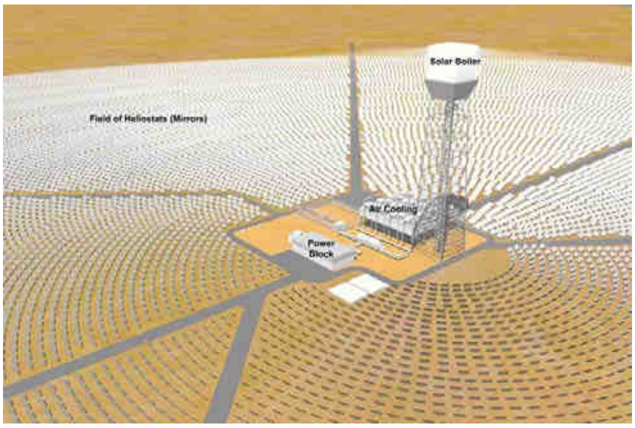

Fig.1- ***Mirror farm focusing a central boiler***

2. The system's problematics

Designing, building and exploiting such solar system involve an intense mixture of many sciences and technologies – automatics, informatics, electrical drives, CAD, CAE and GIS.
Even if from a schematic point-of-view this energy approach seems almost trivial, o huge problem is risen by the fact that the sun rays – reflected by mirrors placed at hundreds meters far away of central boiler – must be kept focalized on the boiler during the whole sun voyage over the sky-

shelter. And, furthermore, if we take into account the fact that in a such plant we have an circular array of thousands flat mirrors (of relative small dimension, 2-3 m), mirrors that heat a collector-boiler positioned on the summit of a 100 meters high tower, the problem gains signification. (Each mirror has to be permanently reoriented such as the perpendicular on his plan, in middle of its surface, to be the bisector of the angle formed by boiler, mirror and sun.)
Each heliostat is driven by an electro-mechanical system able to move it in two directions (2 axis robotics) in order to follow the sun direction during the daylight and according to season. Due to the huge distances between the (more) peripheral mirrors and the central boiler (up to 800 meters), appears like being obvious the need of very high precision in heliostats repositioning in such a way that the reflected sunbeam rigorously reaches on the collecting surface of the boiler. Moreover, this reorienting system must be able to deal also with the stresses and deviation provoked by winds (the wind is often intense in the areas suitable for building such power facilities). In order to obtain the motion on two direction of each mirror assembly/mechanism one can use high efficiency actuators (in a first approach one of the actuators provide the azimuthal rotation (around the vertical axe), and the other provide the elevation movement of the mirror). A control unit (software programmed) is also set up to correct the dynamic relation between the linear velocity of the actuator and the nonlinear rotational velocity. Because the energy amount consumed by the electrical engines of such a double electrical driving subsystem is very small, the heliostat's servomechanism can be fueled by a photovoltaic unit.
There are models using an epicyclic motion driving to control the mirror's azimuth (a trajectory composed from a motion that follows the circumference of a circle whose center follows the circumference of another circle), and this approach drives to command simplification, rigidity improving, and it brings also a gain in motion precision and resolution.

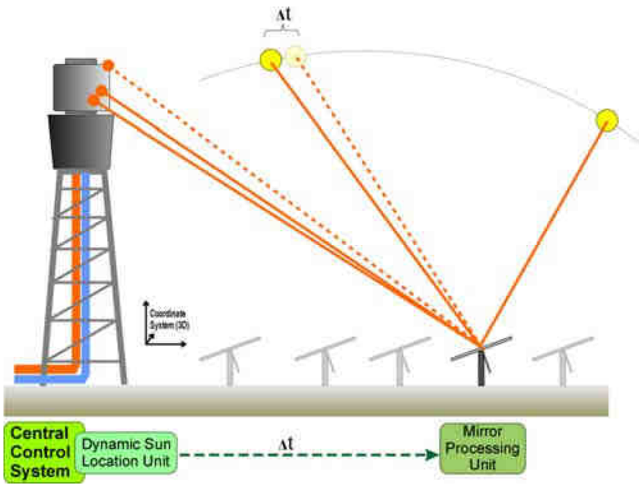

Fig.2- ***Schematics on mirror following the sun***

3. Approaches in schematic solving

The solution for controlling/commanding the subsystems that drive the several hundreds/thousands mirrors around the tower constitutes a challenge of scientific, technical and managerial conception. One can take into account the following scenarios: (see the schematic figure)

» 1st scenario: a dynamic on-sky (canopy) localization unit (based on optical sensors able to sweep the sky) determines periodically (on a time interval computed considering the relative speed of the sun, the distances boiler-heliostats, the receptive dimension of the boiler) the current sun position (in a 3D space coordinate system) and releases the proper instructions to drive the servomechanism/actuators of each mirror;

» 2nd scenario: a central processing and controlling unit knows the sun positions for every day of the year (calendar) and for every hour (from a astrophysics database adapted to the local zenith) and periodically transmits the mirror reorienting statements/commands customized for each heliostat (adapted also about the relative position of the mirror);

» 3rd scenario: each heliostat has its own (embedded) processing unit that knows the sun positions in every moment (from its own memory) and uses them to calculate and to command its own actuators for the current proper reorientation (plus eventual wind corrections).

Nowadays there are studies, researches and even implementations that combine the 2nd and 3rd scenarios, resulting in patented systems (based on hardware and software), whose high complexity can be intuited from the described context.

4. The geoinformatics contribution

Due to the geo-spatial spread of such plant (especially because in practical implementation in desertic areas it is recommended to join more than one such solar-thermal farms), the applicability of the geo-informatics become advisable or even imperative. GIS can be involved in many directions: from addressing design issues, to especially resolving exploiting aspects (dispatching, managing, maintenance). We can engage geoinformatic systems into:

- finding the best location for the farm/plant: by comparative and assessing studies over the solar radiation, by terrain modelling, studies over the possible terrain slopes related to midday direction;

- in the stage of designing the computerized commands/controls for the servomechanisms of heliostats, mainly if we choose a geodetic system as the actual coordinate system;

- in the exploiting stages: for spatial management of the heliostats in diverse internal plant requirements.

We can use GIS for creating average solar radiation maps, showing the irradiance (solar energy falling on unit area per unit time – W/m2), the irradiation (the amount of solar energy falling on unit area over a stated time interval – Wh/m2), the insolation values (the resource available to a flat plate collector facing south, at a vertical angle equal to the latitude of the collector location), and also for revealing the local/particular attenuation factors and the latitude lean condition.

The interaction of solar radiation with the Earth's surface is determined by 3 groups of factors:

1. the Earth's geometry, revolution and rotation (declination, latitude, solar hour angle);

2. the terrain (elevation, surface inclination and orientation, shadows);

3. the atmospheric attenuation (scattering, absorption) by: gases (air molecules, ozone, CO_2 and O_2); solid and liquid particles (aerosols, including non-condensed water); clouds (condensed water).

The global radiation consists in:

1) the radiation, selectively attenuated by the atmosphere, which is not reflected or scattered and reaches the surface directly, is named direct radiation (beam radiation).

2) the scattered radiation that reaches the ground is named diffuse radiation.

3) the small part of radiation that is reflected from the ground onto the inclined receiver is named reflected radiation (related to the "albedo" term). [3]

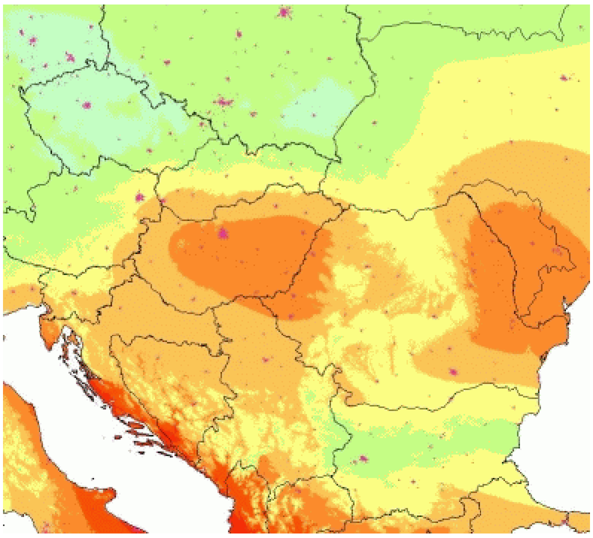

Fig.3 - *Sun radiation map, Romania*

5. Control system formalization

The computerized control of such a system obviously constitutes a special challenge for conception, design, implementation and optimization. And – from all involved aspects – the one, regarding to commanding/monitoring those thousands of mirrors, is proving itself as being the vault key.

By considering a mathematical approach, for the mirrors' motions (movements) in a real three-dimensional space, one can consider a hypothetic spherical calotte, and on this surface the current succeeding sun's positions are to be projected (a trajectory relative at both the boiler position and the whole mirror farm). This hemisphere delimits/defines a 3D space that can be governed (governable) through a local coordinate system, its own coordinate system (rectangular or spherical) chosen as more convenient as possible.

We may resort to a such idealization – considering a local coordinate system (as it is named in geodesy) – in order to avoid working with a geodesic classical coordinate system, whose implications regarding the geodetic projections are still difficult to assimilate in a solution that requires a high 3D precision for its entities (sun, especially). [2] We can observe that the local coordinate system can be a cartesian one (such as the three-orthogonal X, Y, Z), or rather a spherical one, modelling the hypothetic calotte (in spherical coordinates: radius, horizontal angle, vertical angle, but not being a geocentric system).

In this local coordinate system, we can pursue a quasi-algebraic formalization for the mirrors reorientation functions (which can be substituted by the displacement functions for light spots reflected by mirrors):

$$f: R^{n*i} \rightarrow R^{n*o}$$

– the function of reorienting the mirrors, where
n – the number of mirrors (hundreds-thousands)
i – the number of input parameters of each mirror (relative localization and the previous orientation of the mirror)
o – the number of output parameters for each mirror (the next orientation of the mirror)

$$s: T \rightarrow R^3$$

– the function for modelling the sun trajectory by time (day-season and hour)

$$f \circ s$$

– by composing the function we can correlate the mirrors reorientation with the sun motion.

In a rough approach one can work with a reorientation function defined for every mirror, and this coarse solution imposes a simplified mathematical apparatus, but a considerable huge computational effort (inflicting to recording and to simultaneous rerunning many algorithms and data). Perhaps, the ideal approach consists in defining a single multi-scalar function able to work with substantial input data (data concerning the mirrors localization relative at boiler and at current sun position) and able to furnish output data matrix (commanding parameters to be issued towards the mirrors reorienting automated servomechanisms); but yet, a such hypothetic solution do not significantly spare the computing efforts.
Once completely formulated these controlling functions, they can be transposed as binary code for commanding and monitoring the heliostats, and effectively implemented in the computing systems governing the mirror farm. (At this point, the researches regarding the control modelling for such solar systems are protected by commercial confidentiality (NDA), but – as the interest for sustainable energy becomes more general – we can presume that the concrete solutions for such problems will appear as public assets.)

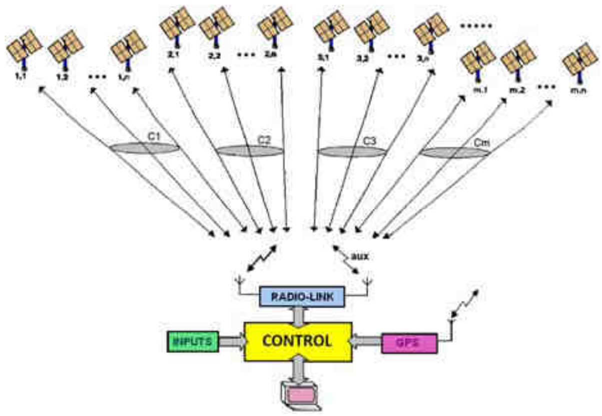

Fig.4 – ***Schematic of controlling the system***

6. Other issues and perspectives

These huge geometrical and computational problems are complicating themselves furthermore by the fact that – especially in some extreme days/hours of season/day, or in sloped terrain situation – the repositioning of mirrors must take into account the effects of shading and blocking by adjacent heliostats. In pursuing high levels of efficiency (lower costs, or higher energy), a computer program can be deployed and applied on a whole basis (involving large plant-managing parameters). The variables which can be considered in an optimization process are: the size and number of heliostats, the height of the tower, the dimensions of the receiver, the parameters of the heat-transfer fluid (thermal capacity, velocity, flow, total volume), the capacity of the storage tanks, the power of the turbine. [8]
Another imperative problem influencing many of the specifications of the computer-based system that controls the mirrors farm consists in settling the time period in which we need to remake the mirror reorientation (see the schematic illustration). Beside the mirrors continuous reorientation issue, this one proves itself as being much simpler, i.e. based on a simple geometric calculus: in how much time the reflected sunbeam will trace the whole collecting surface of the boiler (effective incidence/aiming surface of the collector in mirror's direction). We can observe that for the most peripheral mirrors of the farm – due to the long distance to the central tower, that implies a more risen sensibility to angular deviations (inflicted by the sun continuous movement) – a more frequent reorientation commands update is needed.
As a normal expectation, great improvement perspectives can be foreseen in direction of heat collector efficiency and performance, where the materials physics and the photonic science still have more potential. Yet another key problem in the case of these Concentrated Solar Power

(CSP) consist in the discontinuity of the energy source, and the fact (along with that of the nightly recession of solar power) can be addressed by technical solutions of energy capturing/storing (such as in molten salt cells), but here we risk to go out from the sphere of electrical driven and computerized controls.

7. Instead of conclusions

Nowadays, the electricity produced by means of solar power plant is around one percent of the world's electricity. But - being so non-polluting and cheaper - this energy source is knowing a rising slope, and the perspective are very bright in helping the large power grids, as in balancing the world's energy relationships. Therefore, it is worth to increasingly attract the research in the related fields, including automatics, computers and informatics.

REFERENCES

[1] Băduţ, M., *Sisteme geoinformatice (GIS) pentru electroenergetică*, Editura Polirom, Iaşi, 2008.
[2] Băduţ, M., *Sisteme informatice geografice (GIS) – fundamente practice*, Editura Albastră, Cluj-Napoca, 2007.
[3] Băduţ, M., "Geoinformatics for Renewable and Non-impact Energies", in *GEOinformatics* magazine, The Netherlands, 2/2007.
[4] Băduţ, M., *Sisteme geoinformatice (GIS) pentru administraţie şi interne*, Editura Conphys, 2006.
[5] Băduţ, M. " Sistem solar - termal cu fermă de oglinzi", in "Tehnică & Tehnologie" magazine, nr.6, 2008, p.104.
[6] Ricker, C. "Is the solar thermal power the answer?", in "Photonic Spectra" magazine, Laurin Publishing, Pittsfield Massachusetts, USA, July 2008, pp.58-59.
[7] d'Hoop, Delphine "From heat to megawatts", in research*eu magazine, April 2008, Communication Unit of the European Commissions's Directorate-General for Research.
[8] Sener, Solar Tres. Sensol public information, http://www.sener.es

ISSN 1454 - 8003
Proceedings of 2014 International Conference of Hydraulics and Pneumatics - HERVEX
November 5 – 7, Calimanesti-Caciulata, Romania

PROCEDURE AND PNEUMATIC TRANSDUCER FOR MEASURING HUMIDITY DURING DRYING OF CERAMIC BODIES

Erol MURAD[1], Cătalin DUMITRESCU[2], Liliana DUMITRESCU[2]

[1] Univ. POLITEHNICA Bucureşti erolmurad@yahoo.com

[2] INOE2000 – IHP dumitrescu.ihp@fluidas.ro

[2] INOE2000 – IHP lilianad.ihp@fluidas.ro

Abstract : *For optimal quality and economic management of the process of drying ceramic bodies is necessary to measure in real time the actual humidity variation of bodies. It was developed a procedure and pneumatic transducer to measure the variation of the ceramic body mass in the drying process specifically designed to work precisely and reliably at typical temperatures in the domain 120 - 180 °C. This type of transducer is working in sampled measurement mode and is characterized by very low energy consumptions, something which is typical for low-cost automation. The output of transducer is coupled to the PLC destined for automatic control of the processes in drying chamber. The dynamic behavior and energy consumptions were determined through experiments realised with a model and a numerical simulation program, developed in the environment MEDSIM DP10 simulation. Experiments have confirmed a high precision of measurement and a low consumptions of pneumatic and electric energy.*

Keywords: *drying, humidity, ceramic body, pneumatic, optimisation*

1. Introduction

To increase product quality and reduce scrap ceramic occurring after firing, due mainly to an nonuniform drying and energy and economic optimization is necessary to measure the real-time variation of moisture and shrinkage of ceramic bodies. [6, 11]

There are two possible variants of a body approach to measuring humidity by varying the weight of water evaporated in the drying process. An absolute method which measures the actual mass of the body in a relatively dry and the relative variation of measured body mass ΔMc[i] / Mc[1], actually what interested the drying characteristic.[2, 6, 8, 9]

Drying characteristic F2 (t) - absolute humidity variation Uc (t) of the body over time (kg.w/kg.db•h) - can redefine the discretized form as F2 [i]:

$$F_2[i] = \frac{-\Delta U_c[i]}{\Delta t} = \frac{U_c[i-1] - U_c[i]}{\Delta t} = \frac{\Delta M_w[i]}{M_{db}\Delta t} \quad (1)$$

Where: $U_c[i] = \frac{M_w[i]}{M_{db}}$ is the absolute body humidity at moment [i] (kg.w/kg.db);

$M_{db} = \frac{M_c[1]}{U_c[1]+1}$ is the mass of full dry body (kg.db);

$M_w[i]$ is water mass of body at moment [i] (kg.w);

$M_c[i]$ is the humid body mass measured at moment [i] (kg);

and:

$$\Delta M_w[i] = M_c[i-1] - M_c[i] \quad (2)$$

result:
$$F_2[i] = \frac{U_c[1]+1}{\Delta t} \cdot \frac{M_c[i-1]-M_c[i]}{M_c[1]} \tag{3}$$

To determine the speed of drying is necessary to measure the ratio Mc[i] / Mc[1]. Raw ceramic bodies entering the drying have a maximum relative humidity rh [1] $\leq$ 20% and an absolute humidity Uc [1] <0.25 kg.w / kg.db at ambient temperature 10 - 25 ° C.

At the end of drying, when the index i = n, ceramic bodies having a maximum relative humidity φc [n] <2% and an absolute humidity Uc [n] <0.02 kg.w / kg.db at a temperature Tc $\in$ [120, 180] °C.

This procedure can also be used for drying wet other products, especially vegetables and fruit, where the drying rate is the main factor that determines the quality of the final product.[7, 9,10]

2. Pneumatic load cell

Using pneumatic transducers, largely unconventional, coupled with current numerical technique, is currently an opportunity to achieve automatic control systems precise, safe, very low power consumption and low cost. [1, 5, 8]

The main element of the force transducer is pneumatic load cell, which converts measured force F_{mas} in a force proportional pressure p_{mas}.

Figure 1 shows a functional diagram for pneumatic load cell for the drying process, which can be used for proving that force change occurs slowly and processes take place in a single direction.

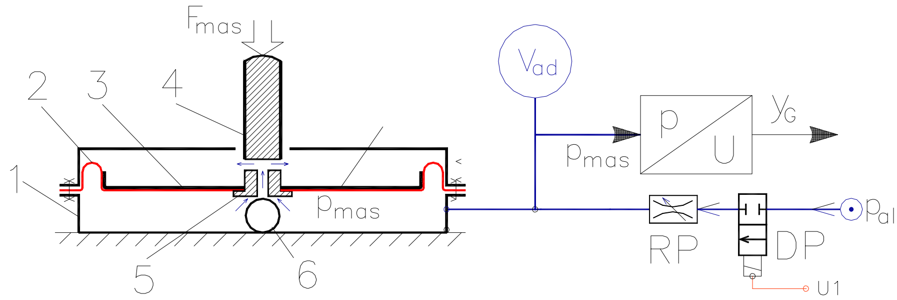

Figure 1 - Functional diagram of pneumatic load cell

Force measuring F_{mas}(t) is applied on top of a rod (4) attached to the rigid center (3) of an embossed flexible membrane (2) with effective diameter D_{ef} and constant effective area S_{ef}, mounted on a body (1). On the rod (4) is attached a nozzle (5), with the diameter d_d, which is based on a ball (6) with diameter d_b, closing the chamber as air access to the outside through holes in the membrane, rigid centre and rod.

The measurement chamber can be connected in parallel with an air capacity V_{ad}. Pneumatic circuit supply is done by RP variable air resistance and DP distributor type 2x2. Pressure source must be $p_{al} \geq 1{,}5\, p_{mas\ max}$.

Pressure measured p_{mas} (t) is applied to a integrated converter p/U, which gives the output voltage $y_F \in$[1, 3] or [1, 5] Vdc.

The steady, the balance of forces, pressure p_{mas} (t) in the enclosure is:

$$p_{mas}(t) = \frac{F_{mas}(t) + G_{em}}{S_{ef}} \tag{4}$$

where: G_{em} is the weight of mobile equipment, which is constant.

For measuring a force with some variation, included in the measurement, the supply with dried compressed gas is sampled with an u_1 order form, short pulse, which provides increased pressure p_{mas} to F_{mas} balance; then the rigid centre, membrane and nozzle amount of the ball with h(t) and excess flow gas D_{ev}(t) is discharged outside.

For measuring a force with a change in one respect, specific processes of drying, the weight of bodies during drying decreases continuously, it is necessary to supply compressed gas only at the beginning of drying burden.

During drying F_{mas} decreases continuously, p_{mas} decreases continuously, and additional gas is discharged outside through the space between the gasket and valve, to maintain balance as it shows the relationship (1).

This method of measurement consumes a very small amount of compressed gas, which means little air power.

As the outdoor temperature is constant and the variation of force $F_{mas}(t)$ is slow, can be considered, in terms of thermodynamics, the measurement is an isothermal process at constant volume. [3, 4]

Variation of the air mass in the enclosure depends on pressure variation $p_{mas}(t)$ produced by the variation of force $F_{mas}(t)$:

$$V_m + V_{ad} = \frac{m_a(t) R_a T_a}{p_{mas}(t)} \tag{5}$$

The position of dynamic equilibrium of cell phone equipment load, if the air distributor DP is closed, the volume of gas is constant V_m. Therefore, thermodynamic equilibrium equation is:

$$p_{mas}(t)\left(V_m + V_{ad}\right) = m_a(t) R_a T_a \tag{6}$$

hence the differential equation of the dynamic behavior of load cell:

$$\left(V_m + V_{ad}\right)\frac{dp_{mas}(t)}{dt} = R_a T_a \frac{dm_a(t)}{dt} \tag{7}$$

and

$$\frac{dm_a(t)}{dt} = \left(\frac{V_m + V_{ad}}{S_{ef} R_a T_a}\right)\frac{dF_{mas}}{dt} \tag{8}$$

When the force produced by the membrane exceeds the loading:

$$\left(p_{mas}(t) \cdot S_{ef} - F_{mas}(t) - G_{em}\right) > 0 \tag{9}$$

is entering a phase characterized by acceleration a(t) that makes lifting the nozzle from the ball to h(t):

$$a(t) = \left(p_{mas}(t) \cdot S_{ef} - F_{mas}(t) - G_{em}\right) / M_{red}(t) \tag{10}$$

M_{red} low mass value (t) at the transducer rod is:

$$M_{red}(t) = \left(F_{mas}(t) + G_{em}\right)\frac{1}{g} \tag{11}$$

D_{mev} exhaust mass flow (t) depends on the distance nozzle-ball h(t), the $p_{mas}(t)$ and external pressure p_{atm}. S_{ev} exhaust section (h, db, dd) is a truncated cone with the tip in the centre of the ball and the base on the nozzle [3], where Rh is hydraulic radius [3]:

$$R_h = 0.5 \cdot \left(\sqrt{h^2 + h\sqrt{d_b^2 - d_d^2} + 0.25 \cdot d_b^2} - 0.5 d_b \right) \tag{12}$$

The k_{ev} rate of contraction of the jet exhaust is calculated from a relationship F(R_e, R_h, R_a, T_a, p_{mas}, p_{atm}) [3].

If $F_{mas}(t)$ decreases continuously, so in drying processes, change $dm_a(t)/dt$ will be negative; over time, the gas is discharged outside for reaching a value $p_{mas}(t)$ with which is balanced $F_{mas}(t)$.

Under these conditions, mass balance for air in the enclosure is:

$$\frac{dm_a(t)}{dt} = D_{mi}(t) - D_{mev}(t) \tag{13}$$

It was made a model and a simulation program of this type of transducer operation in MEDSIMFP.10 simulation environment. Figure 2 presents simulated experiment result of transducer operation with a simulation of decreasing variation of the mass measured in drying processes.

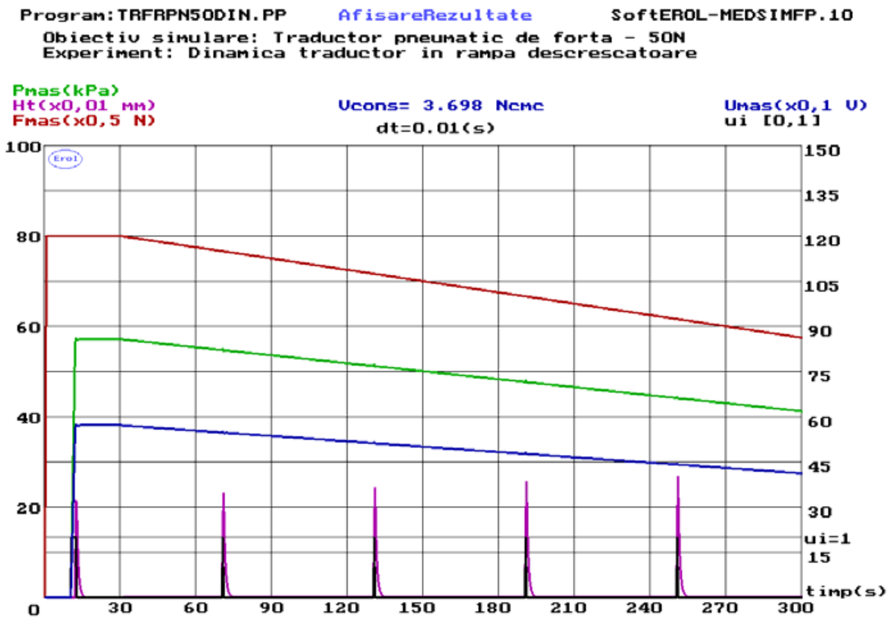

Fig. 2. Experiment simulation for decreasing measurement of force $dF_{mas}(t)/dt < 0$

It finds a good measurement accuracy achieved with a very low consume of compressed gas and electric energy used to action the distributor with a relatively large sampling period - of 60 s.

If the procedure for measuring the relative variation of ceramic body weight is used, according to the equation (3), structure of pneumatic transducer can be simplified requiring a single load cell.

3. Conclusions

It examines the use to measure the speed of drying ceramic body in an environment of relatively high temperature 150 - 180 °C. of pneumatic transducers that can achieve accurate measurements, simple constructive and much cheaper than similar electronic versions.

Combined transducer – pneumatic and electronic - uses the principle of balance of forces, conducted by varying of air pressure, pressure is not influenced by external environmental temperature variation, so it works precise and transitory. Electronic parts work with high precisions in a environment with low temperature .

Due to the measuring principle applied forces of decreasing continuously analyzed pneumatic transducer has a very low energy consumption, a high safety in operation and low cost.

REFERENCES

[1].Berling B., Heinrich B., Thrun W., Vogt W., *Kaspers/Küfner Messen- Steuern- Regeln: Elemente der Automatisierungstechnik*, Springer DE, 2005

[2].Courtois F., *Automatic control of drying processes*, 1996, Automatic Control of Drying Processes, in Computerized Control Systems, Mittal ed., pp 295-316

[3].Dimitriev V.N., Gradeţkii B.G., *Osnovâ pnevmoavtomatiki*, Maşinostroienie, Moskva, 1973

[4].Feidt Michel Louis, *TERMODINAMICA şi optimizarea energetică a sistemelor şi proceselor*, Editura BREN, Bucureşti, 2001

[5].Hitoshi Takeda, and all., *Low Cost Intelligent Automation: Produktivitätsvorteile durch Einfachautomatisierung*, Landsberg am Lech : Mi-Fachverl. Redline, 2006

[6].Murad E., *Măsurarea parametrilor procesului de uscare a produselor ceramice cu traductoare pneumatice neconvenţionale*, Simpozion HERVEX 2007, Călimăneşti, 14-16 noiembrie, 2007

[7].Murad E., Maican E., Marin A., Dumitrescu C., *Dinamica traductoarelor pneumatice cu consum redus de energie pentru măsurarea forţelor în procese lente*, Simpozion HERVEX 2009, Călimăneşti, 18-20 noiembrie 2009

[8].Murad E., Dumitrescu C., Haraga G., Dumitrescu L., *Force pneumatic transducers with low energy consumption in stochastic measurement operations,* Simpozion HERVEX 2010, Călimăneşti, 10-12 noiembrie 2010

[9].Murad E., Sima C., Haraga G., Safta V.V., *Reduction of final humidity dispersion of bodies in convective drying process*, The 4th International Conference on Advanced Concepts on Mechanical Engineering, Iaşi, 17-18 June 2010

[10]. Murad Erol, Vintila Marian, Craciunescu Aurelian, *Uscătoare cu impact ecologic redus pentru zone montane* Sesiunea de comunicări ştiinţifice ICEDIMPH-HORTING, 20 septembrie 2012

[11]. Murad E., Dumitrescu C., Haraga G., Dumitrescu L., HIDRAULICA, nr.1, 2013, pag. 65-62

ISSN 1454 - 8003
Proceedings of 2014 International Conference of Hydraulics and Pneumatics - HERVEX
November 5 – 7, Calimanesti-Caciulata, Romania

SMART FLUIDS FOR SMART FURNITURE

Daniel BANYAI[1], Adriana BANYAI[2], Bela ZALANYI[3], Razvan CURTA[4], Lucian MARCU[5]

[1] Technical University of Cluj-Napoca, daniel.banyai@termo.utcluj.ro

[2] S.C. Smart Furniture S.R.L. Cluj-Napoca

[3] S.C. Smart Furniture S.R.L. Cluj-Napoca

[4] Technical University of Cluj-Napoca

[5] Technical University of Cluj-Napoca

Abstract: *New product development, in any domain, aims to introduce controllable, reconfigurable or multi-functional elements, so that the product can be named "smart". The paper contains an overview of hydraulic elements used inthe furniture manufacturing industry. In this paper are noted the possibilities of using smart fluids (electro and magneto rheological) to achieve shock absorbers for smart furniture, also some technical solutions are illustrated.*

Keywords*: Smart Furniture, Smart Fluid, Shock absorbers, hydraulic elements.*

1. Introduction

Starting from the second half of the last century the hydraulic actuation had an exponential evolution due to their specific advantages, among which the most important is the density of force which reaches 500 bar (in comparison with electrical actuators where the equivalent corresponds to 0.5 ÷ 4 bar), due to the high static pressure. Making a comparison between the hydraulic and electric actuators, the hydraulic ones have a moment of inertia 72 times greater, they weigh 14 times less and they are 26 times smaller, than a corresponding electrical one. [2]

Nowadays, on worldwide level, there are three main concurrent markets for innovative hydraulic products:

- in U.S.A., with an annual turnover of $5.9 \cdot 10^9$ \$, the value of imports exceed the exports;

- in Europe, (Germany having a higher share) with an annual turnover of $3\text{-}4 \cdot 10^9$ Euro and with higher exports;

- in Japan, with an annual turnover of $2 \cdot 10^9$ \$ and with exports eight times larger than imports.

In Germany, in the hydraulic industry there are around 23.000 people employed, in approximately 140 companies (with an average of 160 people / company). [1], [2], [4]

It is well known that the hydro-pneumatic elements increasingly find their application in smart furniture.

A possible definition for smart furniture might be: furniture that uses surrounding environment information to provide functionality and comfort to its users. Other approaches might refer to it as: furniture that provides integrated functionality or furniture that has at least a whole second purpose. Some define it as: furniture that uses smart materials or furniture that integrates latest IT technology to provide remote access to different home devices. [3]

In [3] the authors propose a statement which summarizes all the above: Smart furniture is the furniture which brings added value, functionality, comfort and elegance to fit every personalized requirement issued by the user.

In the furniture sector, the hydro-pneumatic elements are used for: Gas/Oil springs - applied to offset weight or to support the activation of moving components (pushing, lifting, lowering, pulling and positioning) in a controlled manner; Locking springs - provide ergonomics and comfort, are used for the convenient and safe adjustment of sitting and lying positions; Dampers or shock absorbers; Table and Chair lift systems. In the past period designers were using fluid power for urban furniture (See Figure 1).

Figure 1 Hydraulic custom urban bench [8]

2. Smart Fluids

Considering that smart furniture should include smart components, in the following are described the smart fluids that could be used in the furniture industry.

Each individual type of smart material has a different property, which can be significantly altered, such as viscosity, volume or conductivity. The property that can be altered determines what type of application the smart material is used for. [6]

Fluids with controllable properties are also assigned to smart materials. These fluids respond to an applied electric or magnetic field with a change of their rheological behaviour. There are two main classes of smart fluids: electro rheological (ER) and magneto rheological (MR). ER fluids generally consist of semi-conducting particles suspended in dielectric oil, whereas MR fluids use magnetiseable particles suspended in a non-magnetisable carrier liquid. In both cases the flow mechanism is the same: excitation of the fluid by the appropriate field (electric or magnetic, respectively) causes polarization and subsequent alignment of the particles suspended within the liquid. The resulting chain structure is held in place by the applied field, and hence it resists fluid flow. The resulting behavior is analogous to the class of fluids known as Bingham plastics – non-Newtonian fluids capable of developing a yield stress. For smart fluids, this yield stress is a function of the applied electric or magnetic field. However, once this yield stress is exceeded, the behaviour of the smart fluid deviates from that of a Bingham plastic. This is attributable to a breakdown of the chains of particles under the forces of the fluid flow, and results in a shear-stress / shear-rate characteristic that is highly non-linear. When used in a damping device, the result is a damper whose force/velocity characteristic is non-linear, but can be changed by way of the applied electric or magnetic field. [6], [2]

Electro rheological liquids have been discovered in 1949 by Winslow. These liquids are substances whose aggregation state can change in under a millionth of a second, under the influence of a high intensity electrical field. For hydraulic actuations this means a viscous variation controlled through an electrical field. This liquid consists of a dispersion of solid micro granules with good conductibility (polymer particles), immersed into a dielectric liquid, namely a synthetic oil, in which are added activators for amplifying the above mentioned effect. Thus, it results a substance, which, changes its state from liquid into a quasi-solid one. One of the companies that produce these liquids is the German company, Bayer. [2],

The electro-rheological effect can be used to control the pressure or flow using special command resistances. The relation characterizes capillary resistances, resembling a laminar split:

$$\Delta p = \frac{12 \cdot \eta \cdot l \cdot Q}{b \cdot h^2},$$

Where: l, b, h are the length, width and height of the split;

Δp pressure difference on the resistance;

Q is the flow

η dynamic viscousity.

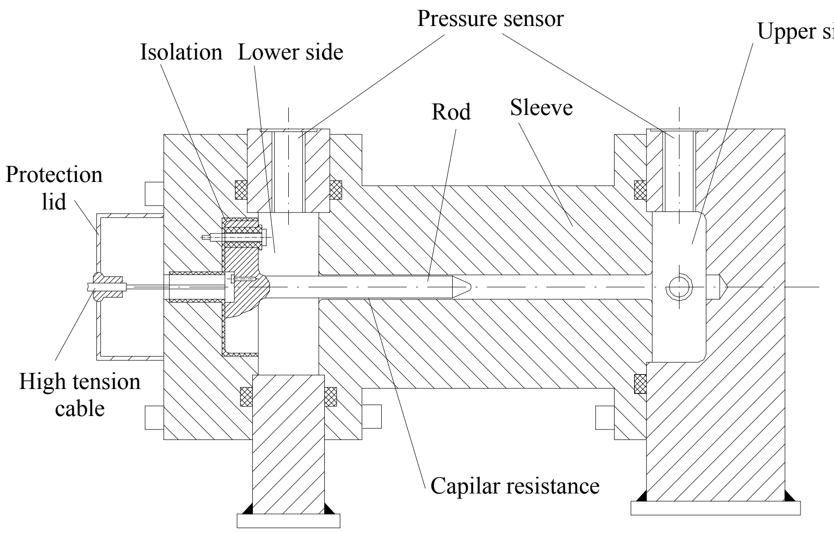

Figure 2 Electro-rheological command resistance

By applying an electrical field, it generates an increase in the shear stress of the liquid layers, thus in the pressure difference.

The electric field, is obtained from a stabilized source of continuous current, whose power field is limited by a maximum voltage of 6.5 kV and a maximum current of 5 mA. [2]

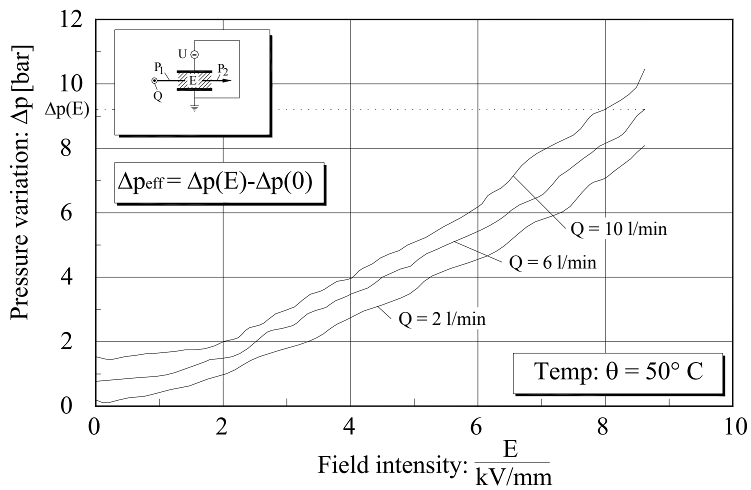

Figure 3 The variation of Δp with the intensity of the field

In 1948 Rabinow invented Magneto-rheological fluid and developed an application device (a clutch). In the following few years more patents and publications related to MR fluids appeared. Classical MR fluids are non-colloidal suspensions of magnetisable particles, having a size of the order of a few microns, in liquids of low permeability.

The main advantages of MR fluids are a yield strength of up to 50–100 kPa, which is one order of magnitude higher than ER fluids, insensitivity to contaminants, using 12–24 V low voltage, relatively broad working temperature range (40 °C to 150 °C). Since the early 1990s there has been a resurgence of interest in MR fluids. In recent years, MR fluid devices have been applied commercially to engineering fields.

The characteristic of MR fluids is the dependence of viscosity of the fluid on the strength of the magnetic field. The change of viscosity proportional to the magnetic field strength is reversible, moreover, it runs within a very short time, a few milliseconds. MR fluid may be changed from liquid state to almost solid and then back to the initial state. Therefore MR fluids are widely used in various types of devices, operating based on hydrodynamics principles. [6], [7]

3. MR fluid dampers

The main parameter of the classical damper is its resisting force. It depends on the dimensions of the cylinder and piston, piston speed, bypass channel dimensions and hydraulic fluid viscosity. When the working fluid in the cylinder is the MR fluid, its viscosity depends on the strength of magnetic field, in which the cylinder is placed. By varying this parameter the resistance force of the cylinder may be controlled [5], [7].

The linear MR fluid damper made by Lord Corporation (Cary, North Carolina), using the single-ended piston-rod structure can be seen in Figure 4, [6]. The damper is 41 mm in diameter, has a 179 mm eye-to-eye length at mid-stroke and has a 29 mm stroke [6]. Current is carried to an electromagnetic coil via the leads through the hollow shaft. An input power of 5 W is required to operate the damper at its nominal design current of 1 A.

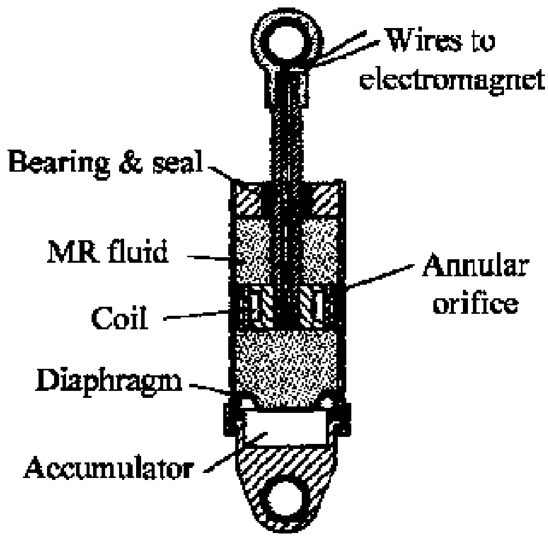

Figure 4 MR fluid damper

In addition to the damper presented above, Carlson et al. [5] and Jolly and Chrzan [6] have applied for patents, for many MR fluid dampers with complicated structures, which can be used in various applications.

The authors propose a shock absorber for furniture elements described in Figure 5.

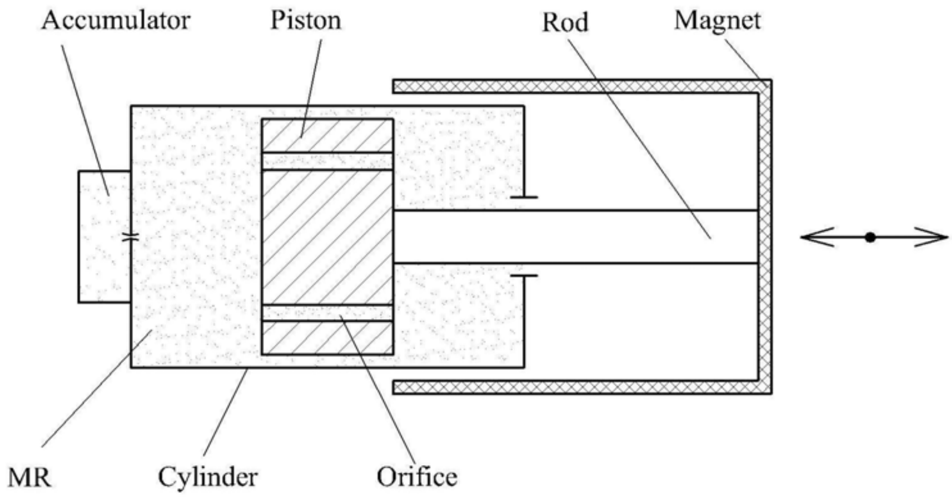

Figure 5 MR fluid damper for furniture parts

A rod-volume compensator (e.g. the accumulator in Fig. 4, 5) needs to be incorporated into the damper because the volume occupied by the piston rod varies when the rod moves. The damper is capable of providing a wide dynamic range of force control for very modest input power levels.

4. Outlook

The key for MR fluid technology is to prepare high-performance MR fluids. This opens new possibilities to design MR fluid devices in as many applications, as dampers are used in smart furniture parts, controlling the force using an electromagnet with low power.

There are some problems that should be noted when working with MR fluid devices in mechanical engineering. The first problem when applying MR fluid devices is the settling stability. The heavy particles in an MR fluid are easy to settle down without suitable additives. The second problem is the durability of the devices, because the MR fluid is abrasive, finally, the third problem is the relative cost of an MR fluid device compared with conventional passive devices.

The research and development of MR fluids and their application devices are increasing. The published literature on MR fluids is increasing gradually, thus MR fluids and their applications have been shown extensive interest by researchers.

ACKNOWLEDGEMENT AND DISCLAIMER

This paper has benefited from the support of the project “Research for the development and implementation into production of innovative furniture”, contract no. 12 P01 001 13 C3, beneficiary Smart Furniture SRL Cluj-Napoca, partner Technical University of Cluj-Napoca. The project is part of the Competitiveness Pole 12 P01 001 “Transylvanian Furniture Cluster” financed through the Sectorial Operational Program “Increase of Economic Competitiveness 2007-2013” by the European Regional Development Fund.

This publication reflects the views only of the authors, and the Commission cannot be held responsible for any use which may be made of the information contained therein.

REFERENCES

[1] A. Plummer "Fluid Power Transmission and Motion Control: Research and Future Trends", Fluid Power Society of India Magazine, vol. 40, no. 2, 2013.
[2] D. Banyai, L. Vaida, L. Năşcuţiu, D. Opruţa, C. Giurgea, L. Marcu, "Synoptic view of the latest trends in hydraulic actuation", Buletinul Institutului Politehnic din Iași, Tom. LVI (LX), Fasc.1, Secția Construcţii de Maşini, pag.148-155, ISSN 1011-2855, 2010.
[3] C. Vaida, B. Gherman, M. Dragomir, O. Iamandi, D. Banyai, "Smart Furniture – Quo Vadis", International Conference on Production Research – Africa, Europe and Middle East; 3rd International Conference on Quality and Innovation in Engineering and Management, 2014.
[4] E. Dragašius, V. Grigas, D. Mažeika, A. Šulginas "Evaluation of the resistance force of magnetorheological fluid damper", Journal of Vibroengineering, Vol 14, no. 1, ISSN 1392-8716, 2012.
[5] J. D. Carlson "Magnetorheological fluid actuators in adaptronics and smart structures", Ed. H. Janocha, Springer-Verlag, Berlin, 1999.
[6] J. Wang, G. Meng " Magnetorheological fluid devices: principles, characteristics and applications in mechanical engineering", Proceedings of the Institution of Mechanical Engineers, Part L: Journal of Materials, Design and Applications, vol. 215, no. 3, pg. 165-174, 2001.
[7] X. Zhu, X. Jing, L. Cheng " Magnetorheological fluid dampers: A review on structure design and analysis", Journal of Intelligent Material Systems and Structures, vol. 23, no. 8, 2012.
[8] www.dornob.com

ISSN 1454 - 8003
Proceedings of 2014 International Conference of Hydraulics and Pneumatics - HERVEX
November 5 – 7, Calimanesti-Caciulata, Romania

FACILITY WITH ENERGY INDEPENDENCE FOR RENATURATION OF LAKES

Gabriela MATACHE[1], Catalin DUMITRESCU[1], Ionel NITA[1]

[1] INOE 2000-IHP, e-mail address: fluidas@fluidas.ro

Abstract: *This article makes an analysis of the criteria for the use of photovoltaic panels produced by different companies in the Solarbee technique for renaturation of lakes. INOE 2000-IHP Bucharest aimed to gather and systematize such data in order to establish a uniform methodology for choosing photovoltaic panels with the new proposed (pneumatic) technology for de-eutrophication of lakes. Depending on the success of this research it is intended the establishment of international collaborations in order to develop renaturation facilities (de-eutrophication stations) based on the new pneumatic technology. INOE 2000-IHP has many achievements in the field of environmental equipment, bio-technology and energy recovery systems, has a specialized laboratory for that, with proper equipment for water quality analysis and monitoring.*
Keywords*: photovoltaic panels, de-eutrophication, environment*

1. Introduction

Eutrophication is the enrichment of standing or running water with nutrients, leading to algal blooms, excessive growth of aquatic macrophytes, high turbidity, oxygen deficiency in bottom waters of the lake bottom, and in some cases a disagreeable odor and taste. Eutrophication is caused in 90% by natural causes (temperature, light). The effects of eutrophication are: a) thermal stratification due to the lack of mixing between the surface and deep layers of the river [1]. The Solarbee technology [8] eliminates this effect by mixing water between the two layers (the hydraulic method); b) plants covering the water surface (due to lack of light there is caused a decrease in oxygen in the water). By pneumatic technology (injection of pressurized air) there is increased oxygen intake causing disappearance of extra algal vegetation. The (pilot) station for renaturation proposed by IHP uses a pneumatic (not electrical) tracker, and provides treatment for eutrophic lakes with a concentration of 5-10 mg/l of algal mass (70% of all lakes in Romania).
SolarBee stations are all independent in terms of energy, they all using solar panels. Our research starts from the peculiarities of using PV panels in pneumatic drive of the tracker installed on floating station, control electronics under conditions of the station swinging on the water, automation of panels with power distribution to the consumers.
Concrete issues that are subject of the research refer to a) study of orientation behavior of PV panels (fixed - with zero degree of freedom; under conditions of swinging on the water – with two degrees of freedom); b) solving their orientation (equatorial, azimuthal or pseudo-equatorial) by automating the pneumatics; c)- maximizing the received solar radiation by using CPV receptors in mono and biaxial orientation systems.

2. Scientific issues that will be approached

In terms of science there is intended a research activity to determine the mathematical correlation between useful photovoltaic power (N_{PV}) and power requirements of pneumatic plant (N_p)[2], at PV panels, to ensure oxygenation of pelagium, up to maximum 0.75 m, ie :

$$\min N_{PV} > N_p$$

Using these measurements there will be possible to extrapolate the results by simulation for 3 new renaturation station sizes (small, medium, large) with dimensions up to 3 times higher than the pilot station proposed by IHP.
Other scientific aspects are related to:

a) Sizing the underwater air injection system;

b) Achieving control ranges for pneumatic flow and pressure, ranges used for levels 3 and 4 of eutrophic water concentration;

c) Mathematical correlations, one of which is the correlation between the speed of de-eutrophication of pelagium (δΔ) and pneumatic parameters pressure (p), flow (Q) of compressed air.

Technical presentation of the pilot station:

a) Structurally, the new pilot station (Figure 1) has as reference model the latest Home version of the Solarbee station [6] developed in 2012 and considered the most efficient in terms of technology and energy.
b) Functionally, it must be within the following performance parameters (the PV parts): useful powers 350-800W (1.2 to 1.6 times higher than at the Solarbee using the hydraulic method) of which 70% distributed in the air injection system, the rest of them in automation; current generated by the station - 24Vdc (similar to the version station - Aerator or the version Home Moderaco [7])
c) Structural diagram of the station (Figure 1) includes the following parts: floating cushion limiting PV panels swing to maximum 5^0; 4 bar pneumatic aerator; 1 panel with 2 degrees of freedom for the pilot station (3 panels arranged equilaterally with 1 degree of freedom for large stations); the pneumatic actuation system; two electronic automation systems (panels and pneumatics).

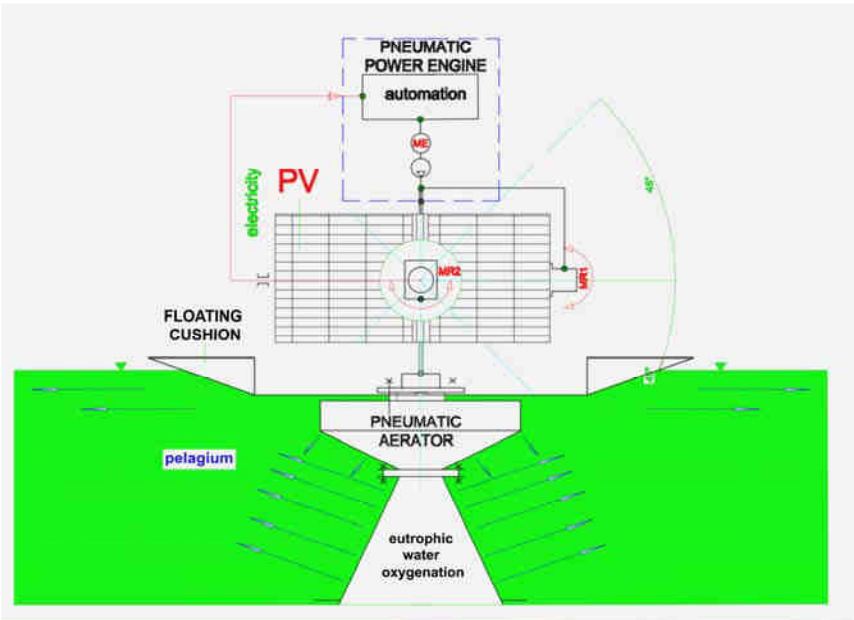

Fig. 1

3. Comparative analysis of the state of the art

Internationally, among the prestigious companies that deal with research and development of PV panels for water renaturation stations we mention: Solarbee.Co- USA- the company that has developed the first technology and equipment for renaturation using only renewable energy; Medoraco- USA – no 1 worldwide in the development of Solarbee type stations. It manufactures and sells whatever is the latest in renaturation equipment [7]; Other companies producing Solarbee equipment: Elsaco- USA [7]; Novasys.Co- Australia [8]; Nanotech- South Africa; Water and Wastewater- Canada.

The model of voltaic PV panel that will be driven by the pneumatic tracker of the SolarBee station

a)- Requirements for use imposed on PV panels used in the version with pneumatic tracker

- Panels to be medium or large size as to the work surface;
- In the latter case there should be eliminated the larger possibilities for shading which they can generate to each other through their proximity, compared to the small area panels;
- They should offer possibility to be adjusted to the zero position relative to an horizontal flat ground;
- In conditions of their swinging on the water the PV panels should have possibilities for orientation relative to the zero position adjusted to maximize the reception of solar radiation;
- transparent protection against radiation and bad weather (rain, wind);
- robust electrical connections;
- protection of solar rigid cells from mechanical actions;
- protection of solar cells and electrical connections from moisture;
- ensuring proper cooling of solar cells;
- contact protection of the electrically conductive components;
- possibility for easy handling and mounting.

b)- Constructive requirements imposed on PV panels used on the renaturation station

Of the many constructive variants of solar panels for our research we chose the following type of panel with the next features:

- It has a toughened glass one layer protection on the side exposed to the sun;
- It is covered by a transparent plastic layer (ethylene vinyl acetate, EVA or silicone rubber) into which solar cells are placed tightly;
- Solar cells can be monocrystalline or polycrystalline, connected by strips of tin;
- Lining the rear face of the panel is made with a plastic laminated foil weather resistant, polyvinylidene fluoride (Tedlar) and Polyester;
- Connection socket is equipped with protection diode respectively by-pass diode;
- The panel is reinforced with aluminum profile frame to protect the glass during transport, handling and installation, for fixing and hardening the connection.

c)- Energy efficiency requirements imposed on PV panels used on the renaturation station

The parameters of this solar panel have been established based on the ones of solar cells, in standard working conditions. Its electrical characteristics (calculated before the acquisition of it) are:

- Idle voltage UOC
- Flask current ISC
- Voltage in optimal operating point UMPP
- Current in maximum power point IMPP
- Maximum power PMPP
- Space factor FF
- Coefficient of power amending to cell temperature
- Solar cell efficiency η

Sustainable encapsulation of components is very important because moisture that might penetrate would affect the lifespan of the solar panel by corrosion and by short-circuiting connections between the elements through which electric current passes.

ISSN 1454 - 8003
Proceedings of 2014 International Conference of Hydraulics and Pneumatics - HERVEX
November 5 – 7, Calimanesti-Caciulata, Romania

d- Schematic diagram of the proposed orientation system

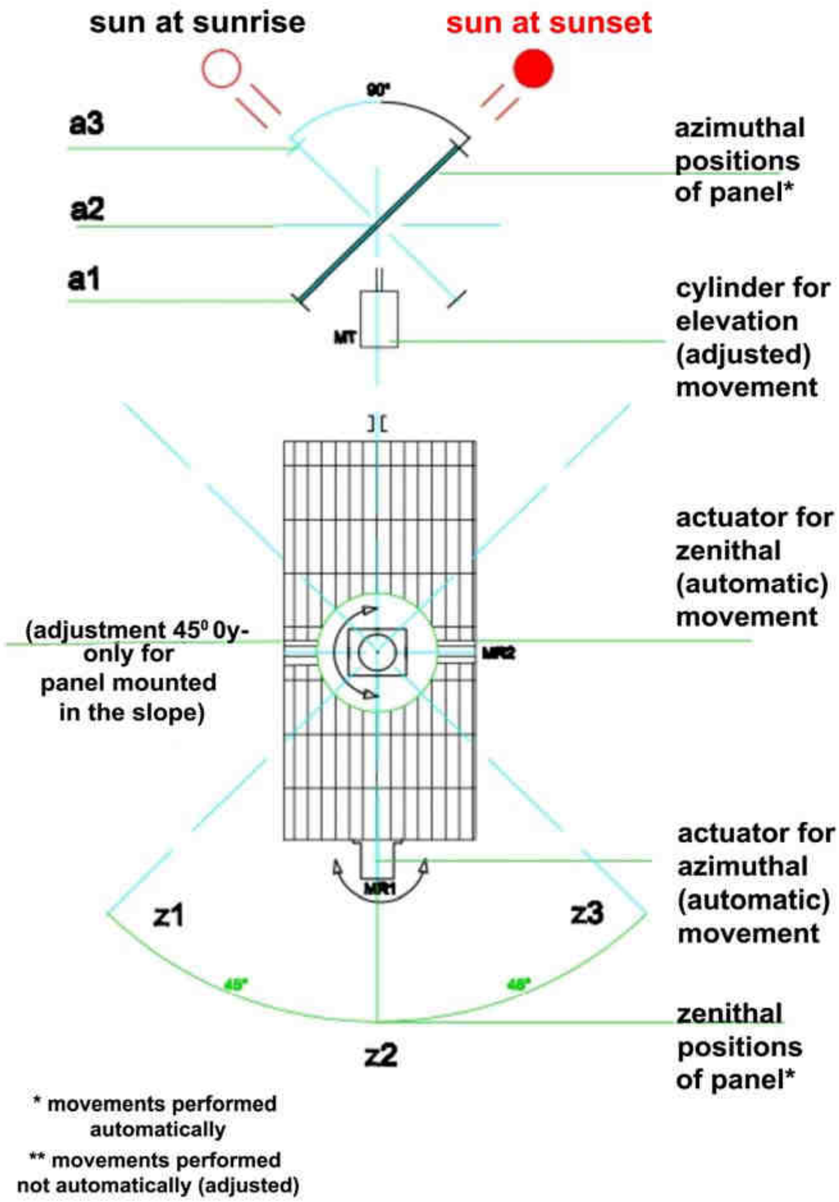

Fig.2

4. Automation diagram proposed for the photovoltaic panel

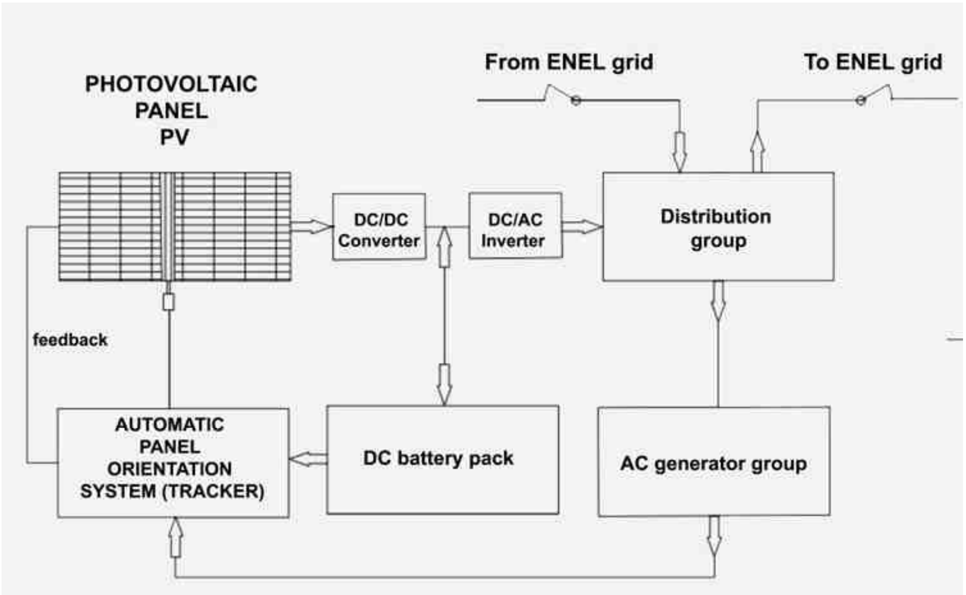

Fig.3 Automation block diagram of PV panel

- Block structure of the panel automation system (equipment for photovoltaic signal acquisition - processing and energy conversion- storage)
Automation diagram of photovoltaic panel is main control support for automation system of the tracker, being composed of the following component parts:
a)- The main automation components of the photovoltaic panel are represented by:
- bicellular solar concentrator of the type below (Figure 4 a)

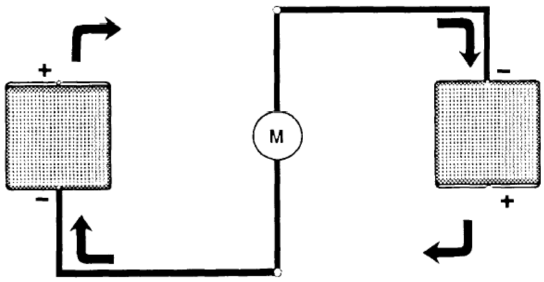

Fig.4 a

- control electronics corresponding to the two position transducers (solar receiving cells), represented in the diagram in Figure 4 b[10]:

Efficiency requirements in functioning of PV panels used in the model of the proposed orientation solution. The idle diode (Bypass). Its role (Figure 4b)
When connecting several modules in series (maximum 3 in our case), it is necessary to mount a diode antiparallel to each panel.[9] Maximum current and breakdown voltage of the diode must be at least equal to the current and voltage of the panel. There can be used recovery diodes of 3 Amp / 100 Volt. Idle diode is connected to the output terminals of each panel so that in normal operation mode (the panel debiting current) it has at its terminals reverse voltage (cathode of the diode connected to the positive pole of the panel). Should the panel be shaded or get damaged it would no longer debit current, voltage polarity at the terminals would change and it would be damaged, or the best case scenario efficiency of that chain of modules would drop. This is prevented by the bypass diode which takes over power in this case.

ISSN 1454 - 8003
Proceedings of 2014 International Conference of Hydraulics and Pneumatics - HERVEX
November 5 – 7, Calimanesti-Caciulata, Romania

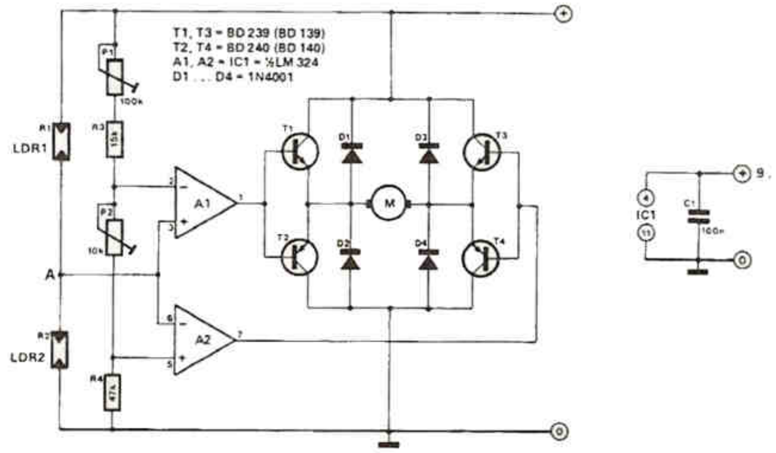

Fig.4 b

b)- Photovoltaic converter
c)- Battery pack
d)- Distribution group

5. Description of principle of operation of the automation system of PV panel

a)- Solar concentrator bicellular type takes over the photon radiation of sunlight and emits a signal for panel positioning, as follows [11]:
- When both cells of the concentrator are equally illuminated (sun rays fall perpendicularly on the concentrator) it results that PV panel is facing correctly, and the electronic system gives a signal confirming this;
- When cells are illuminated unequally (sun rays do not fall perpendicularly on the concentrator), its electronic system will emit the ordering for panel rotation around Oz or Ox (depending on the indications of the solar electronic clock within the automation system) until both cells of the concentrator are equally illuminated again.

In both cases signals from the electronics of the concentrator address work orderings for both proportional distributors and rotational actuators.
b)- Photovoltaic converter - Takes over and converts signals of photovoltaic concentrator into direct current sending it to the battery pack;
c)- Battery pack - stores the new energy and delivers it to the system either to be used as a source of 24Vdc electric commands for the tracker, or to be converted into alternating current through the circuits of the automation system towards the DC / AC inverter in order to be used - in our case – for actuation of the group generating compressed air (Fig.5) .
d)- Via the distribution group the alternating current is routed in two directions:
- for use in internal network of the panels
- to be delivered in the public grid.

When it is delivered to internal use part of the energy converted into alternating current serves for driving the compressed air generator which the pneumatic tracker is actuated by.
When actuating hydraulic or pneumatic trackers, the entire automation system is recommended to be connected to the public grid, as the regenerative energy which is to be used to drive the proportional devices might not fully meet the strict requirements for frequency required for their operation, case in which the systems witches to the public grid.

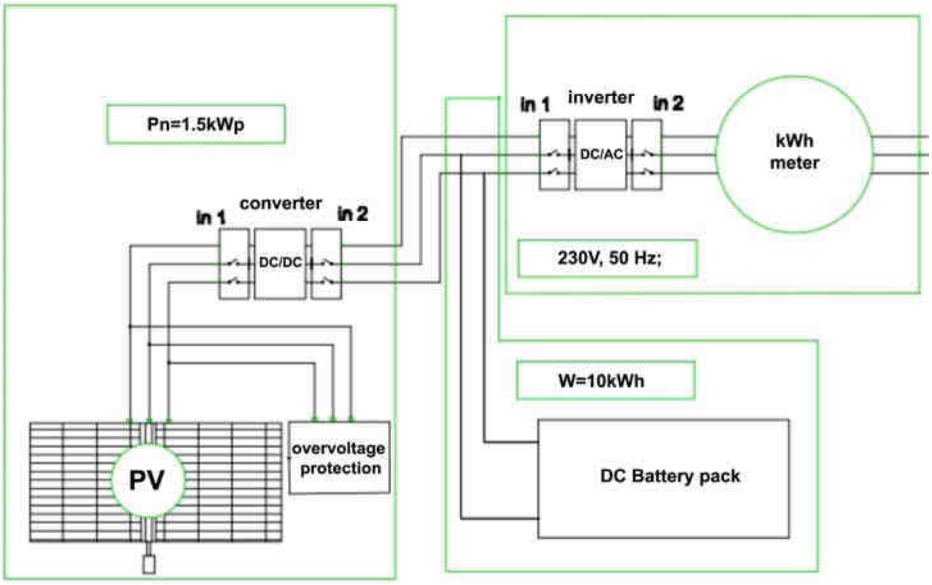

Fig.5

Automation diagram proposed for the orientation system of PV panel (of pneumatic tracker)
Automation diagram of the tracker consists of the following functional blocks:
-The signal processing and amplification system (PID type)
-Electronic block for control-adjustment of proportional distributors D1 and D2 (the controller). Transducers of the block are represented by the (linear) position sensors that equip the distributors used in the diagram.
-The system for conversion and amplification of signals for actuators MR1 and MR2;
- Electronic block for control-adjustment of rotary actuators. Transducers of the block are represented by the (angular) position sensors that equip the rotary actuators used in the diagram.

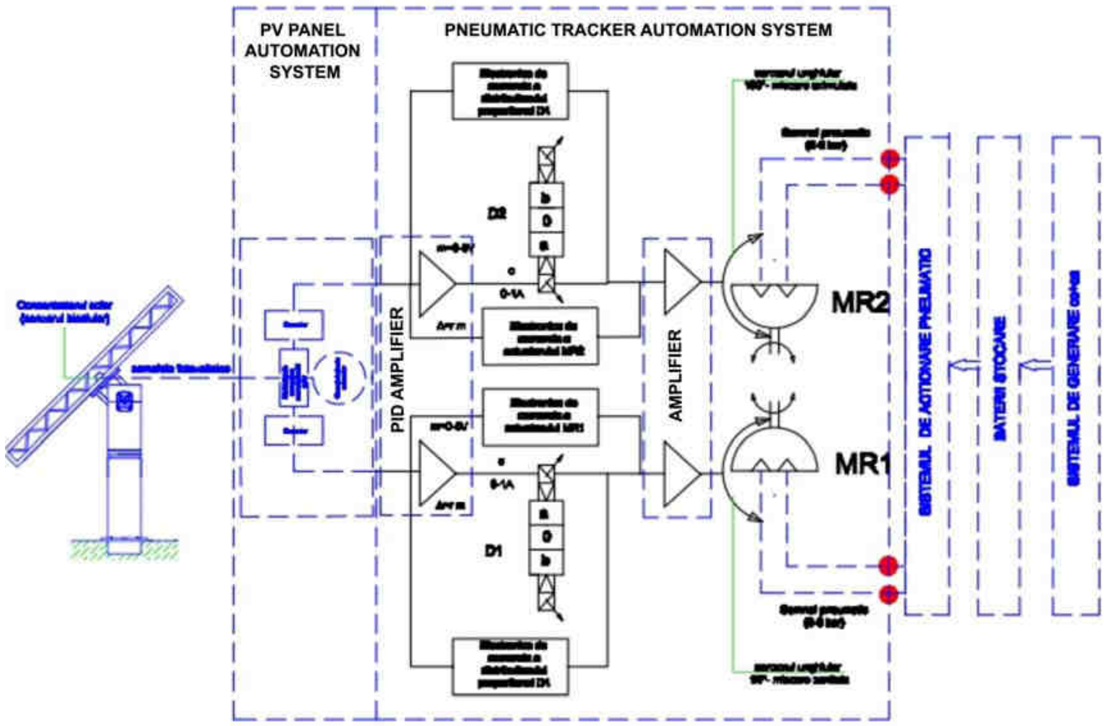

Fig.6 Automation block diagram of the pneumatic tracker

6. Conclusions

This article highlights the following:
a) - The proposed pilot station maintains constructive structure of a classical station, differences are only in terms of actuation.
b) -As to the photovoltaic panels, there is used a new architecture – that this article describes structurally;
c) - Using the pneumatic tracker increases the solar capture power of the panels compensating its large gauge;
d) - As to the air injection system (the proposed pneumatic solution), this one reduces energy requirements.

REFERENCES

[1]. The Romanian Academy - National Institute of Biology, V. Zinevici, L. Parpală – The fito-and zooplankton structure and productivity in lacustrine ecosystems, 2006
[2] Belforte, Bertetto, Mazza: “Pneumatico - corso completo”, Publisher Techniche nueve, Milan, 2004
[3] Dzitac, Manolescu- “Controlers for Pneumatics Actuators” – vol. II- Publisher University of Oradea, 2006
[4] G. Matache, I. Nita - Compressed air at medium and high pressure used in pneumatic automations at maximum pressure - Mecatronica Review No. 2/2011 (en)
[5] www.clearwasterwater.com
[6] www.lakes.moderaco.com/equipament
[7] www.moderaco.com
[8] www.novosys.com.au/solarbee;
[9] D. Diaconescu, I. Visa, M. Vatasescu, I. Hermenean, R. Saulescu: *Synthesis of a bi-axial tracking spatial linkage with a single actuator*. Proceedings of SYROM 2009, The 10th IFToMM International Symposium on Science of Mechanisms and Machines, Springer, 2009, ISBN: 978-90-481-3521-9;
[10] I. Hermenean, I. Visa, A. Duta, D. Diaconescu: *Modeling and Optimization of a Concentrated Hybrid Photovoltaic System with Pseudo- Equatorial Tracking* in: CD Proceedings EVER 10 (Ecologic Vehicles • Renewable Energies), March 2010;
[11] I. Hermenean, I. Visa, D. Diaconescu, N. Creanga: *Kinematic Synthesis of a 3RP Linkage for the Optimal Orientation of a Photovoltaic Platform,* IFToMM World Congress 2011 Proceedings, Guanajuato, Mexico.

ISSN 1454 - 8003
Proceedings of 2014 International Conference of Hydraulics and Pneumatics - HERVEX
November 5 – 7, Calimanesti-Caciulata, Romania

TILLER HYDROSTATIC TRANSMISSION

Gheorghe IVAN[1], Radu CIUPERCA[1], Ioan GANEA[1]

[1] INMA Bucharest, geoivan2006@yahoo.com

Abstract: *The article relates to a hydrostatic transmission intended for the tillers equipped with internal combustion engines for continuous transmission of motion and power of the drive wheels or to a device for digging soil. The state of the art transmission tillers operated internal combustion engines using classical scheme consists of clutch, gearbox, control systems thereof etc. Chaining these elements presents disadvantages, on the one hand because they are complicated, bulky and heavy, requires a large number of control systems for drive and on the other hand that the transmission of the movement is done in steps. The hydrostatic transmission we propose simplifies construction of tillers and control systems for its operation and will mount easily on the transmission instead of classical combustion engine. This transmission is made up of a variable displacement hydraulic pump which is connected to the internal combustion engine, an orbital hydraulic motor to drive the wheels of the driving or digging the ground equipment, on which is mounted a framework for the internal combustion engine, hydraulic pump and motor hydraulic pipes connecting the hydraulic motor and hydraulic pump.*

Keywords*: tiller, hydrostatic transmission.*

1. Introduction

A tiller is a self-propelled vehicle, usually having two drive wheels, internal combustion engine through a gearbox and clutch, operated by a handlebar of a leader who walk. The engines full power more than 15 kW and are powered by gasoline or diesel. The moving of tiller has different speeds, forward or backward, gears and moving purposes are changed using control systems located on the handlebars.
The tillers are used in horticulture and gardening soil processing using specific equipment attachments (plough, milling unit, ridge plough, cultivator, digging canals for irrigation equipment, digging pits equipment, equipment for crown shaped shrubs and trees, irrigation pump etc.). Also, the some tillers can pull a trailer on two wheels, the driver sitting in a chair.
The tiller to replace the mechanical transmission with a hydrostatic transmission is type produced by S.C. RURIS.

2. Technical and functional characteristics of the tiller

Technical and functional characteristics of the tiller with mechanical transmission and hydrostatic transmission are presented in Table 1.

Technical and functional characteristics of the tiller

Table 1

Technical and functional characteristics	Values mechanical transmission	Values hydrostatic transmission
full power engine (net power)	5.5 kW (4.8 kW)	
maximum RPM engine	3600 rpm	
RPM drive wheels	40...125 rpm	
maximum resistant torque, m_{rmax}	30 daNm	
clutch	dry single disc clutch	-
gearbox	2 forward, 1back	-

Technical and functional characteristics	Values mechanical transmission	Values hydrostatic transmission
reducer		-
geometric volume hydraulic pump	-	7.08 cm^3/rot
theoretical flow of hydraulic pump	-	25,5 l/min to 3600 rpm
operating pressure	-	210 bar
geometric volume hydraulic motor	-	125.7 cm^3 / rot
oil flow of the hydraulic motor	-	5.6 ÷ 17.4 l / min
metal wheels diameter	400 mm	
weight	65 kg	42 kg

The mechanical transmission, consists of clutch, gearbox and reducer, is replaced with hydrostatic transmission, consists of variable displacement hydraulic pump which is connected to the internal combustion engine, an orbital hydraulic motor to drive the wheels of the driving or digging the ground equipment, on which is mounted a framework for the internal combustion engine, hydraulic pump and motor hydraulic pipes connecting the hydraulic motor and hydraulic pump. In Figure 1 is presented the tiller with mechanical transmission.

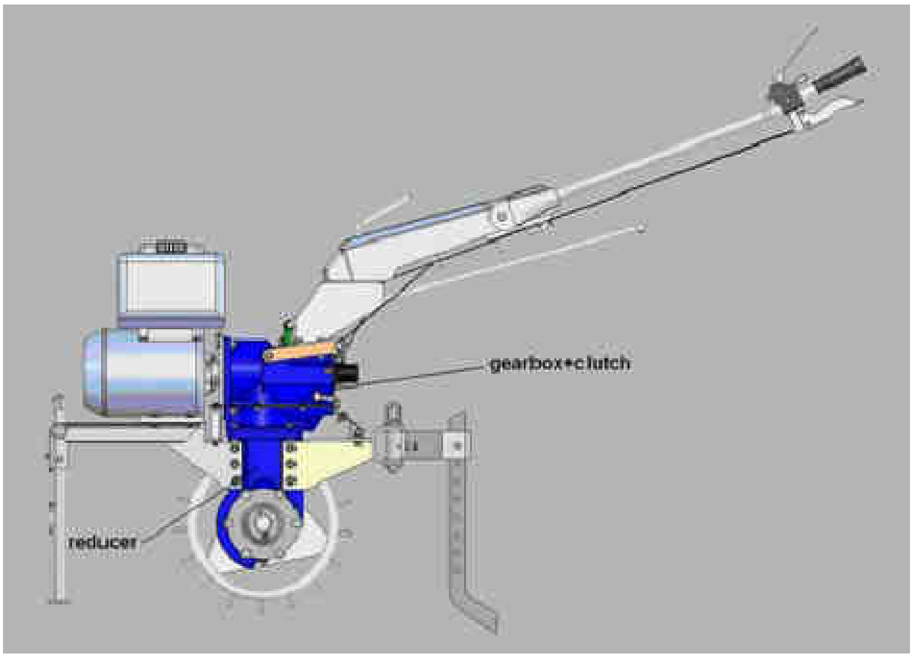

Fig.1 Tiller with mechanical transmission

3. Tiller with hydrostatic transmission

The tiller with hydrostatic transmission is mainly composed of an internal combustion engine, a flexible coupling, a variable hydraulic pump, two frames assembly, a hydraulic orbital motor with two axes, hoses and fittings and pump control system [Fig. 2].

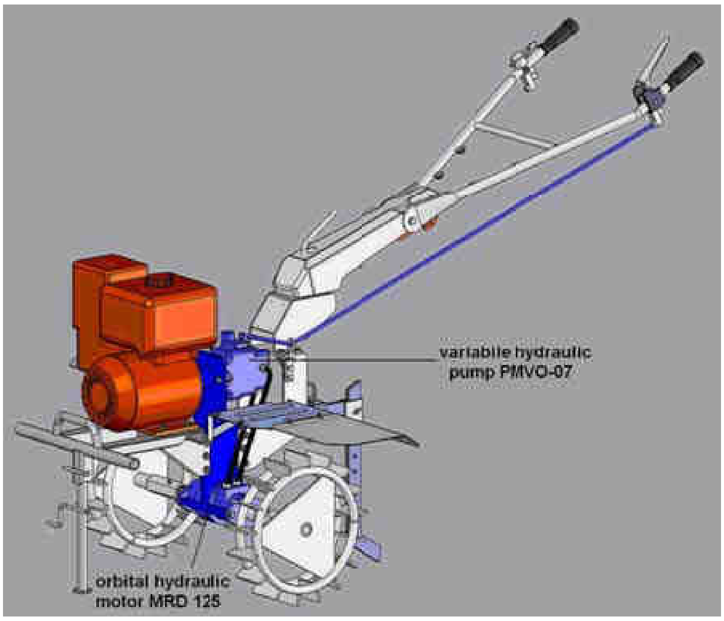

Fig.2 Tiller with hydrostatic transmission

4. Calculation of hydrostatic transmission

Internal combustion engine torque diagram is presented in Figure 3.

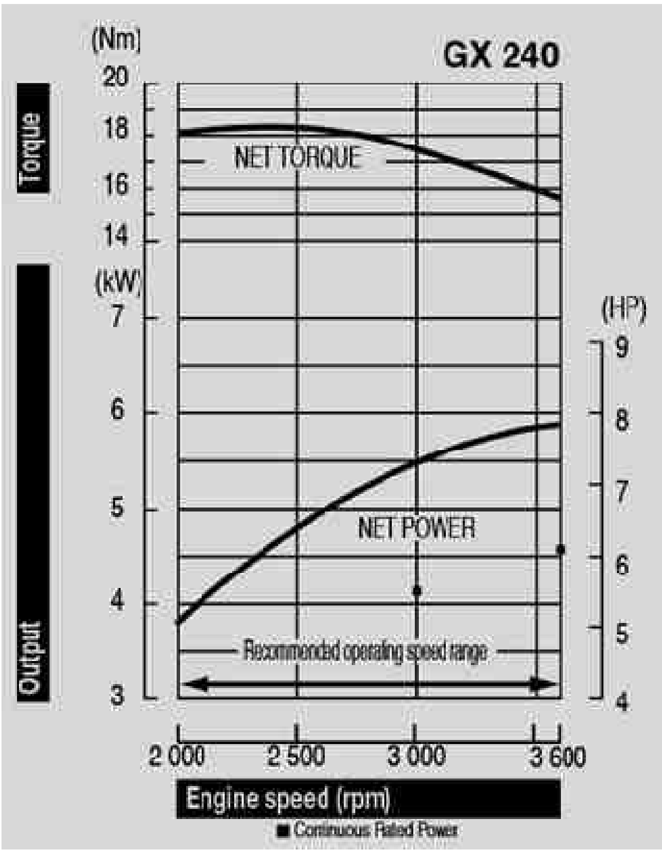

Fig.3 Internal combustion engine torque diagram

The tiller hydrostatic system will have variable flow hydraulic pump PMV0-07, driven by the combustion engine at speed of n_p = 3000 rpm and an orbital hydraulic motor with two-axis output MRB 125, to drive the wheels of the driving or digging the ground equipment.
Hydrostatic installation diagram is presented in Figure 4.

Fig.4 Hydrostatic installation diagram

The total efficiency of the hydraulic motor is calculated with relation 1 [1]:

$$\eta_{tm} = \eta_{vm}\ \eta_{mm} \tag{1}$$

where η_{tm} is total efficiency of the hydraulic motor;
η_{vm} – volumetric efficiency of the hydraulic motor, η_{vm}=0.9 ÷ 0.95; it is choose $\boldsymbol{\eta_{vm}}$**= 0.9;**
η_{mm} – mechanical efficiency of the hydraulic motor; $\boldsymbol{\eta_{mm}}$**= 0.9.**

Resulting: η_{tm} = 0.81…0.85. For the calculation it is chosen**:** $\boldsymbol{\eta_{tm}}$ **= 0.81.**

Geometrical calculation of the hydraulic motor is calculated with relation 2 [1]:

$$V_{gm} = \frac{2\pi\ M_{r\,max}}{(p_n - p_r)\,\eta_{mm}} 10^2 \tag{2}$$

where V_{gm} is geometric volume of the hydraulic motor, in cm^3/rot;
$M_{r\,max}$ - maximum resisting moment, $\boldsymbol{M_{r\,max}}$ **= 30 daNm;**
p_n – nominal pressure of the hydraulic motor, $\boldsymbol{p_n}$ **= 210 bar;**
p_r – the pressure in the return line; $\boldsymbol{p_r}$**=4÷5bar**;
η_{mm} - mechanical efficiency of the hydraulic motor, $\boldsymbol{\eta_{mm}}$**=0.9.**

Resulting: $\boldsymbol{V_{gm}}$ **=102.16** $\boldsymbol{cm^3}$**/rot.**

It is choose hydraulic motor **MRB 125** from Motors Catalog [2], with the following characteristics:
- geometric volume: 125.7 cm^3/rot;
- maximum speed: n_{max}= 475 rpm;
- maximum torque: M_{max} = 30 daNm;
- torque on the shaft A: M_A = 20 daNm;
- torque on the shaft B: M_B = 20 daNm;
- pressure drop: Δp = 175 bar;
- maximum flow: $Q_{m\,max}$ = 60 l/min.

The oil flow of the hydraulic motor is calculated with relation 3 [1]:

$$Q_m = \frac{V_{gm} n_{mh}}{\eta_{vm}} 10^{-3} \tag{3}$$

where Q_m is oil flow of hydraulic motor, in l/min;
n_{mh} - RPM motor hydraulic, $\mathbf{n_{mh} = 40 \div 125}$ **rpm**;
η_{vm} – volumetric efficiency of the hydraulic motor, $\boldsymbol{\eta_{vm}} = \mathbf{0.9}$**.**

Resulting: $\mathbf{Q_m = 5.6 \div 17.4}$ **l/min.**

Total efficiency of hydraulic pump is calculated with the relation 4 [1]:

$$\eta_{tp} = \eta_{vp}\ \eta_{mp} \tag{4}$$

where η_{tp} is total efficiency of the hydraulic pump;
η_{vp} – volumetric efficiency of hydraulic pump, η_{vm}=0.9÷0.95; it is choose $\boldsymbol{\eta_{vp}} = \mathbf{0.9}$**;**
η_{mp} – mecanichal efficiency of hydraulic pump; $\boldsymbol{\eta_{mp}} = \mathbf{0.9}$**.**

Resulting: η_{tp} = 0.81…0.85. For the calculation is chosen $\boldsymbol{\eta_{tp}} = \mathbf{0.81}$**.**

Geometric volume calculation of the hydraulic pump is calculated with the relation 5 [1].

$$V_{gp} = \frac{1000 Q_p}{n_p \eta_{vp}} \tag{5}$$

where V_{gp} is the geometric volume of the hydraulic pump, in cm^3/rot;
Q_p - assured flow of hydraulic pump $\mathbf{Q_p = Q_m = 17.4}$ **l/min.**
n_p – RPM driving pump, $\mathbf{n_p = 3000}$ **rpm;**
η_{vp} – volumetric efficiency of hydraulic pump, $\boldsymbol{\eta_{vp}} = \mathbf{0{,}9}$**.**

Resulting: $\mathbf{V_{gp} = 6.44\ cm^3}$**/rot**

Is chosen hydraulic pump **PMV0 - 07 C1 M 00 A0 00 R** from Poclain Hydraulic Catalog [3], with the following characteristics:

- geometric volume of the hydraulic pump: V_{gp} = 7.08 cm^3/rot;
- RPM driving: n_p = 700÷3600 rpm;
- theoretical flow: 25.5 l/min, to 3600 rpm;
- operating pressure: 210 bar;
- maximum pressure: 300 bar;
- inlet pressure: 0.8 bar;
- mounting flange: SAE A;
- setting: mechanical;
- weight:7.5 kg (for setting mechanical).

The calculation of necessary power the hydraulic pump is made with relation 6 [1]

$$P_p = \frac{Q_p\ p_{max}}{600\ \eta_{tp}} \tag{6}$$

Resulting: $\mathbf{P_P = 4.37}$ **kW**

The calculation of the torque consumed by the pump is made with relation 7:

$$M_p = 973,8\frac{P_p}{n_p} \tag{7}$$

where M_p is the consumed torque by the pump, in daNm.

Resulting: **M_p=1.42 daNm**.

5. Conclusions

Lately it tends to develop technical solutions to achieve tiller that allow much more control over it safely and effectively, given that it is run and handled directly by the operator. More specifically, it is the ability to control the speed, so the movement no load, but especially in the work, knowing that a tiller can work with a very wide range of equipment.
From this point of view it required a much wider range of gear adapted to the work carried out and the nature and state of the ground work, which is not possible with current versions of tillers, they generally having only two working speeds, seldom three. To meet these requests, otherwise justifiable, it was realized a tiller with hydrostatic transmission.
The hydrostatic transmission, with variable displacement hydraulic pump and an orbital hydraulic motor, replace the mechanical transmission (clutch, gearbox and reducer), thus enabling a very wide speed range.
An other advantages of the hydrostatic transmission we propose, simplify construction of the tiller and for the control systems for its operation and will mount easily on the transmission instead of classical combustion engine.
The disadvantage of the hydrostatic transmission is lower efficiency and higher costs.

REFERENCES

[1] P. Babiciu, V. Scripnic, Al. Fratila, "Hydraulic systems of tractors and agricultural machinery" Ceres Publishing House, Bucharest, 1984 - pg.45, 239, 241;
[2] M+S Hydraulic-Spool Valve Hydraulic Motors Catalog / Lyra firm;
[3] Poclain Hydraulic Catalog - Variable Displacement Pump Closed Loop Circuit / Lyra firm.

ISSN 1454 - 8003
Proceedings of 2014 International Conference of Hydraulics and Pneumatics - HERVEX
November 5 – 7, Calimanesti-Caciulata, Romania

INCREASING ENERGY INDEPENDENCE OF AGRICULTURAL INSTALLATIONS BASED ON CHAB CONCEPT

Erol MURAD[1]

[1] POLITEHNICA University of Bucharest, erolmurad@yahoo.com

Abstract: *In the context of sustainable development of agriculture is analyzed using a synergistically actual concept –* ***CHAB*** *–* ***C****ombined* ***H****eat* ***A****nd* ***B****iochar production - and to increase energy independence agricultural processes with local harvestable biomass, with a minimum of machining. Energy balance of the greenhouse and dryer, the halls of intensive poultry heat indicators required ≥ 90% and electricity ≤ 10%, which corresponds to a user's ideal for cogeneration systems. Modern processes of thermo-chemical gasification of biomass harvested locally, machined minimum, allow the production of heat and power in direct correlation with user requirements. The gasifier direct coupling with a burner increases energy efficiency, operational safety and to minimize or eliminate cooling-filtration systems are expensive and encombrante. It is exemplified the energy modules with type TLUD gasification process. Steam engines and Stirling cycles have low energy efficiency cogeneration facilities but meeting necessary to achieve in agriculture, as all residual energy can be converted into useful heat. The use of biomass for local energy production develop profitable economic activities for both community and the environment and increase employment levels and stabilize its labor force in rural areas.*

Keywords: *green energy, gasification, biochar, CHAB, dryer, greenhouse*

1. Introduction

A goal of sustainable agriculture is to increase energy independence farms, mainly based on the use of biomass resources and those locally available solar and wind. Agricultural production is seasonal involving use in relatively short periods of energy required for production processes. This leads to the conclusion that biomass is renewable energy source best suited to the needs of agricultural production because it can be stored after harvest and can be used effectively ***when and as necessary***.[2, 4, 5, 8,11,12]

Free burning agricultural biomass waste produces large amounts of emissions and a massive waste of heat. Modern procedures based on densification biomass processes into pellets or briquettes and burning in combustion chamber with high speed combustion air produce high emissions of PM and CO. Note that indirectly pelletizing produce CO2 emission related to electricity consumed. [1]

Alternatively actual current ways of producing heat from biomass is analyzed using the concept **CHAB** (Combined Heat and biochar production) incorporating heat and biochar production (BCH). BCH is a sterile charcoal produced from biomass pyrolysis in an environment with a substoichiometric concentration. It has a carbon content of 75-90% and is characterized by a very high porosity and adsorption capacity. BCH can be used as agricultural amendment to increase fertility of agricultural soils, and as filter material for air, gas and water. Built in soil is the most economical and ecological way of atmospheric carbon sequestration for long journeys. BCH harness Actual prices varied from 400 - 2000 €/t.bc dependent on zonal conditions, but with a European average of € 680 / t.bc. [4,11,12,13,16]

To apply the concept CHAB is analyzed TLUD biomass gasification process that produces combustible gas, also called gasgen, and biochar. Gasgen produced from gasifier is burned in an efficient and clean in a burner directly coupled to reactor or an another location. With TLUD process can gasify a wide variety of agricultural or other biomass source, shredded to 10..50 mm and humidity below 20%; features that allow the effective use of local sources of biomass and increases energy INDEPENDENCE farms. Minimal mechanical processing, transport distances below 15 km and natural ventilation drying leads to a very low cost thermal energy produced, estimated at up to 5 € / GJ, which is 6 times less than that obtained as the diesel. [7,8,11].

In many cases, agricultural production processes are performed in isolated areas without access to mains electricity net and therefore energy independence of installations must be carried by their own means in cogeneration mode. This aspect will be studied in terms of the use of biomass as an energy source available locally, clean and green energy supply for thermal, mechanical and electrical installations of small and medium agricultural production capacities.

For example it will consider increasing energy independence two types of agricultural systems: convective drying plants and vegetable tunnel greenhouses.

Convective dryers and greenhouses are ideal for users of cogeneration energy systems. They require, in total energy consumption:

- thermal energy for heating the air as thermal or drying agent - 92..95%;
- electricity for the fan drive - 4..6%;
- electricity for automation - 1..2%. [5,6,7,10]

Biomass can be used directly to produce heat through:

- direct combustion that produces flue gas with high entalpy;
- thermochemical gasification to produce used in installations for the production of thermal or electrical energy;
- gasification fermentation - occurs continuously usable biogas plants to produce heat or electricity;

For electricity production traditionally used gazgen or biogas to power internal combustion engines type mas for electro-generators with an overall yield of 20%. There have been attempts to use external combustion Stirling engines but their high cost makes them more economically viable. For agricultural farms, shows that to ensure sufficient electricity demand 5..8% overall yield. Starting from this reality to another level of technology, materials and automation resumed production of mechanical energy at low power with steam engines or free piston impulse turbines, external combustion engines that can use biomass burning or gazgen. However, due to small efficiency of the steam engine these systems are cost-effective only in cogeneration mode. An example is Bison-OTAG cogeneration system operating with chopped biomass or pellets. The most important aspect is that steam engines are ecological heat engines, which corresponds to the current requirements on environmental protection. [17]

Based on these aspects was analyzed applying the concept Chabal to increase energy independence and agricultural installations with small production capacity using biomass as a primary energy source and an energy system cogeneration steam engine. By capitalizing BCH product can achieve a significant reduction in the cost of energy produced. In this study we chose impulse steam turbine, four nozzles, because it has low weight and volume. This does not exclude the use of linear steam generators, free piston dual action, which are currently used in small domestic cogeneration installations. [3.17]

2. Biomass resourses from agriculture

Biomass from agriculture is harvested seasonally in large quantities to be transported, processed and stored; in table 1 are presented the advantages and disadvantages. Table 2 presents general information about the main types of agricultural biomass available in Romania. For chips using standard EN 14961.

There is a wide variety of densities on the basis of the processing and compaction. They influence the way of transformation of biomass into heat, which requires dedicated facilities that are more expensive. This is the main reason that has expanded so much as compaction into pellets, which provides a more uniform use of biomass. Plletizing requires additional costs and energy consumption of 1.5 MJ/kg.bm, so about 10% of the calorific value of the biomass. Chopping into pieces of 10 - 40 mm is conform with the standard EN 14961 value P45A, with maximum M20 and minimum BD200, consumes about 0.12 MJ/kg.bm, so about 10 times less. [1,2,7,14]

To apply the concept **CHAB** was adopted TLUD gasifiers which efficiently produce and 10-20% biochar. This type of gasification process is recommended to be used in agriculture as it can gasifying a wide variety of locally available biomass, chopped to 10..40 mm with humidity below 20%, have a high reliability, is simple and inexpensive. [8, 11, 12]

Table 1 Advantages and Disadvantages of biomass use

Advantages	Disadvantages
Agricultural Biomass is a fuel that is available at a very low cost for use in farms	Is responsible for air pollution when burned in open fires or traditional installations.
You can create large stocks of biomass farms algricole	It is very bulky and requires more storage space protected from the rain on the farm
Agricultural Biomass is safer than LPG, which raises safety issues for local transport and use	□Agricultural biomass □ seasonal availability may limit its use
It is easier to maneuver and transport	Low energetic density

Table 2 Residual agricultural wastes caracteristics

Nr.	Biomass	Volatile	Fixed Carbon	Ash	H.H.V.	Status	Bioma-ss Densi-ty	Bed Densi-ty
		[%]	[%]	[%]	MJ/kg	-	kg/m^3	kg/m^3
1	Tree prunings	75.0	24.0	1.0	19.0	chips	550	300
2	Vine prunings	77.4	20.0	2.6	19.1	chips	600	350
3	Corn stalks	77.2	19.3	5.5	17.7	chips	350	150
4	Corn stalks	77.2	19.3	5.5	17.7	pellets	1000	600
5	Energetic grass	76.0	18.0	6.0	17.5	pellets	1000	600
6	Vegetable stalks	77.0	19.0	4.0	17.0	pellets	1000	600

3. Convective dryer with biomass based cogeneration system

In figure 3 is presented block diagrame of a dryers with energy independence from biomass, in concept CHAB, with steam energy agent. [10]

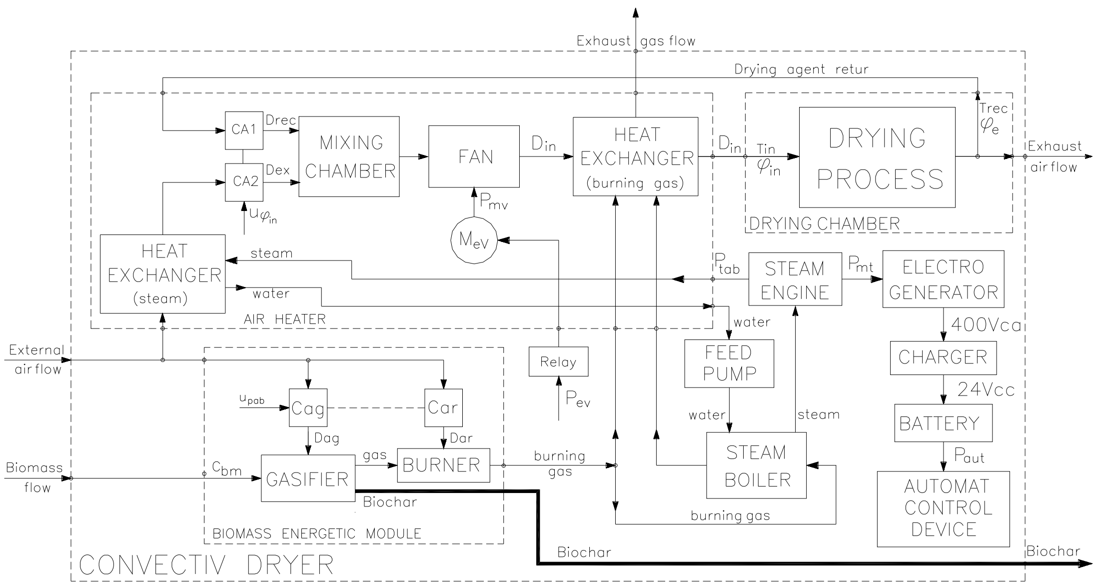

Fig.3 Block diagram of dryers with CHAB concept

For heat production using flow C_{bm} chopped or pelleted biomass gasified in TLUD gasifier with air flow D_{ag}. It produces gasgen which is burned with air flow D_{ar}. The flue gases which have a very low concentration of CO and particulate matter (PM) is discharged into the atmosphere. [6,7,8]

It examines the dryer type USCMER 30/60 AB, with 30 m^2 cassettes and rated thermal input of 60 kWth coupled to a cogeneration system that includes the concept CHAB. For electricity generation is fed with superheated steam turbine impulse action driving three phase electric generator 400 Vac. Generator produces a 4 kVA necessary to operate the dryer. In normal regim steam turbine continuously consumes a power of 13.5 kWth. Saturated steam exits the turbine at 0.5 bar, with a power of about 8.5 kWth waste heat; steam is used to heat outside aspirated air .

In table 4 is presented the energy balance in a cogeneration mode operation for dryer with energy independence obtained with a biomass CHP in CHAB concept.

Table 4 Convective dryer with cogenerativ energetic system

Feature	U.M.	Value
Nominal thermal power drying chamber	kWth	60.00
Electric power produced by the electric generator	kWe	3.64
Yield electric generator	-	0.90
Steam turbine mechanical power	kWm	4.04
Thermal power consumed by the turbine	kWth	13.47
Residual thermal power turbine output	kWth	8.96
Yield steam boiler (minimum)	-	0.85
Nominal thermal power boiler	kWth	64.51
Average thermal power boiler	kWth	34.51
Nominal thermal power boiler burner	kWth	75.90
Average thermal power boiler burner	kWth	40.60
L.H.V of a gasifierd biomass	MJ/kg.bmg	14.00
Production ratio BCH	-	**0.15**
Biomass conversion efficiency	-	0.90
Maximum hourly consumption biomass	kg.bm/h	25.51
Average hourly consumption biomass	kg.bm/h	13.65
Daily use time	h	20.00
Daily biomass consumption	Kg.bm/zi	272.95
Daily BCH production	kg.bc/zi	40.94
Total cogeneration yield	-	**0.64**
Average price chopped biomass	€/t.bm	50.00
Average price of biochar	€/t.bc	400.00
Daily fuel consumption cost	€/zi	-2.73
Drying period	zile/an	100.00
Annual consumption of biomass	t.bm/an	27.30
Annual production of BCH	t.bc/an	4.09
Annual cost of fuel	€/an	-272.95
Annual CO_2 emission	t.CO_2/an	**-14.26**

In this embodiment shows that energy efficiency cogeneration is 64%, which is lower than with diesel due to lower yields of conversion of biomass into useful heat. In this study we have used the lower limit values for yields, leading to the conclusion that the operation can be obtained cogeneration higher overall yields.In this embodiment shows that energy efficiency cogeneration is 64%, which is lower than with diesel due to lower yields of conversion of biomass into useful heat. In this study we have used the lower limit values for yields, leading to the conclusion that the operation can be obtained cogeneration higher overall yields.

4. Heating tunnel greenhouses with biomass

Heating tunnel greenhouses and solariums can be done with simple constructive installation, cheap and secure through application of the CHAB concept. To determine the specific aspects of the greenhouse warming with power modules GAZMER.T was chosen a tunnel type Quonset-based Metric 6 m, height 3 m, which has an area of 200 m2 ground and a volume of 475 m3. It is covered with a double wrap, inflatable polyethylene with high thermal resistance. [8,9,12]

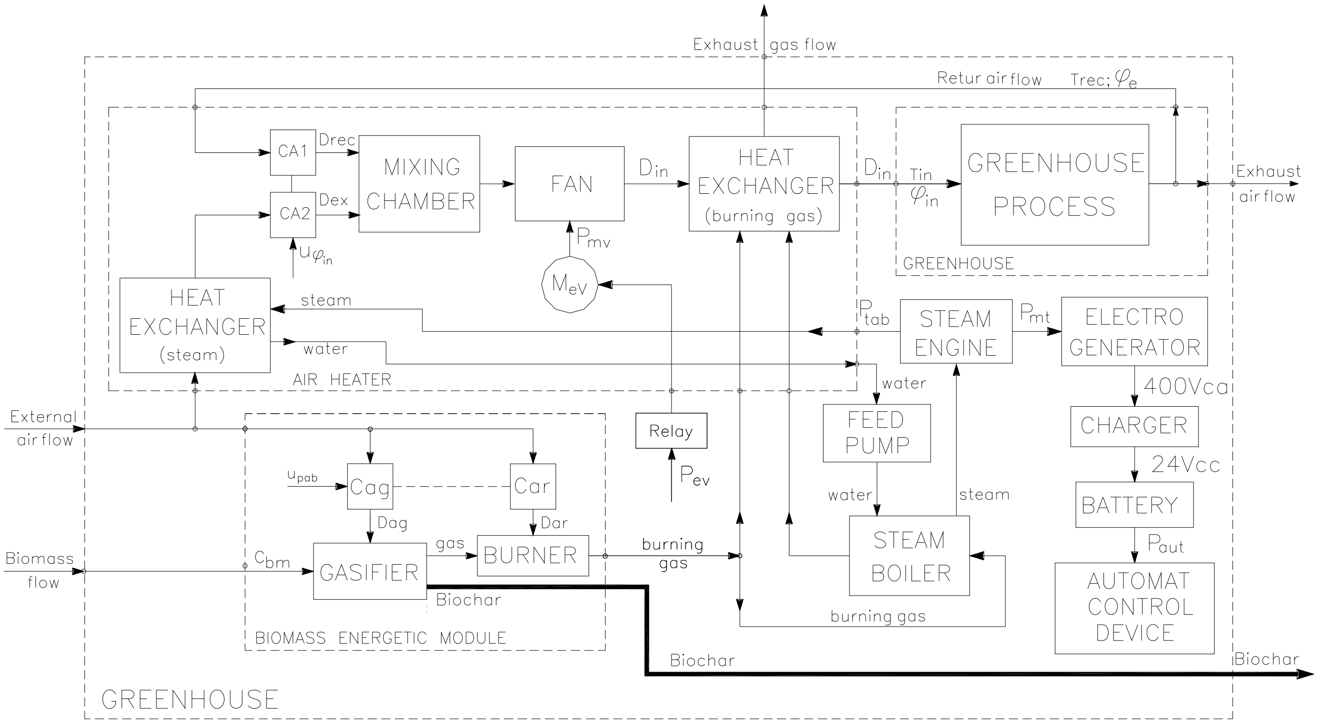

Fig. 4 Block diagram for a tunnel greenhouses with a biomass cogerative energy system

Tunnel greenhouse is heated by hot air through a flexible pipe which has apertures for distribution of the hot air jets. indoor air is partial recirculated and mixed with outside air for ventilation needed greenhouse; mixture was heated with a heat exchanger (HE). Actual yield of the heat exchanger is at least 85% and NTU type analysis confirm that remains almost constant throughout the range of use as D_{in}= 2 kg/s cnt. [9]

Table 5 Results of simulated experiments

		oct.	nov.	dec.	ian.	feb.	mar.	sezon
Heating time	day	**15**	**30**	**31**	**31**	**28**	**15**	**150**
Average calculation outdoor temperature	degree C	7.00	5.20	-0.10	1.20	5.60	7.00	**3.71**
Average indoor temperature	degree C	10.50	10.50	10.50	10.50	10.50	10.50	10.50
Average needed heating	K*day/month	52.50	159.00	328.60	288.30	137.20	52.50	1018.10
Average biomass consumption	kg.bm/K*day	13.20	13.20	13.20	13.20	13.20	13.20	13.20
Average monthly biomass consumption	t.bm/month	0.693	2.099	4.338	3.806	1.811	0.693	13.439
Average monthly biochar production	t.bc/month	0.092	0.278	0.575	0.504	0.240	0.092	1.781
Pellets price	€/t.pl	160.00	160.00	160.00	160.00	160.00	160.00	160.00
Local chopped biomass price	€/t.bm	50.00	50.00	50.00	50.00	50.00	50.00	50.00
Biochar as amendment price	€/t.bc	400.00	400.00	400.00	400.00	400.00	400.00	400.00
Monthly cost biomass for heating	€/month	34.65	104.94	216.88	190.28	90.55	34.65	671.95
Income biochar capitalization	€/month	36.73	111.24	229.89	201.69	95.99	36.73	712.26

Net cost biomass for heating	€/month	-2.08	-6.30	-13.01	-11.42	-5.43	-2.08	-40.32
Specific cost wihtout CHAB	€/m^2*month	0.173	0.525	1.084	0.951	0.453	0.173	0.672
Specific cost with CHAB	€/m^2*month	-0.010	-0.031	-0.065	-0.057	-0.027	-0.010	-0.040
Consumer report pellets/chips	kg.pl/kg.bm	0.738	0.738	0.738	0.738	0.738	0.738	0.738
Monthly cost pellet heating	€/month	81.83	247.83	512.17	449.36	213.85	81.83	1586.87
Specific cost pellet heating	€/m^2*month	0.41	1.24	2.56	2.25	1.07	0.41	1.59
Balance CO_2 sequestration	t.CO_2	-0.32	-0.97	-2.00	-1.76	-0.84	-0.32	*-6.20*

5. Conclusions

1. Agricultural production is seasonal that involve use in relatively short periods of energy necessary for production processes. Biomass is the most reliable and cheap source of energy for agriculture because it can be used **when and as necessary**.
2. Heat and biochar products with ecological CHAB concept, is how economic and ecological way to use agricultural waste biomass to increase energy independence on farms, increasing the productive potential of agricultural land and soil sequestration of CO_2 with a balance negative to -400 kg.CO_2/ t.bm
3. Energy balance of glasshouses, convective dryers and halls growth of broilers, indicating a need for ≥ 90% thermal power and ≤ 10% electricity power, the users ideal for biomass based cogeneration systems, systems that have as ecological thermal agent the steam.
4. Heat production from biomass can be achieved economically and environmentally through TLUD gasification process with high efficiency energy conversion, biochar production, very small emissions of CO and PM and with a large safety functions.

REFERENCES

[1]. Danciu A., Vladuţ V., Matache M., Mihai.M., Lehr C., Mihailov N., *Experimentation of Manufacturing Technology and Equipmens for Pellets/Agro-pellets*, INMATECH-Agricultural Engineering, Vol.31, nr.2, 2010
[2]. Callejon-Ferre A.J., and all, *Green crops residues: Energy potential and models for the prediction of their higher heating value*, Renewable and Sustainable Energy Reviews, vol.15, 948-955, 2011
[3]. Haslinger W., Friedl G., *Biomass micro scale CHP – State of art and recent R&D activities*, 2nd International Pellet forum, Verona, 26 february, 2010
[4]. McLaughlin H., *Biochar and energy linkages in: Biochar and Energy Co-products*, Center for Energy and Environmental Security, June 2010, Colorado, USA
[5]. Murad E., Safta V. V., Haraga G., *Biomass regenerating source of thermal energy for drying installations*, Conferinţa ISIRB, Hunedoara aprilie 2009
[6]. Murad E., Crăciunescu A., Haraga G., Panţiru A., *Instalaţii de uscare convectivă cu independenţă energetică bazată pe biomasă şi panouri fotovoltaice*, Simpozion HERVEX 2010, Călimăneşti, 10-12 noiembrie 2010;
[7]. Murad E., Vintilă M., Crăciunescu A., *Uscătoare cu impact ecologic redus pentru zone montane*, Sesiunea de comunicări ştiinţifice – ICEDIMPH-HORTING, 20 septembrie 2012
[8]. Murad E., Dragomir F., *Heat generators with TLUD gasifier for generating energy from biomass with a negative balance of CO_2*, International Conference HERVEX 2012, Călimăneşti, 7-9 noiembrie 2012
[9]. Murad E., Maican E., Dumitrescu C., Biriş S.S., *Extending the use of hothouses through heating with residual agricultural biomass*, TE-RE-RD-2013, Olăneşti, Vâlcea, 20-22 iunie 2013
[10]. Murad E., *Biomass cogeneration systems with steam cycle for convective dryers with energy independence and negative balance of CO_2*, CIEM – 2013, UPB, Bucureşti, 7- 8 noiembrie 2013
[11]. Murad E., *CHAB din biomasă agricolă cu TLUD – eficienţă economică şi ecologică,* Sesiunea de comunicări ştiinţifice – ICEDIMPH-HORTING, 28 noiembrie 2013
[12]. Murad E., *Applying the CHAB concept at horticultural greenhouses heated with biomass,* International Scientific Congress, LIVE SCIENCES A CHALANGE FOT THE FUTURE, USAMV-Iaşi, 24-25 octombrie 2014
[13]. Schmidt Hans Peter and all., *European Biochar Certificate - Guidelines for biochar production*, 2012 Delinat Institute und Biochar Science Network, Version 4.2 of 13th June 2012
[14]. Sima C., Haraga G., Murad E. *Environmentally drying vegetables using greenhouses crop residues,*TE-RE-RD 2013, 20-22 june, Olăneşti, 2013

[15]. Tomilson T., *Growth in the Biochar Movement and Industry Updates*, The International Biochar Initiative, February 2013
[16]. * * * Biochar for Environmental Management - Science and Technology, Edited by Johannes Lehmann and Stephen Joseph, EARTHSCAN, in the UK and USA, 2009
[17]. *** OTAG.Gmb. Bison –Powerblock, Germany

ISSN 1454 - 8003
Proceedings of 2014 International Conference of Hydraulics and Pneumatics - HERVEX
November 5 – 7, Calimanesti-Caciulata, Romania

RENEWABLE ENERGY SOURCES TO INCREASE ENERGY INDEPENDENCE OF MINI-GREENHOUSES

Gabriela MATACHE, Sava ANGHEL, Ionel PAVEL, Gheorghe SOVAIALA

[1] INOE 2000-IHP, fluidas@fluidas.ro

Abstract: *This paper aims to present research and identify solutions to achieve an innovative technology for a TLUD type biogas generating system (TLUD: Top-Lit Up Draft), which is designed primarily for heating greenhouses and hothouses. The raw material used as fuel should be chopped and dried and it could come from branches, vines or other plant debris from the secondary agricultural production.*

The innovative character consists of hot air generator design, based on TLUD principle, completely automated, allowing implementation of new solutions for preheating and electronic control of combustion and flue air. Technical solutions must be inexpensive, however with energetic and environmental protection results above conventional heating solutions. In parallel it is aimed to successfully use the combustion residue (BIOCHAR) as agricultural fertilizer.

1. The current level of development

For framing within the concepts and requirements of sustainable agriculture development, increasing the energy independence of greenhouses used as hothouse modules in households and in small farms with diversified and flexible production, represents a development direction with major economic and ecological effects, and contributes to the increase of the actual duration of use of the greenhouses.

For thermal energy needs for heating greenhouses, the use of agricultural or other provenience waste is analyzed. From this waste thermal energy is obtained by a gasification process which produces a hot fuel gas which is combusted in a burner specific for this type of gases.

Currently, the wooden and agricultural biomass pelleting and briquetting is widespread. For the production of pellets consumed energy represents an average of 8…10% of the calorific power of the biomass, and is emitted into the atmosphere an amount of CO_2 arising from the production of consumed electricity and from the manufacturing of used equipment. At the same time pelleting involves expensive equipment with high energy consumption, which makes the price to vary between 120 and 180 €/t depending on the biomass type, drying requirements, biomass transportation distances from the place of harvest to the processing place.

As a greener alternative, by means of TLUD (Top-Lit UpDraft) procedure, it is proposed to be used in the gasification process locally sourced biomass chopped at 10…50 mm and dried naturally or by means of ventilation to 10…20% humidity. Power consumption in this version is less than 3% of the calorific energy of the used biomass and far less CO_2 is emitted in the atmosphere. The cost per unit of usable energy decreases below 40% of the average energy cost in case of using pellets.

2. Hot air generating system

The proposed hot air generating system consists of:

1. biofuels supply module;
2. gasification module;
3. burning module;
4. heat exchanger;
5. electronic module for process monitoring and control;
6. piping;
7. chimney.

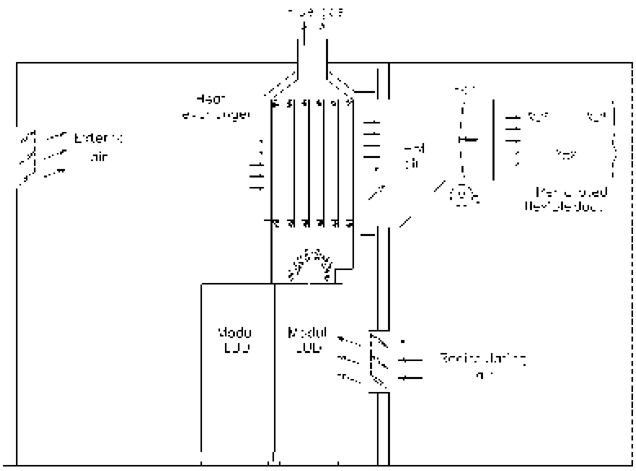

Schematic diagram of biogas hot air generator, TLUD type (Top-Lit UpDraft)

Functioning of the syngas TLUD type generator

The biomass is introduced into the reactor and is supported by a grill, through which the primary air for gasification moves upward. Fast pyrolysis reaches a point of incandescence on the top, and continues down in the biomass from the reactor. From the fast pyrolysis gas, tar and biochar are generated. Tars are passing through the incandescent coal bed, are cracked and totally reduced due to the heat radiated from the pyrolysis front and from the above placed flame. The resulting gas is mixed with secondary combustion air which is preheated by the reactor wall, and which is introduced into the combustion zone through the holes arranged at the top of the reactor. Highly turbulent mixture burns with flame at 900ºC. Thermal power adjustment is made by varying the primary and secondary air flow rates.

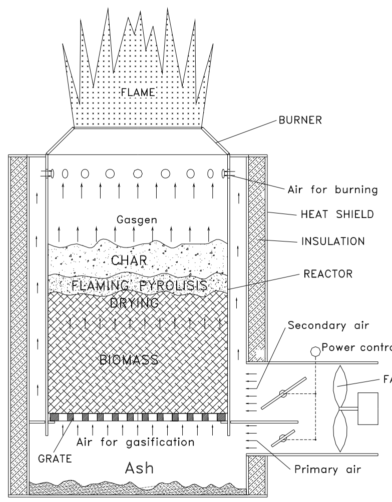

Simplified diagram of the burner with syngas

Within the project it will be studied the use of biomass resulted from the secondary agricultural production, as the main source of energy. It is about locally harvested biomass, minimally mechanically processed and dried to less than 20%. The TLUD energetic modules will use it to produce thermal energy and biochar. The TLUD energetic modules are characterized by low CO and PM emissions, high conversion efficiency, constructive simplicity, reliability and low cost.

The main problem is to bring the heating costs to a level that would justify the functioning time extension of hothouses as mini-greenhouses. Ecological effects will be beneficial also due to produced biochar, which is a good amendment for vegetable farming and which reduces the concentration of environmental CO_2 through carbon sequestration in the soil for long periods, obviously with a negative carbon balance. Below is shown an example estimating the use of biomass from the tree cuttings.

Tree cuttings in fruit groves are made in the non-vegetative period. Therefore, the average humidity of the cutted branches is 30-35%. If we take into account a humidity of 35% of a ton of branches, 765 kg of biomass will be obtained after drying them to an average humidity of 15%. It follows that a ton of cutted branches has an average energetic potential of 11,856 MJ or 3.3 MWh_{th}.

On one hectare of intensive fruit grove, an average of 3000 kg of biomass are annually cutted, which means an energetic potential of 35,628 GJ/ha · year. Biomass from cuttings is transported at the end of the trees row, where is chopped with specialized equipment to 10…50 mm and then stored in containers with perforated walls for a good air circulation. On average, the bulk density of wet tree branches is 250 kg/m^3, which leads to a need for about 12 containers for one hectare of fruit grove. After natural drying or forced ventilation, the biomass reaches an average humidity of 15% and a bulk density of about 200 kg/m^3. One ton of dry biomass has an energetic potential of 15,530 GJ/t.bm or 4.3 MWh_{th}. From the published data, in Europe an average cost of about 40 €/t is estimated for gathe-ring, chopping and transport of a ton of cutted branches. Taking into account a profit margin of 20% and VAT, a ton of biomass used for heat production can be sold by around 80 €/t. Specific price for primary energy in biomass is, in this case study, 5.2 €/GJ or 18.6 €/MWh_{th}. These values are much lower than for diesel (33.22 €/GJ) and LPG (21.52 €/GJ).

For a sustainable development of agriculture it is required an efficient use of its own resources, in order to increase the level of energy independence of its own technological processes. A relevant summary indicator is the energy balance of a crop. It can show what level of energy independence is and how it contributes to the reduction of carbon concentration in the atmosphere. Researches in the use of biomass for energy production have led to the conclusion that biochar, resulting from pyrolysis and gasification processes, is a valuable soil amendment for agriculture and an effective and very economical carbon sequestration method. In viticulture the most valuable byproduct from an energetic point of view is the biomass resulted from vine pruning, giving an average quantity of 2000 kg/ha and an energy potential of 24.8 Gj/(ha year). From an energetical and ecological point of view, the best option for unlocking the potential of this vine biomass is the thermo-chemical gasification, using adapted TLUD modules designed to produce heat and an average of 14% biochar.

The novelty is to use TLUD thermo-chemical gasification modules, for efficient use of local agricultural or forestry biomass, in order to produce hot air and biochar as a valuable agricultural amendment. Since the flue gases are nontoxic, part of them can be used to increase the concentration of CO_2 in the greenhouse, with minimal costs and increased safety. This significantly reduces the costs of heating, which contributes to the economic competitiveness of local vegetable production in winter.

By heating it with hot air, a hothouse will work as a mini-greenhouse. The hot air is driven by an axial fan through a flexible duct which has openings for the jets of hot air distribution in the greenhouse space. A part of the air in the greenhouse is recirculated, mixed with the outside air necessary for venting the greenhouse into a mixing chamber, from where the mixture is sucked by a fan through an internal-flue heat exchanger. This design eliminates the need for regular ventilation, whom are producing energy losses and decreases in temperature, which could prove harmful if not properly managed. Thus, there is the possibility that some of the flue gas with a high CO_2 content (but not toxic) to be introduced in the greenhouse, in order to increase the concentration of CO_2, therefore improving agricultural production with minimal costs. Temperature rigorous control in greenhouses and hothouses eliminates energy losses and decreases the effort and time user a spends for ventilation purposes.

3. Conclusion

As expected technical results it is aimed to research, design, testing and execution of hot air generator system prototype consisting of:

- module of feeding with biofuels,

- gasification module,
- combustion module,
- heat exchanger module,
- energy recovery module
- electronic monitoring and process control module

  Is also aims at:
- production of biochar which is a good agricultural amendment for vegetable growing and reduce the concentration of CO_2 from the environment through carbon sequestration in the soil for long periods, obviously with a negative carbon balance;
- possibility that a part of the flue gas with a high content of CO_2 , but which is not toxic, to be placed in the greenhouse to amplify concentration of CO_2 to improve agricultural production with minimal costs;
- temperature monitoring in the greenhouse eliminating periodic ventilation which leads to energy losses;
- reducing emissions of gases with greenhouse effect;
- submission of two patents that target applied innovative solutions concerning the control and dosage of combustion air and its preheating;
- dissemination of project results and the possibility of applying innovative solutions and other applications of gasification.

ACKNOWLEDGMENT

Presented work was supported by a grant of the Romanian National Authority for Scientific Research CCCDI - UEFISCDI, Project number: PN-II-PT-PCCA-2013-4-76.

REFERENCES

1. http://www.fluidas.ro/hidraulica/2012/3_4/39_44.pdf
2. http://www.youtube.com/playlist?list=FLBQY_0L1cv262M14g92Rl4Q
3. http://ebookbrowse.com/300-xxl-flue-gas-analyser-pdf-d148984747
4. http://ro.farnell.com/testo/510/manometer-0pa-to-100hpa-0-01-res/dp/1471394?crosssellid=1471394&crosssell=true&in_merch=true&
5. http://ro.farnell.com/jsp/displayProduct.jsp?sku=1471401&CMP=KNC-GRO-FRO-GEN-SKU-OTH&mckv=s37r6awCr|pcrid|13698205360|kword|testo%20606-2|match|p|plid|\
6. http://products.ecc.emea.honeywell.com/europe/pdf/en2b0137-ge51r0109.pdf
7. http://www.dynair.it/prodotti.php?idprod=61&numCat=14
8. Adams S., Meyer G., Fitzgerald J.,2008. *Biomass Heating in the Commercial Greenhouse*. University of Nebraska, Biological Sciences Engineering, 2008
9. Mukunda H. s., ş.a, 20*10. Gasifier stoves – science, technology and field outreach,* CURRENT SCIENCE, vol. 98, no. 5, 10 march 2010
10. Murad E., Maican E., Biriş S.S., Vlăduţ V., *Heating greenhouses with TLUD biomass energy modules*, 3rd International Conference „Research People and Actual Tasks on Multidisciplinary Sciences” 8–10 June 2011, Lozenec, Bulgaria
11. Murad E., Dragomir F., *Generatoare termice cu gazogen TLUD pentru producerea din biomasă a energiei cu un bilanţ negativ de* CO_2, HERVEX 2012, Călimăneşti 7-9 noiembrie 2012
12. Varunkunar S., (2012) Packed bed gasification-combustion in biomass domestic stove and combustion systems, Teza de doctorat, Department of Aerospace Engineering Indian Institute of Science, Bangalore, India, feb. 2012

ISSN 1454 - 8003
Proceedings of 2014 International Conference of Hydraulics and Pneumatics - HERVEX
November 5 – 7, Calimanesti-Caciulata, Romania

A SOLUTION TO REDUCE CO_2 EMMISSIONS

Ovidiu PACALA

[1] IFA Magurele, o.pacala@ifa-mg.ro

Abstract: *The appropriate management of the power consumers' networks is an efficient saving solution and hence the equivalent CO2 emissions reduction.*
The present paper describes a system able to significantly reduce the power consumption through the management of outdoor / indoor public lighting.

Keywords*: LED, management, network, lamp*

1. Overview

Reducing CO_2 emissions is an important segment of the global effort in cleaning up terrestrial atmosphere. A lot of actions are supported in this direction. If we assume a usual efficiency of around 30% for a classical thermoelectric plant, a simple evaluation shows that each saved MW leads to 0.58 tons less of CO_2 dump into the atmosphere

Outdoor and indoor public lighting is a high power consumer in the populous area. In this case, two trends of power saving efforts can be observed:

1. Using lighting devices or lamps of increasingly efficiency as shown in Table 1
2. Optimizing the network control, according to the local necessities

Table 1

Filament in vacuum - Edison	Filament and halogen	Florescence	HPS	LED
15 lm/W	25 lm/W	40-50 lm/W	80 lm/W	150 lm/W

The more efficient lamps are the LED ones. Moreover, they are dimmable from 0 to 100% without changing the efficiency and color rendering.

In order to improve the efficiency and capabilities of street lighting lamps, we developed one of the most efficient and simplest street light management and control system available that can be applied on high bays. The technology works effectively for intelligent LED's (light emitting diode) lamps, can drive no matter how many lamps (more than 65,000) and needs no intervention upon the existing network and no inermediary tranceivers.

2. Lighting Management and Control Network System

The Street Lighting Management and Control Network System is comprised of one to 65,000 or more Intelligent LED's Lamps, one computer (any type of PC or Laptop) having a USB connection, one radio transceiver of a mobile phone dimensions and a dedicated software to be installed on the PC, in a location chosen for the centralized management and control. The dedicated software need not a dedicated computer as it runs in background.
It enables to remotely program the entire street light network and/or any number of subgroups of lights or even individual lamps to:

a) turn on, off and dime at specific times and percentage of dimming during off-peak hours or for zonal events (street works, accidents, etc);

b) set dawn/ dusk triggers of photocells.

The programming is made from the center (the chosen location where the data server is located).

Each lamp contains a central unit around a RISC microcontroller and a radio transceiver on 2.4 GHz for data transfer.

A set of smart functions was implemented, as for example:

1. Locals: dimming, self-diagnoses, work after a 24h timing diagram, process the local sensors information – ambient light intensity, presence, etc.
2. A local clock was also implemented, with setting possibility.
3. Network: data transfer, individual or group addressability, report on the local parameters and errors to the central data server. The supported local address has 2 or 4 bytes and covers the largest imaginable lighting network.

The functions can be activated or deactivated from the data server or through the initial settings.

Street Light LED's Lamp

For isolated and not too large areas, the server is not necessary for the local functions are enough to control the lamps. For this kind of applications, the concept of 'chief lamp' was implemented. This is a function that can be activated as any other function and ensures the synchronism of the group. If the clock is never set, the group memorise the moment of the nightfall as a virtual time in order to apply a correct dimming diagram.

A persistent demand of the market is to redesign the lamp using a PLC (Power Line Communication) module for data transfer.

A version of high bay lamp with similar electronic diagram but other local functions was prepared.

Conclusions

The system reduces the electrical energy invoice with more than 70%, according of course to the particularities of the areas. It is ready to be mounted on the existing infrastructure - poles and power network and has the advantages of being power saving, nonpolluting, flexible, esthetic and futuristic.

Moreover, 571 tones less CO_2 per year dump into the atmosphere if 1000 de lamps of 400W each are replaced with equivalent LED lamps of 130 W each, as one see in Table 2

Table 2

Classic Lamps (Na, Hg)	Equivalent LED Lamps	Daily Power Savings for 1000 lamps (~10h/ day)	Yearly Power Savings for 1000 lamps (~ 3650hours/year)	CO_2 savings per year (tones)
100 Wh	35/65 Wh	650/ 350 KW	237.25/ 127.75 MW	137.5/ 74
400 Wh	130 Wh	2.7 MW	985.5 MW	571
1000 Wh	280 Wh	6.2 MW	2.263 GW	1311

REFERENCES

[1] Patent application OSIM A01391/ 22.12.2010 “Sistem si metoda de comanda si control” (*Command and Control Method and System*)– Ovidiu Pacala, Mirela Pacala
[2] **The Vancouver Sun “Going Green: Bright Ideas Vie for the Streets”** Published:Decem-ber 27, 2008 *http://www.streetlightiq.com/About/MediaClippings/MediaClippingDetail/tabid/169/Default.aspx*

ISSN 1454 - 8003
Proceedings of 2014 International Conference of Hydraulics and Pneumatics - HERVEX
November 5 – 7, Calimanesti-Caciulata, Romania

ENVIRONMENTALLY DRYING VEGETABLES USING GREENHOUSES CROP RESIDUES

Cristian SIMA[1], Marina BADILEANU[2], Marius BULEARCA[3]

[1] Centre of Industry and Services Economics, National Institute of Economic Researches, sima60cristian@yahoo.com

[2] Centre of Industry and Services Economics, National Institute of Economic Researches, badmarina@yahoo.com

[3] Centre of Industry and Services Economics, National Institute of Economic Researches, mariusbulearca@yahoo.com

Abstract: *The thermal energy production costs reduction options for vegetable dryers are studied using local biomass from crop residues in greenhouses. The residues used for thermal energy generation can get to an annual average of 5.7 t/ha dry biomass with an energy potential of 73 GJ/ha·year at a cost of up to 60 €/t. The 10-50 mm chopped biomass with a humidity below 15% is gasified using TLUD gasification process with high energy conversion efficiency, stability and security.*

Keywords*: drying, greenhouse residues, gasification, biochar, simulation*

1. Introduction

From the used biomass, the TLUD (Top-Lit-Up-Draft) process generates 10 to 15 percent bio-char that may be used as fuel or agricultural amendment. The team used the biomass resulted from the tomato creeping stalks. The biomass and the resulted bio-char are chemically and energetically defined according to the gasification process TLUD. The experiments are performed with a USCMER 30/60MGB drier, equipped with two energy modules GAZMER type MGB 40/150. [9,11]. The experimental results demonstrate that the biomass utilization resulted from the vegetable crop is feasible, the thermal energy cost being, in average, eight times lower than the diesel one. The biomass is burned with a CO_2 balance close to zero. The bio-char production regime and its incorporation into the soil for fertility purposes results in a long run sequestration of approximately 25% of the carbon generated. From the 8.7 tones/ha and year processed tomato crop biomass residues result 1.13 tones of bio-char containing 910 kg of carbon which, incorporated in soil, generates a CO_2 negative balance of -3.3 tones/ha and year.

2. Greenhouses crop residues properties

The quantities and humidity of the biomass residues vary by crop category and density. Initially, the whole residual quantity is cropped and than the leaves are mechanically separated from the creeping stalks; on average, only 20% remains from the initial quantity. The creeping stalks are chopped to 10-50 mm and dried naturally or mechanically up to a 10% average humidity, with a bulk density ranging between 200-250 kg/m^3 [2,9,10,12]. Table 1 summarizes the residues' characteristics for eight main vegetable species in Romania. We notice the value of the biomass average potential energy, reaching 73 GJ/ha, the equivalent of 20.27 MWh or 2150 L diesel fuel. The crop diversity generates different chemical and energy properties for the biomass residues. A global estimate is possible using the average characteristics depicted in table 1. [2,12]. The tomato crop is credited with high density, generating 9.8 tones/hectare of residual biomass, with a 134 GJ/hectare potential energy, the equivalent of 3988 L diesel oil. Table 2 shows processed biomass characteristics for fuel, gasification or pellet production purposes.

3. Greenhouses crop residues gasification

In a classical gasification process in co-current, the biomass layer descends continuously and enters gradually in the fixed pyrolysis and oxidation areas. In the TLUD process, the biomass layer is fixed in the reactor, and the pyrolysis and oxidation front is continuously descending consuming biomass, insuring a safe and controllable operation. [5, 7, 9, 11]. The TLUD process can be stopped when all the biomass was pyrolyzed and a quantity of unconverted carbon remains (bio-char current); or the gasification can be continued until the bio-char becomes ash.

Table 1. Greenhouse crop residues properties

Crop species	Crop Wastes	Sorted waste	Ash (dry bm)	Humi-dity	HHV BM sorted	HHV (dry)	LHV (dry)	BM (dry)	Energy content
	t/ha·year	t/ha·year	%	%	MJ/kg	MJ/kg	MJ/kg	t/ha·year	GJ/ha·an
Courgette	20.00	4.00	3.42	20	12.85	16.06	14.67	3.20	46.95
Cucumber	24.00	4.80	3.50	20	12.60	15.75	14.36	3.84	55.14
Aubergine	27.00	5.40	2.65	20	16.53	20.66	19.27	4.32	83.26
Tomato	49.00	9.80	3.04	20	14.82	18.53	17.14	7.84	134.34
Bean	23.00	4.60	2.88	20	17.00	21.25	19.86	3.68	73.08
Green pepper	28.00	5.60	3.56	20	15.26	19.08	17.69	4.48	79.23
Water melon	24.00	4.80	3.08	20	14.25	17.81	16.42	3.84	63.06
Melon	33.00	6.60	3.21	20	13.50	16.88	15.49	5.28	81.76
Mean	***28.50***	***5.70***	***3.17***		***14.60***	**18.25**	**16.86**	***4.56***	***77.10***

Table 2. Processed biomass from greenhouses crop residues

Crop Species	BM sorted (dry)	LHV (dry)	Humi-dity	LHV (wet)	BM sorted (wet)	BCH (mean)	LHV BCH (mean)	LHV BM (gasif.)	Energy content (gasif.)
	t/ha·year	MJ/kg	%	MJ/kg	t/ha·year	%	MJ/kg	MJ/kg	GJ/ha·year
Courgette	3.20	14.67	10.00	13.20	3.56	14.00	18.50	12.34	37.74
Cucumber	3.84	14.36	10.00	12.92	4.27	14.00	18.50	12.02	44.09
Aubergine	4.32	19.27	10.00	17.34	4.80	14.00	18.50	17.15	70.81
Tomato	7.84	17.14	10.00	15.43	8.71	14.00	18.50	14.93	111.82
Bean	3.68	19.86	10.00	17.87	4.09	14.00	18.50	17.77	62.49
Green pepper	4.48	17.69	10.00	15.92	4.98	14.00	18.50	15.50	66.36
Water melon	3.84	16.42	10.00	14.78	4.27	14.00	18.50	14.17	52.00
Melon	5.28	15.49	10.00	13.94	5.87	14.00	18.50	13.20	66.59
Mean	***4.56***	***16.86***	***10.00***	***15.18***	***5.07***	***14.00***	***18.50***	***14.64***	***63.99***

The bio-char is ranging between 10 and 15 % from the biomass entered in the gasification process and depends on the lignin content, on the average temperature of the oxidation layer and on the heating speed. The bio-char can be used as fuel, as a filter material or, more efficiently, as an agricultural amendment. [4, 5, 9]. To be used in the TLUD, the vegetable biomass needs to be chopped to 10-50 mm and dried up to a 10 % average humidity. From the TLUD results an average of 14% bio-char and 86% from the biomass is gasified and completely converted in thermal energy.

4. Conclusions

The TLUD is an economical and environmental way to turn to account the greenhouse crop wastes energy potential (thermal energy and bio-char generation) at a production cost between 40 – 60 €/t.
The TLUD is a high energy conversion efficiency process, with CO and PM very low emissions.
The TLUD energy modules are easy to operate, safe, tolerant to the biomass properties' variations.
The USCMER 30/60MGB drier is designed for the agricultural biomass residues, with a drying efficiency of minimum 40% and with thermal energy costs eight times lower than for the diesel fuel.
From the yearly tomatoes crop residues, in bio-char generation regime, one can dry approximately 20 tones of sliced tomatoes with a 25.2 €/tone of sliced tomatoes thermal energy average cost.

REFERENCES

1. Badileanu M., Murad E., Bulearca M., Sima C., *Avantajele economice ale deshidratarii legumelor si fructelor*, Conferinta de Nationala de Pomicultura, INCD Pomicultura Maracineni Argeş, 24 septembrie 2007
2. Callejon-Ferre A.J., and all, *Green crops residues: Energy potential and models for the prediction of their higher heating value*, Renevable and Sustainable Energy Reviews, vol.15, 948-955, 2011
3. Catana L., Murad E., Sima C., s.a., Indrumar pentru realizarea unei unitati de deshidratare a legumelor si fructelor, Ed PRINTECH, mai 2008
4. Mclaughlin H., S. Anderson P., Shields F., Reed Th., *All Biochars are Not Created Equal, and How to Tell Them Apart*, North American Biochar Conference, Boulder, CO, august 2009
5. Mukunda H.S., and all. *Gasifier stoves – science, technology and field outreach*, CURRENT SCIENCE, vol. 98, no. 5, 10 march 2010
6. Murad E., Sima C., Bădileanu M., Bălacianu G., *Modelarea – simularea proceselor de uscare convectivă*; Simpozion: Tehnologii moderne de uscare a legumelor si fructelor*,* IBA, 11 martie 2006
7. Murad E., Sima C., Balacianu G., Ipate G., *Modelarea si simularea proceselor si instalatiilor de uscare convectiva*, AMFI-2007, Bucuresti, 9-10 noiembrie 2007
8. Murad E., Safta V.V., Haraga G., *The control of the convective drying processes of fruits and vegetables according to a model*, International Conference U.T Ghe. Asachi, Iaşi, 22-23 octomber 2009
9. Murad E., Haraga G., Biris S.S., Sima C., *Module energetice TLUD pentru biomasa*, Conference - Alternative Renewable Energy Business Opportunities, Camera de Comert şi Industrie Râmnicu Vâlcea, 1-2 iulie 2010
10. Murad E., Seiculescu M., Sima C., Haraga G., *Utilizarea potenţialului energetic al corzilor de viţă*, Annual Conference, INCVV Valea Călugărească, 10 iunie 2010
11. Murad E., Sima C., Haraga G., Safta V.V., *Reduction of final humidity dispersion of bodies in convective drying process*, The 4th International Conference on Advanced Concepts on Mechanical Engineering, Iaşi, 17-18 iunie 2010
12. * * * GcBiomass – Greenhouses Crop, MORGAN AQUA Environmental Technologies, Madrid, Spain

ISSN 1454 - 8003
Proceedings of 2014 International Conference of Hydraulics and Pneumatics - HERVEX
November 5 – 7, Calimanesti-Caciulata, Romania

TRAINING OF THE HUMAN RESOURCES SPECIALIZED IN TECHNOLOGY TRANSFER AND INNOVATION IN ROMANIA - PAST AND FUTURE

Radu JECU[1]

[1] Research and Development National Institute for Metals and Radioactive Resources - INCDMRR Bucharest, Centre for Technological Information for Mineral Resources CENTIREM, radu.jecu3@gmail.com

Abstract: *The paper summarizes the development and the peculiarities of the training of human resources specialized in technology transfer and innovation in Romania.*

Keywords*: innovation, technology transfer, training, human resources, National RDI Strategy, National RDI Plan*

1. Introduction

The past & the future of the training of specialized human resources in technology transfer and innovation reveal the staff situation of the National Network for Innovation and Technology Transfer - ReNITT in order to improve performance and professional activity in the field in Romania

2. Chapter 1 / The Past.

Innovation & Technology Transfer activities were initiated in Romania around 2000, supported and stimulated by launching the National Program "Development of The Innovation & Technology Transfer Infrastructure – INFRATECH", approved by the Government Decision No. 128/2004 as a tool for supporting the establishment & developing the entities of the innovation & technology transfer infrastructure (scientific & technology parks, technology & business incubators, technology transfer centres, technological information centres, industry liaison offices).

"By the implementation of the INFRATECH Program there were provided:

- the bases of the national innovation & technology transfer system in order to ensure favorable conditions for the generation of a direct innovation current under the demand impulse
- the necessary framework for the reorganization of the RDI system and enhancing its capacity to meet the needs of the economic agents (especially SMEs)"[1]

In this context there was supported the establishment of new entities, the development of their infrastructure and that of the existing ones. Also, the (Romanian) National Innovation & Technology Transfer Network – ReNITT was formed, that integrates the main actors in the field.

In 2006, the innovation culture was still low, both in the enterprise field and in the academic environment. The enterprise innovation level has not been consistently supported by an operational technology transfer system, and the risk capital may be considered absent. In order to reduce disparities and to support the European integration, The National Research, Development and Innovation (RDI) Strategy 2007-2013, approved by the Government Decision No. 217/2007, emphasizes the special role which the innovation & technology transfer entities should have: "Brokerage centres and technology transfer and knowledge centres will provide the interface between the domestic need for innovation and the solutions that may be adapted from the global knowledge stock. The companies will create their own research structures or only interfaces ensuring their integration in open innovation systems and the participation to centres of competence or technology platforms. The universities and public research institutes will develop their own structures capitalizing knowledge and ensuring its transfer into innovative products and services. The technology transfer centres and the high-tech incubators will foster the transfer of knowledge and the development of the entrepreneurial skills. [...] Innovation will also be promoted in relation to the transfer of research outcomes, namely the turning of patents or know-how developed within complex projects into goods and services. For that purpose, the establishment and development of technology transfer entities will be supported, in particular within public research institutes and universities. Due to the cooperation relations they are developing, those centres are the key element promoting the formation of scientific and innovation clusters. Although the international practice shows that such centres cannot become important sources of revenue, the services provided lay the basis for the intersectoral researcher mobility, the use by companies of the experimental facilities in the universities and Research & Development (RD) institutions, and for increased chances regarding innovation and spin-off within those institutions." [2]

Regarding the specific activities in the field of technology transfer and innovation, the document mentioned above

1. shows that one of the specific objectives of the RDI system is: "[The] reinforcement of the role of science in society through science communication, promotion of ethics and equal opportunities in the field of research, development of interfaces dedicated to science-society dialogue." [2]

2. recalls that "taking into account the significance of fundamental research for knowledge development and the training of highly skilled human resources, the excellence, the interdisciplinarity and the international visibility will be emphasized."[2]

3. states that "innovation is in fact an outcome, where research may be just one of the sources, along with other factors such as experience, communication, marketing etc."[2]

4. mentions that "the evaluation of the commercial potential of an idea, the protection and licensing of the intellectual property right will be common elements of innovation management." [2]

In the text, there is one specific reference to the training, specialization and development of the human resource, the first one in an official programmatic document on the personnel formation in technology transfer and innovation: "The success of technology transfer centres depends on the specialized human resources quality, and, in order to support their complex training, the establishment of a system of international exchanges and sharing of good practices will be encouraged." [2]

All these demonstrate a realistic vision of the National Authority for Scientific Research during the strategy preparation, so the innovation and technology transfer activities role in the Romanian science development and the question of human resources quality in line with the European policies.

The National Plan for RDI 2007-2013 PN II, approved by the Government Decision No. 475/2007, was the main instrument used by the (former) National Authority for Scientific Research for the implementation of The National RDI Strategy 2007-2013. One of the principles of the PN II was: "The development of technology transfer infrastructure and services shall also be supported in view of a better valorization of RDI results in the economic environment, while observing the protection of intellectual property." According to the information packets of the PN II programs, the research organization is "an entity, such as a university or a research institute, irrespective of its legal status (public or private) or financing, whose primary goal is to conduct fundamental research, industrial research or experimental development and to disseminate its results through education activities, publication or technology transfer." [3]

Almost all the information packages stipulated the eligibility of expenditure programs for the dissemination of scientific results achieved. "Innovation" Program mentions among its specific objectives: "... 3. Developing the capacity of technology transfer in universities; 4. Stimulation of absorption capacity of RDI results by SMEs." "Capacities" Program was created "to allow researchers to work using modern devices, benefit from an adequate management and maintain a permanent relationship with socio-economic needs".[3] Its Module II was designed exclusively to support projects that aimed market orientation among their objectives and strengthen the role of science in society through activities such as: services, dissemination of information, events, promotional activities for knowledge results, prospective studies etc.

Unfortunately, the implementation of programmatic lines of the National Strategy for RDI 2007-2013 was severely disrupted by the global crisis, which has hit funding and science policy in Romania, especially the programs of The National Plan for RDI II. The financial and economic crisis led to the restriction of funds and activities, thus minimizing the chance of human resources' specialization in the RDI system.

Towards the end of the period, by the initiative of the Directorate of Innovation and Technology Transfer of the former National Authority for Scientific Research, the project "Program of Development of Human Resources within ReNITT in the Field of Management in order to achieve Efficient Technology Transfer Process" (POSDRU/81/3.2/S/48531) was developed. The result of the partnership between the Romanian Institute of Economic and Social Research and Polls (IRECSON) and the Romanian Association for Innovation and Technology Transfer (ARoTT), the project was carried out from 1 November 2010 till 31 March 2013, aiming to develop the professional skills of a minimum number of 300 managers and employees of the Romanian system of innovation and technology transfer in order to increase the competitiveness of the entities in the National Network for Innovation and Technology Transfer.

The project laid the courses foundation of the program "MITT - Management of Innovation and Technology Transfer" ran in the period 2012 - 2013 at the national level in five development regions: Bucharest – Ilfov, North – East, North – West, West and South – West. The program contained the following 9 courses approved by the (former) National Council of Qualifications and Vocational Training of Adults:

- Project Manager
- General Management Skills
- Communication and Public Relations Assistant
- Foreign languages: English / German / French
- Innovation Manager
- Technology Broker
- Marketing / Sales Manager
- Human Resources Manager
- Quality Systems Manager

The continuous vocational training program in the field of innovation and technology transfer developed by the project for the ReNITT personnel is offered to the companies / firms after the project ending.

The project has set up an electronic CVT in ITT (e-Center for Continuous Vocational Training for ITT (e-CVTITT) which includes, in addition to the resources and tools that provide for the e-learning courses, informative resources for developing a partnership network (database of partners, areas of interest, partnership requests, funding opportunities, successful projects etc.) to assist organizations in the area. Results of the project can be included in policies and strategies of integrated human resources training in the area of technology transfer.

In 2009, at university level, the "Management of Innovation and Technology Transfer" master program started through the project entitled "Managers and Employees Competence and Performance through Appropriate Training to Develop Entrepreneurial Culture and Valorization of Business Opportunities through Innovation – PERFORMER" in The Technology and Business Incubator ITA CPRU - University Politehnica of Bucharest. The theme has been currently continued within "Systems Engineering and Management Business" master program at the Faculty of Automatic Control and Computers.

3. Chapter 2 / The Future.

The National Strategy for RDI 2014-2020 has been recently approved by Government Decision No. 929 / 10.21.2014.

"Vision RDI 2020" - an outcome of the "Developing The National Strategy for RDI for 2014-2020" project - considers that in this period the emphasis is on the innovation firms or SMEs, supported by Research Organizations through the innovation and technology transfer entities.

All 3 general objectives of the RDI Strategy 2014-2020 are related to innovation and technology transfer activities.

As Romania continues to be under the European average in terms of indicators of intellectual property, in the document we find special reference on intellectual property services:

- Establishing an action program of indirect support for research, training scientists and engineers in industrial rights issues and intellectual property;
- Developing marketing capacity of public institutions in innovation;
- Encouraging for intellectual property exploitation

One of the subsections (4.2.3) refers only to the innovation and technology transfer infrastructure and innovation incubators. “The absence of an adequate number of professionals well located within public research organizations is a major challenge for the technology and knowledge transfer between public and private space. Public R & D organizations do not have adequate transfer teams, so commercial or social potential research is not optimally valued. As result of efforts to attract European funding to support the professionalization activities for innovation, Romanian incubators supported including the establishment and hosting firms, rather than the full spectrum of relevant services.”[4] Consequently, the strategy supports measures to professionalize the stage of technology transfer from public research organizations and other innovation-oriented organizations by:

- Human resource development program specializing in technology transfer;
- Trading capacity development program in universities, with a focus on training specialized human resources;
- Program of incubators and transfer centers development at regional level;
- Trading platforms for intellectual property demand and supply.”

Among the main transversal actions presented in the document we find "education in science communication", referring only to the popularization of science.

The proposed National Plan for RDI 2014-2020 / PN III does not exactly reflect the provisions of the Strategy; it minimizes human resources specialization in innovation and technology transfer.

4. Conclusions / Final considerations

- At the national strategies level, there is an upward trend of specialized training of the human resources in technology transfer and innovation, their developers gradually noting the importance of specific training for managers and employees to achieve competitive activities;
- At the national plans level, concerns for the professionals’ training in technology transfer and innovation have been neglected, especially because of the financial crisis, which caused a drastic redistribution of funding under the new priorities;
- At the innovation and technology transfer activities and projects level, the gap has increased towards the similar ones from the developed countries.

In conclusion, the dynamics of the European and global integration of the Romanian economy requires rapid and substantial improvement of the training dynamics for specialized human resources in the innovation and technology transfer entities aligned with current and future realities.

REFERENCES

[1] INFRATECH - Prezentare generală http://www.research.ro/ro/articol/1550/programe-nationale-instrumente-suport-acces-baze-de-date-infratech-prezentare-generala
[2] Strategia Naţională de Cercetare, Dezvoltare şi Inovare 2007-2013 http://uefiscdi.gov.ro/userfiles/file/ROST/1188314177strategia%20ro.pdf
[3] Planul Naţional de Cercetare, Dezvoltare şi Inovare II 2007-2013 http://uefiscdi.gov.ro/userfiles/file/ROST/PN2ro.pdf
[4] Versiunea tehnică a strategiei de Cercetare, Dezvoltare şi Inovare 2014-2020 (februarie 2014) http://www.cdi2020.ro/wp-content/uploads/2014/02/STRATEGIA_Versiunea-tehnica_Februarie-2014.pdf

ISSN 1454 - 8003
Proceedings of 2014 International Conference of Hydraulics and Pneumatics - HERVEX
November 5 – 7, Calimanesti-Caciulata, Romania

MOBILE EQUIPMENT FOR SIMULATION OF SIDE SKIDDING AT MOTOR VEHICLES

Corneliu CRISTESCU[1], Cătălin DUMITRESCU[1], Radu RĂDOI[1], Marian BLEJAN[1], Ioan BĂLAN[1], Ioana ILIE[1]

[1] INOE 2000-IHP, cristescu.ihp@fluidas.ro

Abstract: *The paper presents a mobile equipment for simulation of side skidding situations at motor vehicles under glazed frost or slippery ground. It shows the destination, the field of usage, structural composition of the equipment, as well as its usefulness as a support for training in police officer schools, and also in driving schools, to improve driving techniques in special traffic conditions.*

Keywords*: simulation equipment, car simulator, skidding simulator, mobile equipment, hydraulic drive, mechatronics*

1. Introduction

It is known that a particular importance in the training of professional and amateur drivers is palyed by the simulation techniques, which are increasingly used, for which there must be developed also appropriate technical means. These techniques are used both at home and abroad. In the country there are companies that have conducted various simulations with various degrees of freedom, which greatly reduce the actual time for accumulation of knowledge and, especially, of skills required to operate in various conditions.

On this line, the company EDEN-TECH [1] has developed a series of products, such as the intelligent simulator for training and verification in real-time and intelligent simulators for mobile and fixed platforms etc., which reduce learning time by 40%.

Also in Brasov has been developed the first professional motorsport simulator in Romania [2]. There are also other such achievements with outstanding results.

Internationally there are companies that deliver such simulators upon order, some equipped with special software tailored to the requirements.

All these simulation systems have been developed in order to introduce them in driving schools, so as to lead to an improvement of the training process and to the development of skills for defensive driving.

In the driving schools there stands as a necessity the use of simulators for training of drivers also for driving in difficult conditions. To this end, there have been developed simulation scenarios for various situations, leading to the acquisition of necessary skills for driving safely under difficult conditions: glazed frost, ice, skidding, fog, snow, heavy rain etc., [1], [2],

Training techniques have progressed very much, there being developed simulation scenarios for situations increasingly complex and difficult (glazed frost, ice, skidding, fog, night, snow, twilight, heavy rains etc), and good results were not slow in showing.

Recently, in our country, the question arose for achieving a simulator for side skidding, to be implemented in driving schools in ROMANIA. Drivers who attend piloting classes on vehicles provided with mobile simulator for side skidding gain, within few hours, skills and experience for different skidding scenarios, so that they will react instinctively, with minimal risk.

In this context, HYDRAULICS AND PNEUMATICS INSTITUTE in Bucharest has developed an equipment for side skidding simulation with electrohydraulic drive. Such a simulator is cheaper, with maintenance and operating costs lower than other simulators, and more reliable.

The general principle underlying the training activity that will be done with the equipment for side skidding simulation, in Figure 1, consists of controlledly suspending the car from a zero value, when the car rests entirely on its wheels (swivel wheels not touching the ground), up to a maximum value, when the wheels of the vehicle no longer touch the ground, (the unit chassis-vehicle rests entirely on the swivel wheels). Under these varying conditions of contact with the ground it will be possible to reproduce the trajectory of a motor vehicle losing adherence to raceway and skidding under the action of centrifugal force that occurs when cornering [3].

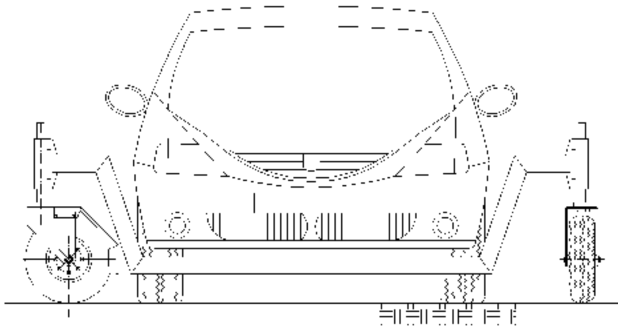

Fig. 1 Mobile equipment for side skidding

To achieve these training scenarios, the side skidding simulation equipment developed was equipped with electro-hydraulic drive, that allows closed loop control on vertical movement of the swivel wheels, becoming thus an advanced mechatronic equipment with safe operating [4].
The results of experimental research conducted during project implementation will be applicable to all entities for training of drivers, entities that use specially equipped DACIA LOGAN cars in testing fields for practical training.
Equipping the testing fields for practical training of drivers with side skidding simulation equipment will have major positive implications for road safety. Among these potential users there are: operational units of the Ministry of Internal Affairs (M.A.I.), driving schools, companies that own motor vehicles, etc.

2. Overview of the simulation equipment

The mobile equipment for side skidding simulation, shown in Figure 2, is a device used for training in testing fields, to simulate situations of car skidding on an icy or slippery ground.
The equipment is used to train drivers to cope with and react correctly in these situations. By taking over, to a greater or lesser extent, the weight of the vehicle by the front and / or rear swivel wheels of the device there is achieved decrease in adhesion to the ground of the vehicle wheels.

Fig. 2 Mobile equipment for side skidding

The device can be attached to the vehicle without doing interventions, dismantling or irreversible changes to the latter. The equipment was designed to be mounted on a car make DACIA LOGAN -

ISSN 1454 - 8003
Proceedings of 2014 International Conference of Hydraulics and Pneumatics - HERVEX
November 5 – 7, Calimanesti-Caciulata, Romania

Model 2010, but it could however be used, with minimal changes, also on other cars of about similar gauge[3].
The equipment has electrohydraulic drive and uses power supplied by the car battery and alternator. Control for changing the ground adhesion of the motor vehicle wheels is remote, by means of a remote controller within reach of the instructor seating next to the driver [4].
Hydraulic and electric installations are mounted in the trunk instead of the spare wheel, which is removed. This is the only intervention to be done.
The equipment is used only inside of a special testing field, provided with a large shunting area and a strictly smooth surface, no bumps or rocks larger than 20 mm.

2.1 Structure of the equipment

Structure of the equipment can be seen in the general assembly drawing shown in Figure 3, where can be noted the main parts of the equipment. The equipment consists generally of the following main parts:
- metal chassis suspended on swivel wheels;
- hydraulic installation;
- electrical drive and control installation;
- accessories for interconnecting and fastening the simulator on the car.

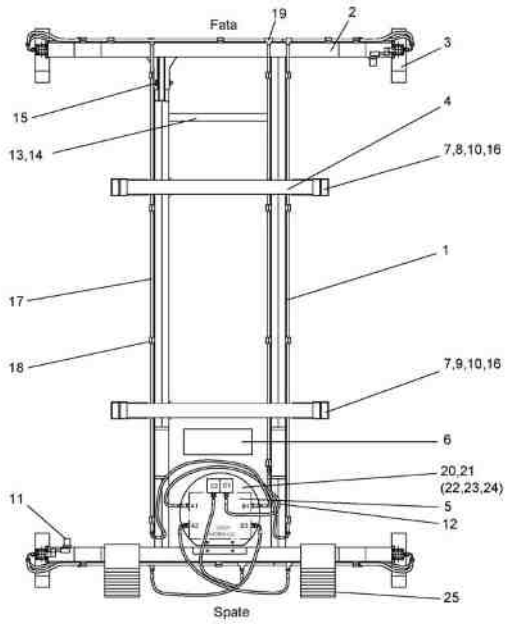

Fig. 3 Overall assembly of the simulator

Fig. 4 Chassis of the side skidding mobile simulator

2.1.1. Metal chassis

Metal chassis, as shown in Figure 3, is a structure consisting of two bridges (front and rear) (item 2) joined by two struts (item 1). On the struts there are placed loose two beams (item 4), which support the car that is simulating the skidding. Placing the car on the beams is done by means of elastic props (item 7) and spacers (items 8; 9). Bridges (item 2) are provided at the ends with swivel wheel hydraulic cylinders (item 3). Hydraulic cylinders lift the car off the ground by a

distance, reducing its adhesion and enabling it to skid. Swivel wheels do not oppose the tendency of the vehicle for side skidding.
On clamping cylinders to the bridges by means of swivel wheels, particular attention is paid to installation of stroke rotary transducers, in order not to damage them by striking [5].
On the bridges and struts there are fastened with clamps (item. 18) hydraulic supply pipes (item. 17), which are connected with each other and with hydraulic cylinders (the consumers) by means of end fittings (item. 19). In Figure 4, can be seen a picture of the metal chassis of the equipment made by INOE 2000-IHP.

2.1.2. Electrical drive and control installation

The electrical installation, shown in Figure 5, is made up of:
- electronic block, placed in the trunk of the car;
- a remote controller available to the instructor;
- cables and jacks for connecting them to the battery and electric consumers;
- electric consumers: electric motor of the pump, electromagnets of electro hydraulic distributors, position and pressure transducers.

The power cord is connected one wire to the plus sign of the battery and the other wire to the chassis, ensuring thus good operating conditions.

Electronic block, in Figure 6, consists of a plastic case comprising the following main parts:
- electronic control board (**controller**), provided with strips for connection;
- one button to power on the electrical installation;
- a signal lamp.

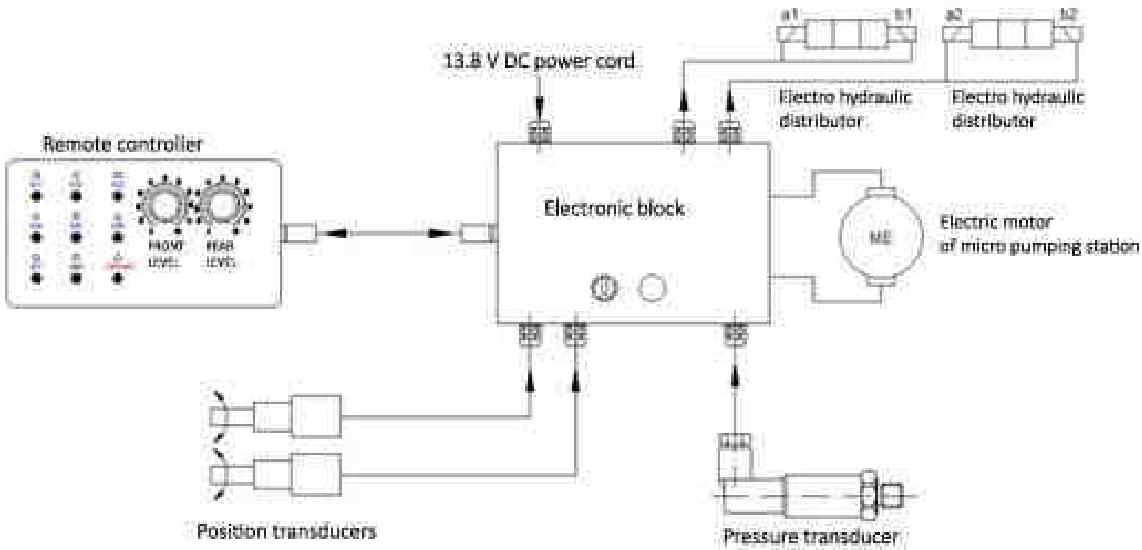

Fig. 5. Assembly of electronic drive and control block

Connecting to the remote controller is made via a jack mounted on the outside of the case. Electronic block case contains no buttons for manual controls. Manual controls to the cylinders can be performed either on the remote controller, or by direct manual operation of the slide valves of hydraulic distributors, or from the mechanical drive buttons in case of necessity (mechanical locking of slide valves), buttons which are located on the sides of the distributors.

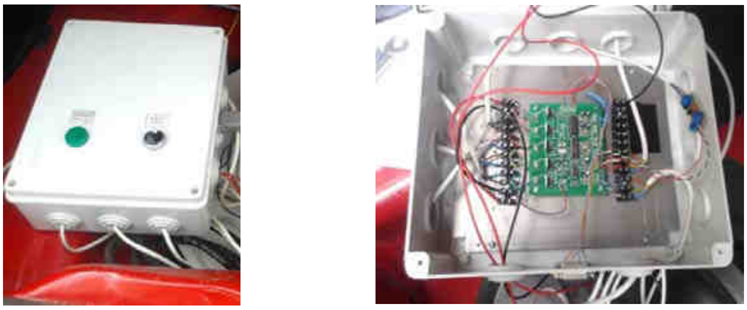

a) b)

Fig. 6 Electronic drive and control block

The remote controller, in Figure 7, is used by driving instructors. With it there can be made both manual and automatic controls. The manual controls are made from the rotating buttons of potentiometers and the emergency button ("Descent"), while the automatic controls by pressing the memory buttons 1÷7. Switching from manual control via buttons of potentiometers to control via memory buttons is done by pressing any memory button. Pressing the button (SET) does the reverse switching from control via memory to manual control.

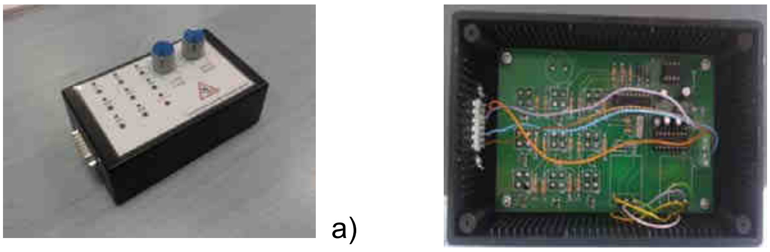

a) b)

Fig.7 Remote controller

3. General technical characteristics of the equipment

- Maximum load (equipment + car + passengers) 1600 daN;
- Drive .... electro hydraulic;
- Supply voltage ......……………...............................12 V DC;
- DC Electric motor power.………………150 W;
- Minimum road clearance (maximum adhesion)..............20 mm;
- Maximum road clearance (minimum adhesion)..................… 150 mm;
- Weight of simulator (including hydraulic system)...........400 kg;
- Sizes ....……..……............3 / 4 /1 m.

4. Presentation of hydraulic drive system

To achieve the training scenarios required to be performed in the testing field, it is necessary to use a flexible way of actuation, the most suitable being the electro-hydraulic drive.
General design of the hydraulic drive system / installation is presented in the hydraulic diagram shown in Figure 8, where can noted, at first glance, the use of electrohydraulic distributors for motion control, which provide the interface with the electronic control system, and also the use of stroke transducers, for closed loop motion control [5].

This hydraulic system works with pressurized hydraulic oil supplied by a hydraulic pump driven by an electric motor, powered to 12 V DC from the battery of the vehicle which is mounted on the chassis.

4.1. Presentation of the hydraulic diagram

Figure 8 shows the hydraulic diagram for actuating the simulation equipment; there one can see the structure, connections between devices and operation of the hydraulic system. Hydraulic cylinders (item 12) are connected in series and grouped by twos on each bridge (front and rear). Each group of two cylinders is actuated by an electro hydraulic distributor (item 14). The cylinders are the same size and the same stroke, which provides a simultaneous and strictly equal movement of the pistons and rods. Rod position is detected by a stroke transducer (item 11) and it is maintained by unlockable double valve (item 8) along the duration the hydraulic cylinders are not actuated.
Lifting speed is controlled by the way throttle (item 13) and nozzle (item 16), while lowering speed only by the nozzle (item 16). Any delays in movement of rods, which can occur after a while, can be removed through the manual distributor (item 15).
To increase the speed of movement of the rods there has been inserted into the system a hydraulic accumulator (item 9), allowing to make five maximum strokes (130 mm) to one bridge or two stokes and a half at both bridges at a single charge of the accumulator. The time to make a maximum stroke with the flow delivered by the hydraulic accumulator is 3.5 – 5.5 sec, while with the flow delivered by the pump (item 2) it is 23 – 25 sec.
Safety valve (item 5) is set to the maximum operating pressure of the system (160 bar), and oil returned to the tank (item 3) is filtered by the return filter (item 7). System pressure can be measured with the manometer (item 6).

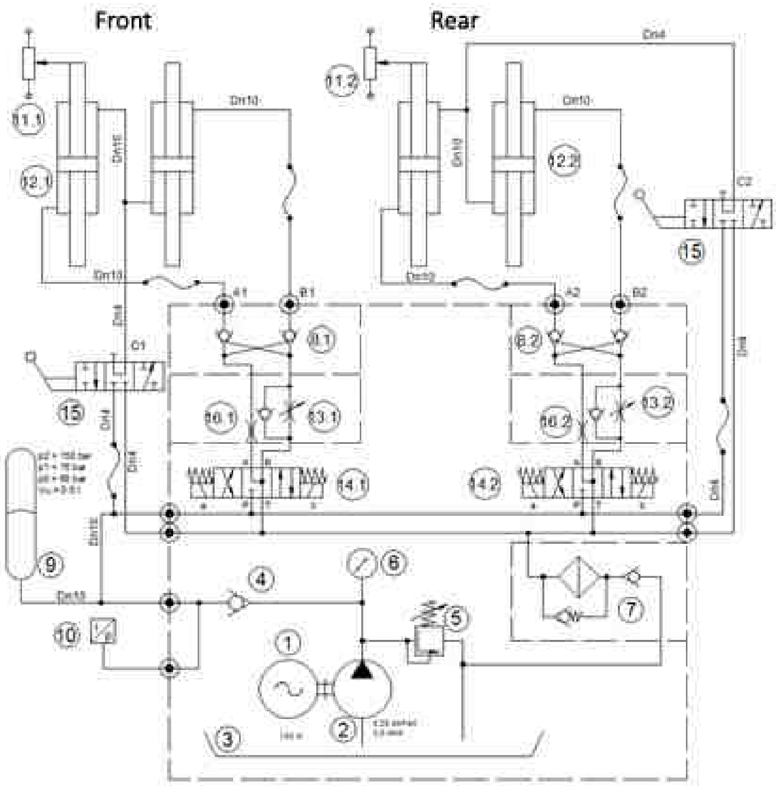

Fig. 8 Diagram of hydraulic drive

The two groups of cylinders (front and rear) can be controlled simultaneously or in turn, by electrical controls to the electromagnets of hydraulic distributors (item 14), given by the operator. Hydraulic drive can be made either via accumulator or via pump, which is indicated visually on the remote controller of the operator.

4.2. The hydraulic unit

In Figure 9 a and b, there is represented the hydraulic unit, also called mini hydraulic station, which is the source of pressurized oil and is made up of the following parts:

- block with devices (item 1), including most of the hydraulic equipment specified in the hydraulic diagram (Figure 2);
- hydraulic accumulator (item 2);
- manual distributors (item 3);
- pressure transducer (item 4).

Hydraulic unit is mounted on the motherboard (item 5) inside the car trunk, together with the electronic control block, Figure 6.

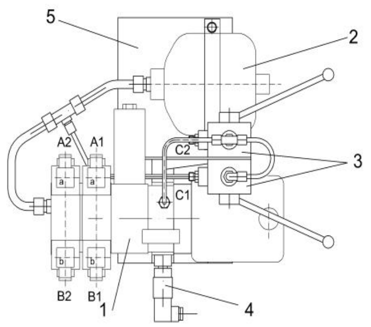

a)

b)

Fig.9 Hydraulic unit

Placing of hydraulic unit and electronic block is done inside the trunk, in the space occupied by the spare wheel, Figure 10.

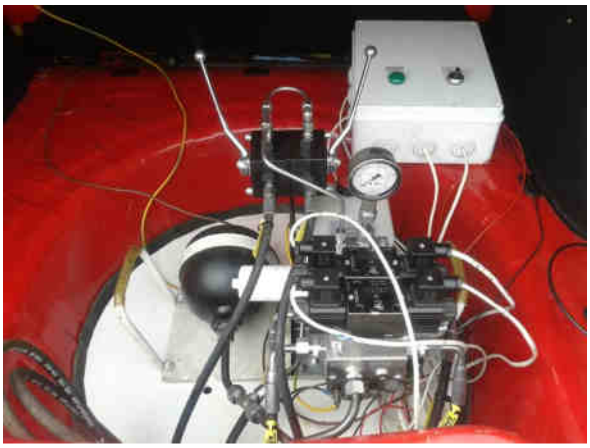

Fig. 10 Placing of hydraulic unit and electronic block inside the car trunk

4.3. Technical characteristics of the hydraulic system

Hydraulic pump:
- Maximum working pressure ......……............150 bar;
- Flow rate (q = 0.25 cm^3/rev).………….........~ 0.5 l/min;
- Time for hydraulic accumulator charge......1.5 min;

Hydraulic cylinders:..4 pcs;
- Piston diameter …………. ………….......ф 63 mm;
- Rod diameter ....……………………..........ф 45 mm;
- Maximum piston stroke …………….............130 mm

5. Conclusions

The paper presents an equipment for simulation of side skidding in motor vehicles, which was done on the request of a beneficiary.

By conducting specific applied experimental research, the equipment has been improved constructively and optimized functionally, being put into operation and approved. Tests carried out during product approval validated the constructive solution adopted and there are chances for its widespread implementation in the country.

The simulator presented is a novelty in our country and it is likely to generalize it in the specialized schools in the country, thereby contributing to the elimination of import and increasing jobs, based on the **advanced solutions** resulting from the research activity of the Institute.

REFERENCES

[1] Justin Gafiuc, Mihai Marinescu a inaugurat la Braşov primul simulator profesional de motorsport din România/ Mihai Marinescu inaugurated in Braşov the first professional motorsport simulator in Romania, In: GAZETA SPORTURILOR/ SPORTS GAZETTE, December 18, 2012. http://www.gsp.ro/sporturi/auto/senzatii-de-formula-1- mihai-marinescu-a-inaugurat-la-brasov-primul-simulator-profesional-de-motorsport-din-romania-379474.html;

[2] *** Sisteme inteligente training în timp real pentru instruirea şoferilor/ Intelligent real-time training systems or drivers training. În : EDEN-Consulting et engineering, http://www.eden-tech.com/simulatoare;

[3] *** Manual de utilizare DACIA LOGAN/ DACIA LOGAN User Manual http://www.automobile-dacia.cz/Dacia_Logan_mk1_(2003-2005)_Manual_utilizare_(ro).pdf ;

[4] Marin V., Marin Al. Sisteme hidraulice automate–constructie reglare exploatare/ Automatic hydraulic systems –building, control, operation, Technical Publishing House, Bucharest, 1987

[5] C. Calinoiu, Senzori si traductoare/ Sensors and transducers, vol. I, Technical Publishing House, Bucharest, 2009.

ISSN 1454 - 8003
Proceedings of 2014 International Conference of Hydraulics and Pneumatics - HERVEX
November 5 – 7, Calimanesti-Caciulata, Romania

VOCABULARUL TERMENILOR FOLOSITI IN HIDRAULICA / VOCABULARY OF TERMS USED IN FLUID POWER

Petrin DRUMEA[1], Gabriela MATACHE[1]

[1] INOE 2000-IHP, Bucharest, fluidas@fluidas.ro

Abstract: *Acest material isi propune sa arate definesca si sa arate sensurile corecte ale diferitelor componente hidraulice folosite in literatura de specialitate*

1. Introducere

Acest material a aparut ca o necesitate a realitatii descoperita pe parcursul anilor, atata in materilele de tehnica traduse din diverse limbi de circulatie internationala cat si in discutiile cu personalul care se ocupa cu aprovizionarea pentru diverse firme din domeniu.

S-a intamplat ca in materiale tehnice traduse in limba romana sa fie definite diferit aceleasi componente in functie de tara (limba) de unde au fost preluate echipamente sau sistemele hidraulice. S-a observat ca se pot da sensuri gresite functionarii aparatelor prin traducerea defectuasa a termenilor. Activitatea personalului de aprovizionare s-a complicat prin faptul ca nu s-au gasit puncte comune cu diversi vanzatori, ajungandu-se chiar la situatia cumpararii altor echipamente decat cele necesare.

Materialul se adreseaza cu precadere tinerilor care se vor descurca greu in cartile, articolele sau materialele tehnice care nu tin cont de normele interne si internationale. De aceea dorim sa preluam denumirile in engleza, germana si franceza din ISO 5598 /2008 si sa le denumim si definim in limba romana

2. Vocabularul

1. **Pompa volumica** (displacement pump; Verdrängerpumpe; pompe volumetrique) – pompa hidraulica la care debitul refulat este in functie de viteza de rotatie a arborelui. Teoretic presiunea nu depinde de turatie
2. **Pompa cu pistoane axiale** (axial piston pump; Axialkolben pumpe; pompe a pistons axiaux) – pompa hidraulica cu mai multe pistoane dispuse axial paralel intre ele
3. **Pompa cu pistoane axiale cu bloc inclinat** (axial piston pump; bent axis design; Axialkolbenpumpe in Schrägachsenbauweise; pompe a pistons axiiaux; conception a axes inclines; pompe a pistons inclines) – pompa cu pistoane axiale la care axa blocului cilindrilor are un unghi fata de axa arborelui de antrenare
4. **Pompa cu pistoane axiale cu disc inclinat** (axial piston pump; swashplate design; Axialkolbenpumpe in Schrägscheibenbauweise; pompe a pistons axiaux; conception a plateau oscillant independent) pompa cu pistoane axiale ale carei arbore de antrenare este parallel cu axa cilindrilor, iar discul inclinat nu este legat cu arborele de antrenare
5. **Pompa cu palete** (vane pump; Flügelzellenpumpe; pompe a palettes)- pompa hidraulica in care fluidul este pus in miscare de un set de palete radiale culisante
6. **Pompa cu pistoane in linie** (in – line pump; Reihenkolbenpumpe; pompe a pistons en ligne) – pompa cu pistoane paralele intre ele dispuse in acelasi plan perpendicular pe arborele de antrenare
7. **Pompa cu pistoane radiale** (radial piston pump; Radialkolbenpumpe; pompe a pistons radiaux) – pompa hidraulica cu pistoane dispuse radial

8. **Pompa cu roti dintate** (gear pump; Zahnradpumpe; pompe a engrenages) – pompa hidraulica cu doua sau mai multe roti dintate (ca elemente de pompare) lucrand impreuna intr-un corp comun
9. **Pompa cu roti dintate cu dantura exterioara** (external gear pump; Aussenzahnradpumpe; pompe a engrenages exterieurs) – pompa cu angrenaje cu roti dintate cu dantura exterioara
10. **Pompa cu roti dintate cu dantura interioara** (internal gear pump; Innenzahnradpumpe; pompe a angrenage interne)- pompa hidraulica cu roti dintate avand o roata dintata la interior ce angreneaza cu una sau mai multe roti dintate cu dantura exterioara
11. **Pompa cu surub** (screw pump; Schrauberpumpe; pompe a vis) – pompa hidraulica in care lichidul este deplasat de unul sau mai multe suruburi care se rotesc
12. **Pompa de supralimentare (**alimentare alta pompa) (charge pump; Speisepumpe; pompe de gavage)- pompa hidraulica avand ca functie cresterea presiunii de alimentare a altei pompe
13. **Pompa reversibila** (overcentre pump; Reversierpumpe; pompe reversible) – pompa la care sensul de curgere poate fi schimbat fara schimbarea sensului de rotatie al arborelui de antrenare
14. **Distribuitor** (directional-control valve; wegeventil; distributeur de comande directe) – aparat de distributie care inchide sau deschide una sau mai multe cai de curgere
15. **Aparat de distributie sau reglare** (valve; Ventil; distributeur)- aparat care controleaza directia, presiunea sau debitul unui fluid
16. **Aparat de distributie si reglare** (valve; Ventil;distributeur) – aparat care controleaza directia, presiunea sau debitul unui fluid
17. **Distribuitor cu 3 orificii de baza** (3 cai) (three – port valve; Drei-Wege-Ventil;distributeur a trios orifices) – distribuitor cu 3 orificii de baza
18. **Distribuitor centrat cu arcuri** (spring – centred valve; Ventil mit Federzentrierung; distributeur centre par resort)- Distribuitor autocentrant, in care elemental de distributie revine in pozitia initiala (central) datorita fortei unuia sau mai multor arcuri
19. **Distribuitor cu sertar** (spool valve; schieberventil; distributeur a tirair) – distribuitor in care elemental de inchidere (distributie) este un element cilindric culisant
20. **Distribuitor cu comanda numerica** (electrically operated valve; elektrisch betätigtes Ventil; distributeur a commande electrique) Distribuitor actionat prin comanda electrica
21. **Supapa anticavitatie** (anti-cavitation valve; Nachaugventil; clapet anticavitation) – Supapa de sens pentru protectia contracavitatiei
22. **Supapa cartus** (cartridge valve; Einbauventil; distributeur a cartouche) – Supapa care poate functiona doar in combinatie cu o carcasa (corp) in care este inclusa avand orificiile de legatura necesare
23. **Supapa de pilotare** (pilot valve; Vasteuerventil; vanne pilote) -Supapa ce furnizeaza un semnal de comanda pentru alt aparat (mai mare)
24. **Supapa de presiune** (pressure control valve; Druckventil; distributeur de commande de pression) – supapa care are rolul de a regla (controla) presiunea
25. **Supapa de reductie** (pressure-reducing valve; Druck minderventil; reducteur de pression) – Supapa care mentine presiunea de iesire (aval) chiar daca variaza presiunea de intrare (amonte) sau debitul
26. **Supapa de selectare** (shuttle valve; wechselventil; vane seleteur de circuit) – Aparat cu doua intrari si o iesire comuna, care permite trecerea fluidului de la o intrare la iesire, in timp ce blocheaza cealalta intrare

27. **Drosel reglabil** (throttle valve; Drosselventil; limiteur de debit) – Aparat de reglare a debitului
28. **Drosel de cale** (one-way flow control valve; Drosselrückschlagventil; limiteur de debit monodirectionnel) – Drosel cu supapa de sens de ocolire. Drosel care permite curgerea libera intr-un sens si curgerea controlata (droselizata) in celalalt sens
29. **Drosel fix** (fixed-restrictor valve; Konstantdrossel; reducteur de debit non reglable) Rezistenta hidraulica la care intrarea si iesirea sunt legate printr-o fanta de droselizare care nu poate fi modificata
30. **Regulator de debit** (flow control valve; stromventil; distributeur de debit) – Aparat de reglare a debitului
31. **Regulator de debit cu 2 cai** (series flow control valve; Zwei – wege- Stromregelventil; distributeur serie compose) Regulator care opereaza intr-o singura directive
32. **Regulator de debit cu 3 cai** (three-port flow control valve (three-way); Drei – wegw-Stromregelventil; distributeur compense de debit a trios orifices
33. **Cilindru cu simpla actiune** (single – acting cylinder; einfach wirkender Zylinder; verin a simple effect) – Cilindru la care forta fluidului poate fi aplicata intr-un singur sens
34. **Cilindru cu tija unilateral** (single-rod cylinder; Zylinder mit einseitiger kolbenstange; verin a simple tige) Cilindru la care tija pistonului iese pe la un singur capat
35. **Servocilindru** (servo-cylinder; Servozylinder; servo-verin) Cilindru capabil sa-si stabileasca pozitia cursei in functie de un semnal de comanda variabil
36. **Servovalva** (servo-valve; Servoventil; Servo-vane) – Aparat de distributie cu comanda electrica modulate la care zona moarta este mai mica de 3%
37. **Racord – Conector** (connector; Verschraubung; connecteur) – Dispozitiv care uneste tevi, furtunuri intre ele sau pe component
38. **Racord rotitor** (swivel connector; Schwenkverschraubung; connecteur pivotant) – Conector (record) ce se poate roti un unghi limitat, insa nu rotatie continua
39. **Efectiv** (adjectiv)(actual; tatsächlich; localise)- Obtinut prin masuratori fizice la un anumit timp si intr-un punct particular
40. **Presiune absoluta** (absolute pressure; Absolutdruck; pression absolue)- Presiunea care utilizeaza vidul absolute ca referinta
41. **Iesire activa** (active output; aktiver Ausgang; sortie active) – Iesire de putere la un aparat care in orice pozitie de comutare depinde doar de puterea de alimentare
42. **Presiune locala** (actual pressure; Istdruck; pression localisee) – Presiune existent intr-un anumit punct la un anumit moment
43. **Pozitie comutata** (actuated position; geschaltete Stellung; position commandee) – Pozitia finala a componentelor active ale valvei realizate sub actiunea fortelor de comanda
44. **Timp de actionare** (actuated time; Einschaltdaur; temps d-actuation) Timpul cuprins intre inceputul si sfarsitul semnalului de comanda
45. **Actuator** (actuator; Antrieb; actionneur) – Component (echipament sau element) care transforma energia hidraulica (a fluidului) in lucru mechanic .Exemplu: motor sau cilindru
46. **Aerare** (aeration;Lufteintrang; aeration) – Proces prin care aerul este introdus (antrenat) in fluidul hidraulic
47. **Amplificare** (amplification; Verstürkung; amplification) Raportul dintre semnalul de iesire si semnalul de intrare
48. **Inel antiextruziune** (anti-extrusion ring (back-up ring); Stützring; bague antiextrusin) – Inel destinat prevenirii extruziunii unui element de etansare (sub actiunea presiunii hidraulice) in spatial dintre suprafetele de etansare

49. **Proprietati antiuzura** (anti-wear properties; Verschleisschutzvermögen; proprieties anti-usure)- Insusirea unui fluid de a rezista unui contact metal-metal prin mentinerea unui film de fluid intre suprafetele aflate in miscare in conditii de functionare continua
50. **Presiune atmosferica** (atmospheric pressure; atmosphärendruck; pression atmospherique)- Presiunea absoluta a atmosferei intr-un anumit loc si la un moment dat

3. Concluzii

Materialul s-a oprit la 50 de definitii pe care autorii le-au intalnit cel mai des in literatura tehnica, urmand sa continue seria acestor termini.

Utilizarea corecta si ciompleta a termenilor din sistemele hidraulice usureaza foarte mult personalul ce deserveste aceste sisteme si instalatii.

REFERENCES

[1] ISO 5598/2008 Fluid power systems and components - Vocabulary;
[2] ISO 1219-1/2006 Fluid power systems and components – Graphic symbols and circuit diagrams
[3] Culegere de standard romanesti
[4] ISO 1219-2 Fluid power systems and components – Grafic Symbols and circuit diagrams – Part 2 – Circuit diagrams


www.hervex.ro